frontiers | Research Topics

The involvement of systemic homeostasis in tumour biology

Edited by
Simin Li, Aneesha Acharya, Wei-Lin Jin, Hongying Pan, Qian Wang and Gerhard Schmalz

Published in
Frontiers in Genetics

ISSN 1664-8714
ISBN 978-2-8325-2820-4
DOI 10.3389/978-2-8325-2820-4

About Frontiers

Frontiers is more than just an open access publisher of scholarly articles: it is a pioneering approach to the world of academia, radically improving the way scholarly research is managed. The grand vision of Frontiers is a world where all people have an equal opportunity to seek, share and generate knowledge. Frontiers provides immediate and permanent online open access to all its publications, but this alone is not enough to realize our grand goals.

Frontiers journal series

The Frontiers journal series is a multi-tier and interdisciplinary set of open-access, online journals, promising a paradigm shift from the current review, selection and dissemination processes in academic publishing. All Frontiers journals are driven by researchers for researchers; therefore, they constitute a service to the scholarly community. At the same time, the *Frontiers journal series* operates on a revolutionary invention, the tiered publishing system, initially addressing specific communities of scholars, and gradually climbing up to broader public understanding, thus serving the interests of the lay society, too.

Dedication to quality

Each Frontiers article is a landmark of the highest quality, thanks to genuinely collaborative interactions between authors and review editors, who include some of the world's best academicians. Research must be certified by peers before entering a stream of knowledge that may eventually reach the public - and shape society; therefore, Frontiers only applies the most rigorous and unbiased reviews. Frontiers revolutionizes research publishing by freely delivering the most outstanding research, evaluated with no bias from both the academic and social point of view. By applying the most advanced information technologies, Frontiers is catapulting scholarly publishing into a new generation.

What are Frontiers Research Topics?

Frontiers Research Topics are very popular trademarks of the *Frontiers journals series*: they are collections of at least ten articles, all centered on a particular subject. With their unique mix of varied contributions from Original Research to Review Articles, Frontiers Research Topics unify the most influential researchers, the latest key findings and historical advances in a hot research area.

Find out more on how to host your own Frontiers Research Topic or contribute to one as an author by contacting the Frontiers editorial office: frontiersin.org/about/contact

The involvement of systemic homeostasis in tumour biology

Topic editors

Simin Li — Southern Medical University, China
Aneesha Acharya — Dr D Y Patil Dental College & Hospital, India
Wei-Lin Jin — First Hospital of Lanzhou University, China
Hongying Pan — University of Michigan, United States
Qian Wang — Tai'an City Central Hospital, China
Gerhard Schmalz — Leipzig University, Germany

Topic Coordinators

Jingjing Luo — Sichuan University, China
Xianda Hu — China Tibetology Research Center, China

Citation

Li, S., Acharya, A., Jin, W.-L., Pan, H., Wang, Q., Schmalz, G., eds. (2023). *The involvement of systemic homeostasis in tumour biology*.
Lausanne: Frontiers Media SA. doi: 10.3389/978-2-8325-2820-4

Table of contents

frontiers | Frontiers in Genetics

ORIGINAL RESEARCH
published: 14 July 2022
doi: 10.3389/fgene.2022.938787

ER Stress–Related Genes EIF2AK3, HSPA5, and DDIT3 Polymorphisms are Associated With Risk of Lung Cancer

Yongshi Liu[1†], Xiaohua Liang[1†], Hongpei Zhang[2], Jiajia Dong[2], Yan Zhang[2], Juan Wang[1], Chunmei Li[2], Xiangbing Xin[1] and Yan Li[1]**

[1]Department of Thoracic Surgery, Tangdu Hospital, The Fourth Military Medical University, Xi'an, China, [2]Department of Respiratory Medicine, Tangdu Hospital, The Fourth Military Medical University, Xi'an, China

Objective: This study aimed to evaluate the associations between endoplasmic reticulum (ER) stress–related genes *EIF2AK3*/PERK, *HSPA5*/GRP78, and *DDIT3*/CHOP polymorphisms and the risk of lung cancer.

Methods: Six single-nucleotide polymorphisms (SNPs) of *EIF2AK3*, *HSPA5*, and *DDIT3* were genotyped in 620 cases and 620 controls using a MassARRAY platform.

Results: The minor allele A of rs6750998 was a protective allele against the risk of lung cancer ($p < 0.001$), while the minor alleles of rs867529, rs391957, and rs697221 were all risk alleles that may lead to multiplied risk of the disease ($rp_{rs867529} = 0.002$; $p_{rs391957} = 0.015$; $p_{rs697221} < 0.001$). Moreover, the rs6750998-TA/AA genotypes were protective genotypes against the risk of lung cancer ($p = 0.005$); however, the rs867529-GC/CC, rs391957-CC, and rs697221-GA/AA genotypes were associated with elevated lung cancer risk ($p_{rs867529} = 0.003$, $p_{rs391957} = 0.028$, and $p_{rs697221} = 0.0001$). In addition, *EIF2AK3*-rs6750998 was associated with a decreased risk of lung cancer under dominant, recessive, and log-additive models ($p < 0.05$). By contrast, the *EIF2AK3*-rs867529 was correlated with an increased risk of the disease under dominant and log-additive models ($p = 0.001$). Moreover, *HSPA5*-rs391957 was related to an elevated risk of the disease under recessive and log-additive models ($p < 0.02$). *DDIT3*-rs697221 was identified to have a significant association with the risk of lung cancer under all three genetic models ($p < 0.01$).

Conclusion: Our results provide new insights on the role of the ER stress–related genes *EIF2AK3*, *HSPA5*, and *DDIT3* polymorphisms for lung cancer risk.

Keywords: lung cancer, gene polymorphisms, single-nucleotide polymorphisms, endoplasmic reticulum stress, case–control study

OPEN ACCESS

Edited by:
Simin Li,
Southern Medical University, China

Reviewed by:
Varun Sharma,
NMC Healthcare (NMC Genetics), India
Mohammad Safiqul Islam,
Noakhali Science and Technology University, Bangladesh

****Correspondence:***
Xiangbing Xin
429392090@qq.com
Yan Li
liyanfmmu@163.com

[†]These authors share first authorship

Specialty section:
This article was submitted to Cancer Genetics and Oncogenomics, a section of the journal Frontiers in Genetics

Received: *08 May 2022*
Accepted: *14 June 2022*
Published: *14 July 2022*

Citation:
Liu Y, Liang X, Zhang H, Dong J, Zhang Y, Wang J, Li C, Xin X and Li Y (2022) ER Stress–Related Genes EIF2AK3, HSPA5, and DDIT3 Polymorphisms are Associated With Risk of Lung Cancer. Front. Genet. 13:938787. doi: 10.3389/fgene.2022.938787

INTRODUCTION

At present, lung cancer is still a malignant tumor with the highest morbidity and mortality worldwide and is one of the biggest enemies that threaten human health (Siegel et al., 2021; Yang et al., 2022). The World Health Organization statistics show that there were approximately 2.2 million new cases and 1.8 million death cases of lung cancer in 2020, the incidence and mortality rates are 11.4% and 18.0%, respectively (Mattiuzzi and Lippi, 2020). In China, due to increasing air pollution in the

process of industrialized urbanization, the highest prevalence of tobacco use, the gradual arrival of an aging society, and changes in lifestyles, the incidence and mortality rates of lung cancer have been on the rise (Cao and Chen, 2019). The treatment of lung cancer mainly includes surgical resection, chemotherapy, radiotherapy, and molecular targeting drugs (Hirsch et al., 2017). Although the treatment of lung cancer has made certain progress in recent years, the overall survival is still dissatisfactory (Patel and Weiss, 2020). Most patients progress to the late stage of this disease at diagnosis and miss the best time and means of treatment, leading to a low five-year survival rate. Therefore, it is extremely important to find biomarkers that can be used in the early diagnosis of lung cancer.

The endoplasmic reticulum (ER) is an organelle that is in charge of the synthesis, processing, and modification of protein and thus plays a pivotal role in maintaining proteostasis. When the cells lack nutrition and have low oxygen, calcium imbalance, or oxidative stress, the unfolded and misfolded protein could accumulate, resulting in ER stress (Walter and Ron, 2011). Accumulating evidence have shown that ER stress is deeply involved in the growth, survival, and differentiation of tumor cells (Chen and Cubillos-Ruiz, 2021). PRKR-like ER kinase (PERK) is one of the main stress sensors that mediates ER stress. Generally, PERK is bound to the molecular partner protein causing glucose-regulated protein 78 (GRP78) to become inactive. Under ER stress, the unfolded or misfolded protein is bound to GRP78 competitively, resulting in the dissociation of GRP78 to PERK and activation of the downstream signaling pathway (Volmer et al., 2013). Moreover, activated PERK phosphorylates elF2α and upregulates ATF4 and CHOP, resulting in the activation of a number of genes involved in the biosynthesis and transport of amino acids and intracellular autophagy (B'Chir et al., 2013; Han et al., 2013). Therefore, PERK, GRP78, and CHOP are important proteins involved in ER stress. Previous studies have reported the crucial functions of these genes in the occurrence and metastasis of several types of cancer (Xie et al., 2015; Xu et al., 2019; Zhang et al., 2019). However, little information is found about the single-nucleotide polymorphisms (SNPs) in *EIF2AK3*/PERK, *HSPA5*/GRP78, and *DDIT3*/CHOP in cancer patients, especially those with lung cancer.

In the present study, a total of six candidate SNPs in *EIF2AK3*, *HSPA5*, and *DDIT3* were chosen from previous association studies. The rs6750998 and rs17037621 are intron SNPs in *EIF2AK3* and associated with insulin resistance, high BMI, and the risk of prediabetes (Feng et al., 2014). The rs867529 is a nonsynonymous SNP in *EIF2AK3* and is correlated with the risk of prediabetes and lower bone mineral density (Liu et al., 2012). Moreover, rs17840761 and rs391957 are promoter SNPs in *HSPA5* and have been investigated in patients with gastric and colorectal cancer (Winder et al., 2011). Additionally, rs697221 is a nonsynonymous SNP in *DDIT3* and has been detected in patients with melanoma in a Brazilian population (Francisco et al., 2013). None of these SNPs have been genotyped in patients with lung cancer. Therefore, we genotyped these candidate SNPs in a case–control cohort with 620 lung cancer patients and 620 healthy controls and evaluated these associations with the risk of lung cancer.

MATERIALS AND METHODS

Participants

In this study, 620 lung cancer patients and 620 healthy controls were recruited at the Tangdu Hospital. The diagnosis of lung cancer was established by histopathological examination of biopsy or resected tissue specimens. The patients who had received chemo- or radiotherapy were excluded. The healthy controls were enrolled from cancer-free individuals from the same hospital and were matched to the cases in gender and age. We obtained written informed consent from all subjects. The study was approved by the Ethics Committee of Tangdu Hospital and carried out in accordance with the World Medical Association Declaration of Helsinki—Ethical Principles for Medical Research Involving Human Subjects.

Genotyping

Six tag SNPs in *EIF2AK3*, *HSPA5*, and *DDIT3* were selected in the present study; these SNPs were with minor allele frequencies (MAFs) >5% in the East Asian populations of 1000 Genomes. The DNA was extracted from the blood samples using the QIAamp DNA Blood Midi Kit (QIAGEN, Germany). The primers were designed using the SEQUENOM MassARRAY Assay Designer 3.0 software. SNP genotyping was performed by SEQUENOM MassARRAY RS1000 (Sequenom Inc., San Diego, CA). The primers used for this study are listed in the **Supplementary Material**.

Statistical Analysis

Statistical analyses were performed with SPSS 21.0 statistical package (SPSS, Chicago, IL, United States). The allele frequencies in the cases and controls were tested for departure from the Hardy–Weinberg equilibrium (HWE). HaploReg v4.1 (https://pubsbroadinstituteorg/mammals/haploreg/ haploregphp) was used to predict the potential functions of the SNPs. Differences in the demographic variables and allele frequencies between the cases and controls were evaluated using chi-square tests and Welch's t-tests. Associations between the genotypes and lung cancer risk were evaluated by unconditional logistic regression analysis and expressed by odds ratios (ORs) and 95% confidence intervals (CIs) using SNPstats (https://www.snpstats.net/start.htm). The interaction between SNPs was analyzed by using multifactor dimensionality reduction (MDR) software. The statistical significance was established when $p < 0.05$.

RESULTS

The basic information of the participants is listed in **Table 1**. The case group included 384 males and 236 females, and 381 smokers and 239 nonsmokers, with a mean age of 57.09 years; the control group included 381 males and 239 females, and 378 smokers and

TABLE 1 | Basic information of the participants.

Characteristics	Case (n = 620)	Control (n = 620)	χ2/t	p
Gender (%)			0.031	0.860
Male	384 (61.9)	381 (61.5)		
Female	236 (38.1)	239 (38.5)		
Age			0.282	0.563
Mean ± SD	57.09 ± 10.41	56.61 ± 10.64		
Smoking (%)			0.031	0.860
Yes	381 (61.5)	378 (61.0)		
No	239 (38.5)	242 (39.0)		
Pathological types				
Adenocarcinoma	294 (47.4)			
Squamous cell carcinoma	188 (30.3)			
Small-cell lung cancer	113 (18.2)			
Others	25 (4.1)			

TABLE 2 | Basic information and predicted functions of candidate SNPs.

SNP	Gene	Position	Allele	Role	Predicted functions
rs6750998	EIF2AK3/PERK	chr2:88583424	T > A	Intron	Motifs changed and eQTL hits
rs17037621	EIF2AK3/PERK	chr2:88606202	T > A	Intron	Promoter/enhancer histone mark, motifs changed, and eQTL hits
rs867529	EIF2AK3/PERK	chr2:88613755	G > C	Missense variant	Ser136Cys
rs17840761	HSPA5/GRP78	chr9:125241700	G > A	Promoter	Promoter histone mark, motifs changed, and eQTL hits
rs391957	HSPA5/GRP78	chr9:125241745	T > C	Promoter	Promoter histone mark, motifs changed, and eQTL hits
rs697221	DDIT3/CHOP	chr12:57517377	G > A	Missense variant	Phe33Leu

SNP, single-nucleotide polymorphism; eQTL, expression quantitative trait locus.

TABLE 3 | The MAF and HWE of candidate SNPs between lung cancer cases and healthy controls.

SNP	Gene	MAF-cases	MAF-controls	HWE *p*-cases	HWE *p*-controls	OR (95% CI)	p
rs6750998	EIF2AK3/PERK	0.21	0.27	0.55	0.61	0.733 (0.609–0.882)	<0.001*
rs17037621	EIF2AK3/PERK	0.34	0.33	0.21	0.99	1.075 (0.910–1.271)	0.394
rs867529	EIF2AK3/PERK	0.40	0.34	0.13	0.93	1.301 (1.105–1.531)	0.002*
rs17840761	HSPA5/GRP78	0.43	0.41	0.74	0.56	1.083 (0.923–1.270)	0.328
rs391957	HSPA5/GRP78	0.26	0.22	0.18	0.99	1.256 (1.045–1.510)	0.015*
rs697221	DDIT3/CHOP	0.23	0.17	0.82	0.32	1.504 (1.234–1.834)	<0.001*

p < 0.05 indicates statistical significance.

SNP, single-nucleotide polymorphism; MAF, minor allele frequency; HWE, Hardy–Weinberg equilibrium.

242 nonsmokers, with a mean age of 56.61 years. No significant difference was observed in the distribution of sex, age, or smoking status between the two groups ($p > 0.05$). The case group consisted of 294 adenocarcinoma patients, 188 squamous cell carcinoma patients, 113 small-cell lung cancer patients, and 25 other types of lung cancer patients.

The basic information for the candidate SNPs is presented in **Table 2**. The predicted function according to the HaploReg database showed that rs6750998 and rs17037621 in *EIF2AK3*, and rs17840761 and rs391957 in *HSPA5* were involved in the regulation of the promoter or enhancer histone, changed motifs, and eQTL hits. Moreover, *EIF2AK3*-rs867529 and *DDIT3*-rs697221 were missense variants and led to changed amino acids.

The genotyping call rate in our study was 100%. The MAFs of SNPs in cases and controls are described in **Table 3**. All of the SNPs were consistent with HWE ($p > 0.05$). By comparing the MAFs of SNPs between the case and control groups, we found that the minor allele A of rs6750998 was a protective allele against the risk of lung cancer (OR = 0.733, 95% CI: 0.609–0.882, $p < 0.001$), while the minor alleles of rs867529, rs391957, and rs697221 were all risk alleles that may lead to the multiplied risk of the disease (rs867529: OR = 1.301, 95% CI: 1.105–1.531, $p = 0.002$; rs391957: OR = 1.256, 95% CI: 1.045–1.510, $p = 0.015$; rs697221: OR = 1.504, 95% CI: 1.234–1.834, $p < 0.001$).

The genotype frequencies of SNPs in the cases and controls are shown in **Table 4**. The wild genotype of each SNP was considered as the reference genotype, and the OR and 95% CI of the heterozygous and homozygous mutational genotypes were evaluated. The results showed that the TA and AA genotypes of rs6750998 were protective genotypes that were associated against the risk of lung cancer ($p = 0.005$); however, the rs867529-GC/CC, rs391957-CC, and rs697221-GA/AA genotypes were all risk genotypes that associated with different

TABLE 4 | Genotype frequency distributions between lung cancer cases and healthy controls.

SNP	Genotype	Control	Case	OR (95%CI)	*p*
rs6750998	TT	335 (54%)	388 (62.6%)	1	0.005*
	TA	238 (38.4%)	202 (32.6%)	0.73 (0.58–0.93)	
	AA	47 (7.6%)	30 (4.8%)	0.55 (0.34–0.89)	
rs17037621	TT	282 (45.5%)	261 (42.1%)	1	0.440
	TA	272 (43.9%)	294 (47.4%)	1.17 (0.92–1.48)	
	AA	66 (10.7%)	65 (10.5%)	1.06 (0.73–1.56)	
rs867529	GG	268 (43.2%)	212 (34.2%)	1	0.003*
	GC	281 (45.3%)	317 (51.1%)	1.44 (1.13–1.83)	
	CC	71 (11.4%)	91 (14.7%)	1.64 (1.14–2.35)	
rs17840761	GG	222 (35.8%)	202 (32.6%)	1	0.490
	GA	292 (47.1%)	308 (49.7%)	1.16 (0.90–1.49)	
	AA	106 (17.1%)	110 (17.7%)	1.14 (0.82–1.58)	
rs391957	TT	374 (60.3%)	342 (55.2%)	1	0.028*
	TC	216 (34.8%)	228 (36.8%)	1.16 (0.91–1.47)	
	CC	30 (4.8%)	50 (8.1%)	1.86 (1.15–2.99)	
rs697221	GG	424 (68.4%)	364 (58.7%)	1	0.0001*
	GA	182 (29.4%)	221 (35.6%)	1.42 (1.11–1.81)	
	AA	14 (2.3%)	35 (5.7%)	2.92 (1.54–5.51)	

*p < *0.05 indicates statistical significance.*

SNP, single-nucleotide polymorphism; OR, odds ratio; CI, confidence interval.

TABLE 5 | Association between SNPs and risk of lung cancer in genetic models.

SNP	Model	Genotype	Control	Case	OR (95%CI)	*p*
rs6750998	Dominant	TT	335 (54%)	388 (62.6%)	1	0.002*
		TA-AA	285 (46%)	232 (37.4%)	0.70 (0.56–0.88)	
	Recessive	TT-TA	573 (92.4%)	590 (95.2%)	1	0.046*
		AA	47 (7.6%)	30 (4.8%)	0.62 (0.38–1.00)	
	Log-additive	---	---	---	0.74 (0.61–0.89)	0.001*
rs17037621	Dominant	TT	282 (45.5%)	261 (42.1%)	1	0.230
		TA-AA	338 (54.5%)	359 (57.9%)	1.15 (0.92–1.44)	
	Recessive	TT-TA	554 (89.3%)	555 (89.5%)	1	0.930
		AA	66 (10.7%)	65 (10.5%)	0.98 (0.68–1.41)	
	Log-additive	---	---	---	1.08 (0.91–1.28)	0.390
rs867529	Dominant	GG	268 (43.2%)	212 (34.2%)	1	0.001*
		GC-CC	352 (56.8%)	408 (65.8%)	1.48 (1.17–1.86)	
	Recessive	GG-GC	549 (88.5%)	529 (85.3%)	1	0.087
		CC	71 (11.4%)	91 (14.7%)	1.34 (0.96–1.86)	
	Log-additive	---	---	---	1.32 (1.12–1.56)	0.001*
rs17840761	Dominant	GG	222 (35.8%)	202 (32.6%)	1	0.240
		GA-AA	398 (64.2%)	418 (67.4%)	1.15 (0.91–1.46)	
	Recessive	GG-GA	514 (82.9%)	510 (82.3%)	1	0.790
		AA	106 (17.1%)	110 (17.7%)	1.04 (0.78–1.40)	
	Log-additive	---	---	---	1.08 (0.92–1.27)	0.340
rs391957	Dominant	TT	374 (60.3%)	342 (55.2%)	1	0.060
		TC-CC	246 (39.7%)	278 (44.8%)	1.24 (0.99–1.56)	
	Recessive	TT-TC	590 (95.2%)	570 (91.9%)	1	0.017*
		CC	30 (4.8%)	50 (8.1%)	1.76 (1.10–2.81)	
	Log-additive	---	---	---	1.26 (1.05–1.51)	0.014*
rs697221	Dominant	GG	424 (68.4%)	364 (58.7%)	1	0.0004*
		GA-AA	196 (31.6%)	256 (41.3%)	1.53 (1.21–1.93)	
	Recessive	GG-GA	606 (97.7%)	585 (94.3%)	1	0.002*
		AA	14 (2.3%)	35 (5.7%)	2.61 (1.39–4.90)	
	Log-additive	---	---	---	1.52 (1.24–1.86)	<0.0001*

*p < *0.05 indicates statistical significance.*

SNP, single-nucleotide polymorphism; OR, odds ratio; CI, confidence interval.

TABLE 6 | Association between SNPs and risk of lung cancer in smokers and nonsmokers.

SNP	Model	Genotype	Smokers		Nonsmokers	
			OR (95% CI)	*p*	OR (95% CI)	*p*
rs6750998	Dominant	TT	1	0.029*	1	0.035*
		TA-AA	0.72 (0.54–0.97)		0.68 (0.47–0.97)	
	Recessive	TT-TA	1	0.450	1	0.031*
		AA	0.79 (0.42–1.46)		0.45 (0.21–0.95)	
	Log-additive	---	0.78 (0.61–0.99)	0.038*	0.68 (0.51–0.92)	0.010*
rs867529	Dominant	GG	1	0.150	1	0.0003*
		GC-CC	1.24 (0.92–1.66)		1.98 (1.36–2.88)	
	Recessive	GG-GC	1	0.750	1	0.023*
		CC	1.07 (0.70–1.66)		1.83 (1.08–3.09)	
	Log-additive	---	1.14 (0.92–1.42)	0.230	1.66 (1.27–2.18)	0.0002*
rs391957	Dominant	TT	1	0.290	1	0.054
		TC-CC	1.17 (0.87–1.57)		1.44 (0.99–2.09)	
	Recessive	TT-TC	1	0.320	1	0.015*
		CC	1.38 (0.73–2.58)		2.35 (1.15–4.78)	
	Log-additive	---	1.17 (0.92–1.48)	0.210	1.44 (1.08–1.92)	0.012*
rs697221	Dominant	GG	1	0.009*	1	0.011*
		GA-AA	1.48 (1.10–2.00)		1.65 (1.12–2.44)	
	Recessive	GG-GA	1	0.018*	1	0.038*
		AA	2.91 (1.13–7.46)		2.39 (1.02–5.60)	
	Log-additive	---	1.50 (1.15–1.96)	0.002*	1.57 (1.15–2.16)	0.004*

*p < *0.05 indicates statistical significance.*
SNP, single-nucleotide polymorphism; OR, odds ratio; CI, confidence interval.

TABLE 7 | Association between SNPs and risk of adenocarcinoma, squamous cell carcinoma, and small-cell lung cancer.

SNP	Model	Genotype	Adenocarcinoma		Squamous cell carcinoma		Small cell lung cancer	
			OR (95%CI)	*p*	OR (95%CI)	*p*	OR (95%CI)	*p*
rs6750998	Dominant	TT	1	0.016*	1	0.130	1	0.070
		TA-AA	0.70 (0.53–0.94)		0.72 (0.51–1.02)		0.68 (0.45–1.04)	
	Recessive	TT-TA	1	0.071	1	0.060	1	0.480
		AA	0.57 (0.31–1.08)		0.62 (0.28–1.36)		0.74 (0.32–1.75)	
	Log-additive	---	0.73 (0.57–0.92)	0.008*	0.75 (0.56–1.00)	0.044*	0.74 (0.53–1.05)	0.081
rs867529	Dominant	GG	1	0.003*	1	0.025*	1	0.092
		GC-CC	1.55 (1.15–2.07)		1.48 (1.05–2.09)		1.43 (0.94–2.18)	
	Recessive	GG-GC	1	0.013*	1	0.900	1	0.560
		CC	1.37 (0.91–2.06)		1.03 (0.62–1.73)		1.20 (0.66–2.18)	
	Log-additive	---	1.36 (1.10–1.67)	0.004*	1.24 (0.97–1.59)	0.088	1.26 (0.94–1.69)	0.130
rs391957	Dominant	TT	1	0.093	1	0.430	1	0.150
		TC-CC	1.28 (0.96–1.70)		1.14 (0.82–1.61)		1.35 (0.90–2.03)	
	Recessive	TT-TC	1	0.260	1	0.0016*	1	0.120
		CC	1.41 (0.78–2.54)		2.77 (1.51–5.11)		1.85 (0.87–3.92)	
	Log-additive	---	1.24 (0.98–1.56)	0.070	1.30 (1.00–1.70)	0.054	1.35 (0.98–1.86)	0.073
rs697221	Dominant	GG	1	0.012*	1	0.030*	1	0.015*
		GA-AA	1.46 (1.09–1.96)		1.51 (1.07–2.12)		1.68 (1.11–2.53)	
	Recessive	GG-GA	1	0.032*	1	0.020*	1	0.012*
		AA	2.25 (1.08–4.72)		2.36 (0.95–5.85)		3.45 (1.40–8.50)	
	Log-additive	---	1.45 (1.13–1.86)	0.004*	1.50 (1.11–2.02)	0.009*	1.70 (1.21–2.41)	0.003*

levels of elevated lung cancer risk ($p_{rs867529}$ = 0.003, $p_{rs391957}$ = 0.028, $p_{rs697221}$ = 0.0001).

Based on the comparison results of allele and genotype, we further assessed the associations between these SNPs and lung cancer risk under three genetic models (**Table 5**). We found that *EIF2AK3*-rs6750998 polymorphism was associated with a decreased risk of lung cancer under dominant, recessive, and log-additive models ($p < 0.05$). By contrast, the *EIF2AK3*-rs867529 was correlated with an increased risk of the disease under dominant and log-additive models (p = 0.001). Moreover, rs391957 in *HSPA5* was related to an elevated risk of the disease under recessive and log-additive models ($p < 0.02$). In addition, *DDIT3*-rs697221 was identified to have a significant association with the risk of lung cancer under all three genetic models ($p < 0.01$).

The smoking information was obtained from all the study participants. Therefore, the stratified analysis was performed

TABLE 8 | Summary of SNP-SNP interactions on the risk of lung cancer analyzed by MDR method.

Model	Training accuracy	Testing accuracy	Cross-validation consistency	OR (95%CI)	*p*
rs697221	0.5513	0.5040	5/10	1.521 (1.205–1.920)	0.0004*
rs6750998 and rs697221	0.5598	0.5218	7/10	1.974 (1.500–2.597)	<0.0001*
rs6750998, rs867529, and rs17840761	0.5791	0.4952	3/10	1.842 (1.465–2.316)	<0.0001*

*p < *0.05 indicates statistical significance.*

based on the smoking status (**Table 6**). We found that the *EIF2AK3*-rs6750998 was a protective factor in both smokers and nonsmokers ($p < 0.05$). In addition, *DDIT3*-rs697221 was still a risk factor in both smokers and nonsmokers ($p < 0.05$). However, *EIF2AK3*-rs867529 and *HSPA5*-rs391957 remained significant only in nonsmokers ($p < 0.02$).

In addition, we also performed a stratification analysis based on the pathological types (**Table 7**). We found that *EIF2AK3*-rs6750998 was only correlated with a decreased risk of adenocarcinoma ($p < 0.0016$). *EIF2AK3*-rs867529 was associated with an increased risk of adenocarcinoma and squamous cell carcinoma ($p < 0.025$), and *HSPA5*-rs391957 was only related to an elevated risk of squamous cell carcinoma ($p = 0.0016$), while *DDIT3*-rs697221 was associated with risk of all three pathological types ($p < 0.032$).

The MDR analysis was further used to evaluate the effect of SNP-SNP interaction on the risk of lung cancer (**Table 8**). The higher accuracy and cross-validation consistency means a stronger interaction between the SNPs. We found that the interaction model of rs6750998 and rs697221 was the best predictor between candidate genes and lung cancer susceptibility with a testing accuracy of 52%, CVC of 7/10, and $p < 0.0001$.

DISCUSSION

Tumor cells are often in some mal-conditions such as ischemia, low oxygen, and lack of nutrients, resulting in the accumulation of unfolded and misfolded proteins in the ER and causing ER stress (Clarke et al., 2014). ER stress could regulate autophagy, mitochondrial and lysosomal dysfunction, oxidative stress, and inflammatory responses in the tumor, thus playing a vital role in tumorigenesis and tumor metastasis (Lin et al., 2019). In this study, we genotyped six SNPs in ER stress–related genes *EIF2AK3*/PERK, *HSPA5*/GRP78, and *DDIT3*/CHOP in lung cancer patients and healthy individuals and found that *EIF2AK3*-rs6750998 was a protective mutation against the risk of lung cancer, and three SNPs (*EIF2AK3*-rs867529, *HSPA5*-rs391957, and *DDIT3*-rs697221) were risk factors for the disease.

PERK, encoded by *EIF2AK3*, is a type I membrane protein located in the ER and could be activated under ER stress caused by malfolded proteins. The activated PERK could phosphorylate and inactivate the alpha subunit of eukaryotic translation–initiation factor 2 (elF2α), resulting in an effective reduction of translational initiation and repression of protein synthesis (Kranz et al., 2020). In addition, PERK was gradually proved to be involved in the regulation of mitochondrial function, serving as a bridge between mitochondrial metabolism and ER homeostasis (Fan and Simmen, 2019). Küper et al. (2021) have reported that PERK-related phosphorylation of NRF2 is important for the proliferation and ROS elimination of pancreatic and lung cancer cells under constant hypoxia, and thus the PERK-NRF2-HIF-axis contributes to cancer growth. Cai et al. (2021) have found that the PERK-eIF2α-ERK1/2 axis could regulate the cancer-associated fibroblasts to adopt an endothelial cell-like phenotype and directly lead to tumor angiogenesis *in vitro* and *in vivo*. Moreover, Lei et al. (2021) have demonstrated that the PERK activator CCT020312 combined with taxol could significantly reduce the tumor growth in colorectal cancer xenograft, suggesting that promoting PERK might be an effective way to improve colorectal cancer for Taxol treatment. In this study, we identified that two SNPs in *EIF2AK3* were associated with the risk of lung cancer: rs6750998 was a protective SNP against the risk of lung cancer, while rs867529 was a susceptible SNP for the disease. The rs867529 was a missense variant, therefore we speculated that rs867529 may influence the ER stress of the patients with lung cancer by altering the level or function of PERK.

HSPA5 encodes the GRP78 that localizes in the lumen of the ER. GRP78 is a member of the HSP70 chaperone family, making it serve as a molecular chaperone in the folding and assembly of proteins and a regulator of ER homeostasis. Under some conditions that may induce ER stress, such as viral infection and tumorigenesis, GRP78 dissociates from the transmembrane stress sensor proteins PERK, IRE1, and ATF6 and acts as a repressor of the unfolded protein response (Xia et al., 2021). Furthermore, GRP78 also takes part in the process of cellular apoptosis and senescence. Zhang et al. (2021) have shown that GRP78 was upregulated during M2 macrophages polarization, and the downregulation of GRP78 in macrophages suppressed M2 macrophage–provoked proliferation and migration of cancer cells. Huang et al. (2021) have identified that mitochondrial protein ATAD3A could interact with GRP78 to enhance protein folding and reduce ER stress for cancer cell survival in colorectal cancer patients who received chemotherapy. In addition, Gonzalez-Gronow et al. (2021) have reviewed the function studies of GRP78 and concluded that abnormal expression and atypical translocation of GRP78 to the cell surface may be involved in viral infections and pathogenesis of cancers and neurological disorders. Our results have shown that *HSPA5*-rs391957 was related to an elevated risk of lung cancer and rs391957 was a promoter SNP and may lead to altering promoter histone and changed motifs. Therefore, rs391957 may

have effects on the risk of the disease due to the altering translocation of GRP78 in lung cancer cells.

CHOP, encoded by *DDIT3*, belongs to the CCAAT/enhancer-binding protein (C/EBP) family. Under ER stress, CHOP was activated by a series of PERK activation and phosphorylation. CHOP could form heterodimers with other C/EBP members to serve as a dominant-negative inhibitor, inhibiting the activity of their binding DNA. Increasing evidence have shown that CHOP was implicated in inflammatory response, poor prognosis, and drug resistance in tumors. Conciatori et al. (2020) have found that the BRAF/ERK2/CHOP axis could regulate the IL-8 transcription *via* regulating the subcellular localization of CHOP and was considered a promising therapeutic target in patients with colorectal cancer. Zhang et al. (2018) have identified that low expression of CHOP was associated with the poor prognosis of patients with advanced gastric cancer, and thus CHOP could be used as a prognostic biomarker for advanced gastric cancer. Xiao et al. (2020) have reported that circRNA_103762 was upregulated in lung cancer tissues, and it could target and inhibit the CHOP expression to enhance the multidrug resistance in lung cancer cells. We identified a missense SNP *DDIT3*-rs697221 that correlated with an elevated risk of lung cancer, suggesting that the minor allele of rs697221 may lead to the dysfunction of CHOP, while the hypothesis needs confirmation through further studies.

Tobacco use is an important risk factor for lung cancer (Raman et al., 2022). We performed a stratified analysis based on smoking status. The results have shown that *EIF2AK3*-rs6750998 was a protective and *DDIT3*-rs697221 remained significant in both smokers and nonsmokers. However, *EIF2AK3*-rs867529 and *HSPA5*-rs391957 were only significant in nonsmokers. The different results may be explained by the limited sample size and other confounding factors such as secondhand smoke exposure, pathological type, and other occupational exposures (de Groot and Munden, 2012). We failed to obtain these information from the participants, which is a main limitation of the present study.

In conclusion, we found that *EIF2AK3*-rs6750998 was a protective variant against the risk of lung cancer, while *EIF2AK3*-rs867529, *HSPA5*-rs391957, and *DDIT3*-rs697221 were all susceptible variants for the disease. These results provided new insights on the role of the ER stress-related gene *EIF2AK3*/PERK, *HSPA5*/GRP78, and *DDIT3*/CHOP polymorphisms for lung cancer risk.

DATA AVAILABILITY STATEMENT

The original contributions presented in the study are included in the article/**Supplementary Material**; further inquiries can be directed to the corresponding authors.

ETHICS STATEMENT

The studies involving human participants were reviewed and approved by the Ethics Committee of Tangdu Hospital. The patients/participants provided their written informed consent to participate in this study.

AUTHOR CONTRIBUTIONS

YL: conceptualization, investigation, data curation, and writing—original draft; XL: investigation, data curation, and writing—original draft; HZ: data curation; JD: data curation; YZ: data curation; JW: formal analysis; CL: formal analysis; XX: writing—review and editing, supervision; YL: conceptualization, writing—review and editing, supervision.

SUPPLEMENTARY MATERIAL

The Supplementary Material for this article can be found online at: https://www.frontiersin.org/articles/10.3389/fgene.2022.938787/full#supplementary-material

REFERENCES

B'Chir, W., Maurin, A. C., Carraro, V., Averous, J., Jousse, C., Muranishi, Y., et al. (2013). The eIF2α/ATF4 Pathway Is Essential for Stress-Induced Autophagy Gene Expression. *Nucleic Acids Res.* 41, 7683–7699. doi:10.1093/nar/gkt563

Cai, W., Sun, X., Jin, F., Xiao, D., Li, H., Sun, H., et al. (2021). PERK-eIF2α-ERK1/2 axis Drives Mesenchymal-Endothelial Transition of Cancer-Associated Fibroblasts in Pancreatic Cancer. *Cancer Lett.* 515, 86–95. doi:10.1016/j.canlet.2021.05.021

Cao, M., and Chen, W. (2019). Epidemiology of Lung Cancer in China. *Thorac. Cancer* 10, 3–7. doi:10.1111/1759-7714.12916

Chen, X., and Cubillos-Ruiz, J. R. (2021). Endoplasmic Reticulum Stress Signals in the Tumour and its Microenvironment. *Nat. Rev. Cancer* 21, 71–88. doi:10.1038/s41568-020-00312-2

Clarke, H. J., Chambers, J. E., Liniker, E., and Marciniak, S. J. (2014). Endoplasmic Reticulum Stress in Malignancy. *Cancer Cell.* 25, 563–573. doi:10.1016/j.ccr.2014.03.015

Conciatori, F., Bazzichetto, C., Amoreo, C. A., Sperduti, I., Donzelli, S., Diodoro, M. G., et al. (2020). BRAF Status Modulates Interelukin-8 Expression through a CHOP-dependent Mechanism in Colorectal Cancer. *Commun. Biol.* 3, 546. doi:10.1038/s42003-020-01263-y

de Groot, P., and Munden, R. F. (2012). Lung Cancer Epidemiology, Risk Factors, and Prevention. *Radiologic Clin. N. Am.* 50, 863–876. doi:10.1016/j.rcl.2012.06.006

Fan, Y., and Simmen, T. (2019). Mechanistic Connections between Endoplasmic Reticulum (ER) Redox Control and Mitochondrial Metabolism. *Cells* 8. doi:10.3390/cells8091071

Feng, N., Ma, X., Wei, X., Zhang, J., Dong, A., Jin, M., et al. (2014). Common Variants in PERK, JNK, BIP and XBP1 Genes Are Associated with the Risk of Prediabetes or Diabetes-Related Phenotypes in a Chinese Population. *Chin. Med. J. Engl.* 127, 2438–2444.

Francisco, G., Gonçalves, F. T., Luiz, O. C., Saito, R. F., Toledo, R. A., Sekiya, T., et al. (2013). Polymorphisms in the P27 Kip-1 and Prohibitin Genes Denote Novel Genes Associated with Melanoma Risk in Brazil, a High Ultraviolet Index Region. *Melanoma Res.* 23, 231–236. doi:10.1097/cmr.0b013e3283612483

Gonzalez-Gronow, M., Gopal, U., Austin, R. C., and Pizzo, S. V. (2021). Glucose-regulated Protein (GRP78) Is an Important Cell Surface Receptor for Viral Invasion, Cancers, and Neurological Disorders. *IUBMB Life* 73, 843–854. doi:10.1002/iub.2502

Han, J., Back, S. H., Hur, J., Lin, Y. H., Gildersleeve, R., Shan, J., et al. (2013). ER-stress-induced Transcriptional Regulation Increases Protein Synthesis Leading to Cell Death. *Nat. Cell. Biol.* 15, 481–490. doi:10.1038/ncb2738

Hirsch, F. R., Scagliotti, G. V., Mulshine, J. L., Kwon, R., Curran, W. J., JR., Wu, Y.-L., et al. (2017). Lung Cancer: Current Therapies and New Targeted Treatments. *Lancet* 389, 299–311. doi:10.1016/s0140-6736(16)30958-8

Huang, K. C. Y., Chiang, S. F., Yang, P. C., Ke, T. W., Chen, T. W., Lin, C. Y., et al. (2021). ATAD3A Stabilizes GRP78 to Suppress ER Stress for Acquired Chemoresistance in Colorectal Cancer. *J. Cell. Physiology* 236, 6481–6495. doi:10.1002/jcp.30323

Kranz, P., Sänger, C., Wolf, A., Baumann, J., Metzen, E., Baumann, M., et al. (2020). Tumor Cells Rely on the Thiol Oxidoreductase PDI for PERK Signaling in Order to Survive ER Stress. *Sci. Rep.* 10, 15299. doi:10.1038/s41598-020-72259-1

Küper, A., Baumann, J., Göpelt, K., Baumann, M., Sänger, C., Metzen, E., et al. (2021). Overcoming Hypoxia-Induced Resistance of Pancreatic and Lung Tumor Cells by Disrupting the PERK-NRF2-HIF-axis. *Cell. Death Dis.* 12, 82. doi:10.1038/s41419-020-03319-7

Lei, Y., He, L., Yan, C., Wang, Y., and Lv, G. (2021). PERK Activation by CCT020312 Chemosensitizes Colorectal Cancer through Inducing Apoptosis Regulated by ER Stress. *Biochem. Biophysical Res. Commun.* 557, 316–322. doi:10.1016/j.bbrc.2021.03.041

Lin, Y., Jiang, M., Chen, W., Zhao, T., and Wei, Y. (2019). Cancer and ER Stress: Mutual Crosstalk between Autophagy, Oxidative Stress and Inflammatory Response. *Biomed. Pharmacother.* 118, 109249. doi:10.1016/j.biopha.2019.109249

Liu, J., Hoppman, N., O'Connell, J. R., Wang, H., Streeten, E. A., Mclenithan, J. C., et al. (2012). A Functional Haplotype inEIF2AK3, an ER Stress Sensor, Is Associated with Lower Bone Mineral Density. *J. Bone Min. Res.* 27, 331–341. doi:10.1002/jbmr.549

Mattiuzzi, C., and Lippi, G. (2020). Cancer Statistics: a Comparison between World Health Organization (WHO) and Global Burden of Disease (GBD). *Eur. J. Public Health* 30, 1026–1027. doi:10.1093/eurpub/ckz216

Patel, S. A., and Weiss, J. (2020). Advances in the Treatment of Non-small Cell Lung Cancer. *Clin. Chest Med.* 41, 237–247. doi:10.1016/j.ccm.2020.02.010

Raman, V., Yong, V., Erkmen, C. P., and Tong, B. C. (2022). Social Disparities in Lung Cancer Risk and Screening. *Thorac. Surg. Clin.* 32, 23–31. doi:10.1016/j.thorsurg.2021.09.011

Siegel, R. L., Miller, K. D., Fuchs, H. E., and Jemal, A. (2021). Cancer Statistics, 2021. *CA A Cancer J. Clin.* 71, 7–33. doi:10.3322/caac.21654

Volmer, R., van der Ploeg, K., and Ron, D. (2013). Membrane Lipid Saturation Activates Endoplasmic Reticulum Unfolded Protein Response Transducers through Their Transmembrane Domains. *Proc. Natl. Acad. Sci. U.S.A.* 110, 4628–4633. doi:10.1073/pnas.1217611110

Walter, P., and Ron, D. (2011). The Unfolded Protein Response: from Stress Pathway to Homeostatic Regulation. *Science* 334, 1081–1086. doi:10.1126/science.1209038

Winder, T., Bohanes, P., Zhang, W., Yang, D., Power, D. G., Ning, Y., et al. (2011). GRP78 Promoter Polymorphism Rs391957 as Potential Predictor for Clinical Outcome in Gastric and Colorectal Cancer Patients. *Ann. Oncol.* 22, 2431–2439. doi:10.1093/annonc/mdq771

Xia, S., Duan, W., Liu, W., Zhang, X., and Wang, Q. (2021). GRP78 in Lung Cancer. *J. Transl. Med.* 19, 118. doi:10.1186/s12967-021-02786-6

Xiao, G., Huang, W., Zhan, Y., Li, J., and Tong, W. (2020). CircRNA_103762 Promotes Multidrug Resistance in NSCLC by Targeting DNA Damage Inducible Transcript 3 (CHOP). *J. Clin. Lab. Anal.* 34, e23252. doi:10.1002/jcla.23252

Xie, W. Y., Zhou, X. D., Li, Q., Chen, L. X., and Ran, D. H. (2015). Acid-induced Autophagy Protects Human Lung Cancer Cells from Apoptosis by Activating ER Stress. *Exp. Cell. Res.* 339, 270–279. doi:10.1016/j.yexcr.2015.11.005

Xu, K., Han, B., Bai, Y., Ma, X. Y., Ji, Z. N., Xiong, Y., et al. (2019). MiR-451a Suppressing BAP31 Can Inhibit Proliferation and Increase Apoptosis through Inducing ER Stress in Colorectal Cancer. *Cell. Death Dis.* 10, 152. doi:10.1038/s41419-019-1403-x

Yang, X., Zhang, T., Zhang, X., Chu, C., and Sang, S. (2022). Global Burden of Lung Cancer Attributable to Ambient Fine Particulate Matter Pollution in 204 Countries and Territories, 1990-2019. *Environ. Res.* 204, 112023. doi:10.1016/j.envres.2021.112023

Zhang, H., Wang, S. Q., Hang, L., Zhang, C. F., Wang, L., Duan, C. J., et al. (2021). GRP78 Facilitates M2 Macrophage Polarization and Tumour Progression. *Cell. Mol. Life Sci.* 78, 7709–7732. doi:10.1007/s00018-021-03997-2

Zhang, X., Zhou, T., Li, W., Zhang, T., Che, N., and Zu, G. (2018). Clinicopathological and Prognostic Significance of C/EBP Homologous Protein (CHOP) in Advanced Gastric Cancer. *Pathology - Res. Pract.* 214, 1105–1109. doi:10.1016/j.prp.2018.06.005

Zhang, Y., Wu, J., Jing, H., Huang, G., Sun, Z., and Xu, S. (2019). Long Noncoding RNA MEG3 Inhibits Breast Cancer Growth via Upregulating Endoplasmic Reticulum Stress and Activating NF-κB and P53. *J Cell. Biochem.* 120, 6789–6797. doi:10.1002/jcb.27982

Conflict of Interest: The authors declare that the research was conducted in the absence of any commercial or financial relationships that could be construed as a potential conflict of interest.

Publisher's Note: All claims expressed in this article are solely those of the authors and do not necessarily represent those of their affiliated organizations, or those of the publisher, the editors, and the reviewers. Any product that may be evaluated in this article, or claim that may be made by its manufacturer, is not guaranteed or endorsed by the publisher.

frontiers | Frontiers in Genetics

TYPE Original Research
PUBLISHED 03 August 2022
DOI 10.3389/fgene.2022.956314

OPEN ACCESS

EDITED BY
Qian Wang,
Tai'an City Central Hospital, China

REVIEWED BY
Jinghai Gao,
Shanghai Changzheng Hospital, China
Qie Fan,
People's Hospital of Guangxi Zhuang Autonomous Region, China

*CORRESPONDENCE
Jian Huang,
huangjian900103@163.com
Li Cai,
caili@ems.hrbmu.edu.cn

†These authors have contributed equally to this work and share first authorship

SPECIALTY SECTION
This article was submitted to Cancer Genetics and Oncogenomics, a section of the journal Frontiers in Genetics

RECEIVED 30 May 2022
ACCEPTED 06 July 2022
PUBLISHED 03 August 2022

CITATION
Lan X, Zhao L, Zhang J, Shao Y, Qv Y, Huang J and Cai L (2022), Comprehensive analysis of karyopherin alpha family expression in lung adenocarcinoma: Association with prognostic value and immune homeostasis.
Front. Genet. 13:956314.
doi: 10.3389/fgene.2022.956314

Comprehensive analysis of karyopherin alpha family expression in lung adenocarcinoma: Association with prognostic value and immune homeostasis

Xiuwen Lan[1†], Lin Zhao[2†], Jian Zhang[3], Yingchun Shao[4], Yunmeng Qv[4], Jian Huang* and Li Cai*

[1]Department of Critical Care Medicine, Harbin Medical University Cancer Hospital, Harbin, China, [2]The Fourth Department of Medical Oncology, Harbin Medical University Cancer Hospital, Harbin, China, [3]Department of Thoracic Surgery, Harbin Medical University Cancer Hospital, Harbin, China, [4]Department of Pharmacology, College of Pharmacy, Harbin Medical University, Harbin, China

Background: Karyopherin alpha (KPNA), a nuclear transporter, has been implicated in the development as well as the progression of many types of malignancies. Immune homeostasis is a multilevel system which regulated by multiple factors. However, the functional significance of the KPNA family in the pathogenesis of lung adenocarcinoma (LUAD) and the impact of immune homeostasis are not well characterized.

Methods: In this study, by integrating the TCGA-LUAD database and Masked Somatic Mutation, we first conducted an investigation on the expression levels and mutation status of the KPNA family in patients with LUAD. Then, we constructed a prognostic model based on clinical features and the expression of the KPNA family. We performed functional enrichment analysis and constructed a regulatory network utilizing the differential genes in high-and low-risk groups. Lastly, we performed immune infiltration analysis using CIBERSORT.

Results: Analysis of TCGA datasets revealed differential expression of the KPNA family in LUAD. Kaplan-Meier survival analyses indicated that the high expression of *KPNA2* and *KPNA4* were predictive of inferior overall survival (OS). In addition, we constructed a prognostic model incorporating clinical factors and the expression level of *KPNA4* and *KPNA5*, which accurately predicted 1-year, 3-years, and 5-years survival outcomes. Patients in the high-risk group showed a poor prognosis. Functional enrichment analysis exhibited remarkable enrichment of transcriptional dysregulation in the high-risk group. On the other hand, gene set enrichment analysis (GSEA) displayed enrichment of cell cycle checkpoints as well as cell cycle mitotic in the high-risk group. Finally, analysis of immune infiltration revealed significant differences between the high-and low-risk groups. Further, the high-risk group was more prone to immune evasion while the inflammatory response was strongly associated with the low-risk group.

Conclusions: the KPNA family-based prognostic model reflects many biological aspects of LUAD and provides potential targets for precision therapy in LUAD.

KEYWORDS

lung adenocarcinoma, the KPNA family, immune homeostasis, biomarker, potential target

Introduction

Lung cancer is among the most prevalent tumors and contributes to about 21% of all cancer-related fatalities (Siegel et al., 2022). Non-small cell lung cancer (NSCLC) is the most common subtype of lung cancer that represents at least 85% of all cases of lung cancer. Histologically, NSCLC can be categorized into three types, namely, large cell carcinoma, lung squamous cell carcinoma (LUSC), and lung adenocarcinoma (LUAD), (Ko et al., 2018; Majem et al., 2020). Currently, the principal treatment modalities for lung cancer include targeted therapy, chemotherapy, radiotherapy, surgery, and immunotherapy (Catania et al., 2021). Due to the highly malignant nature of lung cancer, 5-year survival rates of patients with stage I to IIIA range from 14 to 49%, and those for stage IIIB to IV disease are <5% (Ko et al., 2018). LUAD is the most common subtype of lung cancer, accounting for approximately −40% of all cases (Yin et al., 2019). The 5-years overall survival (OS) rate of patients with LUAD is less than 20% (Wu et al., 2021). Therefore, exploration of the pathogenetic mechanism of LUAD and identification of potential therapeutic targets is a key research imperative.

Karyopherin alpha (KPNA) are nuclear transporters (NTRs) that consist of a cluster of basic amino acids, which selectively through the nuclear pore complex (NPC) (Hazawa et al., 2020; Miyamoto et al., 2020). NPC is composed of 30 nucleoporin (NUP) proteins, which is the sole channel between the nucleus and the cytoplasm (Hazawa et al., 2020). Active transport of proteins from the cytoplasm to the nucleus through NPC usually requires a carrier molecule that identifies the transport signal on the cargo, which is called nuclear localization signal (NLS) (Miyamoto et al., 2016). The classical mechanism of the passage of proteins into the nucleus is as follows: cargoes usually possess NLS that is initially detected by KPNA and then exhibits interaction with karyopherin b1 (KPNB1), and the created trimeric complex diffuses into the nucleus through NPC (Myat et al., 2018). The main role of KPNA in nucleocytoplasmic transport is to function as adaptor molecules that carry protein cargoes carrying NLS and Karyopherin beta (KPNB) from the cytoplasm to the nucleus (Miyamoto et al., 2016). In addition to its function in mediating nucleocytoplasmic transport, KPNA also has non-transport functions such as lamin polymerization, nuclear membrane formation, spindle assembly, protein degradation, cytoplasmic retention, cell surface function, gene expression, and mRNA-related function (Miyamoto et al., 2016). In addition, KPNA is increasingly recognized to have a central in cancer growth and progression (Wang et al., 2012; Xu et al., 2021).

The human type the KPNA family consists of seven subtypes, KPNA1, KPNA2, KPNA3, KPNA4, KPNA5, KPNA6, and KPNA7 (Miyamoto et al., 2016), and these subtypes exhibit 42–86% homology to one another (Oostdyk et al., 2019). The KPNA family can be further divided into three subfamilies based on sequence homology: α1, α2, and α3. The α1 subfamily comprises three members, KPNA1, KPNA5, and KPNA6. α2 subfamily comprises two members, KPNA2 and KPNA7. α3 subfamily comprises two members, KPNA3 and KPNA4 (Miyamoto et al., 2016; Myat et al., 2018). KPNA1 was the founding member of the α1 subfamily. The α2 and α3 subfamilies are known to have evolved through duplication of the founding KPNA, and to have developed cell and tissue-specific roles which facilitate development and differentiation in higher eukaryotes (Oostdyk et al., 2019). Aberrant expression of the KPNA family has been detected in multiple cancers, which was related to poor prognosis. For example, a study identified high KPNA1 expression in breast cancer, which was associated with poor overall survival (OS) (Tsoi et al., 2021). High KPNA2 expression in melanoma was linked to poor OS and disease-free survival (DFS) (Yang et al., 2020). High expression of KPNA2 has been identified in ovarian carcinoma and cervical cancer, which was associated with poor prognosis (Cui et al., 2021; Wang et al., 2021). High KPNA4 expression in liver cancer was shown to be associated with poor OS in patients (Xu et al., 2021).

The KPNA family plays varied roles in different types of malignancies. For example, KPNA1 was shown to modulate the nuclear import of NCOR2 splicing variant BQ323636.1 and thus promote tamoxifen resistance in breast cancer (Tsoi et al., 2021). The expression of KPNA2 in ovarian carcinoma can promote epithelial-mesenchymal transition (EMT), migration, and invasion. The expression of KPNA2 in colorectal cancer tissue was correlated with stage, differentiation status, and metastasis. Overexpression of KPNA2 indicated a poor prognosis in patients (Han and Wang, 2020). KPNA3 was shown to confer sorafenib resistance *via* TWIST-regulated EMT in advanced liver cancer (Hu et al., 2019). The expression of KPNA4 in prostate cancer was shown to promote metastasis through miR-708-KPNA4-TNF axes (Yang et al., 2017), and KPNA4 was found to enhance cancer cell proliferation and cisplatin resistance in cutaneous squamous cell carcinoma (Zhang et al., 2019). KPNA5, KPNA6,

and KPNA1 binding regions can promote the proliferation of breast cancer cells (Kim et al., 2015). KPNA7 promotes cell growth and anchorage-independent growth, and reduces autophagy of pancreatic cancer cells (Laurila et al., 2014). Previous studies have reported overexpression of KPNA4 in LUAD and identified it as a potential key driver of the malignant phenotype (Hu et al., 2020). Nonetheless, the functional role and underlying mechanism of the KPNA family in LUAD are poorly understood.

In this study, we used the TCGA-LUAD database and Masked Somatic Mutation to evaluate the expression, mutation status, and prognostic value of the KPNA family in LUAD. We built a prognostic model for individuals on the basis of the clinical features and the expression of the KPNA family and analyzed the differences in mutational signature in the two risk groups. Next, we did a differential expression analysis, Kyoto Encyclopedia of Genes and Genomes (KEGG) pathway enrichment analysis, and Gene Ontology (GO) enrichment analysis in the two risk groups. Finally, we performed the analysis of immune infiltration in these groups. This is the first investigation to examine the function of the KPNA family in LUAD, as per our best knowledge. Our findings may avail both potential biomarkers and therapeutic targets against LUAD.

Materials and methods

Data acquisition and pretreatment

TCGA-LUAD expression profile data were acquired from UCSC Xena (http://xena.ucsc.edu/); the downloaded data type was count, and the count values were transformed to transcript per million (TPM) values in advance. Transcriptomic data from 594 patients in TCGA-LUAD, 535 tumor samples, and 59 normal samples were included in the current analysis. In addition, we selected "Masked Somatic Mutation" data as the somatic mutation data (n = 561) of LUAD patients from TCGA GDC (https://portal.gdc.cancer.gov/), processed these data using VarScan, and performed an analysis of somatic mutation using the maftools R package (Mayakonda et al., 2018). The copy number information (n = 531) of patients in TCGA-LUAD was downloaded in UCSC Xena, which assessed gene copy number variation (CNV).

In this analysis, we used the clinical information of 594 patients from TCGA-LUAD, including age, sex, survival status, and TNM stage. We matched patient IDs in the clinical database with the transcriptomic data as well as somatic mutation data above and removed samples with unavailable transcriptomic data and somatic mutation data.

The KPNA family (*KPNA1, KPNA2, KPNA3, KPNA4, KPNA5, KPNA6,* and *KPNA7*) expression profiles, mutation data, and CNV data were extracted *via* R languages for subsequent analysis.

Differential expression analyses

Based on information in the TCGA-LUAD datasets, we divided the samples into tumor samples and normal samples and screened out differentially expressed genes (DEGs) utilizing the DESeq2 package. The screening criteria were log2 (fold change) > 1.0 and p-value < 0.05 (Love et al., 2014). Subsequently, differential expression analysis was performed using the DESeq2 package to determine the expression profiles of low-and high-risk groups. The screening criteria were log2 (fold change) > 2.0 and adj. p-value < 0.05. Volcano plots were plotted using package ggplot2, heat maps were drawn using package pheatmap to demonstrate the differential gene expression.

Establishment of the prognostic model

Kaplan-Meier method in conjunction with the log-rank test was utilized for survival analysis to establish the link between high/low expression of the KPNA family genes and OS.

To determine the predictive power of the KPNA family for the prognosis of LUAD individuals, we performed univariate Cox regression analysis, LASSO regression analysis, and multivariate Cox regression analysis based on the TCGA-LUAD to identify independent prognostic factors, and created a prognostic model. First, univariate Cox proportional regression analysis was utilized to investigate the link between the expression levels of genes in the KPNA family and OS; genes with an adjusted p-value < 0.1 were retained. Subsequently, to eliminate the effect of multicollinearity, we used the LASSO algorithm to screen meaningful variables in univariate Cox regression analysis. Then we performed a stepwise regression analysis using multivariate Cox regression to discover independent prognostic factors. Finally, optimized gene expression and correlation estimated Cox regression coefficients were taken into consideration to generate a risk score formula: risk score = (exp-Gene1*coef-Gene1) + (exp-Gene2*coef-Gene2)+……+(exp-Gene*coef-Gene).

The participants were then classified into the aforementioned two risk groups as per the given risk score. Kaplan-Meier analysis and log-rank test were performed to compare OS in the two groups applying the survival package. Additionally, receiver operating characteristic (ROC) curve analysis evaluated the survival predictive value of the risk score. The area under ROC curves (AUC) values were derived utilizing the R package timeROC.

After detection of independent prognostic factors, we combined clinical information such as age, sex, stage, and other factors to establish a nomogram for prognostic assessment of LUAD patients. In particular, we evaluated the prognostic outcomes at 1, 3, and 5 years, correspondingly. The reliability of the model was assessed by plotting the calibration curve.

Construct functional enrichment analysis and regulatory network

We did GO enrichment analysis as well as KEGG pathway enrichment analysis of the differentially expressed genes of two risk groups utilizing the clusterProfiler R package and R package GOPlot (Ogata et al., 1999; Ashburner et al., 2000; Yu et al., 2012). GSEA was instrumental in developing the gene expression matrix with clusterProfiler R package; "c2. cp.all.v7.0. symbols" was chosen as a reference gene set. In addition, false discovery rate (FDR) < 0.25 with $p < 0.05$ denotes substantial enrichment (Suarez-Farinas et al., 2010). Based on the "c2. cp.all.v7.0. symbols" gene set, we utilized the R package Gene set variation analysis (GSVA) on the basis of the gene expression matrix for each sample, calculated the related pathway scores, and generated the Heat maps using the ssGSEA method (Hänzelmann et al., 2013).

Using the STRING protein-protein interactions database, we evaluated the link between the hub genes and their interactions and exported the results; core genes were thoroughly screened with the CytoHubba Plugin in Cytoscape (Chin et al., 2014).

In addition, hub genes-miRNA regulation analysis and transcription factors-target genes regulatory network analysis were performed with NetworkAnalyst (http://www.networkanalyst.ca/NetworkAnalyst). Results were finally exported from Networkanalyst, and miRNA-hub genes and transcription factors-hub genes regulatory network plotted using Cytoscape software.

Analysis of immune cell infiltration

We performed deconvolution with transcriptome matrix using the CIBERSORT algorithm (which is premised on the linear support vector regression principle) and assessed the cellular composition and the abundance of immune cells in the mixed infiltrate (Newman et al., 2015). Gene expression matrices data were uploaded onto the CIBERSORT, and after filtering the outputs (p-value < 0.05), we obtained the matrix of infiltrating immune cells. Bar graphs were plotted using R package ggplot2 to demonstrate the distributions of 22 types of infiltrating immune cells in every sample. In addition, we studied the correlation of two risk groups with immune and inflammation by extracting HLA family-related genes (MHC class I and II) and complement-related genes.

Statistical analysis

The R software (version 4.0.2) performed all the analyses and data processing. Between-group variations with respect to normally distributed continuous variables were investigated with the aid of the Student's t-test, whereas those with respect to non-normally distributed variables were investigated utilizing the Mann-Whitney U test (Wilcoxon's rank-sum test). Additionally, for between-group differences with respect to categorical variables, the Chi-squared test or Fisher exact test was used. Correlation between different genes was assessed using Spearman correlation analysis. Kaplan-Meier survival analyses were done through the utilization of the R package survival and the between-group differences in survival outcomes were assessed using the log-rank test. Univariate as well as multivariate Cox regression analyses were utilized to ascertain the independent prognostic factors. Two-sided p values < 0.05 denoted statistical significance for all analyses.

Results

Aberration of the KPNA family in TCGA-LUAD

First, we extracted the KPNA family from the TCGA-LUAD datasets, which included *KPNA1, KPNA2, KPNA3, KPNA4, KPNA5, KPNA6,* and *KPNA7*, and the details are shown in Supplementary Table S1. We plotted the heatmaps of the KPNA family and found a non-uniform trend in their expression with no significant correlations between them (Figures 1A,B). We identified differential expression of *KPNA2, KPNA3, KPNA5, KPNA6,* and *KPNA7*. Compared with normal tissue, *KPNA2, KPNA6,* and *KPNA7* were highly expressed in LUAD, while *KPNA3* and *KPNA5* expression were decreased in LUAD (Figure 1C). Subsequently, we plotted ROC curves, which clearly showed the discriminative value of these genes in differentiating between tumor samples and non-tumor samples. The AUC values of *KPNA2, KPNA3, KPNA5,* and *KPNA7* were >0.7, which indicated a promising discriminating ability. In addition, we did Kaplan-Meier survival analysis to identify genes that affect the prognosis in LUAD. The expression of *KPNA2* and *KPNA4* was found to affect the OS of LUAD individuals, and the patients with high expression of *KPNA2* and *KPNA4* showed a much worse prognosis (Figures 1D–J).

The panorama of gene mutations was displayed in TCGA-LUAD datasets; missense mutations accounted for the majority of mutations, single-nucleotide polymorphisms (SNPs) occurred more frequently than deletions or insertions, and C>A was most frequently identified in single nucleotide variants (SNVs) among patients with LUAD (Supplementary Figures S1A,B). Subsequently, we extracted the KPNA family information and analyzed the mutational signatures. The frequency of overall the KPNA family mutations was low, and the mutation types were primarily missense mutations (Figure 2A). We plotted the lollipop diagrams according to mutational signatures (Figures 2B–G). In addition, we analyzed CNV changes according to the information on the CNV of the KPNA family. As shown in Figure 2H, the copy number

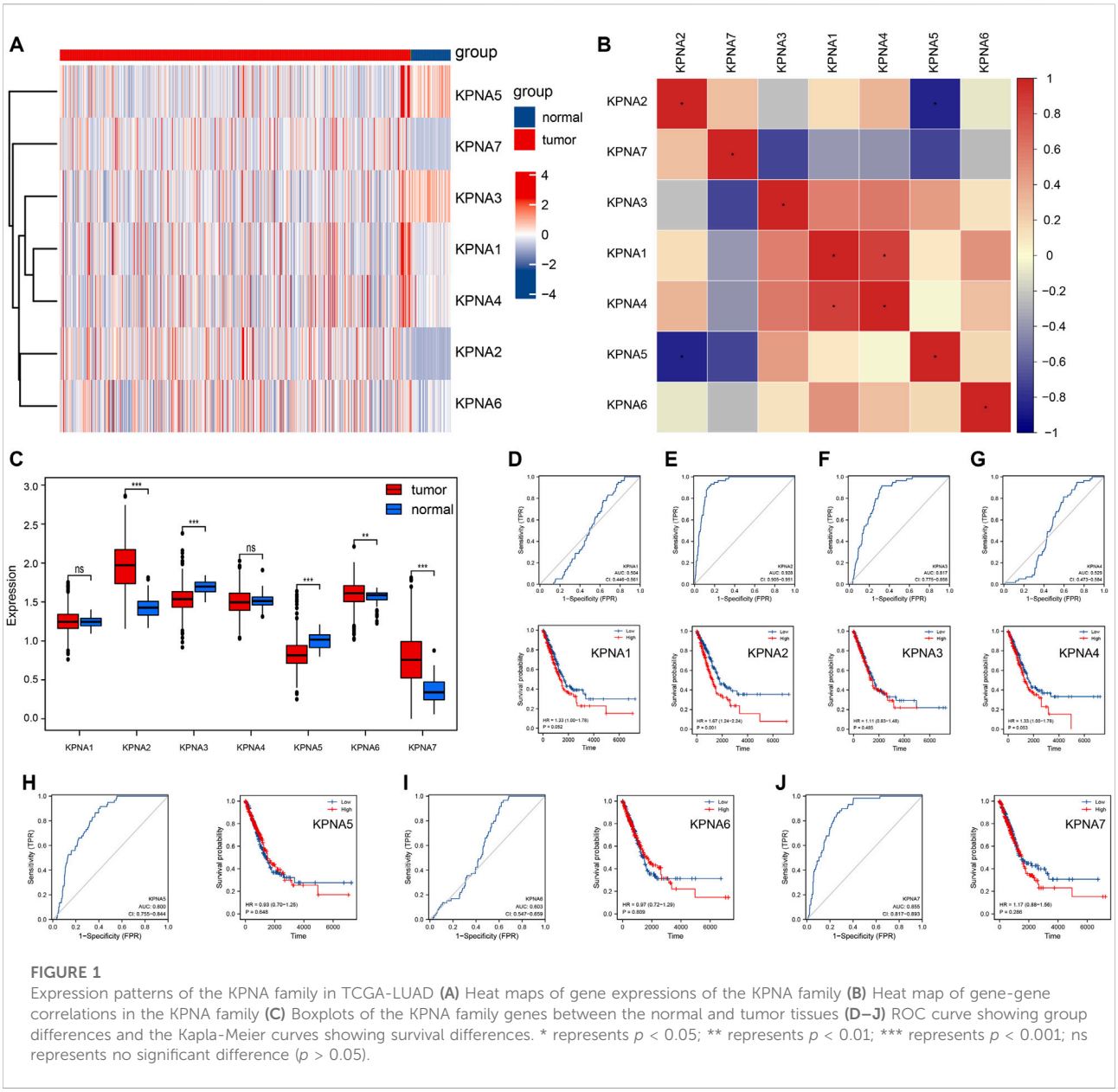

FIGURE 1
Expression patterns of the KPNA family in TCGA-LUAD **(A)** Heat maps of gene expressions of the KPNA family **(B)** Heat map of gene-gene correlations in the KPNA family **(C)** Boxplots of the KPNA family genes between the normal and tumor tissues **(D–J)** ROC curve showing group differences and the Kapla-Meier curves showing survival differences. * represents $p < 0.05$; ** represents $p < 0.01$; *** represents $p < 0.001$; ns represents no significant difference ($p > 0.05$).

amplifications of *KPNA1, KPNA2, KPNA4, KPNA6*, and *KPNA7* in total samples were higher than the copy number deletions, but the copy number amplifications of *KPNA3* and *KPNA5* were lower than the copy number deletions.

Creation of prognostic model based on the KPNA family

We conducted a univariate Cox regression analysis to detect the KPNA family genes linked to the prognosis of LUAD patients. Four genes were discovered to be linked to survival. To further screen the genes associated with prognosis, we screened the genes using LASSO regression analysis and Cox regression analysis and eventually identified *KPNA4* and *KPNA5* as independent prognostic factors (Figures 3A–C). As per their expression values and regression coefficients, we derived the risk score for LUAD specimens and plotted the heatmaps to visualize the distribution of samples in the two risk groups (Figure 3D). We conducted a survival analysis of LUAD individuals utilizing their risk score-based grouping; the findings affirmed that patients in the high-risk group experienced a poor prognosis (Figure 4A). ROC curve analysis indicated good predictive efficacy of risk score-based grouping for 1-year, 3-years, and 5-years survival outcomes (1-year AUC = 0.615, 3-years AUC = 0.645, 5-years AUC = 0.629) (Figure 4B).

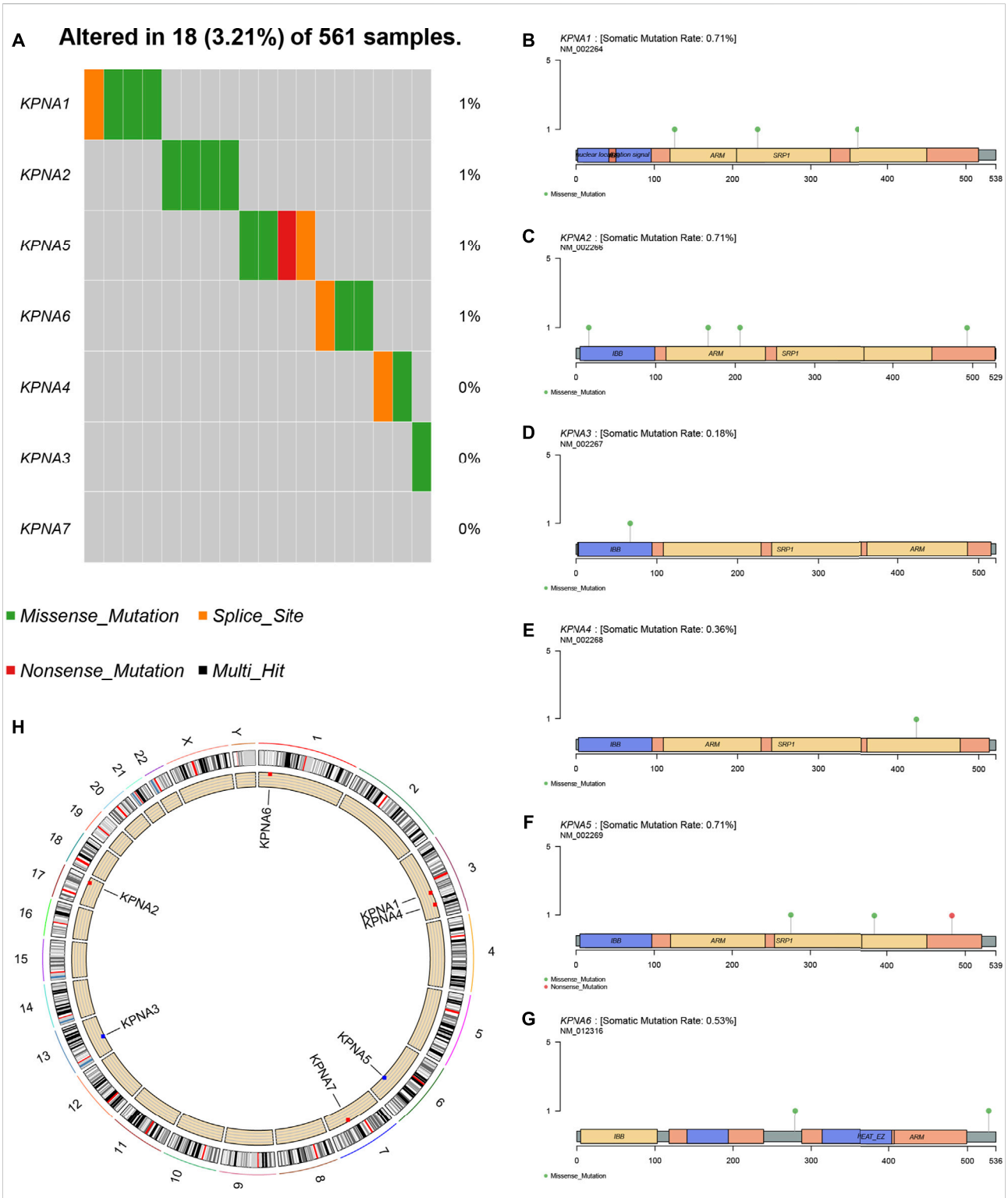

FIGURE 2
Mutations and copy number variations (CNV) of the KPNA family **(A)** Mutation frequency of the KPNA family **(B–G)** Mutated sites of the KPNA family **(H)** Copy number alterations of the KPNA family; red dots indicate that amplifications are greater than deletions while blue dots indicate that deletions are greater than amplifications.

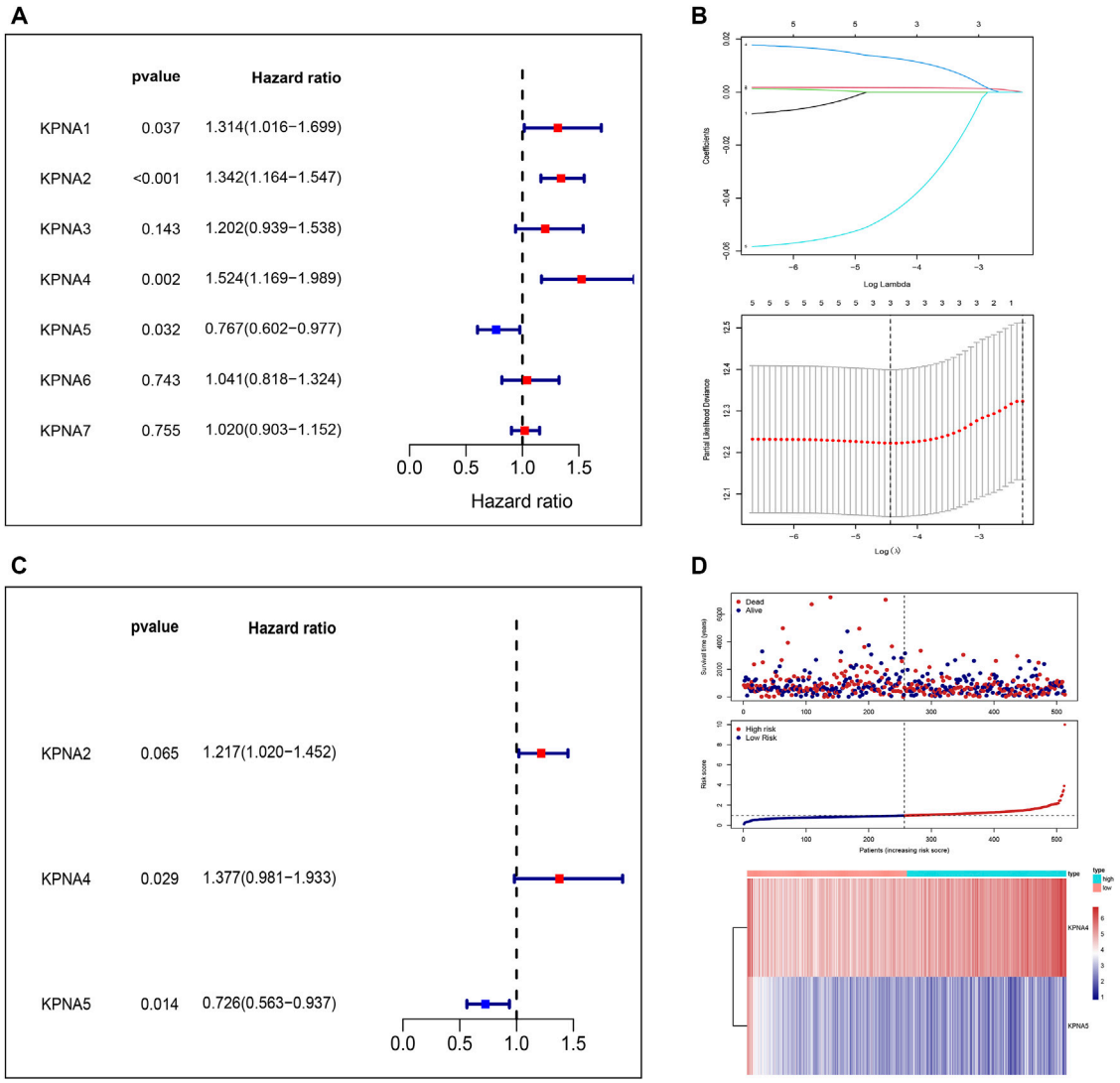

FIGURE 3
Independent prognostic factors of the KPNA family **(A)** Forest plot of univariate Cox regression analysis of the KPNA family **(B)** Lasso regression model of the KPNA family **(C)** Forest plot of multivariate Cox regression analysis of the KPNA family **(D)** Calculated risk score and the heat maps of risk factors based on the findings of multivariate Cox regression analysis.

Subsequently, we constructed a nomogram incorporating age, sex, clinical stage, and the expression level of *KPNA4* and *KPNA5* for prognostic assessment of LUAD patients (Figure 4C). Through calibration curves, we found that the prognostic model for 1-year, 3-years, and 5-years had high reliability (Figure 4D). Additionally, we performed risk stratification based on different factors including age, sex, clinical stage, survival status, and immune subtypes. The results affirmed that there were no remarkable differences between the two risk groups with respect to age or sex; however, there were substantial differences between the two risk groups in terms of clinical stage and immune subtypes (Figures 4E–I).

Comparison of tumor mutation burden and microsatellite instability utilizing risk score

We further compared the mutational signatures between the two groups utilizing the risk score. There were no remarkable differences in MSI scores between the two risk groups, but the high-risk group had greater TMB scores in contrast to the low-risk group (Figures 5A,B). Subsequently, we analyzed the top 30 mutant genes of the two risk groups and ascertained variations in genetic mutations between them (Figure 5C).

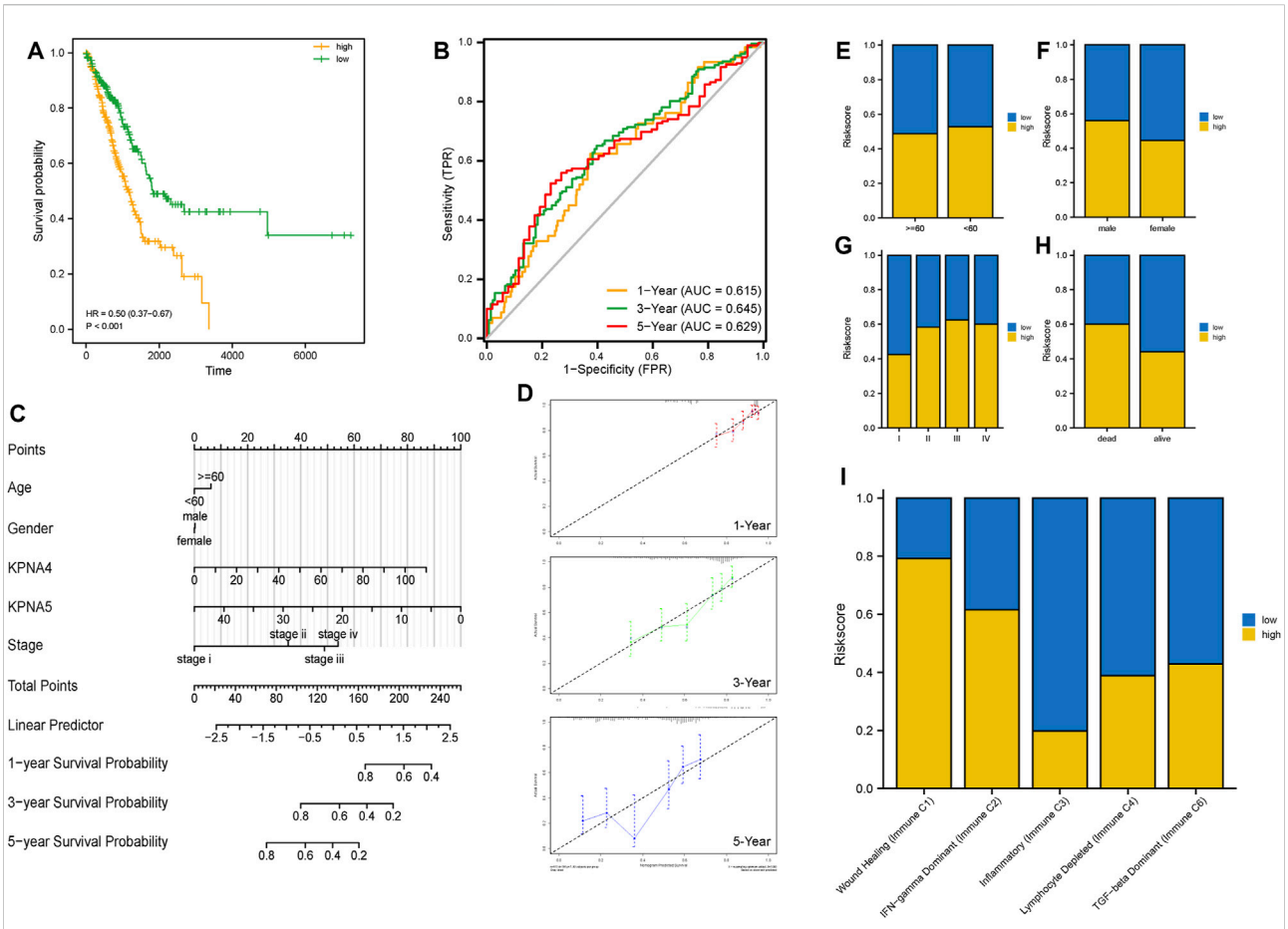

FIGURE 4
Evaluation of prognostic model and correlation analysis of clinical features **(A)** Analysis of prognosis in the two risk groups **(B)** ROC curves displaying the predictive value of the models for 1-year, 3-year, and 5-year survival outcomes **(C,D)** Prognostic nomogram and calibration curves according to clinical factors and the expression of KPNA4 and KPNA5 **(E–I)** Differences in clinical features between the two risk groups.

Differential expression analysis and functional enrichment analysis of high- and low-risk groups

According to the low-and high-risk groups, we did a differential analysis of all genes within the expression profiles in the TCGA cohort using the volcano plots and heat maps (Figures 6A,B). Pathway enrichment analysis, as well as GO enrichment analysis, were performed on DEGs separately (Supplementary Tables S2, S3). GO enrichment analysis included molecular function (MF), biological process (BP), and cellular component (CC). The key DEGs enriched the following principal biological processes: epithelium development, cornification, tissue development, and morphogenesis of a branching epithelium, morphogenesis of a branching structure; the principal aggregation of cellular components was as follows: extracellular region, cornified envelope, and chromatin. The principal enriched molecular functions were as follows: DNA-binding transcription factor activity, sequence-specific double-stranded DNA binding, and amino acid sodium symporter activity (Figures 6C,D). The pathway enrichment was mainly enriched in Neuroactive ligand-receptor interaction, Salivary secretion, Galactose metabolism, Vascular smooth muscle contraction, and Transcriptional dysregulation in cancers (Figures 6E,F).

Subsequently, we constructed PPI networks by STRING databases to identify the hub genes and reveal their potential interactions. First of all, we built protein interaction networks by DEGs and the minimum score of interactions was set to 0.7 (Supplementary Figure S2A). We additionally determined the most relevant genes in the PPI networks by the Cytohubba plugin and 15 genes were regarded as hub genes: *SPANXD, MAGEA4, MAGEC1, SPANXC, CTAG2, MAGEA10, CT45A1, MAGEA1, MAGEA1, MAGEC2, SPRR2D, KRT6A, KRT14, CASP14*, and *SPRR2E* (Supplementary Figure S2B).

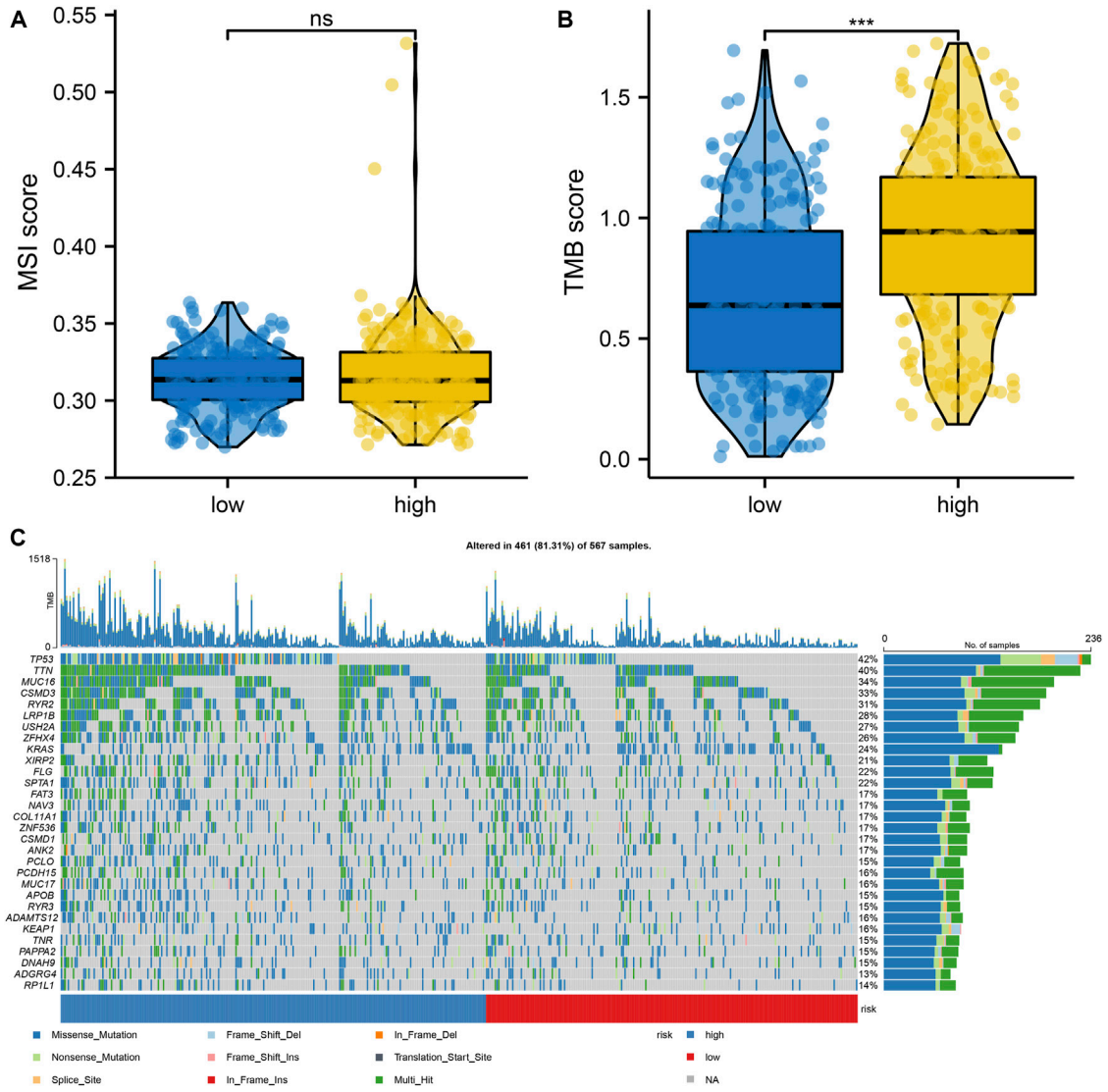

FIGURE 5
Differences in mutation signatures between high-and low-risk groups **(A)** Differences in MSI score between high- and low-risk groups **(B)** Differences in TMB score between high-and low-risk groups **(C)** Differences in the top 30 mutant genes between high-and low-risk groups. *represents $p < 0.05$; ** represents $p < 0.01$; *** represents $p < 0.001$; ns represents no significant difference ($p > 0.05$).

We also predicted the potential miRNAs which regulate the 15 hub genes by the Networkanalyst databases; the final subnetwork contained 49 nodes (i.e., miRNA) and 11 seeds (i.e., matched hub genes) (Supplementary Figure S2C). Similarly, we obtained the transcription factors-hub genes regulatory networks based on the JASPAR databases, the final contained 14 seeds (i.e., hub genes) and 46 nodes (i.e., transcription factors) (Supplementary Figure S2D).

Subsequently, we carried out GSEA between the two risk groups to identify remarkably enriched pathways (p-value < 0.05) (Supplementary Table S4). The GSEA results showed enrichment of cell cycle checkpoints, cell cycle mitotic, retinoblastoma gene in cancer, mitotic metaphase, and anaphase in the high-risk group. CD22 mediated BCR regulation, heme scavenging from plasma, asthma, and antigen activates B cell receptor BCR resulting in the generation of second messengers were enriched in the low-risk group (Figures 7A,B). GSVA findings ascertained that there were variations in a total of six gene sets between the two risk groups, according to the screening of the hallmark gene sets, for example, angiogenesis, apical surface, and apical junction (Figure 7C).

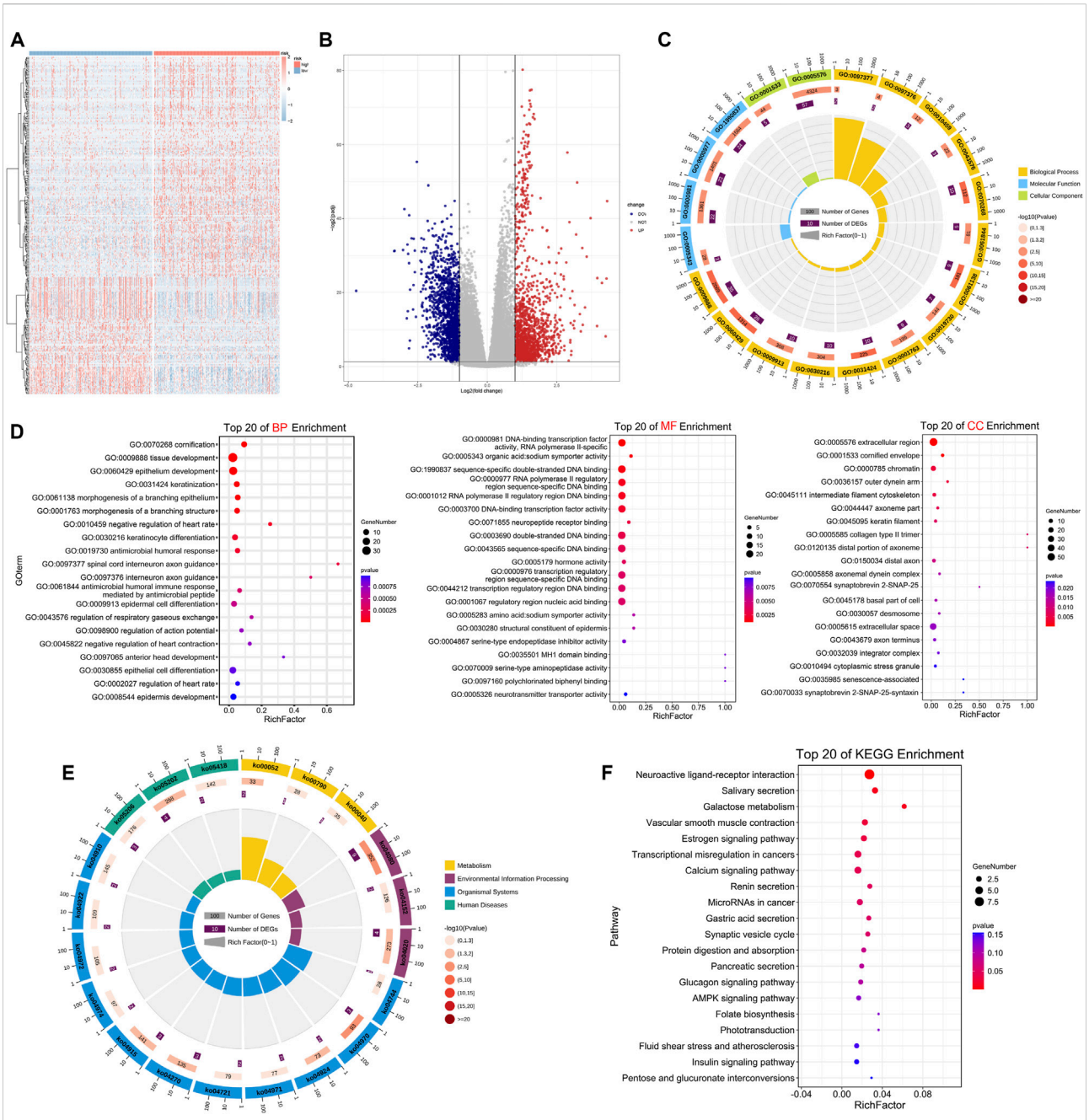

FIGURE 6
Differential expression analysis and functional enrichment analysis of the two risk groups **(A,B)** Heat map and volcano plot of differential expression in high-and low-risk groups **(C)** GO analysis of the two risk groups. Outer circle, GO term; cylindrical of inner circle, number of enriched genes; yellow, BP (Biological Process); blue, MF (Molecular Function); green, CC (Cellular Component) **(D)** Top 20 of BP, MF, CC **(E)** KEGG analysis of high-and low-risk groups. Outer circle, the number of KEGG pathways; inner circle, number of enriched genes; yellow, metabolism; blue, organismal systems; green, human diseases; purple, environmental information processing **(F)** Top 20 of KEGG pathways enrichment.

Analysis of immune infiltration in the high- and low-risk groups

After ranking based on the risk score, the immune cell infiltration for each sample in the TCGA LUAD is shown in the bar graphs. The infiltration scores and correlation analysis between the 22 immune cells were obtained by the CIBERSORT algorithm, respectively (Figures 8A,B). We further evaluated the differences in immune cell infiltrates in the two risk groups. As shown in Figure 8C, the infiltration scores for naive B cells,

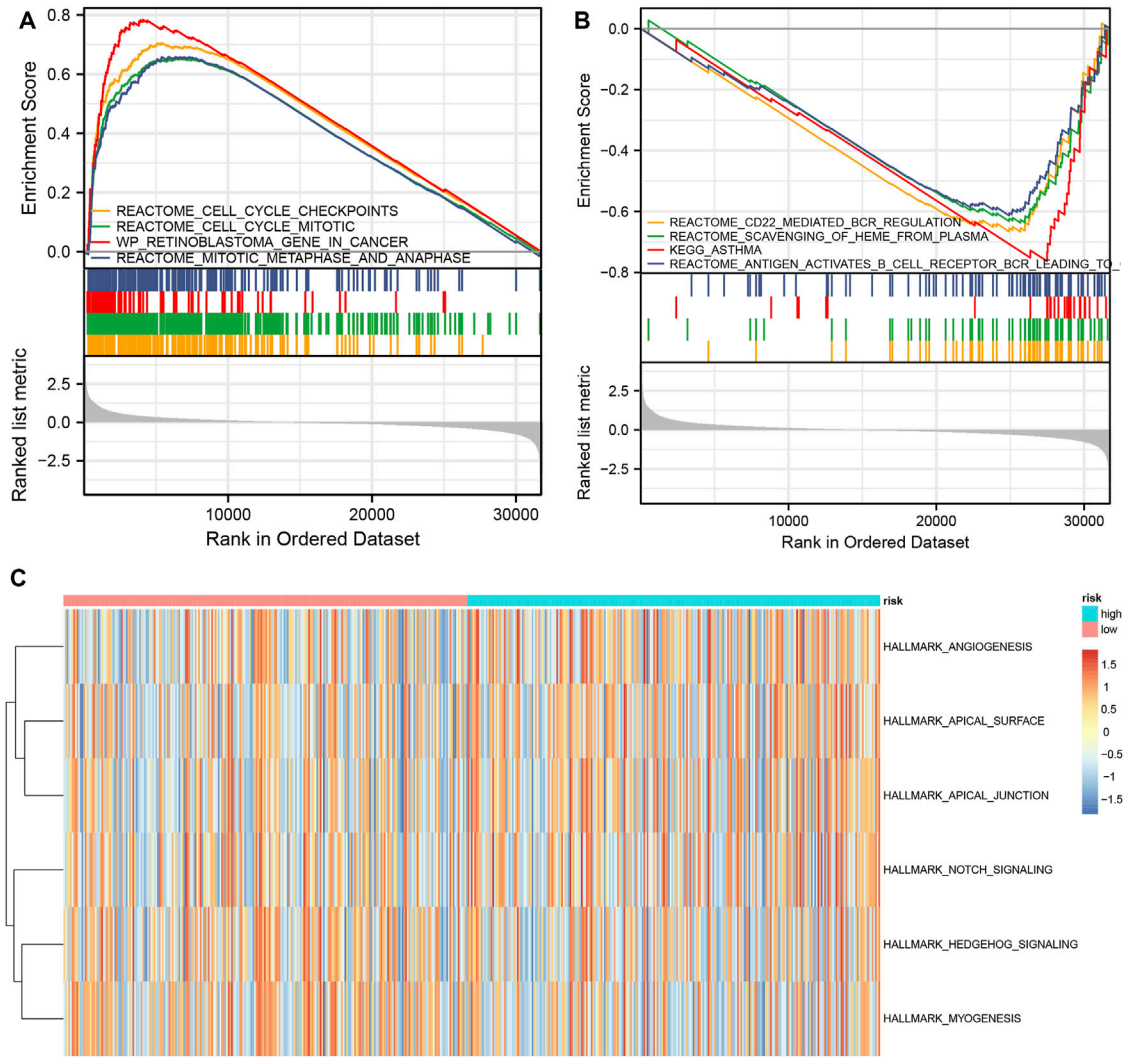

FIGURE 7
GSVA and GSEA analysis of high- and low-risk groups **(A)** Main enriched pathways in the high-risk group **(B)** Main enriched pathways in the low-risk group **(C)** Differential gene sets based on the hallmark gene sets.

plasma cells, $CD4^+$ T cells memory resting T cells, and resting dendritic cells were lower in the high-risk group than in the low-risk group; however, the infiltration scores for $CD8^+$ T cells and M0 Macrophages were greater in the high-risk group. We computed the correlation of the expression level of *KPNA4* and *KPNA5* and various types of immune cells by Spearman's correlation analysis (Supplementary Figures S3, S4). Additionally, we combined the genes related to immunity and inflammation (for example, HLA family and complement-related genes), and analyzed the differences in the two risk groups. We found that the MHC-II family was decreased in the high-risk group, and the main function of the MHC-II gene is antigen-presenting. This suggested that the antigen-presenting function might be affected in the high-risk group (Figures 8D,E). Additionally, there were variations of complement-related genes in both groups, which illustrated a close association with inflammation (Figures 8F,G).

Discussion

Due to its highly malignant nature and a paucity of methods for early diagnosis, LUAD is linked to high incidence as well as mortality rates. Therefore, recognition of particular principal molecular pathways and extensively sensitive, reliable biomarkers is required to improve the early diagnosis and survival outcomes of LUAD patients. Previous investigations have demonstrated the relationship of the KPNA family genes

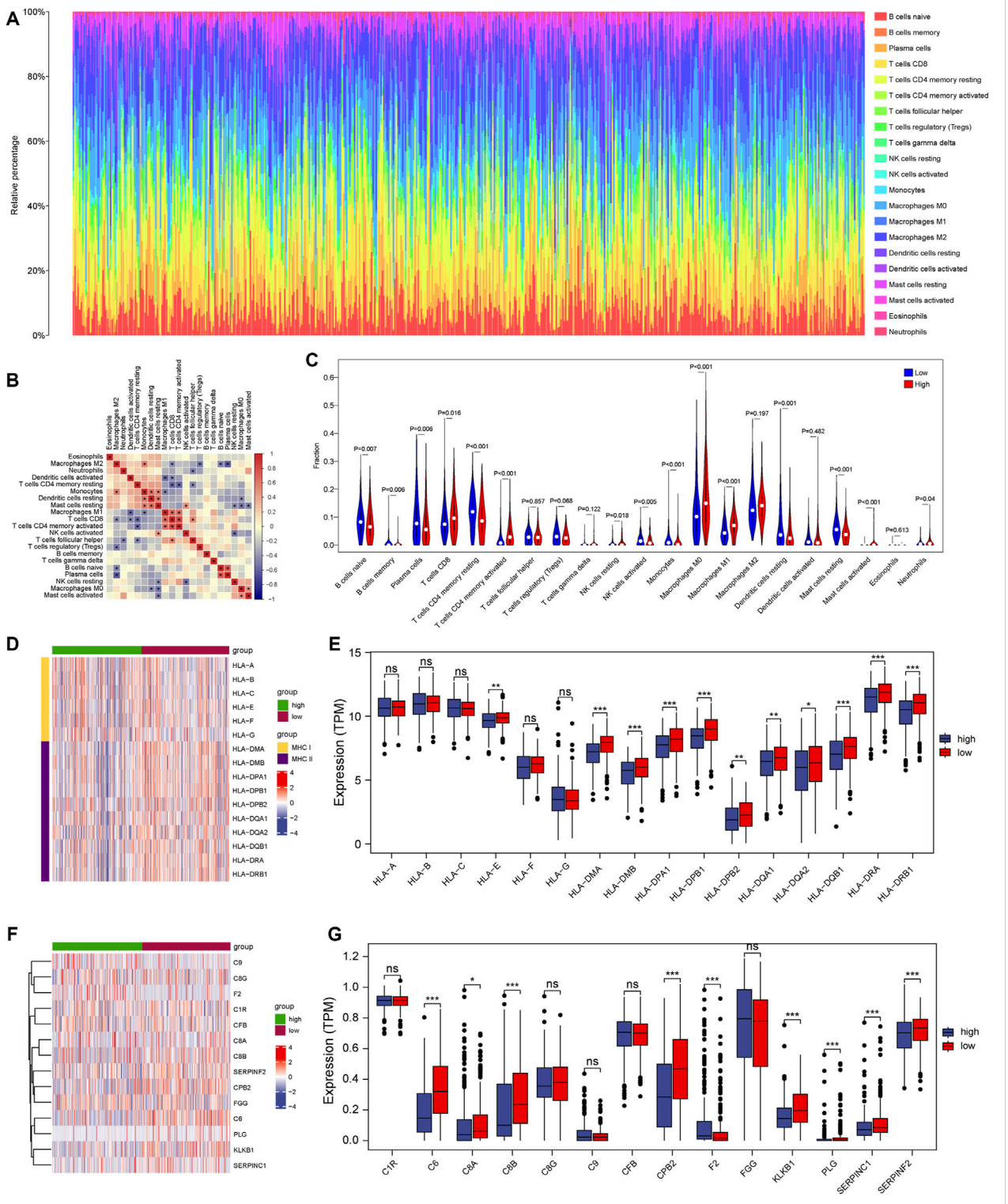

FIGURE 8
Immune infiltration in the two risk groups **(A)** The panorama of 22 immune cell infiltrates **(B)** Correlation analyses of 22 immune cell types **(C)** Differences in the immune cell infiltration between high-and low-risk groups **(D,E)** Differential expression of HLA gene family between the two risk groups **(F,G)** Differential expression of complement-related genes in the two risk groups. * represents $p < 0.05$; ** represents $p < 0.01$; *** represents $p < 0.001$; ns represents no significant difference ($p > 0.05$).

with tumor progression (Wang et al., 2012; Xu et al., 2021). However, there is a lack of in-depth characterization of the role of the KPNA family in LUAD. This is the first investigation to develop a prognostic model premised on the expression of the KPNA family genes, as per our best knowledge. Enrichment analysis revealed the involvement of the KPNA family in transcription, cell cycle, immune infiltration, and inflammatory response, which are tumor-related processes. Thus, our findings may be useful in the development of future investigations to determine patient prognosis and to recognize candidate therapeutic targets in LUAD individuals.

We explored the connection between the KPNA family expression and the OS of patients. High expression of *KPNA2* and *KPNA4* were predictive of inferior OS. *KPNA4* has previously been identified as a tumor promoter gene in some cancers (Wang et al., 2015). For example, high expression of *KPNA4* in cutaneous squamous cell carcinoma was discovered to enhance cancer cell proliferation as well as cisplatin resistance (Zhang et al., 2019). Inhibition of *KPNA4* attenuated prostate cancer metastasis (Yang et al., 2017). Regulating upstream modulators facilitates angiogenesis as well as progression in lung cancer by targeting the miR-340-5p/KPNA4 axis (Li et al., 2020). A previous study identified overexpression of *KPNA2* in NSCLC, and *KPNA2* was identified as a potential biomarker for NSCLC (Wang et al., 2011). These studies support our conclusions that *KPNA2* and *KPNA4* may be useful prognostic biomarkers for LUAD patients.

KEGG enrichment analysis showed transcriptional dysregulation in cancers enriched with DEGs in the high-risk group. Transcription factors serve as a group of sequence-specific binding proteins that can activate or suppress transcription through transactivation or transrepression domains. Transcription factors have been linked to the pathogenesis of a variety of human diseases (including cancers); these account for approximately 20% of all oncogenes identified so far (Lambert et al., 2018). Previous literature reports have displayed the involvement of transcription factors in regulating cell proliferation, differentiation, apoptosis, and their remarkable function in the onset and development of tumors (Sever and Brugge, 2015). Dysregulation of principal transcriptional modulators not only defines the cancer phenotype but is important for its development (Gonda and Ramsay, 2015). Our results suggest that the KPNA family may influence the transcriptional dysregulation in LUAD. Therefore, it is important to study the mechanism of transcriptional dysregulation of the KPNA family in LUAD.

In this study, we found that cell cycle checkpoints and cell cycle mitotic were enriched in the high-risk group. Cell cycle checkpoints are biochemical signaling mechanisms that detect DNA damage or chromosomal dysfunction and trigger a series of sophisticated cellular repair responses (Wu et al., 2005). Typically, cell cycle checkpoints are disrupted in most malignancies and serve a vital function in maintaining genomic integrity and inactivating checkpoint genes (Zheng et al., 2010). In previous research, impaired function of cell cycle checkpoints was found to raise the risk of lung cancer (Wu et al., 2005). Mitosis is the critical stage of the cell cycle, involving the passage of one of the sister chromatids to each of the daughter cells. Therefore, precise regulation of mitosis is essential for the maintenance of chromosome stability in human cells (Pines, 2006). Aberrant mitotic progression leads to chromosomal missegregation, contributing to carcinogenesis (Kops et al., 2005; Holland and Cleveland, 2009; Schvartzman et al., 2010). Our study identified significant enrichment of these two pathways in the high-risk group, which additionally validated the accuracy of the risk prediction model constructed in this study.

The tumor microenvironment (TME) is a heterogeneous system consisting of immune cells, cancer cells, and an extracellular matrix (Hoadley et al., 2014; Warrick et al., 2019). The roles for immune homeostasis similar to a buffering system. While the immune system is constantly stimulated and dampened, the system is maintained at a relatively stable steady state (da Gama Duarte et al., 2018). In this study, the infiltration scores for naive B cells, plasma cells, $CD4^+$ T cells memory resting T cells, and resting dendritic cells were lowered in the high-risk groups than in the low-risk groups, but the infiltration scores for $CD8^+$ T cells, M0 Macrophages were elevated in the high-risk group. This could lead to different responses to immunotherapies in the two risk groups. The purpose of immunotherapy is to alter the environment, and thereby, the equilibrium of the response. Therefore, the sensitivity of immunotherapy in the two risk groups also remains unexplored.

Immune evasion is a significant feature of cancer, and inhibition of HLA gene levels may lead to attenuated antigen presentation, facilitating immune evasion (McGranahan et al., 2017). HLA family genes were decreased in the high-risk group, which suggests that the high-risk group was more prone to immune evasion and thus have a worse prognosis. These results are consistent with our survival analysis. Additionally, we studied the expression of inflammation-related genes in the two risk groups and captured the down-regulation of complement-related genes in the high-risk group. These findings suggest that inflammation was strongly associated with the low-risk group.

This is the first-ever report on the association of the KPNA family expression with survival outcomes of patients with LUAD. Therefore, the KPNA family may potentially serve as a novel prognostic biomarker in patients with LUAD and provide novel targets for LUAD immunotherapy. However, this was bioinformatics research and most of the findings were generated from public databases and bioinformatics analysis. Further *in vitro* and *in vivo* experiments are required to validate our findings.

In conclusion, we found that *KPNA2* and *KPNA4* are potential prognostic markers. We created a prognostic model on the basis of the expression level of the KPNA family, which was shown to accurately predict prognosis. This prognostic model reflects many aspects of LUAD biology and provides

new insights into precision therapy for LUAD. In the future, a lot of basic experiments need to be carried out to validate the applicability and accuracy of this model.

Data availability statement

The original contributions presented in the study are included in the article/Supplementary Material, further inquiries can be directed to the corresponding authors.

Author contributions

JH and LC were responsible for the experimental design and the supervision of this project. XL had the original idea for the study. XL and LZ had access to all data in the study and were in charge of ensuring the data's integrity and accuracy during the data analysis course. XL, LZ, JZ, YS, and YQ participated in analyzing the data and writing the manuscript. All authors have read, edited, and approved the final manuscript.

Funding

This study was supported in part by the grants from the Certificate of China Postdoctoral Science Foundation Grant (2021M693826 and 2021MD703830), the Hei Long Jiang Postdoctoral Foundation (LBH-Z20176 and LBH-Z21187), the Fundamental Research Funds for the Provincial Universities (2020-KYYWF-1462 and 2021-KYYWF-0249), the Haiyan Science Foundation of Harbin Medical University Cancer Hospital (JJZD 2022-13), the Haiyan Youth Fund and Top-Notch Youth Fund from Harbin Medical University Cancer Hospital (JJQN 2021-09, and BJQN 2021-02), and the NSFC (Grant Nos. 82103519 and 82072563).

Acknowledgments

We appreciate all of the professionals and patients who took part in the study, as well as the authors for sharing their essential research findings.

Conflict of interest

The authors declare that the research was conducted in the absence of any commercial or financial relationships that could be construed as a potential conflict of interest.

Publisher's note

Supplementary material

The Supplementary Material for this article can be found online at: https://www.frontiersin.org/articles/10.3389/fgene.2022.956314/full#supplementary-material

References

Ashburner, M., Ball, C. A., Blake, J. A., Botstein, D., Butler, H., Cherry, J. M., et al. (2000). Gene ontology: tool for the unification of biology. The gene ontology consortium. *Nat. Genet.* 25 (1), 25–29. doi:10.1038/75556

Catania, C., Muthusamy, B., Spitaleri, G., Del Signore, E., and Pennell, N. A. (2021). The new era of immune checkpoint inhibition and target therapy in early-stage non-small cell lung cancer. A review of the literature. *Clin. Lung Cancer* 23, 108–115. doi:10.1016/j.cllc.2021.11.003

Chin, C. H., Chen, S. H., Wu, H. H., Ho, C. W., Ko, M. T., Lin, C. Y., et al. (2014). cytoHubba: identifying hub objects and sub-networks from complex interactome. *BMC Syst. Biol.* 8 (Suppl. 4), S11. doi:10.1186/1752-0509-8-S4-S11

Cui, X., Wang, H., Wu, X., Huo, K., and Jing, X. (2021). Increased expression of KPNA2 predicts unfavorable prognosis in ovarian cancer patients, possibly by targeting KIF4A signaling. *J. Ovarian Res.* 14 (1), 71. doi:10.1186/s13048-021-00818-9

da Gama Duarte, J., Woods, K., Andrews, M. C., and Behren, A. (2018). The good, the (not so) bad and the ugly of immune homeostasis in melanoma. *Immunol. Cell Biol.* 96 (5), 497–506. doi:10.1111/imcb.12001

Gonda, T. J., and Ramsay, R. G. (2015). Directly targeting transcriptional dysregulation in cancer. *Nat. Rev. Cancer* 15 (11), 686–694. doi:10.1038/nrc4018

Han, Y., and Wang, X. (2020). The emerging roles of KPNA2 in cancer. *Life Sci.* 241, 117140. doi:10.1016/j.lfs.2019.117140

Hänzelmann, S., Castelo, R., and Guinney, J. (2013). GSVA: gene set variation analysis for microarray and RNA-seq data. *BMC Bioinforma.* 14, 7. doi:10.1186/1471-2105-14-7

Hazawa, M., Sakai, K., Kobayashi, A., Yoshino, H., Iga, Y., Iwashima, Y., et al. (2020). Disease-specific alteration of karyopherin-alpha subtype establishes feed-forward oncogenic signaling in head and neck squamous cell carcinoma. *Oncogene* 39 (10), 2212–2223. doi:10.1038/s41388-019-1137-3

Hoadley, K. A., Yau, C., Wolf, D. M., Cherniack, A. D., Tamborero, D., Ng, S., et al. (2014). Multiplatform analysis of 12 cancer types reveals molecular classification within and across tissues of origin. *Cell* 158 (4), 929–944. doi:10.1016/j.cell.2014.06.049

Holland, A. J., and Cleveland, D. W. (2009). Boveri revisited: chromosomal instability, aneuploidy and tumorigenesis. *Nat. Rev. Mol. Cell Biol.* 10 (7), 478–487. doi:10.1038/nrm2718

Hu, B., Cheng, J. W., Hu, J. W., Li, H., Ma, X. L., Tang, W. G., et al. (2019). KPNA3 confers sorafenib resistance to advanced hepatocellular carcinoma via TWIST regulated epithelial-mesenchymal transition. *J. Cancer* 10 (17), 3914–3925. doi:10.7150/jca.31448

Hu, R. H., Zhang, Z. T., Wei, H. X., Ning, L., Ai, J. S., Li, W. H., et al. (2020). LncRNA ST7-AS1, by regulating miR-181b-5p/KPNA4 axis, promotes the malignancy of lung adenocarcinoma. *Cancer Cell Int.* 20 (1), 568. doi:10.1186/s12935-020-01652-7

Kim, N. H., Yoshimaru, T., Chen, Y. A., Matsuo, T., Komatsu, M., Miyoshi, Y., et al. (2015). BIG3 inhibits the estrogen-dependent nuclear translocation of PHB2 via multiple karyopherin-alpha proteins in breast cancer cells. *PLoS One* 10 (6), e0127707. doi:10.1371/journal.pone.0127707

Ko, E. C., Raben, D., and Formenti, S. C. (2018). The integration of radiotherapy with immunotherapy for the treatment of non-small cell lung cancer. *Clin. Cancer Res.* 24 (23), 5792–5806. doi:10.1158/1078-0432.CCR-17-3620

Kops, G. J., Weaver, B. A., and Cleveland, D. W. (2005). On the road to cancer: aneuploidy and the mitotic checkpoint. *Nat. Rev. Cancer* 5 (10), 773–785. doi:10.1038/nrc1714

Lambert, M., Jambon, S., Depauw, S., and David-Cordonnier, M. H. (2018). Targeting transcription factors for cancer treatment. *Molecules* 23 (6), E1479. doi:10.3390/molecules23061479

Laurila, E., Vuorinen, E., Savinainen, K., Rauhala, H., and Kallioniemi, A. (2014). KPNA7, a nuclear transport receptor, promotes malignant properties of pancreatic cancer cells *in vitro*. *Exp. Cell Res.* 322 (1), 159–167. doi:10.1016/j.yexcr.2013.11.014

Li, X., Yu, M., and Yang, C. (2020). YY1-mediated overexpression of long noncoding RNA MCM3AP-AS1 accelerates angiogenesis and progression in lung cancer by targeting miR-340-5p/KPNA4 axis. *J. Cell. Biochem.* 121 (3), 2258–2267. doi:10.1002/jcb.29448

Love, M. I., Huber, W., and Anders, S. (2014). Moderated estimation of fold change and dispersion for RNA-seq data with DESeq2. *Genome Biol.* 15 (12), 550. doi:10.1186/s13059-014-0550-8

Miyamoto, Y., Sasaki, M., Miyata, H., Monobe, Y., Nagai, M., Otani, M., et al. (2020). Genetic loss of importin α4 causes abnormal sperm morphology and impacts on male fertility in mouse. *FASEB J.* 34 (12), 16224–16242. doi:10.1096/fj.202000768RR

Majem, B., Nadal, E., and Munoz-Pinedo, C. (2020). Exploiting metabolic vulnerabilities of Non small cell lung carcinoma. *Semin. Cell Dev. Biol.* 98, 54–62. doi:10.1016/j.semcdb.2019.06.004

Mayakonda, A., Lin, D. C., Assenov, Y., Plass, C., and Koeffler, H. P. (2018). Maftools: efficient and comprehensive analysis of somatic variants in cancer. *Genome Res.* 28 (11), 1747–1756. doi:10.1101/gr.239244.118

McGranahan, N., Rosenthal, R., Hiley, C. T., Rowan, A. J., Watkins, T. B. K., Wilson, G. A., et al. (2017). Allele-specific HLA loss and immune escape in lung cancer evolution. *Cell* 171 (6), 1259–1271. doi:10.1016/j.cell.2017.10.001

Miyamoto, Y., Yamada, K., and Yoneda, Y. (2016). Importin α: a key molecule in nuclear transport and non-transport functions. *J. Biochem.* 160 (2), 69–75. doi:10.1093/jb/mvw036

Myat, A. B., Ogawa, T., Kadota-Watanabe, C., and Moriyama, K. (2018). Nuclear import of transcriptional corepressor BCOR occurs through interaction with karyopherin alpha expressed in human periodontal ligament. *Biochem. Biophys. Res. Commun.* 507 (1-4), 67–73. doi:10.1016/j.bbrc.2018.10.158

Newman, A. M., Liu, C. L., Green, M. R., Gentles, A. J., Feng, W., Xu, Y., et al. (2015). Robust enumeration of cell subsets from tissue expression profiles. *Nat. Methods* 12 (5), 453–457. doi:10.1038/nmeth.3337

Ogata, H., Goto, S., Sato, K., Fujibuchi, W., Bono, H., Kanehisa, M., et al. (1999). KEGG: kyoto Encyclopedia of genes and Genomes. *Nucleic Acids Res.* 27 (1), 29–34. doi:10.1093/nar/27.1.29

Oostdyk, L. T., McConnell, M. J., and Paschal, B. M. (2019). Characterization of the Importin-beta binding domain in nuclear import receptor KPNA7. *Biochem. J.* 476 (21), 3413–3434. doi:10.1042/BCJ20190717

Pines, J. (2006). Mitosis: a matter of getting rid of the right protein at the right time. *Trends Cell Biol.* 16 (1), 55–63. doi:10.1016/j.tcb.2005.11.006

Schvartzman, J. M., Sotillo, R., and Benezra, R. (2010). Mitotic chromosomal instability and cancer: mouse modelling of the human disease. *Nat. Rev. Cancer* 10 (2), 102–115. doi:10.1038/nrc2781

Sever, R., and Brugge, J. S. (2015). Signal transduction in cancer. *Cold Spring Harb. Perspect. Med.* 5 (4), a006098. doi:10.1101/cshperspect.a006098

Siegel, R. L., Miller, K. D., Fuchs, H. E., and Jemal, A. (2022). Cancer statistics, 2022. *CA. Cancer J. Clin.* 72 (1), 7–33. doi:10.3322/caac.21708

Suarez-Farinas, M., Lowes, M. A., Zaba, L. C., and Krueger, J. G. (2010). Evaluation of the psoriasis transcriptome across different studies by gene set enrichment analysis (GSEA). *PLoS One* 5 (4), e10247. doi:10.1371/journal.pone.0010247

Tsoi, H., Man, E. P., Leung, M. H., Mok, K. C., Chau, K. M., Wong, L. S., et al. (2021). KPNA1 regulates nuclear import of NCOR2 splice variant BQ323636.1 to confer tamoxifen resistance in breast cancer. *Clin. Transl. Med.* 11 (10), e554. doi:10.1002/ctm2.554

Wang, C. I., Chien, K. Y., Wang, C. L., Liu, H. P., Cheng, C. C., Chang, Y. S., et al. (2012). Quantitative proteomics reveals regulation of karyopherin subunit alpha-2 (KPNA2) and its potential novel cargo proteins in nonsmall cell lung cancer. *Mol. Cell. Proteomics* 11 (11), 1105–1122. doi:10.1074/mcp.M111.016592

Wang, C. I., Wang, C. L., Wang, C. W., Chen, C. D., Wu, C. C., Liang, Y., et al. (2011). Importin subunit alpha-2 is identified as a potential biomarker for non-small cell lung cancer by integration of the cancer cell secretome and tissue transcriptome. *Int. J. Cancer* 128 (10), 2364–2372. doi:10.1002/ijc.25568

Wang, H., Tao, T., Yan, W., Feng, Y., Wang, Y., Cai, J., et al. (2015). Upregulation of miR-181s reverses mesenchymal transition by targeting KPNA4 in glioblastoma. *Sci. Rep.* 5, 13072. doi:10.1038/srep13072

Wang, H., Xiao, R., and Yang, B. (2021). MiR-101-3p suppresses progression of cervical squamous cell carcinoma by targeting and down-regulating KPNA2. *Technol. Cancer Res. Treat.* 20, 15330338211055948. doi:10.1177/15330338211055948

Warrick, J. I., Sjodahl, G., Kaag, M., Raman, J. D., Merrill, S., Shuman, L., et al. (2019). Intratumoral heterogeneity of bladder cancer by molecular subtypes and histologic variants. *Eur. Urol.* 75 (1), 18–22. doi:10.1016/j.eururo.2018.09.003

Wu, J., Li, L., Zhang, H., Zhao, Y., Zhang, H., Wu, S., et al. (2021). A risk model developed based on tumor microenvironment predicts overall survival and associates with tumor immunity of patients with lung adenocarcinoma. *Oncogene* 40 (26), 4413–4424. doi:10.1038/s41388-021-01853-y

Wu, X., Roth, J. A., Zhao, H., Luo, S., Zheng, Y. L., Chiang, S., et al. (2005). Cell cycle checkpoints, DNA damage/repair, and lung cancer risk. *Cancer Res.* 65 (1), 349–357. doi:10.1158/0008-5472.349.65.1

Xu, M., Liang, H., Li, K., Zhu, S., Yao, Z., Xu, R., et al. (2021). Value of KPNA4 as a diagnostic and prognostic biomarker for hepatocellular carcinoma. *Aging* 13 (4), 5263–5283. doi:10.18632/aging.202447

Yang, F., Li, S., Cheng, Y., Li, J., and Han, X. (2020). Karyopherin α 2 promotes proliferation, migration and invasion through activating NF-κB/p65 signaling pathways in melanoma cells. *Life Sci.* 252, 117611. doi:10.1016/j.lfs.2020.117611

Yang, J., Lu, C., Wei, J., Guo, Y., Liu, W., Luo, L., et al. (2017). Inhibition of KPNA4 attenuates prostate cancer metastasis. *Oncogene* 36 (20), 2868–2878. doi:10.1038/onc.2016.440

Yin, N., Liu, Y., Khoor, A., Wang, X., Thompson, E. A., Leitges, M., et al. (2019). Protein kinase cι and wnt/β-catenin signaling: Alternative pathways to kras/trp53-driven lung adenocarcinoma. *Cancer Cell* 36 (2), 692–693. e7. doi:10.1016/j.ccell.2019.11.007

Yu, G., Wang, L. G., Han, Y., and He, Q. Y. (2012). clusterProfiler: an R package for comparing biological themes among gene clusters. *OMICS* 16 (5), 284–287. doi:10.1089/omi.2011.0118

Zhang, M., Luo, H., and Hui, L. (2019). MiR-3619-5p hampers proliferation and cisplatin resistance in cutaneous squamous-cell carcinoma via KPNA4. *Biochem. Biophys. Res. Commun.* 513 (2), 419–425. doi:10.1016/j.bbrc.2019.03.203

Zheng, Y. L., Kosti, O., Loffredo, C. A., Bowman, E., Mechanic, L., Perlmutter, D., et al. (2010). Elevated lung cancer risk is associated with deficiencies in cell cycle checkpoints: genotype and phenotype analyses from a case-control study. *Int. J. Cancer* 126 (9), 2199–2210. doi:10.1002/ijc.24771

frontiers | Frontiers in Genetics

TYPE Original Research
PUBLISHED 15 August 2022
DOI 10.3389/fgene.2022.975185

OPEN ACCESS

EDITED BY
Qian Wang,
Tai'an City Central Hospital, China

REVIEWED BY
Pengcheng Zhou,
Hospital of Chengdu University of Traditional Chinese Medicine, China
Xuan Zhou,
Nanjing Drum Tower Hospital, China

*CORRESPONDENCE
Yufeng Zhang,
yufengzhang@njucm.edu.cn
Weilong Jiang,
jwljytcm@163.com
Jia Qi,
qijia@xinhuamed.com.cn

†These authors have contributed equally to this work

SPECIALTY SECTION
This article was submitted to Cancer Genetics and Oncogenomics, a section of the journal Frontiers in Genetics

RECEIVED 22 June 2022
ACCEPTED 05 July 2022
PUBLISHED 15 August 2022

CITATION
Zhang H, Shi Y, Yi Q, Wang C, Xia Q, Zhang Y, Jiang W and Qi J (2022), A novel defined cuproptosis-related gene signature for predicting the prognosis of lung adenocarcinoma.
Front. Genet. 13:975185.
doi: 10.3389/fgene.2022.975185

A novel defined cuproptosis-related gene signature for predicting the prognosis of lung adenocarcinoma

Huizhe Zhang[1†], Yanchen Shi[2†], Qing Yi[2], Cong Wang[3], Qingqing Xia[3], Yufeng Zhang[3*], Weilong Jiang[3*] and Jia Qi[4*]

[1]Department of Respiratory Medicine, Yancheng Hospital of Traditional Chinese Medicine, Yancheng Hospital Affiliated to Nanjing University of Chinese Medicine, Yancheng, China, [2]Department of Pulmonary and Critical Care Medicine, Traditional Chinese and Western Medicine Clinical College of Nanjing University of Chinese Medicine, Nanjing, China, [3]Department of Pulmonary and Critical Care Medicine, Jiangyin Hospital of Traditional Chinese Medicine, Jiangyin Hospital Affiliated to Nanjing University of Chinese Medicine, Jiangyin, China, [4]Department of Pharmacy, Xin Hua Hospital Affiliated to Shanghai Jiao Tong University School of Medicine, Shanghai, China

Lung adenocarcinoma (LUAD) has become the most prevalent histologic subset of primary lung cancer, and effective innovative prognostic models are needed to enhance the feasibility of targeted therapies for the disease. Programmed cell death (PCD) performs an integral function in the origin and treatment of cancer. Some PCD-related effective signatures for predicting prognosis in LUAD patients could provide potential therapeutic options in LUAD. A copper-dependent cell death referred to as cuproptosis is distinct from known PCD. However, whether cuproptosis is associated with LUAD patients' prognoses and the potential roles of cuproptosis-related genes involved is still unknown. For the prediction of LUAD prognosis, we developed a unique cuproptosis-associated gene signature. In The Cancer Genome Atlas (TCGA) cohort, the score derived from the risk signature on the basis of six cuproptosis-related genes was found to independently serve as a risk factor for anticipating lung cancer-related death. The differentially expressed genes between the high- and low-risk groups were linked to the cilium-related function. LUAD patients' prognoses may now be predicted by a unique gene signature identified in this work. This discovery also provides a substantial foundation for future research into the links between cuproptosis-associated genes and cilium-related function in LUAD patients.

KEYWORDS

gene signature, cuproptosis, prognosis, lung adenocarcinoma, cilium

Introduction

Lung adenocarcinoma (LUAD) is currently the most prevalent histologic subset of primary lung cancer, contributing to over 40% of all cases, and its relative prevalence is growing (Barta et al., 2019). The absence of adequate screening strategies and the challenges of performing an early diagnosis have resulted in significantly high recurrence and death rates for LUAD, with an overall five-year survival probability of lower than 15% owing to local and distant metastases (Ali et al., 2013). Despite great efforts having been made to explore the therapeutic effect of LUAD, the clinical outcomes of LUAD remain poor in patients (Zhang et al., 2015). Because of the limits of current LUAD therapies, novel treatment targets are required in order to improve the clinical result of LUAD. As a result, robust innovative prognostic models are needed in order to enhance the feasibility of targeted therapy for LUAD.

Programmed cell death (PCD) is critical for the appropriate development and maintenance of tissue homeostasis, as well as for the removal of damaged, diseased, or defunct cells in multicellular organisms. In the pathophysiology of different illnesses, aberrations in PCD signaling cascades, including ferroptosis, apoptosis, pyroptosis, necroptosis, and cell death linked to autophagy, may be detected (Galluzzi et al., 2018; Moujalled et al., 2021). Nowadays, several studies have established tumor prognostic models associated with PCD (Cai et al., 2021; Fu et al., 2021; Shao et al., 2021; Zhao et al., 2021). PCD performs an integral function in the origin and treatment of cancer (Shao et al., 2019; Strasser and Vaux, 2020). A few studies revealed crosstalk between distinct PCD mechanisms and antitumor immunity (Tang et al., 2020). Immunogenic cell death is a kind of tumor cell death that may be induced by some chemotherapy medicines, oncolytic viruses, physicochemical treatments, and radiotherapy (Ahmed and Tait, 2020). The ability of cancer cells to undergo death when subjected to anti-cancer therapy is mediated by modulated cell death systems, which could either suppress or enhance the immunogenic capacity of cancer cells (Garg and Agostinis, 2017).

The latest research shows that copper mediates cell death by targeting lipoylated tricarboxylic acid (TCA) cycle proteins, and because of this, lipoylated proteins aggregate, and corresponding iron-sulfur cluster proteins are lost, resulting in proteotoxic stress and eventually cell death. The authors demonstrate that copper-dependent modulated cell death in human cells is different from recognized cell death processes and is reliant on mitochondrial respiration (Tsvetkov et al., 2022). Therefore, this copper-dependent cell death was referred to as cuproptosis. There are very few in-depth studies on cuproptosis. There is a strong correlation between the abundance of ferredoxin 1 (FDX1) and the level of lipoylated proteins in a variety of human tumor cells, and cell lines with significant levels of lipoylated proteins are susceptible to cuproptosis, suggesting that copper ionophore intervention ought to be targeted toward malignancies with this metabolic landscape. Consequently, subsequent clinical studies of copper ionophores ought to be conducted utilizing a biomarker-driven strategy (Tsvetkov et al., 2022). According to the above studies on cuproptosis, we obtained cuproptosis-related genes including FDX1, dihydrolipoamide dehydrogenase (DLD), lipoic acid synthetase (LIAS), lipoyltransferase 1 (LIPT1), ATPase copper transporting beta (ATP7B), glycine cleavage system protein H (GCSH), ATPase copper transporting alpha (ATP7A), dihydrolipoamide S-acetyltransferase (DLAT), pyruvate dehydrogenase E1 subunit beta (PDHB), pyruvate dehydrogenase E1 subunit alpha 1 (PDHA1), dihydrolipoamide S-succinyltransferase (DLST), solute carrier family 31 members 1 (SLC31A1), and dihydrolipoamide branched chain transacylase E2 (DBT), which provide the preliminary basis for our next exploration and research.

Recently, a number of studies have established ferroptosis-, pyroptosis-, necroptosis- and autophagy-related effective signatures for predicting prognosis in LUAD patients, which could provide potential therapeutic options in LUAD (Chen et al., 2020; Lin et al., 2021; Yao et al., 2021; Lu et al., 2022). Given these existing findings, we hypothesized that cuproptosis is linked to LUAD patients' prognoses and that cuproptosis-associated genes may be involved in the disease process. As a consequence, we conducted a comprehensive investigation to determine the expression patterns of cuproptosis-associated genes in normal lung and LUAD samples, ascertain the prognostic significance of these genes, and conducted the Gene Ontology (GO) and immune infiltration enrichment analyses.

Materials and methods

Datasets

We acquired the RNA sequencing (RNA-seq) data combined with the corresponding clinical features (phenotype and survival data) from the Genomic Data Commons (GDC) The Cancer Genome Atlas (TCGA) LUAD cohort, all of which were retrieved from the University of California, Santa Cruz (UCSC) Xena (http://xena.ucsc.edu)(Goldman et al., 2020). UCSC Xena is an analysis and visualization platform with excellent performance for both large public databases including TCGA (Chin et al., 2011) and the GDC (Grossman et al., 2016), and private datasets.

The RNA-seq data normalized to fragment per kilobase million (FPKM) values include the gene expression data of 59 normal and 526 tumor tissues samples (https://gdc-hub.s3.us-east-1.amazonaws.com/download/TCGA-LUAD.htseq_fpkm.tsv.gz; version 07-20-2019), the phenotype data include clinicopathologic features of 877 LUAD patients (https://gdc-hub.s3.us-east-1.amazonaws.com/download/TCGA-LUAD.

GDC_phenotype.tsv.gz; version 08-07-2019) and survival data include survival time information of 738 LUAD patients (https://gdc-hub.s3.us-east-1.amazonaws.com/download/TCGA-LUAD.survival.tsv; version 07-20-2019) (Supplementary File S1).

Identification of the cuproptosis-related gene expression levels and interactions

We extracted the 13 cuproptosis-related genes from the recent article (Tsvetkov et al., 2022). The downloaded expression data in the TCGA dataset were presented as FPKM values. The "limma" package (Ritchie et al., 2015) was used to identify differentially expressed genes (DEGs) related to cuproptosis between 59 normal and 526 tumor tissues, and a p-value < 0.05 was defined statistically significant difference. The "pheatmap" package was used to present the RNA levels of these 13 cuproptosis-associated genes. The following are the criteria for the genes linked to cuproptosis with differential expression: $^{*}p < 0.05$, $^{**}p < 0.01$, and $^{***}p < 0.001$. We employed these genes to create a protein-protein interaction (PPI) network with the Search Tool for the Retrieval of Interacting Genes/Proteins (STRING), version 11.5 (https://string-db.org/), which is a repository of PPIs that have been identified and anticipated. There are indirect (functional) and direct (physical) linkages resulting from computerized prediction, information transmission between organisms, and interplay obtained from other repositories (Szklarczyk et al., 2021). The minimum required interaction value for the PPI analysis was established at 0.15 (the lowest confidence level) due to the limited number of genes, which allowed for more interactions to be discovered. Visualization of the correlation network of these genes was accomplished utilizing the "igraph" package, which is a set of network analysis tools that have a focus on portability, efficiency, and simplicity of use.

Tumor classification premised on the cuproptosis-related genes clusters

With the help of the R package "ConsensusClusterPlus" (Wilkerson and Hayes, 2010), a consensus clustering analysis of all 526 LUAD tumor tissues in the TCGA dataset was performed to examine the links between the expression of the 13 cuproptosis-related gene and LUAD subtypes. Once the clustering variable (k) was increased from 2 to 10, a suitable value of k could be found and the 526 LUAD tumor tissues were classified into suitable clusters on basis of the 13 genes, with the highest intragroup correlations and the low intergroup correlations. After collating the phenotype data and survival data and removing the missing values, the data on clustered gene expression and the clinical parameters encompassing the tumor, node, and metastasis (TNM) classification, age, gender, and survival status of 486 LUAD patients were presented via the "pheatmap" package, which allowed for visualization of the differences between the clinical parameters and the classified clusters. A comparison was made for the overall survival (OS) time among the divided clusters *via* the Kaplan–Meier (KM) survival analysis using the "survival" package.

Development of a cuproptosis-associated gene prognostic model

In total, 526 LUAD specimens were paired with the 500 matching patients whose survival data was complete. To examine the predictive significance of the cuproptosis-associated genes, we conducted a Cox regression analysis on the data from the TCGA cohort to determine the relationships between each gene and survival status. We established $p < 0.3$ as the cut-off value to avoid missing important genes and identified genes associated with survival for subsequent evaluation. The least absolute shrinkage and selection operator (LASSO) Cox regression model was then employed to filter out the potential genes and to create the prognostic model, which was done with the help of the R package "glmnet" (Tibshirani, 1997; Engebretsen and Bohlin, 2019). The final decision was made to keep the genes along with their coefficients being retained, and the penalty parameter (λ) was chosen based on the bare minimum requirements. Using a linear combination for each prognostic survival-associated gene's standardized expression level and its associated multivariate Cox regression coefficient (β), the risk score in the derivation, as well as the validation sets, were determined. The following was the equation for calculating the risk score: Risk Score = $\sum(\beta_i \times \text{gene}_i\ \text{EXP})$ (EXP: normalized expression value). After classifying patients into low- and high-risk subgroups premised on their median risk scores, the OS duration was evaluated between the two subgroups utilizing the KM survival analysis method. Using the gene signature as a starting point, principal component analysis (PCA) was done with the help of the function "prcomp" in the R package "stats". The R packages "survival" and "timeROC" were employed to execute analyses of patients' distribution premised on the risk score, each patient's survival status, KM survival curves, and receiver operating characteristic (ROC) curves.

Assessment of the risk score's independent prognosis

Patients with LUAD in the TCGA cohort were categorized into two subgroups premised on their median risk scores. The

clinical features including TNM classification, age, gender, and survival status of LUAD patients in high- and low-risk subgroups were analyzed in conjunction with the risk score derived from our regression model. Univariate and multivariate Cox regression models were utilized in the investigation. After collating the phenotype data and survival data and removing the missing values, the survival-related gene expression data and the clinical parameters encompassing TNM classification, age, gender, and survival status of LUAD patients in low- and high-risk groupings were presented *via* the "pheatmap" package and the differences in the clinical parameters across the two groups were evaluated.

Functional enrichment and immune infiltration analyses of the differentially expressed genes between the low- and high-risk subgroups

Patients with LUAD in the TCGA dataset were categorized into two subgroups premised on their median risk scores. Determining the DEGs that distinguished the patients at low and high risk was done using the criteria of |log2FoldChange (FC)| > 0.5 and adjusted $p < 0.05$. The "org.Hs.eg.db" program was utilized to obtain the entrezIDs of DEGs. By incorporating the "clusterProfiler" and the "GOplot" packages, we were able to conduct analyses of GO functional enrichment on the basis of these DEGs and entrezIDs (Yu et al., 2012; Walter et al., 2015; Wu et al., 2021). GO functional analysis comprises three classifications: biological process (BP), cellular component (CC) and molecular function (MF). Single-sample gene set enrichment analysis (ssGSEA) was performed with the help of the "GSVA" and "GSEABase" packages, which were employed to compute the infiltration scores of immune cells and to assess the functioning of immune-associated pathways (Hanzelmann et al., 2013).

Statistical analysis

The gene expression patterns in the normal lung and LUAD samples were compared utilizing a single-factor analysis of variance, whereas the categorical data were evaluated utilizing the Pearson chi-square test. We used the KM survival analysis approach in conjunction with a two-sided log-rank test to assess the OS of patients across different subgroups. We employed univariate and multivariate Cox regression models to examine the risk model's independent prognostic significance. Through the use of Mann–Whitney test, we evaluated the infiltrating levels of immune cells and the activation of the immune pathway between the two subgroups. RGUI 4.0.3 was employed to execute all analyses of statistical data.

Results

The cuproptosis-related gene expression levels and interactions

The 13 cuproptosis-related gene expression levels were determined after comparing 59 normal and 526 tumor tissues in GDC TCGA LUAD cohort retrieved from UCSC Xena. Among them, 7 genes (DLAT, DLD, GCSH, LIAS, LIPT1, PDHA1, and PDHB) were upmodulated, whereas 3 genes (ATP7B, FDX1, and SLC31A1) were downmodulated in the tumor group in contrast with the normal group ($p < 0.05$). The levels of RNA for these 13 cuproptosis-related genes are displayed as a heatmap, where green and red denote low and high expression levels, respectively (Figure 1A). We undertook a PPI study on these cuproptosis-associated genes in order to learn more about their interactions with one another. Once the minimum required interaction score of the PPI analysis was adjusted to 0.15, the top five interaction proteins/genes were DLD, GCSH, DLAT, PDHA1, and LIAS, which could be considered as hub genes. Figure 1B illustrates the findings of PPI analysis. Figure 1C depicts the correlation network encompassing all genes associated with cuproptosis, where red and blue denote positive and negative correlations, correspondingly.

Characterization of tumors depending on the genes involved in cuproptosis

The expression of the 13 cuproptosis-associated genes was compared to the expression of LUAD subtypes utilizing a consensus clustering analysis of all 526 LUAD tumor specimens from the TCGA cohort in order to investigate the relationship between the two. After adjusting the clustering value (k) from 2 to 10, we discovered that at $k = 3$, the intragroup relationships were the strongest, illustrating that the 526 LUAD tumor tissues may be efficiently classified into three clusters on the basis of the 13 genes (Figure 2A). The 526 LUAD tumor tissues were corresponding to 486 LUAD patients with complete clinical features including TNM classification (stage N: N0, N1, N2, N3 or NX; stage M: M0, M1, or MX; stage T: T1, T2, T3, T4 or TX), age (≤60 or >60 years), gender (male or female) and survival status (dead or alive). An interactive heatmap is used to display the gene expression patterns and clinical parameters of 486 LUAD patients. The heatmap reveals that there are only minor differences in clinical parameters across the three clusters (Figure 2B). The KM survival analysis was utilized to measure the OS duration of the 500 relevant patients who had full survival time information among the three clusters, but differences were not obvious ($p = 0.3091$) (Figure 2C).

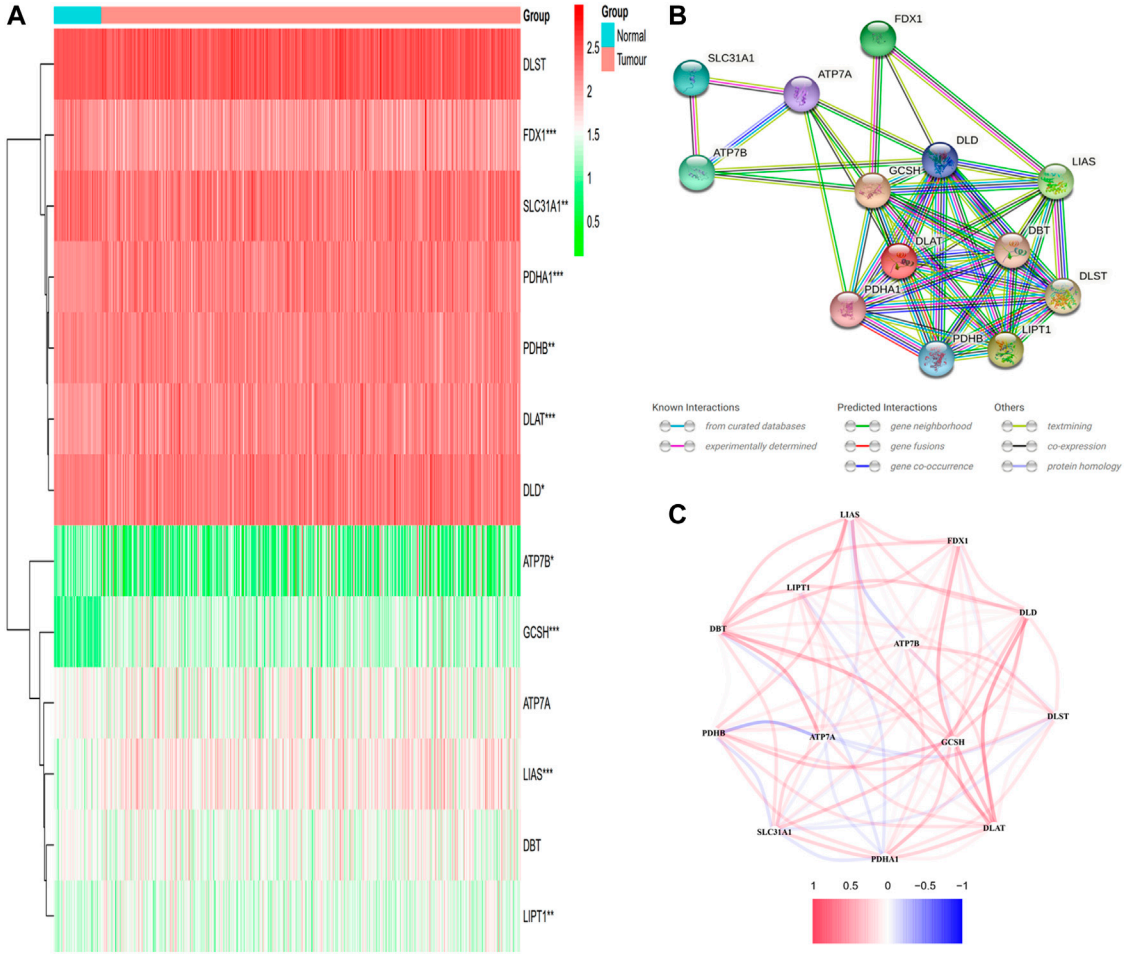

FIGURE 1
The expression and interactions of 13 cuproptosis-related genes. **(A)** The expression of cuproptosis-related genes in normal and tumor samples is shown in a heatmap (with green and red signifying low and high expression levels, respectively). Comparison between the tumor samples and the normal samples *$p < 0.05$; **$p < 0.01$; ***$p < 0.001$. **(B)** PPI network illustrating the connections of genes involved in cuproptosis (interaction score = 0.15). **(C)** The network of genes associated with cuproptosis (red and blue lines depict positive and negative correlations, respectively). The strength of relevance is reflected in the intensity of the colors.

Development of a prognostic gene model in the TCGA dataset

In total, 526 LUAD specimens were paired with the 500 matching patients whose information on survival time was complete. The univariate Cox regression analysis was utilized for the initial filtering of the genes associated with survival. Subsequent investigations were conducted on the 6 genes (DBT, DLAT, DLD, DLST, LIPT1, and PDHA1) that satisfied the criterion of $p < 0.3$. Out of these 6 genes, 2 genes (DBT and LIPT1) were shown to have a protective function with hazard ratios (HRs) < 1, whereas the remaining 4 genes (DLAT, DLD, DLST, and PDHA1) were linked to a greater risk as demonstrated by HRs > 1. LIPT1 independently served as an influencing factor ($p < 0.05$) (Figure 3A). The Cox regression analysis conducted using the LASSO method was utilized to build a 6-gene signature that corresponded to the optimal λ value (Figure 3B). In the next step, we undertook a multivariate Cox regression analysis of the six genes (Figure 3C). The following is the equation for computing the risk score: risk score = (−0.2733 × DBT EXP) + (0.1636 × DLAT EXP) + (0.1974 × DLD EXP) + (0.1606 × DLST EXP) + (−0.4600 × LIPT1 EXP) + (0.1336 × PDHA1 EXP). Five hundred patients were separated into two groups depending on the median score generated by the risk score equation: low- and high-risk subgroups (Figure 3D). When the PCA was performed, it was determined that patients with different risks could be effectively categorized into two clusters (Figure 3E). A higher number of fatalities and a considerably shorter survival duration were observed among

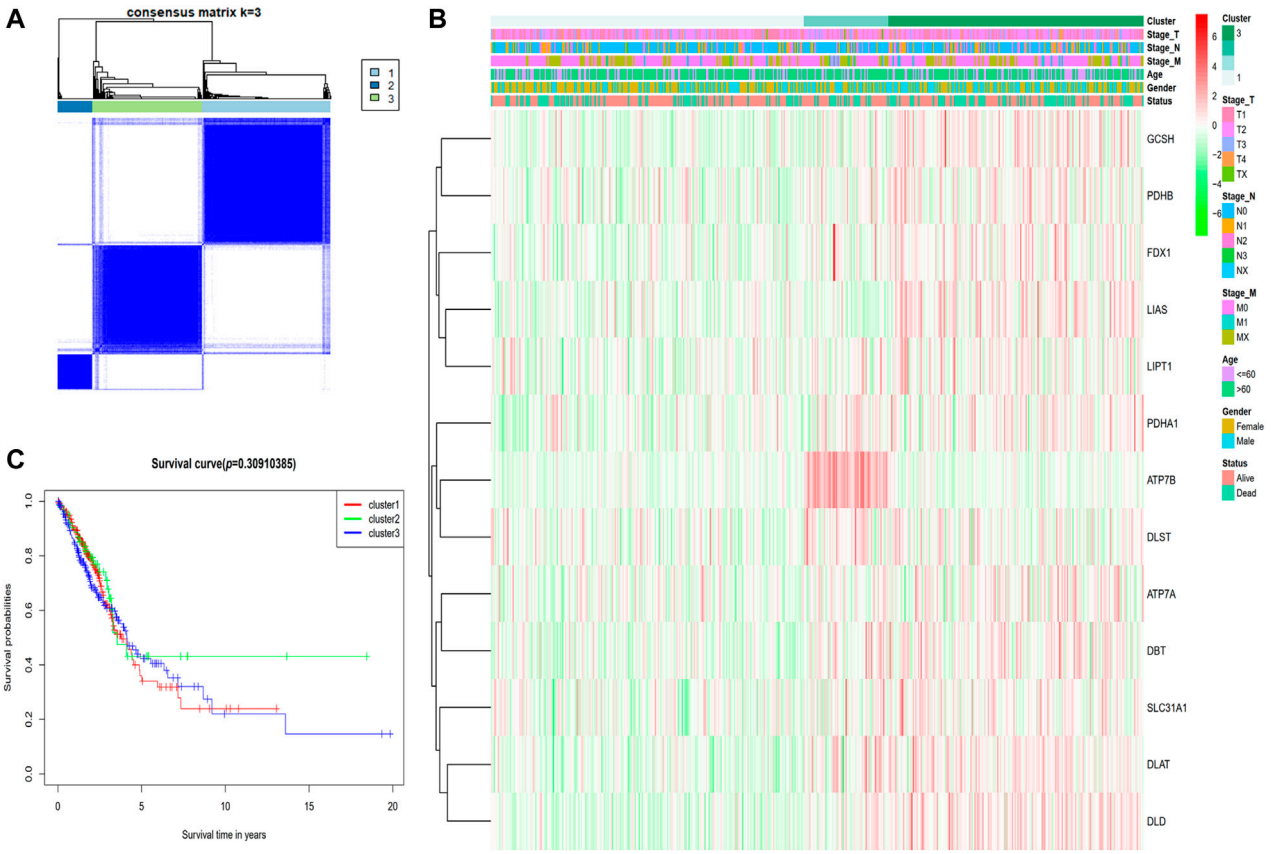

FIGURE 2
Tumor classification premised on the cuproptosis-associated genes. **(A)** Five hundred and twenty-six LUAD tumor samples were classified into three clusters utilizing the consensus clustering matrix (k = 3). **(B)** The heatmap depicting the clinical and pathological parameters of the three cuproptosis-related gene clusters. **(C)** Comparing OS time via KM survival analysis for the three clusters.

patients within the high-risk subgroup (displayed on the right-hand side of the dashed line) relative to those at low risk (Figure 3F). A notable difference (p = 0.0031) in OS duration was discovered between the high- and low-risk groups *via* KM survival analysis (Figure 3G). The prognostic model's specificity and sensitivity were assessed utilizing time-dependent ROC curves. The findings indicated that the area under the ROC curve (AUC) for OS was 0.639, 0.605, and 0.576 for 1-, 2-, and 3-year periods, respectively (Figure 3H).

The risk model's independent prognostic significance

In the TCGA cohort, LUAD patients were classified into two subgroups based on their median risk score. The 482 corresponding patients had complete clinical features including survival status, TNM classification, age, and gender of LUAD patients in low- and high-risk subgroups were examined in combination with the risk score in the regression model. We utilized univariate and multivariate Cox regression analyses to ascertain the possibility of the risk score produced from the gene signature model independently serving as a prognostic factor. The analytical findings from the univariate Cox regression model illustrated that the risk score (HR = 1.5483, 95% CI: 1.973–5.467) independently functions as a predictive factor for unfavorable survival in the TCGA cohort (Figure 4A). Furthermore, after adjusting for possible confounders in the multivariate analysis, the risk score (HR = 1.5014, 95% CI: 1.1042–2.0414), stage T (HR = 1.3345, 95% CI: 1.1170–1.5943) and stage N (HR = 1.3046, 95% CI: 1.1283–1.5086) were found to be prognostic indicators for LUAD patients in TCGA cohort (Figure 4B). As an additional output of our analysis, we established a heatmap of clinical parameters for the TCGA dataset (Figure 4C), and the findings illustrated that the survival duration, stage T, and stage N were diversely distributed between the low- and high-risk subgroups.

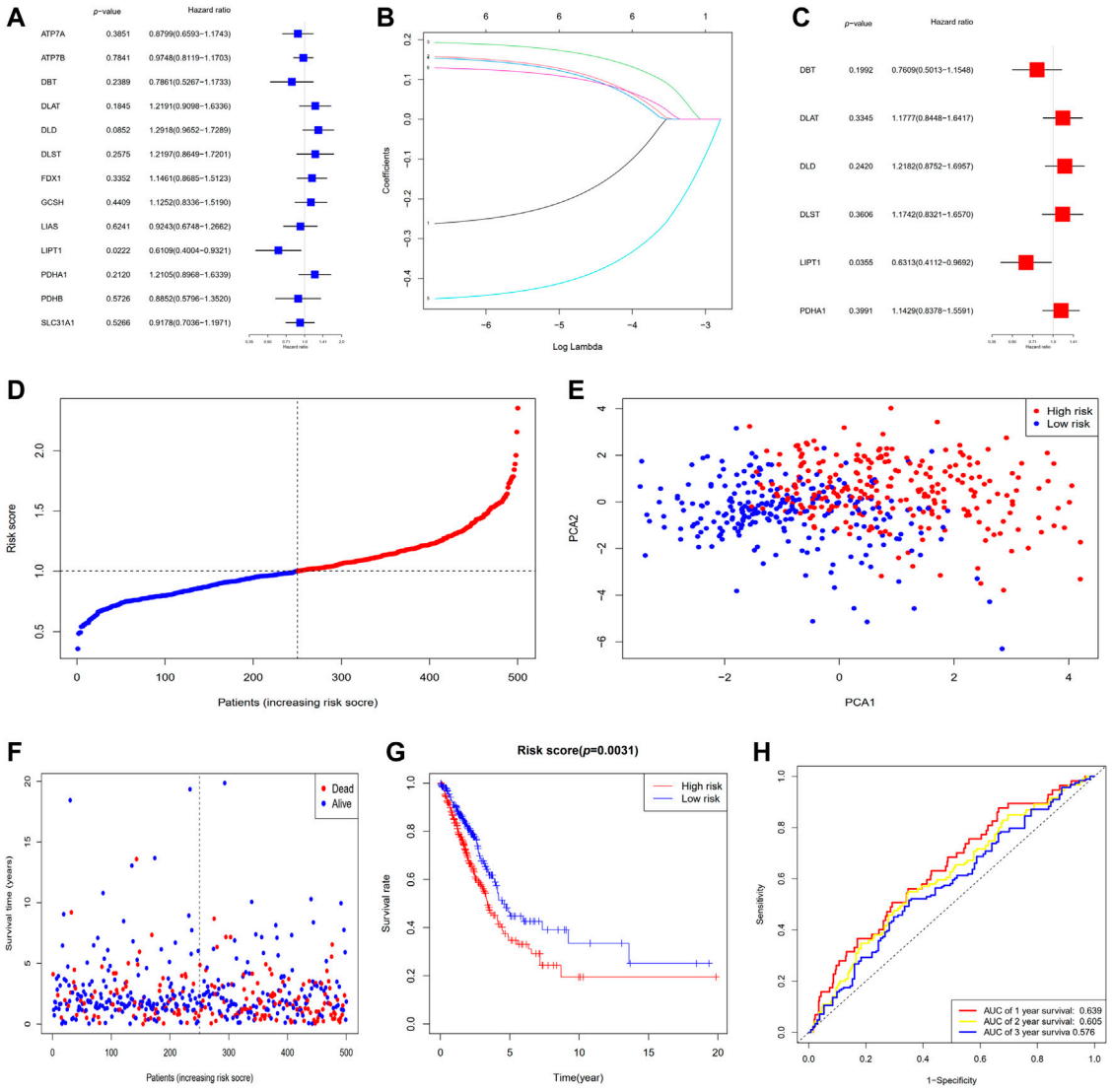

FIGURE 3
The establishment of a risk signature for the TCGA dataset. **(A)** OS analysis utilizing univariate Cox regression for each of the 6 cuproptosis-associated genes with $p < 0.3$. **(B)** LASSO regression analysis of the six genes associated with OS. **(C)** Analysis of OS utilizing multivariate Cox regression for the six genes associated with OS. **(D)** Patients are classified according to their risk scores. **(E)** PCA plot for patients with LUAD depending on their risk scores. **(F)** Each patient's survival probability (low- and high-risk groups are displayed on the left and right sides of the dotted line, respectively). **(G)** KM survival study of patients classified as having high or low risks. **(H)** ROC curves proved the risk score's predictive effectiveness. AUC, area under the ROC curve.

Gene ontology functional analysis premised on the risk model

To additionally examine the difference in the functions of genes between the groups classified by the risk model, we employed the R function "limma" to obtain the DEGs premised on the cutoff values of adjusted $p < 0.05$ and $|\log2FC| > 0.5$. Then, 1292 DEGs were detected between high- and low-risk subgroups in the TCGA dataset. 233 of them were upmodulated in the high-risk group, whereas the remaining 1,059 were downmodulated (Supplementary Table S1). Following that, a GO functional enrichment analysis was carried out using these DEGs. The function enrichment analysis of the GO BP illustrated a considerable enrichment of DEGs in cilium movement, cilium or flagellum-dependent cell motility, cilium-dependent cell motility, microtubule-based movement, cilium movement involved in cell motility and other processes. Analysis of the GO CC illustrated a

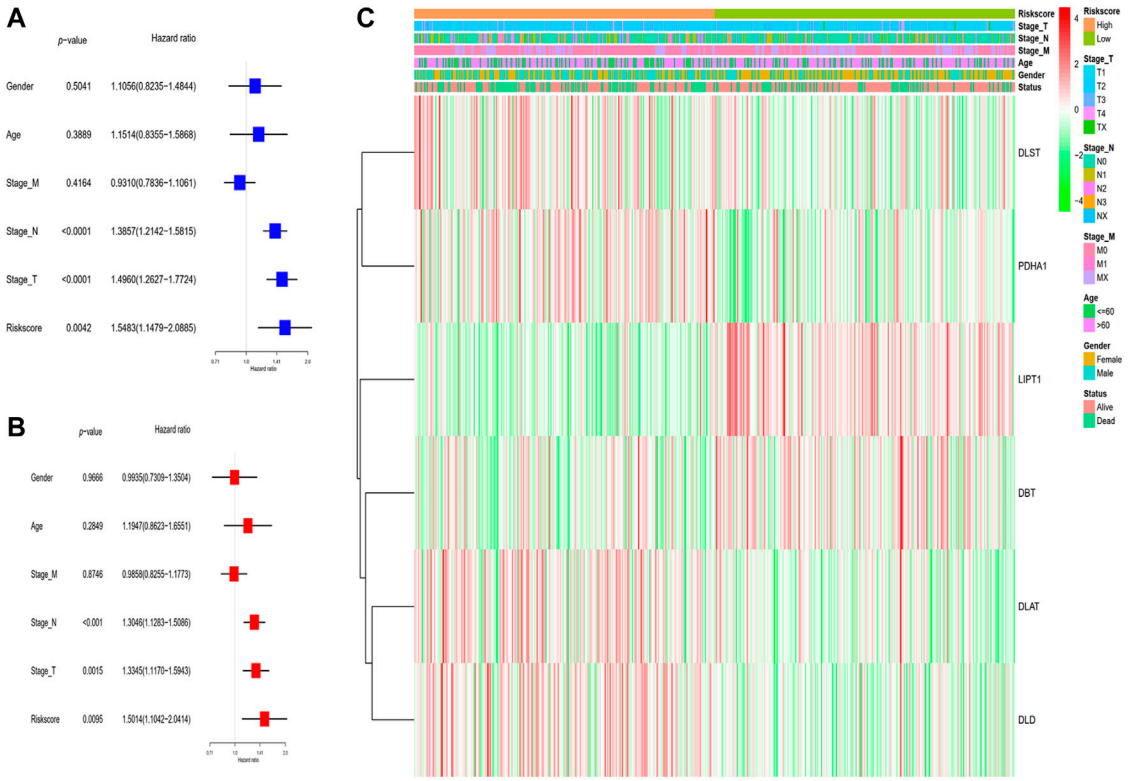

FIGURE 4
Analyses of the risk score utilizing univariate and multivariate Cox regression. **(A)** The TCGA dataset was subjected to a univariate analysis. **(B)** The TCGA cohort was subjected to a multivariate analysis. **(C)** Heatmap depicting the associations between clinical and pathological parameters and risk groups.

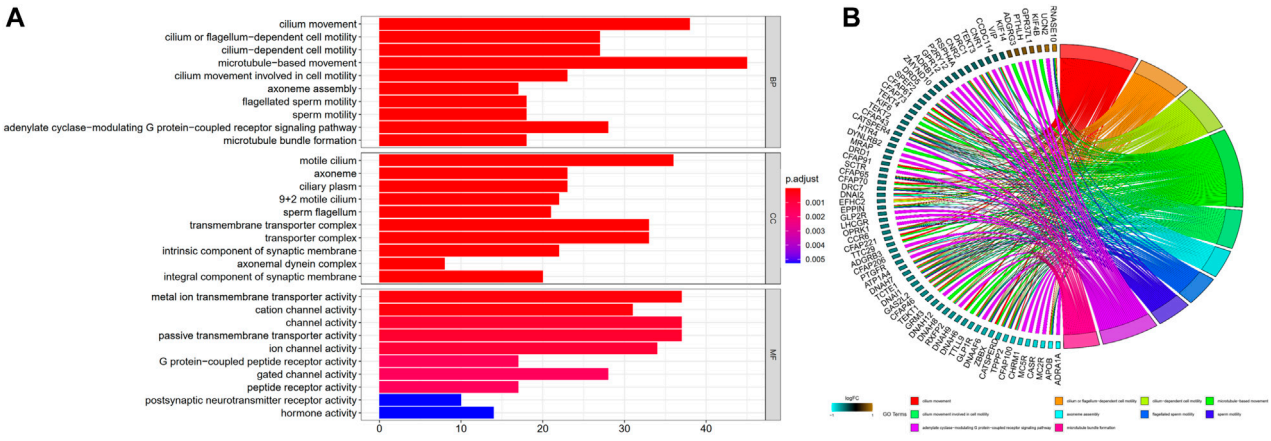

FIGURE 5
GO functional enrichments. **(A)** The top 10 GO functional enrichments included BP, CC, and MF. The smaller the adjusted *p*, the more significant the enrichment. **(B)** GO BP chord plot. GO terms represent the top 10 GO BP functional enrichments, and gene names with the connection represent their enriched genes. BP, biological process; CC, cellular component; MF, molecular function.

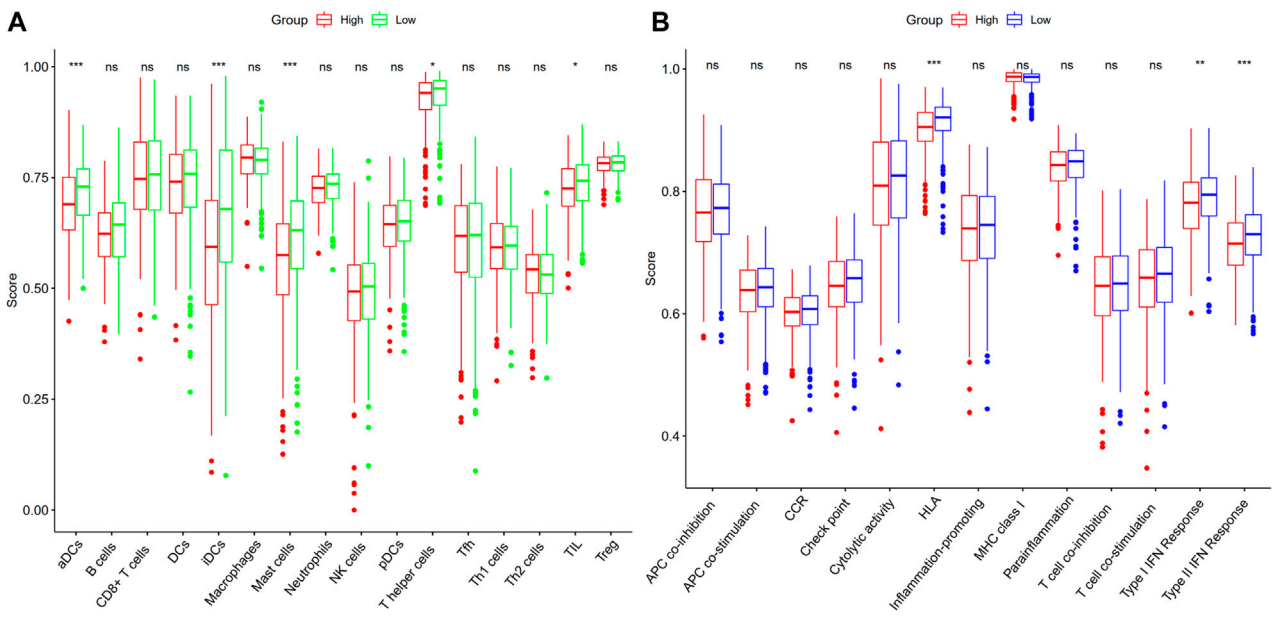

FIGURE 6
ssGSEA score comparison for immune cells and immune pathways. **(A)** Comparison of the enrichment values of 16 different kinds of immune cells in the TCGA dataset between patients at high (red box) and low risks (green box). **(B)** Patients in the high-risk (red box) and low-risk (blue box) groups in the TCGA cohort were compared on the basis of the enrichment values of 13 distinct immune-associated pathways. iDCs, immature dendritic cells; aDCs, activated dendritic cells; TIL, tumor-infiltrating lymphocyte; DCs, dendritic cells; IFN, interferon; NK cells, natural killer cells; MHC, major histocompatibility complex; Th1 cells, type 1 T helper cells; Tfh, T follicular helper cell; Th2 cells, type 2 T helper cells; APC, antigen processing cell; Treg, regulatory T cell; HLA, human leukocyte antigen; CCR, cytokine-cytokine receptor; pDCs, plasmacytoid dendritic cells; ns, not significant; *$p < 0.05$; **$p < 0.01$; ***$p < 0.001$.

substantial enrichment of DEGs in the motile cilium, axoneme, ciliary plasm, 9 + 2 motile cilium, sperm flagellum, and other components. The analysis of GO MF demonstrated a considerable enrichment of DEGs in metal ion transmembrane transporter activity, cation channel activity, channel activity, passive transmembrane transporter activity, ion channel activity, and other functions (Supplementary Table S2). The topmost 10 GO functional enrichments ordered by adjusted *p* are depicted in Figure 5A. The top 10 GO BP functional enrichments with their enriched genes are shown as GO chord plots (Figure 5B).

Assessment of the immune activity across the groups

With the help of the ssGSEA, we were able to additionally evaluate the enrichment scores for 16 distinct kinds of immune cells and the functioning of 13 immune-associated pathways between the high- and low-risk subgroups in the TCGA dataset. In the TCGA cohort, we ascertained that the high-risk subgroup exhibited reduced infiltrating levels of immune cells including T helper cells, immature dendritic cells (iDCs), mast cells, activated dendritic cells (aDCs), and tumor-infiltrating lymphocytes (TILs) in contrast with the low-risk subgroup (Figure 6A). Within the TCGA cohort, three immunological pathways were shown to be less active in the high-risk subgroup as opposed to the low-risk subgroup, including the human leukocyte antigen (HLA), type I interferon (IFN) response, and type II IFN response (Figure 6B).

Discussion

In this work, we initially evaluated the mRNA levels of 13 presently recognized cuproptosis-associated genes in LUAD and normal specimens and discovered a differential expression among several of them. There were interactions and correlations among these genes. Nonetheless, the three clusters generated from the consensus clustering assessment premised on the cuproptosis-related genes, on the other hand, did not exhibit any evident significant differences in clinical parameters or OS time. We conducted univariate and LASSO Cox regression analyses on these cuproptosis-associated genes in order to test their prognostic significance further. We then created a 6-gene risk signature using the results of this investigation. After that, a risk score was established, and the patients were categorized into two subgroups: low-risk and high-risk subgroups. Cox regression

analyses, both univariate and multivariate, were employed to establish if the risk score resulting from the gene signature model independently served as a prognostic indicator. In accordance with the functional analyses, the DEGs that distinguished the low-risk patients from the high-risk ones were linked to cilium-related function. The infiltration of immune cells and the activation of signaling pathways in the low- and high-risk subgroups were also examined. We discovered reduced infiltrating levels of immune cells in the high-risk subgroup, including aDCs, iDCs, T helper cells, mast cells, and TILs, as opposed to the low-risk subgroup. HLA, type I IFN response and type II IFN response showed lower activity in the high-risk in contrast with the low-risk subgroup.

In recent years, PCD was identified as having a dual role in the genesis of tumors and therapeutic processes. As a result of the abundant supply of inflammatory mediators generated by PCD, normal cells are activated, ultimately resulting in their transition into cancer cells. The enhancement of tumor cell PCD, on the other hand, may provide a novel treatment target (Lu et al., 2017; Karki and Kanneganti, 2019; Xia et al., 2019; Al et al., 2021; Koren and Fuchs, 2021). Cell death performs an instrumental function in the origin and treatment of cancer, while several studies have established tumor prognostic models associated with cell death (Cai et al., 2021; Fu et al., 2021; Shao et al., 2021; Zhao et al., 2021).

Cuproptosis, copper-dependent cell death presented by a recent article, as a novel form of PCD (Tsvetkov et al., 2022). Copper is a double-edged sword as it is required as an enzyme cofactor, but it may also be poisonous at even modest intracellular levels, leading to cell death (Ge et al., 2022). As a consequence of cuproptosis, which targets lipoylated TCA cycle proteins, lipoylated protein aggregation and consequent iron-sulfur cluster protein depletion occurs, resulting in proteotoxic stress and eventually inducing the death of cells. These new results may also invigorate studies exploring the use of copper to treat cancer (Kahlson and Dixon, 2022; Tsvetkov et al., 2022). At present, the relevant mechanism research of cuproptosis and tumors should be further deepened. Nonetheless, it may be necessary to first investigate how cuproptosis-associated genes interact with one another and if they are linked to the survival time of patients with LUAD.

Our research established a signature consisting of six cuproptosis-related genes (DBT, DLAT, DLD, DLST, LIPT1, and PDHA1) and discovered that it might anticipate OS among LUAD patients using this signature. Mutation of zebrafish DBT could result in motor dysfunction (Friedrich et al., 2012). DLAT is related to liver cancer metabolism and autophagy with chemotherapeutic resistance (Huang et al., 2019). In patients with head and neck cancer, DLD has been shown to modulate cystine deprivation-mediated ferroptosis (Shin et al., 2020). DLD inhibition could have resulted in lower levels of TCA cycle downstream metabolites, and downmodulation of DLD promoted autophagy in melanoma cells, as well as inhibiting tumor growth and proliferation *in vivo* (Yumnam et al., 2021). The metabolic heterogeneity in TCA cycle utilization amongst triple-negative breast cancer patients is dictated by DLST reliance (Shen et al., 2021). Germline DLST variants promote epigenetic modifications in pheochromocytoma-paraganglioma (Buffet et al., 2021). LIPT1 plays an important role in metabolic regulation (Stowe et al., 2018; Ni et al., 2019). PDHA1 gene deletion in prostate cancer cells causes metabolic remodeling, with the cells becoming more glutamine-reliant (Li et al., 2016). When PDHA1 is downmodulated in breast cancer, the oncoprotein hepatitis B X-interacting protein may help to drive glucose metabolic remodeling (Liu et al., 2015). These genes have some association with the origin and treatment of cancer. However, these genes in the prognostic model, that are cuproptosis promoters or executors should be further studied. Although not all of these promoters and executors were linked to an improved prognosis among patients with LUAD in our analysis, none was linked to a dismal prognosis. It is yet uncertain how these genes interact with one another during cuproptosis, and additional research is warranted.

Cuproptosis has not been thoroughly investigated up to today. A variety of PCD strategies might coexist and interface with one another as tumors grow and progress (Fritsch et al., 2019). For instance, among the 6 cuproptosis-related genes, DLAT is associated with autophagy (Xu et al., 2020); DLD is also known as key regulator ferroptosis (Lu et al., 2017; Park et al., 2018); PDHA1 is closely related to apoptosis (Kwak et al., 2020; Jin et al., 2021). It has been shown that the PCD-related gene correlated with the prognosis of tumor patients, whose mechanism is related to immune cell infiltration (Hong et al., 2021; Ye et al., 2021). Thus, cuproptosis-related genes are certainly associated with other PCD, with the possibility that some genes are involved in multiple ways of PCD. Furthermore, it is possible that low levels of antitumor immunity are responsible for the unfavorable survival results in high-risk patients. They may have an intact cell plasma membrane with no release of contents, which would induce indirect inflammatory reactions, or they could have the opposite properties (Galluzzi et al., 2018; Khan et al., 2021). So, we also performed the immune infiltration enrichment analyses. We found that the infiltration levels of aDCs, iDCs, mast cells, T helper cells and TILs, type I IFN, and type II IFN responses showed lower activity in the high-risk group as opposed to the low-risk group, indicating that the high-risk patients may experience immune system dysfunction. However, no differences were identified between the levels of other main anti-tumor infiltrating immune cells between the two groups. Unlike other PCD, immune infiltration might perform a smaller function in cuproptosis-related genes correlated with the prognosis of LUAD patients, and other deep mechanisms may be involved.

We assessed the DEGs between distinct risk groups and discovered that the DEGs were predominantly implicated in cilium related function, such as movement based on

microtubules, cilium movement, flagellum or cilium-dependent cell motility, cell motility that is mediated by the cilium, cell motility mediated by cilium movement, motile cilium, 9 + 2 motile cilium, and so on. Outside the cell surface, the main cilium is an antenna-like structure that extends beyond the cell membrane. Cilium performs a crucial function in the modulation of cell-signaling transduction, which has an impact on the capacity of cells to proliferate, differentiate, and migrate. Ciliary impairments result in ciliopathies, and ciliary dysregulation performs a critical function in the genesis and progression of cancer. Some cancer cells may undergo growth suppression by restoring the cilia (Wang et al., 2021). Oncogenic signaling pathways, as well as certain specific anticancer treatments, may either stimulate or suppress ciliation. Interactions between the genomic profiles of tumor cells, medication therapy, and ciliary signaling in the tumor microenvironment are expected to have an impact on tumor progression and responsiveness to treatment (Liu et al., 2018). Ciliary disintegration abnormalities are generally linked to the genesis of tumors. The identification of modulators of ciliary disassembly and mitosis is critical in the search for targeted therapies for cancers that are related to these modulators (Doornbos and Roepman, 2021). Ciliogenesis and Hedgehog signaling are suppressed downstream of KRAS all through acinar-ductal metaplasia in mice, which might be employed as a method to limit the progression of early lesions and, therefore, the advancement to pancreatic ductal adenocarcinoma (Bangs et al., 2020). At present, there are still few studies on cilium and tumors, and cilium has the potential to participate in the development of tumors together with cuproptosis, thus affecting the prognosis. The specific mechanisms deserve further investigation.

Cuproptosis is a topic that has received little recent attention, particularly in terms of its mechanisms in LUAD. Our research developed a gene signature associated with cuproptosis. Using these cuproptosis-related genes, we were able to conduct a preliminary analysis of their predictive significance and establish a theoretical foundation for further investigation. We established $p < 0.3$ as the cut-off value to avoid missing important genes and identified 6 genes associated with survival for subsequent evaluation. Therefore, further accurate verification and large sample size verification should be studied in the future. The absence of data, however, prevented us from concluding if these genes also perform similar roles in various cuproptosis pathways in LUAD, and this is an issue that warrants additional investigation.

Conclusion

In summary, our research indicated that cuproptosis is strongly linked to LUAD since the expression levels of most cuproptosis-associated genes differed between normal and LUAD specimens. Furthermore, the score derived from our risk signature, which was on the basis of six cuproptosis-associated genes, was shown to independently serve as a risk indicated for anticipating LUAD outcomes in the TCGA cohort. The DEGs that distinguished the low-risk patients from the high-risk ones were linked to the cilium. LUAD patients' prognoses may now be predicted using a unique gene signature identified in this work. This discovery also offers a substantial foundation for future research into the links between cuproptosis-associated genes and cilium in LUAD patients.

Data availability statement

The data could be download from UCSC Xena (http://xena.ucsc.edu), some data generated or analyzed during this study are included in the article/Supplementary Material, further inquiries can be directed to the corresponding authors.

Author contributions

HZ, YZ, WJ, and JQ performed study concept and design, revised the manuscript. HZ, YS, QY, and YZ analyzed data and wrote the manuscript. YS, CW, QX, and WJ analyzed data, interpretated results and helped to write the manuscript. All authors approved the final manuscript.

Funding

This work was supported by the Grants from the Wuxi Health Commission's Scientific Research Project (M202154 to YZ and T202130 to WJ).

Acknowledgments

We would like to acknowledge TCGA, the GDC and UCSC Xena for providing data. We would like to acknowledge the web database platforms and software programs used for data analysis.

Conflict of interest

The authors declare that the research was conducted in the absence of any commercial or financial relationships that could be construed as a potential conflict of interest.

Publisher's note

All claims expressed in this article are solely those of the authors and do not necessarily represent those of

their affiliated organizations, or those of the publisher, the editors and the reviewers. Any product that may be evaluated in this article, or claim that may be made by its manufacturer, is not guaranteed or endorsed by the publisher.

Supplementary material

The Supplementary Material for this article can be found online at: https://www.frontiersin.org/articles/10.3389/fgene.2022.975185/full#supplementary-material

References

Ahmed, A., and Tait, S. (2020). Targeting immunogenic cell death in cancer. *Mol. Oncol.* 14 (12), 2994–3006. doi:10.1002/1878-0261.12851

Al, M. A., Mimi, A. A., Aziz, M. A., Zaeem, M., Ahmed, T., Munir, F., et al. (2021). Role of pyroptosis in cancer and its therapeutic regulation. *Eur. J. Pharmacol.* 910, 174444. doi:10.1016/j.ejphar.2021.174444

Ali, A., Goffin, J. R., Arnold, A., and Ellis, P. M. (2013). Survival of patients with non-small-cell lung cancer after a diagnosis of brain metastases. *Curr. Oncol.* 20 (4), e300. doi:10.3747/co.20.1481

Bangs, F. K., Miller, P., and O'Neill, E. (2020). Ciliogenesis and Hedgehog signalling are suppressed downstream of KRAS during acinar-ductal metaplasia in mouse. *Dis. Model. Mech.* 13 (7), dmm044289. doi:10.1242/dmm.044289

Barta, J. A., Powell, C. A., and Wisnivesky, J. P. (2019). Global epidemiology of lung cancer. *Ann. Glob. Health* 85 (1), 8. doi:10.5334/aogh.2419

Buffet, A., Zhang, J., Rebel, H., Corssmit, E., Jansen, J. C., Hensen, E. F., et al. (2021). Germline DLST variants promote epigenetic modifications in pheochromocytoma-paraganglioma. *J. Clin. Endocrinol. Metab.* 106 (2), 459–471. doi:10.1210/clinem/dgaa819

Cai, H. J., Zhuang, Z. C., Wu, Y., Zhang, Y. Y., Liu, X., Zhuang, J. F., et al. (2021). Development and validation of a ferroptosis-related lncRNAs prognosis signature in colon cancer. *Bosn. J. Basic Med. Sci.* 21 (5), 569–576. doi:10.17305/bjbms.2020.5617

Chen, C., Chen, S., Hu, X., Wang, J., Wen, T., Fu, J., et al. (2020). Effects of autophagy-associated genes on the prognosis for lung adenocarcinoma. *Transl. Cancer Res.* 9 (3), 1947–1959. doi:10.21037/tcr.2020.02.07

Chin, L., Hahn, W. C., Getz, G., and Meyerson, M. (2011). Making sense of cancer genomic data. *Genes Dev.* 25 (6), 534–555. doi:10.1101/gad.2017311

Doornbos, C., and Roepman, R. (2021). Moonlighting of mitotic regulators in cilium disassembly. *Cell. Mol. Life Sci.* 78 (11), 4955–4972. doi:10.1007/s00018-021-03827-5

Engebretsen, S., and Bohlin, J. (2019). Statistical predictions with glmnet. *Clin. Epigenetics.* 11 (1), 123. doi:10.1186/s13148-019-0730-1

Friedrich, T., Lambert, A. M., Masino, M. A., and Downes, G. B. (2012). Mutation of zebrafish dihydrolipoamide branched-chain transacylase E2 results in motor dysfunction and models maple syrup urine disease. *Dis. Model. Mech.* 5 (2), 248–258. doi:10.1242/dmm.008383

Fritsch, M., Gunther, S. D., Schwarzer, R., Albert, M. C., Schorn, F., Werthenbach, J. P., et al. (2019). Caspase-8 is the molecular switch for apoptosis, necroptosis and pyroptosis. *Nature* 575 (7784), 683–687. doi:10.1038/s41586-019-1770-6

Fu, D., Zhang, B., Wu, S., Zhang, Y., Xie, J., Ning, W., et al. (2021). Prognosis and characterization of immune microenvironment in acute myeloid leukemia through identification of an autophagy-related signature. *Front. Immunol.* 12, 695865. doi:10.3389/fimmu.2021.695865

Galluzzi, L., Vitale, I., Aaronson, S. A., Abrams, J. M., Adam, D., Agostinis, P., et al. (2018). Molecular mechanisms of cell death: recommendations of the nomenclature committee on cell death 2018. *Cell Death Differ.* 25 (3), 486–541. doi:10.1038/s41418-017-0012-4

Garg, A. D., and Agostinis, P. (2017). Cell death and immunity in cancer: from danger signals to mimicry of pathogen defense responses. *Immunol. Rev.* 280 (1), 126–148. doi:10.1111/imr.12574

Ge, E. J., Bush, A. I., Casini, A., Cobine, P. A., Cross, J. R., and Denicola, G. M. (2022). Connecting copper and cancer: from transition metal signalling to metalloplasia. *Nat. Rev. Cancer.* 22 (2), 102–113. doi:10.1038/s41568-021-00417-2

Goldman, M. J., Craft, B., Hastie, M., Repecka, K., Mcdade, F., Kamath, A., et al. (2020). Visualizing and interpreting cancer genomics data via the Xena platform. *Nat. Biotechnol.* 38 (6), 675–678. doi:10.1038/s41587-020-0546-8

Grossman, R. L., Heath, A. P., Ferretti, V., Varmus, H. E., Lowy, D. R., Kibbe, W. A., et al. (2016). Toward a shared vision for cancer genomic data. *N. Engl. J. Med.* 375 (12), 1109–1112. doi:10.1056/NEJMp1607591

Hanzelmann, S., Castelo, R., and Guinney, J. (2013). Gsva: gene set variation analysis for microarray and RNA-seq data. *BMC Bioinforma.* 14, 7. doi:10.1186/1471-2105-14-7

Hong, Y., Lin, M., Ou, D., Huang, Z., and Shen, P. (2021). A novel ferroptosis-related 12-gene signature predicts clinical prognosis and reveals immune relevancy in clear cell renal cell carcinoma. *BMC Cancer* 21 (1), 831. doi:10.1186/s12885-021-08559-0

Huang, X., Gan, G., Wang, X., Xu, T., and Xie, W. (2019). The HGF-MET axis coordinates liver cancer metabolism and autophagy for chemotherapeutic resistance. *Autophagy* 15 (7), 1258–1279. doi:10.1080/15548627.2019.1580105

Jin, L., Cho, M., Kim, B. S., Han, J. H., Park, S., Lee, I. K., et al. (2021). Drug evaluation based on phosphomimetic PDHA1 reveals the complexity of activity-related cell death in A549 non-small cell lung cancer cells. *BMB Rep.* 54 (11), 563–568. doi:10.5483/bmbrep.2021.54.11.101

Kahlson, M. A., and Dixon, S. J. (2022). Copper-induced cell death. *Science* 375 (6586), 1231–1232. doi:10.1126/science.abo3959

Karki, R., and Kanneganti, T. D. (2019). Diverging inflammasome signals in tumorigenesis and potential targeting. *Nat. Rev. Cancer.* 19 (4), 197–214. doi:10.1038/s41568-019-0123-y

Khan, I., Yousif, A., Chesnokov, M., Hong, L., and Chefetz, I. (2021). A decade of cell death studies: breathing new life into necroptosis. *Pharmacol. Ther.* 220, 107717. doi:10.1016/j.pharmthera.2020.107717

Koren, E., and Fuchs, Y. (2021). Modes of regulated cell death in cancer. *Cancer Discov.* 11 (2), 245–265. doi:10.1158/2159-8290.CD-20-0789

Kwak, C. H., Jin, L., Han, J. H., Han, C. W., Kim, E., Cho, M., et al. (2020). Ilimaquinone induces the apoptotic cell death of cancer cells by reducing pyruvate dehydrogenase kinase 1 activity. *Int. J. Mol. Sci.* 21 (17), E6021. doi:10.3390/ijms21176021

Li, Y., Li, X., Li, X., Zhong, Y., Ji, Y., Yu, D., et al. (2016). PDHA1 gene knockout in prostate cancer cells results in metabolic reprogramming towards greater glutamine dependence. *Oncotarget* 7 (33), 53837–53852. doi:10.18632/oncotarget.10782

Lin, W., Chen, Y., Wu, B., Chen, Y., and Li, Z. (2021). Identification of the pyroptosisrelated prognostic gene signature and the associated regulation axis in lung adenocarcinoma. *Cell Death Discov.* 7 (1), 161. doi:10.1038/s41420-021-00557-2

Liu, F., Zhang, W., You, X., Liu, Y., Li, Y., Wang, Z., et al. (2015). The oncoprotein HBXIP promotes glucose metabolism reprogramming via downregulating SCO2 and PDHA1 in breast cancer. *Oncotarget* 6 (29), 27199–27213. doi:10.18632/oncotarget.4508

Liu, H., Kiseleva, A. A., and Golemis, E. A. (2018). Ciliary signalling in cancer. *Nat. Rev. Cancer.* 18 (8), 511–524. doi:10.1038/s41568-018-0023-6

Lu, B., Chen, X. B., Ying, M. D., He, Q. J., Cao, J., Yang, B., et al. (2017). The role of ferroptosis in cancer development and treatment response. *Front. Pharmacol.* 8, 992. doi:10.3389/fphar.2017.00992

Lu, Y., Luo, X., Wang, Q., Chen, J., Zhang, X., Li, Y., et al. (2022). A novel necroptosis-related lncRNA signature predicts the prognosis of lung adenocarcinoma. *Front. Genet.* 13, 862741. doi:10.3389/fgene.2022.862741

Moujalled, D., Strasser, A., and Liddell, J. R. (2021). Molecular mechanisms of cell death in neurological diseases. *Cell Death Differ.* 28 (7), 2029–2044. doi:10.1038/s41418-021-00814-y

Ni, M., Solmonson, A., Pan, C., Yang, C., Li, D., Notzon, A., et al. (2019). Functional assessment of lipoyltransferase-1 deficiency in cells, mice, and humans. *Cell Rep.* 27 (5), 13761386.e6. doi:10.1016/j.celrep.2019.04.005

Park, S., Oh, J., Kim, M., and Jin, E. J. (2018). Bromelain effectively suppresses Kras-mutant colorectal cancer by stimulating ferroptosis. *Anim. Cells Syst.* 22 (5), 334–340. doi:10.1080/19768354.2018.1512521

Ritchie, M. E., Phipson, B., Wu, D., Hu, Y., Law, C. W., Shi, W., et al. (2015). Limma powers differential expression analyses for RNA-sequencing and microarray studies. *Nucleic Acids Res.* 43 (7), e47. doi:10.1093/nar/gkv007

Shao, W., Yang, Z., Fu, Y., Zheng, L., Liu, F., Chai, L., et al. (2021). The pyroptosis-related signature predicts prognosis and indicates immune microenvironment infiltration in gastric cancer. *Front. Cell Dev. Biol.* 9, 676485. doi:10.3389/fcell.2021.676485

Shao, X., Wang, X., Guo, X., Jiang, K., Ye, T., Chen, J., et al. (2019). STAT3 contributes to oncolytic newcastle disease virus-induced immunogenic cell death in melanoma cells. *Front. Oncol.* 9, 436. doi:10.3389/fonc.2019.00436

Shen, N., Korm, S., Karantanos, T., Li, D., Zhang, X., Ritou, E., et al. (2021). DLST-dependence dictates metabolic heterogeneity in TCA-cycle usage among triple-negative breast cancer. *Commun. Biol.* 4 (1), 1289. doi:10.1038/s42003-021-02805-8

Shin, D., Lee, J., You, J. H., Kim, D., and Roh, J. L. (2020). Dihydrolipoamide dehydrogenase regulates cystine deprivation-induced ferroptosis in head and neck cancer. *Redox Biol.* 30, 101418. doi:10.1016/j.redox.2019.101418

Stowe, R. C., Sun, Q., Elsea, S. H., and Scaglia, F. (2018). LIPT1 deficiency presenting as early infantile epileptic encephalopathy, Leigh disease, and secondary pyruvate dehydrogenase complex deficiency. *Am. J. Med. Genet. A* 176 (5), 1184–1189. doi:10.1002/ajmg.a.38654

Strasser, A., and Vaux, D. L. (2020). Cell death in the origin and treatment of cancer. *Mol. Cell.* 78 (6), 1045–1054. doi:10.1016/j.molcel.2020.05.014

Szklarczyk, D., Gable, A. L., Nastou, K. C., Lyon, D., Kirsch, R., Pyysalo, S., et al. (2021). The STRING database in 2021: customizable protein-protein networks, and functional characterization of user-uploaded gene/measurement sets. *Nucleic Acids Res.* 49 (D1), D605–D612. doi:10.1093/nar/gkaa1074

Tang, R., Xu, J., Zhang, B., Liu, J., Liang, C., Hua, J., et al. (2020). Ferroptosis, necroptosis, and pyroptosis in anticancer immunity. *J. Hematol. Oncol.* 13 (1), 110. doi:10.1186/s13045-020-00946-7

Tibshirani, R. (1997). The lasso method for variable selection in the Cox model. *Stat. Med.* 16 (4), 385–395. doi:10.1002/(sici)1097-0258(19970228)16:4<385::aid-sim380>3.0.co;2-3

Tsvetkov, P., Coy, S., Petrova, B., Dreishpoon, M., Verma, A., Abdusamad, M., et al. (2022). Copper induces cell death by targeting lipoylated TCA cycle proteins. *Science* 375 (6586), 1254–1261. doi:10.1126/science.abf0529

Walter, W., Sanchez-Cabo, F., and Ricote, M. (2015). GOplot: an R package for visually combining expression data with functional analysis. *Bioinformatics* 31 (17), 2912–2914. doi:10.1093/bioinformatics/btv300

Wang, B., Liang, Z., and Liu, P. (2021). Functional aspects of primary cilium in signaling, assembly and microenvironment in cancer. *J. Cell. Physiol.* 236 (5), 3207–3219. doi:10.1002/jcp.30117

Wilkerson, M. D., and Hayes, D. N. (2010). ConsensusClusterPlus: a class discovery tool with confidence assessments and item tracking. *Bioinformatics* 26 (12), 1572–1573. doi:10.1093/bioinformatics/btq170

Wu, T., Hu, E., Xu, S., Chen, M., Guo, P., Dai, Z., et al. (2021). clusterProfiler 4.0: a universal enrichment tool for interpreting omics data. *Innovation.* 2 (3), 100141. doi:10.1016/j.xinn.2021.100141

Xia, X., Wang, X., Cheng, Z., Qin, W., Lei, L., Jiang, J., et al. (2019). The role of pyroptosis in cancer: pro-cancer or pro-"host. *Cell Death Dis.* 10 (9), 650. doi:10.1038/s41419-019-1883-8

Xu, Y., Shen, J., and Ran, Z. (2020). Emerging views of mitophagy in immunity and autoimmune diseases. *Autophagy* 16 (1), 3–17. doi:10.1080/15548627.2019.1603547

Yao, J., Chen, X., Liu, X., Li, R., Zhou, X., Qu, Y., et al. (2021). Characterization of a ferroptosis and iron-metabolism related lncRNA signature in lung adenocarcinoma. *Cancer Cell Int.* 21 (1), 340. doi:10.1186/s12935-021-02027-2

Ye, Y., Dai, Q., and Qi, H. (2021). A novel defined pyroptosis-related gene signature for predicting the prognosis of ovarian cancer. *Cell Death Discov.* 7 (1), 71. doi:10.1038/s41420-021-00451-x

Yu, G., Wang, L. G., Han, Y., and He, Q. Y. (2012). ClusterProfiler: an R package for comparing biological themes among gene clusters. *OMICS* 16 (5), 284–287. doi:10.1089/omi.2011.0118

Yumnam, S., Kang, M. C., Oh, S. H., Kwon, H. C., Kim, J. C., and Jung, E. S. (2021). Downregulation of dihydrolipoyl dehydrogenase by UVA suppresses melanoma progression via triggering oxidative stress and altering energy metabolism. *Free Radic. Biol. Med.* 162, 77–87. doi:10.1016/j.freeradbiomed.2020.11.037

Zhang, X., Lou, Y., Zheng, X., Wang, H., Sun, J., Dong, Q., et al. (2015). Wnt blockers inhibit the proliferation of lung cancer stem cells. *Drug Des. devel. Ther.* 9, 2399–2407. doi:10.2147/DDDT.S76602

Zhao, Z., Liu, H., Zhou, X., Fang, D., Ou, X., Ye, J., et al. (2021). Necroptosis-related lncRNAs: predicting prognosis and the distinction between the cold and hot tumors in gastric cancer. *J. Oncol.* 2021, 6718443. doi:10.1155/2021/6718443

frontiers | Frontiers in Genetics

TYPE Original Research
PUBLISHED 17 August 2022
DOI 10.3389/fgene.2022.953580

OPEN ACCESS

EDITED BY
Qian Wang,
Tai'an City Central Hospital, China

REVIEWED BY
Zhi-jie Zhao,
Shanghai Jiao Tong University, China
Run Jieshi,
Shanghai Jiao Tong University School of Medicine, China

*CORRESPONDENCE
Hongze Jin,
hv8wl3z@163.com

†These authors have contributed equally to this work

SPECIALTY SECTION
This article was submitted to Cancer Genetics and Oncogenomics, a section of the journal Frontiers in Genetics

RECEIVED 26 May 2022
ACCEPTED 25 July 2022
PUBLISHED 17 August 2022

CITATION
Wang W, Liu W, Xu J and Jin H (2022), MiR-33a targets FOSL1 and EN2 as a clinical prognostic marker for sarcopenia by glioma.
Front. Genet. 13:953580.
doi: 10.3389/fgene.2022.953580

MiR-33a targets FOSL1 and EN2 as a clinical prognostic marker for sarcopenia by glioma

Wei Wang†, Wei Liu†, Jing Xu and Hongze Jin*

Department of Neurosurgery, Changxing People's Hospital, Changxing, Zhejiang, China

To determine the relationship between glioma and muscle aging and to predict prognosis by screening for co-expressed genes, this study examined the relationship between glioma and sarcopenia. The study identified eight co-downregulated miRNAs, three co-upregulated miRNAs, and seven genes associated with overall glioma survival, namely, KRAS, IFNB1, ALCAM, ERBB2, STAT3, FOSL1, and EN2. With a multi-factor Cox regression model incorporating FOSL1 and EN2, we obtained ROC curves of 0.702 and 0.709, respectively, suggesting that glioma prognosis can be predicted by FOSL1 and EN2, which are differentially expressed in both cancer and aged muscle. FOSL1 and EN2 were analyzed using Gene Set Enrichment Analysis to identify possible functional pathways. RT-qPCR and a dual-luciferase reporter gene system verified that hsa-miR-33a targets FOSL1 and EN2. We found that hsa-mir-33a co-targeting FOSL1 and EN2 has a good predictive value for glioblastoma and skeletal muscle reduction.

KEYWORDS

FOSL1, EN2, mir-33a, glioma, sarcopenia, muscle, systemic homeostasis-related genes

Introduction

Gliomas are the most common primary tumors of the central nervous system (CNS), arising from glial cells or supporting cells (Davis, 2018; Ostrom et al., 2018). The World Health Organization updated their classification system for gliomas in May 2016, taking advantage of advances in molecular genetics and epigenetic research. The revised guidelines aim to allow oncologists to better diagnose, predict treatment outcomes, and improve individualized treatment plans for patients (Louis et al., 2016; Wesseling and Capper, 2018). About 49% of malignant tumors of the CNS are gliomas, which can be found anywhere in the CNS but are most frequently in the frontal and temporal lobes (Schmoldt et al., 1975; Aldape et al., 2015; Ostrom et al., 2018; Miller et al., 2021). Early symptoms of glioma, similar to other benign neurological disorders, include headache, vomiting, loss of vision, seizures, weakness, confusion, and other signs of increased intracranial pressure (Rasmussen et al., 2017; Ozawa et al., 2019). The most common treatment for glioma is surgical resection followed by radiotherapy and chemotherapy (Wen et al., 2020). However, the blood–brain barrier prevents most drugs from reaching the tumor site, so even with combination therapy, the overall survival rate of patients with gliomas is still low (Stummer et al., 2012; Kim et al., 2019; Tan et al., 2020; Miller et al.,

2021). Therefore, for early diagnosis and risk assessment of glioma, transcriptomic and epigenomic screening of neuroblastoma-related biomarkers is critical to facilitate early targeted interventions to improve survival.

Sarcopenia is an age-related syndrome of progressive decline in skeletal muscle mass and function, associated with adverse outcomes such as decreased body function, impaired quality of life, physical disability, and death (Cruz-Jentoft et al., 2019). In patients with chronic diseases, malnutrition, and malignancies, sarcopenia is associated with poor prognosis, increasing the risk of recurrence and death (Xia et al., 2020; Williams et al., 2021). Previous studies suggested that sarcopenia and loss of temporal muscle thickness may be associated with lower overall survival (OS) in glioma patients (An et al., 2021; Guven et al., 2021; Huq et al., 2021). There are, however, relatively few studies investigating the association between glioma prognosis and sarcopenia expression profiles.

Typically, sarcopenia is characterized by muscle aging and loss of function and mass in the elderly (Larsson et al., 2019). Muscle loss and sarcopenia are regulated by microRNAs (miRNAs) (Wang et al., 2020; Javanmardifard et al., 2021). MicroRNAs) are endogenous, small RNAs that have a variety of regulatory functions in living organisms (Sun et al., 2017; Chen et al., 2019; Hill and Tran, 2021; Chen et al., 2022). Glioma miRNAs are known to be potential diagnostic markers (Zhou et al., 2018). In previous studies, miRNAs were differentially expressed in the skeletal muscles of elderly people (Larsson et al., 2019). MiRNA-1245a, for instance, has been identified as a potential key molecule for treating glioma-related sarcopenia (An and Wang, 2021). The regulation of miRNAs in the skeletal muscle is influenced by systemic homeostasis (Kim et al., 2020; Podkalicka et al., 2022). The development of sarcopenia and poor outcome for glioma patients are likely to occur as a result of gliomas deteriorating the body's microenvironmental homeostasis (Magnus et al., 2014; Chen and Kang, 2015). Gliomas may cause sarcopenia by affecting miRNA expression in skeletal muscle.

This study examined miRNAs associated with glioma and sarcopenia and their potentially regulated mRNAs. We screened for co-expressed genes to determine the relationship between glioma and sarcopenia and predict prognosis.

Methods

Data collection and processing

The Gene Expression Omnibus (GEO) database provided glioma-derived exosome miRNA transcript datasets (GSE122488), which included 16 standard samples and 22 glioma samples. The miRNAs that did not appear in more than 10 samples were removed. Additionally, 17 old Basal samples and 19 young Basal samples were obtained from skeletal muscle-derived miRNA transcript datasets (GSE23527). For 143 glioma samples, transcriptomic FPKM expression data were obtained from the UCSC Xena website (https://xenabrowser.net/). Expression data were transformed into $\log_2$ (x+1) when multiple probes corresponded to the same gene.

Differential expression analysis

GSE122488 and GSE23527 datasets were screened for differentially expressed miRNAs associated with GBM and aging, respectively. Differentially expressed miRNAs were those with *p*-values less than 0.05. Differentially expressed miRNA volcanoes were mapped using the ggplot2 package (Version 3.3.5) and the ggrepel package (Version 0.9.1), and differentially expressed miRNA heatmaps were mapped using the pheatmap package (Version 1.0.12).

MiRNA target gene prediction and regulatory network mapping

The miRTarBase database contains a large number of experimentally validated miRNA target gene regulatory pairs, ensuring the reliability of the data (Huang et al., 2019). Based on miRTarBase, co-differentially expressed miRNA target genes were examined, and pairs with at least two validated results in Western blot, qPCR, or CLIPseq were retained. Cytoscape (Version 3.8.0) was used to map the miRNA-target regulatory network.

Gene Ontology and Kyoto Encyclopedia of Genes and Genomes enrichment analyses

For all target genes, the clusterProfiler (Version 4.0.5) package and org. Hs.eg.db (Version 3.13.0) package were used to perform GO and KEGG enrichment analyses, retaining all enriched entries with FDR <0.05 as in previous research studies (Fabris et al., 2020; Huang et al., 2021; Li et al., 2022a; Zhang et al., 2022a; Zhang et al., 2022b; Wang et al., 2022).

Survival risk prediction model

Training (70%, $n = 100$) and validation (30%, $n = 43$) sets of The Cancer Genome Atlas (TCGA) glioblastoma dataset were randomly divided. Based on the training set samples, a survival risk prediction model was constructed and its performance was then validated using the validation set. To identify the miRNA targets associated with overall survival, a univariate Cox proportional risk regression analysis was conducted on all

target genes of common differential miRNAs. The Least absolute shrinkage and selection operator (LASSO) Cox model in the glmnet package (Version 4.1-3) was further used to screen genes with one-way Cox $p < 0.05$ and multicollinearity between the genes was removed. The gene screened by the LASSO regression analysis was then used to construct a multifactorial Cox proportional risk regression model based on the survival package (version 3.2-13) and the survminer package (version 0.4.9). The risk score for each patient was calculated by entering the expression values of the characteristic genes screened by multifactorial Cox regression analysis into the formula. Patients in the training set were segregated into low- and high-risk groups, the relationship between risk score levels was analyzed, and Kaplan–Meier curves were used for prognosis. In addition, the survivalROC (Version 1.0.3) package was used to evaluate the time-dependent subject operating characteristic curve (ROC) of the prediction model over multiple years.

Gene set enrichment analysis

TCGA-glioma samples were classified into high-expression and low-expression groups by median gene expression values for the signature genes screened. The Gene Set Enrichment Analysis (GSEA) was performed on the Kyoto Encyclopedia of Genes and Genomes (KEGG) pathway using the clusterProfiler package (Version 4.0.5), with the nPermSimple parameter set to 10,000.

Cell cultivation

The human glioma cell lines U251 and 293T cells were purchased from the Institute of Cell Research, Chinese Academy of Sciences, Shanghai, and cultured in a constant humidity incubator with 5% CO2 in DMEM+10% FBS+1% double-antibody.

RNA extraction and real-time quantitative PCR

The total RNA was extracted using Trizol (Beyotime, Shanghai, China) according to the instructions and reverse-transcribed into cDNA using the GoScript ™ Reverse Transcription Kit (Promega, Wisconsin, United States), followed by TB Green Premix Ex Taq (Takara, Japan) to determine the mRNA expression levels. The mRNA expression levels were calculated as 2-ΔΔCt, and GAPDH was used as an internal reference.

Dual-luciferase reporter assay

The pmirGLO-FOSL1-3′ UTR-WT and pmirGLO-EN2-3′ UTR-WT vector plasmids were synthesized by Shanghai Biotech, and the corresponding pmirGLO-FOSL1-3′ UTR-MUT and pmirGLO-EN2-3′ UTR-MUT were used as controls. A total of 500 ng of vector plasmid and 100 pmol of hsa-miR-33a mimics were transfected into 293 T cells, and the fluorescence was detected by using a Dual-Luciferase Assay Kit from Promega (United States) after 24 h.

Statistical analysis

All data from at least three independent experiments are expressed as mean ± standard deviation. A *t*-test was used to analyze the statistical differences between two independent samples. $p < 0.05$ was considered to be statistically significant.

Results

Differentially expressed miRNAs in glioma and muscle

The GSE122488 dataset was screened using differential expression analysis to identify 105 downregulated miRNAs and 62 upregulated miRNAs in glioma (Figure 1A). Aged muscle GSE23527 was also screened for 40 downregulated and 15 upregulated miRNAs (Figure 1B). Furthermore, we obtained eight co-downregulated miRNAs (hsa-miR-512, hsa-miR-660, hsa-miR-1304, hsa-miR-30d, hsa-miR-33a, hsa-miR-337, hsa-miR-1277, and hsa-miR-758) and three co-upregulated miRNAs (hsa-miR-25, hsa-let-7b, and hsa-miR-215) (Figures 1C,D). Different subgroups of the samples displayed different expression patterns of differentially expressed miRNAs, as demonstrated by the expression heatmap (Figures 1E,F). The development of glioma with muscle aging may be closely related to those miRNAs.

Analysis of common differential miRNA target genes and their functional enrichment

To identify co-differentially expressed miRNAs, we used the miRTarBase database to predict the target genes and screened for miRNA-gene pairs with at least two validation records in a reporter assay, Western blot, qPCR, and CLIPseq. The results showed that miR-1277 and miR-1304 had no target genes; miR-758 and miR512 both had two target genes; miR-660 had one target gene; miR-337 had three target genes; miR-215 had eight target genes; miR-30d had 11 target genes; miR-25 had 18 target genes; miR-33a had 21 target genes; and let-7b had 32 target genes (Figure 2A). The miRNA–target interaction network showed that HMGA2, IRS2, CASP3, TP53, EZH2, and SMAD7 were regulated by two miRNAs, and there was no

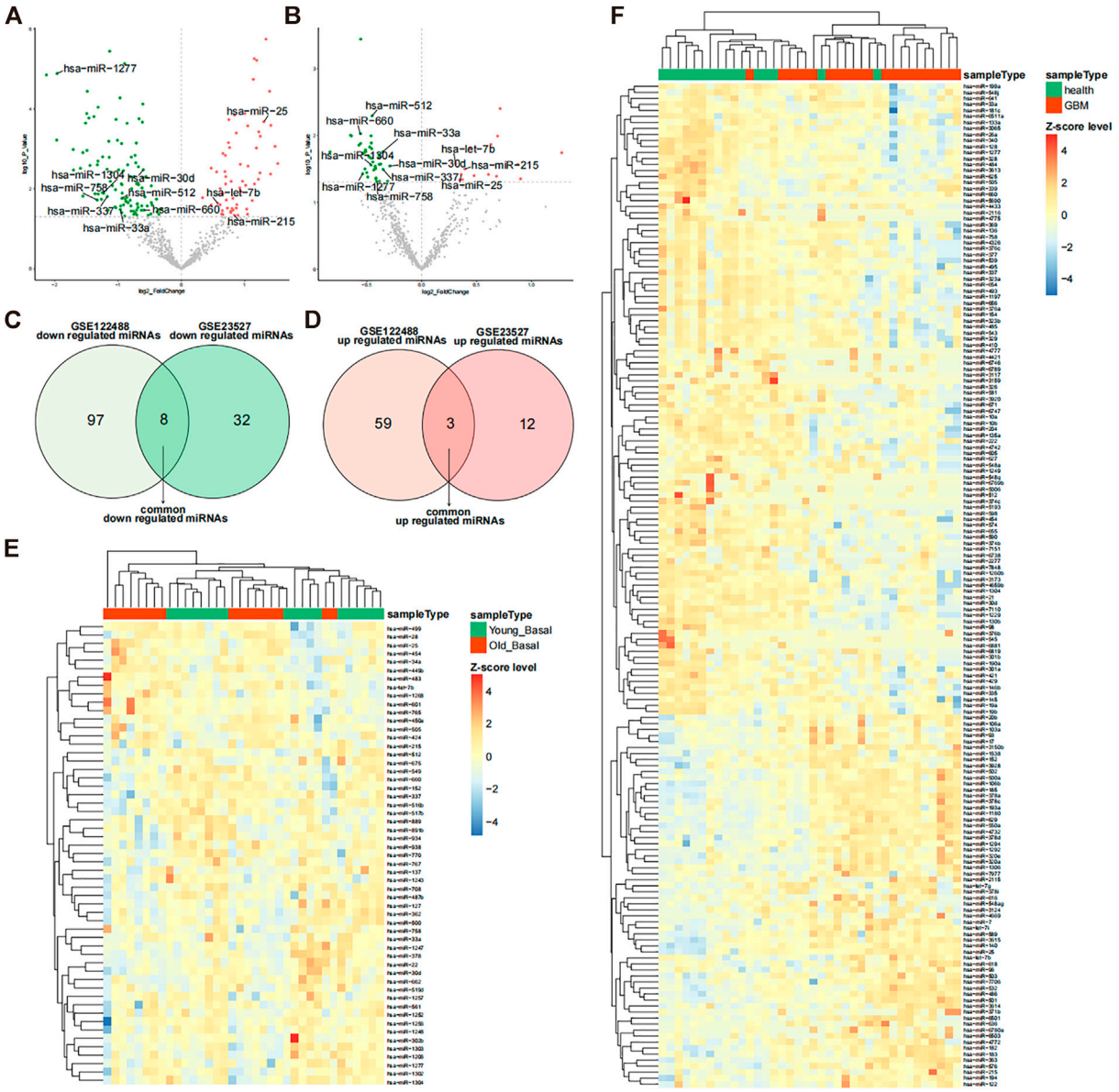

FIGURE 1
Differentially expressed miRNAs in glioma and muscle. **(A)** Volcano plot of differentially expressed miRNAs in the GSE122488 dataset. Green dots indicate downregulated miRNAs and red dots indicate upregulated differential miRNAs. Common differential miRNAs of both datasets are marked on the plot. **(B)** Volcano plot of differentially expressed miRNAs in the GSE23527 dataset (glioma vs. healthy). Green dots indicate downregulated miRNAs and red dots indicate upregulated differential miRNAs. Common differential miRNAs of both datasets are marked on the plot. **(C,D)** Venn diagram of differential downregulated and upregulated miRNAs in the two datasets. **(E)** Expression heatmap of differentially expressed miRNAs in the GSE23527 dataset. MiRNA expression values were Z-score transformed. **(F)** Expression heatmap of differentially expressed miRNAs in the GSE122488 dataset; miRNA expression values were transformed by the Z-score.

common target gene between most of the miRNAs (Figure 2A). To further investigate the biological processes affected by these differential miRNAs (hsa-let7b, hsa-miR-25, hsa-miR-30d, hsa-miR-33a, hsa-miR-337, hsa-miR-512, hsa-miR-660, and hsa-miR-758), GO and KEGG enrichment analyses were performed for all common differential miRNAs, involving 1,173 GO pathways (including 1083 BP, 12 CC, and 78 MF) and 35 KEGG pathways. The enrichment results indicated that these miRNAs might be involved in the cell cycle, gene transcription, and cancer-related pathways (Figures 2B,C). Accordingly, these miRNAs may play an essential role in cancer development by targeting specific mRNAs.

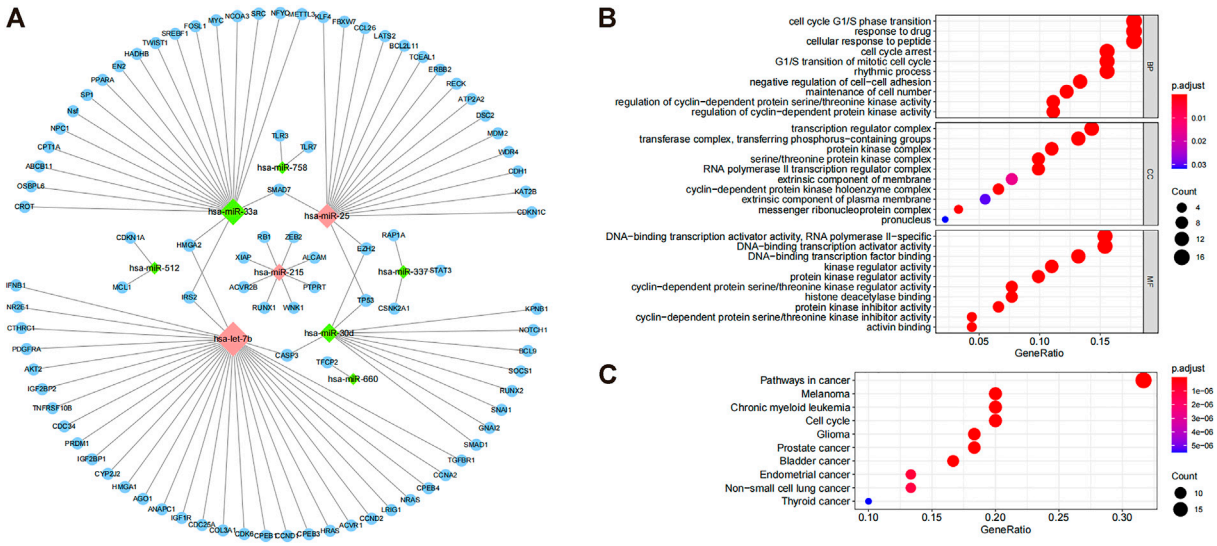

FIGURE 2
Target gene prediction of common differential miRNAs and their functional enrichment analysis. **(A)** Differential regulation of miRNAs. The diamond-shaped dots indicate miRNAs. Green and red dots indicate downregulation and upregulation, respectively, and blue dots indicate miRNA regulatory targets. **(B)** GO enrichment results of miRNA target genes, highlighting the top 10 GO terms of BP, CC, and MF. **(C)** KEGG enrichment results of miRNA target genes show the top 10 enrichment pathways.

Prognostic value of miRNA target genes

TCGA training set samples were used to construct a model of glioma-related survival risk prediction. KRAS, IFNB1, ALCAM, ERBB2, STAT3, FOSL1, and EN2 were screened by univariate Cox proportional risk regression (Figure 3A). ALCAM was a protective factor for patient survival, whereas the others were risk factors. The Cox regression analysis revealed an association between high IFNB1 expression and poor prognosis. We then used LASSO Cox regression to further remove the multicollinearity between genes, and LASSO regression did not reject any genes (Figure 3C). Finally, we obtained a convergent patient survival risk regression model using multifactorial Cox proportional risk regression and stepwise regression with two characteristic genes, FOSL1 (hazard ratio, 1.357; 95% CI, 1.077 to 1.711; p = 0.010), and EN2 (hazard ratio, 1.415; 95% CI, 1.090 to 1.837; p = 0.009) (Figure 3E). The formula for predicting the survival risk is risk score = (FOSL1 expression × 0.3056) + (EN2 expression × 0.3471). FOSL1 and EN2 may affect the prognosis of gliomas independently. The Kaplan–Meier survival analysis was used to compare the survival differences between the high- and low-risk groups based on the median values of the risk scores of the training set samples. The high-risk group's prognosis was worse than the low-risk group's (p = 0.011) (Figure 3D). Therefore, the multifactorial Cox model developed by FOSL1 and EN2 can better predict glioma prognoses.

Prognostic model construction for glioma

Based on the prediction model, we constructed a nomogram (Figure 4A) and plotted the calibration curves for the model predicting overall survival at 1 and 2 years (Figures 4C,D). To evaluate the model's predictive performance, we plotted time-dependent ROC curves. AUCs for the training sets 1, 2, 3, 4, and 5 years were 0.678, 0.748, 0.881, 0.979, and 0.957, respectively (Figure 4B). These results suggest that this nomogram model has good predictive power.

Nomogram prediction model evaluation

We calculated the survival scores of the validation set samples and compared the survival differences between the high-risk and low-risk groups to further validate the performance of the survival risk prediction model. The high-risk group had a poor prognosis in the validation set (Figure 5A). Additionally, we plotted time-dependent ROC curves of the risk model to predict overall survival at 1 and 2 years for the validation set samples with AUC values of 0.702 and 0.709, respectively (Figure 5B). To investigate whether FOSL1 and EN2 are independent prognostic factors, we divided all TCGA-glioma samples into high- and low-expression groups based on median gene expression values. The Kaplan–Meier survival analysis was then used to compare the survival differences between the high- and low-expression groups. The results showed that both the

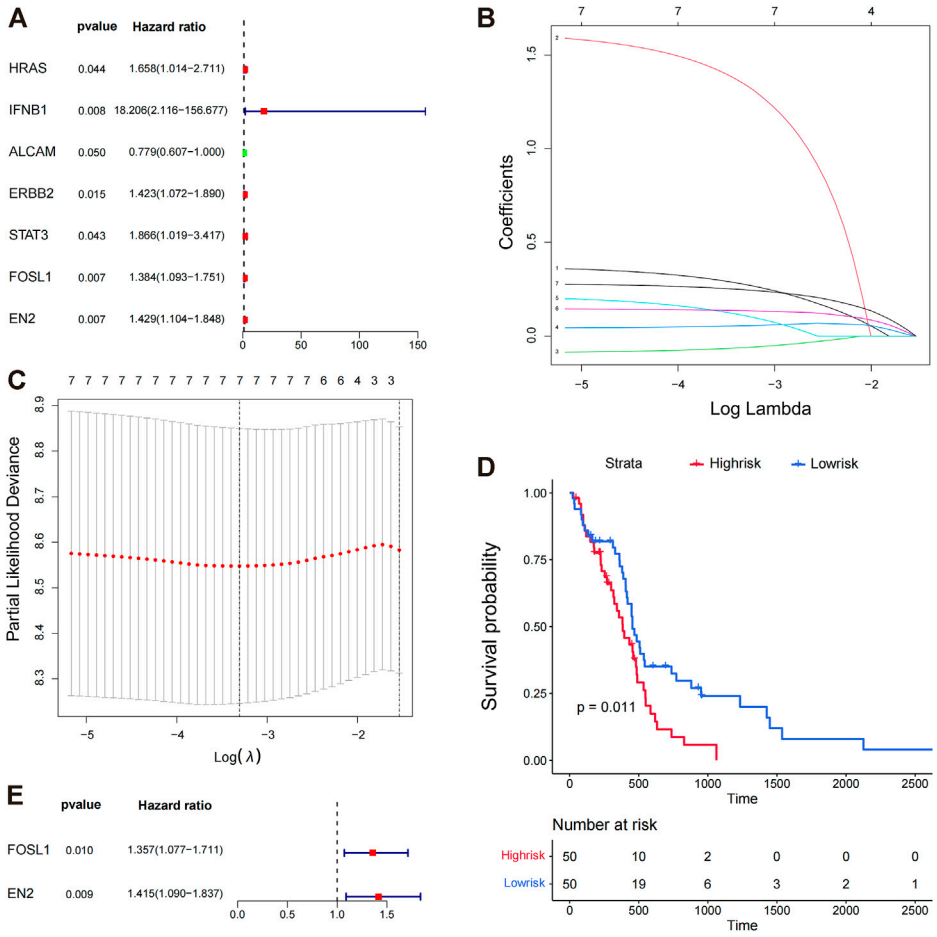

FIGURE 3
Prognostic value of miRNA target genes. **(A)** Genes targeted by significant miRNAs were analyzed by univariate Cox proportional risk regression. **(B,C)** Lasso regression analysis was conducted on the seven target genes screened by univariate Cox proportional risk regression analysis, and the seven best genes were screened again by Lasso regression. **(D)** K–M plots show the survival differences between high- and low-risk groups in the training set samples. **(E)** Survival risk regression model was constructed using multi-factor Cox proportional risk regression and stepwise regression, and two genes were retained, FOSL1 and EN2.

high-expression groups of FOSL1 and EN2 had poor prognosis (Figures 6A,B).

Gene expression analysis of prognostic models

In comparing high- and low-expression groups of FOSL1 and EN2, we examined the functional pathways involved with these proteins. FOSL1-related GSEA analysis significantly enriched 23 KEGG pathways, including 22 activated pathways (NES >0), such as leukocyte transendothelial migration, VEGF signaling pathway, and apoptotic cell death. FOSL1-associated top five pathways were plotted using GSEA (Figure 6C). Based on the EN2-related GSEA analysis, only two functional pathways were enriched, proteasome and ribosome (Figure 6D).

Hsa-miR-33a targets and regulates the expression of *FOSL1* and EN2

FOSL1 and EN2, which are target mRNAs of hsa-miR-33a, can be used to predict the prognosis of glioma based on the results of the bioinformatics analysis. As risk factors for glioma, both FOSL1 and EN2 can be considered and further verified to be regulated and targeted by hsa-miR-33a. Glioma cell lines were treated with mimics of hsa-miR-33a. As shown in Figures 7A,B RT-qPCR analysis of mimics-treated glioma cell lines showed decreased expression of FOSL1 and EN2. We then used the dual-luciferase reporter gene system to detect the regulation of miRNAs and target genes (Figure 7C,D). The results indicate that miR-33a targets and regulates FOSL1 and EN2. In summary, miR-33a with differential expression in glioma and sarcopenia may affect

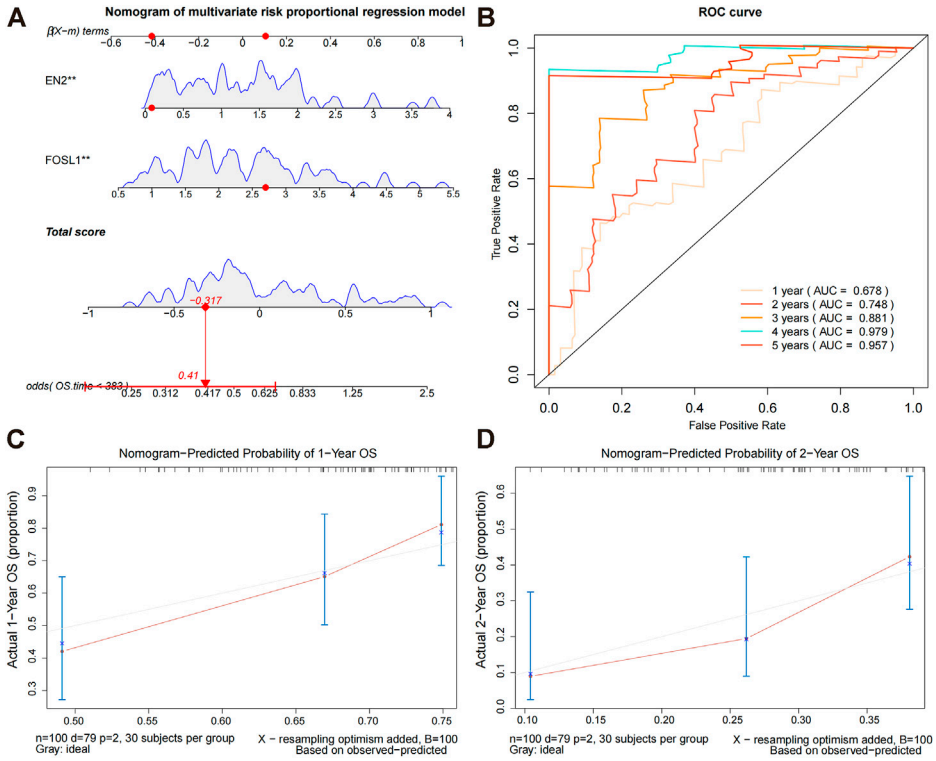

FIGURE 4
Constructing a nomogram prediction model. **(A)** Nomogram prediction model for prognostic risk. **(B)** Time-dependent ROC curves for the overall survival of the training set. During the first, second, third, and fourth years, AUC values were evaluated. **(C,D)** Calibration curves for predicting the overall survival of the training set at 1 and 2 years.

the prognosis of glioma by targeting and regulating FOSL1 and EN2.

Discussion

We identified co-expressed differential miRNA genes in glioma and skeletal muscle miRNA datasets. Target genes were predicted using the miRTarBase database after functional annotation according to GO and KEGG. ROC curves were plotted to evaluate the prognostic value of the aforementioned target genes in glioma. Multivariate Cox regression was used to construct a model of prognosis prediction for glioma. The model was evaluated by plotting ROC curves and K–M curves. This model accurately predicted the prognosis for glioblastoma based on correlation analysis, providing an exciting pathway for clinical applications.

Glioma is the most common type of malignant tumor in the central nervous system, and its pathogenesis is complex, involving genetic background, gene mutation, tumor microenvironment, and other aspects (McKinnon et al., 2021). However, most GBMs have no identifiable risk factors for tumor development. Some rare familial cancer syndromes such as Lynch syndrome, neurofibromatosis type 1, and tuberous sclerosis have increased the risk of developing glioma (Ostrom et al., 2014; Wen et al., 2020). Glioma is characterized by aggressiveness and poor prognosis of the disease. In addition, the early diagnosis of glioblastoma is often tricky due to the lack of specificity of early clinical symptoms and the lack of early diagnostic tools. With the improvement of microsurgery technology, the application of various new radiotherapy techniques, and the introduction of chemotherapy and targeted drugs, the clinical prognosis of glioma has been improved to some extent. However, the overall survival rate of patients is still extremely poor, with a median survival time of only about 1 year, and almost all patients tend to relapse (Jhanwar-Uniyal et al., 2015; Kim et al., 2019). Therefore, developing a validated risk assessment model is essential to guide early clinical diagnosis, prognostic assessment, and individualized treatment.

Sarcopenia is an age-related syndrome of progressive decline in skeletal muscle mass and function, commonly seen in patients with malignancies and associated with poor prognosis in cancer patients (Williams et al., 2021). Several studies have shown that

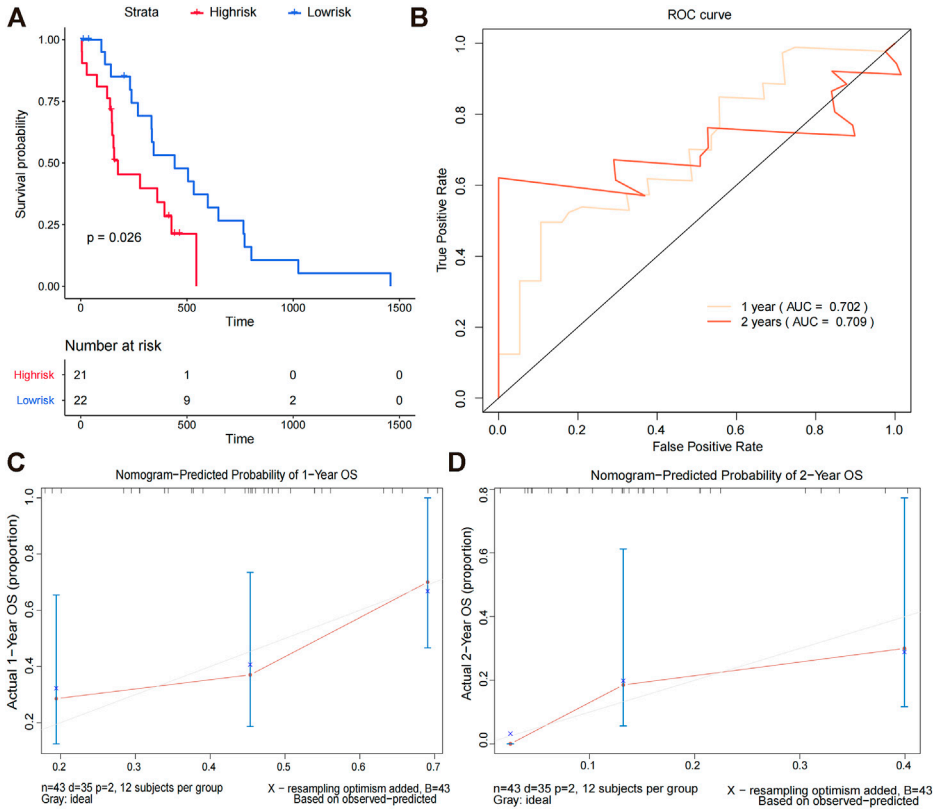

FIGURE 5
Nomogram prediction model evaluation. **(A)** Difference in the overall survival between high-risk and low-risk groups. **(B)**We evaluated the AUC values at 1 and 2 years based on time-dependent ROC curves for the overall survival of the validation set. **(C,D)** Calibration curves for predicting the overall survival in the validation set at 1 and 2 years.

temporalis muscle thickness can be used as a surrogate marker for sarcopenia (Huq et al., 2021). Temporalis muscle thickness was also significantly associated with the expected survival of treated glioma patients with recurrent or concomitant brain metastases (Muglia et al., 2021). Quantifying temporalis muscle thickness has clinical value in the prognostic assessment of glioma (Guven et al., 2021; Mi et al., 2022). This study obtained co-expressed differential miRNA genes by analyzing glioma and skeletal muscle miRNA datasets, followed by multifactorial Cox regression analysis and stepwise regression analysis to obtain a patient survival risk regression model, which included FOSL1 and EN2.

FOSL1 belongs to the Fos gene family and encodes FOS-associated antigen 1 (FRA1), which is involved in forming a transcription factor complex AP-1 (Matsuo et al., 2000). In addition, as a proto-oncogene, FOSL1 also plays a vital role in tumorigenesis and can promote tumor cell metastasis through epithelial–mesenchymal transition (EMT). FOS1 also has prognostic value in various epithelial tumors, and its overexpression is associated with tumor aggressiveness, chemotherapy resistance, tumor progression, and poor survival prognosis (Yu et al., 2013; Gao et al., 2017; Vallejo et al., 2017; Xu et al., 2017; Sobolev et al., 2022). It has been shown that FOSL1 can promote the development and invasion of colorectal cancer through the Smurf1-mediated FBXL2/Wnt/β-catenin axis and the migration, invasion, and proliferation of breast, head, and neck squamous cell carcinoma, pancreatic cancer, bladder cancer, and prostate cancer (Elangovan et al., 2018; Luo et al., 2018; Cui et al., 2020; Dai et al., 2021; Hyakusoku et al., 2021; Liu et al., 2021). In addition, FOSL1 also mediates the dephosphorylation of proliferation and apoptosis bridging protein 15 (PEA15) by upregulating dual-specificity phosphatase 7 (DUSP7), which increases drug resistance in breast cancer (Li et al., 2022b). It is to be noted that FOSL1 was also associated with glioma growth and invasion and was a poor prognostic factor for GBM (Guo et al., 2022). Gliomas overexpress FRA1, which regulates the malignancy of gliomas, including morphology, growth pattern, and tumorigenic potential (Debinski and Gibo, 2005). The engrailed-2 (EN2) gene encodes a transcription factor containing a homology cassette involved in

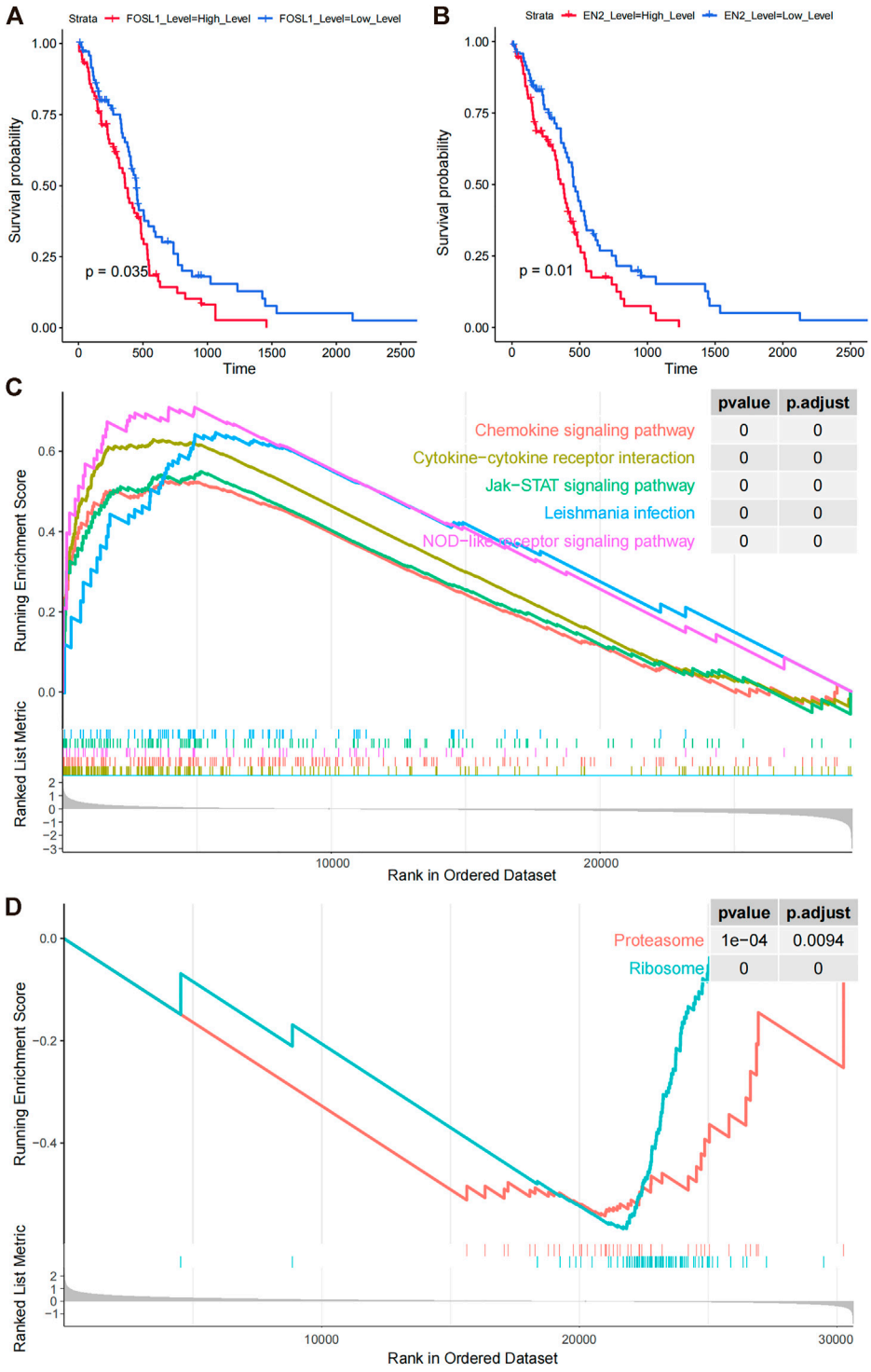

FIGURE 6
Prognostic model signature genes analyzed by GSEA. **(A,B)** Overall survival differences among FOSL1 and EN2 high- and low-expression groups (grouped by median expression values). **(C)** GSEA enrichment of KEGG pathways in FOSL1 high- and low-groups. **(D)** GSEA significantly enriched the KEGG pathway in the high- and low-EN2 expression groups.

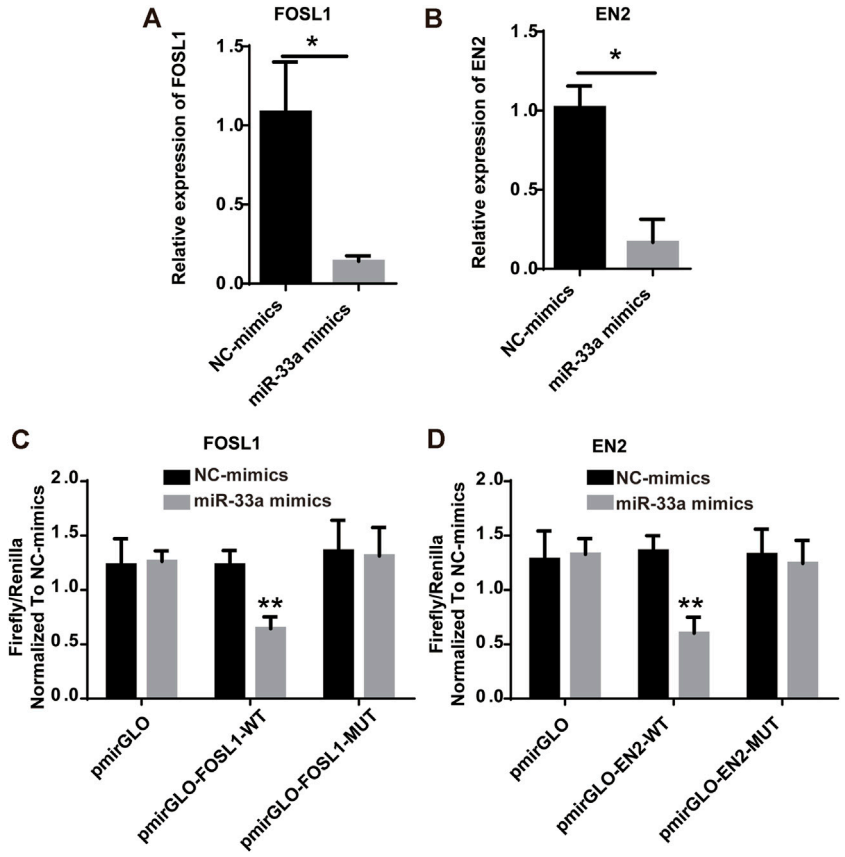

FIGURE 7
Hsa-miR-33a targets and regulates the expression of FOSL1 and EN2. **(A)** RT-qPCR results indicate that FOSL1 expression is lower in miR-33a-treated glioma cell lines than in the control. **(B)** RT-qPCR results indicated that EN2 expression was lower in miR-33a-treated glioma cell lines than in the control. **(C)** Dual-luciferase reporter gene system indicates the targeting relationship between FOSL1 and hsa-miR-33a. **(D)** Dual-luciferase reporter gene system indicates the targeting relationship between EN2 and hsa-miR-33a. *- $p < 0.05$ and **- $p < 0.01$.

regionalization, patterning, and cellular differentiation in early brain development. It plays an essential role during nervous system development. In addition, disorders of EN2 regulation can lead to abnormal cell proliferation, leading to tumorigenesis. Studies show that EN2 plays an important role in the proliferation, migration, and invasion of various tumor cells, including prostate cancer, colorectal cancer, esophageal squamous cell carcinoma, lung cancer, and bladder cancer, and is closely related to the poor prognosis of tumor patients (Zhou et al., 2017; Lin et al., 2018; Cao et al., 2020; Li et al., 2020; Li et al., 2021). EN2 promotes the proliferation and invasion of colorectal cancer cells by regulating CCL20, thus promoting the progression of colorectal cancer. EN2 also promotes the invasion and metastasis of esophageal squamous cell carcinoma by upregulating SPARC expression. It promotes the proliferation, invasion, and metastasis of bladder cancer cells by activating the PI3K/Akt pathway and inhibiting the PTEN gene (Cao et al., 2020; Li et al., 2020) (Li et al., 2021). In addition, it was found that EN2 expression levels are also correlated with the degree of malignancy of gliomas and promoted the malignant progression of glioma (Zeng et al., 2020). These lines of evidence indicate that FOSL1 and EN2, which are involved in our risk assessment model, have prognostic value in various tumors, including glioma.

MiR-33a plays a variety of physiological roles in tumor microenvironments, and it has been proposed as a potential target for cancer prevention and therapy (Gao et al., 2020). By inhibiting phosphorylation of JAK2 and STAT3, which are highly activated in many malignant cells, including glioma cells, miR-33a inhibits the growth, invasion, and EMT of tumor cells (Feng et al., 2016; Chang et al., 2017; Liu et al., 2019a; Liu et al., 2019b). Aside from targeting PDE8A and UVRAG, miR-33a also targets cAMP/PKA and NOTCH signaling pathways in glioma cancer cells (Wang et al., 2014). It is to be noted that both signaling pathways promote self-renewal of glioma-initiating cells only when they are activated simultaneously (Jiang et al., 2019). MiR-33a may exert oncogenic effects by regulating JAK2/STAT3, cAMP/PKA, and NOTCH signaling pathways in gliomas. Further investigation is needed to

determine whether miR-33a overexpression affects glioma cell proliferation, invasion, and other oncogenic features.

In this study, hsa-miR-33a was found to regulate FOSL1 and EN2 and affect the prognosis of gliomas. Furthermore, hsa-miR-33a appeared to be involved in sarcopenia and gliomas. However, a larger sample of data is needed to validate the findings conclusively, and further experimental studies are needed to help understand the specific regulatory mechanisms. Because this study only has data on skeletal muscle age, sarcopenia cannot be fully simulated. Furthermore, miR-33a downregulation caused by glioma and muscle aging may also be caused by sarcopenia, but this remains unclear as we did not investigate which causes miR-33a downregulation.

Conclusion

In conclusion, this study's risk model provides good clinical application and predictive value for assessing the risk and prognosis of glioblastoma and a potential therapeutic target. Moreover, hsa-mir-33a co-targeting FOSL1 and EN2 has a good predictive value for glioma and skeletal muscle reduction.

Data availability statement

The original contributions presented in the study are publicly available. This data can be found here: https://www.ncbi.nlm.nih.gov/geo/ GSE122488; GSE23527.Transcriptomic FPKM expression data was accessed from the UCSC Xena website (https://xenabrowser.net/).

Author contributions

Conceptualization: HJ and WW; methodology: WW and WL; software: WW; validation: WW and JX; writing—original draft preparation: WW, WL, JX, and HJ; writing—review and editing: WW; all authors contributed to the manuscript and approved the submitted version.

Conflict of interest

The authors declare that the research was conducted in the absence of any commercial or financial relationships that could be construed as a potential conflict of interest.

Publisher's note

All claims expressed in this article are solely those of the authors and do not necessarily represent those of their affiliated organizations, or those of the publisher, the editors, and the reviewers. Any product that may be evaluated in this article, or claim that may be made by its manufacturer, is not guaranteed or endorsed by the publisher.

References

Aldape, K., Zadeh, G., Mansouri, S., Reifenberger, G., and von Deimling, A. (2015). Glioblastoma: Pathology, molecular mechanisms and markers. *Acta Neuropathol.* 129, 829–848. doi:10.1007/s00401-015-1432-1

An, G., Ahn, S., Park, J-S., Jeun, S-S., and Hong, Y-K. (2021). Association between temporal muscle thickness and clinical outcomes in patients with newly diagnosed glioblastoma. *J. Cancer Res. Clin. Oncol.* 147, 901–909. doi:10.1007/s00432-020-03386-5

An, L., and Wang, Y. (2021). Potential roles of miRNA-1245a regulatory networks in sarcopenia. *Int. J. Gen. Med.* 14, 6807–6813. doi:10.2147/IJGM.S334501

Cao, Y., Wang, X., Tang, L., Li, Y., Song, X., Liu, X., et al. (2020). Engrailed-2 promotes a malignant phenotype of esophageal squamous cell carcinoma through upregulating the expression of pro-oncogenic genes. *PeerJ* 8, e8662. doi:10.7717/peerj.8662

Chang, M., Qiao, L., Li, B., Wang, J., Zhang, G., Shi, W., et al. (2017). Suppression of SIRT6 by miR-33a facilitates tumor growth of glioma through apoptosis and oxidative stress resistance. *Oncol. Rep.* 38, 1251–1258. doi:10.3892/or.2017.5780

Chen, L., Heikkinen, L., Wang, C., Yang, Y., Sun, H., and Wong, G. (2019). Trends in the development of miRNA bioinformatics tools. *Brief. Bioinform.* 20, 1836–1852. doi:10.1093/bib/bby054

Chen, L., and Kang, C. (2015). miRNA interventions serve as 'magic bullets' in the reversal of glioblastoma hallmarks. *Oncotarget* 6, 38628–38642. doi:10.18632/oncotarget.5926

Chen, Y., Sun, Y., Luo, Z., Lin, J., Qi, B., Kang, X., et al. (2022). Potential mechanism underlying exercise upregulated circulating blood exosome miR-215-5p to prevent necroptosis of neuronal cells and a model for early diagnosis of alzheimer's disease. *Front. Aging Neurosci.* 14, 860364. doi:10.3389/fnagi.2022.860364

Cruz-Jentoft, A. J., Bahat, G., Bauer, J., Boirie, Y., Bruyère, O., Cederholm, T., et al. (2019). Sarcopenia: Revised European consensus on definition and diagnosis. *Age Ageing* 48, 16–31. doi:10.1093/ageing/afy169

Cui, Y-P., Xie, M., Pan, W-X., Zhang, Z-Y., and Li, W-F. (2020). HOXA10 promotes the development of bladder cancer through regulating FOSL1. *Eur. Rev. Med. Pharmacol. Sci.* 24, 2945–2954. doi:10.26355/eurrev_202003_20659

Dai, C., Rennhack, J. P., Arnoff, T. E., Thaker, M., Younger, S. T., Doench, J. G., et al. (2021). SMAD4 represses FOSL1 expression and pancreatic cancer metastatic colonization. *Cell Rep.* 36, 109443. doi:10.1016/j.celrep.2021.109443

Davis, M. E. (2018). Epidemiology and overview of gliomas. *Semin. Oncol. Nurs.* 34, 420–429. doi:10.1016/j.soncn.2018.10.001

Debinski, W., and Gibo, D. M. (2005). Fos-related antigen 1 modulates malignant features of glioma cells. *Mol. Cancer Res.* 3, 237–249. doi:10.1158/1541-7786.MCR-05-0004

Elangovan, I. M., Vaz, M., Tamatam, C. R., Potteti, H. R., Reddy, N. M., and Reddy, S. P. (2018). FOSL1 promotes kras-induced lung cancer through amphiregulin and cell survival gene regulation. *Am. J. Respir. Cell Mol. Biol.* 58, 625–635. doi:10.1165/rcmb.2017-0164OC

Fabris, F., Palmer, D., de Magalhães, J. P., and Freitas, A. A. (2020). Comparing enrichment analysis and machine learning for identifying gene properties that discriminate between gene classes. *Brief. Bioinform.* 21, 803–814. doi:10.1093/bib/bbz028

Feng, J., Yan, P-F., Zhao, H-Y., Zhang, F-C., Zhao, W-H., and Feng, M. (2016). SIRT6 suppresses glioma cell growth via induction of apoptosis, inhibition of oxidative stress and suppression of JAK2/STAT3 signaling pathway activation. *Oncol. Rep.* 35, 1395–1402. doi:10.3892/or.2015.4477

Gao, C., Wei, J., Tang, T., and Huang, Z. (2020). Role of microRNA-33a in malignant cells. *Oncol. Lett.* 20, 2537–2556. doi:10.3892/ol.2020.11835

Gao, X-Q., Ge, Y-S., Shu, Q-H., and Ma, H-X. (2017). Expression of Fra-1 in human hepatocellular carcinoma and its prognostic significance. *Tumour Biol.* 39, 1010428317709635. doi:10.1177/1010428317709635

Guo, S., King, P., Liang, E., Guo, A. A., and Liu, M. (2022). LncRNA HOTAIR sponges miR-301a-3p to promote glioblastoma proliferation and invasion through upregulating FOSL1. *Cell. Signal.* 94, 110306. doi:10.1016/j.cellsig.2022.110306

Guven, D. C., Aksun, M. S., Cakir, I. Y., Kilickap, S., and Kertmen, N. (2021). The association of BMI and sarcopenia with survival in patients with glioblastoma multiforme. *Future Oncol.* 17, 4405–4413. doi:10.2217/fon-2021-0681

Hill, M., and Tran, N. (2021). miRNA interplay: Mechanisms and consequences in cancer. *Dis. Model. Mech.* 14, dmm047662. doi:10.1242/dmm.047662

Huang, H-Y., Lin, Y-C-D., Li, J., Huang, K-Y., Shrestha, S., Hong, H-C., et al. (2019). miRTarBase 2020: updates to the experimentally validated microRNA–target interaction database. *Nucleic Acids Res.* 48, D148–D154. doi:10.1093/nar/gkz896

Huang, J., Liang, X., and Cai, Z. (2021). A potential ceRNA network for neurological damage in preterm infants. *Biomed. Res. Int.* 2021, 2628824. doi:10.1155/2021/2628824

Huq, S., Khalafallah, A. M., Ruiz-Cardozo, M. A., Botros, D., Oliveira, L. A. P., Dux, H., et al. (2021). A novel radiographic marker of sarcopenia with prognostic value in glioblastoma. *Clin. Neurol. Neurosurg.* 207, 106782. doi:10.1016/j.clineuro.2021.106782

Hyakusoku, H., Sawakuma, K., Sano, D., Takahashi, H., Hatano, T., Sato, K., et al. (2021). FosL1 regulates regional metastasis of head and neck squamous cell carcinoma by promoting cell migration, invasion, and proliferation. *Anticancer Res.* 41, 3317–3326. doi:10.21873/anticanres.15119

Javanmardifard, Z., Shahrbanian, S., and Mowla, S. J. (2021). MicroRNAs associated with signaling pathways and exercise adaptation in sarcopenia. *Life Sci.* 285, 119926. doi:10.1016/j.lfs.2021.119926

Jhanwar-Uniyal, M., Labagnara, M., Friedman, M., Kwasnicki, A., and Murali, R. (2015). Glioblastoma: Molecular pathways, stem cells and therapeutic targets. *Cancers* 7, 538–555. doi:10.3390/cancers7020538

Jiang, K., Sun, F., Zhu, J., Luo, G., Ban, Y., and Zhang, P. (2019). *miR-33a* inhibits cell growth in renal cancer by downregulation of MDM4 expression. *Mol. Genet. Genomic Med.* 7, e833. doi:10.1002/mgg3.833

Kim, J., Aydemir, T. B., Jimenez-Rondan, F. R., Ruggiero, C. H., Kim, M-H., and Cousins, R. J. (2020). Deletion of metal transporter Zip14 (Slc39a14) produces skeletal muscle wasting, endotoxemia, Mef2c activation and induction of miR-675 and Hspb7. *Sci. Rep.* 10, 4050. doi:10.1038/s41598-020-61059-2

Kim, J-Y., Jackman, J. G., Woodring, S., McSherry, F., Herndon, J. E., Desjardins, A., et al. (2019). Second primary cancers in long-term survivors of glioblastoma. *Neurooncol. Pract.* 6, 386–391. doi:10.1093/nop/npz001

Larsson, L., Degens, H., Li, M., Salviati, L., Lee, Y., Thompson, W., et al. (2019). Sarcopenia: Aging-Related loss of muscle mass and function. *Physiol. Rev.* 99, 427–511. doi:10.1152/physrev.00061.2017

Li, L., Wang, N., Xiong, Y., Guo, G., Zhu, M., and Gu, Y. (2022). Transcription factor FOSL1 enhances drug resistance of breast cancer through DUSP7-mediated dephosphorylation of PEA15. *Mol. Cancer Res.* 20, 515–526. doi:10.1158/1541-7786.MCR-21-0658

Li, L., Xiao, F., Liu, G., and Chen, Y. (2022). Serum exosomal lncRNA AC007099.1 regulates the expression of neuropeptide-related FAP, as a potential biomarker for hepatocarcinogenesis. *Dis. Markers* 9501008, 1–13. doi:10.1155/2022/9501008

Li, Y., Duan, Q., Gan, L., Li, W., Yang, J., and Huang, G. (2021). microRNA-27b inhibits cell proliferation and invasion in bladder cancer by targeting engrailed-2. *Biosci. Rep.* 41, BSR20201000. doi:10.1042/BSR20201000

Li, Y., Liu, J., Xiao, Q., Tian, R., Zhou, Z., Gan, Y., et al. (2020). EN2 as an oncogene promotes tumor progression via regulating CCL20 in colorectal cancer. *Cell Death Dis.* 11, 604. doi:10.1038/s41419-020-02804-3

Lin, X., Liu, X., and Gong, C. (2018). Expression of engrailed homeobox 2 regulates the proliferation, migration and invasion of non-small cell lung cancer cells. *Oncol. Lett.* 16, 536–542. doi:10.3892/ol.2018.8693

Liu, K., Tian, T., Zheng, Y., Zhou, L., Dai, C., Wang, M., et al. (2019). Scutellarin inhibits proliferation and invasion of hepatocellular carcinoma cells via down-regulation of JAK2/STAT3 pathway. *J. Cell. Mol. Med.* 23, 3040–3044. doi:10.1111/jcmm.14169

Liu, S-C., Huang, C-M., Bamodu, O. A., Lin, C-S., Liu, B-L., Tzeng, Y-M., et al. (2019). Ovatodiolide suppresses nasopharyngeal cancer by targeting stem cell-like population, inducing apoptosis, inhibiting EMT and dysregulating JAK/STAT signaling pathway. *Phytomedicine* 56, 269–278. doi:10.1016/j.phymed.2018.05.007

Liu, Y., Yue, M., and Li, Z. (2021). FOSL1 promotes tumorigenesis in colorectal carcinoma by mediating the FBXL2/Wnt/β-catenin axis via Smurf1. *Pharmacol. Res.* 165, 105405. doi:10.1016/j.phrs.2020.105405

Louis, D. N., Perry, A., Reifenberger, G., von Deimling, A., Figarella-Branger, D., Cavenee, W. K., et al. (2016). The 2016 world health organization classification of tumors of the central nervous system: A summary. *Acta Neuropathol.* 131, 803–820. doi:10.1007/s00401-016-1545-1

Luo, Y-Z., He, P., and Qiu, M-X. (2018). FOSL1 enhances growth and metastasis of human prostate cancer cells through epithelial mesenchymal transition pathway. *Eur. Rev. Med. Pharmacol. Sci.* 22, 8609–8615. doi:10.26355/eurrev_201812_16624

Magnus, N., D'Asti, E., Meehan, B., Garnier, D., and Rak, J. (2014). Oncogenes and the coagulation system – forces that modulate dormant and aggressive states in cancer. *Thromb. Res.* 133, S1–S9. doi:10.1016/S0049-3848(14)50001-1

Matsuo, K., Owens, J. M., Tonko, M., Elliott, C., Chambers, T. J., and Wagner, E. F. (2000). Fosl1 is a transcriptional target of c-Fos during osteoclast differentiation. *Nat. Genet.* 24, 184–187. doi:10.1038/72855

McKinnon, C., Nandhabalan, M., Murray, S. A., and Plaha, P. (2021). Glioblastoma: Clinical presentation, diagnosis, and management. *BMJ* 374, n1560. doi:10.1136/bmj.n1560

Mi, E., Mauricaite, R., Pakzad-Shahabi, L., Chen, J., Ho, A., and Williams, M. (2022). Deep learning-based quantification of temporalis muscle has prognostic value in patients with glioblastoma. *Br. J. Cancer* 126, 196–203. doi:10.1038/s41416-021-01590-9

Miller, K. D., Ostrom, Q. T., Kruchko, C., Patil, N., Tihan, T., Cioffi, G., et al. (2021). Brain and other central nervous system tumor statistics, 2021. *Ca. Cancer J. Clin.* 71, 381–406. doi:10.3322/caac.21693

Muglia, R., Simonelli, M., Pessina, F., Morenghi, E., Navarria, P., Persico, P., et al. (2021). Prognostic relevance of temporal muscle thickness as a marker of sarcopenia in patients with glioblastoma at diagnosis. *Eur. Radiol.* 31, 4079–4086. doi:10.1007/s00330-020-07471-8

Ostrom, Q. T., Bauchet, L., Davis, F. G., Deltour, I., Fisher, J. L., Langer, C. E., et al. (2014). The epidemiology of glioma in adults: A "state of the science" review. *Neuro. Oncol.* 16, 896–913. doi:10.1093/neuonc/nou087

Ostrom, Q. T., Gittleman, H., Truitt, G., Boscia, A., Kruchko, C., and Barnholtz-Sloan, J. S. (2018). *CBTRUS Statistical Report: Primary Brain and Other Central Nervous System Tumors Diagnosed in the United States in 2011–2015*, 20, iv1–iv86. doi:10.1093/neuonc/noy131*Neuro-Oncology*

Ozawa, M., Brennan, P. M., Zienius, K., Kurian, K. M., Hollingworth, W., Weller, D., et al. (2019). The usefulness of symptoms alone or combined for general practitioners in considering the diagnosis of a brain tumour: A case-control study using the clinical practice research database (CPRD) (2000-2014). *BMJ Open* 9, e029686. doi:10.1136/bmjopen-2019-029686

Podkalicka, P., Mucha, O., Kaziród, K., Szade, K., Stępniewski, J., Ivanishchuk, L., et al. (2022). miR-378 affects metabolic disturbances in the mdx model of Duchenne muscular dystrophy. *Sci. Rep.* 12, 3945. doi:10.1038/s41598-022-07868-z

Rasmussen, B. K., Hansen, S., Laursen, R. J., Kosteljanetz, M., Schultz, H., Nørgård, B. M., et al. (2017). Epidemiology of glioma: Clinical characteristics, symptoms, and predictors of glioma patients grade I–iv in the the Danish neuro-oncology registry. *J. Neurooncol.* 135, 571–579. doi:10.1007/s11060-017-2607-5

Schmoldt, A., Benthe, H. F., and Haberland, G. (1975). Digitoxin metabolism by rat liver microsomes. *Biochem. Pharmacol.* 24, 1639–1641. doi:10.1016/0006-2952(75)90094-5

Sobolev, V. V., Khashukoeva, A. Z., Evina, O. E., Geppe, N. A., Chebysheva, S. N., Korsunskaya, I. M., et al. (2022). Role of the transcription factor FOSL1 in organ development and tumorigenesis. *Int. J. Mol. Sci.* 23, 1521. doi:10.3390/ijms23031521

Stummer, W., Meinel, T., Ewelt, C., Martus, P., Jakobs, O., Felsberg, J., et al. (2012). Prospective cohort study of radiotherapy with concomitant and adjuvant temozolomide chemotherapy for glioblastoma patients with no or minimal residual enhancing tumor load after surgery. *J. Neurooncol.* 108, 89–97. doi:10.1007/s11060-012-0798-3

Sun, Y., Li, Y., Wang, H., Li, H., Liu, S., Chen, J., et al. (2017). miR-146a-5p acts as a negative regulator of TGF-β signaling in skeletal muscle after acute contusion. *Acta Biochim. Biophys. Sin.* 49, 628–634. doi:10.1093/abbs/gmx052

Tan, A. C., Ashley, D. M., López, G. Y., Malinzak, M., Friedman, H. S., and Khasraw, M. (2020). Management of glioblastoma: State of the art and future directions. *Ca. Cancer J. Clin.* 70, 299–312. doi:10.3322/caac.21613

Vallejo, A., Perurena, N., Guruceaga, E., Mazur, P. K., Martinez-Canarias, S., Zandueta, C., et al. (2017). An integrative approach unveils FOSL1 as an oncogene vulnerability in KRAS-driven lung and pancreatic cancer. *Nat. Commun.* 8, 14294. doi:10.1038/ncomms14294

Wang, H., Sun, T., Hu, J., Zhang, R., Rao, Y., Wang, S., et al. (2014). miR-33a promotes glioma-initiating cell self-renewal via PKA and NOTCH pathways. *J. Clin. Invest.* 124, 4489–4502. doi:10.1172/JCI75284

Wang, T., Liu, G., Guo, X., and Ji, W. (2022). Single-cell analysis reveals the role of the neuropeptide receptor FPR2 in monocytes in kawasaki disease: A bioinformatic study. *Dis. Markers* 1666240, 1–15. doi:10.1155/2022/1666240

Wang, Y., Zhao, Z-J., Kang, X-R., Bian, T., Shen, Z-M., Jiang, Y., et al. (2020). lncRNA DLEU2 acts as a miR-181a sponge to regulate SEPP1 and inhibit skeletal muscle differentiation and regeneration. *Aging (Albany NY)* 12, 24033–24056. doi:10.18632/aging.104095

Wen, P. Y., Weller, M., Lee, E. Q., Alexander, B. M., Barnholtz-Sloan, J. S., Barthel, F. P., et al. (2020). Glioblastoma in adults: A society for neuro-oncology (SNO) and European society of neuro-oncology (EANO) consensus review on current management and future directions. *Neuro. Oncol.* 22, 1073–1113. doi:10.1093/neuonc/noaa106

Wesseling, P., and Capper, D. (2018). WHO 2016 Classification of gliomas. *Neuropathol. Appl. Neurobiol.* 44, 139–150. doi:10.1111/nan.12432

Williams, G. R., Dunne, R. F., Giri, S., Shachar, S. S., and Caan, B. J. (2021). Sarcopenia in the older adult with cancer. *J. Clin. Oncol.* 39, 2068–2078. doi:10.1200/JCO.21.00102

Xia, L., Zhao, R., Wan, Q., Wu, Y., Zhou, Y., Wang, Y., et al. (2020). Sarcopenia and adverse health-related outcomes: An umbrella review of meta-analyses of observational studies. *Cancer Med.* 9, 7964–7978. doi:10.1002/cam4.3428

Xu, H., Jin, X., Yuan, Y., Deng, P., Jiang, L., Zeng, X., et al. (2017). Prognostic value from integrative analysis of transcription factors c-jun and fra-1 in oral squamous cell carcinoma: A multicenter cohort study. *Sci. Rep.* 7, 7522. doi:10.1038/s41598-017-05106-5

Yu, M., Bardia, A., Wittner, B. S., Stott, S. L., Smas, M. E., Ting, D. T., et al. (2013). Circulating breast tumor cells exhibit dynamic changes in epithelial and mesenchymal composition. *Science* 339, 580–584. doi:10.1126/science.1228522

Zeng, S., Zhou, C., Yang, D-H., Xu, L-S., Yang, H-J., Xu, M-H., et al. (2020). LEF1-AS1 is implicated in the malignant development of glioblastoma via sponging miR-543 to upregulate EN2. *Brain Res.* 1736, 146781. doi:10.1016/j.brainres.2020.146781

Zhang, Y., Kong, X., Zhang, J., and Wang, X. (2022). Functional analysis of bronchopulmonary dysplasia-related neuropeptides in preterm infants and miRNA-based diagnostic model construction. *Comput. Math. Methods Med.* 5682599, 1–17. doi:10.1155/2022/5682599

Zhang, Y., Zhang, J., Sun, C., and Wu, F. (2022). Identification of the occurrence and potential mechanisms of heterotopic ossification associated with 17-beta-estradiol targeting MKX by bioinformatics analysis and cellular experiments. *PeerJ* 9, e12696. doi:10.7717/peerj.12696

Zhou, Q., Liu, J., Quan, J., Liu, W., Tan, H., and Li, W. (2018). MicroRNAs as potential biomarkers for the diagnosis of glioma: A systematic review and meta-analysis. *Cancer Sci.* 109, 2651–2659. doi:10.1111/cas.13714

Zhou, Y., Yang, H., Xia, W., Cui, L., Xu, R., Lu, H., et al. (2017). Down-regulation of miR-605 promotes the proliferation and invasion of prostate cancer cells by up-regulating EN2. *Life Sci.* 190, 7–14. doi:10.1016/j.lfs.2017.09.028

frontiers | Frontiers in Genetics

TYPE Original Research
PUBLISHED 19 August 2022
DOI 10.3389/fgene.2022.959684

OPEN ACCESS

EDITED BY
Qian Wang,
Tai'an City Central Hospital, China

REVIEWED BY
Qiancheng Luo,
Shanghai Pudong New Area Gongli Hospital, China
Xiaoning Zhong,
First Affiliated Hospital of Guangxi Medical University, China
Junming Xu,
Shanghai General Hospital, China

*CORRESPONDENCE
Ning Zhang,
z7755366054764@163.com

†These authors have contributed equally to this work

SPECIALTY SECTION
This article was submitted to Cancer Genetics and Oncogenomics, a section of the journal Frontiers in Genetics

RECEIVED 02 June 2022
ACCEPTED 25 July 2022
PUBLISHED 19 August 2022

CITATION
Ma J, Zhu M, Ye X, Wu B, Wang T, Ma M, Li T and Zhang N (2022), Prognostic microRNAs associated with phosphoserine aminotransferase 1 in gastric cancer as markers of bone metastasis.
Front. Genet. 13:959684.
doi: 10.3389/fgene.2022.959684

Prognostic microRNAs associated with phosphoserine aminotransferase 1 in gastric cancer as markers of bone metastasis

Jingwei Ma[1†], Meng Zhu[2†], Xiaofeng Ye[1], Bo Wu[1], Tao Wang[1], Muyuan Ma[1], Tao Li[1] and Ning Zhang[3*]

[1]The Second Department of Surgical Oncology, General Hospital of Ningxia Medical University, Ningxia, China, [2]College of Basic Medicine, Ningxia Medical University, Yinchuan, China, [3]Department of Pathology, General Hospital of Ningxia Medical University, Ningxia, China

This study analyzed PSAT1-targeted miRNAs as a prognostic predictor for gastric cancer. The relationship between the clinical manifestations of gastric cancer in patients and phosphoserine aminotransferase 1 (PSAT1) was analyzed using correlation analysis. PSAT1 was highly expressed in gastric cancer, and its low expression was associated with a poor prognosis. By pan-cancer analysis, PSAT1 could affect the tumor immune microenvironment by immune infiltration analysis. Nine microRNAs targeting PSAT1 and associated with gastric cancer were screened by miRwalk and microRNA expression in TCGA tumor tissues. Six microRNAs were obtained by survival curve analysis, including hsa-miR-1-3p, hsa-miR-139-5p, hsa-miR-145-5p, hsa-miR-195-5p, hsa-miR-218-5p, and hsa-miR-497-5p. Based on the above six microRNAs, a model for bone metastasis prediction in gastric cancer prediction was constructed. An analysis of a decision curve was performed based on the microRNAs obtained to predict bone metastasis from gastric cancer. It had a positive area under the curve (AUC) value of 0.746, and the decision curve analysis (DCA) indicated that it was clinically significant. Dual-luciferase reporter genes indicated that hsa-miR-497-5p and PSAT1 were targeted, and qRT-PCR results confirmed that hsa-miR-497-5p could down-regulate PSAT1 expression. MicroRNAs targeting the regulation of PSAT1 expression can well predict the prognosis of gastric cancer.

KEYWORDS

PSAT1, exosome, microRNA, gastric cancer, prognosis

Introduction

Cancer of the gastric mucosa arises from the epithelium of the mucosa, and most of its clinical manifestations are indigestion, abdominal pain, early satiety, or anorexia, but it may also present as reflux, dysphagia, and gastrointestinal bleeding (Machlowska et al., 2020). Gastric cancer is a heterogeneous and multifactorial disease caused by a combination of environmental and genetic factors, with a complex pathogenesis (Oliveira et al., 2015). Infections with *H. pylori*, nitrate- and nitrite-rich diets, smoking and drinking alcohol are all risk factors for gastric cancer (Machlowska et al., 2020; Joshi and Badgwell, 2021). Some genetic syndromes, such as CDH1, Lynch, and Peutz-Jegher syndromes, are also associated with gastric cancer (Hansford et al., 2015; Lott and Carvajal-Carmona, 2018). There were approximately 1.089 million new cases of gastric cancer worldwide in 2020, accounting for 5.6% of all cancers, making it the fifth-largest malignant tumor in the world after breast, lung, colorectal, and prostate cancers. (Sung et al., 2021). In addition, since gastric cancer exhibits insidious symptoms in the early stages, metastases are often detected at the time of diagnosis, making the prognosis poor and the mortality rate high. Globally, approximately 769,000 people will die from stomach cancer in 2020, accounting for 7.7% of all cancer-related deaths. The most common sites of metastasis for gastric cancer are the peritoneum, liver, lung, and lymph nodes, while bone metastases are rare, occurring in less than 5% of patients (Park et al., 2013; Turkoz et al., 2014). However, studies have shown that bone metastases from gastric cancer are an independent poor prognostic factor for gastric cancer and are significantly associated with overall patient survival. Bone metastases from gastric cancer have a significantly lower 5-year survival rate than non-bone metastases, with a median survival time of only about four months (Lee et al., 2007; Xiaobin et al., 2022). Because most bone metastases do not show significant clinical symptoms, the actual incidence of bone metastasis may be higher than reported. There is an urgent need for biomolecular markers that can determine the risk factors for bone metastasis in gastric cancer, assess their risk in patients, and detect early and accurately.

PSAT1 encodes the catalytic enzyme phosphoserine aminotransferase, which is associated with cell proliferation and serine anabolism (Hart et al., 2007; Montrose et al., 2021). Researchers have found that PSAT1 is aberrantly expressed in various tumor cells and promotes proliferation, metastasis, invasion, and drug resistance in a variety of malignancies, including breast, lung, and colorectal cancer (Metcalf et al., 2020; Biyik-Sit et al., 2021; Montrose et al., 2021). In addition, PSAT1 was found to promote extracellular vesicle (EV) secretion via the serine-ceramide synthesis pathway in multiple cancer types, affecting the tumor microenvironment. By activating osteoclasts, it could also promote bone metastasis. EVs are a collective term for vesicular structures encased in lipid bilayers released by various cells, including exosomes and particles. Exo is a signaling vesicle involved in normal homeostatic processes or pathological exchanges of nucleic acids, proteins, and other components between cells (Kowal et al., 2016). Exosomes not only play a role in regulating normal physiological processes, such as immune response and cell differentiation, but can also be involved in the pathophysiology of diseases, such as cancer development, progression, and metastasis (Yao et al., 2021). Tumor cells can interact with cells in the bone microenvironment through the secretion of exosomes and transfer tumor-specific contents, such as miRNA, to the bone microenvironment through exosomes, thus promoting tumor bone metastasis (Rossi et al., 2018; Tiedemann et al., 2019). Furthermore, breast cancer cells has been suggested to promote the development of breast cancer bone metastases by releasing exosomes containing miRNA-19a and IBSP (Wu et al., 2021a). However, it remains to be seen whether exosomes can regulate PSAT1.

In this study, we analyzed the clinical and tumor microenvironment of gastric cancer patients to investigate the relationship between PSAT1 and prognosis. We screened the PSAT1-targeting microRNAs with miRWalk, and then analyzed their expression in gastric cancer. Diagnosis and treatment strategies can be provided by screening marker proteins associated with gastric cancer prognosis.

Methods

Downloading and processing of data

We downloaded PSAT1 pan-cancer data from the UCSC Xena database for a total of 18 cancer types, including bladder uroepithelial carcinoma (BLCA), breast invasive carcinoma (BRCA), cholangiocarcinoma (CHOL), colon adenocarcinoma (COAD), esophageal carcinoma (ESCA), glioblastoma multiforme (GBM), head and neck squamous cell carcinoma (HNSC), kidney chromophobe (KICH), kidney renal clear cell carcinoma (KIRC), kidney renal papillary cell carcinoma (KIRP), liver hepatocellular carcinoma (LIHC), lung adenocarcinoma (LUAD), lung squamous carcinoma (LUSC), prostate adenocarcinoma (PRAD), rectal adenocarcinoma (READ), stomach adenocarcinoma (STAD), thyroid carcinoma (THCA), and uterine corpus endometrial carcinoma (UCEC). From the Cancer Genome Atlas (TCGA) database (https://www.cancer.gov/about-nci/organization/ccg/research), raw RNA sequencing data and clinical information were downloaded from gastric cancer patients (Wang et al., 2016; Goldman et al., 2020). Information about survival time, survival status, age, sex, tumor grade, clinical stage, pathological stage, TNM stage, OS, DSS, and PFI were collected from the patients.

Clinicopathological and survival analysis of phosphoserine aminotransferase 1 in gastric cancer

Patients' clinical information included age, gender, clinical stage, and TMN stage. To investigate the relationship between PSAT1 expression and clinical characteristics, we selected clinical, pathological, and TNM stages as representative outcomes with significant differences. The gastric cancer samples were then divided into high and low expression groups based on their median PSAT1 expression values. Kaplan-Meier survival curves were plotted using this method. We analyzed the relationship between PSAT1 expression and prognostic DSS (disease-specific survival) in gastric cancer taking into account the possibility of non-tumor death during follow-up. The relationship between PSAT1 expression and PFI (progression-free interval) was also examined.

Immune infiltration analysis

CIBERSORT deconvolution algorithm is a computational method for identifying 22 types of immune cells in tissues (Bindea et al., 2013; Hänzelmann et al., 2013; Wu et al., 2021b). With R software, the CIBERSORT deconvolution algorithm was used to simulate the transcriptional features matrix of 22 immune cells, including B cells, plasma cells, T cells, natural killer cells, monocytes, macrophages, dendritic cells, mast cells, eosinophils, and neutrophils. Calculations were set at 100, and data with $p < 0.05$ were analyzed. In order to analyze the correlation between PSAT1 and immune cells, R software calculated correlation coefficients between immune cells and PSAT1. Additionally, the ESTIMATE algorithm in the R language estimation package was used to estimate the ratio of immune to stromal components in tumor microenvironments. Three types of scores were presented: immune, stromal, and ESTIMATE. Based on the correlation between PSAT1 and these three scores, we were able to analyze the correlation between PSAT1 and the tumor microenvironment. The relationships between PSAT1 expression, immune cell infiltration score, and tumor microenvironment were assessed by Spearman correlation analysis.

Gastric cancer microRNAs associated with upregulation of phosphoserine aminotransferase 1 expression

All microRNAs that may target PSAT1 were predicted using the online miRNA target gene prediction tool miRWalk2.0 as previous researches (http://zmf.umm.uni-heidelberg.de/apps/zmf/mirwalk2) (Dweep et al., 2014; Sticht et al., 2018; Feng et al., 2021; Chen et al., 2022; Zhao and Jiang, 2022). MiRWalk integrated with several different miRNA target gene prediction tools, including miRanda, RNA22, miRDB, Targetscan, etc., which can perform multiple databases of miRNA co-screening and find the common target genes among them, maximizing the prediction confidence. Then, we conducted correlation analysis of the miRNAs that correlated negatively with PSAT1.

MicroRNA expression and survival in gastric cancer

The microRNAs obtained above were calculated as the expression between gastric cancer tissues and normal tissues, and the microRNAs with statistically significant differences in expression were screened by the $p < 0.05$. Survival curves were plotted by Kaplan-Meier method based on the median expression value of each microRNA as previous researches (Rich et al., 2010; Lacny et al., 2015; Sun et al., 2022; Xuan et al., 2022).

Model construction and evaluation

Using the Akaike information criterion (AIC), the optimal logistic nomogram model was constructed. We evaluated the expressiveness of the model using ROC curves and calibration curves. We also performed the Hosmer-Lemeshow goodness-of-fit test. Decision curve analysis (DCA) was used to examine the effect of the model on net clinical benefit rates at different positive thresholds. Threshold probability is the horizontal coordinate of DCA. When the nomogram model assessment value reached a certain value, bone metastasis probability was denoted as p.

Cell culture and transfection

Chinese Academy of Sciences, Shanghai, provided 293T and SGC-7901 cells, which were cultured at 37 °C in a constant humidity CO_2 incubator with DMEM + 10% FBS + 1% double antibody. Afterwards, we transfected 293T cells with 100 pmol hsa-miR-497-5p, purchased from Bioindustries, for 48 h before RNA extraction.

RNA extraction by qRT-PCR analysis

SGC-7901 cells were treated with Trizol (Sangon, China) according to Trizol's guidelines. In order to measure mRNA expression levels, RNA was reverse-transcribed into cDNA using Promega's Reverse Transcription Kit (GoScriptTM Reverse Transcription Kit), followed by qRT-PCR analysis using Biotech's qRT-PCR reagents (2X SG Fast qPCR Master Mix).

TABLE 1 Gastric cancer patients' demographic characteristics and PSAT1 expression.

Characteristic	Low expression of PSAT1 (n = 187)	High expression of PSAT1 (n = 188)	p value
Age, n (%)			0.032
≤65	93 (25.1%)	71 (19.1%)	
>65	93 (25.1%)	114 (30.7%)	
Gender, n (%)			0.073
Female	58 (15.5%)	76 (20.3%)	
Male	129 (34.4%)	112 (29.9%)	
T stage, n (%)			0.471
T1	10 (2.7%)	9 (2.5%)	
T2	38 (10.4%)	42 (11.4%)	
T3	90 (24.5%)	78 (21.3%)	
T4	44 (12%)	56 (15.3%)	
N stage, n (%)			0.638
N0	58 (16.2%)	53 (14.8%)	
N1	49 (13.7%)	48 (13.4%)	
N2	35 (9.8%)	40 (11.2%)	
N3	32 (9%)	42 (11.8%)	
M stage, n (%)			0.219
M0	168 (47.3%)	162 (45.6%)	
M1	9 (2.5%)	16 (4.5%)	
Pathologic stage, n (%)			0.112
Stage I	23 (6.5%)	30 (8.5%)	
Stage II	65 (18.5%)	46 (13.1%)	
Stage III	69 (19.6%)	81 (23%)	
Stage IV	16 (4.5%)	22 (6.2%)	
Histologic grade, n (%)			0.112
G1	8 (2.2%)	2 (0.5%)	
G2	64 (17.5%)	73 (19.9%)	
G3	112 (30.6%)	107 (29.2%)	
Primary therapy outcome, n (%)			0.769
PD	35 (11%)	30 (9.5%)	
SD	9 (2.8%)	8 (2.5%)	
PR	1 (0.3%)	3 (0.9%)	
CR	116 (36.6%)	115 (36.3%)	
Race, n (%)			0.062
Asian	47 (14.6%)	27 (8.4%)	
Black or African American	4 (1.2%)	7 (2.2%)	
White	118 (36.5%)	120 (37.2%)	
Histological type, n (%)			0.028
Diffuse Type	40 (10.7%)	23 (6.1%)	
Mucinous Type	12 (3.2%)	7 (1.9%)	
Not Otherwise Specified	103 (27.5%)	104 (27.8%)	
Papillary Type	2 (0.5%)	3 (0.8%)	
Signet Ring Type	6 (1.6%)	5 (1.3%)	
Tubular Type	24 (6.4%)	45 (12%)	
Residual tumor, n (%)			0.867
R0	144 (43.8%)	154 (46.8%)	
R1	8 (2.4%)	7 (2.1%)	
R2	7 (2.1%)	9 (2.7%)	

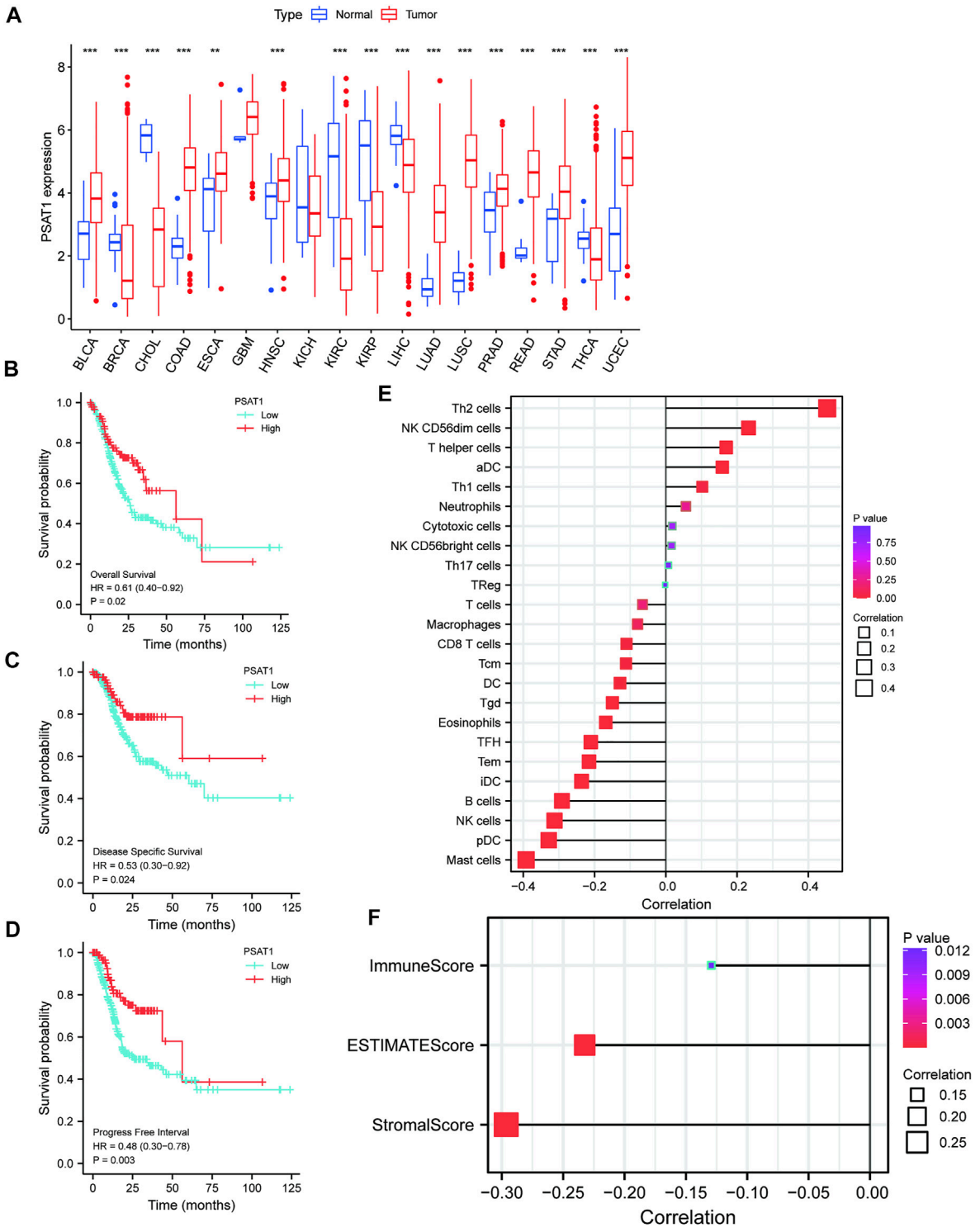

FIGURE 1
A correlation between PSAT1 expression levels and cancer patient prognosis. **(A)**. Box plot showing the level of PSAT1 mRNA expression in different cancer tissues and normal tissues; data from UCSC database; ***$p < 0.001$, **$p < 0.01$; **(B)**. Survival analysis demonstrating the overall survival of gastric cancer patients with high PSAT1 expression (OS, HR = 0.61, 95% CI: 0.40–0.92, $p = 0.02$); **(C)**. Survival analysis demonstrating the relationship between PSAT1 expression levels and DSS of gastric cancer patients (DSS, HR= 0.53, 95% CI: 0.30–0.92, $p = 0.024$); **(D)**. Survival analysis demonstrating the relationship between PSAT1 expression levels and progress-free interval of gastric cancer patients (PFI, HR = 0.48, 95% CI: 0.30–0.78, $p = 0.003$); **(E)**. Correlation analysis of PSAT1 expression with immune cell infiltration displaying that TH2 cells and NK cells are positively correlated with PSAT1, whereas plasmacytoid dendritic cells and mast cells are negatively correlated with PSAT1; **(F)**. PSAT1 correlation analysis with ImmuneScore, StromalScore, and ESTIMATEScore.

As an internal reference, GAPDH was used and $2^{-\Delta\Delta Ct}$ was used to calculate mRNA expression levels.

Dual luciferase reporter gene system

PmirGLO-PSAT1-3' UTR-WT and pmirGLO-PSAT1-3' UTR-MUT vector plasmids were purchased from Shanghai Sangon Biotech. 500 ng of vector plasmid and 100 pmol of hsa-miR-497-5p mimics were transfected into 293T cells and the fluorescence situation was determined 24 h after transfection using Dual Luciferase Assay Kit (Promega).

Statistical methods

Statistical analysis was performed using the R software package (version 3.6.3). The Spearman correlation test was used to determine whether the two variables were correlated. Differences with $p < 0.05$ were considered statistically significant.

Results

Phosphoserine aminotransferase 1 expression and general health of gastric cancer patients

From the TCGA database, clinical information was downloaded for 375 gastric cancer patients. PSAT1 expression was divided into low and high groups based on median expression. Their median ages were 65.5 and 69, respectively, statistically significantly different ($p < 0.05$). In addition, there was a statistically significant difference in pathological types between low and high expression groups ($p = 0.028$) (Table 1). PSAT1 expression was statistically significantly different between pathological Stage IV, TNMF Stage IV, and clinical Stage IV based on patient's clinical data [HR = 1.70 (1.09–2.68), $p = 0.021$]. There was a difference in PSAT1 expression at pathological stage IV. However, there were no significant differences in the other clinical-pathological symptoms.

Pan-cancer phosphoserine aminotransferase 1 expression

UCSC database was used to analyze PSAT1 mRNA expression levels in tumor and normal tissue samples (Figure 1A). The results disclosed that PSAT1 was highly expressed in ten cancer types relative to normal tissues, including BLCA, COAD, ESCA, HNSC, LUAD, LUSC, PRAD, READ, STAD, and UCEC. In contrast, PSAT1 expression was low in BRCA, CHOL, KIRC, KIRP, LIHC, and THCA. PSAT1 expression was not significant in GBM and KICH.

Survival analysis of phosphoserine aminotransferase 1 in gastric cancer and immune infiltration analysis

Patients with high PSAT1 expression had significantly longer overall survival (OS, HR= 0.61, 95% CI: 0.40–0.92, $p = 0.02$), disease-specific survival (DSS, HR= 0.53, 95% CI: 0.30–0.92, $p = 0.024$), and progression-free interval (PFI, HR= 0.48, 95% CI: 0.30–0.78, $p = 0.003$) (Figures 1B–D). In gastric cancer, low expression of PSAT1 was associated with worse OS, DSS, and PFI. Therefore, patients with gastric cancer with low expression of PSAT1 had a poor prognosis.

The percentage of immune cell infiltration was calculated by Cibersort software, and samples that met the requirements were screened according to the $p < 0.05$ criterion. According to our analysis, each immune cell shows a positive correlation with PSAT1 expression, while plasmacytoid dendritic cells and mast cells have a negative correlation with PSAT1 (Figure 1E). Furthermore, ImmuneScore, StromalScore, and ESTIMATEScore were calculated using the ESTIMATE algorithm in R language estimate package. PSAT1 expression and these three scores were negatively correlated (Figure 1F). PSAT1 expression levels can influence the immune activity of tumor microenvironments, according to these results.

Prognostic analysis of microRNAs negatively associated with phosphoserine aminotransferase 1

MiRNAs targeting and regulating PSAT1 gene expression were identified using miRwalk database and visualized using Cytoscope (Figure 2A). We calculated the expression of the above 116 miRNAs in TCGA in gastric cancer. By analyzing the correlation between their expression and PSAT1 expression, we found that the following were negatively correlated with PSAT1 expression: hsa-miR-1-3p ($r = -0.3$, $p < 0.05$), hsa-miR-29c-3p ($r = -0.25$, $p < 0.05$), hsa-miR-101 -3p ($r = -0.25$, $p < 0.05$), hsa-miR-129-5p ($r = -0.34$, $p < 0.05$), hsa-miR-139-5p ($r = -0.29$, $p < 0.05$), hsa-miR-145-5p ($r = -0.29$, $p < 0.05$), hsa-miR-195-5p ($r = -0.34$, $p < 0.05$), hsa-miR-497-5p ($r = -0.36$, $p < 0.05$), and hsa-miR-218-5p ($r = -0.36$, $p < 0.05$) (Figure 2B). Eight miRNAs were found to have low expression and be significantly different between tumors and normal tissue, namely: hsa-miR-1-3p, hsa-miR-29c-3p, hsa-miR-129-5p, hsa-miR-139-5p, hsa-miR-145-5p, hsa-miR-195-5p, hsa-miR-497-5 (Figure 2C). We calculated the p-value for each miRNA in relation to patient survival using KM survival curves of the eight differential miRNAs

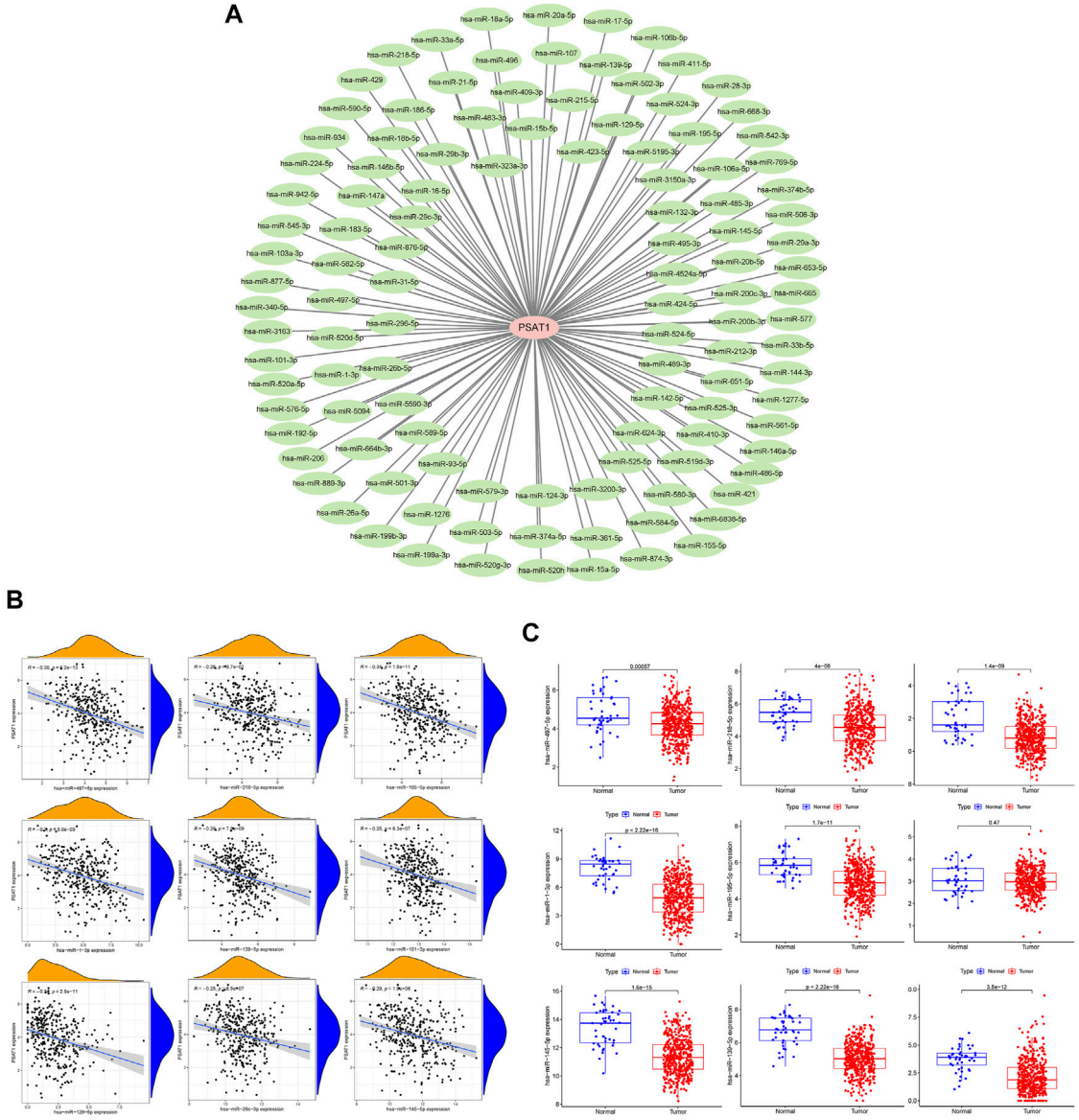

FIGURE 2
The microRNAs associated with gastric cancer expression of PSAT1. **(A)**. The miRwalk database and correlation analysis identified microRNAs that could target PSAT1 in gastric cancer; **(B)**. MicroRNAs negatively correlated with PSAT1 expression; **(C)**. Gastric tumor tissues and normal tissue samples showed negative correlations between miRNA levels and PSAT1 expression levels.

listed above. Six miRNAs were found to have significant correlations with prognosis, including hsa-miR-1-3p, hsa-miR-139-5p, hsa-miR-145-5p, hsa-miR-195-5p, hsa-miR-218-5p (Figure 3A). Then, we constructed a regulatory relationship map targeting PSAT1 using cytoscope software (Figure 3B). There was a negative correlation between these nine miRNAs (Figure 3C). Therefore, these six miRNAs (hsa-miR-1-3p, hsa-miR-139-5p, hsa-miR-145-5p, hsa-miR-195-5p, hsa-miR-218-5p, and hsa-miR-497-5p) may be associated with (hsa-miR-1-3p, hsa-miR-139-5p, hsa-miR-145-5p, hsa-miR-195-5p, hsa-miR-218-5p, and hsa-miR-497-5p) the expression of PSAT1 and the prognosis of patients.

Construction of the nomogram predictive model and clinical utility assessment

The six miRNAs (hsa-miR-1-3p, hsa-miR-139-5p, hsa-miR-145-5p, hsa-miR-195-5p, hsa-miR-218-5p, and hsa-

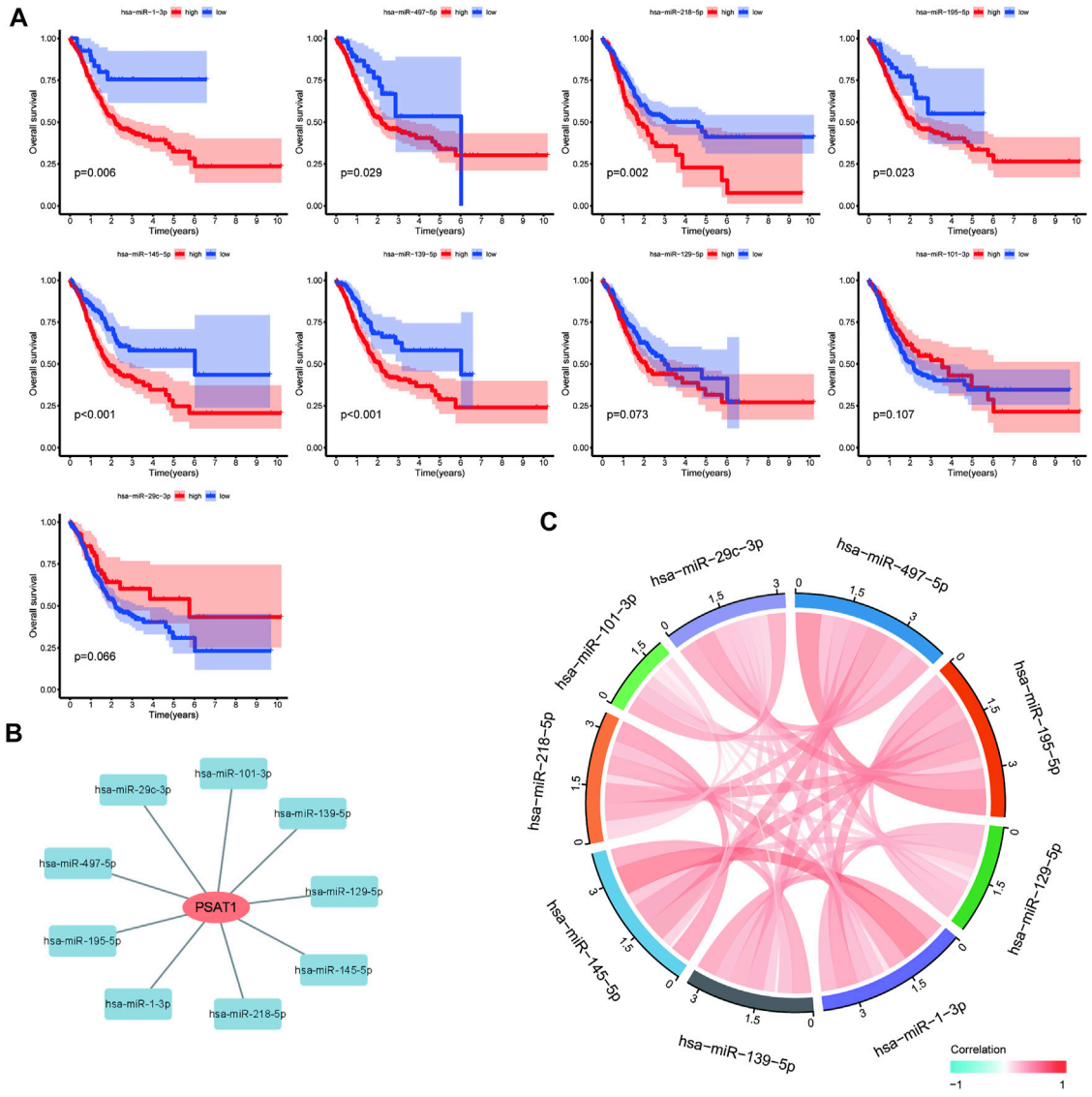

FIGURE 3
Prognostic analysis of microRNAs negatively associated with PSAT1. **(A)**. Survival analysis of miRNAs (hsa-miR-218-5p, hsa-miR-129-5p, hsa-miR-145-5p, hsa-miR-139-5p, hsa-miR-195-5p, hsa-miR-1-3p, hsa-miR-29c-3p, and hsa-miR-497-5p) significantly associated with tumor prognosis; **(B)**. PSAT1-related microRNA regulatory network; **(C)**. Correlation analysis circle diagram between PSAT1 and its negatively associated microRNAs.

miR-497-5p) were built into a nomogram model (Figure 4A). Each miRNA's corresponding scale was determined based on its actual situation in the patient. By projecting upward to the top scale points, each miRNA's score was calculated, and the scores were summed. The risk probability of bone metastasis in the patient was calculated by projecting downward based on the total score. Validating the model, we found that it had a good AUC value (AUC = 0.746), calibration, and goodness of fit, suggesting that it could predict the risk of bone metastasis in gastric cancer (Figures 4B,C). DCA illustrating the benefits of using the miRNA nomogram model (Figure 4D). Overall, we established a predictive model for gastric cancer bone metastasis.

Hsa-miR-497-5p targets and regulates phosphoserine aminotransferase 1

Among the six miRNAs targeted by PSAT1, hsa-miR-1-3p, hsa-miR-139-5p, hsa-miR-145-5p, hsa-miR-195-5p, hsa-miR-218-5p, and hsa-miR-497-5p were most closely related to gastric cancer prognosis. PSAT1 and hsa-miR-497-5p were

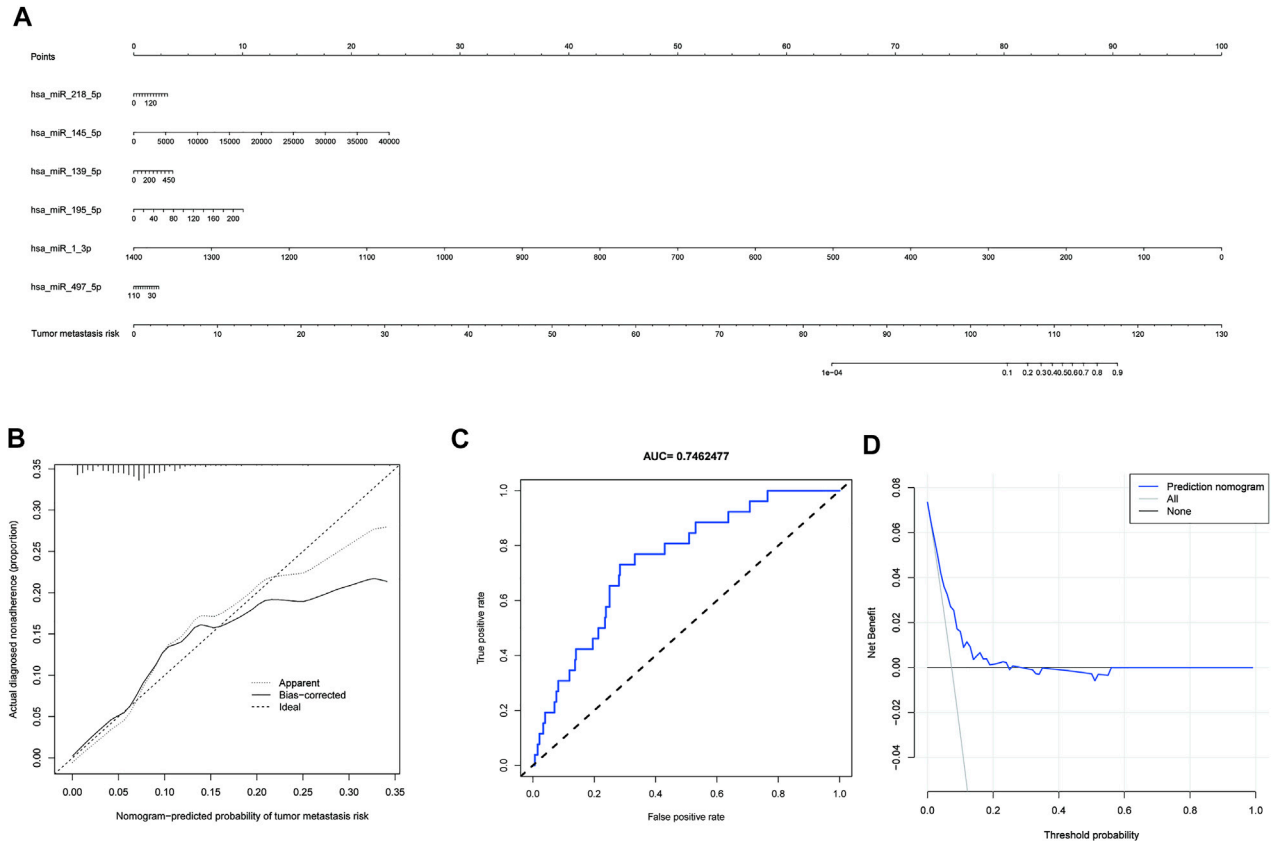

FIGURE 4
A predictive model for gastric cancer metastasis risk based on microRNAs associated with downregulated PSAT1 expression. **(A)**. Nomogram models based on six miRNAs (hsa-miR-1-3p, hsa-miR-139-5p, hsa-miR-145-5p, hsa-miR-195-5p, hsa-miR-218-5p, and hsa-miR-497-5p); **(B)**. Calibration curve for nomogram model; **(C)**. ROC curve of nomogram model (AUC = 0.746); **(D)**. Clinical decision curves illustrating the benefits of using the miRNA nomogram model.

detected using a dual-luciferase reporter gene system and qRT-PCR. Figure 5A shows that hsa-miR-497-5p mimics reduced the fluorescence ratio compared to the control, demonstrating a targeting relationship between hsa-miR-497-5p and PSAT1. PSAT1 expression was reduced by hsa-miR-497-5p in further qRT-PCR experiments (Figure 5B). As a result of the above findings, hsa-miR-497-5p appears to be capable of targeting PSAT1 expression in order to affect gastric cancer prognosis.

Discussion

The rapid development of precision medicine has improved the survival rate of gastric cancer by combining surgery with targeted therapy and chemotherapy, but the prognosis remains poor (Li et al., 2022). Early symptoms of gastric cancer are atypical, so early diagnosis is mainly based on endoscopic biopsy, which is a limited method. Distant metastases are often diagnosed in most patients (Dohi et al., 2017). Recently, with the continuous improvement of imaging technology, related studies have found that the percentage of patients with bone metastases from gastric cancer detected by bone scan screening can be as high as 25–45.3% (Choi et al., 1995). Several studies have demonstrated that bone metastasis, as an independent risk factor for gastric cancer, often indicated rapid deterioration of the clinical course, which seriously affected the treatment outcome and prognosis of patients (Ahn et al., 2011; Qiu et al., 2018). Moreover, patients with bone metastases may suffer from complications such as bone pain, pathological fracture, and spinal cord compression, which seriously affect their quality of life (Mikami et al., 2017). Bone metastases from gastric cancer were found to be lower than the actual rate because there were often no obvious clinical symptoms in the early stages, and skeletal screening for gastric cancer patients was not routine (Clézardin, 2017). Therefore, a predictive risk model should be developed to help detect and diagnose gastric cancer bone metastases early, enabling effective treatment plans to be developed.

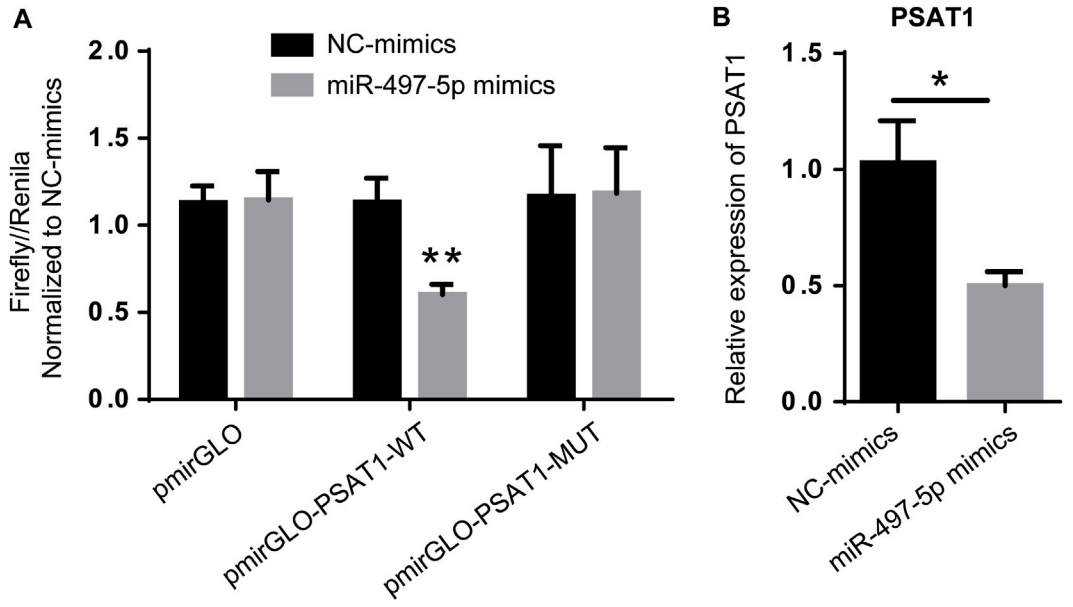

FIGURE 5
PSAT1 expression is regulated by has-miR-497-5p. **(A)**. PSAT1 and has-miR-497-5p targeting relationship revealed by dual-luciferase reporter gene system. **(B)**. The expression of PSAT1 was lower in has-miR-497-5p-treated gastric cancer cell lines compared to control cells. *$p < 0.05$, **$p < 0.01$.

PSAT1 regulates serine anabolism, playing an important role in cell proliferation, and is also essential for osteoclastogenesis (de KONING et al., 2003; Ogawa et al., 2006). Furthermore, it was found that high PSAT1 expression was closely associated with bone metastasis in malignant tumors. High expression of PSAT1 has been suggested to regulate serine anabolism, promotes osteoclast differentiation and enhances their activity, regulates the tumor microenvironment, and thus promotes bone metastasis in breast cancer (Pollari et al., 2011). PSAT1 expression was highly correlated with poor prognosis in gastric cancer in this study based on pan-cancer analysis. According to immune infiltration analysis, PSAT1 affects the tumor immune microenvironment, which indicates that PSAT1 plays a critical role in invasion and gastric cancer prognosis. Furthermore, we identified miRNAs targeting PSAT1 in TCGA tumor tissues and associated them with gastric cancer. We found that multiple miRNAs regulated PSAT1 expression (Figure 2B). The survival curve analysis identified six microRNAs, including hsa-miR-1-3p, hsa-miR-139-5p, hsa-miR-145-5p, hsa-miR-195-5p, hsa-miR-218-5p, and hsa-miR-497-5p (Figure 3A). Based on the above six microRNAs, we constructed the prognostic prediction model for gastric cancer.

MicroRNAs (miRNAs) belong to a family of non-coding RNAs of 20–24 nucleotides in length. MiRNAs are significantly associated with tumor development and metastasis (Liu et al., 2019; Wang et al., 2019; Chen et al., 2021; Zhang and Liu, 2021; Cao et al., 2022). Compared with normal tissues, miRNA expression is down-regulated in various cancers. They are widely involved in tumor metastasis and invasion by suppressing target genes and have an important role in tumor diagnosis and prognosis assessment (Daoud et al., 2019). Previous studies found that all six microRNAs used to construct predictive models were associated with malignant tumorigenesis, invasion, or metastasis. Hsa-miR-139-5p expression was low in various tumor tissues, including gastric cancer, liver cancer, and thyroid cancer (Yang et al., 2013; Montero-Conde et al., 2020; Chi et al., 2021). Bioinformatics analysis revealed that hsa-miR-139-5p was closely associated with gastric cancer prognosis (Wang et al., 2022). Furthermore, hsa-miR-139-5p/MYB axis has been suggested to promote the proliferation, invasion, and metastasis of gastric cancer (Xie et al., 2021). The expression of hsa-miR-145-5p was down-regulated in various tumor cells, including gastric cancer, and the down-regulation of hsa-miR-145-5p expression was associated with lymph node metastasis and distant metastasis in gastric cancer, suggesting a poor prognosis (Hang et al., 2018). In addition, it was found that the exosomes secreted by ovarian cancer cells also contained hsa-miR-145-5p, and its abnormal expression was associated with distant metastasis of cancer cells (Hang et al., 2018). Hsa-miR-195-5p is also a suppressor of multiple tumor types, and its dysregulated expression is involved in the development of multiple tumors and is associated with poor tumor prognosis

and drug resistance (Jin et al., 2018; Rezaei et al., 2019). It has been suggested that hsa-miR-195-5p was involved in regulating the invasion and metastasis of gastric cancer cells by binding to PD-L1 and regulating E-calmodulin expression, which was closely associated with poor prognosis for patients with gastric cancer (Zou et al., 2019; Liu et al., 2020; Liu et al., 2021). Expression of hsa-miR-218-5p is downregulated in various malignancies, including gastric, prostate, and cervical cancers, and is associated with tumor invasion and migration (Gao et al., 2009). Researchers found that hsa-miR-218-5p regulated KIT protein expression and inhibited proliferation and invasion of gastrointestinal mesenchymal tumors (Fan et al., 2014). Upregulation of hsa-miR-218-5p expression inhibits cancer progression in cervical and bladder cancer, by reducing cell migration and invasion (Chiyomaru et al., 2012; Yamamoto et al., 2013). Hsa-miR-497-5p expression is down-regulated in gastric, hepatocellular, and colorectal cancers, and is also associated with tumorigenesis, invasion, and poor prognosis (Falzone et al., 2018; Liu et al., 2021; Tian et al., 2021). In addition, abnormal expression of hsa-miR-1-3p is associated with poor prognosis of malignant tumors, such as breast cancer and small cell lung cancer (Li et al., 2020; Yan et al., 2021). Gene expression levels are closely connected to tumor metastasis according to the prediction model obtained in this study, which implicates genes involved in cancer development and metastasis. Furthermore, we developed and validated a prognostic prediction model using nine microRNAs for gastric cancer and found that AUC value with good calibration and good fit was 0.746 (Figures 4B,C). A good prediction of the risk of bone metastases in patients with gastric cancer could be obtained through this model, and it could have some application in the assessment of gastric cancer prognoses.

Conclusion

Gastric cancers expressed high levels of PSAT1, and low levels were associated with poor prognoses. Furthermore, microRNAs targeting PSAT1 can predict gastric cancer prognosis and bone metastasis risk. Based on the results of this study, it can be concluded that the prediction model provides good predictive value in the risk assessment of bone metastasis in gastric cancer, in addition to showing some clinical application in the prognosis evaluation of gastric cancer. The study has, however, some limitations. To validate the findings of this study, a larger sample size is required. It is also necessary to conduct further experimental studies in order to clarify the specific mechanisms involved in regulation.

Data availability statement

The datasets presented in this study can be found in online repositories. The names of the repository/repositories and accession number(s) can be found in the article/supplementary material.

Author contributions

JM, MZ, XY, BW, and NZ performed the data curation and analysis. JM, MZ, XY, BW, TW, MM, TL, and NZ analyzed and interpreted the results. JM and NZ drafted and reviewed the manuscript. JM and NZ provided funding. All authors read and approved the final manuscript.

Acknowledgments

The language touch-up services provided by Home for Researchers [www.home-for-researchers.com] are greatly appreciated.

Conflict of interest

The authors declare that the research was conducted in the absence of any commercial or financial relationships that could be construed as a potential conflict of interest.

Publisher's note

All claims expressed in this article are solely those of the authors and do not necessarily represent those of their affiliated organizations, or those of the publisher, the editors and the reviewers. Any product that may be evaluated in this article, or claim that may be made by its manufacturer, is not guaranteed or endorsed by the publisher.

References

Ahn, J. B., Ha, T. K., and Kwon, S. J. (2011). Bone metastasis in gastric cancer patients. *J. Gastric Cancer* 11, 38–45. doi:10.5230/jgc.2011.11.1.38

Bindea, G., Mlecnik, B., Tosolini, M., Kirilovsky, A., Waldner, M., Obenauf, A. C., et al. (2013). Spatiotemporal dynamics of intratumoral immune cells reveal the immune landscape in human cancer. *Immunity* 39, 782–795. doi:10.1016/j.immuni.2013.10.003

Biyik-Sit, R., Kruer, T., Dougherty, S., Bradley, J. A., Wilkey, D. W., Merchant, M. L., et al. (2021). Nuclear pyruvate kinase M2 (PKM2) contributes to phosphoserine

aminotransferase 1 (PSAT1)-Mediated cell migration in EGFR-activated lung cancer cells. *Cancers* 13, 3938. doi:10.3390/cancers13163938

Cao, T., Hong, J., Qi, F., Zheng, B., Chen, G., Yu, B., et al. (2022). A hyperglycemic microenvironment inhibits tendon-to-bone healing through the let-7b-5p/CFTR pathway. *Comput. Math. Methods Med.* 2022, 82680671–82680710. doi:10.1155/2022/8268067

Chen, C., Zhao, J., Liu, J., and Sun, C. (2021). Mechanism and role of the neuropeptide LGI1 receptor ADAM23 in regulating biomarkers of ferroptosis and progression of esophageal cancer. *Dis. Markers* 9227897, 1–15. doi:10.1155/2021/9227897

Chen, Y., Sun, Y., Luo, Z., Lin, J., Qi, B., Kang, X., et al. (2022). Potential mechanism underlying exercise upregulated circulating blood exosome miR-215-5p to prevent necroptosis of neuronal cells and a model for early diagnosis of alzheimer's disease. *Front. Aging Neurosci.* 14, 860364. doi:10.3389/fnagi.2022.860364

Chi, F., Cao, Y., and Chen, Y. (2021). Analysis and validation of circRNA-miRNA network in regulating m6A RNA methylation modulators reveals CircMAP2K4/miR-139-5p/YTHDF1 Axis involving the proliferation of hepatocellular carcinoma. *Front. Oncol.* 11, 560506. doi:10.3389/fonc.2021.560506

Chiyomaru, T., Enokida, H., Kawakami, K., Tatarano, S., Uchida, Y., Kawahara, K., et al. (2012). Functional role of LASP1 in cell viability and its regulation by microRNAs in bladder cancer. *Urol. Oncol.* 30, 434–443. doi:10.1016/j.urolonc.2010.05.008

Choi, C. W., Lee, D. S., Chung, J-K., Lee, M. C., Kim, N. K., Choi, K. W., et al. (1995). Evaluation of bone metastases by Tc-99m MDP imaging in patients with stomach cancer. *Clin. Nucl. Med.* 20, 310–314. doi:10.1097/00003072-199504000-00005

Clézardin, P. (2017). Pathophysiology of bone metastases from solid malignancies. *Jt. Bone Spine* 84, 677–684. doi:10.1016/j.jbspin.2017.05.006

Daoud, A. Z., Mulholland, E. J., Cole, G., and McCarthy, H. O. (2019). MicroRNAs in pancreatic cancer: Biomarkers, prognostic, and therapeutic modulators. *BMC Cancer* 19, 1130. doi:10.1186/s12885-019-6284-y

de Koning, T. J., Snell, K., Duran, M., Berger, R., Poll-The, B-T., and Surtees, R. (2003). l-Serine in disease and development. *Biochem. J.* 371, 653–661. doi:10.1042/bj20021785

Dohi, O., Yagi, N., Majima, A., Horii, Y., Kitaichi, T., Onozawa, Y., et al. (2017). Diagnostic ability of magnifying endoscopy with blue laser imaging for early gastric cancer: A prospective study. *Gastric Cancer* 20, 297–303. doi:10.1007/s10120-016-0620-6

Dweep, H., Gretz, N., and Sticht, C. (2014). "miRWalk database for miRNA–target interactions," in *RNA mapping. Methods in molecular biology*. Editors M. L. Alvarez and M. Nourbakhsh (New York, NY: Springer), 289–305. doi:10.1007/978-1-4939-1062-5_25

Falzone, L., Scola, L., Zanghì, A., Biondi, A., Di Cataldo, A., Libra, M., et al. (2018). Integrated analysis of colorectal cancer microRNA datasets: Identification of microRNAs associated with tumor development. *Aging* 10, 1000–1014. doi:10.18632/aging.101444

Fan, R., Zhong, J., Zheng, S., Wang, Z., Xu, Y., Li, S., et al. (2014). MicroRNA-218 inhibits gastrointestinal stromal tumor cell and invasion by targeting KIT. *Tumour Biol.* 35, 4209–4217. doi:10.1007/s13277-013-1551-z

Feng, W., Yang, J., Song, W., and Xue, Y. (2021). Crosstalk between heart failure and cognitive impairment via hsa-miR-933/RELB/CCL21 pathway. *Biomed. Res. Int.* 2021, 2291899–2291916. doi:10.1155/2021/2291899

Gao, C., Zhang, Z., Liu, W., Xiao, S., Gu, W., and Lu, H. (2009). Reduced microRNA-218 expression is associated with high nuclear factor kappa B activation in gastric cancer. *Cancer* 116 (1), 41–49. doi:10.1002/cncr.24743

Goldman, M. J., Craft, B., Hastie, M., Repečka, K., McDade, F., Kamath, A., et al. (2020). Visualizing and interpreting cancer genomics data via the Xena platform. *Nat. Biotechnol.* 38, 675–678. doi:10.1038/s41587-020-0546-8

Hang, W., Feng, Y., Sang, Z., Yang, Y., Zhu, Y., Huang, Q., et al. (2018). Downregulation of miR-145-5p in cancer cells and their derived exosomes may contribute to the development of ovarian cancer by targeting CT. *Int. J. Mol. Med.* 43 (1), 256–266. doi:10.3892/ijmm.2018.3958

Hansford, S., Kaurah, P., Li-Chang, H., Woo, M., Senz, J., Pinheiro, H., et al. (2015). Hereditary diffuse gastric cancer syndrome: *CDH1* mutations and beyond. *JAMA Oncol.* 1, 23–32. doi:10.1001/jamaoncol.2014.168

Hänzelmann, S., Castelo, R., and Guinney, J. (2013). Gsva: Gene set variation analysis for microarray and RNA-seq data. *BMC Bioinforma.* 14, 7. doi:10.1186/1471-2105-14-7

Hart, C. E., Race, V., Achouri, Y., Wiame, E., Sharrard, M., Olpin, S. E., et al. (2007). Phosphoserine aminotransferase deficiency: A novel disorder of the serine biosynthesis pathway. *Am. J. Hum. Genet.* 80, 931–937. doi:10.1086/517888

Jin, Y., Wang, M., Hu, H., Huang, Q., Chen, Y., and Wang, G. (2018). Overcoming stemness and chemoresistance in colorectal cancer through miR-195-5p-modulated inhibition of notch signaling. *Int. J. Biol. Macromol.* 117, 445–453. doi:10.1016/j.ijbiomac.2018.05.151

Joshi, S. S., and Badgwell, B. D. (2021). Current treatment and recent progress in gastric cancer. *Ca. Cancer J. Clin.* 71, 264–279. doi:10.3322/caac.21657

Kowal, J., Arras, G., Colombo, M., Jouve, M., Morath, J. P., Primdal-Bengtson, B., et al. (2016). Proteomic comparison defines novel markers to characterize heterogeneous populations of extracellular vesicle subtypes. *Proc. Natl. Acad. Sci. U. S. A.* 113, E968–E977. doi:10.1073/pnas.1521230113

Lacny, S., Wilson, T., Clement, F., Roberts, D. J., Faris, P. D., Ghali, W. A., et al. (2015). Kaplan-meier survival analysis overestimates the risk of revision arthroplasty: A meta-analysis. *Clin. Orthop. Relat. Res.* 473, 3431–3442. doi:10.1007/s11999-015-4235-8

Lee, J., Lim, T., Uhm, J. E., Park, K. W., Park, S. H., Lee, S. C., et al. (2007). Prognostic model to predict survival following first-line chemotherapy in patients with metastatic gastric adenocarcinoma. *Ann. Oncol.* 18, 886–891. doi:10.1093/annonc/mdl501

Li, X., Ma, C., Luo, H., Zhang, J., Wang, J., and Guo, H. (2020). Identification of the differential expression of genes and upstream microRNAs in small cell lung cancer compared with normal lung based on bioinformatics analysis. *Medicine* 99, e19086. doi:10.1097/MD.0000000000019086

Li, Y., Feng, A., Zheng, S., Chen, C., and Lyu, J. (2022). Recent estimates and predictions of 5-year survival in patients with gastric cancer: A model-based period analysis. *Cancer Control.* 29, 10732748221099227. doi:10.1177/10732748221099227

Liu, F., Qiu, F., Fu, M., Chen, H., and Wang, H. (2020). Propofol reduces epithelial to mesenchymal transition, invasion and migration of gastric cancer cells through the MicroRNA-195-5p/snail Axis. *Med. Sci. Monit.* 6, e920981. doi:10.12659/MSM.920981

Liu, J., Wang, P., Zhang, P., Zhang, X., Du, H., Liu, Q., et al. (2019). An integrative bioinformatics analysis identified miR-375 as a candidate key regulator of malignant breast cancer. *J. Appl. Genet.* 60, 335–346. doi:10.1007/s13353-019-00507-w

Liu, W., Chen, H., and Wang, D. (2021). Protective role of astragaloside IV in gastric cancer through regulation of microRNA-195-5p-mediated PD-L1. *Immunopharmacol. Immunotoxicol.* 43, 443–451. doi:10.1080/08923973.2021.1936013

Lott, P. C., and Carvajal-Carmona, L. G. (2018). Resolving gastric cancer aetiology: An update in genetic predisposition. *Lancet. Gastroenterol. Hepatol.* 3, 874–883. doi:10.1016/S2468-1253(18)30237-1

Machlowska, J., Baj, J., Sitarz, M., Maciejewski, R., and Sitarz, R. (2020). Gastric cancer: Epidemiology, risk factors, classification, genomic characteristics and treatment strategies. *Int. J. Mol. Sci.* 21, E4012. doi:10.3390/ijms21114012

Metcalf, S., Dougherty, S., Kruer, T., Hasan, N., Biyik-Sit, R., Reynolds, L., et al. (2020). Selective loss of phosphoserine aminotransferase 1 (PSAT1) suppresses migration, invasion, and experimental metastasis in triple negative breast cancer. *Clin. Exp. Metastasis* 37, 187–197. doi:10.1007/s10585-019-10000-7

Mikami, J., Kimura, Y., Makari, Y., Fujita, J., Kishimoto, T., Sawada, G., et al. (2017). Clinical outcomes and prognostic factors for gastric cancer patients with bone metastasis. *World J. Surg. Oncol.* 15, 8. doi:10.1186/s12957-016-1091-2

Montero-Conde, C., Graña-Castro, O., Martín-Serrano, G., Martínez-Montes, Á. M., Zarzuela, E., Muñoz, J., et al. (2020). Hsa-miR-139-5p is a prognostic thyroid cancer marker involved in HNRNPF-mediated alternative splicing. *Int. J. Cancer* 146, 521–530. doi:10.1002/ijc.32622

Montrose, D. C., Saha, S., Foronda, M., McNally, E. M., Chen, J., Zhou, X. K., et al. (2021). Exogenous and endogenous sources of serine contribute to colon cancer metabolism, growth, and resistance to 5-fluorouracil. *Cancer Res.* 81, 2275–2288. doi:10.1158/0008-5472.CAN-20-1541

Ogawa, T., Ishida-Kitagawa, N., Tanaka, A., Matsumoto, T., Hirouchi, T., Akimaru, M., et al. (2006). A novel role of l-serine (l-Ser) for the expression of nuclear factor of activated T cells (NFAT)2 in receptor activator of nuclear factor κB ligand (RANKL)-induced osteoclastogenesis *in vitro*. *J. Bone Min. Metab.* 24, 373–379. doi:10.1007/s00774-006-0705-0

Oliveira, C., Pinheiro, H., Figueiredo, J., Seruca, R., and Carneiro, F. (2015). Familial gastric cancer: Genetic susceptibility, pathology, and implications for management. *Lancet. Oncol.* 16, e60–e70. doi:10.1016/S1470-2045(14)71016-2

Park, J. M., Song, K. Y., O, J. H., Kim, W. C., Choi, M-G., and Park, C. H. (2013). Bone recurrence after curative resection of gastric cancer. *Gastric Cancer* 16, 362–369. doi:10.1007/s10120-012-0193-y

Pollari, S., Käkönen, S-M., Edgren, H., Wolf, M., Kohonen, P., Sara, H., et al. (2011). Enhanced serine production by bone metastatic breast cancer cells stimulates osteoclastogenesis. *Breast Cancer Res. Treat.* 125, 421–430. doi:10.1007/s10549-010-0848-5

Qiu, M-Z., Shi, S-M., Chen, Z-H., Yu, H-E., Sheng, H., Jin, Y., et al. (2018). Frequency and clinicopathological features of metastasis to liver, lung, bone, and brain from gastric cancer: A SEER-based study. *Cancer Med.* 7, 3662–3672. doi:10.1002/cam4.1661

Rezaei, Z., Sebzari, A., Kordi-Tamandani, D. M., and Dastjerdi, K. (2019). Involvement of the dysregulation of miR-23b-3p, miR-195-5p, miR-656-5p, and miR-340-5p in trastuzumab resistance of HER2-positive breast cancer cells and system biology approach to predict their targets involved in resistance. *DNA Cell Biol.* 38, 184–192. doi:10.1089/dna.2018.4427

Rich, J. T., Neely, J. G., Paniello, R. C., Voelker, C. C. J., Nussenbaum, B., and Wang, E. W. (2010). A practical guide to understanding Kaplan-Meier curves. *Otolaryngol. Head. Neck Surg.* 143, 331–336. doi:10.1016/j.otohns.2010.05.007

Rossi, M., Battafarano, G., D'Agostini, M., and Del Fattore, A. (2018). The role of extracellular vesicles in bone metastasis. *Int. J. Mol. Sci.* 19, 1136. doi:10.3390/ijms19041136

Sticht, C., De La Torre, C., Parveen, A., and Gretz, N. (2018). miRWalk: An online resource for prediction of microRNA binding sites. *PLoS ONE* 13, e0206239. doi:10.1371/journal.pone.0206239

Sun, C., Ma, S., Chen, Y., Kim, N. H., Kailas, S., Wang, Y., et al. (2022). Diagnostic value, prognostic value, and immune infiltration of LOX family members in liver cancer: Bioinformatic analysis. *Front. Oncol.* 12, 843880. doi:10.3389/fonc.2022.843880

Sung, H., Ferlay, J., Siegel, R. L., Laversanne, M., Soerjomataram, I., Jemal, A., et al. (2021). Global cancer statistics 2020: GLOBOCAN estimates of incidence and mortality worldwide for 36 cancers in 185 countries. *Ca. Cancer J. Clin.* 71, 209–249. doi:10.3322/caac.21660

Tian, L-L., Qian, B., Jiang, X-H., Liu, Y-S., Chen, T., Jia, C-Y., et al. (2021). MicroRNA-497-5p is downregulated in hepatocellular carcinoma and associated with tumorigenesis and poor prognosis in patients. *Int. J. Genomics* 2021, 6670390–6670416. doi:10.1155/2021/6670390

Tiedemann, K., Sadvakassova, G., Mikolajewicz, N., Juhas, M., Sabirova, Z., Tabariès, S., et al. (2019). Exosomal release of L-plastin by breast cancer cells facilitates metastatic bone osteolysis. *Transl. Oncol.* 12, 462–474. doi:10.1016/j.tranon.2018.11.014

Turkoz, F. P., Solak, M., Kilickap, S., Ulas, A., Esbah, O., Oksuzoglu, B., et al. (2014). Bone metastasis from gastric cancer: The incidence, clinicopathological features, and influence on survival. *J. Gastric Cancer* 14, 164–172. doi:10.5230/jgc.2014.14.3.164

Wang, W., Zhou, R., Wu, Y., Liu, Y., Su, W., Xiong, W., et al. (2019). PVT1 promotes cancer progression via MicroRNAs. *Front. Oncol.* 9, 609. doi:10.3389/fonc.2019.00609

Wang, Y., Wei, Y., Fan, X., Xu, F., Dong, Z., Cheng, S., et al. (2022). Construction of a miRNA signature using support vector machine to identify microsatellite instability status and prognosis in gastric cancer. *J. Oncol.* 6586354, 1–13. doi:10.1155/2022/6586354

Wang, Z., Jensen, M. A., and Zenklusen, J. C. (2016). "A practical guide to the cancer Genome Atlas (TCGA)," in *Statistical genomics. Methods in molecular biology*. Editors E. Mathé and S. Davis (New York, NY: Springer), 111–141. doi:10.1007/978-1-4939-3578-9_6

Wu, J-Y., Qin, J., Li, L., Zhang, K-D., Chen, Y-S., Li, Y., et al. (2021). Roles of the immune/methylation/autophagy landscape on single-cell genotypes and stroke risk in breast cancer microenvironment. *Oxid. Med. Cell. Longev.* 2021, 5633514. doi:10.1155/2021/5633514

Wu, K., Feng, J., Lyu, F., Xing, F., Sharma, S., Liu, Y., et al. (2021). Exosomal miR-19a and IBSP cooperate to induce osteolytic bone metastasis of estrogen receptor-positive breast cancer. *Nat. Commun.* 12, 5196. doi:10.1038/s41467-021-25473-y

Xiaobin, C., Zhaojun, X., Tao, L., Tianzeng, D., Xuemei, H., Fan, Z., et al. (2022). Analysis of related risk factors and prognostic factors of gastric cancer with bone metastasis: A SEER-based study. *J. Immunol. Res.* 2022, 3251051. doi:10.1155/2022/3251051

Xie, Y., Rong, L., He, M., Jiang, Y., Li, H., Mai, L., et al. (2021). LncRNA SNHG3 promotes gastric cancer cell proliferation and metastasis by regulating the miR-139-5p/MYB axis. *Aging* 13, 25138–25152. doi:10.18632/aging.203732

Xuan, Z., Ma, T., Qin, Y., and Guo, Y. (2022). Role of ultrasound imaging in the prediction of TRIM67 in brain metastases from breast cancer. *Front. Neurol.* 13, 889106. doi:10.3389/fneur.2022.889106

Yamamoto, N., Kinoshita, T., Nohata, N., Itesako, T., Yoshino, H., Enokida, H., et al. (2013). Tumor suppressive microRNA-218 inhibits cancer cell migration and invasion by targeting focal adhesion pathways in cervical squamous cell carcinoma. *Int. J. Oncol.* 42, 1523–1532. doi:10.3892/ijo.2013.1851

Yan, L., Wang, A., Lv, Z., Yuan, Y., and Xu, Q. (2021). Mitochondria-related core genes and TF-miRNA-hub mrDEGs network in breast cancer. *Biosci. Rep.* 41, BSR20203481. doi:10.1042/BSR20203481

Yang, M., Liu, R., Sheng, J., Liao, J., Wang, Y., Pan, E., et al. (2013). Differential expression profiles of microRNAs as potential biomarkers for the early diagnosis of esophageal squamous cell carcinoma. *Oncol. Rep.* 29, 169–176. doi:10.3892/or.2012.2105

Yao, X., Mao, Y., Wu, D., Zhu, Y., Lu, J., Huang, Y., et al. (2021). Exosomal circ_0030167 derived from BM-MSCs inhibits the invasion, migration, proliferation and stemness of pancreatic cancer cells by sponging miR-338-5p and targeting the Wif1/Wnt8/β-catenin axis. *Cancer Lett.* 512, 38–50. doi:10.1016/j.canlet.2021.04.030

Zhang, P., and Liu, B. (2021). Integrative bioinformatics analysis reveals that infarct-mediated overexpression of potential miR-662/CREB1 pathway-induced neuropeptide VIP is associated with the risk of atrial fibrillation: A correlation analysis between myocardial electrophysiology and neuroendocrine. *Dis. Markers* 2021, 81166331–81166417. doi:10.1155/2021/8116633

Zhao, B., and Jiang, X. (2022). hsa-miR-518-5p/hsa-miR-3135b regulates the REL/SOD2 pathway in ischemic cerebral infarction. *Front. Neurol.* 13, 852013. doi:10.3389/fneur.2022.852013

Zou, J., Liao, X., Zhang, J., and Wang, L. (2019). Dysregulation of miR-195-5p/-218-5p/BIRC5 axis predicts a poor prognosis in patients with gastric cancer. *J. Biol. Regul. Homeost. Agents* 33, 1377–1385. doi:10.23812/19-146-A

frontiers | Frontiers in Genetics

TYPE Original Research
PUBLISHED 24 August 2022
DOI 10.3389/fgene.2022.994003

OPEN ACCESS

EDITED BY
Qian Wang,
Tai'an City Central Hospital, China

REVIEWED BY
Wenquan Hu,
Chongqing Medical University, China
Pengzhi Dong,
Tianjin University of Traditional Chinese Medicine, China

*CORRESPONDENCE
Meixiu Jiang,
jiangmxs@163.com

SPECIALTY SECTION
This article was submitted to Cancer Genetics and Oncogenomics, a section of the journal Frontiers in Genetics

RECEIVED 14 July 2022
ACCEPTED 27 July 2022
PUBLISHED 24 August 2022

CITATION
Li S and Jiang M (2022), Elevated insulin-like growth factor 2 mRNA binding protein 1 levels predict a poor prognosis in patients with breast carcinoma using an integrated multi-omics data analysis. *Front. Genet.* 13:994003. doi: 10.3389/fgene.2022.994003

Elevated insulin-like growth factor 2 mRNA binding protein 1 levels predict a poor prognosis in patients with breast carcinoma using an integrated multi-omics data analysis

Shiqi Li[1] and Meixiu Jiang[2]*

[1]Queen Mary School, Nanchang University, Nanchang, China, [2]The National Engineering Research Center for Bioengineering Drugs and the Technologies, Institute of Translational Medicine, Nanchang University, Nanchang, China

Background: Insulin-like growth factor 2 mRNA binding protein 1 (IGF2BP1) controls the cytoplasmic fate of certain mRNAs and is hypothesized to predict a poor patient prognosis in several malignant tumors. However, the prognostic relevance of IGF2BP1 in breast cancer remains debatable.

Methods: We interrogated large publicly available datasets from the Gene Expression Omnibus (GEO), The Cancer Genome Atlas (TCGA), and cBioportal databases to analyze the genetic alterations in the expression levels of IGF2BP1 in patients with invasive breast carcinoma (BRCA), and to discern the prognostic value of IGF2BP1 in BRCA. We applied Gene Ontology (GO), the Kyoto Encyclopedia of Genes and Genome (KEGG), and gene set enrichment analysis (GSEA) to uncover a functional association between IGF2BP1 and BRCA using differentially expressed genes (DEGs), and we screened genes and proteins related to BRCA.

Results: We determined that both genetic alterations in IGF2BP1 (approximately 10%) and an increase in IGF2BP1 mRNA levels were related to certain cancer subtypes and an unfavorable prognosis in BRCA patients, and we then established an OS nomogram upon our multivariate regression model. The DEGs and IGF2BP1-correlated genes/proteins that implied the involvement of cornification, keratinization, drug/xenobiotic metabolism by cytochrome P450, chemical carcinogenesis, cell interactions, and cell adhesion to the extracellular matrix (ECM) pathways with respect to the prognostic relevance of IGF2BP1.

Conclusion: In summary, our results indicated that both genetic alterations in IGF2BP1 and increased levels of IGF2BP1 mRNA and protein predict a poor patient prognosis in BRCA patients.

KEYWORDS

IGF2BP1, BRCA, prognosis, enrichment analysis, differentially expressed genes, genetic correlation

1 Introduction

Breast cancer constitutes the most prevalent form of cancer found in women globally, and its incidence in China is rising annually in recent years. It is firmly established that breast cancer is a biologically heterogeneous disease, and four intrinsic molecular subtypes (luminal A, luminal B, HER2-positive, and basal-like) facilitate prognostication. However, although prediction of therapeutic has improved survival over the past 30 years relative to clinicopathologic categories, breast cancer remains one of the leading causes of cancer death in women principally due to recurrence, metastasis, or therapeutic failure (e.g., with acquired drug resistance to tamoxifen). Given the heterogeneous clinical outcomes of any one subtype, the challenge is now to identify tumors that portend a less favorable prognosis. Growth, metastasis, and even responses to breast cancer therapy are closely related to deregulation, mutation, and epigenetic mechanisms with respect to certain genes, and the use of integrated multi-omics such as integrated genomics, transcriptomics, and proteomics is thus critical to providing prognostic factors and to refining clinically relevant subtypes by data-mining (Perou et al., 2000; Sorlie et al., 2003).

IGF2BP1—also known as IMP1, ZBP1, CRDBP, and VICKZ1—belongs to the insulin-like growth factor 2 mRNA-binding protein family, the IGF2BPs. The proteins in this family bind to the mRNAs of certain genes and regulate their translation, decay, and transport, or promote the formation of "stable" protein–mRNA complexes (Huang et al., 2018a). There are still numerous unidentified target mRNAs for IGF2BP1—including ACTB, CTNNB1, GLI1, IGF2, MAPK4, MDR1, PPP1R9B, CD44, MYC, PTEN, and BTRC which indicate that this protein modulates multiple important aspects of cellular function during both normal development and cancer (Bell et al., 2013). In fact, IGF2BP1 has been found to be frequently overexpressed in many cancers, such as head and neck squamous cell carcinoma (HNSCC) (Paramasivam et al., 2021), melanoma (Kim et al., 2018; Mahapatra et al., 2019), cervical cancer (Wang et al., 2018), ovarian carcinoma (Kobel et al., 2007; Mahapatra et al., 2017) and lung cancer (Shi et al., 2017). Because of its strong correlation with unfavorable prognosis and drug resistance, IGF2BP1 is also considered one of the most promising therapeutic targets (Bell, et al., 2013; Huang et al., 2018b; Kim, et al., 2018).

A role for IGF2BP1 in breast cancer, however, remains controversial. Some investigative groups reported that IGF2BP1 was downregulated and that it suppressed the invasive phenotype of human breast carcinoma cells both *in vitro* (Gu et al., 2012) and in a mouse xenograft model through the regulation of its target mRNAs (Wang et al., 2016) or *via* an interaction with the lncRNA urethral carcinoma-associated 1 (UCA1) (Zhou et al., 2018). In contrast, another group reported that IGF2BP1 was reactivated in breast cancer cells by beta-catenin, and that this interaction stabilized beta-catenin (Gu et al., 2008). To clarify this area of focus, we analyzed the functional relationships between IGF2BP1 and clinical values in patients with invasive breast carcinoma (BRCA) *via* data mining of multiple databases and enrichment analysis.

2 Materials and methods

2.1 Correlation between genetic alterations in insulin-like growth factor 2 mRNA binding protein 1 and breast cancer prognosis using cBioPortal

We analyzed the genomic profiles of IGF2BP1 using a dataset from the Molecular Taxonomy of Breast Cancer International Consortium (METABRIC) and retrieved an integrated genomic and transcriptomic targeted sequencing of 2,509 primary breast tumors and 548 matched normal tissues (Curtis et al., 2012; Pereira et al., 2016) in cBioPortal (www.cbioportal.org) (Gao et al., 2013). IGF2BP1 mRNA levels (RNA Seq V2 RSEM) were also determined and visualized by constructing a heatmap with cBioPortal. Comparisons of survival (overall survival [OS] or relapse free survival [RFS]) and clinical attributes between the genetically altered IGF2BP1 group and nonaltered group were then executed using genome data and clinical data in cBioportal.

2.2 Insulin-like growth factor 2 mRNA binding protein 1 expression levels in TCGA-breast carcinoma

RNAseq TPM data were obtained from UCSC XENA (https://xenabrowser.net/datapages/) for the TCGA and GTEx samples using the Toil pipeline (Vivian et al., 2017), and then log2-transformed. We evaluated the comparisons of IGF2BP1 expression in 33 types of human cancers and adjacent normal tissues (n = 15,776), in 1,109 unmatched BRCA tissues and 292 normal tissues, and in 112 paired BRCA tissues and adjacent normal breast issues. Gene-expression profiles of GSE7904 were further extracted from the GEO database to validate the expression of IGF2BP1 in BRCA.

2.3 Correlation analysis of insulin-like growth factor 2 mRNA binding protein 1 expression and clinical value

The histologic information and intrinsic molecular subtype information were retrieved from the TCGA database, and we conducted a correlation analysis of IGF2BP1 expression and breast cancer subtypes using ggplot2 (version 3.3.3) in R. We

determined the differences between groups using the nonparametric Kruskal–Wallis test on ranks, and Student's t-test or paired t-test for parametric data.

2.4 Correlation analysis of insulin-like growth factor 2 mRNA binding protein 1 expression with breast cancer prognosis

Our cohort including 1,082 patients was divided into low and high-expression subgroups according to the median level of IGF2BP1 mRNA. Kaplan–Meier curves for OS or/disease-specific survival (DSS) rates were generated using the survminer package (version 0.4.9) with gene expression data from TCGA-BRCA and the supplementary dataset from the TCGA pan-cancer clinical data resource (TCGA-CDR) (Liu et al., 2018). We utilized log-rank test to compare survival curves among high- and low- expression subgroups using the survival R package (version 3.2–10), and the differences of $p < 0.05$ were considered statically significant.

2.5 Creation of nomogram model

Univariate and multivariate Cox regression analyses were used to assess the effects of selected variables on OS. Variables that were significant upon univariate Cox regression analysis ($p < 0.1$) were subsequently subjected to multivariate Cox regression analysis, and we developed nomograms using the nomogram package in R with the independent predictors identified in the Cox proportional hazards model. The nomogram-predicted survival probabilities were compared with the observed survival probabilities by Cox analysis and visualized in the calibration curve using the rms (version 3.6.3) and survival packages (version 3.2–10) (Liu, et al., 2018).

2.6 Biological functional analysis and enrichment of differentially expressed genes

We downloaded and analyzed gene expression data of TCGA-BRCA in HTSeq-TPM, and compared the expression profiles (HTSeq-TPM) between the high- and low-IGF2BP1 mRNA expression groups so that to identify the DEGs with DESeq2 (version 1.26.0) (Love et al., 2014), applying filtering thresholds of |log2 fold-change| > 1.0 and adjusted $p < 0.05$. Then DEGs with |log2 fold change| > 2.0 and adjusted $p < 0.05$ were subjected to functional analysis with the clusterProfiler R package and the org. Hs.eg.db package for biological process GO terms and KEGG pathways (Yu et al., 2012). Gene set enrichment analysis (GSEA) against the MSigDB category (c2. cp.v7.2. symbols.gmt) was also performed to assess the enrichment of gene sets between IGF2BP1 high-expression and low-expression groups using the clusterProfiler R package (Version 3.14.3) (Subramanian et al., 2005). A false discovery rate (FDR) of <0.25 and p. adjust<0.05 were considered to reflect significant enrichment.

2.7 Screening of insulin-like growth factor 2 mRNA binding protein 1 correlated genes and proteins from different databases for breast carcinoma

Gene expression HTSeq-FPKM data from the TCGA-BRCA database were downloaded from TCGA, converted to TPM using the formula TPM = (FPKM ×106)/(sum of FPKM), and then log2 transformed. The IGF2BP1-correlated genes were screened with Pearson's correlation coefficient ($|r| > 0.3$ and $p < 0.05$) using the stat package in R (version 3.6.3). The top 10 IGF2BP1-correlated genes, proteins, and lncRNAs were visualized with R ggplot2 (version 3.3.3), respectively. We also zbscreened correlated proteins from the QExact platform proteome datasets with LinkedOmics (Vasaikar et al., 2018) which is a unique online analytical platform that provides comprehensive multi-omics data analysis using default settings, and visualized them with heatmaps.

2.8 Statistical methods

We employed the R package to perform statistical analysis. Differences between groups were compared using the Student's t-test, paired t-test, or nonparametric Wilcoxon rank-sum test, as appropriate. We computed correlations in R using cor with options for Pearson or Spearman correlation tests, as appropriate. Kaplan-Meier plots were generated and log-rank tests were executed to identify significant differences between survival curves, and differences of $p < 0.05$ were considered statistically significant.

3 Results

3.1 Relationship between genetic alterations in insulin-like growth factor 2 mRNA binding protein 1 and survival and clinical attributes in the cBioportal dataset

To elucidate the role of IGF2BP1 in breast cancer, we first interrogated large publicly available datasets from METABRIC using cBioPortal and analyzed genetic alterations in IGF2BP1 that included mRNA amplifaction, deletion or level changes and their correlation with clinical values. Using a dataset from the targeted sequences of 2,509 primary breast tumors and

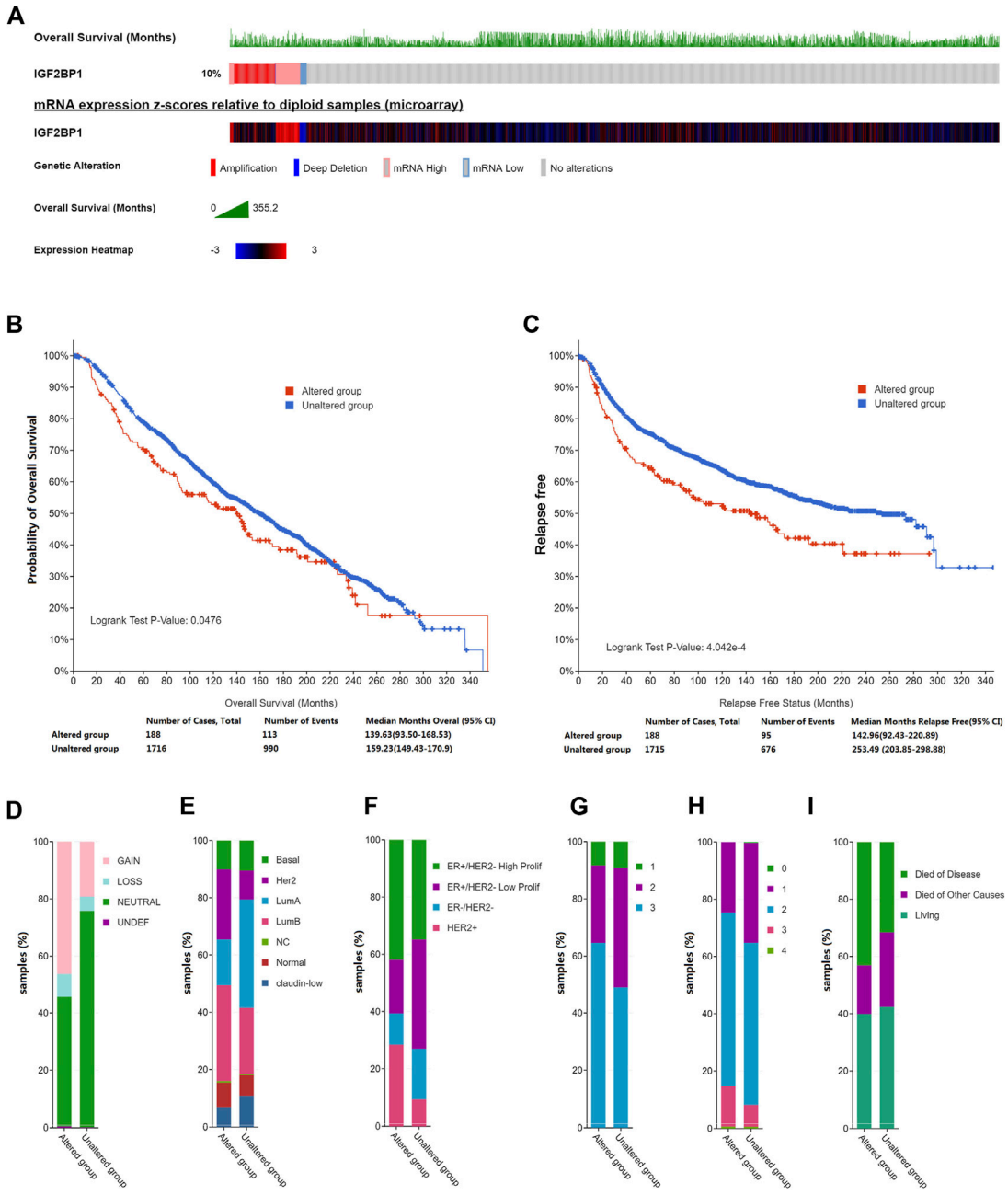

FIGURE 1
Genetic alterations in IGF2BP1 and their relation to clinical attributes by cBioportal. **(A)**, Genetic alterations and mRNA expression of IGF2BP1. **(B)** and **(C)**, The relationship between genetic alterations in IGF2BP1 and OS or RFS. **(D–I)**, The relationship between genetic alterations of IGF2BP1 and clinical attributes.

548 matched normal controls (Curtis, et al., 2012; Pereira, et al., 2016), we analyzed IGF2BP1-gene alterations in 1904 patients/samples with available mutation and CNA data and observed a change for IGF2BP1 mRNA in breast cancer of 10% (188/1904). Amplification and elevated mRNA levels accounted for the majority of the genetic alterations in IGF2BP1 (Figure 1A). Genetically altered IGF2BP1 predicted a poor prognosis for both OS and relapse-free status ($p < 0.05$, Figures 1B,C), while alterations in IGF2BP1 demonstrated a robust relationship with clinical attributes. Specifically, the IGF2BP1 altered group exhibited a greater incidence of HER2 mRNA gain (Figure 1D), higher proportion of HER2 and luminal B

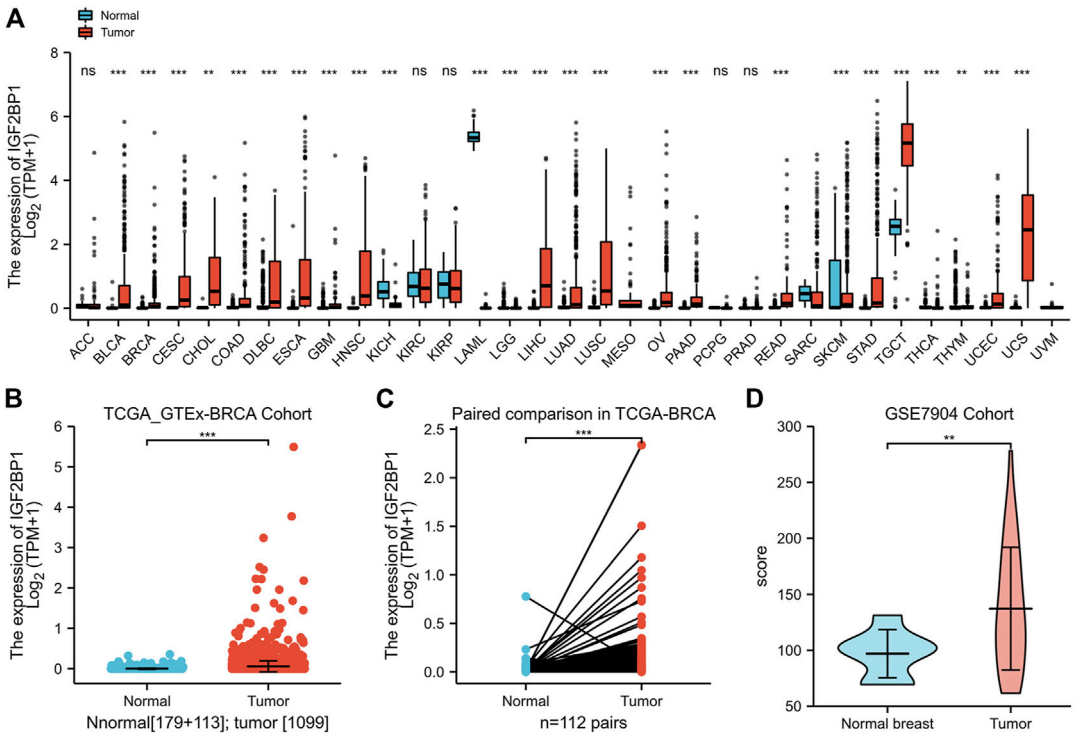

FIGURE 2
Expression of IGF2BP1 in various cancers and BRCA in particular. **(A)**, The expression of IGF2BP1 in various cancers. **(B)**, The expression of IGF2BP1 in TCGA-GTEx-BRCA cohort samples. **(C)**, The expression of IGF2BP1 in TCGA -BRCA paired samples. **(D)**, The expression of IGF2BP1 in the GSE7904 cohort. *$p < 0.05$; **$p < 0.01$; ***$p < .001$.

subtypes by prediction analysis of microarray 50 (PAM50) (Figure 1E) or HER2 and ER+/HER2- with high proliferating subtypes by three genes classifiers (Figure 1F), a tendancy to manifest, grade-3 histology (Figure 1G), higher clinical tumor stages (Figure 1H), and an increased probability of disease-specific death (Figure 1I).

3.2 Insulin-like growth factor 2 mRNA binding protein 1 expression is augmented in breast cancer tissues using TCGA and gene expression omnibus databases

As amplification and elevated mRNA levels accounted for most of the genetic alterations of prognostic IGF2BP1, we consequently analyzed mRNA levels in a large patient cohort of 15,776 samples with 33 types of human cancer and 31 types of adjacent normal tissues in TCGA datasets and GTEx samples accessible through UCSC Xena. We ascertained IGF2BP1 was significantly upregulated in most cancer types as compared with the corresponding normal tissues, but not in adrenocortical carcinoma (ACC), kidney, renal clear cell carcinoma (KIRC), kidney renal papillary cell carcinoma (KIRP), pheochromocytoma and paraganglioma (PCPG), and prostate adenocarcinoma (PRAD) (Figure 2A). We specifically noted that IGF2BP1 was more highly expressed in BRCA tissues in both unmatched (tumor, $n = 1,109$ vs. adjacent and normal, $n = 292$) and paired (112 paired tumors vs. adjacent normal) comparisons of TCGA-BRCA datasets compared to normal tissues (Figures 2B,C). A majority of paired samples also exhibited upregulation, while a minute subset demonstrated downregulation of IGF2BP1 in cancer tissue (Figure 2C). Our analysis of gene expression data of the GSE7904 cohort (seven normals vs. 43 tumors) validated the overexpression of IGF2BP1 at the mRNA level (Figure 2D).

3.3 Insulin-like growth factor 2 mRNA binding protein 1 expression correlates with histologic and intrinsic subtyping of breast cancer

Using the expression and clinical data from the TCGA-BRCA dataset, we demonstrated that the expression of IGF2BP1 mRNA was markedly correlated with histologic type (Figure 3A), and that molecular subtypes of breast cancer were

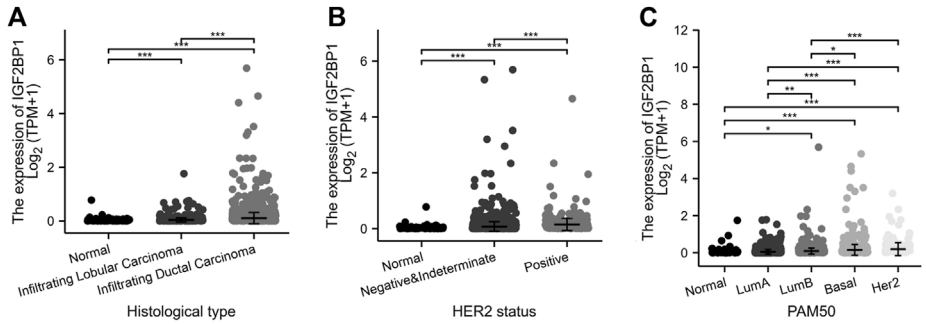

FIGURE 3
Relationship between IGF2BP1 expression and histologic and molecular features in TCGA-BRCA datasets. **(A)**, Relationship between IGF2BP1 expression and histologic types. **(B)**, Relationship between IGF2BP1 expression and HER2 status of breast cancer. **(C)**, Relationship between IGF2BP1 expression and PAM50 molecular subtypes of breast cancer. *$p < 0.05$; **$p < 0.01$; ***$p <.001$.

defined by HER2 status (Figure 3B) or PAM50 (Figure 3C). In addition to discriminating cancerous from normal cells, the mRNA levels of IGF2BP1 were found to be significantly increased in certain subgroups of breast cancer. For example, the highest level was found in invasive ductal carcinoma (IDC) ($n = 772$) when compared to invasive lobular carcinoma (ILC) ($n = 205$) and normal breast tissues ($n = 111$), as well as in the HER2-positive subgroup ($n = 157$) when compared to the HER2-negative group ($n = 570$) or normal breast tissues ($n = 111$). Our data revealed IGF2BP1 at differential levels among intrinsic subtypes of breast cancer (Normal, $n = 40$; LumA, $n = 562$; LumB, $n = 204$; Basal, $n = 195$; Her2, $n = 82$: Kruskal–Wallis test, $p < 0.001$), which raised the question whether IGF2BP1 was related to breast cancer prognosis.

3.4 Relationships of insulin-like growth factor 2 mRNA binding protein 1 expression with OS and disease-specific survival in breast carcinoma patients in TCGA database

We divided the cohorts into low or high-expression subgroups according to the median expression of IGF2BP1 mRNA to compare IGF2BP1 expression-related outcomes of the patients. Kaplan–Meier curves for OS and DSS revealed that BRCA patients with high IGF2BP1 expression possessed a generally worse prognosis than patients with low IGF2BP1 expression ($p < 0.01$, Figures 4A,B). Further analysis indicated that high IGF2BP1 expression argued an unfavorable prognosis for both OS and DSS in the subgroups of IDC and women in postmenopausal status ($p < 0.01$, Figures 4C–F), while it was prognostic for DSS but not for OS in the subgroup that did not undergo radiation therapy (Figures 4G,H). The analysis of other subgroups (including histologic ILC subgroup, peri- and pre-menopausal status, HER2 status, ER status, and PR status) achieved no significant prognostic relevance with respect to IGF2BP1 overexpression (data not shown). The 5- and 10-year OS rates in the database were higher among patients with low IGF2BP1 expression relative to those with high expression (85.95 ± 2.4% vs. 77.3 ± 2.8% and 58.2 ± 5.8% vs.46.1 ± 6.5%, respectively; $p < 0.001$).

3.5 Generation of nomogram model

Using survival data from 876 of 1,082 patient cohorts in the TCGA database, we further implemented uni- and multivariate survival analyses using Cox proportional hazards models for survival-related factors; and the results showed that T stage, N stage, and M stage of the tumor; PAM50 subtyping; and IGF2BP1 expression were predictors of OS upon univariate Cox analysis. Importantly, N stage, M stage, and IGF2BP1 expression were independent variables in our multivariate Cox analysis, with a concordance index of 0.694 (0.661–0.726) (Table 1). When we then constructed a nomogram for predicting overall survival at 5 years, 10 years, and 20 years based on these models (Figure 5A), we discern that the nomogram calibration plot showed acceptable agreement between nomogram-predicted and observed events (an example of five-year OS is depicted in Figure 5B.

3.6 Functional-enrichment analysis of differentially expressed genes between high and low-insulin-like growth factor 2 mRNA binding protein 1 expression samples

To explore the potential prognostic mechanisms underlying IGF2BP1 action, we analyzed DEGs in the high- and low-IGF2BP1 expression groups and identified a total of 2,405 DEGs of 56,493 genes, of which 2,199 genes were upregulated and

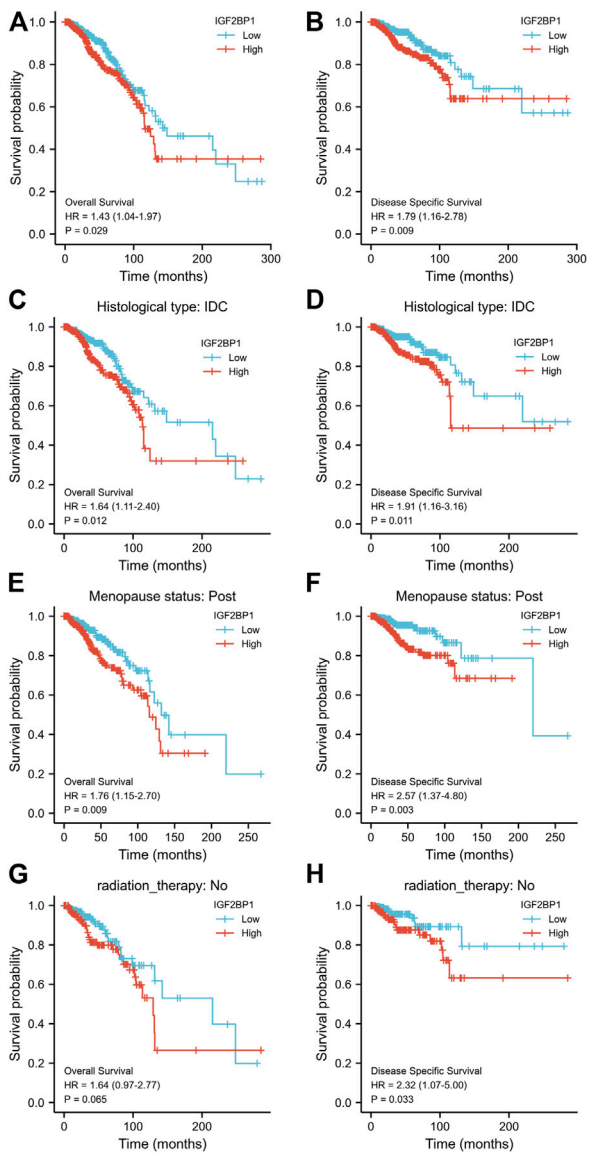

FIGURE 4
Relationship between IGF2BP1 expression and the prognosis of BRCA patients in TCGA database. **(A)** and **(B)**, Comparison of Kaplan–Meier curves for OS or DSS between high- and low-IGF2BP1 expressing groups. **(C–H)**, Compared Kaplan–Meier curves for OS or DSS between high- and low-IGF2BP1 expression in subgroups of IDC, post menopause or without radiation therapy, respectively.

206 were downregulated. When filtering with |log2 fold-change| > 1.5, we identified 875 genes, of which 828 were upregulated and 47 downregulated, and 303 genes were identified when filtering with |log2 fold-change| > 2.0, with 290 upregulated and 13 downregulated (Supplementary Table S1). DEG expression is displayed in Figure 6A in the volcano plot encompassing the top five upregulated and five downregulated genes. Functional analysis of DEGs with a |log2 fold change|> 2.0 revealed 81 GO terms and 13 KEGG pathways at p. adj<0.05 and qvalue<0.2. The top GO terms were cornification, keratinization, keratinocyte differentiation, cornified envelope, keratin filament, glucuronosyltransferase activity, alcohol dehydrogenase (NADP+) activity, aldo-keto reductase (NADP) activity, and monocarboxylic acid binding for biological process (BP), molecular function (MF), and cellular component (CC). The top KEGG pathways were drug metabolism—cytochrome P450, metabolism of xenobiotics by cytochrome P450, and chemical carcinogenesis (Figure 6B, Supplementary Tables S2, S3). The GSEA-enrichment method and the Reactome pathway enrichment analysis for the DEG set exhibited some similar functionally relevant gene networks (Figure 6C). The 28 significantly enriched categories with FDR filtering (qvalue) < 0.25 and p. adjust<0.05 included formation of the cornified envelope (NES = 1.959; p. adjust = 0.020; FDR = 0.019), FCGR activation (NES = 1.942; p. adjust = 0.020; FDR = 0.019), CD22-mediated BCR regulation (NES = 1.979; p. adjust = 0.020; FDR = 0.019), integrin cell surface interactions (NES = 1.844; p. adjust = 0.020; FDR = 0.019), glucuronidation (NES = 1.792; p. adjust = 0.040; FDR = 0.038), and keratinization (NES = 1.788; p. adjust = 0.020; FDR = 0.019) (complete GSEA results are provided in Supplementary Table S4).

3.7 Functional enrichment analysis of correlated genes between high and low-insulin-like growth factor 2 mRNA binding protein 1 expression samples

We then analyzed IGF2BP1-correlated genes and proteins from both the RNAseq dataset and proteome datasets to a screen for IGF2BP1 functional partners. Using the R package, we screened 134 genes that were positively correlated with IGF2BP1 mRNA expression from a total of 56,493 IDs, filtering them with Pearson's correlation coefficient |cor| >0.3 and $p < 0.05$, and the top 10 genes, genes coding proteins, and genes for lncRNAs are displayed in our heatmaps (Figures 7A–C). LinkedOmics is a unique online analytical platform that provides comprehensive multi-omics data analysis (Vasaikar, et al., 2018), and we employed this platform to analyze IGF2BP1 protein partners using proteome datasets from 105 patients. We uncovered 1712 IGF2BP1-correlated proteins from 9,733 entries, and the most positively and negatively correlated proteins are displayed in our heatmaps (Figures 7D,E). We will in future investigations analyze the correlated genes, proteins, and lncRNAs using an interaction network and hub genes, and validate them in clinical samples.

4 Discussion

IGF2BP1 is principally expressed in embryos and in cancerous cells in contrast with comparatively lower or

TABLE 1 Results of Cox univariate and multivariate analyses.

Characteristics	Univariate analysis		Multivariate analysis	
	Hazard ratio (95% CI)	*p* value	Hazard ratio (95% CI)	*p* value
T stage				
T1	Reference			
T2	1.332 (0.887–1.999)	0.166	1.123 (0.697–1.810)	0.634
T3&T4	1.953 (1.221–3.123)	**0.005**	1.448 (0.799–2.624)	0.222
N stage				
N0	Reference			
N1	1.956 (1.329–2.879)	**<0.001**	1.767 (1.148–2.719)	**0.010**
N2	2.519 (1.482–4.281)	**<0.001**	2.245 (1.253–4.023)	**0.007**
N3	4.188 (2.316–7.574)	**<0.001**	3.467 (1.561–7.698)	**0.002**
M stage				
M0	Reference			
M1	4.254 (2.468–7.334)	**<0.001**	2.014 (1.025–3.961)	**0.042**
PAM50				
LumA	Reference			
LumB	1.663 (1.088–2.541)	**0.019**	1.400 (0.887–2.208)	0.148
Her2	2.261 (1.325–3.859)	**0.003**	1.719 (0.933–3.167)	0.082
Basal	1.285 (0.833–1.981)	0.257	1.413 (0.874–2.285)	0.158
IGF2BP1				
Low	Reference			
High	1.463 (1.060–2.018)	**0.021**	1.458 (1.003–2.119)	**0.048**

Bold values reprsents that the *p* value of less than 0.05 indicated statistical significance.

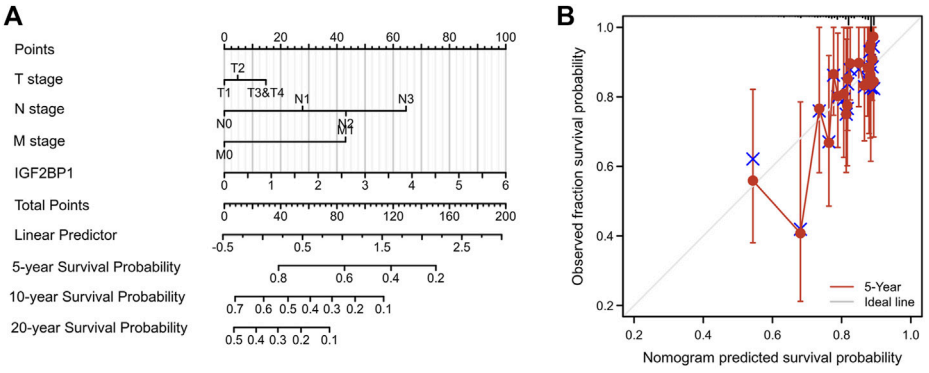

FIGURE 5
Nomogram model for predicting overall survival. **(A)**, Nomogram for predicting overall survival at 5 years, 10 years and 20 years. **(B)**, Nomogram calibration plot for five-year OS as a representative index.

negligible levels in adult normal tissues, reflecting an ideal biomarker for disease. The prognostic overexpression of IGF2BP1 has been reported in over 16 cancers, whereas the overexpression of IGF2BP1 in colon (Hamilton et al., 2015) and breast cancer (Wang, et al., 2016) relative to normal tissues remains controversial. Breast cancer is a highly heterogeneous disease that shows substantial variations in molecular and clinical characteristics, and the discrepancy among studies regarding IGF2BP1 expression in breast cancer might be due to this sample heterogeneity (Huang et al., 2018b) that extends from histologic heterogeneity to subtypes, cellular, and even molecular heterogeneity; these disparities include metastatic status

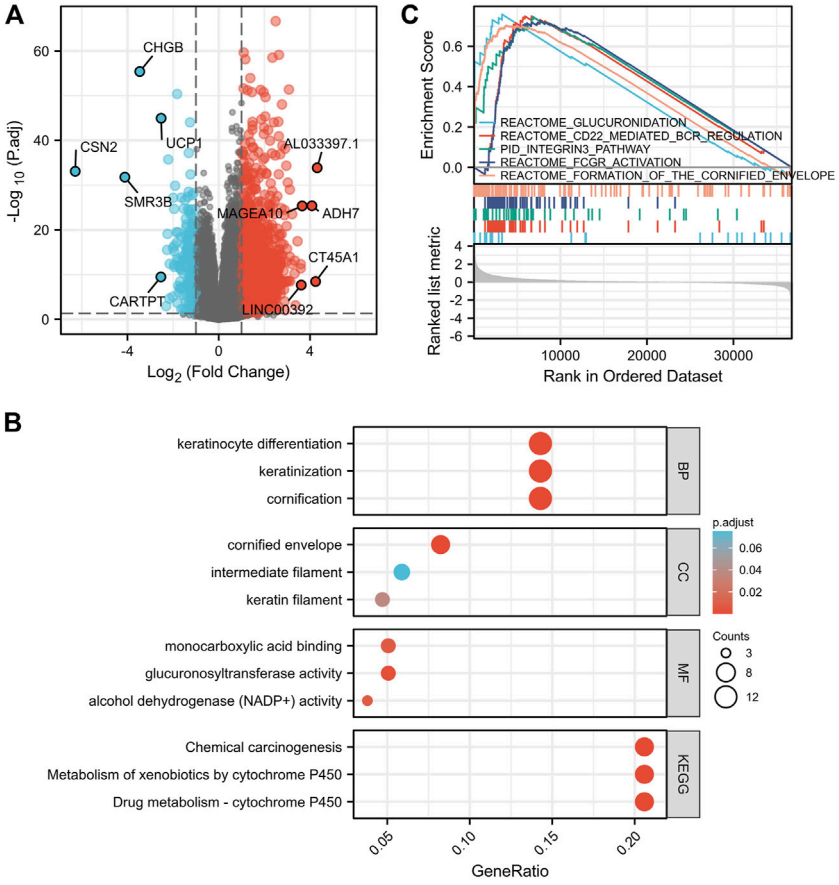

FIGURE 6
Pathway-enrichment analyses of DEGs between high- and low-IGF2BP1 expression samples. **(A)**, Volcano plot for the DEGs expression with the top five upregulated and five down-regulated genes displayed. **(B)**, Bubble diagram of the top enriched GO|KEGG pathway results for DEGs. **(C)**, GSEA of DEGs using the Reactome Pathway Database.

differences, cell types of different origins, phenotypic-functional heterogeneity, genomic discordances, expression-pattern changes, or genetic variations in certain molecules themselves during cancer development. For example, significantly augmented promoter methylation of IGF2BP1 leads to more common silencing events with respect to IGF2BP1 in metastatic breast tumor cells compared to methylation observed in non-metastatic breast tumor cells (Gu, et al., 2012). Moreover, IGF2BP1 was reported to be as a conserved 'oncogenic' m^6A (N6-methylation of adenosine)-reader and could enhance mRNAs stability and translation through m^6A modification (Huang et al., 2018a; Hao et al., 2020). Therefore, it is crucial to elucidate the detailed expression patterns of IGF2BP1 in heterogeneous breast cancer.

In the present study, we demonstrated genetic alterations (particularly amplification and overall upregulation) of IGF2BP1 in invasive breast cancer using large and publicly available datasets from METABRIC, TCGA, and GEO. We also determined that elevated IGF2BP1 mRNA expression was related to histologic and molecular subtypes, especially HER2 status in breast cancer a result not as controversial as that noted by others in the literature, and we found a very small subset of significantly downregulated IGF2BP1 in breast cancer tissues in our paired analysis. What drives the heightened expression of IGF2BP1 in the HER2-positive subtype is unknown, and the discrepancy between relative upregulation and downregulation of IGF2BP1 in paired analyses requires the elucidation of large and deep data mining. The clarification of these underlying mechanisms will facilitate the personalization of subtyping and treatment.

IGF2BP1 is functionally considered to promote tumor growth and invasion *via* the transport of certain mRNAs that play essential roles in embryogenesis, carcinogenesis, and chemo-resistance by affecting mRNA stability, translatability, or localization within most cancers (Huang et al., 2018b). IGF2BP1's potential promotion of tumor invasiveness and progression in breast cancer, however, remains debatable. We also herein confirmed IGF2BP1 to be a promising prognostic indicator in overall invasive

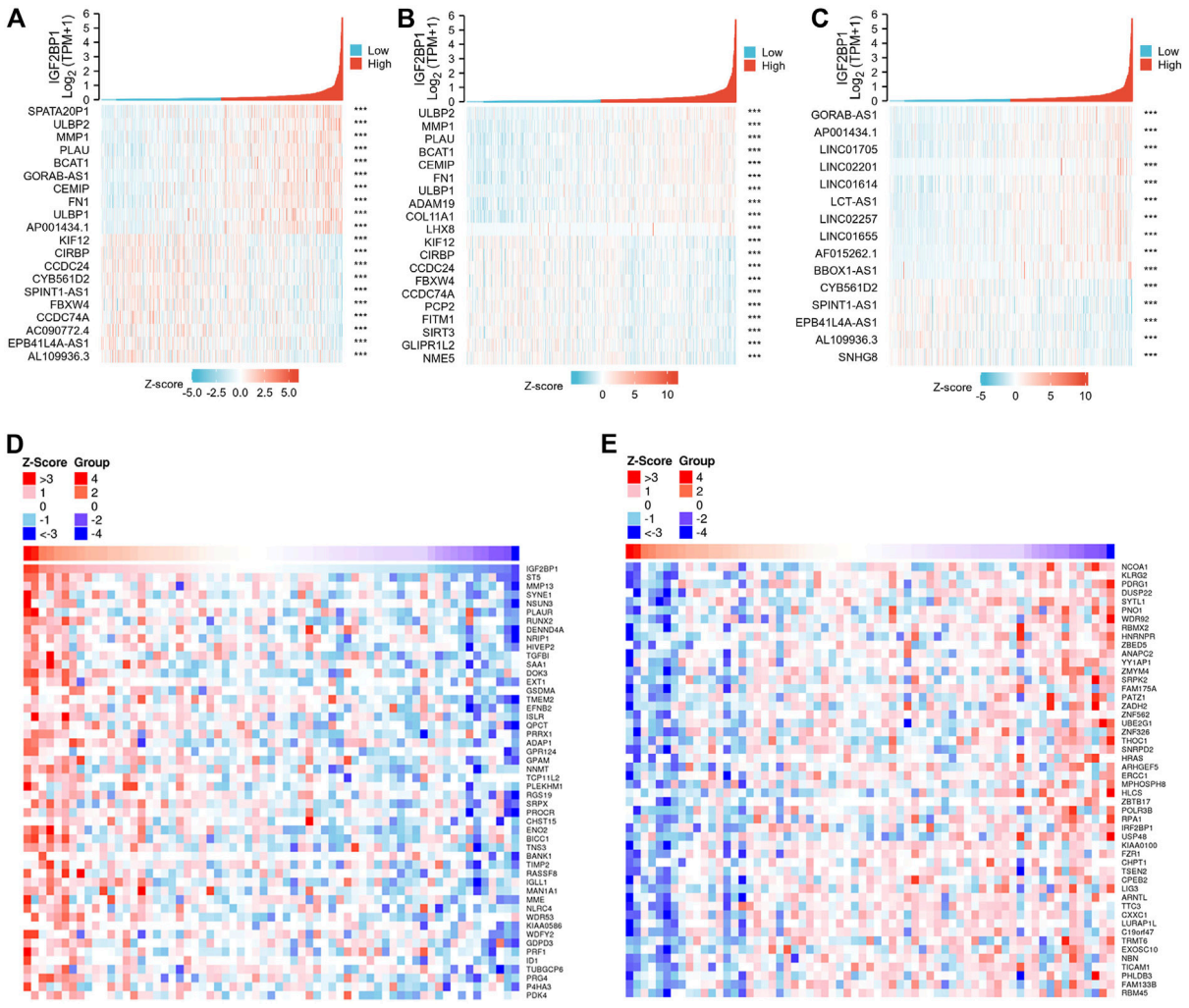

FIGURE 7
IGF2BP1-correlated genes and proteins from TCGA-BRCA databases and the LinkedOmics database. **(A–C)**, Heatmaps of top 10 positive and top 10 negative IGF2BP1-correlated genes, proteins and lncRNAs in TCGA-BRCA gene-expression database. **(D–E)**, Heatmaps of significantly positive and negatively IGF2BP1-correlated proteins in the proteome database using the LinkedOmics platform.

breast cancer and in certain subgroups, including histologic types of IDC and postmenopausal subgroups and patients who did not undergo radiotherapy. We additional analyzed the prognostic relevance of IGF2BP1 in breast cancer by applying enrichment analysis of DEGs, and our data revealed the involvement of pathways such as glucuronidation, cytochrome P450 (CYP) enzyme-related drug metabolism, cornification, and keratinization. Glucuronidation is a drug clearance and resistance mechanism (Mazerska et al., 2016) and cytochrome P450 (CYP) enzymes are responsible for the biotransformation of drugs involved in drug interactions and therapeutic efficacy (Stipp and Acco, 2021) in many diseases. In addition, keratinization and cornified envelope formation associated with proliferation and differentiation of keratinocytes and their progenitor cells (e.g., multipotent stem cells) remain generally stable during carcinogenesis and are correlated with disease aggressiveness and clinical outcomes (Choi et al., 2014; Blommel et al., 2020). We thereby hypothesized that an IGF2BP1-related unfavorable prognosis might be (at least partially) attributable to cellular differentiation as well as acquired drug resistance by altered drug biotransformation and clearance. We also executed correlation analysis using proteome datasets by mining the functional partners of IGF2BP1, as it has been shown that MMP family members were downregulated by IGF2BP1 silencing in ovarian carcinoma, thus reducing the invasive nature of tumor (Davidson et al., 2014). We thus plan to implement a systematic and exhaustive study as well as an experimental validation of the underlying mechanisms with respect to prognostic IGF2BP1 in breast cancer, with particular emphasis on hub genes in IGF2BP1 regulatory networks.

There were several limitations to the present study. First limitation was the lack of validation of the relative expression of IGF2BP1, its prognostic relevance in breast cancer, and the predictive capability of our established nomogram using external datasets such as large, multicenter cohorts. Second, the nomogram we implemented necessitates improvement to satisfy the requirement for convenience and accuracy using routine clinical data and laboratory tests such as the assessment of immune status of lymphocyte subsets. Finally, hub genes in IGF2BP1-targeted mRNA networks need to be identified, and our hypothesis of IGF2BP1 functional pathways based on enrichment analysis of DEGs and genetic correlation remains to be tested experimentally. The detailed molecular mechanisms by which IGF2BP1 regulates target mRNAs or vice versa warrants future investigation.

In summary, our results indicated that both genetic alterations in IGF2BP1 and increased levels of IGF2BP1 mRNA and protein predict a poor patient prognosis in BRCA patients. The findings will represent a potential therapeutic target for the treatment of BRCA.

Data availability statement

The datasets presented in this study can be found in online repositories. The names of the repository/repositories and accession number(s) can be found in the article/ Supplementary Material.

Author contributions

SL contributed to study concept and design, data analysis and interpretation, make tables and figures, and write the manuscript; MJ edited the paper before submission.

Funding

This study was supported by National Natural Science Foundation of China grants (82160094 to MJ) and Natural Science Foundation of Jiangxi Province, China (20202BAB206087 to MJ).

Acknowledgments

The authors thank XIANTAO Academy Platform (https://www.xiantao.love) for aid with data processing.

Conflict of interest

The authors declare that the research was conducted in the absence of any commercial or financial relationships that could be construed as a potential conflict of interest.

Publisher's note

Supplementary material

The Supplementary Material for this article can be found online at: https://www.frontiersin.org/articles/10.3389/fgene.2022.994003/full#supplementary-material

References

Bell, J. L., Wachter, K., Muhleck, B., Pazaitis, N., Kohn, M., Lederer, M., et al. (2013). Insulin-like growth factor 2 mRNA-binding proteins (IGF2BPs): post-transcriptional drivers of cancer progression? *Cell. Mol. Life Sci.* 70, 2657–2675. doi:10.1007/s00018-012-1186-z

Blommel, K., Knudsen, C. S., Wegner, K., Shrestha, S., Singhal, S. K., Mehus, A. A., et al. (2020). Meta-analysis of gene expression profiling reveals novel basal gene signatures in MCF-10A cells transformed with cadmium. *Oncotarget* 11, 3601–3617. doi:10.18632/oncotarget.27734

Choi, W., Porten, S., Kim, S., Willis, D., Plimack, E. R., Hoffman-Censits, J., et al. (2014). Identification of distinct basal and luminal subtypes of muscle-invasive bladder cancer with different sensitivities to frontline chemotherapy. *Cancer Cell* 25, 152–165. doi:10.1016/j.ccr.2014.01.009

Curtis, C., Shah, S. P., Chin, S. F., Turashvili, G., Rueda, O. M., Dunning, M. J., et al. (2012). The genomic and transcriptomic architecture of 2, 000 breast tumours reveals novel subgroups. *Nature* 486, 346–352. doi:10.1038/nature10983

Davidson, B., Rosenfeld, Y. B., Holth, A., Hellesylt, E., Trope, C. G., Reich, R., et al. (2014). VICKZ2 protein expression in ovarian serous carcinoma effusions is associated with poor survival. *Hum. Pathol.* 45, 1520–1528. doi:10.1016/j.humpath.2014.03.005

Gao, J., Aksoy, B. A., Dogrusoz, U., Dresdner, G., Gross, B., Sumer, S. O., et al. (2013). Integrative analysis of complex cancer genomics and clinical profiles using the cBioPortal. *Sci. Signal.* 6, pl1. doi:10.1126/scisignal.2004088

Gu, W., Wells, A. L., Pan, F., and Singer, R. H. (2008). Feedback regulation between zipcode binding protein 1 and beta-catenin mRNAs in breast cancer cells. *Mol. Cell. Biol.* 28, 4963–4974. doi:10.1128/MCB.00266-08

Gu, W., Katz, Z., Wu, B., Park, H. Y., Li, D., Lin, S., et al. (2012). Regulation of local expression of cell adhesion and motility-related mRNAs in breast cancer cells by IMP1/ZBP1. *J. Cell Sci.* 125, 81–91. doi:10.1242/jcs.086132

Hamilton, K. E., Chatterji, P., Lundsmith, E. T., Andres, S. F., Giroux, V., Hicks, P. D., et al. (2015). Loss of stromal IMP1 promotes a tumorigenic microenvironment in the colon. *Mol. Cancer Res.* 13, 1478–1486. doi:10.1158/1541-7786.MCR-15-0224

Hao, J., Hu, H., Jiang, Z., Yu, X., Li, C., Chen, L., et al. (2020). microRNA-670 modulates Igf2bp1 expression to regulate RNA methylation in parthenogenetic mouse embryonic development. *Sci. Rep.* 10, 4782. doi:10.1038/s41598-020-61816-3

Huang, H., Weng, H., Sun, W., Qin, X., Shi, H., Wu, H., et al. (2018a). Recognition of RNA N(6)-methyladenosine by IGF2BP proteins enhances mRNA stability and translation. *Nat. Cell Biol.* 20, 285–295. doi:10.1038/s41556-018-0045-z

Huang, X., Zhang, H., Guo, X., Zhu, Z., Cai, H., and Kong, X. (2018b). Insulin-like growth factor 2 mRNA-binding protein 1 (IGF2BP1) in cancer. *J. Hematol. Oncol.* 11, 88. doi:10.1186/s13045-018-0628-y

Kim, T., Havighurst, T., Kim, K., Albertini, M., Xu, Y. G., and Spiegelman, V. S. (2018). Targeting insulin-like growth factor 2 mRNA-binding protein 1 (IGF2BP1) in metastatic melanoma to increase efficacy of BRAF(V600E) inhibitors. *Mol. Carcinog.* 57, 678–683. doi:10.1002/mc.22786

Kobel, M., Weidensdorfer, D., Reinke, C., Lederer, M., Schmitt, W. D., Zeng, K., et al. (2007). Expression of the RNA-binding protein IMP1 correlates with poor prognosis in ovarian carcinoma. *Oncogene* 26, 7584–7589. doi:10.1038/sj.onc.1210563

Liu, J., Lichtenberg, T., Hoadley, K. A., Poisson, L. M., Lazar, A. J., Cherniack, A. D., et al. (2018). An integrated TCGA pan-cancer clinical data resource to drive high-quality survival outcome analytics. *Cell* 173, 400–416. doi:10.1016/j.cell.2018.02.052

Love, M. I., Huber, W., and Anders, S. (2014). Moderated estimation of fold change and dispersion for RNA-seq data with DESeq2. *Genome Biol.* 15, 550. doi:10.1186/s13059-014-0550-8

Mahapatra, L., Andruska, N., Mao, C., Le, J., and Shapiro, D. J. (2017). A novel IMP1 inhibitor, BTYNB, targets c-myc and inhibits melanoma and ovarian cancer cell proliferation. *Transl. Oncol.* 10, 818–827. doi:10.1016/j.tranon.2017.07.008

Mahapatra, L., Andruska, N., Mao, C., Gruber, S. B., Johnson, T. M., Fullen, D. R., et al. (2019). Protein kinase C-alpha is upregulated by IMP1 in melanoma and is linked to poor survival. *Melanoma Res.* 29, 539–543. doi:10.1097/CMR.0000000000000558

Mazerska, Z., Mroz, A., Pawlowska, M., and Augustin, E. (2016). The role of glucuronidation in drug resistance. *Pharmacol. Ther.* 159, 35–55. doi:10.1016/j.pharmthera.2016.01.009

Paramasivam, A., George, R., and Priyadharsini, J. V. (2021). Genomic and transcriptomic alterations in m6A regulatory genes are associated with tumorigenesis and poor prognosis in head and neck squamous cell carcinoma. *Am. J. Cancer Res.* 11, 3688–3697.

Pereira, B., Chin, S. F., Rueda, O. M., Vollan, H. K., Provenzano, E., Bardwell, H. A., et al. (2016). The somatic mutation profiles of 2, 433 breast cancers refines their genomic and transcriptomic landscapes. *Nat. Commun.* 7, 11479. doi:10.1038/ncomms11479

Perou, C. M., Sorlie, T., Eisen, M. B., van de Rijn, M., Jeffrey, S. S., Rees, C. A., et al. (2000). Molecular portraits of human breast tumours. *Nature* 406, 747–752. doi:10.1038/35021093

Shi, R., Yu, X., Wang, Y., Sun, J., Sun, Q., Xia, W., et al. (2017). Expression profile, clinical significance, and biological function of insulin-like growth factor 2 messenger RNA-binding proteins in non-small cell lung cancer. *Tumour Biol.* 39, 1010428317695928. doi:10.1177/1010428317695928

Sorlie, T., Tibshirani, R., Parker, J., Hastie, T., Marron, J. S., Nobel, A., et al. (2003). Repeated observation of breast tumor subtypes in independent gene expression data sets. *Proc. Natl. Acad. Sci. U. S. A.* 100, 8418–8423. doi:10.1073/pnas.0932692100

Stipp, M. C., and Acco, A. (2021). Involvement of cytochrome P450 enzymes in inflammation and cancer: A review. *Cancer Chemother. Pharmacol.* 87, 295–309. doi:10.1007/s00280-020-04181-2

Subramanian, A., Tamayo, P., Mootha, V. K., Mukherjee, S., Ebert, B. L., Gillette, M. A., et al. (2005). Gene set enrichment analysis: A knowledge-based approach for interpreting genome-wide expression profiles. *Proc. Natl. Acad. Sci. U. S. A.* 102, 15545–15550. doi:10.1073/pnas.0506580102

Vasaikar, S. V., Straub, P., Wang, J., and Zhang, B. (2018). LinkedOmics: Analyzing multi-omics data within and across 32 cancer types. *Nucleic Acids Res.* 46, D956–D963. doi:10.1093/nar/gkx1090

Vivian, J., Rao, A. A., Nothaft, F. A., Ketchum, C., Armstrong, J., Novak, A., et al. (2017). Toil enables reproducible, open source, big biomedical data analyses. *Nat. Biotechnol.* 35, 314–316. doi:10.1038/nbt.3772

Wang, G., Huang, Z., Liu, X., Huang, W., Chen, S., Zhou, Y., et al. (2016). IMP1 suppresses breast tumor growth and metastasis through the regulation of its target mRNAs. *Oncotarget* 7, 15690–15702. doi:10.18632/oncotarget.7464

Wang, P., Zhang, L., Zhang, J., and Xu, G. (2018). MicroRNA-124-3p inhibits cell growth and metastasis in cervical cancer by targeting IGF2BP1. *Exp. Ther. Med.* 15, 1385–1393. doi:10.3892/etm.2017.5528

Yu, G., Wang, L. G., Han, Y., and He, Q. Y. (2012). clusterProfiler: an R package for comparing biological themes among gene clusters. *OMICS* 16, 284–287. doi:10.1089/omi.2011.0118

Zhou, Y., Meng, X., Chen, S., Li, W., Li, D., Singer, R., et al. (2018). IMP1 regulates UCA1-mediated cell invasion through facilitating UCA1 decay and decreasing the sponge effect of UCA1 for miR-122-5p. *Breast Cancer Res.* 20, 32. doi:10.1186/s13058-018-0959-1

frontiers | Frontiers in Genetics

TYPE Original Research
PUBLISHED 13 September 2022
DOI 10.3389/fgene.2022.1009141

OPEN ACCESS

EDITED BY
Qian Wang,
Tai'an City Central Hospital, China

REVIEWED BY
Zhenhao Zhang,
Nanjing Medical University, China
He Wang,
Xuzhou Medical University, China

*CORRESPONDENCE
Yi Shao,
freebee99@163.com

†These authors have contributed equally to this work

SPECIALTY SECTION
This article was submitted to Cancer Genetics and Oncogenomics, a section of the journal Frontiers in Genetics

RECEIVED 01 August 2022
ACCEPTED 24 August 2022
PUBLISHED 13 September 2022

CITATION
Tang J, Shu H-Y, Sun T, Zhang L-J, Kang M, Ying P, Ling Q, Zou J, Liao X-L, Wang Y-X, Wei H and Shao Y (2022), Potential factors of cytokeratin fragment 21-1 and cancer embryonic antigen for mediastinal lymph node metastasis in lung cancer. *Front. Genet.* 13:1009141. doi: 10.3389/fgene.2022.1009141

Potential factors of cytokeratin fragment 21-1 and cancer embryonic antigen for mediastinal lymph node metastasis in lung cancer

Jing Tang[1†], Hui-Ye Shu[2†], Tie Sun[2†], Li-Juan Zhang[2], Min Kang[2], Ping Ying[2], Qian Ling[2], Jie Zou[2], Xu-Lin Liao[3], Yi-Xin Wang[4], Hong Wei[2] and Yi Shao[2]*

[1]Department of Oncology, The Affiliated Zhuzhou Hospital Xiangya Medical College, Central South University, Zhuzhou, Hunan, China, [2]Department of Ophthalmology, Jiangxi Branch of National Clinical Research Center for Ocular Disease, The First Affiliated Hospital of Nanchang University, Nanchang, Jiangxi, China, [3]Department of Ophthalmology and Visual Sciences, The Chinese University of Hong Kong, Hong Kong, China, [4]School of Optometry and Vision Science, Cardiff University, Cardiff, United Kingdom

Objective: Lung cancer is a common malignant tumor, characterized by being difficult to detect and lacking specific clinical manifestations. This study aimed to find out the risk factors of mediastinal lymph node metastasis and explore the correlation between serum tumor markers and mediastinal lymph node metastasis and lung cancer prognosis.

Methods: A retrospective study of 3,042 lung cancer patients (330 patients with mediastinal lymph node metastasis and 2,712 patients without mediastinal lymph node metastasis) collected from the First Affiliated Hospital of Nanchang University from April 1999 to July 2020. The patients were divided into two groups, namely, mediastinal lymph node metastasis group and non-mediastinal lymph node metastasis group. Student's t test, non-parametric rank sum test and chi-square test were used to describe whether there is a significant difference between the two groups. We compared the serum biomarkers of the two groups of patients, including exploring serum alkaline phosphatase (ALP), calcium hemoglobin (HB), alpha-fetoprotein (AFP), carcinoembryonic antigen (CEA), CA125, CA-199, CA -153, cytokeratin fragment 19 (CYFRA 21-1), total prostate specific antigen (TPSA), neuron-specific enolase (NSE) levels and the incidence and prognosis of lung cancer mediastinal lymph node metastasis. Binary logistic regression analysis was used to determine its risk factors, and receiver operating curve (ROC) analysis was used to evaluate its diagnostic value for mediastinal lymph node metastasis.

Abbreviations: AFP, alpha fetoprotein; ALP, alkaline phosphatase; AUC, area under the curve; CEA, Cancer embryonic antigen; CT,Computerized tomography; CYFRA 21-1, cytokeratin fragment 19; HB, calcium hemoglobin; MRI, magnetic resonance imaging; NSE, and neuron-specific enolase; ROC, receiver operating curve; TPSA, total prostate specific antigen.

Results: Binary logistic regression analysis showed that carcinoembryonic antigen and CYFRA 21-1 were independent risk factors for mediastinal lymph node metastasis in patients with lung cancer ($p < 0.001$ and $p = 0.002$, respectively). The sensitivity and specificity of CEA for the diagnosis of mediastinal lymph node metastasis were 90.2 and 7.6%, respectively; CYFRA 21-1 were 0.6 and 99.0%, respectively.

Conclusion: Serum CEA and CYFRA 21-1 have predictive value in the diagnosis of mediastinal lymph node metastasis in patients with lung cancer.

KEYWORDS

lung cancer, mediastinal lymph node metastasis potential indicators, tumor blood markers, cancer, risk factors

Introduction

The morbidity and mortality of lung cancer remain high, and the prognosis of lung cancer patients has not been effectively improved. The preferred treatment for lung cancer is surgery. Postoperative radiotherapy, chemotherapy, biological immunotherapy, and the advent of targeted drugs have all led to increases in the survival time of patients. Lymph node metastasis is one of the main metastatic pathways of lung cancer and is an important determinant of lung cancer stage. Lung cancer has no specific symptoms in the early stages. The cancer cells pass through the bronchus and the lymphatic vessels around the pulmonary blood vessels. They first invade the adjacent lung or lymph nodes around the bronchi and then reach the hilar or subcarinal lymph nodes. They may then spread to the mediastinum and paratracheal lymph nodes, and further to the clavicular or cervical lymph nodes. Immune checkpoint inhibitors is a currently widely used tumor treatment method. Through the development of various related clinical trials, immune checkpoint inhibitors have made many breakthroughs in the efficacy, prognosis and disease prediction of lung cancer (Jain et al., 2018; Bai et al., 2020).

Tumor marker detection has become one a routine detection method, but there is still no ideal marker for clinical use as an indicator of lung cancer metastasis and prognosis. Single marker detection systems often suffer from low specificity (Weinberger et al., 2002). The same tumor can contain a variety of tumor markers. Different tissue types of the same tumor can express the same tumor markers or different tumor markers, so combined detection of multiple tumor markers can improve the diagnostic sensitivity of cancer.

A number of studies have identified distinct factors that are associated with lymph node metastasis in lung cancer. Specific substances detected in the lymph nodes or blood can predicts tumor. In this study, the medical records of lung cancer patients from the First Affiliated Hospital of Nanchang University were collected. Based on serological examination of a large number of lung cancer patients, we screened patients with lung cancer mediastinal lymph node metastasis and analyzed their tumor marker content to identify risk factors. We aimed to establish a standard by which to distinguish between mediastinal lymph node metastasis and non-mediastinal lymph node metastasis and to facilitate the development of further targeted anticancer treatment strategies for lung cancer patients.

Materials and methods

Ethics statement and study design

All patients in this study volunteered to participate, and the study was approved by the Medical Research Ethics Committee of the First Affiliated Hospital of Nanchang University. In this study, patients diagnosed with lung cancer between September 1999 and July 2020 were selected. Patients with mediastinal lymph node metastasis were screened, and their medical records and serological data were compared with those of patients without mediastinal lymph node metastasis. A pathological section obtained by surgical resection or biopsy was used to accurately diagnose the lung cancer of the patient. Computerized tomography (CT) and magnetic resonance imaging (MRI) were used to diagnose mediastinal lymph node metastasis in lung cancer, and data on serum tumor markers were recorded. Patients with primary mediastinal malignancies, benign mediastinal tumors, and secondary mediastinal cancer were excluded. The inclusion criteria for the without mediastinal lymph node metastasis group were patients without organ metastases.

Data collection

We collected various clinical data, including age, gender, time of diagnosis, lesion metastasis, and treatment, from medical records of patients with mediastinal lymph node metastasis and analyzed serum tumor markers, including alkaline phosphatase, serum calcium, HB, alpha-fetoprotein (AFP), carcinoembryonic antigen (CEA), neuron-specific enolase

TABLE 1 The clinical characteristics of patients with lung cancer.

Patient characteristics	Group with mediastinal lymph node metastasis (%)	Group without mediastinal lymph node metastasis (%)	*p* value[d]
	(*n* = 330)	(*n* = 2,712)	
Gender[a]			
Male	249 (75.5)	1988 (73.3)	0.485
Female	81 (24.5)	724 (26.7)	
Age[b]			
Mean	59.6 ± 10.5	60.3 ± 10.8	0.553
Histopathological type[c]			
Adenocarcinoma	143 (45.2)	1,128 (41.6)	0.012
Squamous cell carcinoma	119 (34.2)	1,041 (38.4)	
Small cell carcinoma	33 (10.0)	370 (13.6)	
Other	35 (10.6)	173 (6.4)	

[a]Chi-squared test.
[b]Student's t-test.
[c]Comparison between the lung cancer group with brain metastasis and the lung cancer group without brain metastasis.
[d]p value < 0.05 was considered statistically significant.

(NSE), cytokeratin fragment 19 (CYFRA 21-1), CA-125, CA-153, CA-199, and free prostate-specific antigen (FPSA).

Statistical analyses

We analyzed the differences between tumor markers in the mediastinal lymph node metastasis group and the non-mediastinal lymph node metastasis group by an independent *t*-test. A binary logistic regression model was then applied to identify independent risk factors for mediastinal lymph node metastasis. A receiver operating curve (ROC) curve was generated, and the area under the curve (AUC) was calculated. Then, we used Microsoft Excel 2010 software (Microsoft corporation,United States) to calculate the cut-off value, sensitivity, and specificity of risk factors. All statistical analyses were performed using SPSS 20.0 (SPSS, IBM, United States) and Excel 2010 software. p values < 0.05 indicates statistical significance.

Results

Demographics and clinical characteristics

In this study, 330 cases of lung cancer with mediastinal lymph node metastasis and 2,712 cases of lung cancers without mediastinal lymph node metastasis were collected. The mean ages of lung cancer patients with and without mediastinal lymph node metastasis were 59.6 ± 10.5 and 60.3 ± 10.8 years, respectively. According to the chi-squared test and Student's t-test, there were no significant differences in gender or age between the lung cancer groups with and without mediastinal lymph node metastasis (p > 0.05). In contrast, significant differences were noted for the different histopathological types between the two groups (p < 0.05). There was a statistically significant difference in the pathological type between the mediastinal lymph node metastasis group and lung cancers without mediastinal lymph node metastasis (p = 0.012). Furthermore, the incidence of adenocarcinoma was the highest among the different histopathological types. Most patients had been treated with chemotherapy since the onset of the disease. Detailed clinical data of all patients involved in the study are provided in Table 1 and Figures 1–3.

Clinical data and risk factors of mediastinal lymph node metastasis in lung cancer

After comparing data on tumor biomarkers in lung cancer patients with and without mediastinal lymph node metastasis, we found that the concentrations of AFP, CEA, and CYFRA 21-1 were significantly higher in patients with mediastinal lymph node metastasis, while HB was higher in patients without mediastinal lymph node metastasis (p < 0.05) (Table 2). There were no significant differences in serum ALP, calcium, CA-125, CA-199, CA-153, TPSA, NSE, between the two groups (p > 0.05) (Table 2). Based on binary logistic regression, CEA and CYFRA 21-1 appear to be independent risk factors for mediastinal lymph node metastasis in lung cancer. More detailed results are shown in Table 3.

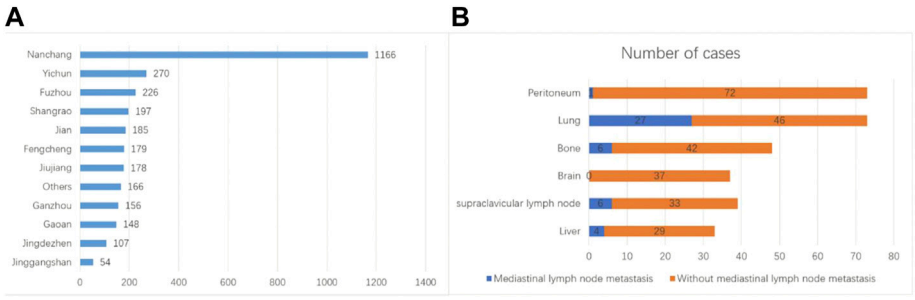

FIGURE 1
Clinical features of the patients. **(A)** Geographic location of the patients. **(B)** Anatomical locations of metastasis and corresponding incidences.

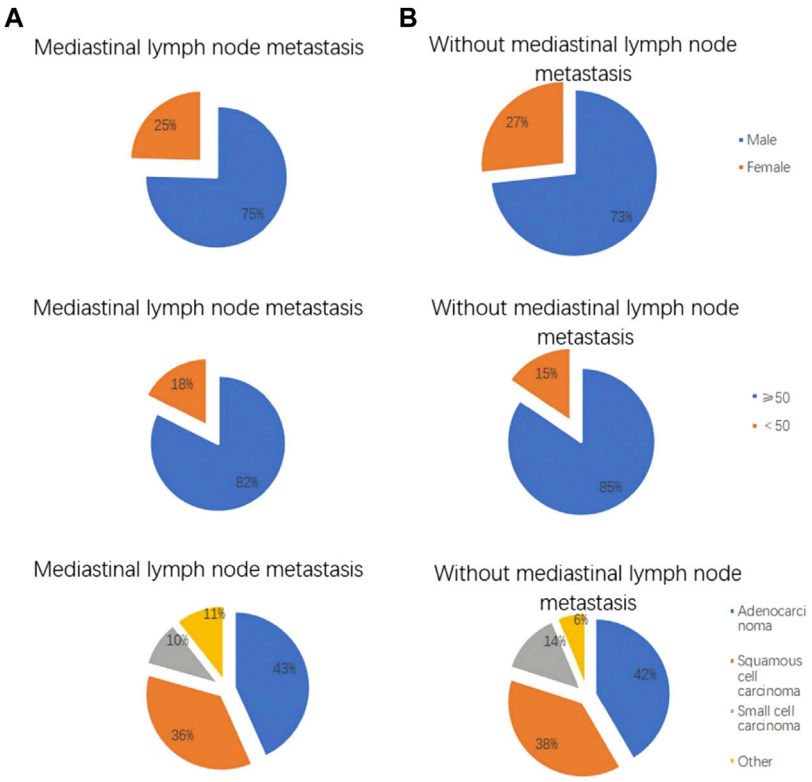

FIGURE 2
Clinical features of lung cancer patients with and without mediastinal lymph node metastasis. The **(A)** shows lung cancer patients with mediastinal lymph node metastasis, and the **(B)** shows lung cancer patients without mediastinal lymph node metastasis. Gender distribution of lung cancer patients with and without mediastinal lymph node metastasis. Age distribution of lung cancer patients with and without mediastinal lymph node metastasis. Pathological features of lung cancer patients with and without mediastinal lymph node metastasis.

Cut-off value, sensitivity, and specificity of CEA and CYFRA 21-1 for the diagnosis of mediastinal lymph node metastasis in lung cancer

Table 4 shows that the cut-off values for CEA and CYFRA 21-1 are 1.005 ng/ml and 135.31 ng/ml, respectively, and the area under the curve (AUC) of CYFRA 21-1 is the highest. The sensitivity and specificity for the diagnosis of mediastinal lymph node metastasis were CEA, 90.2 and 7.6%, respectively; CYFRA 21-1 was 0.6 and 99.0%, respectively. Figure 4A shows the receiver operating curve (ROC) curves for CEA and CYFRA 21-1, each as a single factor. We then tested the combination of these two risk factors in pairs, and Figure 4B shows the ROC

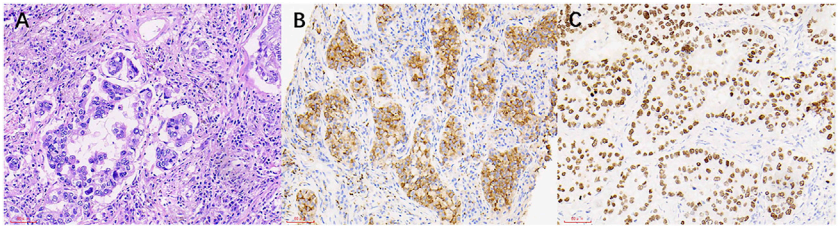

FIGURE 3
The HE staining and IHC images from lung cancer patients with mediastinal lymph node metastasis. **(A)** Lung cancer (HE × 200). **(B)** NapsinA (+) (SP × 200). **(C)** TTF-1 (+) (SP × 200).

TABLE 2 Differences in tumor biomarkers between lung cancer patients with and without mediastinal lymph node metastasis.

Tumor biomarkers	Mediastinal lymph node metastasis group	Without mediastinal lymph node metastasis group	t	*p* value
ALP (U/L)	92.48 ± 100.03	93.18 ± 77.32	0.159	0.8736
Calcium (nmol/L)	2.20 ± 0.22	2.29 ± 15.29	0.624	0.5325
AFP (ng/ml)	2.16 ± 1.04	1.75 ± 1.61	4.981	<0.001
CEA (ng/ml)	69.12 ± 340.77	44.25 ± 231.54	1.680	<0.001
CA-125 (U/ml)	76.03 ± 163.6	71.44 ± 191.25	0.396	0.6915
CA-199 (U/ml)	46.72 ± 199.1	46.28 ± 439.44	0.005	0.9960
CA-153 (U/ml)	21.96 ± 33.6	20.53 ± 34.54	0.694	0.4875
CYFRA 21-1 (ng/ml)	11.3 ± 26.55	9.56 ± 30.42	1.01	0.003
TPSA (ng/L)	2.02 ± 4.37	1.63 ± 3.73	1.71	0.0871
NSE (μg/L)	26.81 ± 41.57	26.12 ± 42.89	0.258	0.7963
HB (g/L)	115.75 ± 19.18	119.44 ± 19.15	3.10	0.0019

Notes: Apply *t*-test analysis. $p < 0.05$ indicated statistically significant differences. Abbreviations: ALP, alkaline phosphatase; HB, calcium hemoglobin; AFP, alpha fetoprotein; CEA,Cancer embryonic antigen; CYFRA 21-1, cytokeratin fragment 19; TPSA, total prostate specific antigen ;NSE, and neuron-specific enolase.

TABLE 3 Risk factors in lung cancer patients with mediastinal lymph node metastasis.

Factors	B	Exp(B)	OR (95% CI)	*p* value
AFP	0.127	1.135	1.059–1.216	0.134
CEA	0.000	1.000	1.000–1.001	<0.001
CYFRA 21-1	0.001	1.001	0.998–1.004	0.002
HB (g/L)	−0.009	0.991	0.985–0.997	0.068

Notes: Binary logistic regression analysis was applied. $p < 0.05$ indicated statistically significant differences. Abbreviations: HB, calcium hemoglobin; AFP, alpha fetoprotein; CEA, Cancer embryonic antigen; CYFRA 21-1, cytokeratin fragment 19.

curve for the CEA + CYFRA 21-1 combination. We found that the combination of CEA + CYFRA 21-1 has a higher AUC value of 0.585. The sensitivity and specificity of CEA + CYFRA 21-1 are shown in Table 4, and results were statistically significant ($p < 0.05$).

Discussion

Studies have shown that lymphatic metastasis occurs in papillary thyroid cancer. (Wang et al., 2019; Wen et al., 2019). Another scholar found that (Shimazu et al., 2019) used a one-step nucleic acid amplification test to detect lymph node metastasis of breast cancer, and in our study, serological tests were also found to predict lymph node metastasis of lung cancer. Studies have shown that (Han et al., 2019) lung cancer is prone to various types of metastasis, such as non-small cell lung cancer will occur bone metastasis.

Marchi et al. (Marchi et al., 2008). Used proteomics technology to screen the serum markers of lung cancer brain metastasis and found that patients with lung cancer brain metastasis had higher levels of ProApolipoprotein A1 and S100beta than those with lung cancer and cerebral ischemia. Roberts et al. (Roberts et al., 2002) first discovered the relationship between abnormal expression of retinol binding protein (RBP) and malignant metastasis of ovarian cancer

TABLE 4 Critical value, sensitivity, specificity and AUC of CEA and CYFRA 21-1 in lung cancer patients with mediastinal lymph node metastasis.

Factor	Cut-off value	Sensitivity (%)	Specificity (%)	AUC	*p* value
CYFRA 21-1 (ng/ml)	135.31	0.6	99.0	0.596	0.002
CEA (ng/ml)	1.005	90.2	7.6	0.533	<0.001
CEA + CYFRA 21-1	1,228.6	0.3	99.6	0.585	<0.001

Notes: Sensitivity and specificity were obtained at the cut-off value. $p < 0.05$ indicates statistically significant differences. Abbreviations: CEA, Cancer embryonic antigen; CYFRA 21-1, cytokeratin fragment 19.

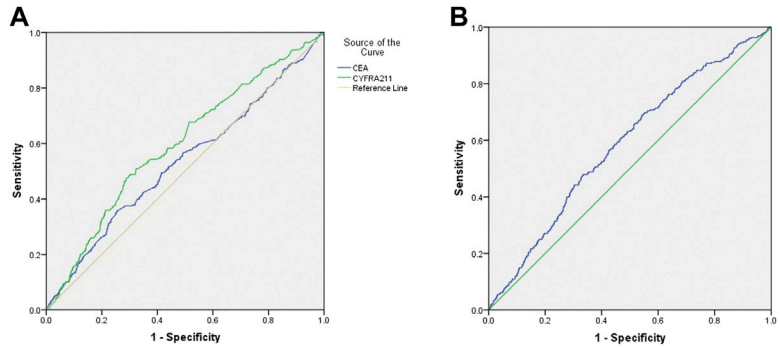

FIGURE 4
(A)ROC curve of CEA and CYFRA 21-1 levels in lung cancer patients with mediastinal lymph node metastasis. **(B)**ROC curve of CEA + CYFRA 21-1 in lung cancer patients with mediastinal lymph node metastasis.

epithelial cells, and speculated that due to the down-regulation and loss of RBP expression, it destroyed the metabolism of retinol and the production of retinoic acid. Promotes gene damage, leading to malignant transformation of ovarian epidermal cells.

At present, most clinicians' method of clinical staging of lung cancer is a multidisciplinary diagnosis method based on chest CT scan (Liam et al., 2015), but chest CT is not specific for the diagnosis of intrapulmonary lymph node metastasis of lung cancer, and accuracy is not accurate. Cannot be used as a basis for surgical clearance (Zhang et al., 2019). Xu et al. (Xu et al., 2003) reported that the sensitivity, specificity and accuracy of PET in the diagnosis of mediastinal lymph node metastasis were 100, 93 and 94%, respectively, and the number and location of positive lymph nodes were completely consistent with pathological results.

The relationship between tumor size and invasion and lymph node metastasis is currently reported. Li Yu et al. (Li et al., 2000) summarized 386 cases of pathological data and thought that with the increase of tumor and increased invasion, the chance of lymph node metastasis increased significantly. Min Kong et al. (Kong et al., 2017) analyzed 1,156 patients, and the test results showed that there is some correlation between lymph node metastasis and the size of the primary tumor.

The intrathoracic lymphatic drainage route of lung cancer is usually performed according to a certain rule, that is, from the near to the far side, from the top to the bottom, from the lung to the mediastinum to the mediastinum, (Ndiaye et al., 2016), regardless of the location and severity, most cases are one station. In some cases, the transfer order of each station can change, or even jump. This situation has been reported in the literature at home and abroad. (Yoshino et al., 1996; Celikoglu et al., 2010).

According to the original location of the tumor, Watanabe et al. (Watanabe et al., 1990) divided the mediastinal lymph nodes into upper and lower parts according to the tracheal bifurcation. The incidence of lung cancer in the lower lobe was 22%, and the incidence of lung cancer in the upper lobe was 8%. Advocate extensive mediastinal lymph node dissection. However, extensive lymph node dissection can directly affect the patient's survival. Funatsu et al. (Funatsu et al., 1994) found that the difference in survival rate may be related to the low immunity caused by mediastinal lymph node dissection. Additionally, the higher the Topography; Lymph Node; Metastasis (TNM)stage, the higher the serum CEA level. Some studies have found that the preoperative CEA level is related to non-small cell carcinoma survival. There have reported important factors related to independence (Okada et al., 2003; Yu et al., 2014).

CYFRA 21-1 is currently considered to be the main tumor marker used for the diagnosis of lung cancer. It is primarily distributed throughout the cytoplasm of the stratified tumor epithelium. When a cell dies, CYFRA 21-1 is released into the blood as a lysed fragment, resulting in an increase in serum levels.

TABLE 5 The risk factors of metastases of lung cancer.

Author	Year	Histopathological type	Metastatic sites	Risk factor
Morita et al. (Morita et al., 2019)	2019	NSCLC	Intertrabecular Vertebral	CEA
Zhou et al. (Zhou et al., 2017)	2017	NS	Bone	CA-125, ALP
Liu et al. (Zhang et al., 2017)	2017	Adenocarcinoma	Brain, Lymph node	CYFRA21-1
Wu et al. (Wu et al., 2017)	2017	NSCLC	Lymph node	MicroRNA-422a
Chu et al. (Chu et al., 2017)	2017	Adenocarcinoma	Lymph node	CLSTNI, CLU, NGAL
Chen et al. (Chen et al., 2015a)	2015	NSCLC	Brain	NSE
Chen et al. (Chen et al., 2015b)	2015	NS	Lymph node	CYFRA21-1, CEA
Lee et al. (Lee et al., 2012)	2012	NSCLC	Brain	CEA
Cabreraalarcon (Cabreraalarcon et al., 2011)	2011	NS	NS	CYFRA21-1
Cedres (Cedrés et al., 2011)	2011	NSCLC	Brain	CEA, CYFRA21-1, CA-125
Oshiro et al. (Oshiro et al., 2004)	2004	Adenocarcinoma	Liver	AFP
Pollan et al. (Pollan et al., 2003)	2003	NSCLC	NS	CA-125
Niklinskij (Nikliúski et al., 1992)	1992	NSCLC	Lymph node	SCC

Pujol et al. reported that CYFRA 21-1 is an independent prognostic factor in lung cancer (Pujol et al., 2004).

In our study, we collected serum and assessed ALP, calcium, HB, AFP, CEA, CA-125, CA-199, CA-153, CYFRA 21-1, TPSA, and NSE levels. Relative to lung cancer patients without mediastinal lymph node metastasis, the concentrations of AFP, CEA, and CYFRA 21-1 in lung cancer patients with mediastinal lymph node metastasis were found to be extremely high, while HB was found to be lower ($p < 0.05$). Based on previous studies, we chose CEA and CYFRA 21-1 as independent risk factors for lung cancer patients with mediastinal lymph node metastasis ($p < 0.01$ and $p = 0.002$, respectively). Furthermore, we assessed the cut-off, sensitivity, specificity, and AUC of CEA and CYFRA 21-1 levels. Finally, we conclude that CEA, and CYFRA 21-1 are risk factors for mediastinal lymph node metastasis in lung cancer.

By using the final ROC curve of these serum biomarkers to provide reliable clinical indicators, we can conclude that CEA and CYFRA 21-1 have cut-off values of 1.005 ng/ml and 135.31 ng/ml, respectively, in lung cancer patients with mediastinal lymph node metastasis. CYFRA 21-1 had the highest AUC, demonstrating that it had the highest accuracy in distinguishing between lung cancer patients with and without mediastinal lymph node metastasis. On this basis, we utilized further detailed diagnostic techniques to diagnose or rule out mediastinal lymph node metastasis without providing a basis for follow-up treatment. Unlike previous studies, this study showed that the combination of CEA + CYFRA 21-1 had a higher AUC value of 0.585. Therefore, we believe that the combination of CEA + CYFRA 21-1 can also be used as a predictor of mediastinal lymph node metastasis in lung cancer (the higher the level of CEA + CYFRA 21-1, the greater the likelihood of mediastinal lymph node metastasis in lung cancer patients). We also summarized the risk factors for lung cancer metastasis in previous studies (Table 5).

In summary, the high expression of serum CEA and CYFRA 21-1 may be related to the occurrence of mediastinal lymph node metastasis in lung cancer patients. At the same time, assessment of the combination of CEA + CYFRA 21-1 can aid in the diagnosis of mediastinal lymph node metastasis in lung cancer patients. The positive expression of serum CEA + and CYFRA 21-1 is associated with the prognosis of patients with mediastinal lymph node metastasis.

However, there are some limitations, because of the large individual differences in some patients, and the small number of samples in this study, the statistical significance is not very significant, and the difference between the minimum and maximum values of CEA in patients is large, which leads to the standard deviation is too high, also The error and statistical difference that would cause the experiment are not significant, and the minimum and maximum values with obvious individual differences can be removed while ensuring the number of samples, thereby reducing the error.

Data availability statement

The original contributions presented in the study are included in the article/Supplementary Material, further inquiries can be directed to the corresponding author.

Ethics statement

The study methods and protocols were approved by the Medical Ethics Committee of the First Affiliated Hospital of Nanchang University (Nanchang, China) and followed the

principles of the Declaration of Helsinki. All subjects were notified of the objectives and content of the study and latent risks, and then provided written informed consent to participate.

Author contributions

JT and TS conceived and designed the present study. MK, H-YS, and TS were responsible for acquiring the data, designing the figures and tables and drafting the manuscript. X-LL and PY contributed to the acquisition of the data and interpreting the results. JZ, QL, and Y-XW assisted in the acquisition of the data and drafting the manuscript. TS, HW, and YS assisted in the acquisition and analysis of the data with constructive discussion.

Conflict of interest

The authors declare that the research was conducted in the absence of any commercial or financial relationships that could be construed as a potential conflict of interest.

Publisher's note

All claims expressed in this article are solely those of the authors and do not necessarily represent those of their affiliated organizations, or those of the publisher, the editors and the reviewers. Any product that may be evaluated in this article, or claim that may be made by its manufacturer, is not guaranteed or endorsed by the publisher.

References

Bai, R., Li, L. Y., Chen, X., Chen, N., Song, W., and Cui, J. (2020). Neoadjuvant and adjuvant immunotherapy: Opening new horizons for patients with early-stage non-small cell lung cancer. *Front. Oncol.* 9, 575472. doi:10.3389/fonc.2020.575472

Cabreraalarcon, J. L., Carrillovico, A., Santotoribio, J. D., CArrillo-Vico, A., Leon-Justel, A., GonzAlez-CAstro, A., et al. (2011). CYFRA 21-1 as a tool for distant metastasis detection in lung cancer. *Clin. Lab.* 57 (11-12), 1011–1014.

Cedrés, S., Nuñez, I., Longo, M., Martinez, P., Checa, E., Torrejon, D., et al. (2011). Serum tumor markers CEA, CYFRA21-1, and CA-125 are associated with worse prognosis in advanced non-small-cell lung cancer (NSCLC). *Clin. Lung Cancer* 12 (3), 172–179. doi:10.1016/j.cllc.2011.03.019

Celikoglu, F., Celikoglu, S. I., and Goldberg, E. P. (2010). Intratumoural chemotherapy of lung cancer for diagnosis and treatment of draining lymph node metastasis. *J. Pharm. Pharmacol.* 62 (3), 287–295. doi:10.1211/jpp.62.03.0001

Chen, F., Yan, C. E., Li, J., Han, X. H., Wang, H., and Qi, J. (2015). Diagnostic value of CYFRA 21-1 and CEA for predicting lymph node metastasis in operable lung cancer. *Int. J. Clin. Exp. Med.* 8 (6), 9820–9824.

Chen, Y., Peng, W., Huang, Y., Chen, J., Su, G., Jiang, C., et al. (2015). Significance of serum neuron-specificenolase before treatment in predicting brain metastases and prognosis of advanced non-small cell lung cancer. *Zhonghua Zhong Liu Za Zhi* 37 (7), 508–511.

Chu, Y., Lai, Y-H., Lee, M-C., Yeh, Y. J., Wu, Y. K., Tsao, W., et al. (2017). Calsyntenin-1, clusterin and neutrophil gelatinase-associated lipocalin are candidate serological biomarkers for lung adenocarcinoma. *Oncotarget* 8 (64), 107964–107976. doi:10.18632/oncotarget.22438

Funatsu, T., Matsubara, Y., Ikeda, S., Hatakenaka, R., Hanawa, T., and IsHida, H. (1994). Preoperative mediastinoscopic assessment of N factors and the need for mediastinal lymph node dissection in T1 lung cancer. *J. Thorac. Cardiovasc. Surg.* 108 (2), :321–328. doi:10.1016/s0022-5223(94)70014-1

Han, S., Wang, T., Chen, Y. M., Han, Z., Guo, L., Wu, Z., et al. (2019). High CCL7 expression is associated with migration, invasion and bone metastasis of non-small cell lung cancer cells. *Am. J. Transl. Res.* 11 (1), 442–452.

Jain, P., Jain, C., and Velcheti, V. (2018). Role of immune-checkpoint inhibitors in lung cancer. *Ther. Adv. Respir. Dis.* 12, 1753465817750075. doi:10.1177/1753465817750075

Kong, M., Jiang, J., Cai, X., Shen, J., Ma, D., Ye, M., et al. (2017). Characteristics of lymph node metastasis in resected adenosquamous lung cancer. *Med. Baltim.* 96 (48), e8870. doi:10.1097/MD.0000000000008870

Lee, D. S., Kim, Y. S., Jung, S. L., Lee, K. Y., Kang, J. H., Park, S., et al. (2012). The relevance of serum carcinoembryonic antigen as an indicator of brain metastasis detection in advanced non-small cell lung cancer. *Tumour Biol.* 33 (4), 1065–1073. doi:10.1007/s13277-012-0344-0

Li, Y., Li, H. W., and Tong, Y. J. (2000). Clinical study of lymph node metastasis in lung cancer. *Chin. J. Thorac. Cardiovasc Surg.* 16 (1), 1012.

Liam, C-K., Andarini, S., Lee, P., Ho, J. C. M., Chau, N. Q., and Tscheikuna, J. (2015). Lung cancer staging now and in the future. *Respirology* 20 (4), 526–534. doi:10.1111/resp.12489

Marchi, N., Peter, M., Fazio, V., Mekhail, T., Masaryk, T., and Janigro, D. (2008). ProApolipoprotein A1: A serum marker of brain metastases in lung cancer patients. *Cancer* 112 (6), 1313–1324. doi:10.1002/cncr.23314

Morita, S., Suda, T., Oda, C., Kobayashi, M., Hoshi, T., Kanefuji, T., et al. (2019). The value of 18F-fdg PET in the diagnosis of intertrabecular vertebral metastasis in a small cell lung cancer patient with a high serum CEA level. *Intern. Med.* 58 (3), 415–418. doi:10.2169/internalmedicine.1394-18

Ndiaye, A., Di-Marino, V., Ba, P. S., Gaye., M., and Nazarian, S. (2016). Anatomical variations in lymphatic drainage of the right lung: Applications in lung cancer surgery. *Surg. Radiol. Anat.* 38 (10), 1143–1151. doi:10.1007/s00276-016-1685-y

Nikliński, J., Furman, M., Laudanski, J., and Kozhowski, M. (1992). Evaluation of squamous cell carcinoma antigen (SCC-Ag) in the diagnosis and follow-up of patients with non-small cell lung carcinoma. *Neoplasma* 39 (5), 279–282.

Okada, M., Sakamoto, T., Nishio, W., Uchino, K., and Tsubota, N. (2003). Characteristics and prognosis of patients after resection of non-small cell lung carcinoma measuring 2 cm or less in greatest dimension. *Cancer* 98 (3), 535–541. doi:10.1002/cncr.11530

Oshiro, Y., Takada, Y., Enomoto, T., Fukao, K., Ishikawa, S., and Iijima, T. (2004). A resected case of metachronous liver metastasis from lung cancer producing alpha-fetoprotein (AFP) and protein induced by vitamin K absence or antagonist II (PIVKA-II). *Hepatogastroenterology.* 51 (58), 1144–1147.

Pollan, M., Varela, G., Torres, A., de la Torre, M., Ludena, M. D., Ortega, M. D., et al. (2003). Clinical value of p53, c-erbB-2, CEA and CA125 regarding relapse, metastasis and death in resectable non-small cell lung cancer. *Int. J. Cancer* 107 (5), 781–790. doi:10.1002/ijc.11472

Pujol, J. L., Molinier, O., Ebert, W., Daurès, J. P., Barlesi, F., Buccheri, G., et al. (2004). CYFRA 21-1 is a prognostic determinant in non-small-cell lung cancer: Results of a meta-analysis in 2063 patients. *Br. J. Cancer* 90 (11), 2097–2105. doi:10.1038/sj.bjc.6601851

Roberts, D., Williams, S. J., Cvetkovic, D., Weinstein, J. K., Godwin, A. K., Johnson, S. W., et al. (2002). Decreased expression of retinol-binding proteins is associated with malignant transformation of the ovarian surface epithelium. *DNA Cell Biol.* 21 (1), 11–19. doi:10.1089/10445490252810276

Shimazu, K., Tanei, T., Tamaki, Y., Saeki, T., Osaki, A., Hasebe, T., et al. (2019). Performance of a new system using a one-step nucleic acid amplification assay for detecting lymph node metastases in breast cancer. *Med. Oncol.* 36, 54–58. doi:10.1007/s12032-019-1277-x

Wang, Y. J., Guan, Q., and Xiang, J. (2019). Nomogram for predicting level V lymph node metastases in papillary thyroid carcinoma with clinically lateral lymph node metastases: A large retrospective cohort study of 1037 patients from fduscc. *J. Cancer* 10, 772–778. doi:10.7150/jca.28527

Watanabe, Y., Shimizu, J., Tsubota, M., and Iwa, T. (1990). Mediastinal spread of metastatic lymph nodes in bronchogenic carcinoma. Mediastinal nodal metastases in lung cancer. *Chest* 97 (5), 1059–1065. doi:10.1378/chest.97.5.1059

Weinberger, S. R., Dalmasson, E. A., and Fung, E. T. (2002). Current achievements using protein chip array technology. *Curr. Opin. Chem. Biol.* 6, 86–91. doi:10.1016/s1367-5931(01)00282-4

Wen, X. Z., Wang, B., Jin, Q. M., Zhang, W., and Qiu, M. (2019). Thyroid antibody status is associated with central lymph node metastases in papillary thyroid carcinoma patients with hashimoto's thyroiditis. *Ann. Surg. Oncol.* 26, 1751–1758. doi:10.1245/s10434-019-07256-4

Wu, L., Hu, B., Zhao, B., Liu, Y., Yang, Y., Zhang, L., et al. (2017). Circulating microRNA-422a is associated with lymphatic metastasis in lung cancer. *Oncotarget* 8 (26), 42173–42188. doi:10.18632/oncotarget.15025

Xu, B. X., Liu, Y. L., Yao, S. L., Shao, M., Chen, Y., Wang, K., et al. (2003). Value of FDG PET for mediastinal lymph node staging in non-small cell lung cancer. *Chin. J. Lung Cancer* 6 (3), 198–200. doi:10.3779/j.issn.1009-3419.2003.03.09

Yoshino, I., Yokoyama, H., Yano, T., Ueda, T., Takai, E., Mizutani, K., et al. (1996). Skip metastasis to the mediastinal lymph nodes in non-small cell lung cancer. *Ann. Thorac. Surg.* 62 (4), 1021–1025. doi:10.1016/0003-4975(96)00470-5

Yu, Z., Chen, X. Z., Cui, L. H., Si, H. Z., Lu, H. J., and Liu, S. H. (2014). Prediction of lung cancer based on serum biomarkers by gene expression programming methods. *Asian pac. J. Cancer Prev.* 15 (21), 9367–9373. doi:10.7314/apjcp.2014.15.21.9367

Zhang, D. G., Chen, X. C., Zhu, D., Qin, C., Dong, J., Qiu, X., et al. (2019). Intrapulmonary lymph node metastasis is common in clinically staged IA adenocarcinoma of the lung. *Thorac. Cancer* 10 (2), 123–127. doi:10.1111/1759-7714.12908

Zhang, L., Liu, D., Li, L., Pu, D., Zhou, P., Jing, Y., et al. (2017). The important role of circulatingCYFRA21-1 in metastasis diagnosis and prognostic value compared with carcinoembryonic antigen and neuron-specific enolase in lung cancer patients. *BMC Cancer* 17, 96. doi:10.1186/s12885-017-3070-6

Zhou, Y., Yu, Q. F., Peng, A. F., Tong, W. L., Liu, J. M., and Liu, Z. L. (2017). The risk factors of bone metastases inpatients with lung cancer. *Sci. Rep.* 7 (1), 8970. doi:10.1038/s41598-017-09650-y

frontiers | Frontiers in Genetics

TYPE Original Research
PUBLISHED 19 September 2022
DOI 10.3389/fgene.2022.1010903

OPEN ACCESS

EDITED BY
Qian Wang,
Tai'an City Central Hospital, China

REVIEWED BY
Zhirong Lin,
Xiamen University, China
Wensi Tao,
University of Miami Health System, United States

*CORRESPONDENCE
Yi Shao,
freebee99@163.com

†These authors have contributed equally to this work

SPECIALTY SECTION
This article was submitted to Cancer Genetics and Oncogenomics, a section of the journal Frontiers in Genetics

RECEIVED 03 August 2022
ACCEPTED 30 August 2022
PUBLISHED 19 September 2022

CITATION
Tang J, Zhang L-J, Kang M, Huang R, Shu H-Y, Wei H, Zou J, Pan Y-C, Ling Q and Shao Y (2022), AFP and CA-125 as an accurate risk factor to predict eye metastasis in hypertension patients with liver carcinoma: A STROBE-compliant article.
Front. Genet. 13:1010903.
doi: 10.3389/fgene.2022.1010903

AFP and CA-125 as an accurate risk factor to predict eye metastasis in hypertension patients with liver carcinoma: A STROBE-compliant article

Jing Tang[1†], Li-Juan Zhang[2†], Min Kang[2†], Rong Huang[2], Hui-Ye Shu[2], Hong Wei[2], Jie Zou[2], Yi-Cong Pan[2], Qian Ling[2] and Yi Shao[2*]

[1]Department of Oncology, The First Affiliated Hospital of Nanchang University, Jiangxi Center of National Ocular Disease Clinical Research Center, Nanchang, Jiangxi, China, [2]Department of Ophthalmology, The First Affiliated Hospital of Nanchang University, Jiangxi Center of National Ocular Disease Clinical Research Center, Nanchang, Jiangxi, China

Purpose: In this study, we analyzed the differences between hypertension patients with ocular metastasis of liver cancer and those with metastases to other sites, the correlation between history of HBV and liver cancer metastasis, and independent risk factors for ocular metastasis.

Methods: We used treatment records from 488 patients with metastases of primary liver cancer from August 2001 to May 2015, divided into two groups based on metastatic sites: OM (ocular metastasis) and NOM (non-ocular, other sites of metastasis) groups. The Student's *t*-test and Chi-square test were used to assess the significance of differences between the groups and define the relationship between history of HBV and ocular metastasis of liver cancer. Binary logistic regression analysis was used to identify indicators of ocular metastasis of liver cancer and receiver operating curve (ROC) analyses to estimate their diagnostic value.

Results: No significant differences in sex, age, tumor stage, pathological type, or treatment were identified between the OM and NOM groups, while the prevalence of HBV was higher in the former than that in latter. Binary logistic regression demonstrated that AFP and CA-125 were independent indicators of liver metastasis (both $p < 0.001$). ROC curve analyses generated cut-off values for AFP and CA-125 of 957.2 ng/ml and 114.25 U/ml, respectively, with corresponding AUC values of 0.739 and 0.810. The specificity of the combination of AFP and CA-125 was higher than either factor separately.

Discussion: To explore the diagnostic value of AFP and CA125 in predicting the development of ocular metastases of hypertensive patients with liver cancer, which will help us to diagnose the occurrence and development of the disease more accurately and make the best clinical diagnosis and treatment measures.

KEYWORDS

AFP, CA-125, ocular metastasis, primary liver cancer, hypertension, history of hepatitis B

Introduction

Hypertension is a chronic disease with functional or organic damage of heart, brain, kidney, and other organs, which brings a huge health burden to the society. Primary liver cancer (PLC) is a common disease worldwide, particularly in developing countries (Zhang et al., 2015). Hepatocellular carcinoma (HCC) is the main pathological type of PLC, and exhibits high malignancy and strong invasiveness, resulting in poor prognosis and a heavy economic burden of treatment (Wang et al., 2016). Worldwide, patients with hepatitis B virus (HBV) infection exceed 300 million, and many liver diseases, including liver cancer, can be secondary to HBV infection (Liang, 2009). Moreover, chronic hepatitis virus infection not only affects the liver, but also extrahepatic organs, leading to severe extrahepatic lesions such as dry eye, Mooren's ulcer, and retinopathy. HBV infection is clearly linked to dry eye syndrome (Tsoumani et al., 2013). Extrahepatic metastasis is an indicator of prognosis in patients with PLC, and different metastatic sites are associated with distinct survival rates (Wu et al., 2017). A survey of 419 patients with HCC who had extrahepatic metastases found that the most common sites of extrahepatic metastases are lung, bone, lymph node, and adrenal gland in that order (Aino et al., 2014). The eye is a rare site of distant hepatic metastasis of PLC, and most patients with ocular metastases also have metastases at other sites. Hypertensive patients are prone to arteriosclerosis, which leads to liver blood supply insufficiency and liver function damage. Related clinical symptoms can cover up the signs of liver cancer, and the early clinical symptoms of HCC are not obvious; hence, patients can be completely unaware of their disease progression and even metastasis (McMahon et al., 2016). Once a distant metastasis occurs, treatment is extremely difficult, and patient prognosis is poor. At present, the diagnosis of PLC mainly depends on imaging [ultrasound and magnetic resonance imaging (MRI)] (Cassinotto et al., 2017), clinicopathological correlation, and application of immunohistochemical markers (Vyas and Jain, 2018); however, these methods are inefficient for early detection of metastases, hence a simple and effective clinical diagnostic indicator is needed to improve the early diagnosis rate of ocular metastasis from PLC.

Materials and methods

Study design

This study met the requirements of the Declaration of Helsinki and was licensed by the Medical Ethics Committee of the First Affiliated Hospital of Nanchang University. The study design followed relevant regulations and guidelines. Hypertensive patients with PLC metastases (n = 488), admitted from August 2001 to May 2015, were enrolled in the study. The inclusion criteria are: 1) hypertension (systolic blood pressure >140 mmHg or diastolic blood pressure >90 mmHg); 2) without contraindications in MRI, CT and other imaging examinations; 3) Canceration of liver tissue; 4) ocular metastasis of hepatocellular carcinoma (Figure 1). Diagnosis was determined by imaging [ultrasound, computed tomography (CT), MRI] and histopathological biopsy. A review of the medical records of the patients revealed that those with ocular metastases of liver cancer also had metastases at other sites. Therefore, patients were divided into two groups, according to the tumor metastasis sites: OM (PLC with ocular metastasis) and NOM group (PLC with non-ocular, but other metastasis sites) groups. Exclusion criteria for the OM group were: 1) primary malignant tumor of the eye; 2) benign tumor of the eye; 3) primary liver cancer patients with metastases in other sites (intrahepatic, portal system, lung, bone, etc.).

Data collection

Relevant clinical data were collected retrospectively from the medical records of each subject, including sex, age, history of HBV, clinical stage, pathological type, treatment methods, and other clinical features, serum markers (AFP, CEA, CA-125, CA-199, CA-153, and CA-724), blood lipid indicators {lipoprotein a [Lp(a)], apolipoprotein B (ApoB), apolipoprotein A1 (ApoA1), low-density lipoprotein (LDL), high-density lipoprotein (HDL), triglycerides (TG), and total cholesterol (TC)}, serum calcium concentration, hemoglobin concentration, ferritin, alkaline phosphatase (ALP), and other serum indicators. All clinical data were collected at initial diagnosis.

Statistical analysis

Student's t-tests and Chi-square tests were used to evaluate the significance of differences in clinical characteristics between the OM and NOM groups. Binary logistic regression analysis was used to identify indicators of ocular metastasis of liver cancer. ROC curve analysis was conducted and the area under the curve (AUC) used to assess the accuracy of risk factors as diagnostic indicators. $p < 0.05$ was considered statistically significant. SPSS

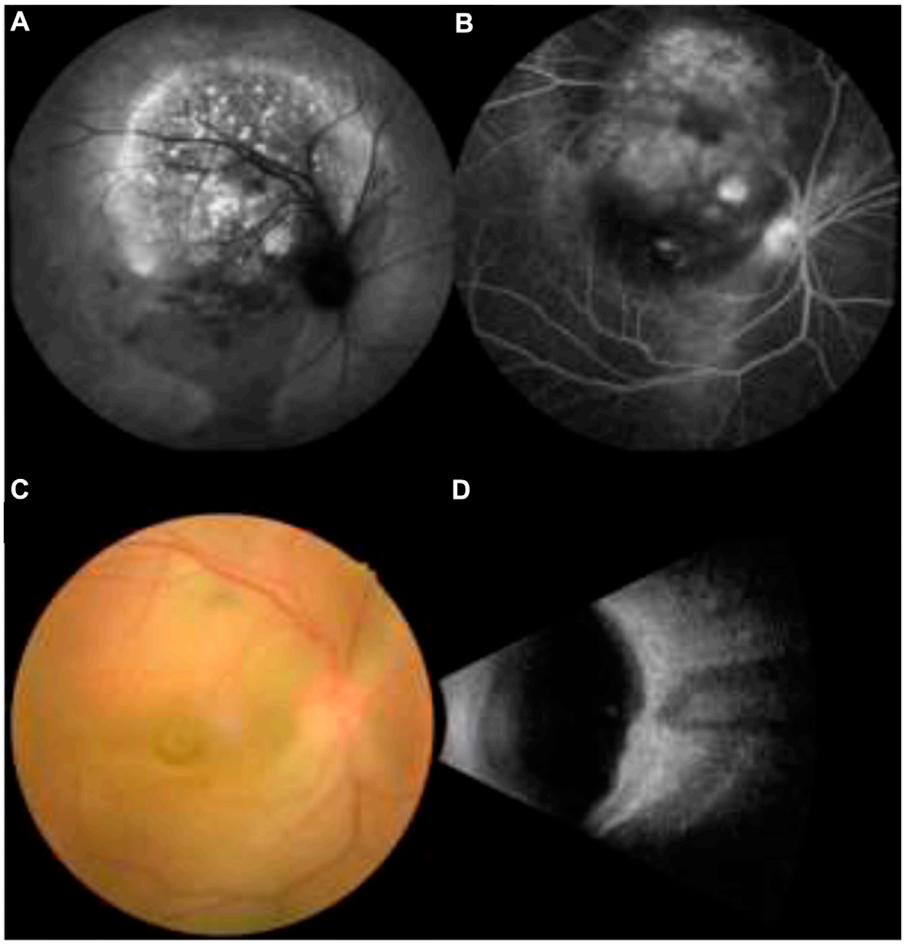

FIGURE 1
(A,B) Fundus fluorescein angiography in patients with primary liver cancer, **(C,D)** Funduscopy in patients with primary liver cancer.

25.0 (SPSS, IBM, United States), MedCalc 19.0.5 (MedCalc Ostend, Belgium), and Excel 2019 (Microsoft Corp, Redmond, WA, United States) software were used for statistical analyses.

Results

Demographic and clinical characteristics

In this study we reviewed data from 488 patients, including 21 in the OM and 467 in the NOM groups. Clinical characteristics, including sex, clinical stage, pathological type, and treatment methods did not differ significantly between the OM and NOM groups (Student's *t*-test and Chi-square test). The OM group was significantly older (57.7 ± 12.2 years) than the NOM group (51.5 ± 13.8 years) ($p < 0.05$). There was also a significant difference in history of HBV between the two groups ($p < 0.05$), confirming that ocular metastasis of PLC is associated with history of HBV. The clinical details of all subjects are presented in Table 1.

Differences in clinical characteristics and risk factors for OM

CEA, CA-199, CA-153, CA-724, TC, TG, HDL, LDL, ApoA1, ApoB, Lp(a), calcium, Hb, ferritin, ALP, and other serological indicators did not differ significantly between the OM and NOM groups, while AFP and CA-125 were significantly higher in the OM group ($p < 0.001$) (Table 2). Binary logistic regression analysis determined that AFP and CA-125 were associated with liver cancer metastasis (Table 3).

Cut-off, sensitivity, specificity, and AUC values of AFP and CA-125 for diagnosing ocular metastases of PLC

Figure 2 shows the ROC curves for AFP and CA-125, as independent risk factors for ocular metastasis of liver cancer, and their AUC, specificity, sensitivity, and cut-off values. The cut-off

TABLE 1 The clinical characteristics of patients with metastases of primary liver cancer.

Clinical characteristics	OM group (%) (n = 21)	NOM group (%) (n = 467)	P value[c]
Sex[a]			
Male	16 (76.2)	401 (85.9)	0.219
Female	5 (23.8)	66 (14.1)	
Age (years)[b]			
Mean ± SD	57.7 ± 12.2	51.5 ± 13.8	0.044
History of HBV[a]			
With (+)	18 (85.7)	267 (57.2)	0.018
Without (-)	3 (14.3)	200 (42.8)	
Tumor clinical stage[a]			
Stage 2	0 (0)	15 (3.2)	0.084
Stage 3	3 (14.3)	98 (21.0)	
Stage 4	5 (23.8)	33 (7.1)	
Unknown	13 (61.9)	321 (68.7)	
Pathological type[a]			
Hepatocellular carcinoma (HCC)	0 (0)	38 (8.1)	0.327
Cholangiocarcinoma	0 (0)	24 (5.1)	
Mixed hepatocellular carcinoma	0 (0)	2 (0.4)	
Unknown	21 (0)	403 (86.4)	
Treatment[a]			
Surgery	4 (19.0)	85 (18.2)	0.261
Chemotherapy	3 (14.3)	38 (8.1)	
Protect liver treatment	9 (42.8)	137 (29.3)	
TACE	3 (14.3)	148 (31.6)	
Radiation and chemotherapy	1 (4.8)	7 (1.5)	
Refuse treatment	1 (4.8)	32 (6.8)	
Other	0 (0)	21 (4.5)	

[a]Chi-square test was used.
[b]Student's t-test was used.
[c]Comparison between OM, group and NOM, metastases group.
Notes: $p < 0.05$ was considered statistically significant.
Abbreviations: OM, ocular metastasis; NOM, non-ocular, other sites of metastasis; SD, standard deviation; HBV, hepatitis B virus; TACE, transcatheter arterial chemoembolization.

values for AFP and CA-125 were 957.2 and 114.25 U/ml and AUC values were 0.739 and 0.810, respectively. AFP had a higher sensitivity value than CA-125, while the specificity of CA-125 was higher than that of AFP. Figure 3 shows a comparison of the ROC curves for AFP, CA-125, and the combination of AFP and CA-125 (AFP + CA-125). The AUC, sensitivity, specificity, and cut-off values for AFP, CA-125, and AFP + CA-125 are presented in Table 4. Among them, AFP + CA-125 had the largest AUC (0.875), AFP the highest sensitivity (95.2%), and AFP + CA-125 the highest specificity (88.4%); all results were statistically significant.

Discussion

Liver carcinoma ranks second among the causes of cancer mortality globally (McGlynn et al., 2015). PLC pathological types include: intrahepatic cholangiocarcinoma (iCCA), HCC, and other rare types (Sia et al., 2017). Among these, HCC is the primary pathological type, accounting for approximately 80% of the total (Adigun et al., 2021). Wang et al. confirmed this through statistical analysis of 2,172 patients with histologically confirmed PLC, among which were 1,823 HCC and 238 iCCA patients, accounting

TABLE 2 The serum indicators of patients with metastases of primary liver cancer.

Serum indicators	OM group	NOM group	*t*	*p* Value
Tumor markers				
AFP (ng/ml)	1,048.80 ± 273.95	559.00 ± 553.48	7.529	<0.001
CEA (ng/ml)	19.78 ± 46.90	19.93 ± 82.97	−0.008	0.994
CA-125 (U/ml)	481.74 ± 356.55	167.26 ± 318.36	4.404	<0.001
CA-199 (U/ml)	221.34 ± 338.41	156.12 ± 292.84	0.992	0.322
CA-153 (u/ml)	18.71 ± 12.76	22.36 ± 25.41	−0.655	0.513
CA-724 (U/ml)	8.60 ± 9.76	6.86 ± 7.16	1.070	0.285
Blood lipid indicators				
TC (mmol/L)	4.63 ± 1.87	4.12 ± 1.46	1.566	0.118
TG (mmol/L)	1.82 ± 1.38	1.24 ± 0.88	1.895	0.072
HDL (mmol/L)	1.57 ± 1.30	1.37 ± 0.95	0.905	0.366
LDL (mmol/L)	2.91 ± 1.97	2.40 ± 1.27	1.148	0.265
ApoA1 (g/L)	1.64 ± 0.47	1.55 ± 0.47	0.825	0.410
ApoB (g/L)	1.01 ± 0.59	0.97 ± 0.58	0.299	0.765
Lp(a) (mg/L)	148.20 ± 182.73	224.15 ± 238.04	−1.407	0.16
Calcium (mmol/L)	2.12 ± 0.24	2.16 ± 0.28	−0.665	0.506
Hb (g/L)	114.71 ± 36.00	116.02 ± 24.02	−0.237	0.812
Ferritin (μg/L)	235.13 ± 243.46	264.73 ± 207.33	−0.635	0.526
ALP (U/L)	225.95 ± 122.46	199.78 ± 189.18	0.628	0.530

Notes: Student's *t*-test was uesd. $p < 0.05$ represented statistically significant. Abbreviations: OM, ocular metastasis; NOM, non-ocular, other sites of metastasis; TC, total cholesterol; TG, triglycerides; HDL, high-density lipoprotein; LDL, low-density lipoprotein; ApoA1, apolipoprotein A1; ApoB, apolipoprotein B; Lp(a), lipoprotein a; Hb, hemoglobin; ALP, alkaline phosphatase.

TABLE 3 Independent risk factors of OM in patients with primary liver cancer.

Factor	B	Exp(B)	OR (95%CI)	*p*
AFP	0.001	1.001	1.001–1.002	<0.001
CA-125	0.001	1.001	1.001–1.002	<0.001

Notes: Binary logistic analysis was used. $p < 0.05$ represented statistically significant. Abbreviations: B, coefficient of regression; OR, odds ratio; CI, confidence interval; OM, ocular metastasis.

for 83.9 and 11.0%, respectively (Wang et al., 2017). Therefore, we chosed HCC as the main research object.

The incidence and mortality of HCC are increasing. Cirrhosis caused by HBV and hepatitis C is a significant risk factor for HCC globally (Mittal and El-Serag, 2013); however, in most areas of China, HBV is the most important pathogen in the context of PLC. (Li et al., 2015; Ye et al., 2015; Wang et al., 2017). The pathogenesis of HBV is clear. The integrated viral sequence produces different mutations in the preS/S gene, due to replication defects, which can induce various tumorigenesis mechanisms, thereby contributing to HCC (Li et al., 2016).

Infection with HBV can cause a variety of liver lesions and illness; for example, fulminant cirrhosis, chronic hepatitis, hepatic failure, acute hepatitis, and HCC (Liang, 2009). Cirrhosis is an intermediate process, through which viral hepatitis develops into liver cancer. Most HCC patients with a history of viral hepatitis have experienced cirrhosis (Ringelhan et al., 2017). Mahmood et al. (2008) conducted a study on cirrhosis and found that, among the 137 patients with cirrhosis who participated in the trial, the causes of cirrhosis included: hepatitis C virus (61%), HBV (32%), alcoholism (3%), and primary biliary cirrhosis (3%). In addition, 47% of participants had ocular complications. Martín LL et al. (Martín et al., 2021) reported a case of severe multiple and recurrent spontaneous corneal perforation in a patient with primary biliary cirrhosis**.** It is clear that HBV contributes to liver cirrhosis and even liver cancer, and the former can cause ocular complications; therefore, there is evidence for an indirect relationship between history of HBV and ocular lesions. The mechanism underlying this relationship is currently unclear; however, experiments in mice confirmed that SMAD3 mediates the majority of profibrotic activity, since liver cirrhosis, proliferative vitreoretinopathy, and ocular capsule injury are alleviated in SMAD3-null mice (Flanders, 2004).

HBV can also cause eye lesions directly. A 72-year-old chronic HBV patient was also diagnosed with orbital MALT lymphoma, with a clinical manifestation of bilateral ocular protrusion and slight limitation of eye movement, providing evidence for a possible association between HBV and ocular lesions (Lin et al., 2017). There is a risk of eye complications during the prevention and treatment of HBV. HBV vaccine, either alone or administered with other vaccines, appears to be

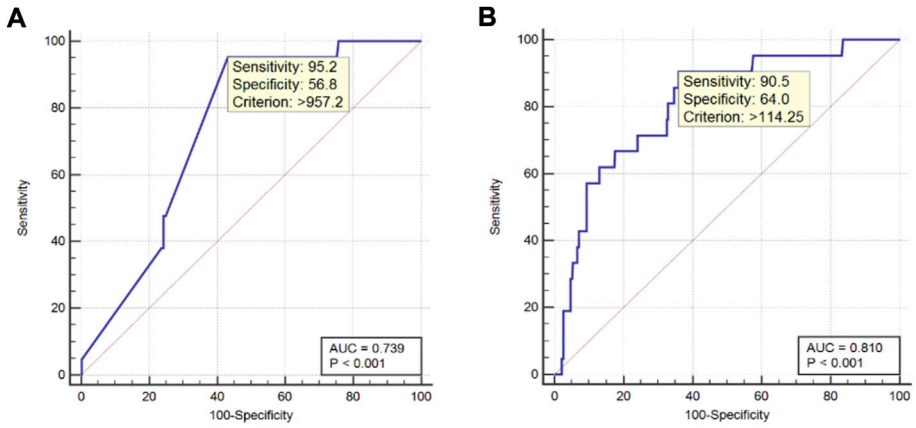

FIGURE 2
ROC curve of independent risk factors for ocular metastasis from liver cancer. Notes: **(A)**. ROC curve of AFP; **(B)**. ROC curve of CA-125. Abbreviations: AUC, area under the curve; ROC, receiver operating curve.

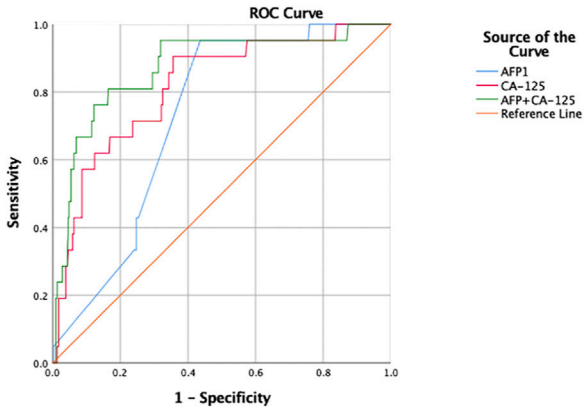

FIGURE 3
ROC curve of respective and combination of independent risk factors for ocular metastasis from liver cancer. Abbreviations: AUC, area under the curve; ROC, receiver operating curve.

chronic HBV. The glaucoma symptoms were improved after discontinuation of interferon therapy.

Liver cancer is frequently occult; 70% of patients with PLC have detectable metastases at initial diagnosis, while metastases account for 90% of the total cancer-related mortality rate (Arvelo et al., 2016). Different distant extrahepatic metastases vary greatly in terms of mortality rates. The lung is common metastatic site of PLC, while brain metastasis is rare, and patients with brain metastasis have the worst prognosis (Wu et al., 2017). Other rarer cases of HCC metastatic sites include thyroid (Liang et al., 2007) and nodal (Liu et al., 2017).

As there is no lymphatic system in the eye, it is rarely a site of malignant tumor metastasis; however, malignant tumors can still be transferred to the eye *via* the blood system. Therefore, blood-rich areas, such as the posterior choroid of the uveal structure, are prone to ocular metastases. The appearance of ocular metastases is also conclusive evidence of tumor metastasis (Konstantinidis and Damato, 2017).

TABLE 4 The AUC, sensitivity, specificity and cut-off value for single risk factors in predicting OM from primary liver cancer.

Factor	AUC	Sensitivity (%)	Specificity (%)	Cut-off value U/ml	*p*
AFP	0.739	95.2	56.8	957.2	<0.001
CA-125	0.810	90.2	64.0	14.25	<0.001
AFP + CA-125	0.875	76.2	88.4	—	<0.001

Notes: Sensitivity and specificity were obtained at the point of cut-off value. $p < 0.05$ represented statistically significant. Abbreviations: AUC, area under the curve; OM, ocular metastasis.

the leading offender in causing uveitis (Benage and Fraunfelder, 2016). Kwon et al. (2001) reported a 15-year-old boy who developed glaucoma while using interferon alpha therapy for

Most patients with stage 4 cancer (distal tumor metastasis), including distant ocular metastases, have clear primary sites (Cohen, 2013). The most common among them for ocular metastases are

breast and lung (Konstantinidis and Damato, 2017). Primary cancer sites also include: pancreas (1%), thyroid (1%), prostate (2%), lung carcinoid (2%), cutaneous melanoma (2%), gastrointestinal (GI) tract (4%), kidney (4%), lung (26%), breast (37%), other sites (3%), and unknown (16%) (Shields et al., 2018). All of the patients in our study with eye metastases also had other sites of metastasis. The eye is the terminal organ of liver cancer metastasis. Once metastasis occurs, treatment is difficult and the prognosis poor. Therefore, we compared patients with ocular metastasis to those with other metastasis sites, to identify indicators of ocular metastasis of liver cancer and improve the early diagnosis rate. We found that the OM group was older than the NOM group ($p < 0.05$), likely because elderly patients have a higher prevalence of diabetes, poorer physical fitness, and cannot tolerate higher-intensity treatment (Guo et al., 2017). In addition, due to the association between HBV and ocular lesions, patients with a history of HBV had higher rate of metastases to the eye than to other sites. During clinical diagnosis of PLC, whether the patient has a history of HBV should be determined, to inform subsequent treatment.

Lp(a), ApoB, ApoA1, LDL, HDL, TG, TC, hemoglobin, ferritin, and ALP are commonly used as indicators for evaluating blood lipids and liver function. Statistical analysis did not identify any significant differences between the above indicators in the OM and NOM groups. The serum biomarkers, CA-153, CA-199, CA-125, CEA, AFP, and CA-724 are tumor markers and have clear predictive significance for a variety of tumors (Zou et al., 2006; Zhao et al., 2015; Hogendorf et al., 2017; Kim et al., 2017). In patients with HBV and hepatitis C virus, particularly combined evaluation of AFP, CEA, CA-125, CA-153, and CA-199 have already been implemented (Assmar et al., 2016). Among them, multiple roles for AFP and CA-125 have been confirmed. AFP is a plasma protein produced by embryonic tissue. Healthy adult adults have very low levels of AFP, and some primary cancers can cause significant increases in this factor; therefore, it can be used to screen for tumors and other pathologies in adults (Adigun and Khetarpal, 2019), including primary HCC (Ahmed Mohammed and Roberts, 2017), and gastric cancer (Sun et al., 2017). CA-125 levels are associated with lymphangioleiomyomatosis (LAM), and elevated CA-125 may indicate LAM with pleural effusion, leading to decreased lung function (Glasgow et al., 2018). Karimi-Zarchi et al. (2016) reported that CA-125 can be used for clinical prediction of endometriosis, while another report showed CA-125 as useful for surveillance in ovarian cancer (Esselen et al., 2016).

Non-invasive standard imaging methods, such as MRI, dynamic multi-phase multi-row computed tomography, and ultrasound, are used to diagnose HCC (Wang et al., 2015). Serum biomarker assays are reproducible, simple, and rapid, relative to traditional diagnostic methods. Our statistical analyses confirmed the diagnostic value of AFP and CA-125 for liver metastasis.

Finally, we determined the value of AFP, CA-125, and AFP + CA-125 as diagnostic indicators for ocular metastasis of liver cancer by binary logistic regression analysis and plotting ROC curves. The results indicate that AFP has the highest sensitivity and can be used for early screening of ocular metastases from liver cancer. If AFP rises above 957.2 U/ml, the patient has a higher probability of terminal ocular metastasis. AFP + CA-125 has the highest specificity, and is of great significance for the diagnosis of ocular metastasis from liver cancer.

Our research has certain limitations. First, the sample size of this retrospective study was small, particularly for the OM group. Second, because all patients in the OM group had other sites of metastases simultaneously, confounding factors were inevitable. Furthermore, there were missing items in various clinical statistical analyses, which will have reduced the accuracy of the results. Finally, all subjects were diagnosed and treated in the same hospital, and it is difficult to exclude selection bias; therefore, the accuracy of the conclusions from the results of this study require confirmation in investigations with large samples and multiple centers.

Conclusion

In summary, we found that patients who had PLC metastasis with a history of HBV were more likely to have ocular metastases than those without. Increases in the serum biomarkers, AFP and CA-125, are associated with an increased likelihood of ocular metastasis. AFP, CA-125, and AFP combined with CA-125 can be used as diagnostic indicators for ocular metastasis in patients with PLC with metastasis.

Data availability statement

The original contributions presented in the study are included in the article/supplementary material, further inquiries can be directed to the corresponding author.

Ethics statement

The studies involving human participants were reviewed and approved by the Medical Ethics Committee of the First Affiliated Hospital of Nanchang University. The patients/participants provided their written informed consent to participate in this study.

Author contributions

JT was responsible for conceiving and designing the work and writing the manuscript; L-JZ and MK played an important role in interpreting the results and analyze dates; RH helped acquire data and gave some advice; HW helped perform the analysis with constructive discussions; JZ helped make the figures; Y-CP contributed to helping make the tables; QL

revised the manuscript; and YS helped design the work and approved the final version.

Conflict of interest

The authors declare that the research was conducted in the absence of any commercial or financial relationships that could be construed as a potential conflict of interest.

Publisher's note

References

Adigun, O. O., and Khetarpal, S. (2019). "Alpha fetoprotein (AFP, maternal serum alpha fetoprotein, MSAFP)," in *StatPearls. Treasure island (FL)* (StatPearls Publishing LLC).

Adigun, O. O., Yarrarapu, S. N. S., and Khetarpal, S. (2021). *Alpha Fetoprotein* In: StatPearls [Internet]. Treasure Island, FL: StatPearls Publishing.

Ahmed Mohammed, H. F., and Roberts, L. R. (2017). Should AFP (or any biomarkers) be used for HCC surveillance? *Curr. Hepatol. Rep.* 16 (2), 137–145. doi:10.1007/s11901-017-0349-7

Aino, H., Sumie, S., Niizeki, T., Kuromatsu, R., Tajiri, N., Nakano, M., et al. (2014). Clinical characteristics and prognostic factors for advanced hepatocellular carcinoma with extrahepatic metastasis. *Mol. Clin. Oncol.* 2 (3), 393–398. doi:10.3892/mco.2014.259

Arvelo, F., Sojo, F., and Cotte, C. (2016). Cancer and the metastatic substrate. *Ecancermedicalscience* 10, 701. doi:10.3332/ecancer.2016.701

Assmar, M., Yeganeh, S., Mansourghanaei, F., and Amirmozafari, N. (2016). Combined evaluation of AFP, CA15-3, CA125, CA19-9, and CEA tumor markers in patients with hepatitis B and C. *Iran. J. Public Health* 45 (12), 1645–1651.

Benage, M., and Fraunfelder, F. W. (2016). Vaccine-associated uveitis. *Mo. Med.* 113 (1), 48–52.

Cassinotto, C., Aube, C., and DohAn, A. (2017). Diagnosis of hepatocellular carcinoma: An update on international guidelines. *Diagn. Interv. Imaging* 98 (5), 379–391. doi:10.1016/j.diii.2017.01.014

Cohen, V. M. (2013). Ocular metastases. *Eye (Lond)* 27 (2), 137–141. doi:10.1038/eye.2012.252

Esselen, K. M., Cronin, A. M., Bixel, K., Bookman, M. A., Burger, R. A., Cohn, D. E., et al. (2016). Use of CA-125 tests and computed tomographic scans for surveillance in ovarian cancer. *JAMA Oncol.* 2 (11), 1427–1433. doi:10.1001/jamaoncol.2016.1842

Flanders, K. C. (2004). Smad3 as a mediator of the fibrotic response. *Int. J. Exp. Pathol.* 85 (2), 47–64. doi:10.1111/j.0959-9673.2004.00377.x

Glasgow, C. G., Pacheco-Rodriguez, G., Steagall, W. K., Haughey, M. E., Julien-Williams, P. A., Stylianou, M. P., et al. (2018). CA-125 in disease progression and treat ment of lymphangioleiomyomatosis. *Chest* 153 (2), 339–348. doi:10.1016/j.chest.2017.05.018

Guo, H., Wu, T., Lu, Q., Dong, J., Ren, Y. F., Nan, K. J., et al. (2017). Hepatocellular carcinoma in elderly: Clinical characteristics, treatments and outcomes compared with younger adults. *PLoS One* 12 (9), e0184160. doi:10.1371/journal.pone.0184160

Hogendorf, P., Skulimowski, A., Durczyński, A., Kumor, A., Poznańska, G., Oleśna, A., et al. (2017). A panel of CA19-9, Ca125, and Ca15-3 as the enhanced test for the differential diagnosis of the pancreatic lesion. *Dis. Markers* 2017, 8629712. doi:10.1155/2017/8629712

Karimi-Zarchi, M., Dehshiri-Zadeh, N., Sekhavat, L., and Nosouhi, F. (2016). Correlation of CA-125 serum level and clinico-pathological characteristic of patients with endometriosis. *Int. J. Reprod. Biomed.* 14 (11), 713–718. doi:10.29252/ijrm.14.11.713

Kim, N. H., Lee, M. Y., Park, J. H., Park, D. I., Sohn, C. I., Choi, K., et al. (2017). Serum CEA and CA 19-9 levels are associated with the presence and severity of colorectal neoplasia. *Yonsei Med. J.* 58 (5), 918–924. doi:10.3349/ymj.2017.58.5.918

Konstantinidis, L., and Damato, B. (2017). Intraocular metastases--A review. *Asia. Pac. J. Ophthalmol.* 6 (2), 208–214. doi:10.22608/APO.201712

Kwon, Y. S., Choe, Y. H., and Chin, H. S. (2001). Development of glaucoma in the course of interferon alpha therapy for chronic Hepatitis B. *Yonsei Med. J.* 42 (1), 134–136. doi:10.3349/ymj.2001.42.1.134

Li, H. M., Wang, J. Q., Wang, R., Zhao, Q., Li, L., Zhang, J. P., et al. (2015). Hepatitis B virus genotypes and genome characteristics in China. *World J. Gastroenterol.* 21 (21), 6684–6697. doi:10.3748/wjg.v21.i21.6684

Li, Y. W., Yang, F. C., Lu, H. Q., and Zhang, J. S. (2016). Hepatocellular carcinoma and Hepatitis B surface protein. *World J. Gastroenterol.* 22 (6), 1943–1952. doi:10.3748/wjg.v22.i6.1943

Liang, H. H., Wu, C. H., Tam, K. W., Chai, C. Y., Lin, S. E., and Chen, S. C. (2007). Thyroid metastasis in a patient with hepatocellular carcinoma: Case report and review of literature. *World J. Surg. Oncol.* 5, 144. doi:10.1186/1477-7819-5-144

Liang, T. J. (2009). Hepatitis B: The virus and disease. *Hepatology* 49, S13–S21. doi:10.1002/hep.22881

Lin, P. H., Kitaguchi, Y., Mupas-Uy, J., Takahashi, Y., and Kakizaki, H. (2017). Bilateral orbital marginal zone B-cell lymphoma of the mucosa-associated lymphoid tissue in a patient with Hepatitis B virus infection. *Am. J. Ophthalmol. Case Rep.* 7, 27–30. doi:10.1016/j.ajoc.2017.05.002

Liu, Y. J., Ng, K. F., Huang, S. C., Wu, R. C., and Chen, T. C. (2017). Composite hepatocellular carcinoma and small cell carcinoma with early nodal metastasis: A case report. *Med. Baltim.* 96 (34), e7868. doi:10.1097/MD.0000000000007868

Mahmood, K., Samo, A. H., Jairamani, K. L., Ali, G., Talib, A., and Qazmi, W. (2008). Serum retinol binding protein as an indicator of vitamin A status in cirrhotic patients with night blindness. *Saudi J. Gastroenterol.* 14 (1), 7–11. doi:10.4103/1319-3767.37794

Martín, L. L., Rocha-de-Lossada, C., Marín-Martínez, S., and Peraza-Nieves, J. E. (2021). Sterile, recurrent, and bilateral corneal perforation related to primary biliary cirrhosis complicated by secondary Sjögren syndrome and vitamin A deficiency. *Arq. Bras. Oftalmol.* 84 (6), 606–609. doi:10.5935/0004-2749.20210100

McGlynn, K. A., Petrick, J. L., and London, W. T. (2015). Global epidemiology of hepatocellular carcinoma: An emphasis on demographic and regional variability. *Clin. Liver Dis.* 19 (2), 223–238. doi:10.1016/j.cld.2015.01.001

McMahon, B., Block, J., Block, T., Cohen, C., Evans, A. A., Hosangadi, A., et al. (2016). Hepatitis-associated liver cancer: Gaps and opportunities to improve care. *J. Natl. Cancer Inst.* 108 (4), djv359. doi:10.1093/jnci/djv359

Mittal, S., and El-Serag, H. B. (2013). Epidemiology of hepatocellular carcinoma: Consider the population. *J. Clin. Gastroenterol.* 47, S2–S6. doi:10.1097/MCG.0b013e3182872f29

Ringelhan, M., McKeating, J. A., and Protzer, U. (2017). Viral hepatitis and liver cancer. *Philos. Trans. R. Soc. Lond. B Biol. Sci.* 372, 20160274. doi:10.1098/rstb.2016.0274

Shields, C. L., Welch, R. J., Malik, K., Acaba-Berrocal, L. A., Selzer, E. B., Newman, J. H., et al. (2018). Uveal metastasis: Clinical features and survival outcome of 2214 tumors in 1111 patients based on primary tumor origin. *Middle East Afr. J. Ophthalmol.* 25 (2), 81–90. doi:10.4103/meajo.MEAJO_6_18

Sia, D., Villanueva, A., Friedman, S. L., and Llovet, J. M. (2017). Liver cancer cell of origin, molecular class, and effects on patient prognosis. *Gastroenterology* 152 (4), 745–761. doi:10.1053/j.gastro.2016.11.048

Sun, W., Liu, B., Chen, J., Gong, P., Wu, X., Liu, C., et al. (2017). Novel characteristics of alpha-fetoprotein (AFP)-producing gastric cancer. *Oncotarget* 8 (60), 101944–101951. doi:10.18632/oncotarget.22109

Tsoumani, A., Katsanos, K., AsproudIs, I., and Tsianos, E. V. (2013). Treatment and non-treatment related ocular manifestations in patients with chronic Hepatitis B or C. *Eur. Rev. Med. Pharmacol. Sci.* 17 (8), 1123–1131.

Vyas, M., and Jain, D. (2018). A practical diagnostic approach to hepatic masses. *Indian J. Pathol. Microbiol.* 61 (1), 2–17. doi:10.4103/IJPM.IJPM_578_17

Wang, C. H., Wey, K. C., Mo, L. R., Chang, K. K., Lin, R. C., and Kuo, J. J. (2015). Current trends and recent advances in diagnosis, therapy, and prevention of hepatocellular carcinoma. *Asian pac. J. Cancer Prev.* 16, 3595–3604. doi:10.7314/apjcp.2015.16.9.3595

Wang, M., Wang, Y., Feng, X., Wang, R., Wang, Y., Zeng, H., et al. (2017). Contribution of Hepatitis B virus and hepatitis C virus to liver cancer in China north areas: Experience of the Chinese National Cancer Center. *Int. J. Infect. Dis.* 65, 15–21. doi:10.1016/j.ijid.2017.09.003

Wang, S., Sun, H., Xie, Z., Li, J., Hong, G., Li, D., et al. (2016). Improved survival of patients with hepatocellular carcinoma and disparities by age, race, and socioeconomic status by decade, 1983-2012. *Oncotarget* 7 (37), 59820–59833. doi:10.18632/oncotarget.10930

Wu, W., He, X., Andayani, D., Yang, L., Ye, J., Li, Y., et al. (2017). Pattern of distant extrahepatic metastases in primary liver cancer: A SEER based study. *J. Cancer* 8 (12), 2312–2318. doi:10.7150/jca.19056

Ye, Y. F., Xiang, Y. Q., Fang, F., Gao, R., Zhang, F., Xie, S. H., et al. (2015). Hepatitis B virus infection and risk of nasopharyngeal carcinoma in southern China. *Cancer Epidemiol. Biomarkers Prev.* 24 (11), 1766–1773. doi:10.1158/1055-9965.EPI-15-0344

Zhang, Y., Ren, J. S., Shi, J. F., Li, N., Wang, Y. T., Qu, C., et al. (2015). International trends in primary liver cancer incidence from 1973 to 2007. *BMC Cancer* 15, 94. doi:10.1186/s12885-015-1113-4

Zhao, S., Mei, Y., Wang, Y., Zhu, J., Zheng, G., and Ma, R. (2015). Levels of CEA, CA153, CA199, CA724 and AFP in nipple discharge of breast cancer patients. *Int. J. Clin. Exp. Med.* 8 (11), 20837–20844.

Zou, D., Zhang, B., Ba, J., Ye, Q., and Wu, G. (2006). Expression and significance of CEA and CA153 in pleural fluid of patients with lung cancer. *Zhongguo Fei Ai Za Zhi* 9 (4), 337–339. doi:10.3779/j.issn.1009-3419.2006.04.08

frontiers | Frontiers in Genetics

TYPE Original Research
PUBLISHED 29 September 2022
DOI 10.3389/fgene.2022.1013253

OPEN ACCESS

EDITED BY
Qian Wang,
Tai'an City Central Hospital, China

REVIEWED BY
Raluca Ioana Stefan-van Staden,
National Institute of Research and Development for Electrochemistry and Condensed Matter (INCEMC), Romania
Zhiyuan Li,
The First People's Hospital Affliate to University of South China, China
Yuan Liu,
University of Miami Health System, United States

*CORRESPONDENCE
Yi Shao,
freebee99@163.com

SPECIALTY SECTION
This article was submitted to Cancer Genetics and Oncogenomics, a section of the journal Frontiers in Genetics

RECEIVED 06 August 2022
ACCEPTED 12 September 2022
PUBLISHED 29 September 2022

CITATION
Cheng T, Chen J, Ying P, Wei H, Shu H, Kang M, Zou J, Ling Q, Liao X, Wang Y and Shao Y (2022), Clinical risk factors of carbohydrate antigen-125, cytokeratin fragment 19, and neuron-specific enolase in liver metastases from elderly lung cancer patients.
Front. Genet. 13:1013253.
doi: 10.3389/fgene.2022.1013253

Clinical risk factors of carbohydrate antigen-125, cytokeratin fragment 19, and neuron-specific enolase in liver metastases from elderly lung cancer patients

Tao Cheng[1], Jun Chen[2], Ping Ying[2], Hong Wei[2], Huiye Shu[2], Min Kang[2], Jie Zou[2], Qian Ling[2], Xulin Liao[3], Yixin Wang[4] and Yi Shao[2]*

[1]Department of Respiratory, Shangrao People's Hospital of Nanchang University, Shangrao, Jiangxi, China, [2]Department of Ophthalmology, Jiangxi Branch of National Clinical Research Center for Ocular Disease, The First Affiliated Hospital of Nanchang University, Nanchang, Jiangxi, China, [3]Department of Ophthalmology and Visual Sciences, The Chinese University of Hong Kong, Hong Kong, Hong Kong SAR, China, [4]School of Optometry and Vision Science, Cardiff University, Cardiff, United Kingdom

Objective: Lung cancer is a common malignant tumor characterized by challenging detection and lack of specificity in clinical manifestations. To investigate the correlation of tumor markers in the serum with liver metastasis and prognosis of lung cancer.

Methods: A total of 3,046 elderly lung cancer patients were retrospectively studied between September 1999 and July 2020. Divided into liver metastasis group and non-liver metastasis group. We compared a series of serum biomarkers between the two groups of elderly patients to predict the prognosis in patients with lung cancer by fluorescence *in situ* hybridization (FISH), advanced flow cytometry (FCM) and multi tumor marker protein chip, including tumor markers in the serum included alkaline phosphatase (ALP), serum calcium, hemoglobin (HB), alpha-fetoprotein (AFP), carcinoembryonic antigen (CEA), neuron-specific enolase (NSE), cytokeratin fragment 19 (Cyfra21-1), carbohydrate antigen-125 (CA-125), carbohydrate antigen-153 (CA-153), carbohydrate antigen-199 (CA-199), and free prostate specific antigen (free PSA). We used binary logistic regression analysis to determine risk factors, and used receiver operating curve (ROC) analysis to evaluate the diagnostic value of liver metastases in elderly patients with lung cancer.

Results: The proportion of lung cancer in the liver metastasis group was higher than that observed in the non-liver metastases group. The expression levels of CA-125, Cyfra21-1, and NSE in the liver metastasis group of lung cancer were significantly higher than those reported in the non-liver metastases group ($p < 0.05$). ROC curve analysis shows that the area under the curve of CA-125, Cyfra21-1, and NSE are 0.614, 0.616 and 0.608, respectively. The sensitivity and specificity of CA-125 were 45.70% and 76.20%, the sensitivity and specificity of

Cyfra21-1 were 60.10% and 57.10%, and the sensitivity and specificity of NSE were 44.10% and 75.00%, respectively.

Conclusion: High levels of CA-125, Cyfra21-1, and NSE in the serum may be associated with liver metastasis in elderly patients with lung cancer. CA-125 and NSE are factors influencing the prognosis of elderly patients with liver metastasis of lung cancer.

KEYWORDS

lung cancer, liver metastasis, risk factors, potential indicators, CA-125, CYFRA21-1, NSE

Introduction

The morbidity and mortality of lung cancer remain high. This type of cancer has become one of the most important life-threatening diseases in humans. According to studies, the incidence and mortality of lung cancer rank first among all types of cancer in men, accounting for 17% of the total number of new cancer cases and 23% of the total number of cancer-related deaths. (Jemal et al., 2011) Following the rapid development of medical care witnessed in recent years, the treatment of various diseases has been very successful. However, the prognosis of elderly lung cancer patients has not been effectively improved. The reason for this may be that lung cancer is a very complicated tumor, and characterized by the occurrence of metastasis. In addition, it is the main cause of treatment failure and patient death. Liver metastasis of lung cancer is one of the most common sites of hematogenous metastasis of lung cancer, and It is one of the third most common sites of liver metastasis the disease progresses rapidly and the prognosis is poor. In all elderly patients with lung cancer metastasis, the incidence of liver metastasis and adrenal metastasis was 33–40% and 18–38%, respectively. (Quint et al., 1996) Elderly patients with liver metastasis of lung cancer may not present obvious symptoms in the early stage. Thus, the diagnosis mainly depends on imaging. Computed tomography (CT) is an accurate method for the diagnosis of liver metastasis. The advantage of this approach is that the scanning section is fixed, and can be dynamically compared during the observation of the lesions. In addition, it is more objective and sensitive than ultrasound. However, the disadvantage of this method is that the specificity and sensitivity to diffuse small nodules and small cancerous lesions are poor. Hence, several cases may be misdiagnosed. Traditional CT scan and magnetic resonance imaging (MRI) cannot diagnose lung cancer in the early stage, owing to the absence of the corresponding clinical symptoms and lesions. This also hinders the early detection of liver metastasis. Therefore, the discovery of factors affecting metastasis is of great importance for the early treatment of lung cancer metastasis to the liver. Markers in the serum are widely used for the screening of clinical tumors. The detection of tumor markers in human blood, body fluids, or tissue cells can assist in determining the presence, pathogenesis, and prognosis of tumors.

Currently, numerous tumor markers in the serum have been associated with lung cancer. Mal (Ma et al., 2015) found that the levels of CEA, CA-125, and Cyfra21-1 are high in lung cancer, and can be used for the diagnosis of lung cancer. Moreover, previous studies have shown that CEA, Cyfra21-1, and CA-125 are associated with poor prognosis in non-small cell lung cancer (Cedrés et al., 2011). In addition, tumor markers may be potentially effective in predicting metastasis. However, currently, there is no evidence showing the difference between liver metastasis and non-liver metastasis of lung cancer. Therefore, in this study, the medical records of elderly patients with lung cancer from the First Affiliated Hospital of Nanchang University (Nanchang, China) were reviewed. We screened for liver metastasis based on the serological examination of a large number of elderly patients with lung cancer. The content of tumor markers in elderly patients was also compared to study the correlation between risk factors. Furthermore, we attempted to establish a standard for distinguishing between liver metastasis and non-liver metastases of lung cancer, and targeted anticancer treatment strategies for elderly patients with this disease.

The reason for choosing these biomarkers is that there have been related studies that have shown that these biomarkers are related to liver metastasis of lung cancer or other tumors, but there is no clear level indicator that when a certain biomarker exceeds how much, lung cancer may be suspected Liver metastases occur. Therefore, we can select these indicators and hope to obtain relevant biomarker levels through big data research.

Materials and methods

Study design

In this study, the clinical data of 3,046 elderly patients with lung cancer (188 and 2,858 elderly patients with liver and non-liver metastases, respectively) were selected in the First Affiliated Hospital of Nanchang University (Nanchang,

China) from September 1999 to July 2020. Elderly patients with liver metastasis were screened, and their medical records and serological data were compared with those without liver metastasis. All elderly patients volunteered to participate in this study. The study was approved by the Medical Research Ethics Committee of the First Affiliated Hospital of Nanchang University, Nanchang, China. A pathological section, obtained through surgical resection or biopsy, was used to clearly diagnose lung cancer. Liver metastasis of lung cancer was diagnosed by CT and MRI, and data related to tumor markers in the serum were recorded.

Data collection

We collected various clinical data from the medical records of elderly patients with liver metastasis of lung cancer, including age, gender, time of diagnosis, lesion metastasis, and treatment. The examined tumor markers in the serum included ALP, HB, AFP, CEA, NSE, Cyfra21-1, CA-125, CA-153, CA-199, and free PSA.

Statistical analyses

We analyzed the differences between tumor markers in the liver metastasis group and the non-liver metastases group using an independent *t*-test. A binary logistic regression model was subsequently applied to identify independent risk factors of liver metastasis. We constructed a receiver operating characteristic (ROC) curve, and calculated the area under the curve (AUC). Subsequently, we calculated the cut-off value, sensitivity, and specificity of risk factors. $p < 0.05$ indicated statistical significance. All statistical analyses were performed using the SPSS 20.0 software (SPSS, IBM, United States) and Excel 2010 software (Excel, Microsoft, United States).

Results

Demographics and characteristics of elderly patients

In this study, 188 cases of liver metastasis from lung cancer and 2,858 cases of lung cancer non-liver metastases were collected. The mean ages in the lung cancer liver metastasis and non-liver metastases from lung groups were 60.3 ± 4.9 and 60.6 ± 3.2 years, respectively. According to the chi-squared test and Student's t-test, there was no significant difference between the groups in terms of gender and age ($p > 0.05$). In addition, the statistical analysis showed differences in the histopathological types between the two groups ($p < 0.05$). There was a statistically significant difference in the pathological type ratio between the liver metastasis group and non-liver metastases group ($p = 0.003$), and the proportion of adenocarcinoma was the highest. The expression of small cell carcinoma in the liver metastasis group was higher than that observed in the non-liver metastases group. The majority of elderly patients had received chemotherapy since the onset of the disease (Table 1; Figure 1). More detailed clinical data of the patients are provided in Figure 2.

Clinical data and risk factors for liver metastasis of lung cancer

After comparing the data for tumor biomarkers in elderly patients with lung cancer liver metastasis and lung cancer non-liver metastases, we found that the levels of ALP, AFP, CEA, CA-125, CA-199, CA-153, Cyfra21-1, and NSE were extremely high compared with those measured in elderly patients lung cancer non-liver metastases. In contrast, the level of HB was lower in the former group ($p < 0.05$). There were no significant differences between the two groups in the levels of calcium, CA-724, and total PSA in the serum ($p > 0.05$) (Table 2). Through binary logistic regression, CA-125, Cyfra21-1, and NSE were identified as independent risk factors for the liver metastasis of lung cancer (Table 3).

Cut-off values, sensitivity, specificity, and AUC of CA-125, Cyfra21-1, and NSE for the diagnosis of lung cancer metastasis to the liver

Table 4 shows that the cut-off values for CA-125, Cyfra21-1, and NSE were 53.00 U/ml, 4.15 U/ml, and 23.39 ng/ml, respectively. The AUC of Cyfra21-1 was the highest. Figure 3A shows the ROC curves for CA-125, Cyfra21-1, and NSE as a single factor. We subsequently tested the possible combinations of these three risk factors and all combinations in pairs. Figure 3B shows CA-125 + Cyfra21-1, CA-125 + NSE, Cyfra21-1+NSE, and CA-125 + Cyfra21-1+ NSE combinations. We found that the combination of CA-125 + Cyfra21-1+NSE exhibited AUC value of 0.672. The sensitivity and specificity of CA-125 + Cyfra21-1, CA-125 + NSE, Cyfra21-1+NSE, and CA-125 + Cyfra21-1+NSE can be observed in Table 4 ($p < 0.05$).

TABLE 1 Clinical data of liver metastasis of lung cancer and elderly patients with lung cancer non-liver metastases.

Patient characteristics	Lung cancer liver metastasis group (%) (n = 188)	Lung cancer non-liver metastasis group (%) (n = 2,858)	p Value
Gender			
Male	124 (66.0)	1,892 (66.2)	0.214
Female	64 (34.0)	966 (33.8)	—
Age			
Mean	66.3 ± 4.9	64.6 ± 3.2	0.220
Histopathological type			
Adenocarcinoma	76 (40.4)	1,195 (41.8)	0.001
Squamous cell carcinoma	60 (31.9)	1,100 (38.5)	—
Small cell carcinoma	28 (14.9)	329 (11.5)	—
Other	24 (12.8)	234 (8.2)	—
Smoking history	101 (53.1)	1,495 (48.9)	0.253
Other transfers	131 (69.7)	538 (18.8)	—
Eyes	17 (9.0)	45 (1.5)	—
Brain	35 (18.6)	216 (7.5)	—
Bone	23 (12.2)	250 (8.7)	—

$p < 0.05$ is statistically significant.

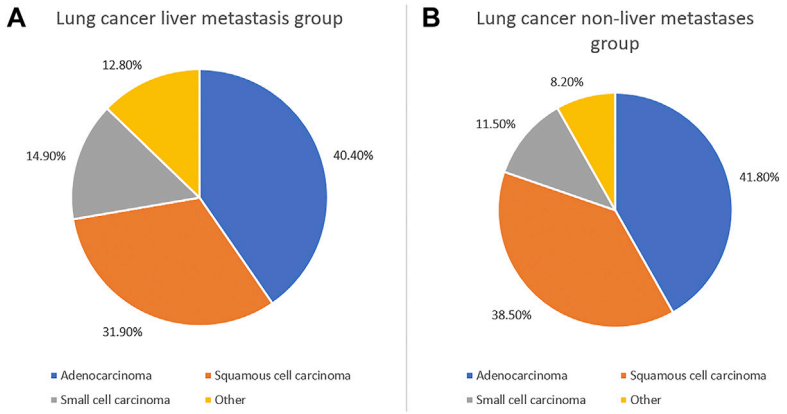

FIGURE 1
Clinical characteristics of elderly lung cancer patients with liver metastasis and without liver metastasis. The clinical characteristics of elderly patients with lung cancer liver metastasis **(A)** and without liver metastasis **(B)**.

Limitation

We performed serological experiments on elderly patients with liver metastases from lung cancer and those without liver metastases from lung cancer and approved the consent of the elderly patients and their families. Environmental factors may affect the experiment (for example, the contamination of individual serum by the instrument) is the limitation of the experiment. We still need more sample sizes to reduce the impact of these changes on the experimental results.

Discussion

Lung cancer is a common malignant tumor characterized by challenging detection and lack of specificity in clinical manifestations. Most elderly patients develop distant metastasis or present with Late stage diseases such as pleural effusion, and the prognosis is poor. Therefore, early diagnosis and treatment of this disease is especially important. Tumor markers in the serum are substances that reflect the presence and growth of tumors. They mainly include proteins, polyamines,

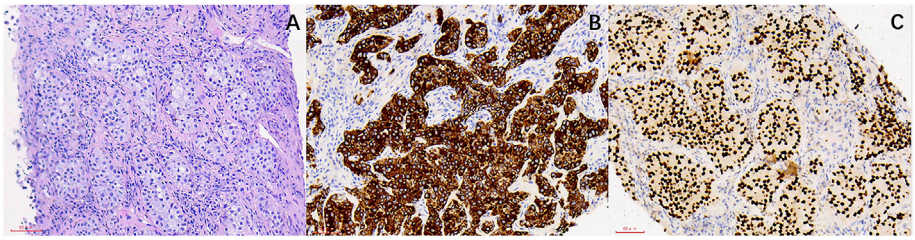

FIGURE 2
The HE staining and IHC images from lung cancer patients with liver metastasis. **(A)** Lung cancer (HE ×200). **(B)** CK7(+) (SP ×200). **(C)** TTF-1 (+) (SP ×200).

TABLE 2 Differences in tumor biomarkers between liver metastasis of elderly lung cancer and non-liver metastases of elderly lung cancer.

Tumor biomarkers	Lung cancer liver metastasis group	Lung cancer non-liver metastasis group	t	P
ALP (U/L)	150.30 ± 11.3	89.37 ± 1.34	10.25	<0.001
Calcium (mmol/L)	2,023 ± 0.02	2.37 ± 0.09	0.41	0.068
AFP (ng/ml)	3.22 ± 0.39	1.72 ± 0.03	7.85	<0.001
CEA (ng/ml)	100.5 ± 16.57	44.07 ± 4.63	3.04	0.0024
CA-125 (U/ml)	171.2 ± 27.59	65.30 ± 3.12	7.53	<0.001
CA-199 (U/ml)	148.7 ± 51.37	40.15 ± 7.37	3.43	0.0006
CA-153 (U/ml)	33.98 ± 5.51	19.72 ± 0.96	5.48	<0.001
CA-724 (U/ml)	16.60 ± 7.52	8.30 ± 4.13	0.51	0.55
CYFRA21-1 (ng/ml)	16.07 ± 2.83	9.43 ± 0.55	2.92	0.0035
TPSA (ng/L)	1.83 ± 0.14	1.66 ± 0.07	0.58	0.5630
NSE (μg/L)	41.77 ± 5.49	24.85 ± 0.74	6.97	<0.001
HB (g/L)	112.1 ± 1.52	119.5 ± 0.36	5.15	<0.001

Independent sample Student's t-test was used. $p < 0.05$ indicates statistical significance.
Abbreviationalkaline phosphatase (ALP), serum calcium, hemoglobin (HB), alpha-fetoprotein (AFP), carcinoembryonic antigen (CEA), neuron-specific enolase (NSE), cytokeratin fragment 19 (Cyfra21-1), carbohydrate antigen-125 (CA-125), carbohydrate antigen-153 (CA-153), carbohydrate antigen-199 (CA-199), carbohydrate antigen-724 (CA-724), total prostate-specific antigen (TPSA).

hormones, enzymes, and oncogenes. They are produced by tumor cells during tumor development or by the host. Tumor cells are released into the bloodstream. The detection of tumor markers is helpful in diagnosing tumors, evaluating treatment outcomes and prognosis, and providing guidance for treatment options. Table 5 are studies on other metastasis of lung cancer, Table 6 is the study of liver metastasis in different cancer elderly patients.

Currently, the mechanism involved in the metastasis of lung cancer has not been fully elucidated. However, it is generally thought that lung cancer tissues contain subcellular populations with different invasive and metastatic potentials. During the metastatic process, lung cancer cells complete a series of selections and sequential steps. Recent studies have shown that there are numerous similar abnormal molecules in primary tumors and brain metastases. However, these differ in terms of certain molecular changes, such as abnormalities in human epidermal growth factor receptor family receptors and expression of ligands. Although several studies have shown that CEA, CA-125, and Cyfra21-1 are prognostic factors for stage III-IV non-small cell lung cancer, (Zhang et al., 2015; Chen et al., 2018) they did not investigate the liver metastasis of lung cancer. Interestingly, the results of the present study showed that CEA and Cyfra21-1 are not independent prognostic factors for the metastasis of lung cancer to the liver. CEA was initially discovered in 1965 by Gold and Freeman. (Gold and Freedman, 1965) Since then, a large number of studies have confirmed its effectiveness as a tumor marker. However, thus far, only few studies have investigated the tumor markers in the sera of elderly patients with liver metastasis of lung cancer. Numerous

TABLE 3 Risk factors for elderly patients with liver metastasis of lung cancer.

Factors	B	Exp(B)	Or (95% CI)	P
ALP	0.006	1.006	0.994–1.018	0.316
AFP	0.409	1.505	0.930–2.436	0.096
CEA	0.007	1.007	0.996–1.018	0.0024
CA-125	−0.032	0.969	0.908–1.033	< 0.001
CA-199	−0.001	0.999	0.961–1.039	<0.001
CA-153	0.049	1.003	0.999–1.006	<0.001
CYFRA21-1	−0.013	0.987	0.797–1.224	0.004
NSE	0.003	1.003	0.989–1.017	<0.001
HB	0.033	0.983	0.976–0.991	<0.001

Binary logistic analysis was applied. $p < 0.05$ indicates statistical significance. AbbreviationsB, coefficient of regression; OR, odds ratio; CI, confidence interval, alkaline phosphatase (ALP), serum calcium, hemoglobin (HB), alpha-fetoprotein (AFP), carcinoembryonic antigen (CEA), neuron-specific enolase (NSE), cytokeratin fragment 19 (Cyfra21-1), carbohydrate antigen-125 (CA-125), carbohydrate antigen-153 (CA-153), carbohydrate antigen-199 (CA-199).

studies have shown that the levels of CEA in the serum can be used as a risk factor for the prognosis of lung cancer. (Arrieta et al., 2009; Tomita et al., 2010; Grunnet and Sorensen, 2012) In addition, studies have shown that lung cancer and brain metastases in elderly patients with lower CEA concentration exhibit a better prognosis *versus* CEA-positive elderly patients. Moreover, the levels of CA-125 in the serum are independent factors affecting the prognosis of elderly patients with brain metastasis of non-small cell lung cancer. (Liu et al., 2015b) This study showed that the positive expression of CEA in the serum does not serve as a prognostic risk factor for elderly patients with liver metastasis of lung cancer. The levels of CA19-9 and CA-125 in the sera of elderly patients with liver metastasis of colorectal cancer are independent factors affecting prognosis. (Zhang et al., 2013; Sakamoto et al., 2015) However, there are few studies investigating the relationship between the levels of CA19-9 and CA-125 in the serum and prognosis of elderly patients with lung cancer. In recent years, studies have also shown that the levels of NSE in the serum are independent factors influencing the prognosis of elderly patients with lung cancer. Cyfra21-1 is a fragment of cytokeratin-19, which is present in the cytoplasm of monolayer and stratified epithelial tumor cells. It exhibits high levels in epithelial-derived tumor tissues, and can be used for the diagnosis of non-small cell lung cancer and lung squamous cell carcinoma with high specificity. (Zheng et al., 2014) CEA is one of the earliest markers for the diagnosis of lung cancer, and is mainly present in the epithelial tissue of the fetal digestive tract, pancreas, and liver. Under normal circumstances, the levels of CEA in the serum are low. However, CEA levels are high in elderly patients with gastrointestinal malignant tumors, breast cancer, lung cancer, *etc.* Different pathological types have different sensitivities. NSE is a glycolytic enzyme found in neurons and neuroendocrine tissues. It is a marker for the diagnosis of small cell lung cancer and neuroblastoma, and its levels are used to evaluate the diagnosis, treatment effect, prognosis and clinical stage of small cell carcinoma. CA-125 is a carbohydrate antigen used to diagnose epithelial ovarian cancer and endometrial cancer. It is a broad-spectrum tumor marker, especially in the diagnosis of lung adenocarcinoma. In this study, the accuracy, sensitivity, and negative predictive value of the combined detection of tumor markers in the serum were significantly higher than those observed with single markers. It is worth noting that serum tumor markers can be clinically diagnosed in lung cancer, although there is no significant difference in specificity and positive predictive value. The combined detection of tumor markers has a high diagnostic value, and can improve the sensitivity and accuracy of diagnosis. The reason for this may be that different tumor markers exhibit varied sensitivities to the detection of lung cancer, whereas single-marker detection cannot provide high sensitivity. Moreover, the combined detection of different markers may offer complementary advantages, and promote the sensitivity and accuracy of diagnosis.

However, few studies have comprehensively analyzed the distribution of liver metastasis in lung cancer. In the present study, we examined the levels of ALP, calcium, HB, AFP, CEA, CA-125, CA-199, CA-153, CA-724, Cyfra21-1, total PSA, and NSE in the sera of elderly patients The concentrations of ALP, AFP, CEA, CA-125, CA-199, CA-153, Cyfra21-1, and NSE were found to be extremely high in elderly patients with liver metastasis of lung cancer. Notably, the levels of HB were lower in elderly patients with lung cancer non-liver metastases ($p < 0.05$). AFP (Gold and Freedman, 1965; Zhang et al., 2015) has been associated with the development of liver cancer. In addition, it has also been associated with the concentration of CEA in a rat animal model. (Zhang et al., 2011) CA-199 was originally found to be expressed in the pancreas and bile ducts, and has been used as a risk factor for the diagnosis of liver metastasis of advanced pancreatic cancer. (Dong et al., 2017) Clinically, small cell lung cancer (Qu et al., 2019) can be diagnosed according to the levels of Cyfra21-1. Therefore, based on the data analyses of previous studies, we selected CEA, CA-125, and Cyfra21-1 ($p < 0.01$, $p < 0.01$, and $p = 0.03$, respectively) as independent risk factors of liver metastasis in elderly patients with lung cancer. In addition, by determining the levels of CA-125, CEA, and Cyfra21-1 (including the cut-off values, sensitivity, specificity, and AUC), we concluded that these are specific risk factors of lung cancer metastasis.

Using the final ROC curves of these serum biomarkers, we demonstrated that the cut-off values for CA-125, Cyfra21-1 and NSE were 53.00 U/ml, 4.15 U/ml, and 23.39 ng/ml, respectively. NSE concentration 53.00 U/ml is the key point for liver metastasis in elderly patients with lung cancer. Cyfra21-1 yielded the largest AUC, showing the highest accuracy in

TABLE 4 Cut-off value, sensitivity, specificity, and AUC of CA-125, Cyfra21-1, and NSE for the diagnosis of liver metastasis in elderly patients with lung cancer.

Factor	Cut-off value	Sensitivity (%)	Specificity (%)	AUC	P
CA-125 (U/ml)	53.00	45.70	76.20	0.614	<0.001
Cyfra21-1 (U/ml)	4.15	60.10	57.10	0.616	<0.001
NSE (ng/ml)	23.39	44.10	75.00	0.608	<0.001
CA-125 + Cyfra21-1	62.36	46.80	76.70	0.631	<0.001
CA-125 + NSE	87.57	51.10	78.40	0.663	<0.001
Cyfra21-1+NSE	32.01	50.50	72.80	0.633	<0.001
CA-125 + Cyfra21-1+NSE	92.44	53.20	76.80	0.672	<0.001

Sensitivity and specificity were obtained at the point of the cut-off value. $p < 0.05$ indicates statistical significance.
AbbreviationsAUC, area under the curve; CI, confidence interval; NSE, neuron-specific enolase, Cyfra21-1, cytokeratin fragment 19, CA-125, carbohydrate antigen-125.

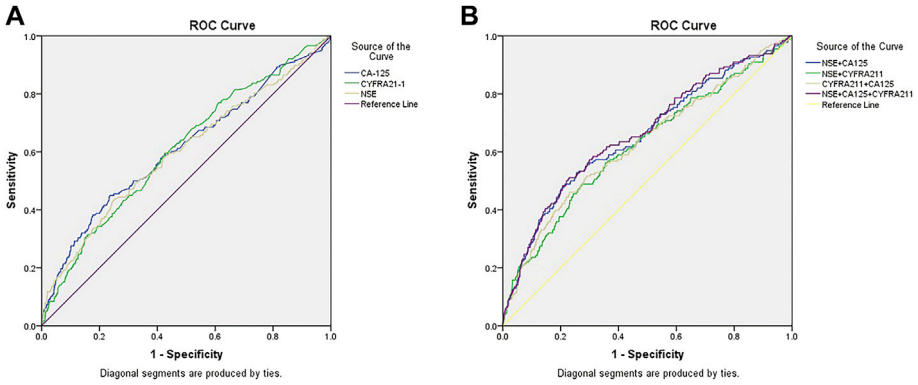

FIGURE 3
The receiver operating characteristics (ROC) curves of risk factor CA-125, CYFRA21-1, and NSE for detecting elderly lung cancer patients with liver metastasis. ROC curve of the levels of [3CA-125, CYFRA21-1, and NSE in elderly patients with liver metastasis of lung cancer **(A)**. ROC curve of the CA-125+CYFRA21-1, CA-125+NSE, CYFRA21-1+NSE combination and CA-125+CYFRA21-1+NSE combinations in elderly patients with liver metastasis of lung cancer **(B)**.

TABLE 5 Studies on other metastasis of lung cancer.

Author	Year	Metastasis
Ayan., et al. (Ayan et al., 2016)	2016	Bone
Roato I., et al. (Roato, 2014)	2014	Bone
Liu Y., et al. (Liu et al., 2015a)	2015	Bone
Yang F., et al. (Yang et al., 2010)	2010	Lymph node
Suzuki K., et al. (Suzuki et al., 2001)	2001	Lymph node

distinguishing elderly patients with lung cancer. On this basis, we conducted further detailed diagnostic analysis for liver metastasis, without providing evidence for follow-up treatment. Unlike previous studies, this study showed that the best diagnostic values for CA-125 + Cyfra21-1, CA-125 + NSE, Cyfra21-1+NSE, and CA-125 + Cyfra21-1+NSE combinations were 62.36, 87.57, 32.01, and 92.44 U/ml, respectively. We observed that the combination of CA-125 + Cyfra21-1+NSE exhibited the highest AUC value of 0.672. The CA-125 + NSE

TABLE 6 Studies on the liver cancer from different cancers.

Author	Year	Diseases
Higashins K. et al. (Higashino et al., 1975)	2012	Lung cancer
Willyard C. et al. (Willyard, 2007)	2007	Lung cancer, Breast cancer, *etc.*
Marrero JA. et al. (Marrero et al., 2005)	2005	Lung cancer, Breast cancer, *etc.*

group showed high specificity. In other words, the higher levels of CA-125 and NSE are more likely to be observed in liver metastasis of lung cancer. Therefore, we suggest that the combination of CA-125 with NSE may be a useful risk factor for the prediction of liver metastasis of lung cancer.

In summary, high expression of CA-125, Cyfra21-1, and NSE in the serum may be associated with liver metastasis of lung cancer. In addition, the combination of CA-125 + Cyfra21-1+NSE may assist in the diagnosis of liver metastasis of lung cancer. The positive expression of CA-125 and NSE in the serum is a factor affecting the prognosis of elderly patients with liver metastasis of lung cancer.

Data availability statement

The datasets presented in this study can be found in online repositories. The names of the repository/repositories and accession number(s) can be found in the article/Supplementary Material.

Ethics statement

The studies involving human participants were reviewed and approved by the Medical Ethics Committee of the First Affiliated Hospital of Nanchang University (Nanchang, China). The patients/participants provided their written informed consent to participate in this study.

Author contributions

All authors listed have made a substantial, direct, and intellectual contribution to the work and approved it for publication.

Conflict of interest

The authors declare that the research was conducted in the absence of any commercial or financial relationships that could be construed as a potential conflict of interest.

Publisher's note

All claims expressed in this article are solely those of the authors and do not necessarily represent those of their affiliated organizations, or those of the publisher, the editors and the reviewers. Any product that may be evaluated in this article, or claim that may be made by its manufacturer, is not guaranteed or endorsed by the publisher.

References

Arrieta, O., Saavedra-Perez, D., Kuri, R., Aviles-Salas, A., Martinez, L., Mendoza-Posada, D., et al. (2009). Brain metastasis development and poor survival associated with carcinoembryonic antigen (CEA) level in advanced non-small cell lung cancer: A prospective analysis. *BMC Cancer* 9, 119. doi:10.1186/1471-2407-9-119

Ayan, A. K., Erdemci, B., Orsal, E., Bayraktutan, Z., Akpinar, E., Topcu, A., et al. (2016). Is there any correlation between levels of serum ostepontin, CEA, and FDG uptake in lung cancer patients with bone metastasis? *Rev. Esp. Med. Nucl. Imagen Mol.* 35, 102–106. doi:10.1016/j.remn.2015.09.002

Cedrés, S., Nunez, I., Martinez, P., Marina, L., Checa, E., Torrejon, D., et al. (2011). Serum tumor markers CEA, cyfra21-1, and CA-125 are associated with worse prognosis in advanced non–small-cell lung cancer (NSCLC). *Clin. Lung Cancer* 12, 172–179. doi:10.1016/j.cllc.2011.03.019

Chen, Z. Q., Huang, L. S., and Zhu, B. (2018). Assessment of seven clinical tumor markers in diagnosis of non-small-cell lung cancer. *Dis. Markers* 2018, 9845123. doi:10.1155/2018/9845123

Dong, S., Wang, L., Guo, Y. B., Fy. H.,H, S. X., Q, M. Z., et al. (2017). Risk factors of liver metastasis from advanced pancreatic adenocarcinoma: A large multicenter cohort study. *World J. Surg. Oncol.* 15, 120. doi:10.1186/s12957-017-1175-7

Gold, P., and Freedman, S. O. (1965). Specific carcinoembryonic antigens of the human digestive system. *J. Exp. Med.* 122, 467–481. doi:10.1084/jem.122.3.467

Grunnet, M., and Sorensen, J. B. (2012). Carcinoembryonic antigen (CEA) as tumor marker in lung cancer. *Lung Cancer* 76, 138–143. doi:10.1016/j.lungcan.2011.11.012

Higashino, K., Otani, R., Kudo, S., HashinostuMeM.,and Hada, T. (1975). Hepatocellular carcinoma and a variant alkaline phosphatase. *Ann. Intern. Med.* 83, 74–78. doi:10.7326/0003-4819-83-1-74

Jemal, A., Bray, F., Center, M. M., Ferlay, J., Ward, E., and Forman, D. (2011). Global cancer statistics. *Ca. Cancer J. Clin.* 61, 69–90. doi:10.3322/caac.20107

Liu, Y. P., Zeng, A. P., and Song, X. Q. (2015). Relationship between serum tumor markers and brain metastasis in patients with advanced non-small cell lung cancer. *Mod. Oncol.* 23, 2777–2781.

Liu, Y. S., Qing, H. F., Su, X. Y., Wang, C., Li, Z., and Liu, S. (2015). Association of CD44 gene polymorphism with survival of NSCLC and risk of bone metastasis. *Med. Sci. Monit.* 21, 2694–2700. doi:10.12659/MSM.894357

Ma, L., Xie, X. W., Wang, H. Y., and Wen, Z. G. (2015). Clinical evaluation of tumor markers for diagnosis in patients with non-small cell lung cancer in China. *Asian pac. J. Cancer Prev.* 16, 4891–4894. doi:10.7314/apjcp.2015.16.12.4891

Marrero, J. A., Romano, P. R., Nikolaeva, O., Steel, L., Mehta, A., Fimmel, C. J., et al. (2005). GP73, a resident Golgi glycoprotein, is a novel serum marker for hepatocellular carcinoma. *J. Hepatol.* 43, 1007–1012. doi:10.1016/j.jhep.2005.05.028

Qu, T., Zhang, J., Xu, N., Liu, B., Li, M., Liu, A., et al. (2019). Diagnostic value analysis of combined detection of Trx, CYFRA21-1 and SCCA in lung cancer. *Oncol. Lett.* 17, 4293–4298. doi:10.3892/ol.2019.10073

Quint, L. E., Tummala, S., Brisson, L. J., Francis, I. R., Krupnick, A. S., Kazerooni, E. A., et al. (1996). Distribution of distant metastases from newly diagnosed non-small cell lung cancer. *Ann. Thorac. Surg.* 62, 246–250. doi:10.1016/0003-4975(96)00220-2

Roato, I. (2014). Bone metastases: When and how lung cancer interacts with bone. *World J. Clin. Oncol.* 5, 149–155. doi:10.5306/wjco.v5.i2.149

Sakamoto, Y., Miyamoto, Y., Beppu, T., Nitta, H., Imai, K., Hayashi, H., et al. (2015). Post-chemotherapeutic CEA and CA19-9 are prognostic factors in patients with colorectal liver metastases treated with hepatic resection after oxaliplatin-based chemotherapy. *Anticancer Res.* 35, 2359–2368.

Suzuki, K., Nagai, K., Yoshida, J., NishiMuraM.,and Nishiwaki, Y. (2001). Predictors of lymph node and intrapulmonary metastasis in clinical stage IA non-small cell lung carcinoma. *Ann. Thorac. Surg.* 72, 352–356. doi:10.1016/s0003-4975(01)02748-5

Tomita, M., Shimizu, T., Ayabe, T., Yonei, A., and Onitsuka, T. (2010). Prognostic significance of tumour marker index based on preoperative CEA and CYFRA 21-1 in non-small cell lung cancer. *Anticancer Res.* 30, 3099–3102.

Willyard, C. (2007). Researchers look for 'sweet 'method to diagnose cancer. *Nat. Med.* 13, 1267. doi:10.1038/nm1107-1267

Yang, F., Chen, H. Q., Xiang, J., Zhang, Y., Zhou, J., Hu, H., et al. (2010). Relationship between tumor size and disease stage in non-small cell lung cancer. *BMC Cancer* 10, 474. doi:10.1186/1471-2407-10-474

Zhang, D., Yu, M. X., Xu, T. P., and Bin, X. (2013). Predictive value of serum CEA, CA19-9 and CA-125 in diagnosis of colorectal liver metastasis in Chinese population. *Hepatogastroenterology* 60, 1297–1301. doi:10.5754/hge121125

Zhang, H. X., Liu, D. D., Jin, B. J., Wang, Y. W., Liu, Q., Duan, R. B., et al. (2011). Changes of serum trace elements, AFP, CEA, SF, T3, T4 and IGF-II in different periods of rat liver cancer. *Chin. J. Cancer Res.* 23, 301–305. doi:10.1007/s11670-011-0301-2

Zhang, Z. H., Han, Y. W., Liang, H., and Wang, L. M. (2015). Prognostic value of serum Cyfra21-1and CEA for non-small-cell lung cancer. *Cancer Med.* 4, 1633–1638. doi:10.1002/cam4.493

Zheng, L., Gong, W., Liang, P., Huang, X., You, N., Han, K. Q., et al. (2014). Effects of AFP-activated PI3K/Akt signaling pathway on cell proliferation of liver cancer. *Tumour Biol.* 35, 4095–4099. doi:10.1007/s13277-013-1535-z

frontiers | Frontiers in Genetics

TYPE Original Research
PUBLISHED 29 September 2022
DOI 10.3389/fgene.2022.981222

OPEN ACCESS

EDITED BY
Qian Wang,
Tai'an City Central Hospital, China

REVIEWED BY
Su-Ding Fei,
Ningbo College of Health Sciences, China
Chen Chen,
The First Affiliated Hospital of Soochow University, China
Cheng Hu,
The Third Hospital of Quzhou, China

*CORRESPONDENCE
Runjie Shi,
runjieshi@hotmail.com

†These authors have contributed equally to this work

SPECIALTY SECTION
This article was submitted to Cancer Genetics and Oncogenomics, a section of the journal Frontiers in Genetics

RECEIVED 29 June 2022
ACCEPTED 05 September 2022
PUBLISHED 29 September 2022

CITATION
Chen B, Luo Y, Kang X, Sun Y, Jiang C, Yi B, Yan X, Chen Y and Shi R (2022), Development of a prognostic prediction model based on a combined multi-omics analysis of head and neck squamous cell carcinoma cell pyroptosis-related genes. *Front. Genet.* 13:981222. doi: 10.3389/fgene.2022.981222

Development of a prognostic prediction model based on a combined multi-omics analysis of head and neck squamous cell carcinoma cell pyroptosis-related genes

Bin Chen[1,2,3†], Yuanbo Luo[1,2,3†], Xueran Kang[1,2,3], Yuxing Sun[1,2,3], Chenyan Jiang[1,2,3], Bin Yi[1,2,3], Xiaojun Yan[1,2,3], Yisheng Chen[4] and Runjie Shi[1,2,3*]

[1]Department of Otorhinolaryngology Head and Neck Surgery, Ninth People's Hospital, Shanghai Jiaotong University, School of Medicine, Shanghai, China, [2]Ear Institute, School of Medicine, Shanghai Jiaotong University, Shanghai, China, [3]Shanghai Key Laboratory of Translational Medicine on Ear and Nose Diseases, Shanghai, China, [4]Department of Sports Medicine, Huashan Hospital, Fudan University, Shanghai, China

This study aimed to understand the prognosis of patients with head and neck squamous cell carcinoma (HNSCC) and to develop and validate a prognostic model for HNSCC based on pyroptosis-associated genes (PAGs) in nasopharyngeal carcinoma. The Cancer Genome Atlas database was used to identify differentially expressed PAGs. These genes were analyzed using the Kyoto Encyclopedia of Genes and Genomes functional annotation analyses and Gene Ontology analyses. The NLR family pyrin domain containing 1 (*NLRP1*) gene, charged multivesicular body protein 7 (*CHMP7*) gene, and cytochrome C (*CYCS*) gene were used to create a prognostic model for HNSCC. The results of the Kaplan-Meier (K-M) and Cox regression analyses indicated that the developed model served as an independent risk factor for HNSCC. According to the K-M analysis, the overall survival of high-risk patients was lower than that of low-risk patients. The hazard ratios corresponding to the risk scores determined using the multivariate and univariate Cox regression analyses were 1.646 (95% confidence interval (CI): 1.189–2.278) and 1.724 (95% CI: 1.294–2.298), respectively, and the area under the receiver operator characteristic curve was 0.621. The potential mechanisms associated with the functions of the identified genes were then identified, and the tumor microenvironment and levels of immune cell infiltration achieved were analyzed. The immune infiltration analysis revealed differences in the distribution of Th cells, tumor-infiltrating lymphocytes, regulatory T cells, follicular helper T cells, adipose-derived cells, interdigitating dendritic cells, $CD8^+$ T cells, and B cells. However, validating bioinformatics analyses through biological experiments is still recommended. This study developed a prognostic model for HNSCC that included *NLRP1*, *CHMP7*, and *CYCS*.

KEYWORDS

prognostic model, nasopharyngeal carcinoma (NPC), pyroptosis, immune infiltration, head and neck squamous cell carcinoma (HNSCC)

Introduction

Head and neck squamous cell carcinoma (HNSCC) is a highly heterogeneous malignancy of various anatomical sites in the upper respiratory and digestive tracts. The sites of its origin are the paranasal sinuses, nasal cavity, oropharynx, oral cavity, and larynx. HNSCC accounts for 90% of all HNSCC cases (Bray et al., 2018; Ferlay et al., 2019). Each year, approximately 450,000 deaths and 890,000 new cases of HNSCC are recorded worldwide (Bray et al., 2018; Ferlay et al., 2019). HNSCC causes include smoking, alcohol consumption, and viral infections (Stein et al., 2015; Johnson et al., 2020). More than half the patients with HNSCC are diagnosed at an advanced stage of HNCC due to the lack of effective clinical risk assessment tools and early-stage diagnostic resources, resulting in a low survival rate (34.9%) (Chauhan et al., 2015). Currently, treatment options are selected, and the overall survival (OS) of HNSCC patients is primarily determined using the tumor–lymph node–metastasis (TNM) staging system developed by the American Joint Committee on Cancer (AJCC) (Amin et al., 2017; Keung and Gershenwald, 2018). Though this system is simple to implement and useful in a wide range of fields, it only considers tumor-related anatomical information and ignores biological heterogeneity. As a result, the ability to predict risk and assess the prognosis for patients with HNSCC is limited. Therefore, developing a novel, valid, and robust risk prediction and prognosis-assessment model is critical to improving the risk prediction accuracy and individualized treatment process.

Intracellular genes regulate cell death (including apoptosis, necroptosis, ferroptosis, pyroptosis, necrosis, autophagy, and others), which significantly impacts the process of immune system development (Fink and Cookson, 2005; Bedoui et al., 2020; Chen et al., 2021; Shi et al., 2021). Pyroptosis, a novel form of caspase-1-mediated programmed cell death, is characterized by the rapid rupture of the plasma membrane. Following the rupture, cellular contents and pro-inflammatory substances such as interleukins are released. This triggers an inflammatory cascade response, resulting in cellular damage. The process has a significant impact on tumor progression, including tumor proliferation, metastasis, and invasion (He et al., 2016; Tsuchiya, 2020). Pyroptosis induces the onset and progression of various diseases, including hepatocellular carcinoma, leukemia, lung cancer, breast cancer, gastric cancer, cervical cancer, and colorectal cancer (He et al., 2016). The dual role of pyroptosis significantly affects tumor pathogenesis. During pyroptosis, multiple signals are generated, and inflammatory mediators are released. The generation of these signals and the release of these mediators have an impact on tumorigenesis and resistance to chemotherapeutic agents. The high expression level of the pyroptosis effector gasdermin D promotes the process of tumor metastasis. For example, it is associated with a poor prognosis in patients with lung adenocarcinoma (Gao et al., 2018). Moreover, the increased susceptibility of cells to caspase-3-dependent signaling pathways that trigger pyroptosis can increase melanoma cells' resistance to etoposide (Lage et al., 2001). Pyroptosis, on the other hand, may inhibit tumor onset and progression (Fiddian-Green and Silen, 1975; Yu et al., 2021). The expression of the pyroptosis effector gasdermin E accelerates tumor cell phagocytosis. The action of the tumor-associated macrophages mediates the process. As a result, the number of $CD8^+$ T lymphocytes and tumor-infiltrating natural killer lymphocytes increases (Ding et al., 2016). $CD8^+$ T lymphocytes and tumor-infiltrating natural killer lymphocytes have also shown improved function. Additionally, downregulation of the oncogene LncRNA–XIST inhibits the progression of non-small cell lung cancer. The activation of the miR-335/SOD2/ROS cascade-related pyroptosis process results in the downregulation of the oncogene (Liu et al., 2019). However, more research into the link between HNSCC and pyroptosis is needed.

Researchers recently discovered that pyroptosis is crucial in developing nasopharyngeal carcinoma (NPC) (Cai et al., 2021; Xia et al., 2021). NPC arises from epithelial cells in the nasopharynx, and squamous carcinoma is the most common type (Chen et al., 2019). Exploring the relationship between NPC and pyroptosis-associated genes (PAGs) could aid in the understanding of HNSCC. Basic medical research can benefit from bioinformatics as it can provide information at multiple levels and aspects about molecular mechanisms of disease (Holtsträter et al., 2020; Lin et al., 2021; Chen et al., 2022; Luo et al., 2022; Sun et al., 2022; Yan et al., 2022). Biomarkers related to PAGs for NPC-related bioinformatics can provide effective treatment for HNSCC. This study combined genomic, transcriptomic, proteomic, metabolomic, and immunomics data to explore the microenvironmental composition of head and neck tumors and identify indicators associated with patient prognosis. A prognostic model for HNSCC was developed and validated based on PAGs in NPC.

Methods

Data download and pre-processing

Nasopharyngeal carcinoma (NPC)-related gene expression profiles was obtained from the Gene Expression Omnibus (GEO) database. The keyword "nasopharyngeal carcinoma" was selected to obtain three eligible mRNA microarray datasets (GSE12452, GSE53819, and GSE64634). GSE12452 and GSE64634 were from

the GPL570 platform, whereas GSE53819 was based on GPL6480. 61 NPC samples and 32 normal samples were obtained and normalized using R 4. 0. 3 software. In cases where a single gene was associated with multiple probes, the value for the expression of that gene was set to the average expression value corresponding to the multiple probes. Additionally, a batch correction was performed using the ComBat function in the sva package to eliminate the effect of different biological companies, researchers, and experimental batches on the results. Raw ribonucleic acid (RNA) sequencing data and clinical information were also downloaded from the TCGA database. Information on the survival time, age, survival status, clinical stage, gender, tumor grade, TNM staging, and pathological stage was obtained.

Identification of pyroptosis-related long non-coding RNAs

A total of 52 pyroptosis-related lncRNAs were obtained from literature reports (Broz et al., 2020; Wang et al., 2020; Zhou et al., 2020; Tan et al., 2021). Subsequently, the co-expression for lncRNAs and PAGs was studied using the Person correlation analysis method and the limma package in R was used to study the pyroptosis-related lncRNAs (correlation coefficient ≥0. 4; $p < 0.001$).

Expression analysis of *BAK1, NLRP1, CHMP7, RIPK1*

We used the Gene Expression Profiling Interactive Analysis (GEPIA) 2. 0 (http://gepia.cancer-pku.cn/), which integrates gene expression data from the Cancer Genome Atlas (TCGA) database, to analyze the expression of *BAK1*, *NLRP1*, *CHMP7*, and *RIPK1* genes (Tang et al., 2017). The Cancer Genome Atlas (GSCA) (http://bioinfo.life.hust.edu.cn/web/GSCALite/) was also used to analyze target gene expression in tumors (Liu et al., 2018). UALCAN (http://ualcan.path.uab.edu) analyzes cancer and paracancer gene expression data in depth using TCGA data (Chandrashekar et al., 2017). In addition, it can be used to analyze the correlation between gene expression and clinical information, including age, gender, tumor clinical staging, tumor pathological staging, and other clinical data.

Mutation and correlation analysis of *BAK1*, *NLRP1*, *CHMP7*, and *RIPK1* genes

CbioPortal (cBio Cancer Genomics Portal) (http://www.cbioportal.org/) was used to study gene mutation information in tumors, and we identified *BAK1*, *NLRP1*, *CHMP7*, and *RIPK1* gene mutations in HNSCC using the TCGA-HNSCC status (Gao et al., 2013). Meanwhile, GeneMANIA (http://genemania.org/), a website for constructing gene networks and functional prediction, was used to study the interaction of *BAK1*, *NLRP1*, *CHMP7*, and *RIPK1* genes (Warde-Farley et al., 2010).

Survival analysis

We used the kaplan-meier plotter (http://kmplot.com/analysis/) to analyze the survival curves of different genes in HNSCC, where we chose the best cutoff value for the selection, where higher than this value is considered high expression and lower than this value is low expression, where the vertical lines are censored data (Lánczky and Győrffy, 2021). In addition to overall survival (OS), we analyzed Disease Free Survival (DFS), progression-free interval (PFI), and progression-free interval survival data.

Combined indicator long non-coding RNAs (lncRNAs) receiver operator characteristic (ROC) curves for NPC diagnosis

The diagnostic effectiveness and diagnostic value of single or multiple combined indicators (biomarkers) were determined using ROC curves. The pROC package (R4. 0.3 software) was used to conduct the analysis. The area under the curve (AUC) represents the clinical significance of the experiment. Generally, an AUC value closer to 1.0 indicates high accuracy, and vice versa. Multiple lncRNAs (identified using the preceding procedures) were subjected to the process of single or multiple combined-indicator ROC curve analysis. The pROC package in the R4. 0.3 software was used for analysis and determining diagnostic values.

Enrichment analysis of NPC-related PAGs

The ROC analysis method was used on 52 PAGs to screen genes with AUC values >0.5. As in previous studies, the "clusterProfiler" and "org. Hs. eg. db" packages (R 4.0.3 software) were used for the Kyoto Encyclopedia of Genes and Genomes (KEGG) pathway and Gene Ontology (GO) enrichment analyses (Lin et al., 2021; Wu et al., 2021; Zhao and Jiang, 2022). In addition, the "clusterProfiler" package was used to analyze and visualize the genes and gene clusters in functional profiles (GO and KEGG). Biological process (BP), molecular function (MF), and cellular component (CC) are the three components associated with GO analyses (screening criteria: Q-value < 0. 05; p-value < 0. 05).

We analyzed the functional enrichment of *BAK1*, *NLRP1*, *CHMP7*, and *RIPK1* genes in the TCGA-HNSCC status and applied the LinkedOmics database (http://www.linkedomics.org/login.php) for analysis. We chose TCGA_HNSCC and RNA-seq

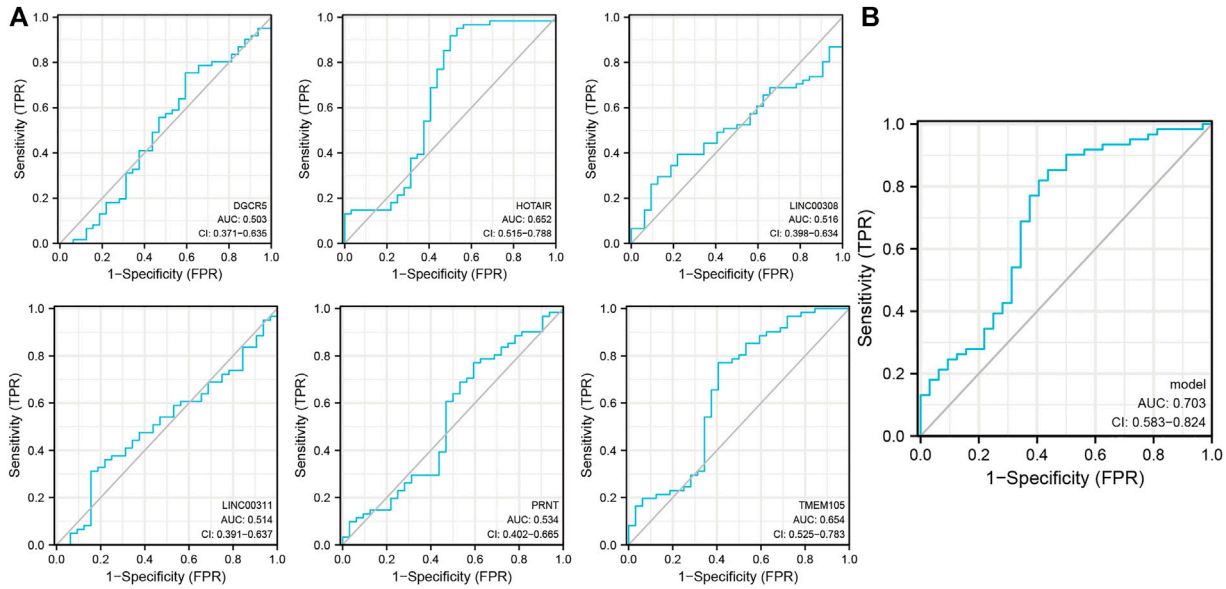

FIGURE 1
Single- and combined-indicator receiver operating characteristic curve (ROC) curves of pyroptosis-related long non-coding RNA (lncRNAs) for nasopharyngeal carcinoma (NPC) diagnosis. **(A)**. Single-indicator ROC curves for *DGCR5*, *HOTAIR*, *LINC00308*, *LINC00311*, *PRNT*, and *TMEM105* for NPC diagnosis; **(B)**. Six lncRNAs as co-diagnostic biomarkers.

data on this website and entered *BAK1*, *NLRP1*, *CHMP7*, and *RIPK1* genes using the Pearson Correlation test. Later, we selected over-representation analysis (ORA) as an enrichment tool, PANTHER pathway data as functional data, and rank criteria as *p*-value, with <0.05 being considered statistically significant (Vasaikar et al., 2018).

Immunomodulator analysis

We used the TISIDB database (http://cis.hku.hk/TISIDB/index.php) to analyze the correlation between genes and immunomodulation-related genes in HNSCC, where immunosuppressive markers included CD244, CD274, CTLA4, and LGALS9, the immune activation marker was ICOS, and major histocompatibility complex (MHC) molecules included HLA-E (Ru et al., 2019).

Immuno-infiltration analysis

For immune infiltration analysis, we used the tumor immune estimation resource (TIMER) database (https://cistrome.shinyapps.io/timer/). Immune cells were selected as B cells, $CD8^+$ T cells, $CD4^+$ T cells, macrophages, neutrophils, and dendritic cells (DCs). The correlation between the aforementioned immune cells and the genes *BAK1*, *NLRP1*, *CHMP7*, and *RIPK1* was analyzed (Li et al., 2016; Li et al., 2017). Subsequently, we used the TIMER database to analyze the correlation between the degrees of immune cell infiltration of HNSCC tumors and the variation in the copy number of different somatic cells of the gene.

Construction of the prognostic model

The survival analyses method was used to screen the genes associated with the prognosis of patients with HNSCC. The gene expressions were combined with the clinical prognostic information of the patients. After the false discovery rate (FDR) is corrected for both univariate Cox regression analysis and Kaplan-Meier (KM) survival analysis results, we identified the other genes that affected the prognosis of HNSCC patients using the univariate Cox regression analysis method (criterion: $p < 0.05$). Genes were used as dependent variables for curve fitting to obtain an optimal Cox proportional risk regression model. The model characterized by the minimum Akaike information criterion (AIC) value was selected. The low AIC value indicated that the model contained few free parameters and could be used to analyze the data efficiently.

Validation of the prognostic model

Following the identification of the optimal model, the risk scores were calculated. The risk scores were analyzed, and based on the risk scores at the maximum of the Youden index in the ROC curve, the patients were classified into low- and high-risk groups. The following

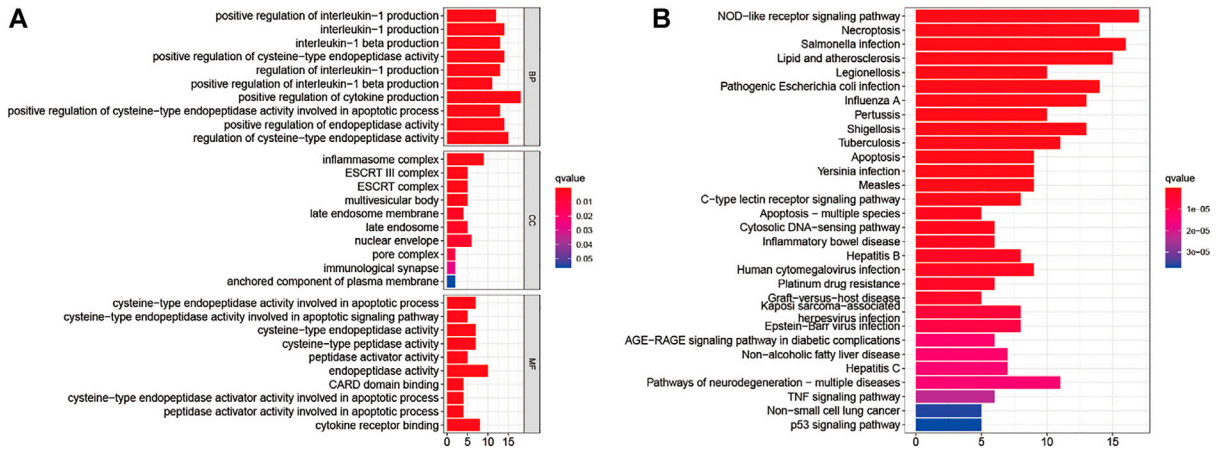

FIGURE 2
Gene Ontology **(A)** and The Kyoto Encyclopedia of Genes and Genomes **(B)** Enrichment analyses for nasopharyngeal carcinoma-related pyroptosis-associated genes.

methods were used to determine whether the risk scores could influence a patient's prognosis for hepatocellular carcinoma (Bray et al., 2018): non-parametric tests were conducted to compare the differences in risk scores by studying various clinicopathological factors (sex, age, pathological stage, clinical stage, grading, and TNM stage) (Ferlay et al., 2019); the survival curves of the prediction model for patients with HNSCC were plotted using the survival analysis method (Johnson et al., 2020); the prediction accuracy was studied by analyzing the time-dependent ROC curves generated using R software; and (Stein et al., 2015) Cox regression analysis results were used to determine if the risk score and other clinicopathological factors contributed to patients' poor prognosis for HNSCC.

Nomogram construction and calibration curve plotting

A nomogram was generated with the "rms" package in R, and the calibration curves were plotted for 1-, 3-, and 5-years OS. The risk score, sex, age, grading, clinical stage, and tumor stage were analyzed to obtain the results. Additionally, the Hosmer-Lemeshow test was employed to check whether the predicted and actual outcomes agreed.

Analysis of the level of immune cell infiltration and the tumor microenvironment

Various analytical methods for detecting immune cell infiltration are currently available. These methods include TIMER, CIBERSORT, XCELL, QUANTISEQ, McCounter, EPIC, and CIBERSORT on TIMER2 (Newman et al., 2015; Becht et al., 2016; Aran et al., 2017; Li et al., 2017; Racle et al., 2017; Chen et al., 2018; Finotello et al., 2019; Deng et al., 2021; Mei et al., 2022; Sun et al., 2022). The correlation coefficients for the correlation between different risk scores (obtained using different calculation methods) and certain immune cells can be obtained by determining the relationship between the immune cells and risk scores. The R software packages limma, ggplot2, scales, ggtext, ggpubr, and tidyverse were used for analysis, and the results were visualized using bubble plots. The scores for immune cells and immune-related functions were obtained using the single-sample gene set enrichment analysis (ssGSEA) technique. Additionally, using limma, ggpubr, and reshape2 (R software) were used to determine the differences between the immune cells and immune-related functions corresponding to the low- and high-risk groups. Finally, the TME was scored using the estimate package (R software) to compare the TME between the two groups.

Statistical analysis

Statistical results were presented as mean ± standard deviation, and statistical differences between the two samples were analyzed using two-tailed t-tests or analysis of variance. p-value ≤ 0.05 was considered statistically significant.

Results

Data download and pre-processing

Three NPC datasets (GSE12452, GSE53819, and GSE64634) were downloaded from the Gene Expression Omnibus (GEO) database, normalized, and batch corrected to form a dataset with

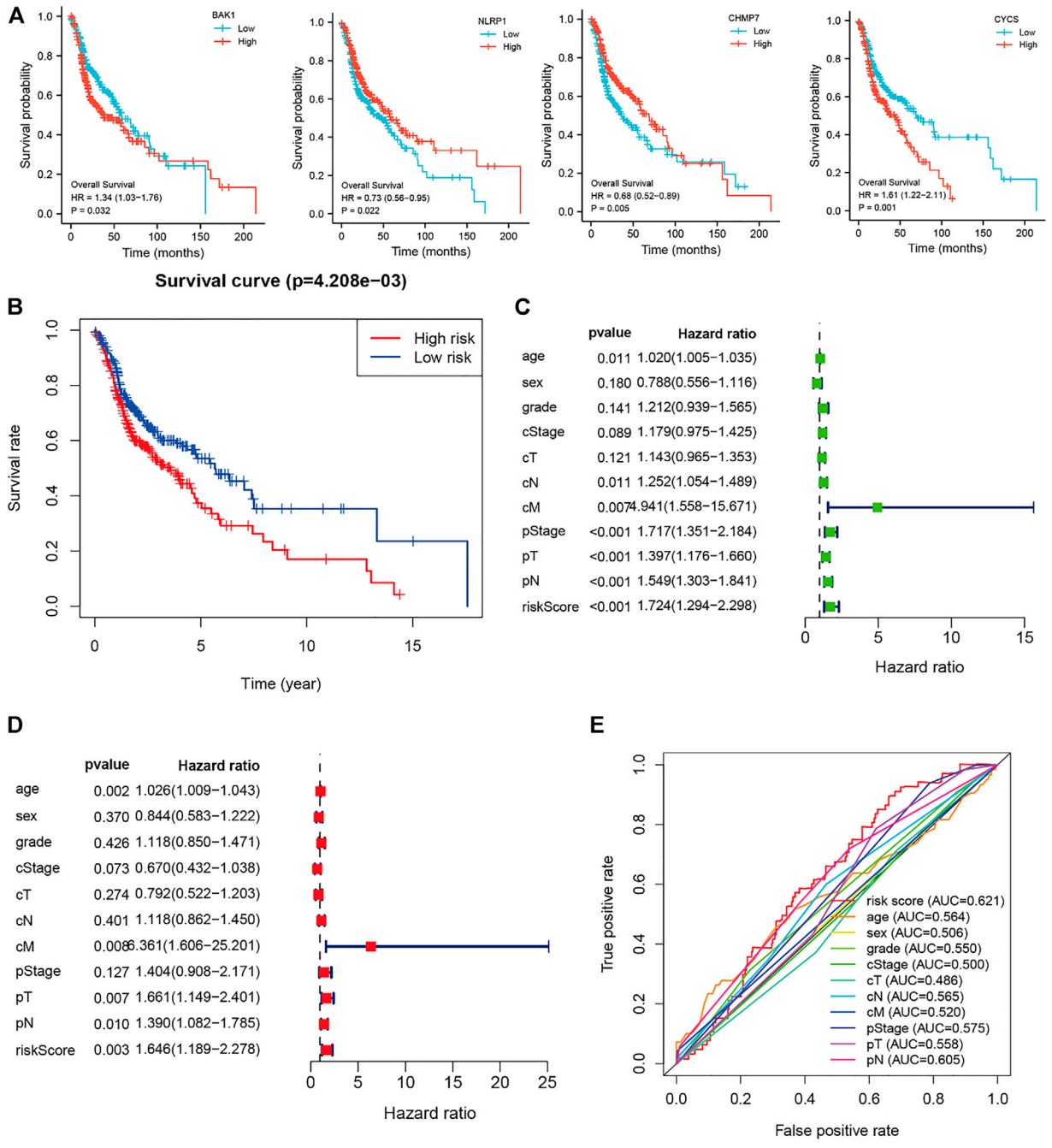

FIGURE 3
Risk and prognostic analysis of the single gene. **(A)**. Survival analysis to determine the correlation between the expressions of *BAK1*, *NLRP1*, *CHMP7*, and *CYCS* and head and neck squamous cell carcinoma (HNSCC); **(B)**. Kaplan-Meier survival curves present the correlation between the prognostic risk scores of patients suffering from HNSCC and the corresponding overall survival rates; **(C–D)**. The forest plot shows the univariate **(C)** and multivariate **(D)** Cox regression results; and **(E)**. Receiver operating characteristic curves are calculated for determining risk scores based on the sensitivity and specificity of the prognosis of patients with HNSCC.

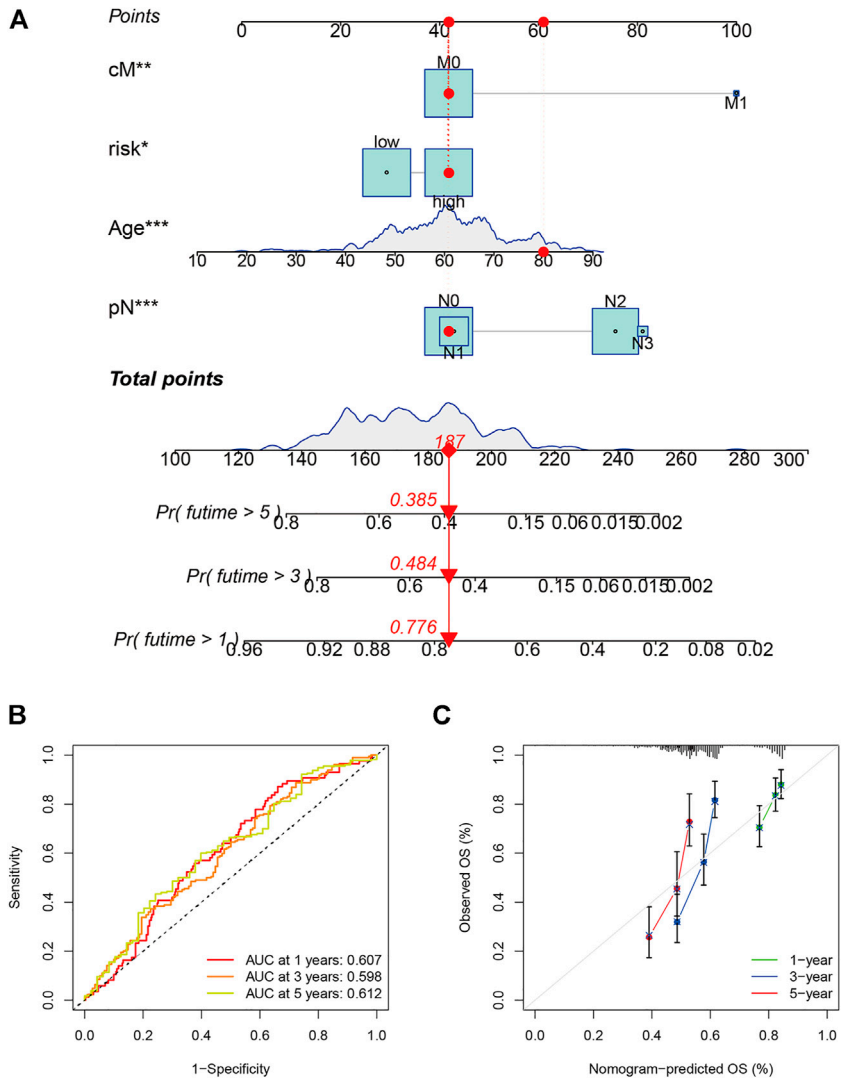

FIGURE 4
Evaluation and development of the prognostic model. **(A)** Prognostic model (nomogram) constructed using the "rms" R package; **(B)** The area under the curves for 1-, 3-, and 5-years clinical outcomes (0.607, 0.598, and 0.612, respectively). The values indicate good predictive power; and **(C)** Calibration plots reflect the agreement between the predicted and actual survival rates.

61 NPC samples and 32 normal samples (16,820 genes). The TCGA database was analyzed, and the transcript data and relevant clinical information for HNSCC patients ($n = 360$) were downloaded from it.

Pyroptosis-related lncRNAs ROC curves for NPC diagnosis

The raw dataset included 15,153 messenger RNA (mRNAs) and 199 lncRNAs. Previously reported results were analyzed to extract 52 PAGs to obtain the relevant expression profile (Supplementary Table 1). Subsequently, six pyroptosis-related lncRNAs (*DGCR5*, *HOTAIR*, *LINC00308*, *LINC00311*, *PRNT*, and *TMEM105*) were identified ($p < 0.001$; correlation coefficient ≥0.4) using three NPC datasets (GSE12452, GSE53819, and GSE64634). The lncRNAs were analyzed using the single-indicator ROC curve analysis method. The following results have been presented: DGCR5: (AUC = 0.503, 95% confidence interval (CI): 0.371–0.635), HOTAIR: (AUC = 0.652, 95% CI: 0.515–0.788), LINC00308: (AUC = 0.516, 95% CI: 0.398–0.634), LINC00311: (AUC = 0.514, 95% CI: 0.391–0.637), PRNT: (AUC = 0.534, 95% CI: 0.402–0.665), and TMEM105: (AUC = 0.654, 95% CI: 0.525–0.783) (Figure 1A). Subsequently, the combined-indicator ROC curves for the six lncRNAs were plotted with an AUC of 0.703 and a 95% CI of 0.583–0.824 (Figure 1B). These results suggest that the six lncRNAs (DGCR5, HOTAIR, LINC00308, LINC00311, PRNT, and TMEM105) have

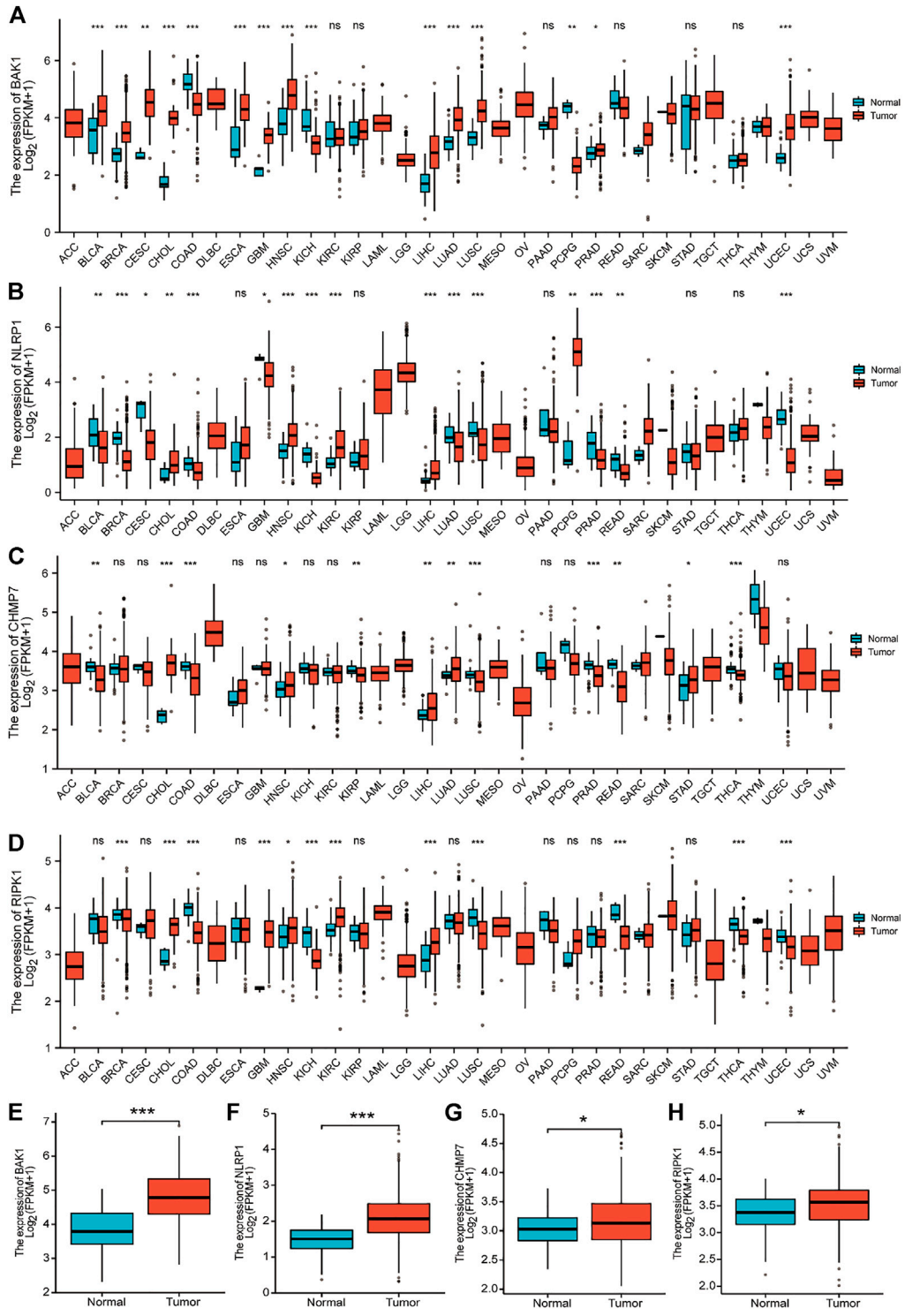

FIGURE 5
Expression of *BAK1*, *NLRP1*, *CHMP7*, and *RIPK1* markers in tumors. **(A)** BAK1 expression in 33 tumor species in the Cancer Genome Atlas (TCGA) database; **(B)** Expression of NLRP1 in tumor of 33 species in the TCGA database; **(C)** CHMP7 expression in 33 tumor species in the TCGA database; **(D)** TCGA database of RIPK1 expression in 33 tumor species; **(E)** BAK1 expression is increased in head and neck squamous cell carcinoma (HNSCC) tissues; **(F)** NLRP1 expression is elevated in HNSCC tissues; **(G)** CHMP7 expression is elevated in HNSCC tissues; **(H)** RIPK1 expression was elevated in HNSCC tissues. *$p < 0.05$, **$p < 0.01$, ***$p < 0.001$.

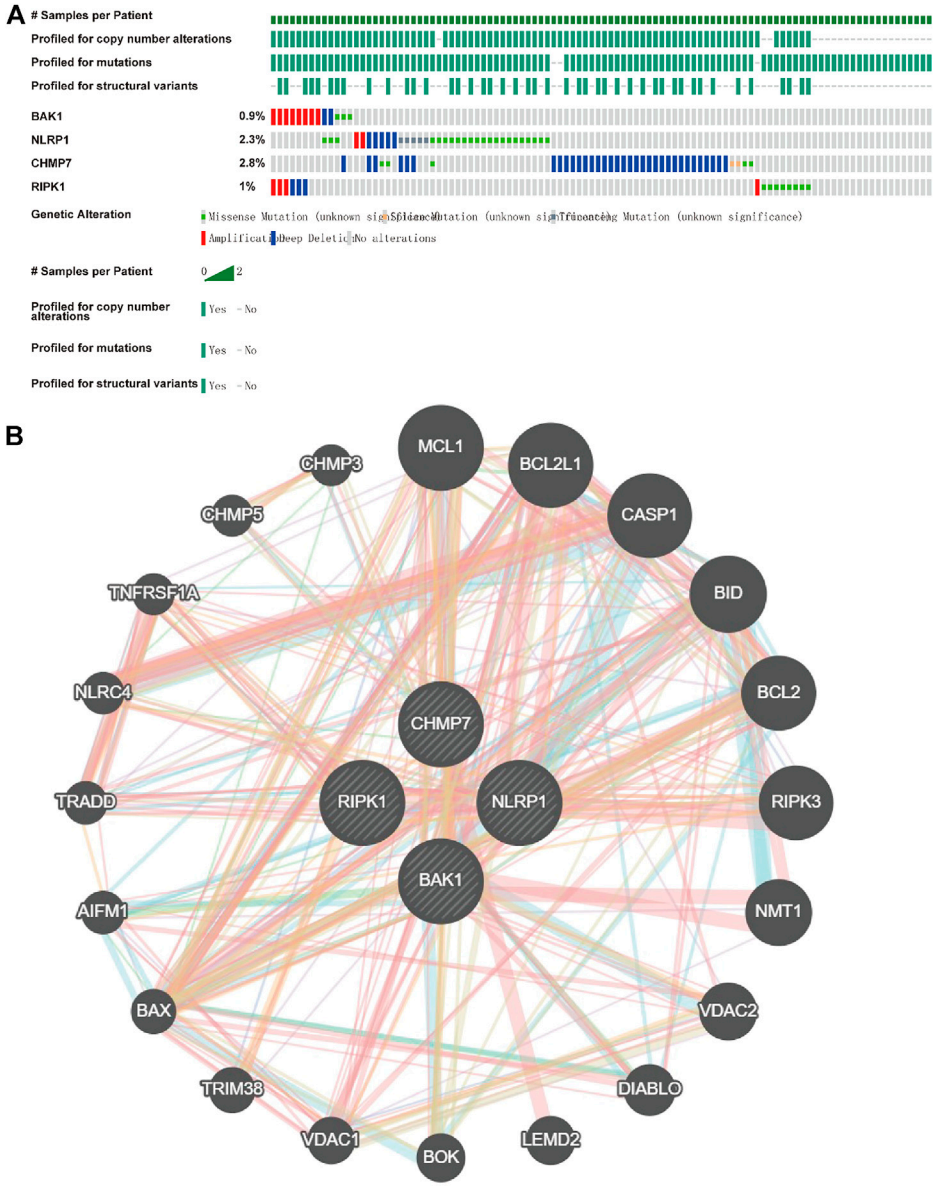

FIGURE 6
Mutations of *BAK1*, *NLRP1*, *CHMP7*, and *RIPK1* genes in head and neck squamous cell carcinoma (HNSCC) and their interplay network. **(A)** Total mutations of *BAK1*, *NLRP1*, *CHMP7*, and *RIPK1* in HNSCC; **(B)** GeneMANIA demonstrates the gene interaction network of *BAK1*, *NLRP1*, *CHMP7*, and *RIPK1*.

good diagnostic values and can function as co-diagnostic biomarkers.

Enrichment analysis of NPC-related PAGs

Analyzing the ROCs yielded NPC-related 42 genes with AUC values >0.5 (p-value < 0.05; Q-value < 0.05; Supplementary Table S2). GO and KEGG analyses were performed on these genes. These 42 genes were enriched in BPs (positive regulation of cytokine production; positive regulation of cysteine-type endopeptidase activity involved in the apoptotic process; positive regulation of interleukin-1 production; and others); CCs (inflammasome complex, ESCRT III complex, multivesicular body, nuclear envelope, and others); and MFs (cysteine-type endopeptidase activity involved in the apoptotic signaling pathway; cysteine-type endopeptidase activator activity involved in apoptotic process; peptidase activator activity involved in apoptotic process; cytokine

receptor binding; and others) (Figure 2A). The NOD-like receptor signaling pathway was the most enriched in KEGG pathways. *Salmonella* infection, necroptosis, lipid and atherosclerosis, legionellosis, pathogenic *Escherichia coli* infection, influenza A, pertussis, shigellosis, tuberculosis, apoptosis, *Yersinia* infection, measles, C-type lectin receptor signaling pathway, apoptosis-multiple species, cytosolic DNA-sensing pathway, inflammatory bowel disease, hepatitis B, human cytomegalovirus infection, platinum drug resistance, graft-versus-host disease, Kaposi sarcoma-associated herpesvirus infection, Epstein-Barr virus infection, AGE/RAGE signaling pathway in diabetic complications, non-alcoholic fatty liver disease, hepatitis C, pathways of neurodegeneration-multiple diseases, TNF signaling pathway, and non-small cell lung cancer p53 signaling pathway respectively (Figure 2B).

Construction and evaluation of a prognostic model

The 42 PAGs were incorporated into the TCGA database and four genes [*BAK1* (p = 0.032, HR = 1.34 (1.03–1.76)], *NLRP1* [p = 0.022, HR = 0.73 (0.56–0.95)], *CHMP7* [p = 0.005, HR = 0.68 (0.52–0.89)], and *CYCS* [p = 0.001, HR = 1.61 (1.22–2.11)] associated with the prognosis of HNSCC patients were identified following the process of survival analysis (Figure 3A). Subsequently, the minimum AUC value was considered when selecting the best model, which consisted of three genes (*NLRP*, *CHMP7*, and *CYCS*). The risk score was calculated as follows: risk score = *NLRP1**(−0. 067) + *CHMP7**(−0. 044) + *CYCS**(0. 111). The patients were then classified into two groups (low-risk and high-risk) based on their risk scores. The median risk score was used as the cut-off value. Analyzing the K-M survival curves showed that the OS of patients in the high-risk group was lower than that of patients in the low-risk group (p = 4.208e-03) (Figure 3B). This indicated that the prognosis could be predicted using the risk scores. The multivariate and univariate Cox regression analysis method was used to assess the clinical prognostic factors (sex, age, stage, pathological TNM staging, and clinical TNM staging) and risk scores to determine whether the survival model could function as an independent prognostic factor for HNSCC. The HR values for the risk scores obtained using the multivariate and univariate Cox regression analyses were 1.646 (95% CI: 1.189–2.278, p = 0.003) and 1. 724 (95% CI: 1.294–2.298, p < 0.001), respectively (Figures 3C,D). This indicated that the risk model could be used as an independent prognostic factor for HNSCC. Furthermore, the AUC value (0.621) for the risk score was calculated to assess its predictive sensitivity and specificity (Figure 3E). The findings suggested that the developed risk model was a viable independent prognostic factor for HNSCC patients. Moreover, to predict patient prognosis, "rms" (an R package) was used to construct a nomogram based on risk score, age, sex, grade, clinical stage, and tumor stage (Figure 4A). The survival rate for each individual was calculated using the total score obtained by adding all the scores corresponding to each variable. The process was used to obtain the 1-, 3-, and 5-years OS. The corresponding AUCs were 0.607, 0.598, and 0.612, indicating good predictive performance (Figure 4B). The analysis of nomogram calibration plots revealed that the predicted survival rate was in good agreement with the actual survival rate (Figure 4C).

Expression of *BAK1, NLRP1, CHMP7*, and *RIPK1* in HNSCC and normal tissues

Figures 5A–D show the expression of BAK1, NLRP1, CHMP7, and RIPK1 markers in 33 tumors. These four markers were overexpressed in cholangiocarcinoma (CHOL), HNSCC, and liver hepatocellular carcinoma (LIHC), and they were all statistically different. Figures 5E–H show that the expression of BAK1, NLRP1, CHMP7, and RIPK1 was higher in HNSCC tumor tissues than in paraneoplastic tissues.

Mutation of *BAK1*, *NLRP1*, *CHMP7*, and *RIPK1* genes in HNSCC and gene interaction network

Because all the above genes were expressed at higher levels in HNSCC, we investigated their mutations in HNSCC using cBioportal and found that *BAK1*, *NLRP1*, *CHMP7*, and *RIPK1* genes were highly conserved in HNSCC (Figure 6A). The interaction of the genes above was then investigated using GeneMANIA (http://genemania.org). The interplay network of the *BAK1*, *NLRP1*, *CHMP7*, and *RIPK1* genes may include 20 potential target genes (Figure 6B).

Prognostic role of *BAK1*, *NLRP1*, *CHMP7*, and *RIPK1* in HNSCC

We analyzed the relationship between *BAK1, NLRP1, CHMP7*, and *RIPK1* mRNA and HNSCC survival. Figure 7A demonstrates the relationship between *BAK1, NLRP1, CHMP7*, and *RIPK1* mRNAs and tumor survival. The Kaplan-Meier (K-M) plotter was also used to analyze its relationship with the prognosis of HNSCC patients. As shown in Figures 7B–D, the higher expression of *BAK1* worsens the HNSCC prognosis. Unlike *BAK1*, the higher expression of *NLRP1, CHMP7*, and *RIPK1* improves HNSCC prognosis, as shown in Figures 7E–M.

Relationship between *BAK1, NLRP1, CHMP7*, and *RIPK1* mRNAs and clinical characteristics in HNSCC

Because the above results showed that *BAK1, NLRP1, CHMP7*, and *RIPK1* mRNAs and HNSCC prognosis were

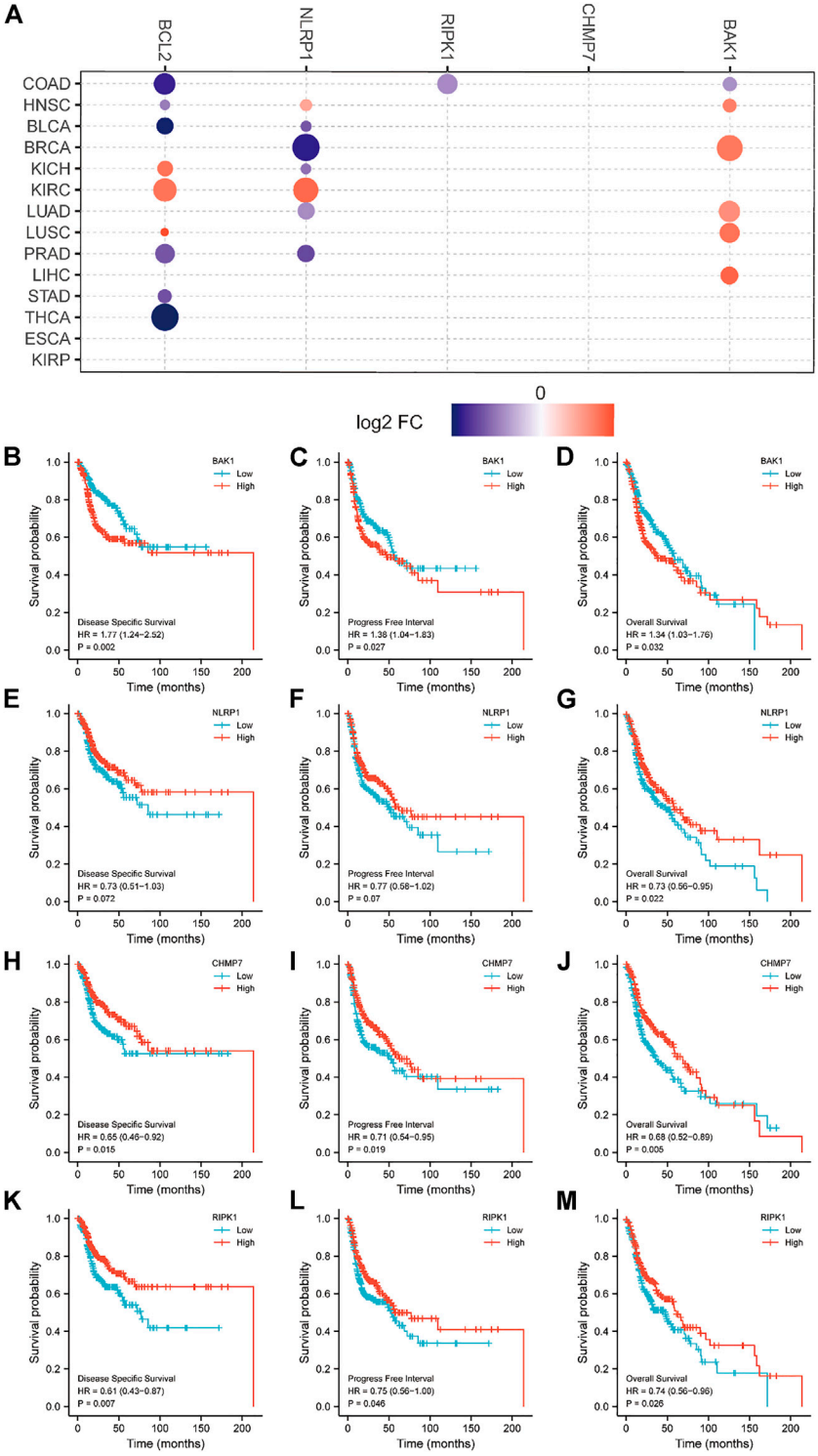

FIGURE 7
Relationship between BAK1, NLRP1, CHMP7, and RIPK1 messenger RNAs (mRNAs) and prognosis of head and neck squamous cell carcinoma (HNSCC) patients. **(A)** Relationship between BAK1, NLRP1, CHMP7, and RIPK1, Bcl-2 mRNAs expression and tumor survival in the Cancer Genome Atlas database; Kaplan-Meier (K-M) plotter showing survival curves for disease free survival (DFS); **(B)** Progression-free interval (PFI); **(C)** Overall survival (OS); **(D)** For BAK1 and HNSCC; the K-M plotter shows DFS for NLRP1 and HNSCC; **(E)** PFI; **(F)** OS; **(G)** Survival plots; K-M plotter showing DFS; **(H)** PFI; **(I)** OS; **(J)** Survival plots for CHMP7 and HNSCC; K-M plotter showing DFS; **(K)** PFI; **(L)** OS; **(M)** Survival plots for RIPK1 and HNSCC.

TABLE 1 Demographic characteristics of the patients.

Variable	Total
Age	60.84 ± 11.85
Sex	
Male	264
Female	96
Grade	
G1	43
G2	229
G3	87
G4	1
cStage	
Stage I	16
Stage II	60
Stage III	81
Stage IV	203
cT	
T1	27
T2	85
T3	96
T4	152
cN	
N0	183
N1	69
N2	103
N3	5
cM	
M0	356
M1	4
pSatge	
Stage I	20
Stage II	46
Stage III	64
Stage IV	230
pT	
T1	31
T2	94
T3	82
T4	153
pN	
N0	154
N1	56
N2	143
N3	7

closely related, we investigated the relationship between the above genes and the clinical characteristics of HNSCC further. Table 1 shows that in HNSCC, BAK1 and CHMP7 are associated with sex, clinical staging, and tumor histological grading, NLRP1 is associated with sex and clinical staging, and RIPK1 is not associated with any of these clinical characteristics.

Functional analysis of the genes *BAK1*, *NLRP1*, *CHMP7*, and *RIPK1* in HNSCC

The LinkedOmics database was used to further analyze the predicted function of the above genes in HNSCC. As shown in Figure 8A, *BAK1* is primarily enriched in pathways such as pyrimidine metabolism, androgen/estrogen/progesterone biosynthesis, 2-arachidonoylglycerol biosynthesis, and gamma-aminobutyric acid synthesis. As shown in Figure 8B, *NLRP1* functions are mainly enriched in purine metabolism, valine biosynthesis, isoleucine biosynthesis, and alanine synthesis. As shown in Figure 8C, the functions of *CHMP7* are primarily enriched in pathways such as P53 pathway feedback loops, tetrahydrofolate biosynthesis, ascorbate degradation, and succinate to propionate conversion. Similarly, the functions of *RIPK1* are mainly enriched in pathways such as purine metabolism, valine biosynthesis, isoleucine biosynthesis, and salvage pyrimidine deoxyribonucleotides, as shown in Figure 8D.

Analysis of immune cell infiltration levels and TME

The immune cells and risk scores were correlated using different calculation methods. The findings suggested a correlation between the immune cells and low-risk populations. The low-risk population, in particular, was associated with the $CD4^+$ T cells, immune score, and DCs using the XCELL algorithm; $CD4^+$ T cells and $CD8^+$ T cells using the TIMER algorithm; macrophages using the QUANTISEQ algorithm; $CD8^+$ T cells using the MCPCOUNTER algorithm; B cells using the EPIC algorithm; $CD4^+$ T cells, B cells, and $CD8^+$ T cells using the CIBERSORT-ABS algorithm; and $CD8^+$ T and B cells using the CIBERSORT algorithm (Figure 9A). Moreover, the ssGSEA scores for immune cells and immune-related functions revealed a difference in the distribution patterns of Th cells, regulatory T cells, tumor-infiltrating lymphocytes, follicular helper T cells, adipose-derived cells, interdigitating dendritic cells, $CD8^+$ T cells, and B cells between the high- and low-risk groups. Furthermore, a difference was observed in the immune functions (for the antigen-presenting cells, T cells, and immune checkpoints) associated with the two groups (Figures 9B,C). The TMEs corresponding to the low- and high-risk groups were analyzed, and the results indicated that the immune scores of the high-risk patients were lower than those of the low-risk patients (Figures 9D–F).

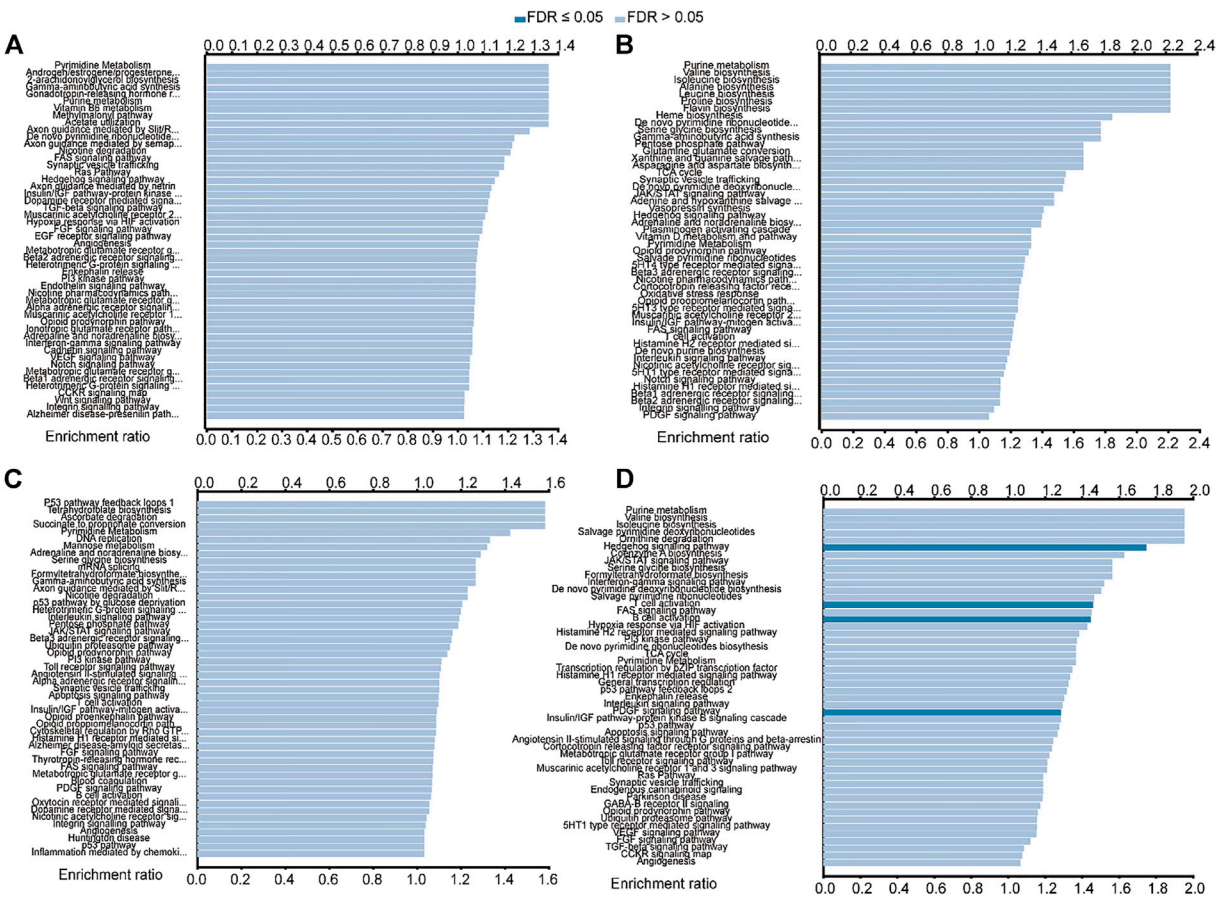

FIGURE 8
Functional enrichment analysis of *BAK1*, NLRP1, CHMP7, and RIPK1 in head and neck squamous cell carcinoma (HNSCC) from the LinkedOmics database. **(A)** Functional enrichment analysis of *BAK1* in HNSCC; **(B)** Functional enrichment analysis of NLRP1 in HNSCC; and **(C)** Functional enrichment analysis of CHMP7 in HNSCC; and **(D)** Functional enrichment analysis of RIPK1 in HNSCC.

Correlation between *BAK1*, *NLRP1*, *CHMP7*, and *RIPK1* genes and immunomodulators

Interaction network results revealed that *BAK1*, *NLRP1*, *CHMP7*, and *RIPK1* genes could interact with immune factors, including TNF-α, suggesting their influence on the immune microenvironment of the HNSCC tumor. We used the TISIDB database to investigate the relationship between the above genes and immunomodulators. As shown in Figure 10A, in HNSCC, *BAK1* has a positive correlation with CD244, CD274, CTLA4, HLA-E, and ICOS, while having a negative correlation with LGALS9; as shown in Figure 10B, *NLRP1* has a positive correlation with CD244, CD274, CTLA4, HLA-E, and ICOS, while having a negative correlation with LGALS9; as shown in Figure 10C, *CHMP7* correlates positively with CD244, CTLA4, ICOS, and LGALS9, and negatively with CD274 and HLA-E; similarly, as shown in Figure 10D, *RIPK1* correlates positively with CD244, CD274, CTLA4, HLA-E, ICOS, and LGALS9.

Correlation of *BAK1*, *NLRP1*, *CHMP7*, and *RIPK1* genes' expression and immune infiltration

In HNSCC, the expression of *BAK1*, NLRP1, CHMP7, and RIPK1 genes and numerous immunomodulatory markers showed a certain relationship. We used the TIMER database to analyze the relationship between different genes and immune infiltration. We selected B cells, $CD8^+$ T cells, $CD4^+$ T cells, macrophages, neutrophils, and DCs for immune cell infiltration analysis. As shown in Figure 11A, in HNSCC, *BAK1* has a positive correlation with $CD8^+$ T cells, $CD4^+$

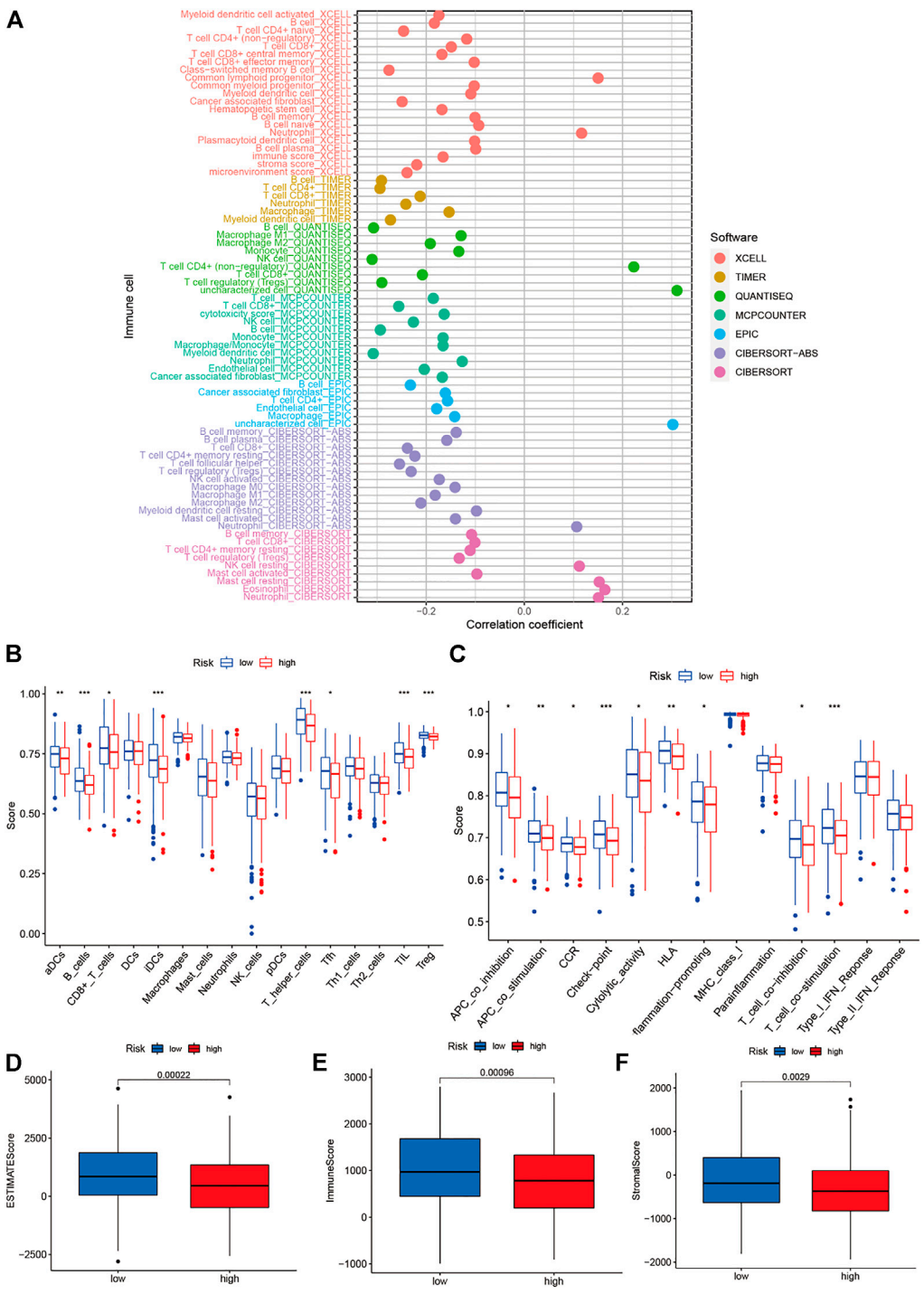

FIGURE 9
Analysis of tumor microenvironment and of degrees mmune cell infiltration. **(A)** Determination of the relationship between immune cells and risk scores using different calculation methods; **(B–C)** Immune cell and immune-related function scores were obtained using the single-sample gene set enrichment analysis technique; and **(D–F)** The differences between the immune cell infiltration levels in the low- and high-risk groups.

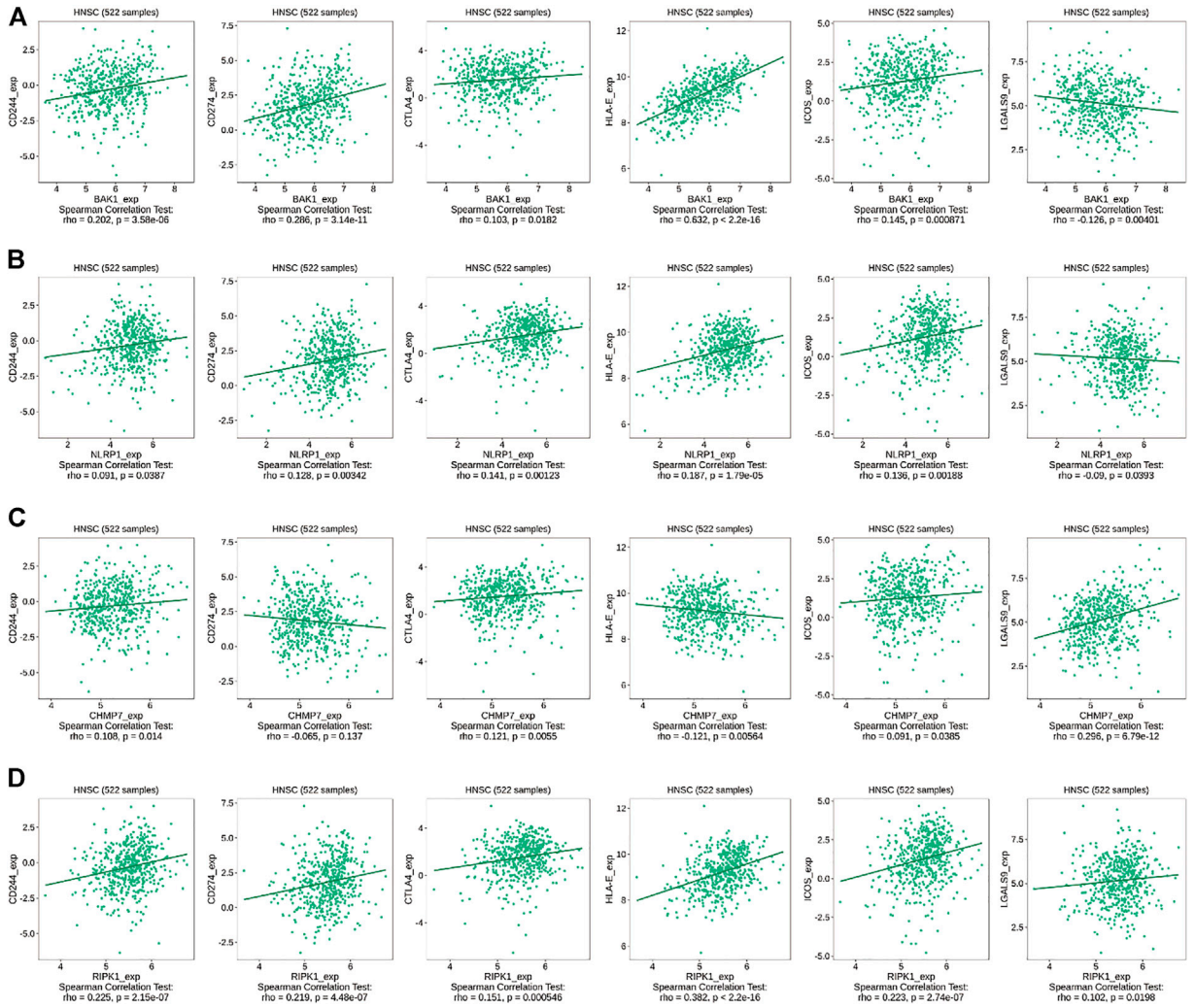

FIGURE 10
Correlation between *BAK1*, *NLRP1*, *CHMP7*, and *RIPK1* genes and immunomodulators. **(A)** Correlation between *BAK1* gene and CD244, CD274, CTLA4, HLA-E, ICOS, and LGALS9 in HNSCC according to TISIDB database; **(B)** Correlation between *NLRP1* gene and CD244, CD274, CTLA4, HLA-E, ICOS, and LGALS9 in HNSCC according to TISIDB database; **(C)** Correlations between *CHMP7* gene and CD244, CD274, CTLA4, HLA-E, ICOS, and LGALS9 in HNSCC according to TISIDB database; and **(D)** Correlations between *RIPK1* gene and CD244, CD274, CTLA4, HLA-E, ICOS, and LGALS9 in HNSCC according to TISIDB database.

T cells, neutrophils, and DC infiltration while having a negative correlation with B cells and macrophage cell infiltration; as shown in Figures 11B–D, *NLRP1*, *CHMP7*, and *RIPK1* genes and immune cell infiltration all show some positive correlation.

All the above genes can influence tumor development by affecting immune infiltration. We used the TIMER database to analyze the correlation between the level of immune cell infiltration and gene copy number variation in HNSCC tumors. As shown in Figure 12A, the levels of B cell, $CD8^+$ T cell, $CD4^+$ T cell, macrophage, neutrophil, and DC infiltration decrease as the copy number of the *BAK1* gene increases. As shown in Figure 12B, the levels of B cell, $CD4^+$ T cell, and DC infiltration increase as the copy number of the *NLRP1* gene increases, whereas the levels of $CD8^+$ T cell, neutrophil, and macrophage decrease, and the changes in macrophage are not statistically significant. As shown in Figure 12C, when the *CHMP7* gene copy number is increased, B cell, $CD8^+$ T cell, $CD4^+$ T cell, and DC infiltration levels decrease; macrophages and neutrophils do not show statistical differences. As shown in Figure 12D, when the *RIPK1* gene copy number is increased, B cell, $CD8^+$ T cell, $CD4^+$ T cell, macrophage, neutrophil, and DC infiltration levels decrease.

In summary, the *BAK1*, *CHMP7*, and *RIPK1* genes can reduce immune cell infiltration by activating immunosuppressive markers, whereas *NLRP1* can both reduce immune infiltration by activating immunosuppressive markers

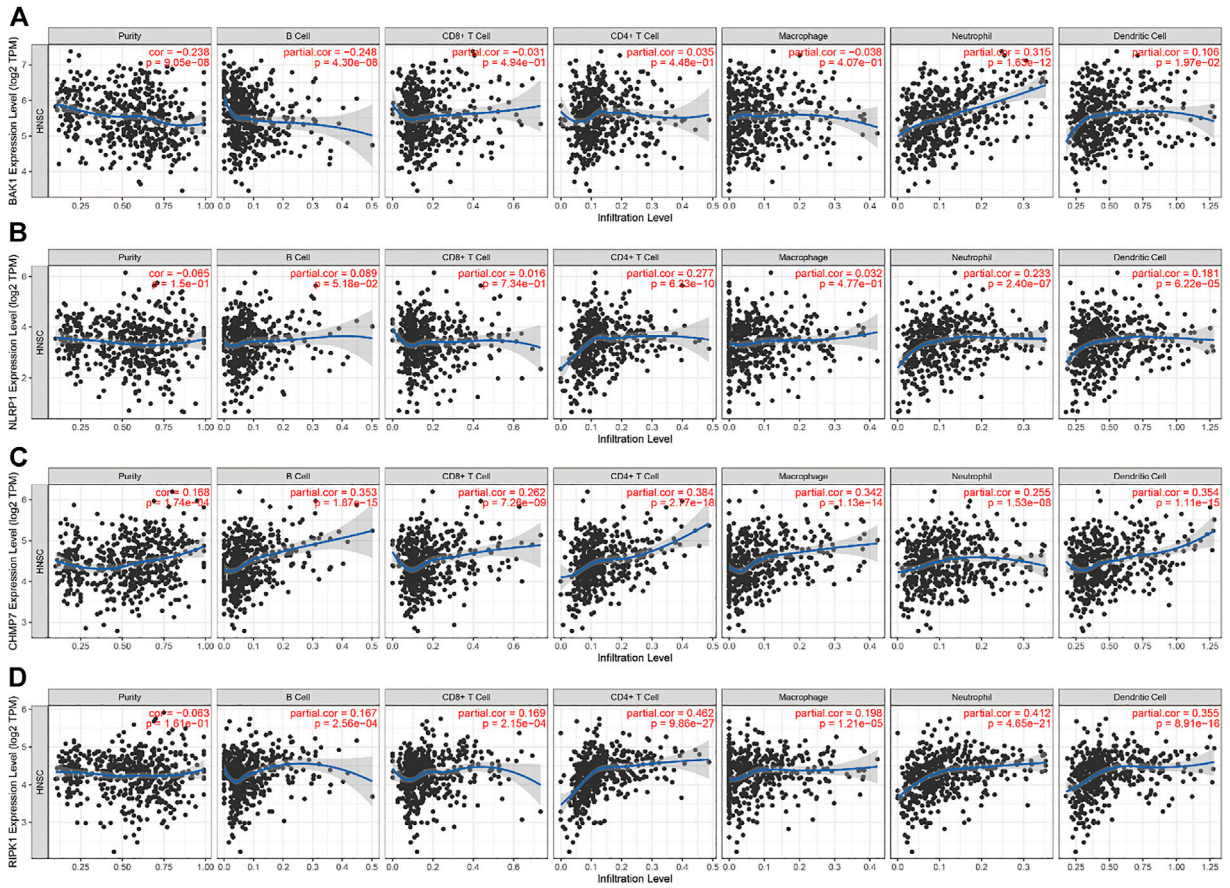

FIGURE 11
Correlation between *BAK1*, *NLRP1*, *CHMP7*, and *RIPK1* genes' expression and immune infiltration. **(A)** Correlation between *BAK1* expression levels and B cell, $CD8^+$ T cell, $CD4^+$ T cell, macrophage, neutrophil, dendritic cell (DC) infiltration; **(B)** Correlation between *NLRP1* expression levels and B cells, $CD8^+$ T cells, $CD4^+$ T cells, macrophages, neutrophils, and DC infiltration; **(C)** Correlation between *CHMP7* expression levels and the infiltration of B cells, $CD8^+$ T cells, $CD4^+$ T cells, macrophages, neutrophils, and DCs; and **(D)** Correlation between *RIPK1* expression levels and the infiltration of B cells, $CD8^+$ T cells, $CD4^+$ T cells, macrophages, neutrophils, and DCs.

and promote immune infiltration by activating immune activation markers.

Discussion

HNSCC is a group of heterogeneous solid tumors originating from upper respiratory tract epithelial cells. It tends to metastasize and recur, increasing mortality, morbidity, and disability rates (Bray et al., 2018). Effective clinical risk assessment and early-stage diagnostic tools for HNSCC are scarce. Poor prognosis is primarily associated with local invasion, drug resistance, recurrence, and metastasis (Pulte and Brenner, 2010; Leemans et al., 2011). Traditional clinicopathological indicators, such as tumor size, vascular invasion, and TNM staging, cannot be used to stratify patients' risks or predict their prognosis (Cheng et al., 2009). As a result, transcriptionomics and epigenetics should be used for screening potential biomarkers that aid in the early detection of the disease. The biomarkers have the potential for risk assessment, treatment, and monitoring of the prognosis of patients with HNSCC.

We obtained 52 PAGs by analyzing the NPC-related gene expression profile obtained from the GEO database. Six PAG-related lncRNAs were identified based on the correlation coefficient (r) and *p*-value (≥0.4 and <0.001, respectively). The single- and combined-indicator ROC curve analysis results suggested that the six lncRNAs had good diagnostic values and could be used as co-diagnostic biomarkers. These were accurate predictors of NPC. Moreover, 42 genes with AUC values of >0.5 were screened using the ROC analysis method. Their association with MF, CC, and BP was analyzed using the GO and KEGG enrichment analysis methods. Subsequently, the 42 genes were incorporated into the TCGA database, and the four

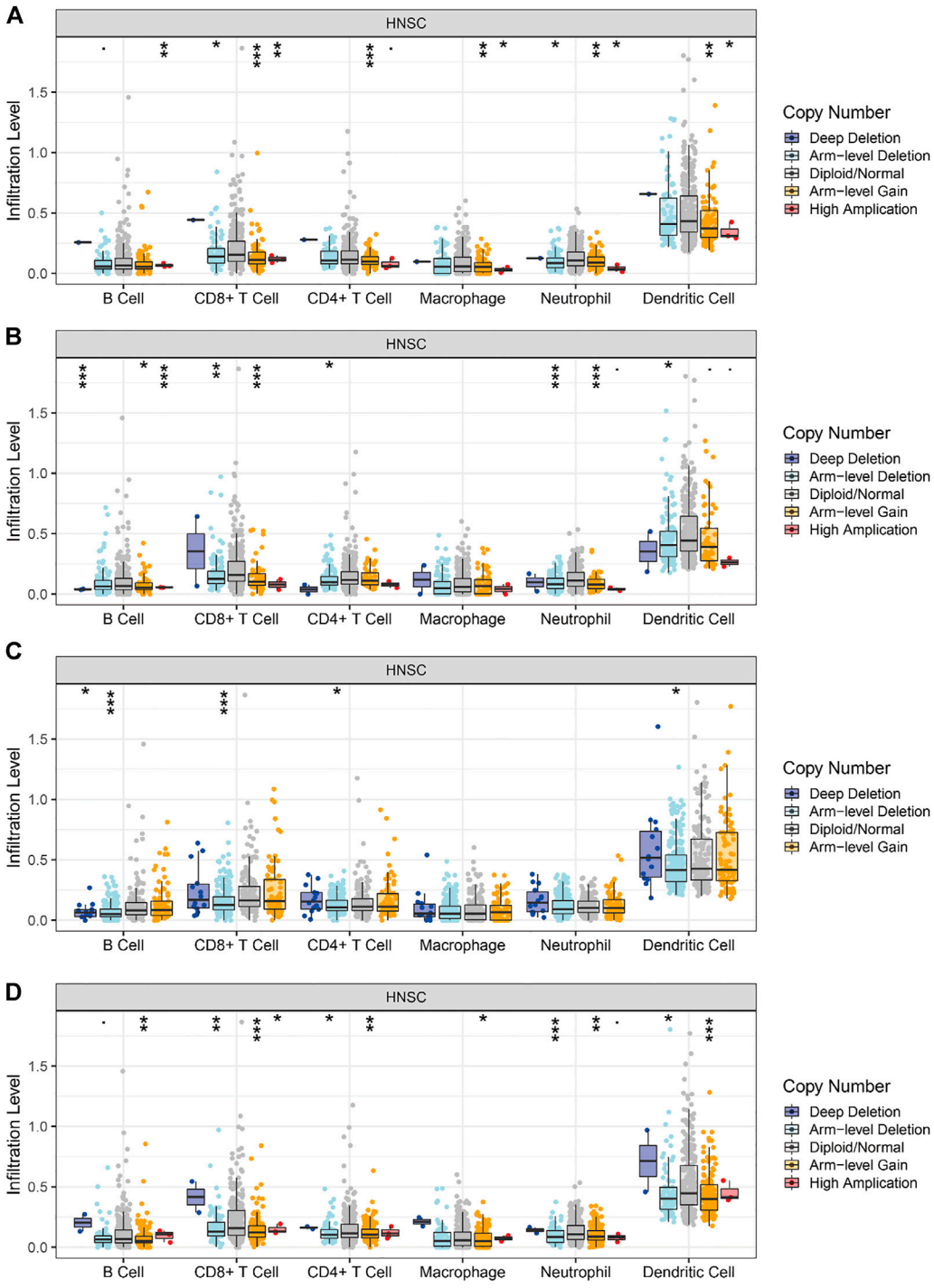

FIGURE 12
Correlation of *BAK1*, *NLRP1*, *CHMP7*, and *RIPK1* gene copy number variation and immune infiltration. **(A)** Correlation between *BAK1* gene copy number variation and B cell, $CD8^+$ T cell, $CD4^+$ T cell, macrophage, neutrophil, dendritic cell (DC) infiltration; **(B)** Correlation between *NLRP1* gene copy number variation and B cell, $CD8^+$ T cell, $CD4^+$ T cell, macrophage, neutrophil, DC infiltration; **(C)** Correlation between *CHMP7* gene copy number variation and B cell, $CD8^+$ T cell, $CD4^+$ T cell, macrophage, neutrophil, and DC infiltration; and **(D)** Correlation between *RIPK1* gene copy number variation and B cell, $CD8^+$ T cell, $CD4^+$ T cell, macrophage, neutrophil, and DC infiltration. $^*p < 0.05$, $^{**}p < 0.01$, $^{***}p < 0.001$.

genes (*BAK1*, *NLRP1*, *CHMP7*, and *CYCS*) associated with the prognosis of HNSCC patients were screened using the survival analysis method. The obtained genes were used as dependent variables for curve fitting to select the best Cox proportional risk regression model, which consisted of three genes (*NLRP1*, *CHMP7*, and *CYCS*). It has previously been reported that the genes incorporated into this model regulate tumor progression and significantly influence the process associated with the onset of oral squamous cell carcinoma, cutaneous squamous cell carcinoma, melanoma, breast cancer, and lung cancer (Sand et al., 2019; Xu et al., 2021).

NLRP1, a NOD-like receptor family protein, is widely expressed in various cell types. It is associated with the formation of inflammasomes. NLRP1 is linked to the production of IL-1 β and IL-18 and pyroptosis and plays a crucial role in developing innate immunity and generating inflammation. Thus, it influences the processes involved in the onset and progression of multiple diseases, including tumors, autoimmune diseases, neurological diseases, and metabolic diseases (Tupik et al., 2020). The downregulation of NLRP1 expression promotes the progression of human cutaneous squamous cell carcinoma (Sand et al., 2019). NLRP1 is also linked to the progression of various malignancies. It has also been reported that the regulation of TME by NLRP1 affects the prognosis of patients with lung adenocarcinoma (Shen et al., 2021). Moreover, elevated NLRP1 expression levels promote breast cancer cell proliferation, metastasis, and invasion. These processes are mediated by the induction of the process of epithelial-mesenchymal transition (Wei et al., 2017). The inflammasome is activated, and apoptotic pathways are inhibited in these conditions, resulting in the rapid progression of melanoma (Ehrhart et al., 1975).

As a component of the endosomal sorting complex (ESCRT III), CHMP7 significantly influences the processes of endosomal sorting, nuclear envelope formation, and neurodevelopment (Olmos et al., 2016; Sadoul et al., 2018). CHMP7 is also associated with the pathogenesis of amyotrophic lateral sclerosis. These conditions cause spinal cord damage, and bulbar muscular atrophy is observed under these conditions (Fairfield et al., 2019; Malik et al., 2019). A statistical relationship was found between CHMP7 expression levels and the clinical prognosis of cancer patients, and protein phosphorylation and immune cell infiltration processes were established (Guo et al., 2021).

CYCS is a central component of the mitochondrial electron transport chain. It is primarily associated with energy production in normal and tumor cells (Hüttemann et al., 2011). Mutations in this gene cause autosomal dominant thrombocytopenia, and apoptosis in oral squamous cell carcinoma cells is also triggered under these conditions (Ong et al., 2017; Uchiyama et al., 2018; Sabit et al., 2021).

To our knowledge, we are the first to report NPC-related PAGs. HNSCC was retrieved to screen the genes associated with the prognosis of HNSCC patients. A novel and robust prognosis assessment model for HNSCC patients has been developed. However, this study still has some limitations, and the sample size is small. Due to data set restrictions, there is a risk of racial bias in this study. In addition, bioinformatics analysis does not provide comprehensive results and should be supplemented with biological experiments. Further experimental studies are needed to gain a comprehensive understanding.

Conclusion

In this study, NPC and PAGs were investigated in relation to nasopharyngeal carcinoma, and indicators related to the prognosis of HNSCC patients were identified. PAGs were used to develop and validate a prognostic model for NPC, and the genes incorporated into the model were closely related to the tumor microenvironment. Therefore, this study suggests that prognosis-related PAGs of NPC also predict the prognosis of HNSCC, which helps to improve our understanding of the treatment of NPC and HNSCC.

Data availability statement

Publicly available datasets were analyzed in this study. This data can be found here: The gene expression profile data related to nasopharyngeal carcinoma were obtained from GEO database (https://www.ncbi.nlm.nih.gov/geo/): GSE12452, GSE53819, and GSE64634. From TCGA database (https://www.cancer.gov/about-nci/organization/ccg/research), we downloaded the original RNA sequences and clinical data for HNSCC.

Author contributions

BC, YL, and RS: Conceptualization, methodology, software; BC, YL, XK, YS, CJ, BY, XY, YC, and RS: Data curation, writing-original draft preparation; BC and YL: Visualization, investigation; RS: Supervision; BC, YL, XK, YS, CJ, BY, XY, and YC, and RS: Software, validation; BC, YL, and RS: Writing-reviewing and editing.

Acknowledgments

We thank Bullet Edits Limited for the linguistic editing and proofreading of the manuscript.

Conflict of interest

The authors declare that the research was conducted in the absence of any commercial or financial relationships that could be construed as a potential conflict of interest.

Publisher's note

All claims expressed in this article are solely those of the authors and do not necessarily represent those of their affiliated organizations, or those of the publisher, the editors and the reviewers. Any product that may be evaluated in this article, or claim that may be made by its manufacturer, is not guaranteed or endorsed by the publisher.

Supplementary material

The Supplementary Material for this article can be found online at: https://www.frontiersin.org/articles/10.3389/fgene.2022.981222/full#supplementary-material

References

Amin, M. B., Greene, F. L., Edge, S. B., Compton, C. C., Gershenwald, J. E., Brookland, R. K., et al. (2017). The Eighth Edition AJCC Cancer Staging Manual: Continuing to build a bridge from a population-based to a more "personalized" approach to cancer staging. *Ca. Cancer J. Clin.* 67, 93–99. doi:10.3322/caac.21388

Aran, D., Hu, Z., and Butte, A. J. (2017). xCell: digitally portraying the tissue cellular heterogeneity landscape. *Genome Biol.* 18, 220. doi:10.1186/s13059-017-1349-1

Becht, E., Giraldo, N. A., Lacroix, L., Buttard, B., Elarouci, N., Petitprez, F., et al. (2016). Estimating the population abundance of tissue-infiltrating immune and stromal cell populations using gene expression. *Genome Biol.* 17, 218. doi:10.1186/s13059-016-1070-5

Bedoui, S., Herold, M. J., and Strasser, A. (2020). Emerging connectivity of programmed cell death pathways and its physiological implications. *Nat. Rev. Mol. Cell Biol.* 21, 678–695. doi:10.1038/s41580-020-0270-8

Bray, F., Ferlay, J., Soerjomataram, I., Siegel, R. L., Torre, L. A., and Jemal, A. (2018). Global cancer statistics 2018: GLOBOCAN estimates of incidence and mortality worldwide for 36 cancers in 185 countries. *Ca. Cancer J. Clin.* 68, 394–424. doi:10.3322/caac.21492

Broz, P., Pelegrín, P., and Shao, F. (2020). The gasdermins, a protein family executing cell death and inflammation. *Nat. Rev. Immunol.* 20, 143–157. doi:10.1038/s41577-019-0228-2

Cai, J., Yi, M., Tan, Y., Li, X., Li, G., Zeng, Z., et al. (2021). Natural product triptolide induces GSDME-mediated pyroptosis in head and neck cancer through suppressing mitochondrial hexokinase-II. *J. Exp. Clin. Cancer Res.* 40, 190. doi:10.1186/s13046-021-01995-7

Chandrashekar, D. S., Bashel, B., Balasubramanya, S. A. H., Creighton, C. J., Ponce-Rodriguez, I., Chakravarthi, B. V. S. K., et al. (2017). Ualcan: A portal for facilitating tumor subgroup gene expression and survival analyses. *Neoplasia* 19, 649–658. doi:10.1016/j.neo.2017.05.002

Chauhan, S. S., Kaur, J., Kumar, M., Matta, A., Srivastava, G., Alyass, A., et al. (2015). Prediction of recurrence-free survival using a protein expression-based risk classifier for head and neck cancer. *Oncogenesis* 4, e147. doi:10.1038/oncsis.2015.7

Chen, B., Khodadoust, M. S., Liu, C. L., Newman, A. M., and Alizadeh, A. A. (2018). "Profiling tumor infiltrating immune cells with CIBERSORT," in *Cancer systems biology. Methods in molecular biology*. Editor L. von Stechow (New York, NY: Springer New York), 243–259. doi:10.1007/978-1-4939-7493-1_12

Chen, C., Zhao, J., Liu, J-N., and Sun, C. (2021). Mechanism and role of the neuropeptide LGI1 receptor ADAM23 in regulating biomarkers of ferroptosis and progression of esophageal cancer. *Dis. Markers* 2021, 9227897. doi:10.1155/2021/9227897

Chen, Y., Sun, Y., Luo, Z., Chen, X., Wang, Y., Qi, B., et al. (2022). Exercise modifies the transcriptional regulatory features of monocytes in alzheimer's patients: A multi-omics integration analysis based on single cell technology. *Front. Aging Neurosci.* 14, 881488. doi:10.3389/fnagi.2022.881488

Chen, Y-P., Chan, A. T. C., Le, Q-T., Blanchard, P., Sun, Y., and Ma, J. (2019). Nasopharyngeal carcinoma. *Lancet* 394, 64–80. doi:10.1016/S0140-6736(19)30956-0

Cheng, A-L., Kang, Y-K., Chen, Z., Tsao, C-J., Qin, S., Kim, J. S., et al. (2009). Efficacy and safety of sorafenib in patients in the asia-pacific region with advanced hepatocellular carcinoma: A phase III randomised, double-blind, placebo-controlled trial. *Lancet. Oncol.* 10, 25–34. doi:10.1016/S1470-2045(08)70285-7

Deng, C., Guo, H., Yan, D., Liang, T., Ye, X., and Li, Z. (2021). Pancancer analysis of neurovascular-related NRP family genes as potential prognostic biomarkers of bladder urothelial carcinoma. *Biomed. Res. Int.* 2021, 5546612. doi:10.1155/2021/5546612

Ding, J., Wang, K., Liu, W., She, Y., Sun, Q., Shi, J., et al. (2016). Pore-forming activity and structural autoinhibition of the gasdermin family. *Nature* 535, 111–116. doi:10.1038/nature18590

Ehrhart, I. C., Parker, P. E., Weidner, W. J., Dabney, J. M., Scott, J. B., and Haddy, F. J. (1975). Coronary vascular and myocardial responses to carotid body stimulation in the dog. *Am. J. Physiol.* 229, 754–760. doi:10.1152/ajplegacy.1975.229.3.754

Fairfield, C. J., Wigmore, S. J., and Harrison, E. M. (2019). Gallstone disease and the risk of cardiovascular disease. *Sci. Rep.* 9, 5830. doi:10.1038/s41598-019-42327-2

Ferlay, J., Colombet, M., Soerjomataram, I., Mathers, C., Parkin, D. M., Piñeros, M., et al. (2019). Estimating the global cancer incidence and mortality in 2018: GLOBOCAN sources and methods. *Int. J. Cancer* 144, 1941–1953. doi:10.1002/ijc.31937

Fiddian-Green, R. G., and Silen, W. (1975). Mechanisms of disposal of acid and alkali in rabbit duodenum. *Am. J. Physiol.* 229, 1641–1648. doi:10.1152/ajplegacy.1975.229.6.1641

Fink, S. L., and Cookson, B. T. (2005). Apoptosis, pyroptosis, and necrosis: Mechanistic description of dead and dying eukaryotic cells. *Infect. Immun.* 73, 1907–1916. doi:10.1128/IAI.73.4.1907-1916.2005

Finotello, F., Mayer, C., Plattner, C., Laschober, G., Rieder, D., Hackl, H., et al. (2019). Molecular and pharmacological modulators of the tumor immune contexture revealed by deconvolution of RNA-seq data. *Genome Med.* 11, 34. doi:10.1186/s13073-019-0638-6

Gao, J., Aksoy, B. A., Dogrusoz, U., Dresdner, G., Gross, B., Sumer, S. O., et al. (2013). Integrative analysis of complex cancer genomics and clinical profiles using the cBioPortal. *Sci. Signal.*, 6, pl1. doi:10.1126/scisignal.2004088

Gao, J., Qiu, X., Xi, G., Liu, H., Zhang, F., Lv, T., et al. (2018). Downregulation of GSDMD attenuates tumor proliferation via the intrinsic mitochondrial apoptotic pathway and inhibition of EGFR/Akt signaling and predicts a good prognosis in non-small cell lung cancer. *Oncol. Rep.* 40, 1971–1984. doi:10.3892/or.2018.6634

Guo, Y., Shi, J., Zhao, Z., and Wang, M. (2021). Multidimensional analysis of the role of charged multivesicular body protein 7 in pan-cancer. *Int. J. Gen. Med.* 14, 7907–7923. doi:10.2147/IJGM.S337876

He, Y., Hara, H., and Núñez, G. (2016). Mechanism and regulation of NLRP3 inflammasome activation. *Trends biochem. Sci.* 41, 1012–1021. doi:10.1016/j.tibs.2016.09.002

Holtsträter, C., Schrörs, B., Bukur, T., and Löwer, M. (2020). "Bioinformatics for cancer immunotherapy," in *Bioinformatics for cancer immunotherapy. Methods in molecular biology*. Editor S. Boegel (New York, NY: Springer US), 1–9. doi:10.1007/978-1-0716-0327-7_1

Hüttemann, M., Pecina, P., Rainbolt, M., Sanderson, T. H., Kagan, V. E., Samavati, L., et al. (2011). The multiple functions of cytochrome c and their regulation in life and death decisions of the mammalian cell: From respiration to apoptosis. *Mitochondrion* 11, 369–381. doi:10.1016/j.mito.2011.01.010

Johnson, D. E., Burtness, B., Leemans, C. R., Lui, V. W. Y., Bauman, J. E., and Grandis, J. R. (2020). Head and neck squamous cell carcinoma. *Nat. Rev. Dis. Prim.* 6, 92. doi:10.1038/s41572-020-00224-3

Keung, E. Z., and Gershenwald, J. E. (2018). The eighth edition American Joint committee on cancer (AJCC) melanoma staging system: Implications for melanoma treatment and care. *Expert Rev. Anticancer Ther.* 18, 775–784. doi:10.1080/14737140.2018.1489246

Lage, H., Helmbach, H., Grottke, C., Dietel, M., and Schadendorf, D. (2001). DFNA5 (ICERE-1) contributes to acquired etoposide resistance in melanoma cells. *FEBS Lett.* 494, 54–59. doi:10.1016/S0014-5793(01)02304-3

Lánczky, A., and Győrffy, B. (2021). Web-based survival analysis tool tailored for medical research (KMplot): Development and implementation. *J. Med. Internet Res.* 23, e27633. doi:10.2196/27633

Leemans, C. R., Braakhuis, B. J. M., and Brakenhoff, R. H. (2011). The molecular biology of head and neck cancer. *Nat. Rev. Cancer* 11, 9–22. doi:10.1038/nrc2982

Li, B., Severson, E., Pignon, J-C., Zhao, H., Li, T., Novak, J., et al. (2016). Comprehensive analyses of tumor immunity: Implications for cancer immunotherapy. *Genome Biol.* 17, 174. doi:10.1186/s13059-016-1028-7

Li, T., Fan, J., Wang, B., Traugh, N., Chen, Q., Liu, J. S., et al. (2017). Timer: A web server for comprehensive analysis of tumor-infiltrating immune cells. *Cancer Res.* 77, e108–e110. doi:10.1158/0008-5472.CAN-17-0307

Lin, W., Wang, Y., Chen, Y., Wang, Q., Gu, Z., and Zhu, Y. (2021). Role of calcium signaling pathway-related gene regulatory networks in ischemic stroke based on multiple WGCNA and single-cell analysis. *Oxid. Med. Cell. Longev.*, 2021. doi:10.1155/2021/8060477

Liu, C-J., Hu, F-F., Xia, M-X., Han, L., Zhang, Q., and Guo, A-Y. (2018). GSCALite: A web server for gene set cancer analysis. *Bioinformatics* 34, 3771–3772. doi:10.1093/bioinformatics/bty411

Liu, J., Yao, L., Zhang, M., Jiang, J., Yang, M., and Wang, Y. (2019). Downregulation of LncRNA-XIST inhibited development of non-small cell lung cancer by activating miR-335/SOD2/ROS signal pathway mediated pyroptotic cell death. *Aging* 11, 7830–7846. doi:10.18632/aging.102291

Luo, Z., Qi, B., Sun, Y., Chen, Y., Lin, J., Qin, H., et al. (2022). Engineering bioactive M2 macrophage-polarized, anti-inflammatory, miRNA-based liposomes for functional muscle repair: From exosomal mechanisms to biomaterials. *Small* 18, 2201957. doi:10.1002/smll.202201957

Malik, B., Devine, H., Patani, R., La Spada, A. R., Hanna, M. G., and Greensmith, L. (2019). Gene expression analysis reveals early dysregulation of disease pathways and links Chmp7 to pathogenesis of spinal and bulbar muscular atrophy. *Sci. Rep.* 9, 3539. doi:10.1038/s41598-019-40118-3

Mei, S., Li, Y., and Kang, X. (2022). Prognostic and functional analysis of NPY6R in uveal melanoma using bioinformatics. *Dis. Markers*, 2022. doi:10.1155/2022/4143447

Newman, A. M., Liu, C. L., Green, M. R., Gentles, A. J., Feng, W., Xu, Y., et al. (2015). Robust enumeration of cell subsets from tissue expression profiles. *Nat. Methods* 12, 453–457. doi:10.1038/nmeth.3337

Olmos, Y., Perdrix-Rosell, A., and Carlton, J. G. (2016). Membrane binding by CHMP7 coordinates ESCRT-III-dependent nuclear envelope reformation. *Curr. Biol.* 26, 2635–2641. doi:10.1016/j.cub.2016.07.039

Ong, L., Morison, I. M., and Ledgerwood, E. C. (2017). Megakaryocytes from *CYCS* mutation-associated thrombocytopenia release platelets by both proplatelet-dependent and -independent processes. *Br. J. Haematol.* 176, 268–279. doi:10.1111/bjh.14421

Pulte, D., and Brenner, H. (2010). Changes in survival in head and neck cancers in the late 20th and early 21st century: A period analysis. *Oncologist* 15, 994–1001. doi:10.1634/theoncologist.2009-0289

Racle, J., de Jonge, K., Baumgaertner, P., Speiser, D. E., and Gfeller, D. (2017). Simultaneous enumeration of cancer and immune cell types from bulk tumor gene expression data. *eLife* 6, e26476. doi:10.7554/eLife.26476

Ru, B., Wong, C. N., Tong, Y., Zhong, J. Y., Zhong, S. S. W., Wu, W. C., et al. (2019). Tisidb: An integrated repository portal for tumor–immune system interactions. *Bioinformatics* 35, 4200–4202. doi:10.1093/bioinformatics/btz210

Sabit, H., Tombuloglu, H., Cevik, E., Abdel-Ghany, S., El-Zawahri, E., El-Sawy, A., et al. (2021). Knockdown of c-MYC controls the proliferation of oral squamous cell carcinoma cells *in vitro* via dynamic regulation of key apoptotic marker genes. *Int. J. Mol. Cell. Med.* 10, 45–55. doi:10.22088/IJMCM.BUMS.10.1.45

Sadoul, R., Laporte, M. H., Chassefeyre, R., Chi, K. I., Goldberg, Y., Chatellard, C., et al. (2018). The role of ESCRT during development and functioning of the nervous system. *Semin. Cell Dev. Biol.* 74, 40–49. doi:10.1016/j.semcdb.2017.08.013

Sand, J., Fenini, G., Grossi, S., Hennig, P., Di Filippo, M., Levesque, M., et al. (2019). The NLRP1 inflammasome pathway is silenced in cutaneous squamous cell carcinoma. *J. Invest. Dermatol.* 139, 1788–1797. doi:10.1016/j.jid.2019.01.025

Shen, E., Han, Y., Cai, C., Liu, P., Chen, Y., Gao, L., et al. (2021). Low expression of NLRP1 is associated with a poor prognosis and immune infiltration in lung adenocarcinoma patients. *Aging* 13, 7570–7588. doi:10.18632/aging.202620

Shi, Q., Yan, X., Wang, J., and Zhang, X. (2021). Collagen family genes associated with risk of recurrence after radiation therapy for vestibular schwannoma and pan-cancer analysis. *Dis. Markers*, 2021. doi:10.1155/2021/7897994

Stein, A. P., Saha, S., Kraninger, J. L., Swick, A. D., Yu, M., Lambert, P. F., et al. (2015). Prevalence of human papillomavirus in oropharyngeal cancer: A systematic review. *Cancer J.* 21, 138–146. doi:10.1097/PPO.0000000000000115

Sun, C., Ma, S., Chen, Y., Kim, N. H., Kailas, S., Wang, Y., et al. (2022). Diagnostic value, prognostic value, and immune infiltration of LOX family members in liver cancer: Bioinformatic analysis. *Front. Oncol.* 12, 843880. doi:10.3389/fonc.2022.843880

Tan, L-L., Jiang, X-L., Xu, L-X., Li, G., Feng, C-X., Ding, X., et al. (2021). TP53-induced glycolysis and apoptosis regulator alleviates hypoxia/ischemia-induced microglial pyroptosis and ischemic brain damage. *Neural Regen. Res.* 16, 1037–1043. doi:10.4103/1673-5374.300453

Tang, Z., Li, C., Kang, B., Gao, G., Li, C., and Zhang, Z. (2017). Gepia: A web server for cancer and normal gene expression profiling and interactive analyses. *Nucleic Acids Res.* 45, W98–W102. doi:10.1093/nar/gkx247

Tsuchiya, K. (2020). Inflammasome-associated cell death: Pyroptosis, apoptosis, and physiological implications. *Microbiol. Immunol.* 64, 252–269. doi:10.1111/1348-0421.12771

Tupik, J. D., Nagai-Singer, M. A., and Allen, I. C. (2020). To protect or adversely affect? The dichotomous role of the NLRP1 inflammasome in human disease. *Mol. Asp. Med.* 76, 100858. doi:10.1016/j.mam.2020.100858

Uchiyama, Y., Yanagisawa, K., Kunishima, S., Shiina, M., Ogawa, Y., Nakashima, M., et al. (2018). A novel *CYCS* mutation in the α-helix of the CYCS C-terminal domain causes non-syndromic thrombocytopenia. *Clin. Genet.* 94, 548–553. doi:10.1111/cge.13423

Vasaikar, S. V., Straub, P., Wang, J., and Zhang, B. (2018). LinkedOmics: Analyzing multi-omics data within and across 32 cancer types. *Nucleic Acids Res.* 46, D956–D963. doi:10.1093/nar/gkx1090

Wang, Q., Wang, Y., Ding, J., Wang, C., Zhou, X., Gao, W., et al. (2020). A bioorthogonal system reveals antitumour immune function of pyroptosis. *Nature* 579, 421–426. doi:10.1038/s41586-020-2079-1

Warde-Farley, D., Donaldson, S. L., Comes, O., Zuberi, K., Badrawi, R., Chao, P., et al. (2010). The GeneMANIA prediction server: Biological network integration for gene prioritization and predicting gene function. *Nucleic Acids Res.* 38, W214–W220. doi:10.1093/nar/gkq537

Wei, Y., Huang, H., Qiu, Z., Li, H., Tan, J., Ren, G., et al. (2017). NLRP1 overexpression is correlated with the tumorigenesis and proliferation of human breast tumor. *Biomed. Res. Int.*, 2017, 4938473–4938479. doi:10.1155/2017/4938473

Wu, T., Hu, E., Xu, S., Chen, M., Guo, P., Dai, Z., et al. (2021). clusterProfiler 4.0: A universal enrichment tool for interpreting omics data. *Innovation.* 2, 100141. doi:10.1016/j.xinn.2021.100141

Xia, T., Tian, H., Zhang, K., Zhang, S., Chen, W., Shi, S., et al. (2021). Exosomal ERp44 derived from ER-stressed cells strengthens cisplatin resistance of nasopharyngeal carcinoma. *BMC Cancer* 21, 1003. doi:10.1186/s12885-021-08712-9

Xu, D., Ji, Z., and Qiang, L. (2021). Molecular characteristics, clinical implication, and cancer immunity interactions of pyroptosis-related genes in breast cancer. *Front. Med.* 8, 702638. doi:10.3389/fmed.2021.702638

Yan, C., Chen, Y., Sun, C., Ahmed, M. A., Bhan, C., Guo, Z., et al. (2022). Does proton pump inhibitor use lead to a higher risk of coronavirus disease 2019 infection and progression to severe disease? A meta-analysis. *Jpn. J. Infect. Dis.* 75, 10–15. doi:10.7883/yoken.JJID.2021.074

Yu, P., Zhang, X., Liu, N., Tang, L., Peng, C., and Chen, X. (2021). Pyroptosis: Mechanisms and diseases. *Signal Transduct. Target. Ther.* 6, 128. doi:10.1038/s41392-021-00507-5

Zhao, B., and Jiang, X. (2022). hsa-miR-518-5p/hsa-miR-3135b regulates the REL/SOD2 pathway in ischemic cerebral infarction. *Front. Neurol.* 13, 852013. doi:10.3389/fneur.2022.852013

Zhou, Z., He, H., Wang, K., Shi, X., Wang, Y., Su, Y., et al. (2020). Granzyme A from cytotoxic lymphocytes cleaves GSDMB to trigger pyroptosis in target cells. *Science*, 368, eaaz7548. doi:10.1126/science.aaz7548

frontiers | Frontiers in Genetics

TYPE Original Research
PUBLISHED 11 October 2022
DOI 10.3389/fgene.2022.1013737

OPEN ACCESS

EDITED BY
Qian Wang,
Tai'an City Central Hospital, China

REVIEWED BY
Yiheng Ye,
First Affiliated Hospital of Wenzhou Medical University, China
Qiancheng Luo,
Shanghai Pudong New Area Gongli Hospital, China
Xingju Zheng,
Guizhou Provincial People's Hospital, China

*CORRESPONDENCE
Yuan Song,
sypw@qq.com
Xianyou Zheng,
zhengxianyou@126.com
Hai Hu,
xmhuhai@hotmail.com

†These authors have contributed equally to this work

SPECIALTY SECTION
This article was submitted to *Cancer Genetics and Oncogenomics*, a section of the journal Frontiers in Genetics

RECEIVED 07 August 2022
ACCEPTED 26 September 2022
PUBLISHED 11 October 2022

CITATION
Xu N, Wang X, Wang L, Song Y, Zheng X and Hu H (2022), Comprehensive analysis of potential cellular communication networks in advanced osteosarcoma using single-cell RNA sequencing data.
Front. Genet. 13:1013737.
doi: 10.3389/fgene.2022.1013737

Comprehensive analysis of potential cellular communication networks in advanced osteosarcoma using single-cell RNA sequencing data

Ning Xu[1†], Xiaojing Wang[2†], Lili Wang[1†], Yuan Song[1*], Xianyou Zheng[3*] and Hai Hu[1,3*]

[1]Departments of Orthopedics, Shanghai Eighth People's Hospital, Shanghai, China, [2]Department of Neurology, The First Affiliated Hospital of Anhui Medical University, Hefei, China, [3]Departments of Orthopedics, Sixth People's Hospital Affiliated to Shanghai Jiao Tong University, Shanghai, China

Osteosarcoma (OS) is a common bone cancer in children and adolescents, and metastasis and recurrence are the major causes of poor treatment outcomes. A better understanding of the tumor microenvironment is required to develop an effective treatment for OS. In this paper, a single-cell RNA sequencing dataset was taken to a systematic genetic analysis, and potential signaling pathways linked with osteosarcoma development were explored. Our findings revealed 25 clusters across 11 osteosarcoma tissues, with 11 cell types including "Chondroblastic cells", "Osteoblastic cells", "Myeloid cells", "Pericytes", "Fibroblasts", "Proliferating osteoblastic cells", "Osteoclasts", "TILs", "Endothelial cells", "Mesenchymal stem cells", and "Myoblasts". The results of Cell communication analysis showed 17 potential cellular communication networks including "COLLAGEN signaling pathway network", "CD99 signaling pathway network", "PTN signaling pathway network", "MIF signaling pathway network", "SPP1 signaling pathway network", "FN1 signaling pathway network", "LAMININ signaling pathway network", "FGF signaling pathway network", "VEGF signaling pathway network", "GALECTIN signaling pathway network", "PERIOSTIN signaling pathway network", "VISFATIN signaling pathway network", "ITGB2 signaling pathway network", "NOTCH signaling pathway network", "IGF signaling pathway network", "VWF signaling pathway network", "PDGF signaling pathway network". This research may provide novel insights into the pathophysiology of OS's molecular processes.

KEYWORDS

osteosarcoma, cell types, cellular communication networks, regulon activity, ScRNA-seq

Introduction

Osteosarcoma (OS) is a highly malignant solid bone tumor characterized by malignant mesenchymal cells producing pathological osteoid and/or bony matrix; it accounts for roughly 60% of all pediatric malignancies (Bousquet et al., 2016; Guo et al., 2022; Ho et al., 2017), and the incidence of OS in the overall population is two to three million per year (Shao et al., 2022). Clinical signs of OS affect the proximal tibia, proximal humerus, and distal femur, and consist predominantly of local discomfort, edema, and reduced joint movement (Rothzerg et al., 2021). Currently, this cancer is treated with surgical excision and chemotherapy with many agents. Unfortunately, the 5-years overall survival rate for osteosarcoma patients was just approximately 60% among patients with localized osteosarcoma but is only 20% among patients presenting with metastases or recurrent disease (Meltzer and Helman, 2021). The pathophysiology of OS is characterized by the substantial infiltration of complex cells, including malignant mesenchymal stem cells, proliferating osteoblastic cells, osteoblastic cells, immunological cells, and vascular networks, indicating the existence of a highly complex tumor microenvironment (TME) (Kansara et al., 2014). Nonetheless, the potential cellular communication networks of these cells are still not fully elucidated.

To understand cancer biology and immunology and to get the most out of tumor immunotherapy, it is important to figure out how this ecosystem's cells work together and how they might talk to each other. The ultimate unit of biological activity is a single cell, where genetic processes interact with the cellular environment to determine the development and function of complex structures including tissues and organs. Understanding the biology of virtually all living phenomena in normal and disease states necessitates dissecting and characterization of their composition and characterization, as well as evaluating their interactions, dynamics, and function at the single-cell level (Ren et al., 2018). Technically, however, previous genomic, transcriptomic, and proteomic cancer investigations have been unable to comprehensively elaborate on TME due to its complexity.(Liu et al., 2021). The emergence of new technologies based on single-cell sequencing has enabled unparalleled resolution and scale in capturing diverse tumor stages and understanding tumor heterogeneity (Vegliante et al., 2022). Rapid advancements in single-cell technology provide us with a potent approach to examine the multiple allosteric states and potential cellular communication networks of the TME at the single cell level.

This study employed scRNA-seq to investigate potential cellular communication networks in the OS's TME, as well as trajectory analysis and transcription factor enrichment analysis among mesenchymal stem cells, proliferating osteoblastic cells, and osteoblastic cells.

Materials and methods

Data source collection and processing

The 11 OS samples with scRNA-seq data based on the 10X Genomics platform were downloaded from GSE152048 via the Gene Expression Omnibus database (https://www.ncbi.nlm.nih.gov/geo/). The Seurat package (v4.1.1) was used to load the 10X genomics data for each individual sample into R software (v4.1.3). We excluded cells with identified genes <300 or a percentage of mitochondrial genes over 10% of total expressed genes. We eliminated low-quality cells with ≥7,500 detected genes, as well as genes detected in fewer than three cells. Furthermore, using the DoubletFinder package (v2.0.3), we eliminated any doublets that might have happened during encapsulation or as random pairings of cells that were not separated during sample preparation.

This research did not need ethical approval for our work because we used data from a publicly accessible database.

Identification of cell types

For each cell, gene expression was expressed as a fraction of the gene multiplied by 10,000, The log (x+1) method was used to perform natural log transformation. We identified, and scaled the top 2000 highly variable genes (HVGs) from the normalized expression matrix before doing principal component analysis (PCA) on these HVGs. Based on the top 50 PCA components identified, the batch effects were removed using the R Harmony package (version 1.0) (Zhou et al., 2020). On the basis of harmony-corrected data, k-nearest neighbors were estimated, and a shared nearest neighbor (SNN) graph was formed. The modular function was then adjusted to achieve cluster recognition based on the clustering algorithm. On the 2D map generated with the t-distributed stochastic neighbor embedding (tSNE) or uniform manifold approximation and projection for dimension reduction (UMAP) approach, the identified clusters were displayed.

Using the "FindAllMarkers" function, each cluster's marker genes were identified according to the following criteria: logfc.threshold = 0.25, min. pct = 0.25, and min. diff.pct = 0.25. Using the "DotPlot" tool in Seurat, the expression pattern of each marker gene across clusters was shown. The cell groupings were annotated based on the DEGs and well-known cellular markers described in the scientific literature (Zhou et al., 2020).

Pseudotemporal ordering of single cells

The Monocle package (v2.22.0) was used to produce the single-cell pseudotime trajectories. Using pseudotemporal profiling of scRNA-seq data, Monocle aims to decipher

cellular changes during differentiation. After inputting the scale of raw UMI counts into the "newCellDataSet" function with its clustering information, it was computed into a lower dimensional space using the discriminative dimensionality reduction with trees (DDRTree) method, a more recent manifold learning algorithm. Mesenchymal stem cells, proliferating osteoblastic cells, and osteoblastic cells were then ordered according to pseudotime. The plot pseudotime heatmap was used to compute and illustrate the genes whose expression varied in tandem with pseudotime.

Cell-cell communication

The CellChat package (version 1.4.0) predicted cell–cell communication across all cell types based on single-cell RNA sequencing data (Jin et al., 2021). Only the ligand–receptor interaction with a *p*-value 0.05 was utilized to predict cell–cell interaction in the various cell types.

SCENIC analysis

SCENIC is a technique that uses scRNA-seq data to rebuild gene regulation networks while also recognizing stable cell states. Transcription factor enrichment and regulon activity were assessed using SCENIC package (version 1.3.1) is introduced (Aibar et al., 2017). Based on co-expression and DNA motif analysis, the gene regulatory network was created, and the network activity in each cell was assessed to determine the cell state. For transcription factor regulatory network development, two gene-motif rankings (10 kb around the transcription start site or 500 bp upstream and 100 bp downstream of the transcription start site) were used as a guide to set the search space around the transcription start site. The gene-motif rankings for humans are obtained from https://resources.aertslab.org/cistarget/. The database used was Hallmark Gene Set from Molecular Signatures database (MsigDB) (Liberzon et al., 2015). In addition, Gene regulation was constructed using the R package GENIE3 (version 1.16.0), RcisTarget (version 1.14.0) and AUCell (version 1.16.0).

Results

Quality control and removal of batch effect

Eleven OS patients with scRNA-seq data enrolled in this research. Using the R Harmony package (version 1.0), batch effects between samples were eliminated based on the top 50 PCA components. After removal of batch effect, we used the t-SNE and UMAP techniques to decrease dimensionality, and then plotted the result as a 2D scatter plot (Figure 1A). In the process of quality control, we eliminated cells with fewer than 300 identified genes or a proportion of mitochondrial genes exceeding 10% of all expressed genes (Figure 1B). Dot plot of data quality control in scRNA-seq data were shown in Figure 1C.

Identification of 25 cell clusters in osteosarcoma microenvironment using scRNA-seq data reveals high cell heterogeneity

Following the quality control standard, 110,042 cells were finally included in our analysis. These cells were clustered into 25 primary cell clusters (Figures 2A,B; Figures 3A,C). A value of adjusted p value <0.01 is displayed in red, whereas a value of adjusted p value ≥0.01 is displayed in black (Figure 2B). Analysis of differential gene expression revealing up- and down-regulated genes in all clusters. The cluster-specific markers were utilized to label cell types (Figures 3B,D,E): chondroblastic cells (Sox9, Acan, Pth1r), osteoblastic cells (Runx2, Col1a1, Cdh11, Ibsp), myeloid cells (Cd74, Cd14, Fcgr3a), pericytes (Rgs5, Acta2), fibroblasts (Dcn, Col1a1), proliferating osteoblastic cells (Mki67, Top2a, Pcna), osteoclasts (ACP5, Ctsk, Mmp9), TILs (IL7R, CD3D, NKG7), endothelial cells (Pecam1, Vwf), mesenchymal stem cells (Mme, Thy1, Cxcl12, Sfrp2), and myoblasts (Myl1, Mylpf).

Potential cellular communication networks in the osteosarcoma microenvironment

To identify the potential molecular connections between cells, CellChat package (version 1.4.0) of R was utilized to find the potential molecular interactions between ligand-receptor pairings and main cell types in order to build cellular communication networks. First, CellChat was used to analyze cellular communication among the chondroblastic cells, osteoblastic cells, myeloid cells, pericytes, fibroblasts, proliferating osteoblastic cells, osteoclasts, TILs, endothelial cells, mesenchymal stem cells, and myoblasts. The results of the CellChat analysis revealed the numbers and weights of ligand receptors among all cell types (Figures 4A,B). The outgoing and incoming signaling patterns were shown in (Figures 4C,D). The outgoing and incoming interaction strength were shown in (Figures 4B,C) (B: all signaling pathway networks identified; C: selected signaling pathway networks). In addition, all of their ligand-receptor interactions have been identified (Figure 5D).

The details of all signaling pathway networks identified were also shown in Figures 6A-C (A: numbers of ligand receptors among all cell types; B: weights of ligand receptors among all cell

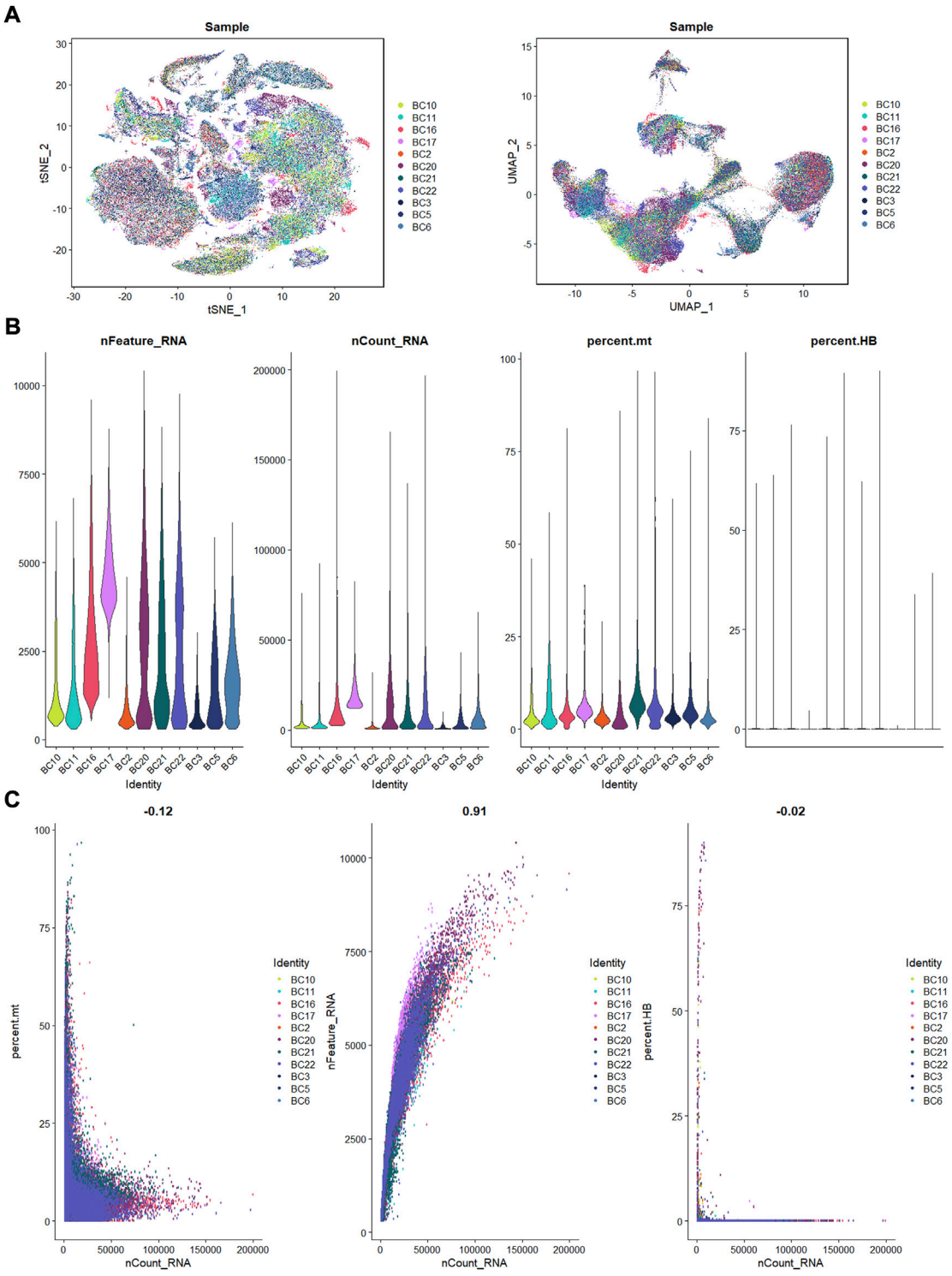

FIGURE 1
The process of quality control. **(A)**: t-SNE and UMAP plots after harmony. **(B)**: violin plots of feature, count, percent. mt, and percent.HB. **(C)**: correlation plots for count and feature, percent. mt, percent. HB.

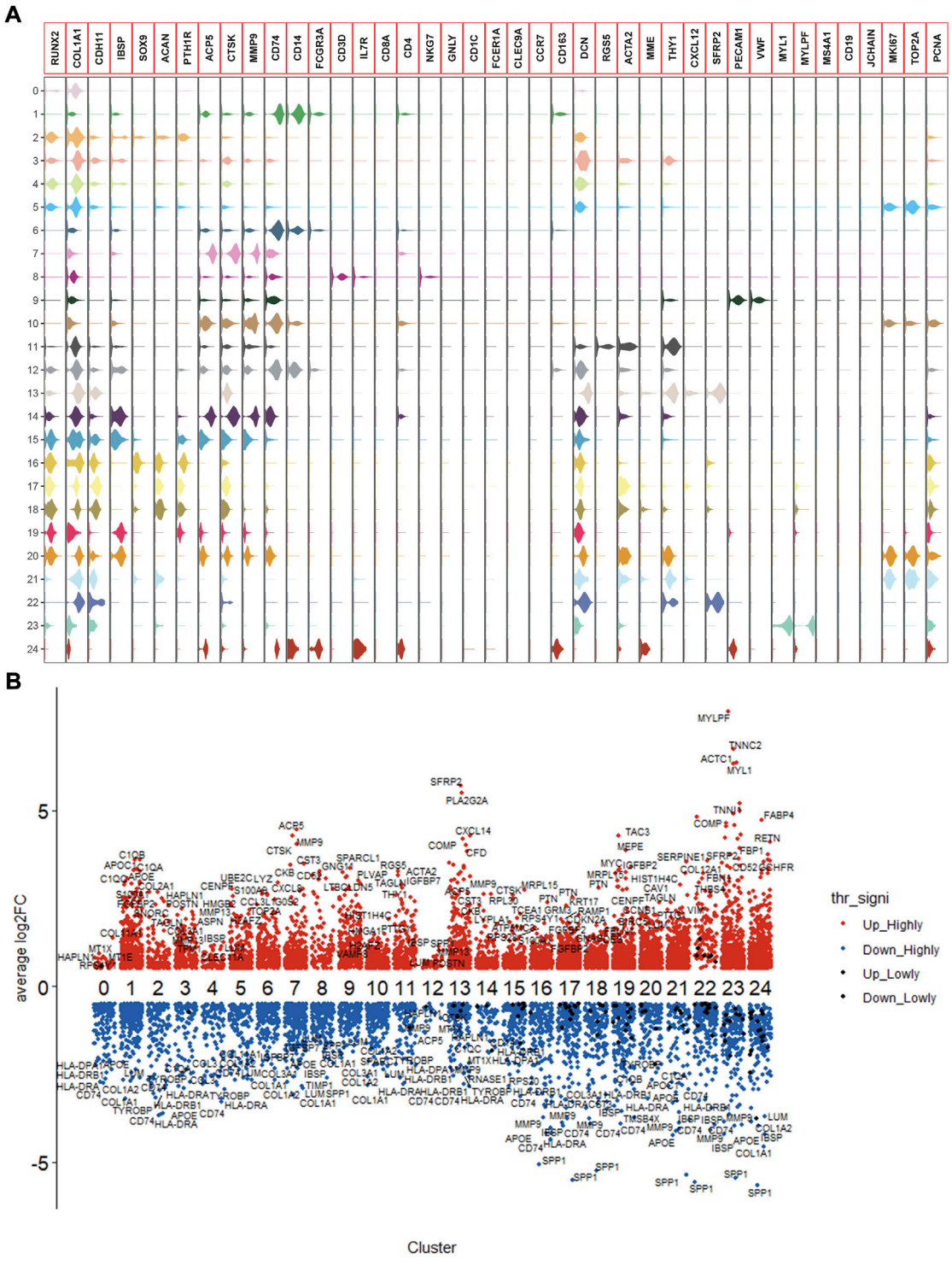

FIGURE 2
Expression of marker genes in the OS. **(A)**: violin plot of marker genes. **(B)**: columnar scatter plot of DEGs.

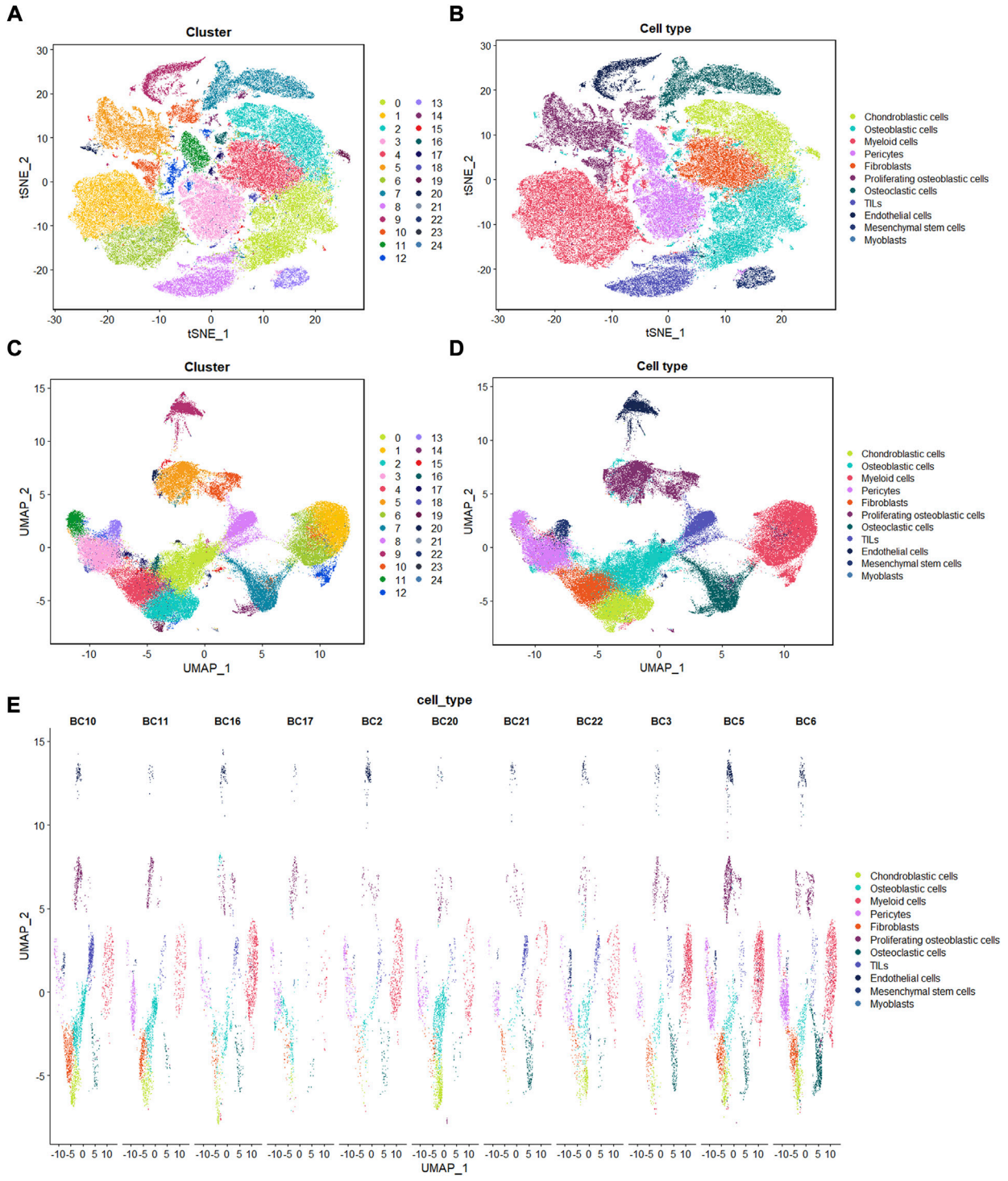

FIGURE 3
Single-cell transcriptomic analysis of OS lesions. **(A,C)**: t-SNE and UMAP analysis showing the results of descending clustering. **(B,D,E)**: t-SNE and UMAP analysis showing the results of annotation of cell subpopulations in cells of OS tissues.

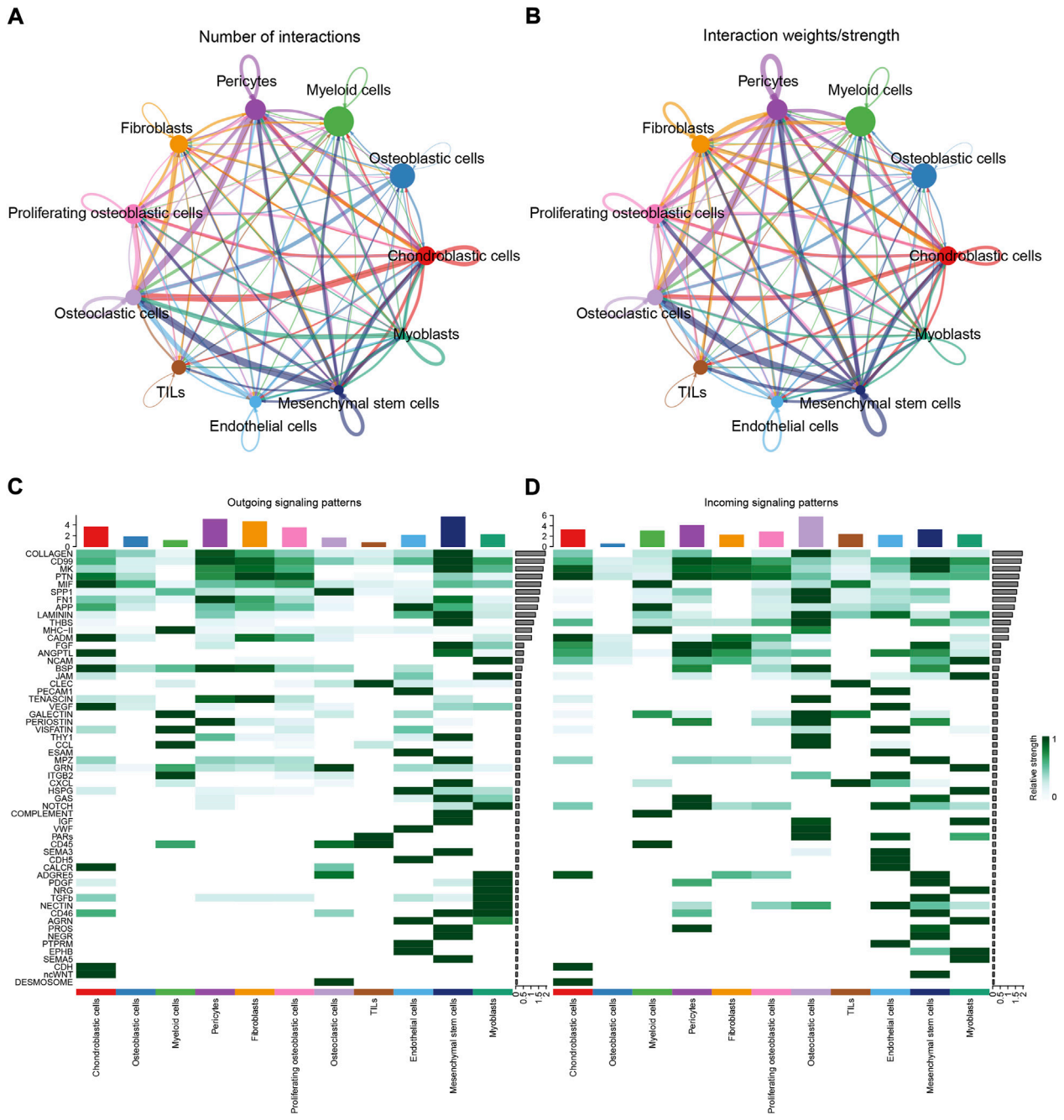

FIGURE 4
Cell–cell communication network among different cell types. **(A,B)**: the numbers and weights of ligand receptors among all cell types. **(C,D)**: the outgoing and incoming interaction strength among all cell types.

types; C: chordal graph of ligand-receptor interactions among all cell types). Among the total of 57 signaling pathways, the following signaling pathways were related to osteosarcoma: COLLAGEN (Baumann and Hennet, 2016; Elenjord et al., 2009; Levinson et al., 2002; Yamaguchi et al., 2005), CD99 (Manara et al., 2006; Sciandra et al., 2014; Zucchini et al., 2014), PTN (He et al., 2019; Qin et al., 2022; Sun et al., 2020), MIF(Liu et al., 2014), SPP1(Dalla-Torre et al., 2006; Li et al., 2017), FN1(Saba et al., 2019; Zhou et al., 2019), LAMININ(Heino and Massague, 1989), FGF (Kurogi et al., 1996; Laulederkind et al., 2000; Li et al., 2019; Xu et al., 2010), VEGF (Ji et al., 2020; Lei et al., 2018; Oda et al., 2006; Tsai et al., 2017; Zhang et al.,

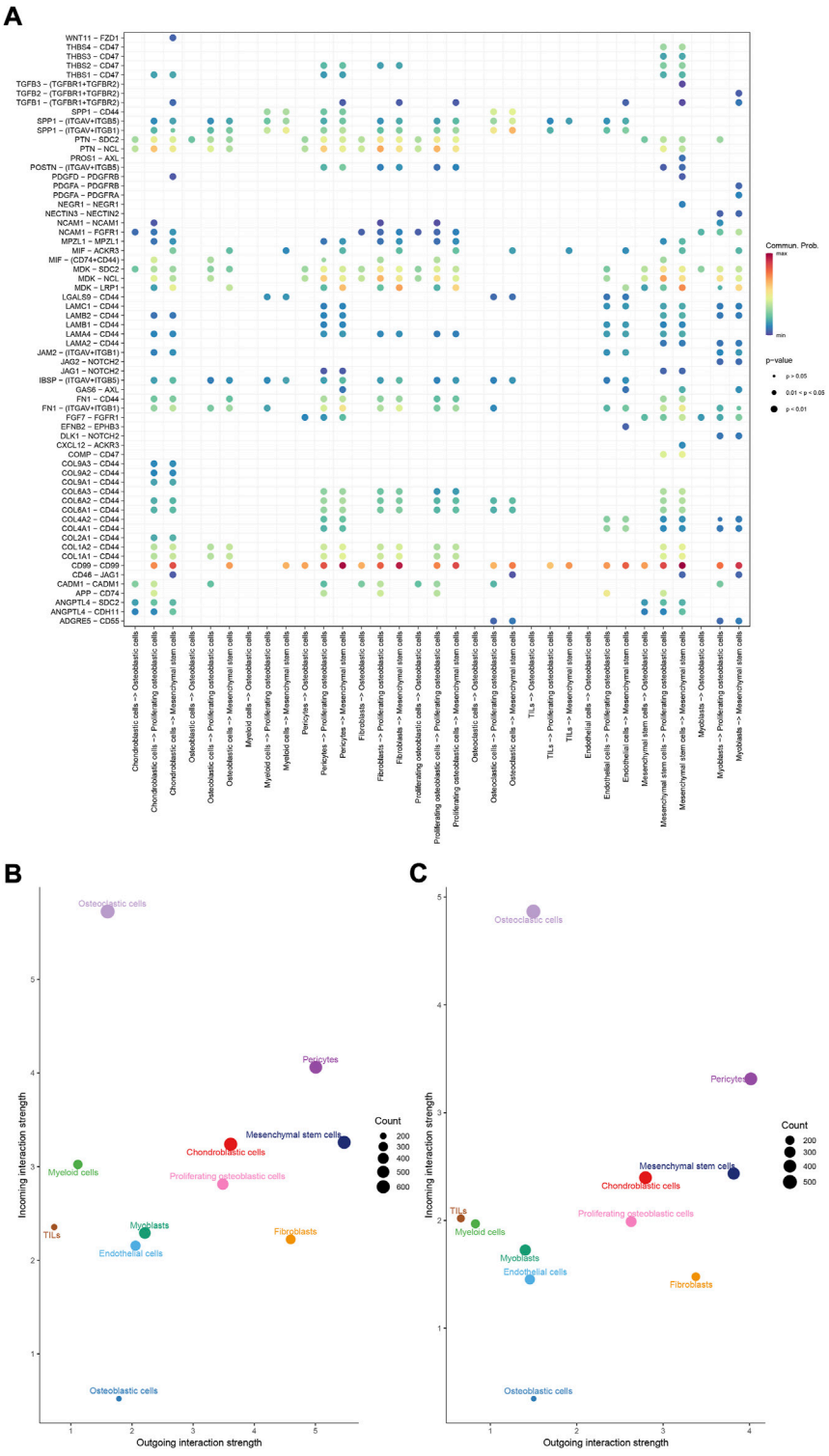

FIGURE 5
Overview of all ligand-receptor interactions of cells in OS. **(A)**: all ligand-receptor interactions of cells in OS. **(B,C)**: all signaling pathway networks identified, selected signaling pathway networks.

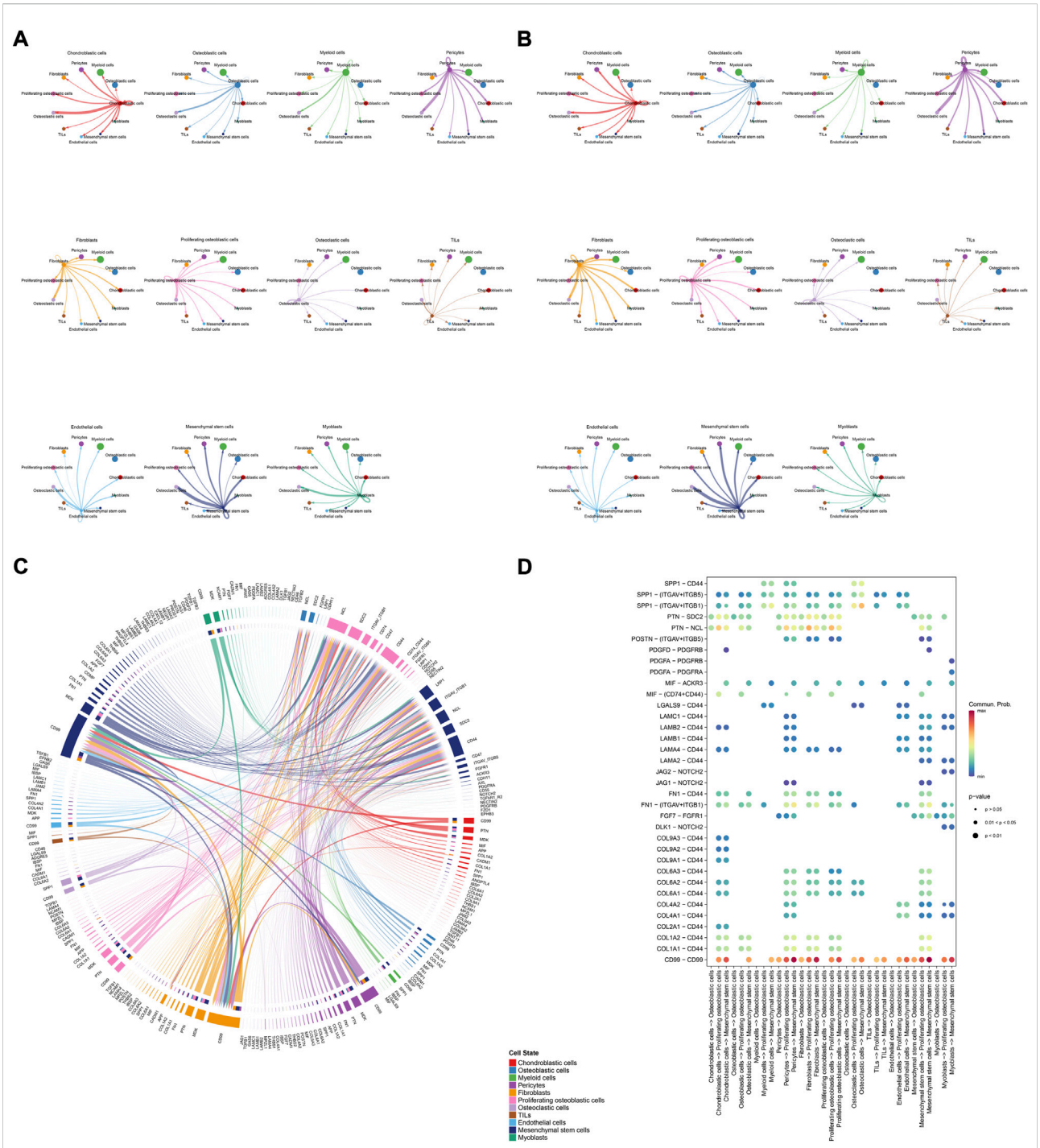

FIGURE 6
Detailed view of the ligands expressed by each major cell type. **(A)**: a detailed perspective of the ligands expressed by each major cell type and the cells expressing the signal-receiving receptors is provided, the thickness of the lines indicated the numbers of ligand-receptor pairs for each intercellular link. **(B)**: the thickness of the lines indicated the weights of ligand-receptor pairs for each intercellular link. **(C)**: chordal graphs showing potential cellular crosstalk within the OS microenvironment. **(D)**: the selected ligand-receptor interactions related to OS.

2019), GALECTIN(Gomez-Brouchet et al., 2010; Miao et al., 2014; Park et al., 2015; Zhou et al., 2014), PERIOSTIN(Ma et al., 2020; Xu et al., 2022), VISFATIN(Cheng et al., 2015; Wang et al., 2019, 2016), ITGB2 (Dai et al., 2018), NOTCH(Jin et al., 2017; Mu et al., 2013; Ongaro et al., 2016; Tanaka et al., 2009; Zhang et al., 2010), IGF (Armakolas et al., 2016; Giatagana et al., 2022;

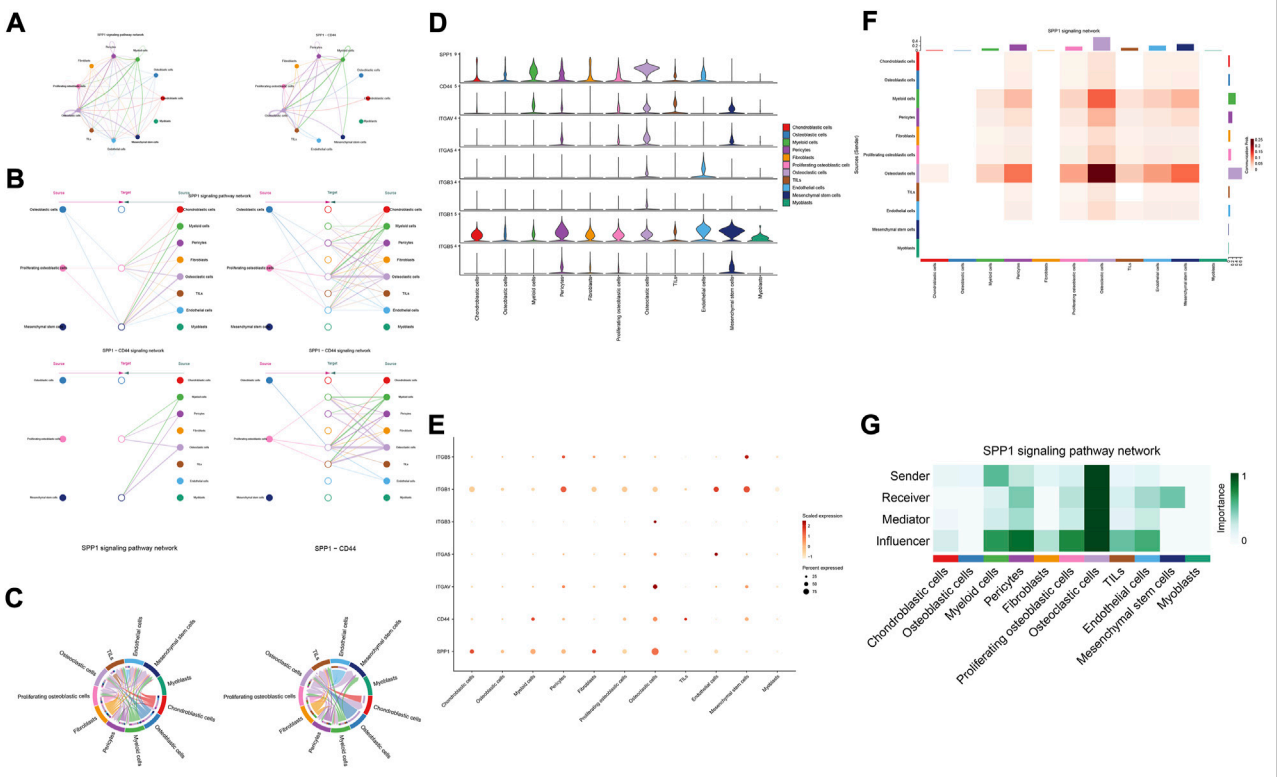

FIGURE 7
SPP1 signaling pathway. **(A–C)**: ligand-receptor interactions of cells. **(D,E)**: the ligand-receptors expressed by each major cell type. **(F,G)**: the network of SPP1 signaling pathway.

Gvozdenovic et al., 2017; Molina et al., 2019; Tan et al., 2015), VWF(Wang et al., 2020), and PDGF (Chen et al., 2009; Egners et al., 2018; Heldin et al., 1986). The ligand-receptor interactions of these signaling pathways related to osteosarcoma were shown in Figure 6D. Furthermore, according to the results of this research, the potential communication of mesenchymal stem cells, proliferating osteoblastic cells, and osteoblastic cells mainly revolved around SPP1 (Figure 7), FGF (Figure 8), NOTCH (Figure 9).

Differentiation trajectory analysis of mesenchymal stem cells, proliferating osteoblastic cells, and osteoblastic cells

Cell state transmission was evaluated using pseudotime analysis based on the Monocle package. The mesenchymal stem cells, proliferating osteoblastic cells, and osteoblastic cells were subjected to differentiation trajectory analysis. We performed pseudotime analysis to explore the cell-state transitions among mesenchymal stem cells, proliferating osteoblastic cells, and osteoblastic cells (Figures 10A–E). Furthermore, we plotted the heatmap of the differentiation trajectory among these cells (Figure 10F). The results of trajectory analysis revealed that osteoblastic cells followed a differentiation trajectory that primarily began with clusters of mesenchymal stem cells and proliferating osteoblastic cells, from which they differentiated into osteoblastic cells.

Single-cell regulatory network of mesenchymal stem cells, proliferating osteoblastic cells, and osteoblastic cells

A SCENIC analysis was conducted to detect the TFs of mesenchymal stem cells, proliferating osteoblastic cells, and osteoblastic cells. The genes of TFs (XBP1(Yang et al., 2015; Yu et al., 2022), ATF4 (Luo et al., 2017, 2019; Xian et al., 2017), and SOX9(Y. Chen S. et al., 2020; He et al., 2017; Wang et al., 2018)) were significantly activated in osteoblastic cells (Figures 11A–D), and were demonstrated to be expressed in osteosarcoma.

Discussion

Osteosarcoma is the most common malignant bone tumor in children, teens, and young adults with a median age of 16 years. It

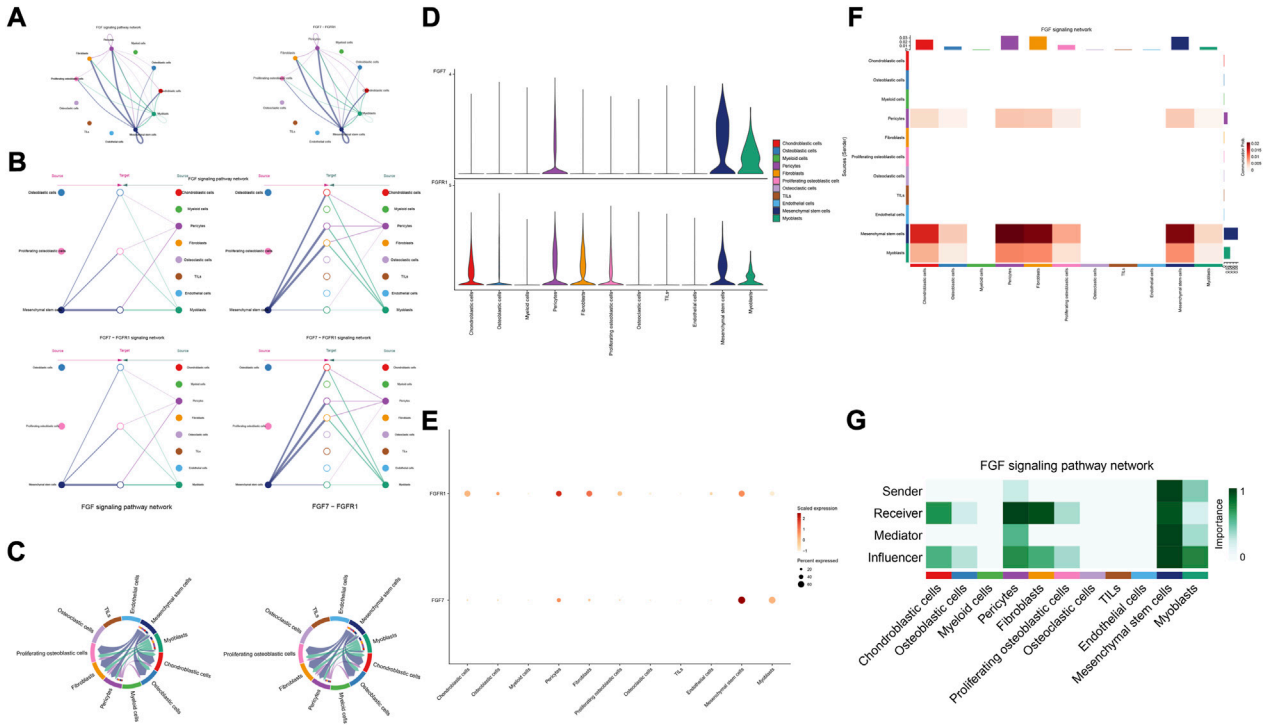

FIGURE 8
FGF signaling pathway. **(A–C)**: ligand-receptor interactions of cells. **(D,E)**: the ligand-receptors expressed by each major cell type. **(F,G)**: the network of FGF signaling pathway.

accounts for approximately 56% of bone sarcomas, and metastasis is the primary reason why treatment fails and the prognosis is poor (Chen et al., 2021). Despite previous molecular biology investigations having offered considerable information on the pathogenesis of osteosarcoma, the mechanisms that regulate its several oncogenic insults necessary for osteosarcoma start and development remain unknown (Isakoff et al., 2015; Kansara et al., 2014). It remains a serious concern due to poorly characterized carcinogenesis processes and restricted therapeutic options. So, it is essential to find important subpopulation driver mutations that promote diversity, expansion, invasion, and eventual colonization of other areas of the body. In addition, the potential cellular communication networks in osteosarcoma and the influence of tumor heterogeneity on cell aggregation are crucial.

Single-cell RNA sequencing (scRNA-seq) can show variation within cell populations. It could discriminate tumor cells from non-tumor cells and examine intercellular connections within the tumor microenvironment by analyzing transcripts inside individual cells. It is helpful to find unique cell types, look into tumor heterogeneity and potential networks of cell-to-cell communication, and show different developmental paths. This can give a theoretical foundation for future research into the molecular processes of OS growth and metastasis (Guo et al., 2022).

Mounting clinical and experimental data suggests that osteosarcoma stem cells, which originate from mesenchymal stem cells, may be the biological genesis of osteosarcomas and demonstrate osteoblastic differentiation, producing malignant osteoid (Brown et al., 2017; Xi et al., 2000). In addition, osteosarcoma is strongly connected with the osteoblastic lineage and displays osteogenic differentiation-related activities in proliferation, extracellular matrix secretion, and induction of ossification (Zeng et al., 2022). So, in this study, potential cellular communication networks among mesenchymal stem cells, proliferating osteoblastic cells, and osteoblastic cells were identified through comprehensive analysis of osteosarcoma single-cell RNA sequencing (scRNA-seq), illustrating the complex regulatory network in the advanced osteosarcoma microenvironment. Moreover, we performed transcription factor regulatory network analysis and trajectory analysis on these cells.

The results of cellular communication networks showed that mesenchymal stem cells, proliferating osteoblastic cells, and osteoblastic cells are mainly involved in SPP1, FGF, and NOTCH signaling pathways. The SPP1 gene (osteopontin, secreted phosphoprotein 1) encodes a protein with several activities, including bone remodeling, adhesion, tumor invasion, and metastasis (Dalla-Torre et al., 2006). It is

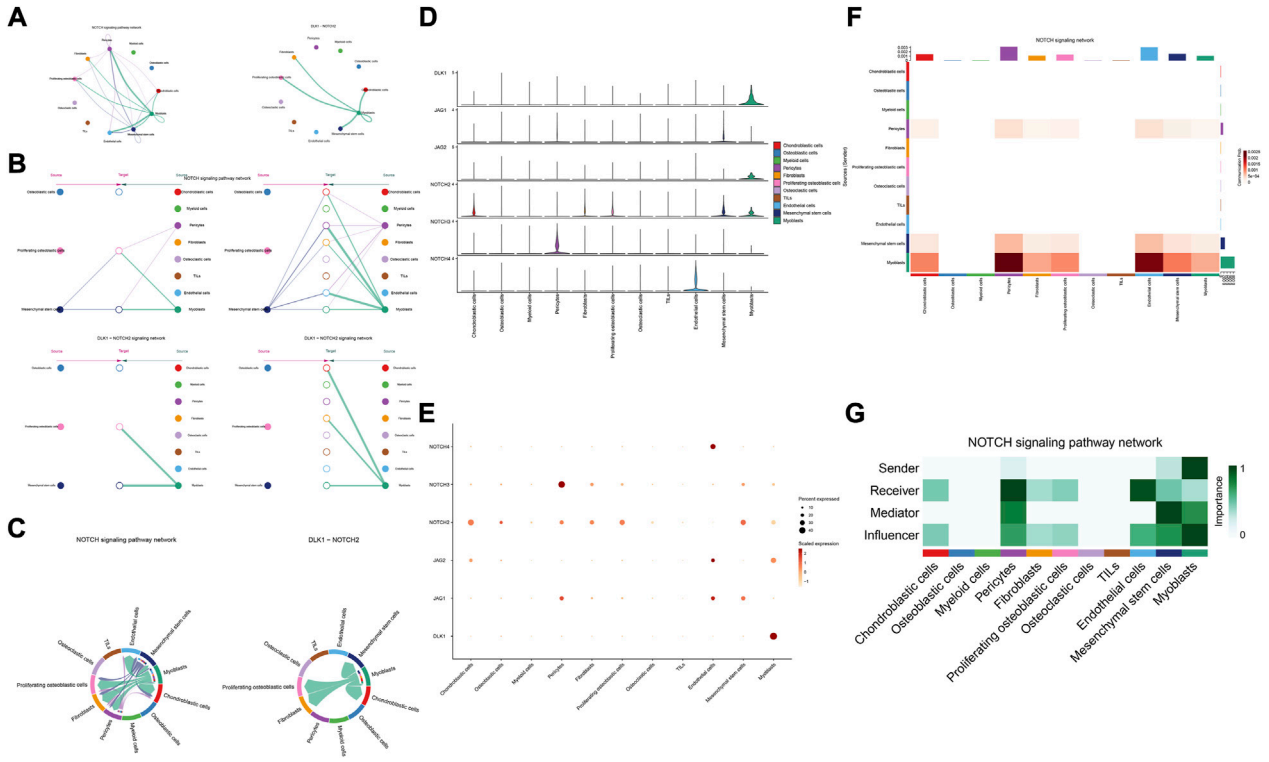

FIGURE 9
NOTCH signaling pathway. **(A–C)**: ligand-receptor interactions of cells. **(D,E)**: the ligand-receptors expressed by each major cell type. **(F,G)**: the network of NOTCH signaling pathway.

generated by a variety of cell types, including osteoblasts, osteoclasts, and endothelial cells (Liu et al., 2013; Wang and Yang, 2015). SPP1 is now of interest in carcinogenesis, Lysosomal-associated membrane protein 3 (LAMP3) enhances osteosarcoma cell invasion via SPP1 signaling (Li et al., 2017). In colorectal cancer (CRC), SPP1 was highly upregulated and increased CRC metastasis by promoting epithelial-mesenchymal transition (EMT) (Xu et al., 2017). In addition, previous research found inhibition of the SPP1 gene may have therapeutic benefits for tongue cancer and may be a useful target for therapy (Zhang et al., 2020). Moreover, in pancreatic tumor microenvironment factors, the SPP1-CD44 axis can promote cancer stemness (Nallasamy et al., 2021). In head and neck squamous cell carcinoma (HNSCC), SPP1 overexpression is prognostic of worse survival results (Bie and Zhang, 2021). However, some scholars found that overexpression of SPP1 was correlated with improved overall survival, event-free survival, and relapse-free survival at diagnosis in osteosarcoma (Dalla-Torre et al., 2006). The results of our study revealed that through the SPP1-CD44 signaling pathway, myeloid cells, pericytes, and osteoclast cells can impact on mesenchymal stem cells and proliferating osteoblastic cells. Moreover, in these cellular communication networks, osteoclasts play a role as major senders, mediators, and influencers of the signal.

Fibroblast growth factor (FGF) signaling is essential for embryonic organ development and the progression of tumors (Brewer et al., 2016) and increases proliferation, invasion, and epithelial-to-mesenchymal transformation of tumor cells. (Bono et al., 2013). In the majority of malignancies, numerous FGFs are increased, and different FGF receptor (FGFR) subtypes are activated on tumor and stromal cells. (Turner and Grose, 2010). In addition, cancer, inflammation, and the resistance of tumor vascularization to VEGF inhibitor therapy have all been linked to FGFR signaling. (Beenken and Mohammadi, 2009; Casanovas et al., 2005; Fischer et al., 2007; Turner and Grose, 2010). Moreover, in the development of cancer, pathological FGF/FGFR signaling enhances cross-talk between oncogenic cells and its microenvironment, ultimately causing cancer cell proliferation, angiogenesis, and migration. (Li et al., 2018). For example, in the tumor microenvironment of esophageal cancer, NCAM- and FGF-2-mediated FGFR1 signaling modulates the survival and migration of tumor-associated macrophages and cancer cells (Takase et al., 2016). Additionally, FGFs activate myeloid cells, macrophages linked with tumors, cancer-related

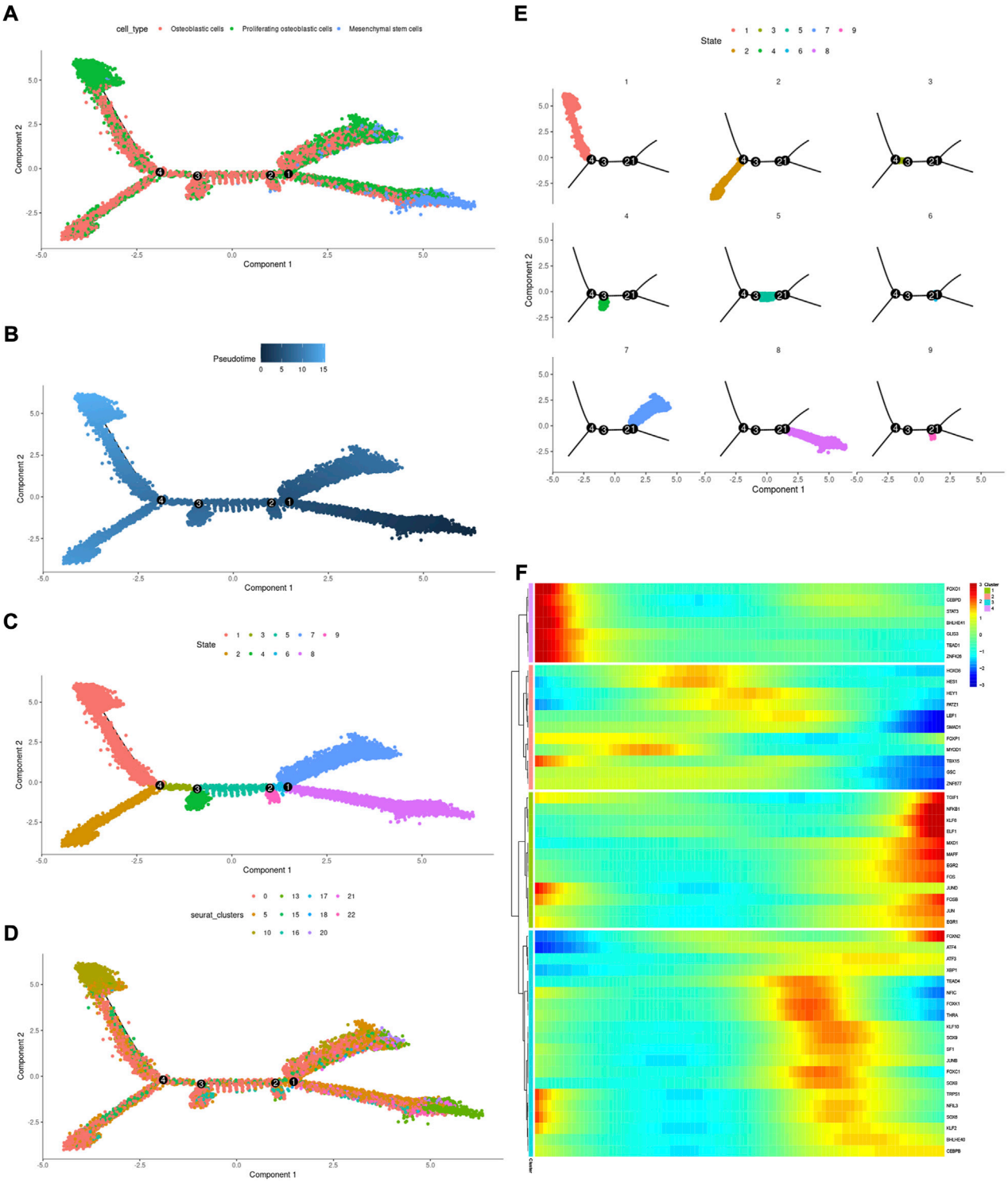

FIGURE 10
Trajectory analysis of mesenchymal stem cells, proliferating osteoblastic cells, and osteoblastic cells. **(A–E)**: trajectory plots showing the differentiation of these cell types. **(F)**: heatmap displaying the scaled expression of dynamic genes across time. The rows of the heatmap reflect genes exhibiting dynamic changes along the pseudotime, and these genes have been grouped into four categories based on their expression pattern over the pseudotime.

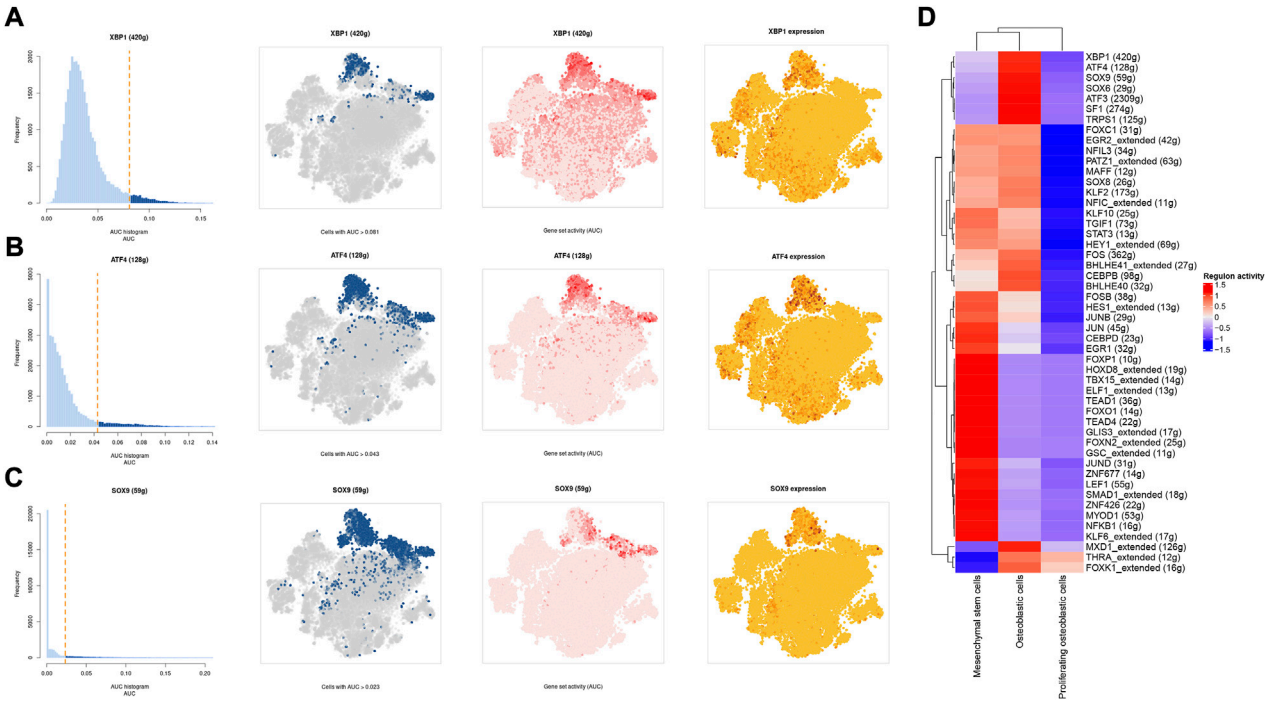

FIGURE 11
The SCENIC analysis predicted the TF. **(A–C)**: tSNE plots and histograms show the top three TF activities in mesenchymal stem cells, proliferating osteoblastic cells, and osteoblastic cells. **(D)**: Heatmap showing the top 50 TF in these cell types.

fibroblasts, and osteoclasts (Berardi et al., 1995; Collin-Osdoby et al., 2002; Itoh, 2007). Recent studies have found that in the evolution of osteosarcoma, FGF has emerged as a crucial regulator. According to previous research, LHX9 is critical for the proliferation, migration, invasion, and metastasis of OS cells via the FGF and TGF−/−catenin signaling pathways (Li et al., 2019). Some scholars have found that through the FRS2/TGF−/−catenin pathway, FGF-induced LHX9 controls osteosarcoma development and migration (Li et al., 2019).

Our research found, through the FGF7-FGFR1 signaling pathway, mesenchymal stem cells, pericytes, and myoblasts may influence mesenchymal stem cells, proliferating osteoblastic cells, and osteoblastic cells. High quantities of FGFR1 and FGF7 were detected in mesenchymal stem cells and pericytes. In addition, in these cellular communication networks, mesenchymal stem cells and pericytes serve as important signal senders, mediators, and influencers.

The Notch pathway regulates various mechanisms that control morphogenesis, lineage determination, apoptosis, and proliferation in some malignancies (Bray, 2006), and has been identified as both a tumor suppressor and an oncogene (Jin et al., 2017; Tanaka et al., 2009; Zhang et al., 2010). The Delta-Serrate-Lag (DSL) family of ligands (jagged 1/Jag1, Jag2, delta-like-1/DLL1, DLL3, and DLL4) on the surface of a cell connect with a membrane-bound Notch receptor (Notch1-4) on a different cell to start the Notch signaling pathway, a crucial step in normal bone growth that is also implicated as a critical mediator in a variety of different malignancies (Iso et al., 2003).

According to previous research, the notch pathway is strongly related to the development of osteosarcoma. Erk phosphorylation promotes osteosarcoma proliferation and migration in response to Notch stimulation (Qin et al., 2019). By activating cell division cycle 20, Notch-1 increases the evolution of osteosarcoma to a malignant state (Gao et al., 2020). The elevated expression of Jagged1 is intimately associated with osteosarcoma metastasis and recurrence. On the contrary, the knockdown of Jagged1 significantly reduced osteosarcoma cell proliferation, migration, and invasion (Zhang et al., 2021). Additionally, Notch signaling also regulates the immune system of the tumor microenvironment. Inhibiting the Notch signaling system enhances the polarization of TAM towards the M2 genotype, which in turn promotes the growth and spread of osteosarcoma (Ren et al., 2020). Our research found, through the DLK1- NOTCH2 signaling pathway, myoblasts may influence mesenchymal stem cells, proliferating osteoblastic cells. Additionally, myoblasts serve as important signal senders, mediators, and influencers.

One of the most prevalent issues in the development of human cancer is the dysregulation of transcription factors, which plays a role in the pathogenesis of the disease. The

SCENIC analysis revealed that the regulon activity of XBP1, ATF4, and SOX9 were down-regulation in both mesenchymal stem cells and proliferating osteoblastic cells. X-box binding protein (XBP1) is a significant transcriptional regulator of the unfolded protein response. Lack of oxygen stimulated the transcription and translation of XBP1 mRNA, resulting in an increase in the activity of XBP1 protein (Romero-Ramirez et al., 2004). It was initially identified as a crucial regulator of major histocompatibility complex class II (MHC) gene expression in B cells (S. Chen Y. et al., 2020). High XBP1 levels were associated with advanced clinical stages, a high malignancy index, and a poor tumor necrosis rate in OS. XBP1 knockdown decreased OS cell growth and survival in culture (Yang et al., 2015). Recent studies have shown that XBP1 increases the susceptibility of HOS osteosarcoma cells to pyropheophorbide- α methyl ester-mediated photodynamic remedies (Yu et al., 2022). Activating transcription factor 4 (ATF4), a major regulator of the integrated stress response system, activates transcription of a group of transcriptional silencing genes that regulate cell survival and death (Ishizawa et al., 2016). In recent years, numerous investigations on the involvement of ATF4 in osteosarcoma have been reported. In human osteosarcoma, suppression of GRP78 increases ATF4-induced cell death via deubiquitination and stability of CHOP(Luo et al., 2017). Moreover, through endoplasmic reticulum (ER) stress-mediated PERK/eIF2/ATF4/CHOP activation and Wnt/β-catenin signal suppresses the development of human osteosarcoma (Zhao et al., 2020). ATF4 devastates RET by inhibiting nonclassical GRP78 to increase osteosarcoma chemosensitivity to bortezomib (Luo et al., 2019). Sex-determining region Y (SRY)- box 9 protein (SOX9) is a crucial transcription factor in a variety of illnesses, particularly in malignancies. Recent research has revealed that SOX9 plays an important function in the control of the tumor microenvironment (TME). Furthermore, SOX9 signaling or SOX9 controlled signaling pathways play an important role in cancer development and metastasis (Panda et al., 2021). Additionally, by means of a Sox9-Mediated positive feedback loop, MAFB contributes towards the progression of cancer stemness and tumorogenesis in osteosarcoma (Y. Chen S. et al., 2020). Moreover, previous study has found the cFOS-SOX9 axis of chondroblastic osteosarcoma reprograms bone marrow derived mesenchymal stem cells into chondroblastic cells (He et al., 2017).

In conclusion, this study uncovered the potential cellular communication networks between several cell types in advanced osteosarcoma. The SPP1, FGF, and NOTCH signaling pathways may play a crucial role in osteosarcoma TME regulation. This research may bring fresh insights into the pathophysiology of osteosarcoma's molecular processes. However, this paper has the following limitations: no additional experiments were conducted to validate the data mining findings presented in this study; no further validation using the bulk RNA-seq database of osteosarcoma.

Data availability statement

The datasets presented in this study can be found in online repositories. The names of the repository/repositories and accession number(s) can be found in the article/ Supplementary Material.

Ethics statement

Ethical review and approval was not required for the study on human participants in accordance with the local legislation and institutional requirements. Written informed consent for participation was not required for this study in accordance with the national legislation and the institutional requirements.

Author contributions

NX, XW, LW, YS, XZ, and HH conceived and designed the research. LW and YS downloaded and collected the data. NX, XW analyzed the data, XW and NX wrote the article. LW, YS, XZ, and HH conducted quality control on the articles and guided the submission. All authors read and approved the final manuscript.

Conflict of interest

The authors declare that the research was conducted in the absence of any commercial or financial relationships that could be construed as a potential conflict of interest.

Publisher's note

Supplementary material

The Supplementary Material for this article can be found online at: https://www.frontiersin.org/articles/10.3389/fgene.2022.1013737/full#supplementary-material

References

Aibar, S., Gonzalez-Blas, C. B., Moerman, T., Huynh-Thu, V. A., Imrichova, H., Hulselmans, G., et al. (2017). Scenic: Single-cell regulatory network inference and clustering. *Nat. Methods* 14 (11), 1083–1086. doi:10.1038/nmeth.4463

Armakolas, N., Armakolas, A., Antonopoulos, A., Dimakakos, A., Stathaki, M., and Koutsilieris, M. (2016). The role of the igf-1 ec in myoskeletal system and osteosarcoma pathophysiology. *Crit. Rev. Oncol. Hematol.* 108, 137–145. doi:10.1016/j.critrevonc.2016.11.004

Baumann, S., and Hennet, T. (2016). Collagen accumulation in osteosarcoma cells lacking glt25d1 collagen galactosyltransferase. *J. Biol. Chem.* 291 (35), 18514–18524. doi:10.1074/jbc.M116.723379

Beenken, A., and Mohammadi, M. (2009). The FGF family: Biology, pathophysiology and therapy.Research support. *Rev. Drug Discov.* 8 (3), 235–253. doi:10.1038/nrd2792

Berardi, A. C., Wang, A., Abraham, J., and Scadden, D. T. (1995). Basic fibroblast growth factor mediates its effects on committed myeloid progenitors by direct action and has no effect on hematopoietic stem cells. *Blood* 86 (6), 2123–2129. doi:10.1182/blood.v86.6.2123.bloodjournal8662123

Bie, T., and Zhang, X. (2021). Higher expression of spp1 predicts poorer survival outcomes in head and neck cancer. *J. Immunol. Res.* 2021, 8569575. doi:10.1155/2021/8569575

Bono, F., De Smet, F., Herbert, C., De Bock, K., Georgiadou, M., Fons, P., et al. (2013). Inhibition of tumor angiogenesis and growth by a small-molecule multi-fgf receptor blocker with allosteric properties. *Cancer Cell* 23 (4), 477–488. doi:10.1016/j.ccr.2013.02.019

Bousquet, M., Noirot, C., Accadbled, F., Sales, D. G. J., Castex, M. P., Brousset, P., et al. (2016). Whole-exome sequencing in osteosarcoma reveals important heterogeneity of genetic alterations. *Ann. Oncol.* 27 (4), 738–744. doi:10.1093/annonc/mdw009

Bray, S. J. (2006). Notch signalling: A simple pathway becomes complex. *Nat. Rev. Mol. Cell Biol.* 7 (9), 678–689. doi:10.1038/nrm2009

Brewer, J. R., Mazot, P., Soriano, P., and Extramural, N. I. H., (2016). Genetic insights into the mechanisms of Fgf signaling. *Genes Dev.* 30 (7), 751–771. doi:10.1101/gad.277137.115

Brown, H. K., Tellez-Gabriel, M., Heymann, D., and Gov't], Non-U. S. (2017). *Review; Research Support*, 386, 189–195. doi:10.1016/j.canlet.2016.11.019Cancer stem cells in osteosarcoma*J. Artic. Lett.*

Casanovas, O., Hicklin, D. J., Bergers, G., and Hanahan, D. (2005). Drug resistance by evasion of antiangiogenic targeting of vegf signaling in late-stage pancreatic islet tumors. *Cancer Cell* 8 (4), 299–309. doi:10.1016/j.ccr.2005.09.005

Chen, C., Xie, L., Ren, T., Huang, Y., Xu, J., and Guo, W. (2021). Immunotherapy for osteosarcoma: Fundamental mechanism, rationale, and recent breakthroughs. *Cancer Lett.* 500, 1–10. doi:10.1016/j.canlet.2020.12.024

Chen, S., Chen, J., Hua, X., Sun, Y., Cui, R., Sha, J., et al. (2020a). The emerging role of xbp1 in cancer. *Biomed. Pharmacother.* 127, 110069. doi:10.1016/j.biopha.2020.110069

Chen, Y. C., Chang, C. N., Hsu, H. C., Chiou, S. J., Lee, L. T., and Hseu, T. H. (2009). Sennoside b inhibits pdgf receptor signaling and cell proliferation induced by pdgf-bb in human osteosarcoma cells. *Life Sci.* 84 (25-26), 915–922. doi:10.1016/j.lfs.2009.04.003

Chen, Y., Wang, T., Huang, M., Liu, Q., Hu, C., Wang, B., et al. (2020b). Mafb promotes cancer stemness and tumorigenesis in osteosarcoma through a sox9-mediated positive feedback loop. *Cancer Res.* 80 (12), 2472–2483. doi:10.1158/0008-5472.CAN-19-1764

Cheng, G., Liu, C., Sun, X., Zhang, L., Liu, L., Ouyang, J., et al. (2015). Visfatin promotes osteosarcoma cell migration and invasion via induction of epithelial-mesenchymal transition. *Oncol. Rep.* 34 (2), 987–994. doi:10.3892/or.2015.4053

Collin-Osdoby, P., Rothe, L., Bekker, S., Anderson, F., Huang, Y., and Osdoby, P. (2002). Basic fibroblast growth factor stimulates osteoclast recruitment, development, and bone pit resorption in association with angiogenesis *in vivo* on the chick chorioallantoic membrane and activates isolated avian osteoclast resorption *in vitro*. *J. Bone Min. Res.* 17 (10), 1859–1871. doi:10.1359/jbmr.2002.17.10.1859

Dai, J., Xu, L. J., Han, G. D., Jiang, H. T., Sun, H. L., Zhu, G. T., et al. (2018). Down-regulation of long non-coding RNA ITGB2-AS1 inhibits osteosarcoma proliferation and metastasis by repressing Wnt/β-catenin signalling and predicts favourable prognosis. *Artif. Cells Nanomed. Biotechnol.* 46, S783–S790. doi:10.1080/21691401.2018.1511576

Dalla-Torre, C. A., Yoshimoto, M., Lee, C. H., Joshua, A. M., de Toledo, S. R., Petrilli, A. S., et al. (2006). Effects of thbs3, sparc and spp1 expression on biological behavior and survival in patients with osteosarcoma. *BMC Cancer* 6, 237. doi:10.1186/1471-2407-6-237

Egners, A., Rezaei, M., Kuzmanov, A., Poitz, D. M., Streichert, D., Muller-Reichert, T., et al. (2018). Phd3 acts as tumor suppressor in mouse osteosarcoma and influences tumor vascularization via pdgf-c signaling. *Cancers (Basel)* 10 (12), E496. doi:10.3390/cancers10120496

Elenjord, R., Allen, J. B., Johansen, H. T., Kildalsen, H., Svineng, G., Maelandsmo, G. M., et al. (2009). Collagen i regulates matrix metalloproteinase-2 activation in osteosarcoma cells independent of s100a4. *FEBS J.* 276 (18), 5275–5286. doi:10.1111/j.1742-4658.2009.07223.x

Fischer, C., Jonckx, B., Mazzone, M., Zacchigna, S., Loges, S., Pattarini, L., et al. (2007). Anti-plgf inhibits growth of vegf(r)-inhibitor-resistant tumors without affecting healthy vessels. *Cell* 131 (3), 463–475. doi:10.1016/j.cell.2007.08.038

Gao, Y., Bai, L., and Shang, G. (2020). Notch-1 promotes the malignant progression of osteosarcoma through the activation of cell division cycle 20. *Aging (Albany NY)* 13 (2), 2668–2680. doi:10.18632/aging.202314

Giatagana, E. M., Berdiaki, A., Gaardlos, M., Samsonov, S. A., Tzanakakis, G. N., and Nikitovic, D. (2022). Biglycan interacts with type i insulin-like receptor (igf-ir) signaling pathway to regulate osteosarcoma cell growth and response to chemotherapy. *Cancers (Basel)* 14 (5), 1196. doi:10.3390/cancers14051196

Gomez-Brouchet, A., Mourcin, F., Gourraud, P. A., Bouvier, C., De Pinieux, G., Le Guelec, S., et al. (2010). Galectin-1 is a powerful marker to distinguish chondroblastic osteosarcoma and conventional chondrosarcoma. *Hum. Pathol.* 41 (9), 1220–1230. doi:10.1016/j.humpath.2009.10.028

Guo, J., Tang, H., Huang, P., Guo, J., Shi, Y., Yuan, C., et al. (2022). Single-cell profiling of tumor microenvironment heterogeneity in osteosarcoma identifies a highly invasive subcluster for predicting prognosis. *Front. Oncol.* 12, 732862. doi:10.3389/fonc.2022.732862

Gvozdenovic, A., Boro, A., Born, W., Muff, R., and Fuchs, B. (2017). A bispecific antibody targeting igf-ir and egfr has tumor and metastasis suppressive activity in an orthotopic xenograft osteosarcoma mouse model. *Am. J. Cancer Res.* 7 (7), 1435–1449.

He, M., Shen, P., Qiu, C., and Wang, J. (2019). Mir-627-3p inhibits osteosarcoma cell proliferation and metastasis by targeting ptn. *Aging (Albany NY)* 11 (15), 5744–5756. doi:10.18632/aging.102157

He, Y., Zhu, W., Shin, M. H., Gary, J., Liu, C., Dubois, W., et al. (2017). Cfos-sox9 axis reprograms bone marrow-derived mesenchymal stem cells into chondroblastic osteosarcoma. *Stem Cell Rep.* 8 (6), 1630–1644. doi:10.1016/j.stemcr.2017.04.029

Heino, J., and Massague, J. (1989). Transforming growth factor-beta switches the pattern of integrins expressed in mg-63 human osteosarcoma cells and causes a selective loss of cell adhesion to laminin. *J. Biol. Chem.* 264 (36), 21806–21811. doi:10.1016/s0021-9258(20)88255-6

Heldin, C. H., Johnsson, A., Wennergren, S., Wernstedt, C., Betsholtz, C., and Westermark, B. (1986). A human osteosarcoma cell line secretes a growth factor structurally related to a homodimer of pdgf a-chains. *Nature* 319 (6053), 511–514. doi:10.1038/319511a0

Ho, X. D., Nguyen, H. G., Trinh, L. H., Reimann, E., Prans, E., Koks, G., et al. (2017). Analysis of the expression of repetitive dna elements in osteosarcoma. *Front. Genet.* 8, 193. doi:10.3389/fgene.2017.00193

Isakoff, M. S., Bielack, S. S., Meltzer, P., and Gorlick, R. (2015). Osteosarcoma: Current treatment and a collaborative pathway to success. *J. Clin. Oncol.* 33 (27), 3029–3035. doi:10.1200/JCO.2014.59.4895

Ishizawa, J., Kojima, K., Chachad, D., Ruvolo, P., Ruvolo, V., Jacamo, R. O., et al. (2016). Atf4 induction through an atypical integrated stress response to onc201 triggers p53-independent apoptosis in hematological malignancies. *Sci. Signal.* 9 (415), a17. doi:10.1126/scisignal.aac4380

Iso, T., Kedes, L., and Hamamori, Y. (2003). Hes and herp families: Multiple effectors of the notch signaling pathway. *J. Cell. Physiol.* 194 (3), 237–255. doi:10.1002/jcp.10208

Itoh, N. (2007). The fgf families in humans, mice, and zebrafish: Their evolutional processes and roles in development, metabolism, and disease. *Biol. Pharm. Bull.* 30 (10), 1819–1825. doi:10.1248/bpb.30.1819

Ji, X., Shan, L., Shen, P., and He, M. (2020). Circular rna circ_001621 promotes osteosarcoma cells proliferation and migration by sponging mir-578 and regulating vegf expression. *Cell Death Dis.* 11 (1), 18. doi:10.1038/s41419-019-2204-y

Jin, H., Luo, S., Wang, Y., Liu, C., Piao, Z., Xu, M., et al. (2017). miR-135b stimulates osteosarcoma recurrence and lung metastasis via notch and wnt/β-catenin signaling. *Mol. Ther. Nucleic Acids* 8, 111–122. doi:10.1016/j.omtn.2017.06.008

Jin, S., Guerrero-Juarez, C. F., Zhang, L., Chang, I., Ramos, R., Kuan, C. H., et al. (2021). Inference and analysis of cell-cell communication using cellchat. *Nat. Commun.* 12 (1), 1088. doi:10.1038/s41467-021-21246-9

Kansara, M., Teng, M. W., Smyth, M. J., and Thomas, D. M. (2014). Translational biology of osteosarcoma. *Nat. Rev. Cancer* 14 (11), 722–735. doi:10.1038/nrc3838

Kurogi, T., Nabeshima, K., Kataoka, H., Okada, Y., and Koono, M. (1996). Stimulation of gelatinase b and tissue inhibitors of metalloproteinase (timp) production in co-culture of human osteosarcoma cells and human fibroblasts: Gelatinase b production was stimulated via up-regulation of fibroblast growth factor (fgf) receptor. *Int. J. Cancer* 66 (1), 82–90. doi:10.1002/(SICI)1097-0215(19960328)66:1<82::AID-IJC15>3.0.CO;2-D

Laulederkind, S. J., Kirtikara, K., Raghow, R., and Ballou, L. R. (2000). The regulation of pge(2) biosynthesis in mg-63 osteosarcoma cells by il-1 and fgf is cell density-dependent. *Exp. Cell Res.* 258 (2), 409–416. doi:10.1006/excr.2000.4961

Lei, Z., Duan, H., Zhao, T., Zhang, Y., Li, G., Meng, J., et al. (2018). Park2 inhibits osteosarcoma cell growth through the jak2/stat3/vegf signaling pathway. *Cell Death Dis.* 9 (3), 375. doi:10.1038/s41419-018-0401-8

Levinson, H., Hopper, J. E., and Ehrlich, H. P. (2002). Overexpression of integrin alphav promotes human osteosarcoma cell populated collagen lattice contraction and cell migration. *J. Cell. Physiol.* 193 (2), 219–224. doi:10.1002/jcp.10164

Li, Q., Alsaidan, O. A., Ma, Y., Kim, S., Liu, J., Albers, T., et al. (2018). Pharmacologically targeting the myristoylation of the scaffold protein FRS2α inhibits FGF/FGFR-mediated oncogenic signaling and tumor progression. *J. Biol. Chem.* 293 (17), 6434–6448. doi:10.1074/jbc.RA117.000940

Li, S. Q., Tu, C., Wan, L., Chen, R. Q., Duan, Z. X., Ren, X. L., et al. (2019). FGF-induced LHX9 regulates the progression and metastasis of osteosarcoma via FRS2/TGF-β/β-catenin pathway. *Cell Div.* 14, 13. doi:10.1186/s13008-019-0056-6

Li, Y., Du, W., Han, J., and Ge, J. (2017). Lamp3 promotes the invasion of osteosarcoma cells via spp1 signaling. *Mol. Med. Rep.* 16 (5), 5947–5953. doi:10.3892/mmr.2017.7349

Liberzon, A., Birger, C., Thorvaldsdottir, H., Ghandi, M., Mesirov, J. P., and Tamayo, P. (2015). The molecular signatures database (msigdb) hallmark gene set collection. *Cell Syst.* 1 (6), 417–425. doi:10.1016/j.cels.2015.12.004

Liu, J., Qu, S., Zhang, T., Gao, Y., Shi, H., Song, K., et al. (2021). Applications of single-cell omics in tumor immunology. *Front. Immunol.* 12, 697412. doi:10.3389/fimmu.2021.697412

Liu, L., Xu, Y., and Reiter, R. J. (2013). Melatonin inhibits the proliferation of human osteosarcoma cell line mg-63. *Bone* 55 (2), 432–438. doi:10.1016/j.bone.2013.02.021

Liu, Y., Zhao, L., Ju, Y., Li, W., Zhang, M., Jiao, Y., et al. (2014). A novel androstenedione derivative induces ros-mediated autophagy and attenuates drug resistance in osteosarcoma by inhibiting macrophage migration inhibitory factor (mif). *Cell Death Dis.* 5, e1361. doi:10.1038/cddis.2014.300

Luo, J., Xia, Y., Luo, J., Li, J., Zhang, C., Zhang, H., et al. (2017). Grp78 inhibition enhances atf4-induced cell death by the deubiquitination and stabilization of chop in human osteosarcoma. *Cancer Lett.* 410, 112–123. doi:10.1016/j.canlet.2017.09.021

Luo, J., Xia, Y., Yin, Y., Luo, J., Liu, M., Zhang, H., et al. (2019). Atf4 destabilizes ret through nonclassical grp78 inhibition to enhance chemosensitivity to bortezomib in human osteosarcoma. *Theranostics* 9 (21), 6334–6353. doi:10.7150/thno.36818

Ma, K., Zhang, C., and Li, W. (2020). Gamabufotalin suppressed osteosarcoma stem cells through the TGF-β/periostin/PI3K/AKT pathway. *Chem. Biol. Interact.* 331, 109275. doi:10.1016/j.cbi.2020.109275

Manara, M. C., Bernard, G., Lollini, P. L., Nanni, P., Zuntini, M., Landuzzi, L., et al. (2006). Cd99 acts as an oncosuppressor in osteosarcoma. *Mol. Biol. Cell* 17 (4), 1910–1921. doi:10.1091/mbc.e05-10-0971

Meltzer, P. S., and Helman, L. J. (2021). New horizons in the treatment of osteosarcoma. *N. Engl. J. Med.* 385 (22), 2066–2076. doi:10.1056/NEJMra2103423

Miao, J. H., Wang, S. Q., Zhang, M. H., Yu, F. B., Zhang, L., Yu, Z. X., et al. (2014). Knockdown of galectin-1 suppresses the growth and invasion of osteosarcoma cells through inhibition of the mapk/erk pathway. *Oncol. Rep.* 32 (4), 1497–1504. doi:10.3892/or.2014.3358

Molina, E. R., Chim, L. K., Salazar, M. C., Mehta, S. M., Menegaz, B. A., Lamhamedi-Cherradi, S. E., et al. (2019). Mechanically tunable coaxial electrospun models of yap/taz mechanoresponse and igf-1r activation in osteosarcoma. *Acta Biomater.* 100, 38–51. doi:10.1016/j.actbio.2019.09.029

Mu, X., Isaac, C., Greco, N., Huard, J., and Weiss, K. (2013). Notch signaling is associated with aldh activity and an aggressive metastatic phenotype in murine osteosarcoma cells. *Front. Oncol.* 3, 143. doi:10.3389/fonc.2013.00143

Nallasamy, P., Nimmakayala, R. K., Karmakar, S., Leon, F., Seshacharyulu, P., Lakshmanan, I., et al. (2021). Pancreatic tumor microenvironment factor promotes cancer stemness via spp1-cd44 axis. *Gastroenterology* 161 (6), 1998–2013.e7. doi:10.1053/j.gastro.2021.08.023

Oda, Y., Yamamoto, H., Tamiya, S., Matsuda, S., Tanaka, K., Yokoyama, R., et al. (2006). Cxcr4 and vegf expression in the primary site and the metastatic site of human osteosarcoma: Analysis within a group of patients, all of whom developed lung metastasis. *Mod. Pathol.* 19 (5), 738–745. doi:10.1038/modpathol.3800587

Ongaro, A., Pellati, A., Bagheri, L., Rizzo, P., Caliceti, C., Massari, L., et al. (2016). Characterization of notch signaling during osteogenic differentiation in human osteosarcoma cell line mg63. *J. Cell. Physiol.* 231 (12), 2652–2663. doi:10.1002/jcp.25366

Panda, M., Tripathi, S. K., and Biswal, B. K. (2021). Sox9: An emerging driving factor from cancer progression to drug resistance. *Biochim. Biophys. Acta. Rev. Cancer* 1875 (2), 188517. doi:10.1016/j.bbcan.2021.188517

Park, G. B., Kim, D. J., Kim, Y. S., Lee, H. K., Kim, C. W., and Hur, D. Y. (2015). Silencing of galectin-3 represses osteosarcoma cell migration and invasion through inhibition of fak/src/lyn activation and beta-catenin expression and increases susceptibility to chemotherapeutic agents. *Int. J. Oncol.* 46 (1), 185–194. doi:10.3892/ijo.2014.2721

Qin, J., Wang, R., Zhao, C., Wen, J., Dong, H., Wang, S., et al. (2019). Notch signaling regulates osteosarcoma proliferation and migration through erk phosphorylation. *Tissue Cell* 59, 51–61. doi:10.1016/j.tice.2019.07.002

Qin, T., Zhu, W., Kan, X., Li, L., and Wu, D. (2022). Luteolin attenuates the chemoresistance of osteosarcoma through inhibiting the PTN/β-catenin/MDR1 signaling axis by upregulating miR-384. *J. Bone Oncol.* 34, 100429. doi:10.1016/j.jbo.2022.100429

Ren, S., Zhang, X., Hu, Y., Wu, J., Ju, Y., Sun, X., et al. (2020). Blocking the notch signal transduction pathway promotes tumor growth in osteosarcoma by affecting polarization of tam to m2 phenotype. *Ann. Transl. Med.* 8 (17), 1057. doi:10.21037/atm-20-3881

Ren, X., Kang, B., and Zhang, Z. (2018). Understanding tumor ecosystems by single-cell sequencing: Promises and limitations. *Genome Biol.* 19 (1), 211. doi:10.1186/s13059-018-1593-z

Romero-Ramirez, L., Cao, H., Nelson, D., Hammond, E., Lee, A. H., Yoshida, H., et al. (2004). Xbp1 is essential for survival under hypoxic conditions and is required for tumor growth. *Cancer Res.* 64 (17), 5943–5947. doi:10.1158/0008-5472.CAN-04-1606

Rothzerg, E., Ho, X. D., Xu, J., Wood, D., Martson, A., and Koks, S. (2021). Upregulation of 15 antisense long non-coding rnas in osteosarcoma. *Genes (Basel)* 12 (8), 1132. doi:10.3390/genes12081132

Saba, K. H., Cornmark, L., Rissler, M., Fioretos, T., Astrom, K., Haglund, F., et al. (2019). Genetic profiling of a chondroblastoma-like osteosarcoma/malignant phosphaturic mesenchymal tumor of bone reveals a homozygous deletion of cdkn2a, intragenic deletion of dmd, and a targetable fn1-fgfr1 gene fusion. *Genes Chromosom. Cancer* 58 (10), 731–736. doi:10.1002/gcc.22764

Sciandra, M., Marino, M. T., Manara, M. C., Guerzoni, C., Grano, M., Oranger, A., et al. (2014). Cd99 drives terminal differentiation of osteosarcoma cells by acting as a spatial regulator of erk 1/2. *J. Bone Min. Res.* 29 (5), 1295–1309. doi:10.1002/jbmr.2141

Shao, H., Ge, M., Zhang, J., Zhao, T., and Zhang, S. (2022). Osteoclasts differential-related prognostic biomarker for osteosarcoma based on single cell, bulk cell and gene expression datasets. *BMC Cancer* 22 (1), 288. doi:10.1186/s12885-022-09380-z

Sun, X., Tian, C., Zhang, H., Han, K., Zhou, M., Gan, Z., et al. (2020). Long noncoding rna oip5-as1 mediates resistance to doxorubicin by regulating mir-137-3p/ptn axis in osteosarcoma. *Biomed. Pharmacother.* 128, 110201. doi:10.1016/j.biopha.2020.110201

Takase, N., Koma, Y., Urakawa, N., Nishio, M., Arai, N., Akiyama, H., et al. (2016). Ncam- and fgf-2-mediated fgfr1 signaling in the tumor microenvironment of esophageal cancer regulates the survival and migration of tumor-associated macrophages and cancer cells. *Cancer Lett.* 380 (1), 47–58. doi:10.1016/j.canlet.2016.06.009

Tan, X., Fan, S., Wu, W., and Zhang, Y. (2015). Microrna-26a inhibits osteosarcoma cell proliferation by targeting igf-1. *Bone Res.* 3, 15033. doi:10.1038/boneres.2015.33

Tanaka, M., Setoguchi, T., Hirotsu, M., Gao, H., Sasaki, H., Matsunoshita, Y., et al. (2009). Inhibition of notch pathway prevents osteosarcoma growth by cell cycle regulation. *Br. J. Cancer* 100 (12), 1957–1965. doi:10.1038/sj.bjc.6605060

Tsai, H. C., Tzeng, H. E., Huang, C. Y., Huang, Y. L., Tsai, C. H., Wang, S. W., et al. (2017). Wisp-1 positively regulates angiogenesis by controlling vegf-a expression in human osteosarcoma. *Cell Death Dis.* 8 (4), e2750. doi:10.1038/cddis.2016.421

Turner, N., and Grose, R. (2010). Fibroblast growth factor signalling: From development to cancer. *Nat. Rev. Cancer* 10 (2), 116–129. doi:10.1038/nrc2780

Vegliante, R., Pastushenko, I., and Blanpain, C. (2022). Deciphering functional tumor states at single-cell resolution. *EMBO J.* 41 (2), e109221. doi:10.15252/embj.2021109221

Wang, D., Qian, G., Wang, J., Wang, T., Zhang, L., Yang, P., et al. (2019). Visfatin is involved in the cisplatin resistance of osteosarcoma cells via upregulation of snail and zeb1. *Cancer Biol. Ther.* 20 (7), 999–1006. doi:10.1080/15384047.2019.1591675

Wang, G. J., Shen, N. J., Cheng, L., Yehan, F., Huang, H., and Li, K. H. (2016). Visfatin triggers the *in vitro* migration of osteosarcoma cells via activation of NF-κB/IL-6 signals. *Eur. J. Pharmacol.* 791, 322–330. doi:10.1016/j.ejphar.2016.08.029

Wang, Q., Liu, W., Fan, J., Guo, J., Shen, F., Ma, Z., et al. (2020). Von willebrand factor promotes platelet-induced metastasis of osteosarcoma through activation of the vwf-gpib axis. *J. Bone Oncol.* 25, 100325. doi:10.1016/j.jbo.2020.100325

Wang, W. T., Qi, Q., Zhao, P., Li, C. Y., Yin, X. Y., and Yan, R. B. (2018). Mir-590-3p is a novel microrna which suppresses osteosarcoma progression by targeting sox9. *Biomed. Pharmacother.* 107, 1763–1769. doi:10.1016/j.biopha.2018.06.124

Wang, Y. P., and Yang, Z. P. (2015). Effects of melatonin combined with cis-platinum or methotrexate on the proliferation of osteosarcoma cell line saos-2. *Zhongguo Yi Xue Ke Xue Yuan Xue Bao.* 37 (2), 215–220. doi:10.3881/j.issn.1000-503X.2015.02.013

Xi, S. C., Tam, P. C., Brown, G. M., Pang, S. F., and Shiu, S. Y. (2000). Potential involvement of mt1 receptor and attenuated sex steroid-induced calcium influx in the direct anti-proliferative action of melatonin on androgen-responsive lncap human prostate cancer cells. *J. Pineal Res.* 29 (3), 172–183. doi:10.1034/j.1600-079x.2000.d01-64.x

Xian, M., Cao, H., Cao, J., Shao, X., Zhu, D., Zhang, N., et al. (2017). Bortezomib sensitizes human osteosarcoma cells to adriamycin-induced apoptosis through ROS-dependent activation of p-eIF2α/ATF4/CHOP axis. *Int. J. Cancer* 141 (5), 1029–1041. doi:10.1002/ijc.30792

Xu, C. J., Song, J. F., Su, Y. X., and Liu, X. L. (2010). Expression of b-fgf and endostatin and their clinical significance in human osteosarcoma. *Orthop. Surg.* 2 (4), 291–298. doi:10.1111/j.1757-7861.2010.00102.x

Xu, C., Sun, L., Jiang, C., Zhou, H., Gu, L., Liu, Y., et al. (2017). Spp1, analyzed by bioinformatics methods, promotes the metastasis in colorectal cancer by activating emt pathway. 91, 1167–1177. doi:10.1016/j.biopha.2017.05.056

Xu, C., Wang, Z., Zhang, L., Feng, Y., Lv, J., Wu, Z., et al. (2022). Periostin promotes the proliferation and metastasis of osteosarcoma by increasing cell survival and activates the pi3k/akt pathway. *Cancer Cell Int.* 22 (1), 34. doi:10.1186/s12935-021-02441-6

Yamaguchi, K., Matsuo, N., Sumiyoshi, H., Fujimoto, N., Iyama, K. I., Yanagisawa, S., et al. (2005). Pro-alpha3(v) collagen chain is expressed in bone and its basic n-terminal peptide adheres to osteosarcoma cells. *Matrix Biol.* 24 (4), 283–294. doi:10.1016/j.matbio.2005.03.006

Yang, J., Cheng, D., Zhou, S., Zhu, B., Hu, T., and Yang, Q. (2015). Overexpression of x-box binding protein 1 (xbp1) correlates to poor prognosis and up-regulation of pi3k/mtor in human osteosarcoma. *Int. J. Mol. Sci.* 16 (12), 28635–28646. doi:10.3390/ijms161226123

Yu, H., Zhang, Y., Zuo, Q., Zhong, S., Chen, Y., Zhang, M., et al. (2022). Targeting x box-binding protein-1 (xbp1) enhances the sensitivity of hos osteosarcoma cells to pyropheophorbide- alpha methyl ester-mediated photodynamic therapy. *Photodiagnosis Photodyn. Ther.* 37, 102646. doi:10.1016/j.pdpdt.2021.102646

Zeng, Z., Li, W., Zhang, D., Zhang, C., Jiang, X., Guo, R., et al. (2022). Development of a chemoresistant risk scoring model for prechemotherapy osteosarcoma using single-cell sequencing. *Front. Oncol.* 12, 893282. doi:10.3389/fonc.2022.893282

Zhang, J., Li, N., Lu, S., Chen, Y., Shan, L., Zhao, X., et al. (2021). The role of notch ligand jagged1 in osteosarcoma proliferation, metastasis, and recurrence. *J. Orthop. Surg. Res.* 16 (1), 226. doi:10.1186/s13018-021-02372-y

Zhang, P., Yang, Y., Nolo, R., Zweidler-McKay, P. A., and Hughes, D. P. (2010). Regulation of notch signaling by reciprocal inhibition of hes1 and deltex 1 and its role in osteosarcoma invasiveness. *Oncogene* 29 (20), 2916–2926. doi:10.1038/onc.2010.62

Zhang, Q., Li, L., Lai, Y., and Zhao, T. (2020). Silencing of spp1 suppresses progression of tongue cancer by mediating the pi3k/akt signaling pathway. *Technol. Cancer Res. Treat.* 19, 1533033820971306. doi:10.1177/1533033820971306

Zhang, Y., Cheng, H., Li, W., Wu, H., and Yang, Y. (2019). Highly-expressed P2X7 receptor promotes growth and metastasis of human HOS/MNNG osteosarcoma cells via PI3K/Akt/GSK3β/β-catenin and mTOR/HIF1α/VEGF signaling. *Int. J. Cancer* 145 (4), 1068–1082. doi:10.1002/ijc.32207

Zhao, A., Zhang, Z., Zhou, Y., Li, X., Li, X., Ma, B., et al. (2020). β-Elemonic acid inhibits the growth of human Osteosarcoma through endoplasmic reticulum (ER) stress-mediated PERK/eIF2α/ATF4/CHOP activation and Wnt/β-catenin signal suppression. *Phytomedicine* 69, 153183. doi:10.1016/j.phymed.2020.153183

Zhou, X., Jing, J., Peng, J., Mao, W., Zheng, Y., Wang, D., et al. (2014). Expression and clinical significance of galectin-3 in osteosarcoma. *Gene* 546 (2), 403–407. doi:10.1016/j.gene.2014.04.066

Zhou, Y., Yang, D., Yang, Q., Lv, X., Huang, W., Zhou, Z., et al. (2020). Single-cell rna landscape of intratumoral heterogeneity and immunosuppressive microenvironment in advanced osteosarcoma. *Nat. Commun.* 11 (1), 6322. doi:10.1038/s41467-020-20059-6

Zhou, Y., Yin, L., Li, H., Liu, L. H., and Xiao, T. (2019). The lncrna linc00963 facilitates osteosarcoma proliferation and invasion by suppressing mir-204-3p/fn1 axis. *Cancer Biol. Ther.* 20 (8), 1141–1148. doi:10.1080/15384047.2019.1598766

Zucchini, C., Manara, M. C., Pinca, R. S., De Sanctis, P., Guerzoni, C., Sciandra, M., et al. (2014). Cd99 suppresses osteosarcoma cell migration through inhibition of rock2 activity. *Oncogene* 33 (15), 1912–1921. doi:10.1038/onc.2013.152

frontiers | Frontiers in Genetics

TYPE Original Research
PUBLISHED 18 October 2022
DOI 10.3389/fgene.2022.1038174

OPEN ACCESS

EDITED BY
Qian Wang,
Tai'an City Central Hospital, China

REVIEWED BY
Haiyang Wu,
Tianjin Medical University, China
Yaying Sun,
Fudan University, China

*CORRESPONDENCE
Yuanliang Yan,
yanyuanliang@csu.edu.cn

†These authors have contributed equally to this work

SPECIALTY SECTION
This article was submitted to Cancer Genetics and Oncogenomics, a section of the journal Frontiers in Genetics

RECEIVED 06 September 2022
ACCEPTED 05 October 2022
PUBLISHED 18 October 2022

CITATION
Liu Y, Luo G, Yan Y and Peng J (2022), A pan-cancer analysis of copper homeostasis-related gene lipoyltransferase 1: Its potential biological functions and prognosis values.
Front. Genet. 13:1038174.
doi: 10.3389/fgene.2022.1038174

A pan-cancer analysis of copper homeostasis-related gene lipoyltransferase 1: Its potential biological functions and prognosis values

Ying Liu[1†], Gengqiu Luo[2,3†], Yuanliang Yan[4*] and Jinwu Peng[2,3]

[1]Department of Pathology, Xiangya Changde Hospital, Changde, China, [2]Department of Pathology, Xiangya Hospital, Basic School of Medicine, Central South University, Changsha, China, [3]National Clinical Research Center for Geriatric Disorders, Xiangya Hospital, Central South University, Changsha, China, [4]Department of Pharmacy, Xiangya Hospital, Central South University, Changsha, China

As a key copper homeostasis-related molecule, lipoyltransferase 1 (LIPT1) is an essential enzyme for the activation of mitochondrial 2-ketoacid dehydrogenase, participating in fatty acylation. However, the biological significances of LIPT1 in the pan-cancer are unclear. Here, we comprehensively analyzed the functional characteristics of LIPT1 in human cancers and its roles in immune response. We found that LIPT1 was down-regulated in some cancers. And LIPT1 overexpression is associated with favorable prognosis in these patients, such as breast cancer, clear cell renal cell carcinoma, ovarian cancer and gastric cancer. We also explored the mutational status and methylation levels of LIPT1 in human cancers. Gene enrichment analysis indicated that abnormally expressed LIPT1 was significantly associated with immune cells infiltration, such as B cells, $CD8^+$ T cells and cancer-associated fibroblast cells. The result from single cell sequencing reflected the important roles of LIPT1 in the regulation of several biological behaviors of cancer cells, such as DNA damage response and cell apoptosis. Taken together, our research could provide a comprehensive overview about the significances of LIPT1 in human pan-cancer progression, prognosis and immune.

KEYWORDS

LIPT1, pan-cancer, biological functions, prognosis, immune

Introduction

Cancers are global health problems, affecting human health and quality of life. According to the statistics from World Health Organization, cancers are the main endangering cause of human life (Tao et al., 2021; Yu and Mitrofanova, 2021). Identifying the valuable pan-cancer genes would be crucial to clarify the underlying mechanisms for occurrence and development of different tumors (He et al., 2021; Shi et al., 2021).

Lipoic acid (LA), an eight-carbon fatty acid, serves as an important cofactor for the mitochondrial glycine cleavage system (Habarou et al., 2017). Lipoyltransferase 1 (LIPT1), as a lipoate-specific sequential enzymes, could be used to maintain the oxidative and reductive glutamine metabolism (Ni et al., 2019). Recent studies have established the functional link between aberrant LIPT1expression and tumorigenesis, including bladder cancer (Chen et al., 2021) and melanoma (Lv et al., 2022). In melanoma patients, Lv and colleague found that upregulated LIPT1 expression might suppress the infiltration of regulatory T cells (Tregs), thereby enhancing the immunotherapy efficacy (Lv et al., 2022). However, the detailed roles of LIPT1 in different tumor types remains elusive.

In this study, by using multiple bioinformatics methods, we explored the underlying molecular mechanisms of LIPT1 in the pathogenesis and clinical prognosis of multiple human cancers. The expression profiles of LIPT1 and corresponding survival status were comprehensively analyzed using the datasets from TCGA and GEO. Meanwhile, gene enrichment indicated the roles of LIPT1-related molecules in tumorigenesis. Meanwhile, the potential implications of LIPT1 in anti-tumor immune response were also explored.

Materials and methods

Gene expression analysis

TIMER2.0 (Li et al., 2020) was used to investigate the different expression profiles of LIPT1 between pan-cancer and adjacent normal tissues. The gene expression levels were shown using a log2 (TPM + 1) scale, where TPM stands for transcripts per million. The clinical proteomic tumor analysis consortium (CPTAC) (Edwards et al., 2015) in UALCAN database (Chandrashekar et al., 2022) was used to analyze the protein expression of LIPT1 in pan-cancers. Gene Expression Profiling Interactive Analysis 2 (GEPIA2.0) (Tang et al., 2017) was used to analyze the relationship between LIPT1 expression and patients' pathological stage in all TCGA cancers. The Human Protein Atlas (HPA) (Colwill et al., 2011) was further used to confirm the intensity of LIPT1 immunohistochemical staining in several cancer tissues, including kidney cancer, breast carcinoma, and uterus endometrium adenocarcinoma.

Survival analysis

The expression of LIPT1 on the patients' prognostic values, including overall survival (OS) and disease-free survival (DFS), was obtained from GEPIA2.0. TCGA tumor patients were divided into the high-expression and low-expression cohorts based on the cut-off values (50% and 50%). The hazards ratio was calculated based on Cox PH Model. With the log-rank test, Kaplan-Meier plotter (Lanczky and Gyorffy, 2021) was used to perform the survival analysis in tumors.

Genetic alteration analysis

cBioPortal (Gao et al., 2013) was used to collect the alteration frequency, mutation type, mutation site information, and three-dimensional (3D) structure of candidate proteins in all TCGA tumors. In the "Comparison" module, clinical prognosis data, including progression-free survival (PFS), disease-specific survival (DSS), DFS, and OS, for all TCGA cancer types with or without LIPT1 gene alterations were downloaded and analyzed.

The infiltration of immune cells

Using multiple algorithms, such as TIMER, EPIC, MCPCOUNTER, XCELL and TIDE, we applied TIMER2.0 tool to evaluate the correlation of LIPT1 expression with immune infiltration levels in different TCGA cancers.

Single cell sequencing

CancerSEA (Yuan et al., 2019) is a specialized single cell sequencing database, which can provide different functional status of cancer cells at the single cell level. The correlation data between LIPT1 expression and different tumor function based on single cell sequencing data were analyzed. T-SNE diagrams demonstrated the expression profiles of LIPT1 at single cells in TCGA samples.

Gene enrichment analysis

BioGRID website (Oughtred et al., 2021) was used to analysis the protein-protein interaction network. GEPIA2.0 was used to obtain the top 100 LIPT1-correlated genes from all TCGA tumor and normal tissues. Then we conducted a pairwise gene-gene Pearson correlation analysis between LIPT1 and the selected genes. Gene ontology (GO) and Kyoto encyclopedia of genes and genome (KEGG) enrichment analyses were used to investigate the underlying biological functions and signaling pathways affected by LIPT1 in TCGA tumors. p-value < 0.05 was considered to be statistically significant.

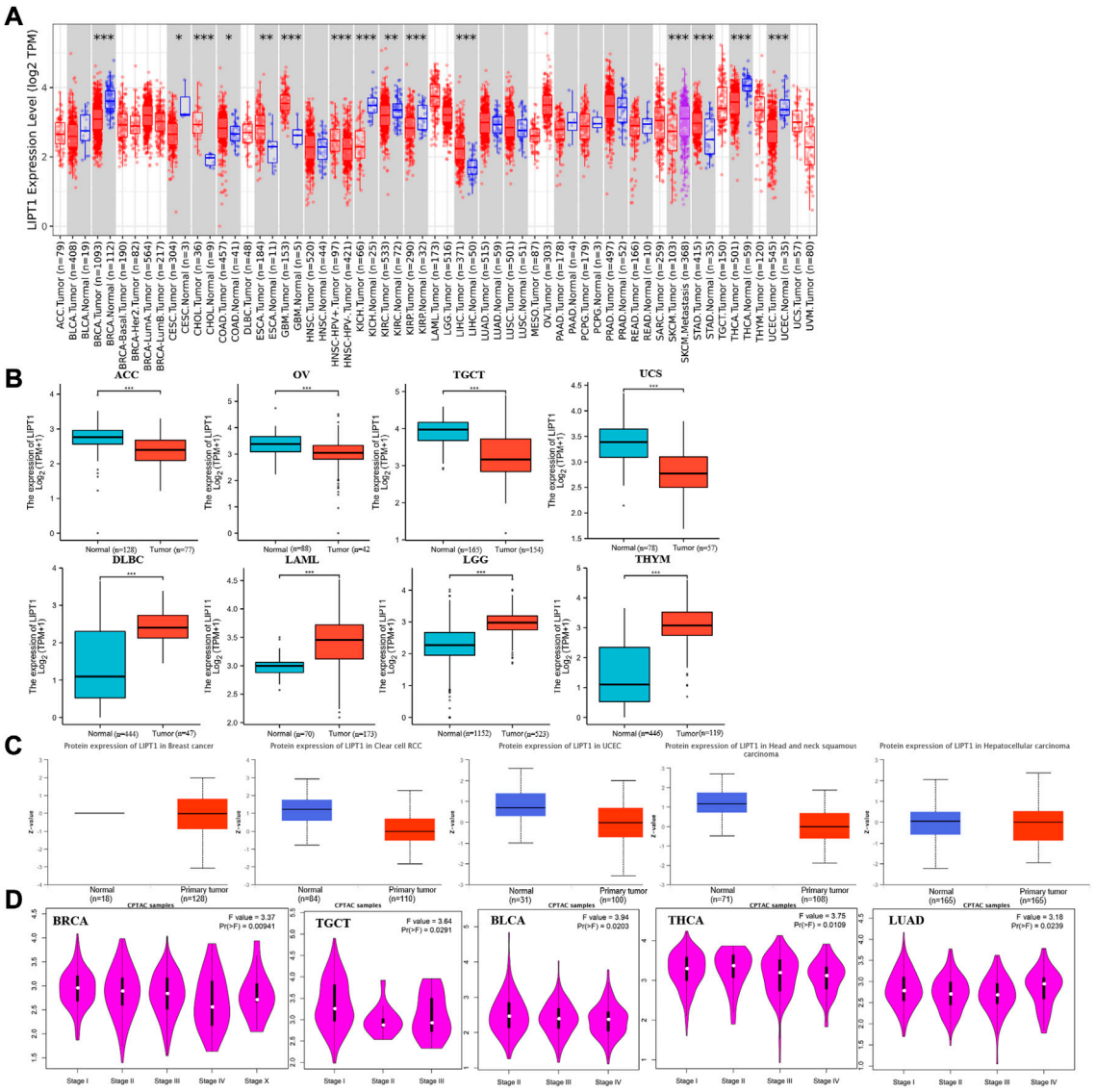

FIGURE 1
The expression of LIPT1 in pan-cancer. **(A)** LIPT1 expression in different cancers from TIMER2.0. *$p < 0.05$; **$p < 0.01$; ***$p < 0.001$. **(B)** The expression differences of LIPT1 in ACC, OV, TGCT, UCS, DLBC, LAML, LGG, and HNSC from GTEx and TCGA. ***$p < 0.001$. **(C)** The protein levels of LIPT1 in BRCA, KIRC, UCEC, HNSC, and LIHC were analyzed using CPTAC. **(D)** LIPT1 expression levels and the pathological stages were analyzed using GEPIA2.0.

Results

The different expression profiles of lipoyltransferase 1 in human pan-cancer

Initially, we examined LIPT1 expression levels in pan-cancer by TIMER2.0. As shown in Figure 1A, the analysis revealed that LIPT1 expression was significantly lower in various tumors than in the adjacent normal tissues, including breast invasive carcinoma (BRCA), cervical squamous cell carcinoma and endocervical adenocarcinoma (CESC), kidney renal clear cell carcinoma (KIRC), kidney renal papillary cell carcinoma (KIRP), thyroid carcinoma (THCA), uterine corpus endometrial carcinoma (UCEC), kidney chromophobe (KICH). Conversely, LIPT1 expression was significantly up-regulated in some other tumors, including cholangiocarcinoma (CHOL), colon adenocarcinoma (COAD), esophageal carcinoma (ESCA), glioblastoma multiforme (GBM), liver hepatocellular carcinoma (LIHC) and stomach adenocarcinoma (STAD). However, no significantly differential expression of LIPT

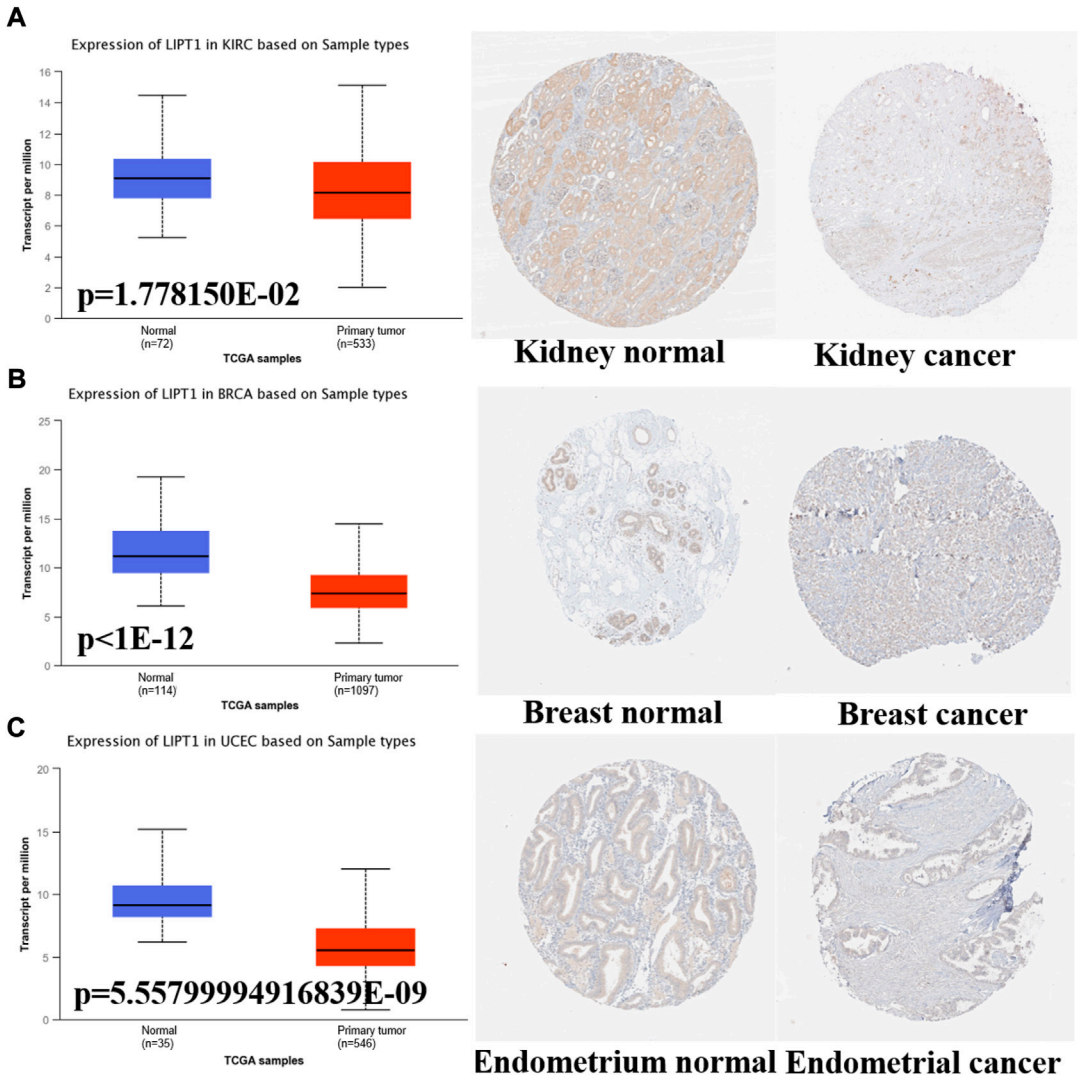

FIGURE 2
The different expression of LIPT1 between normal tissues and tumor tissues. **(A–C)** UALCAN and HPA platforms displayed the downregulated expression of LIPT1 in tumor tissue derived from kidney, breast and endometrium.

could be found in other tumors, such as bladder urothelial carcinoma (BLCA), head and neck squamous cell carcinoma (HNSC), and so on. Given some data in the normal tissues were not available, we further examined the expression differences of LIPT1 using the TCGA and GTEx datasets. As shown in Figure 1B, we found the down-regulated LIPT1 in adrenocortical carcinoma (ACC), ovarian serous cystadenocarcinoma (OV), testicular germ cell tumors (TGCT) and uterine carcinosarcoma (UCS). Meanwhile, we found the up-regulated LIPT1 in lymphoid neoplasm diffuse large B-cell lymphoma (DLBC), acute myeloid leukemia (LAML), brain lower grade glioma (LGG) and thymoma (THYM).

Then, the National Cancer Institute's CPTAC dataset was used to assessed LIPT1 expression at a protein level. We found that the total protein expression of LIPT1 was significantly down-regulated in BRCA, KIRC, UCEC, HNSC, and LIHC (Figure 1C). We also used GEPIA2.0 to explore the correlation between LIPT1 expression level and the pathological stages of tumors. And we found the obvious effect of LIPT1 expression on the patients' stages in BRCA, TGCT, BLCA, THCA and lung adenocarcinoma (LUAD) (Figure 1D; Supplementary Figure S1).

Meanwhile, we further confirmed the LIPT1 expression using the IHC results provided by the HPA database. The IHC staining of LIPT1 was mainly weakly or negatively expressed in tumor tissue derived from kidney cancer, breast cancer and endometrial

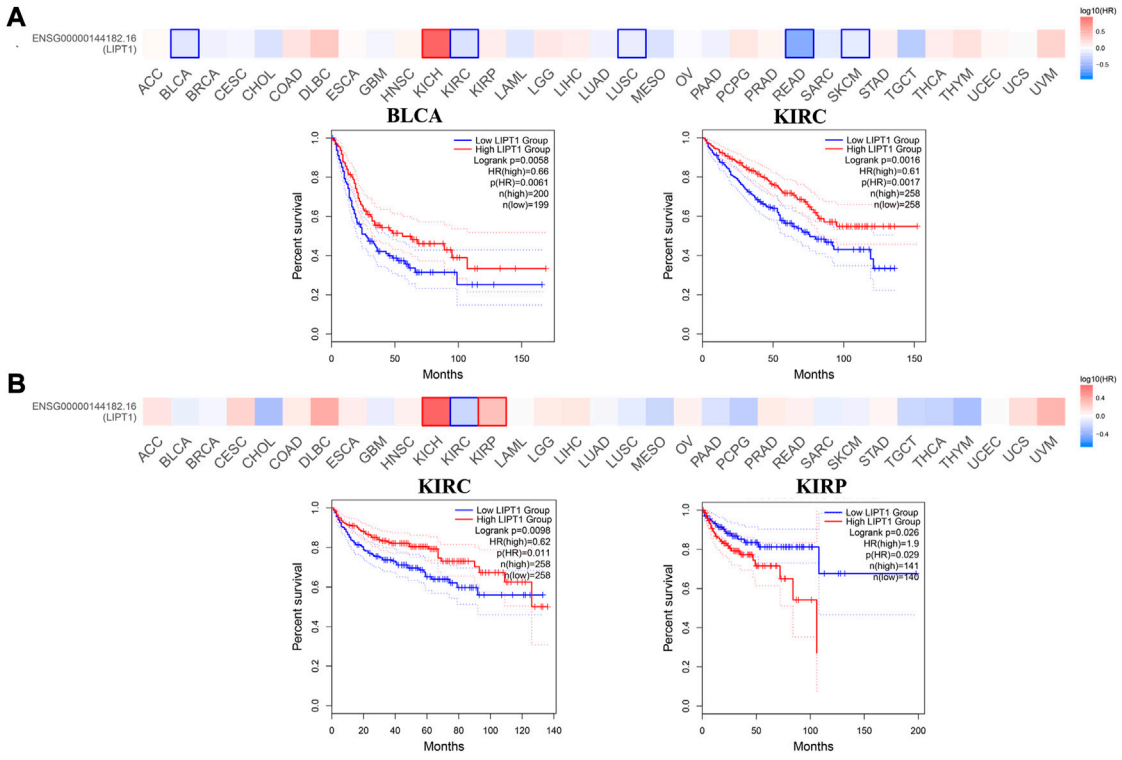

FIGURE 3
Prognostic values of LIPT1 expression in pan-cancer. **(A,B)** GEPIA2.0 was used to analyze the effects of LIPT1 gene expression on the patients' prognosis in pan-cancer, including OS **(A)** and DFS **(B)**.

cancer (Figures 2A–C). Overall, we demonstrated the decreased LIPT1 expression in these tumors.

The prognostic values of lipoyltransferase 1 on the patients' survival

Next, GEPIA2.0 database was used to evaluate the values of LIPT1 on patients' prognosis, including OS and DFS. We found that higher LIPT1 expression was significantly associated with increased OS in BLCA (p = 0.0061) and KIRC (p = 0.0017) (Figure 3A). And DFS analysis data showed that high expression LIPT1 was associated with favorable prognosis in KIRC (p = 0.011). In contrast, in KIRP patients, high expression of LIPT1 is associated with poor prognosis (p = 0.029) (Figure 3B). Meanwhile, we also used the Kaplan-Meier plotter tool to analyze the survival data. Correspondingly, in breast cancer, high expression of LIPT1 was related to good PFS (p = 1.9e-06), OS (p = 3.1e-06) and distant metastasis-free survival (DMFS) (p = 2e-07). In addition, high LIPT1 expression was significantly associated with increased DMFS in ovarian cancer (p = 0.013) and decreased post progression survival (PPS) in gastric cancer (p = 0.00077) (Supplementary Figures S2A–C). Therefore, these results demonstrated that LIPT1 may be a potential prognostic marker in various cancers. Especially, the expression profiles and prognostic values indicated that LIPT1 might act as a tumor suppressor gene in breast cancer patients.

Lipoyltransferase 1 mutation in various tumors

To explore the gene mutation of LIPT1 in various cancers, we analyzed its mutation status through cBioPortal platform based on TCGA data. Pan-cancer analysis suggested the high LIPT1 amplification in BLCA (>2%) and high mutation in UECE (>3%). Mature B cell neoplasms had the highest incidence of "deep deletion" with the frequency of ~2% (Figure 4A). As shown in Figure 4B, we found that missense and truncating were the predominant mutation styles in LIPT1. For instance, a truncating mutation within the BPL_LplA_LipB domain, K123sf*8 alteration, could be detected in five STAD cases. Figure 4C displayed the K123sf*8 alteration in the 3D structure of LIPT1 protein. In addition, we analyzed the potential links between genetic alterations of LIPT1 and the survival prognosis of patients in pan-cancers. However, we could not

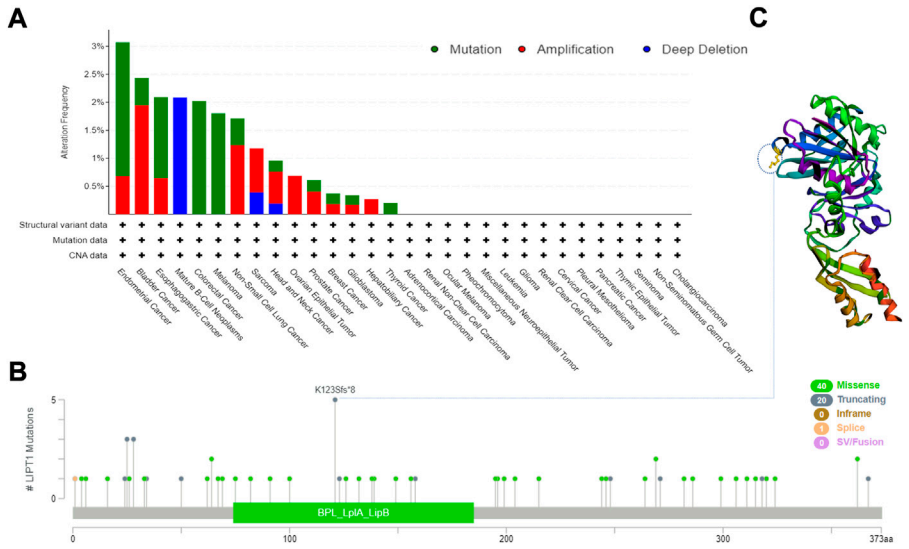

FIGURE 4
LIPT1 gene mutation in various cancers. **(A,B)** cBioPortal was used to display the alteration frequency of different mutation types **(A)** and mutation site **(B)** of LIPT1 in pan-cancer. **(C)** K123sf*8 mutation site was shown in the 3D protein structure of LIPT1.

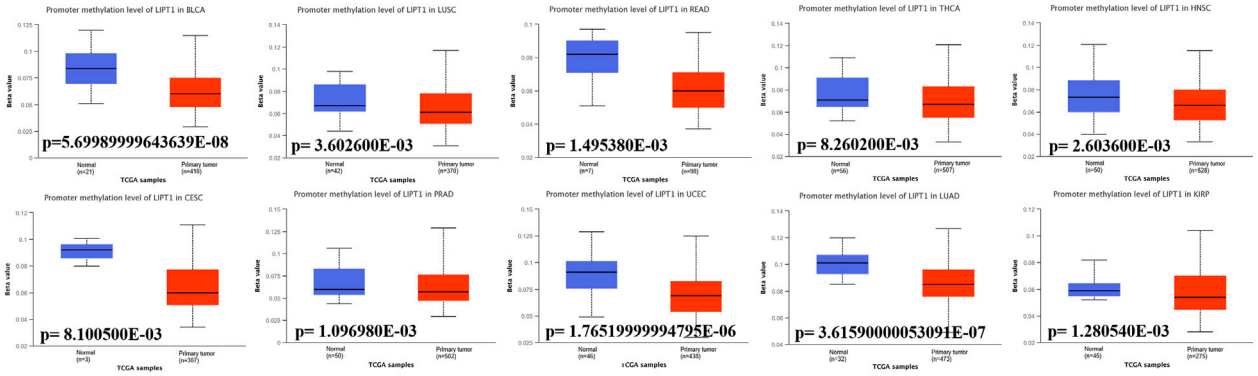

FIGURE 5
Promoter methylation levels of LIPT1 in cancers. The methylation values of LIPT1 between normal and primary tumor tissues were analyzed using UALCAN tool.

find the obvious effect of LIPT1 genetic alterations on the patients' prognosis (Supplementary Figures S3A–F, S4A–F). These unexpected results need to be further verified with more clinical patient data.

Promoter methylation of lipoyltransferase 1 in human cancers

Promoter DNA methylation has been proved to affect the transcriptional repression and participate in the tumor oncogenesis (Smith et al., 2020). We compared the methylation values of LIPT1 between normal and tumor tissues. Our analysis results displayed that promoter methylation levels of LIPT1 were significantly reduced in several tumor tissues, including BLCA, lung squamous cell carcinoma (LUSC), rectum adenocarcinoma (READ), THCA, HNSC, CESC, prostate adenocarcinoma (PRAD), UCEC, LUAD, and KIRP (Figure 5). In contrast, the promoter methylation levels of LIPT1were not significantly different in other tumors (Supplementary Figure S5). These results suggested that the transcriptional

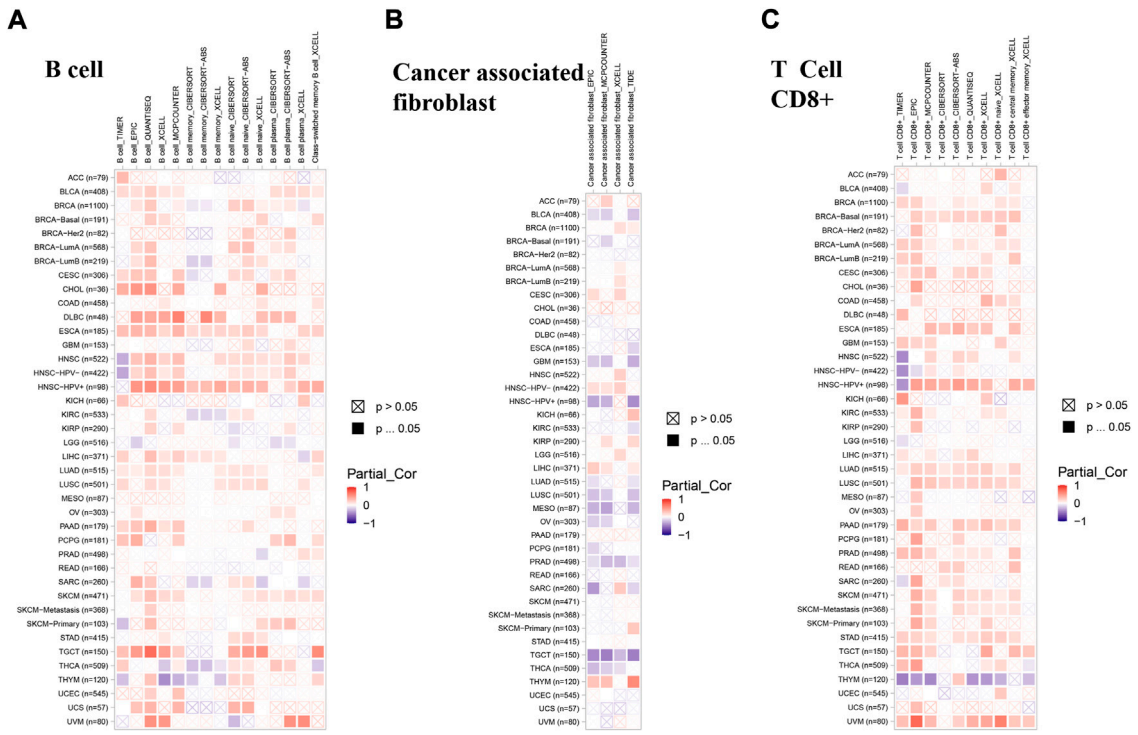

FIGURE 6
The correlation between immune cells and LIPT1 expression in cancers. **(A–C)** The relationship between LIPT1 expression and immune infiltration of B cell **(A)**, cancer-associated fibroblast **(B)** and T cell $CD8^+$ **(C)** was depicted by TIMER2.0 database. Several algorithms, such as TIMER, EPIC, QUANTISEQ, XCELL, MCPCOUNTER, CIBERSORT, CIBERSORT-ABS, and TIDE, were applied to explore the correlation. Positive correlation (0–1) are indicated with the red color, while negative correlation (–1 to 0) are indicated with the blue color. *p*-value < 0.05 is considered as statistically significant. A cross indicates non-significant correlations.

expression of LIPT1 may be due to the alterations of promoter methylation.

The roles of lipoyltransferase 1 on the regulation of immune cell infiltration

Recent researches have shown that immune infiltration is associated with the initiation, progression, and metastasis in human cancers (Stenstrom et al., 2021; Ren et al., 2022; Shan et al., 2022). Several algorithms, such as TIMER, EPIC, QUANTISEQ, XCELL, MCPCOUNTER, CIBERSORT, CIBERSORT-ABS, and TIDE, were applied to explore the correlation between LIPT1 expression and the infiltration of different immune cells in pan-cancer. We found a positive correlation between the infiltration of B cells and LIPT1 expression in BLCA, ESCA, pancreatic adenocarcinoma (PAAD) and TGCT (Figure 6A). Meanwhile, a negative correlation between the infiltration of cancer-associated fibroblasts and LIPT1 expression could be found in PRAD and TGCT (Figure 6B). In LUAD, LIPT1 expression was positively correlated with $CD8^+$ T cells infiltration (Figure 6C). We found no significantly correlation between LIPT1 expression and the infiltration values of dendritic cells (DC), monocyte, regulatory T cells (Treg), natural killer cells (NK), neutrophil and macrophage (Supplementary Figure S6). These findings demonstrated that LIPT1 may act as a novel immune-associated biomarkers for tumor development.

The expression pattern of lipoyltransferase 1 at single-cell levels

Single-cell transcriptome sequencing is a key technique for analyzing the underlying functions of candidate molecules at single-cell levels (He et al., 2021; Li et al., 2021). In retinoblastoma (RB), the expression of LIPT1 was negatively associated with cell cycle, DNA repair response, EMT and invasion. By contrast, LIPT1 expression was positively related to angiogenesis, differentiation, inflammation and stemness. LIPT1 expression in uveal melanoma (UM) had a negative relationship with almost all tumor biological behaviors, such as cell death, DNA damage response, invasion and metastasis. In addition, the results demonstrated that LIPT1 expression was

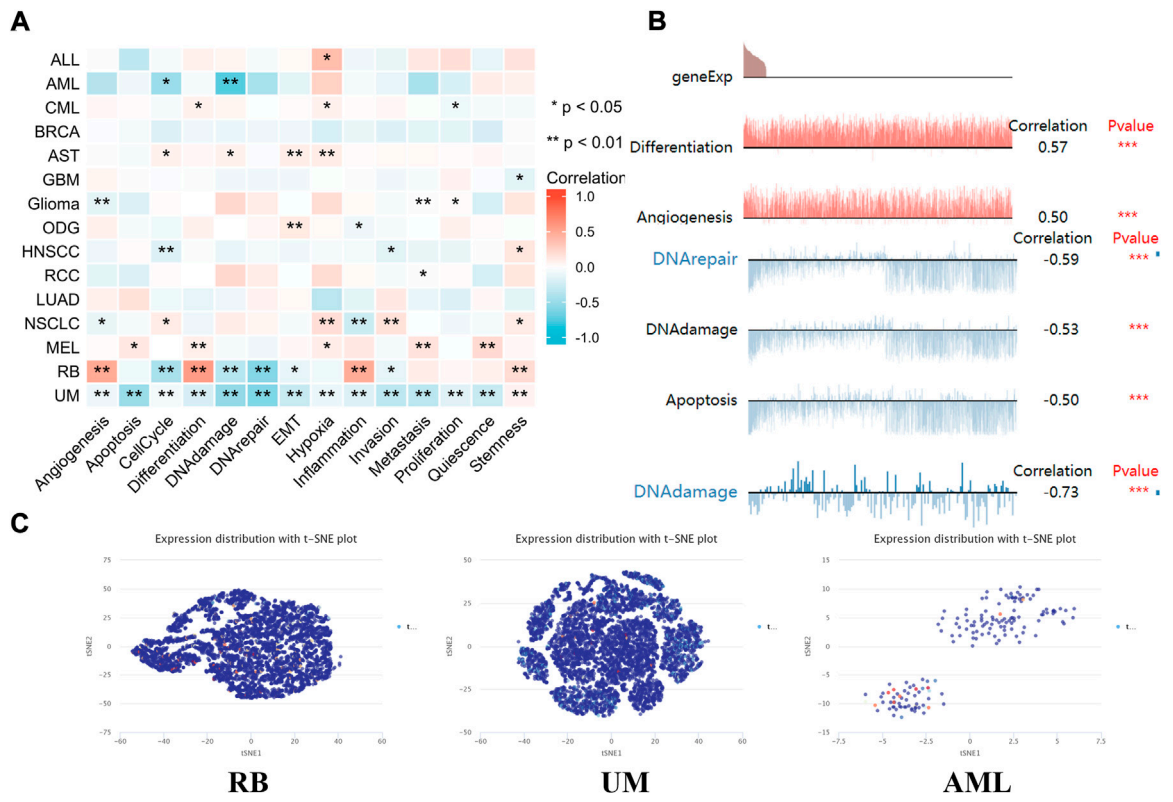

FIGURE 7
The expression levels of LIPT1 at single-cell levels. **(A,B)** The relationship between LIPT1 expression and different functional states in tumors was explored by the CancerSEA tool. *$p < 0.05$; **$p < 0.01$; ***$p < 0.001$. **(C)** LIPT1 expression profiles were shown at single cells from RB, UM and AML by T-SNE diagram.

negatively related with cell cycle and DNA damage in acute myelocytic leukemia (AML) (Figure 7A). In addition, Figure 7B displayed the significant correlation between the LIPT1 expression and differentiation in RB, angiogenesis, DNA damage, DNA repair, and apoptosis in UM, and DNA damage in AML. Moreover, LIPT1 expression profiles were shown at single cell levels from RB, UM, and AML by T-SNE diagram (Figure 7C).

Functional enrichment analysis of lipoyltransferase 1-related genes in cancers

Next, we used functional enrichment analysis to evaluate the underlying molecular mechanisms of LIPT1 in tumorigenesis and development. As shown in Figure 8A, the 15 interacting molecules with LIPT1 were obtained from BioGRID web tool. In addition, we acquired the top 100 LIPT1 co-expressed genes (Supplementary Table S1) in pan-cancer from GEPIA2.0. Among these, testis specific 10 (TSGA10), zinc finger protein 14 (ZNF14), enhancer of polycomb homolog 2 (EPC2), o-sialoglycoprotein endopeptidase like 1 (OSGEPL1), cereblon (CRBN) and wd repeat, sterile alpha motif and u-box domain containing 1 (WDSUB1) showed high correlations with LIPT1 in the majority of cancer types (Figures 8B,C). Meanwhile, GO and KEGG enrichment analyses in Figure 8D indicated that the roles of LIPT1 co-expressed genes on the regulation of herpes simplex virus one infection and acetyltransferase complex in tumorigenesis and development.

Discussion

Emerging studies have shown that copper death plays an important role in the occurrence and treatment of human tumors (Jiang et al., 2022). In our research, we performed a comprehensive analysis of LIPT1, the copper death-related gene, in a total of 33 different tumors. The expression of LIPT1 was significantly decreased in several tumor tissues, including BRCA, CESC, KIRC, KIRP, THCA, UCEC, and KICH. Overexpression of LIPT1 is associated with favorable

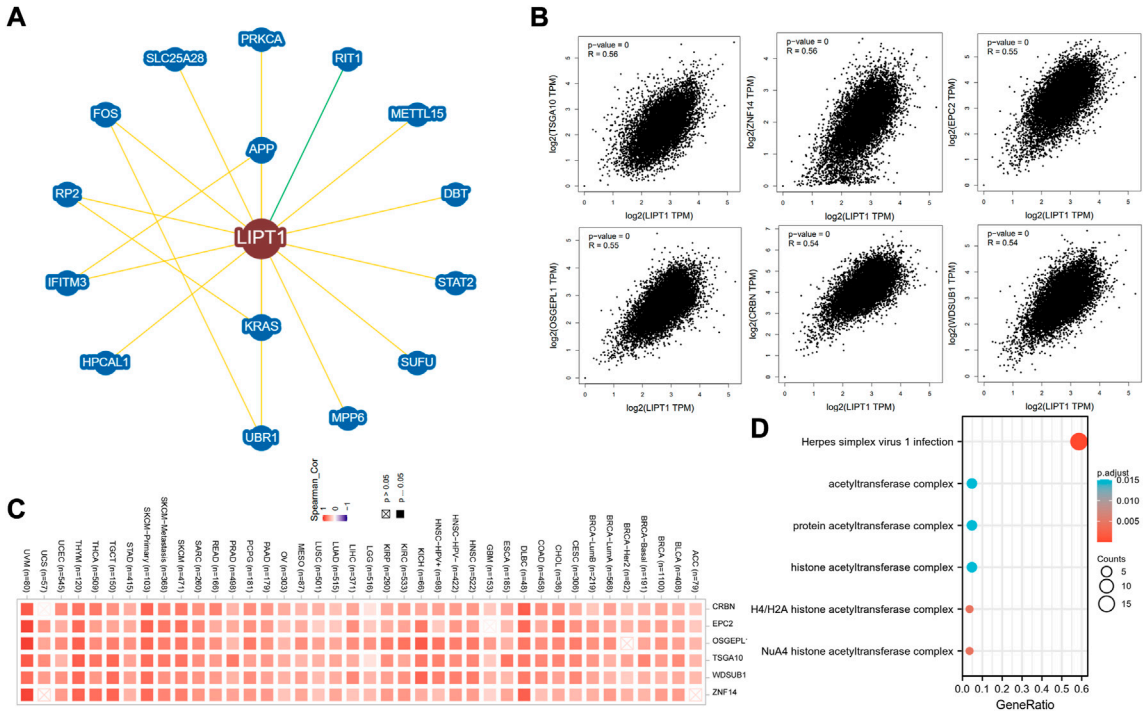

FIGURE 8
Functional enrichment analysis of LIPT1-related genes. **(A)** LIPT1-related genes were obtained from the BioGRID web tool, and 15 proteins were displayed. **(B)** GEPIA2.0 showed the positive correlations between LIPT1 and six genes (TSGA10, ZNF14, EPC2, OSGEPL1, CRBN, and WDSUB1). *p*-value < 0.001. **(C)** The heatmap confirmed that LIPT1 expression was positively correlated with the six genes (TSGA10, ZNF14, EPC2, OSGEPL1, CRBN, and WDSUB1) in pan-cancer. **(D)** GO and KEGG enrichment analyses of LIPT1-related genes.

prognosis in tumor patients, such as breast cancer, clear cell renal cell carcinoma, ovarian cancer, and gastric cancer. In addition, abnormally expressed LIPT1 was significantly associated with immune cells infiltration, such as B cells, $CD8^+$ T cells, and cancer associated fibroblast cells. Therefore, LIPT1 might be a potential prognosis biomarker and immune target for tumor patients.

Copper is a co-factor for important enzymes in all organisms (Kahlson and Dixon, 2022). Unbalanced copper homeostasis affects tumor cell growth, causing irreversible damage (Jiang et al., 2022). Studies showed that copper homeostasis might be regulated by protein lipoylation (Tsvetkov et al., 2022), protein misfolding (Gupta et al., 2022) and DNA damage response (He et al., 2020). Abnormal accumulation of intracellular copper induces a new mode of cell death, copper drooping (Kahlson and Dixon, 2022). The copper homeostasis has been associated with the development and prognosis of patients with various tumors (Feng et al., 2022; Huang et al., 2022; Lei et al., 2022; Li et al., 2022; Wang et al., 2022). As a copper death-related gene, LIPT1 is required for lipoylation and activation of 2-ketoacid dehydrogenases in humans (Tort et al., 2014). LIPT1 genetic alterations, including mutation and deep deletion, cause a variety of human diseases, such as Leigh disease (Soreze et al., 2013) and nonketotic hyperglycinemia with early-onset convulsions (Mayr et al., 2014). However, few studies have established the functional link between LIPT1 and tumorigenesis. Even though LIPT1 has been proved to be upregulated in melanoma (Chen et al., 2021), the detailed roles and underlying mechanisms of LIPT1 in human cancers are unclear and warrant further exploration. Our exploratory findings demonstrated that LIPT1 genetic alterations, including mutation and deep deletion, could be observed in a variety of cancers. At the same time, there were significant differences in LIPT1 methylation levels between tumor tissues and normal tissues. And single cell sequencing and gene enrichment indicated that LIPT1-correlated gene might regulate several cancer biological functions, such as DNA damage response and cell death.

The infiltrating immune cells play essential roles in regulating cancer cell recognition and tumor growth (Shihab et al., 2020; Talty and Olino, 2021). The most well-known function of B cells is to produce antibodies, such as IgM, IgG, IgE, and IgA (Kim et al., 2021). The depleted effector B and T cells could help tumor cells to evade immune surveillance, thereby reducing overall survival in tumor patients (Chakraborty et al., 2022). In this study, we found that LIPT1 expression was strongly correlated with the infiltration of immune cells, including B cell, cancer-

associated fibroblast and $CD8^+$ T cells. These results suggested that LIPT1 could be an effective target for immunotherapy, and provided new hope for clinical treatment of tumor patients. The association between LIPT1 expression and immune checkpoints in cancer patients still needs to be explored in more preclinical and clinical trials.

In conclusion, using comprehensive bioinformatics analysis techniques, we explored the expression levels, clinical prognosis, methylation values, genetic alterations, and immunomodulatory effects of LIPT1 in pan-cancer. The results suggested that LIPT1 may be a novel potential prognostic and immune-associated biomarker for cancer patients. This study lays the foundation for further research on the specific mechanisms of LIPT1 in the development and treatment of different tumors.

Data availability statement

The datasets presented in this study can be found in online repositories. The names of the repository/repositories and accession number(s) can be found in the article/ Supplementary Material.

Author contributions

Acquisition of Data: YL. Analysis and Interpretation of Data: JP. Conception and Design: YY and GL. Writing the Manuscript: YL and YY. All authors contributed to the article and approved the submitted version.

Funding

This study is supported by grants from the National Natural Science Foundation of China (82272659) and the horizontal project (2022, 1 43010100; 2021-021, 1 43010100).

Acknowledgments

All authors thank the GEO and TCGA databases for providing the useful data, and all the bioinformatics tools for data analysis.

Conflict of interest

The authors declare that the research was conducted in the absence of any commercial or financial relationships that could be construed as a potential conflict of interest.

Publisher's note

All claims expressed in this article are solely those of the authors and do not necessarily represent those of their affiliated organizations, or those of the publisher, the editors and the reviewers. Any product that may be evaluated in this article, or claim that may be made by its manufacturer, is not guaranteed or endorsed by the publisher.

Supplementary material

The Supplementary Material for this article can be found online at: https://www.frontiersin.org/articles/10.3389/fgene.2022.1038174/full#supplementary-material

SUPPLEMENTARY FIGURE S1
LIPT1 expression levels and the pathological stages of tumors was analyzed using GEPIA2.0.

SUPPLEMENTARY FIGURE S2
(A-C) Kaplan-Meier plotter tool was used to analyze the effects of LIPT1 expression on the patients' prognosis from breast cancer, ovarian cancer and gastric cancer.

SUPPLEMENTARY FIGURE S3
(A-F) cBioPortal tool was used to explore the effects of LIPT1 mutation on the prognosis of patients from KIRC, SKCM, BLCA, GBM, UCEC, and BRCA, including OS, DSS, DFS, and PFS.

SUPPLEMENTARY FIGURE S4
(A-F) cBioPortal tool was used to explore the effects of LIPT1 mutation on the prognosis of patients from LIHC, stomach and esophageal carcinoma (STES), COAD, HNSC, THCA, and OV, including OS, DSS, DFS, and PFS.

SUPPLEMENTARY FIGURE S5
The methylation values of LIPT1 between normal and primary tumor tissues were analyzed by UALCAN dataset.

SUPPLEMENTARY FIGURE S6
The relationship between LIPT1 expression and immune infiltration of DC, monocyte, Treg, NK, neutrophil, macrophage was depicted by TIMER2.0 database.

SUPPLEMENTARY TABLE S1
The top 100 LIPT1 co-expressed genes in pan-cancer from GEPIA2.0.

References

Chakraborty, S., Khamaru, P., and Bhattacharyya, A. (2022). Regulation of immune cell metabolism in health and disease: Special focus on T and B cell subsets. *Cell Biol. Int.* doi:10.1002/cbin.11867

Chandrashekar, D. S., Karthikeyan, S. K., Korla, P. K., Patel, H., Shovon, A. R., Athar, M., et al. (2022). Ualcan: An update to the integrated cancer data analysis platform. *Neoplasia* 25, 18–27. doi:10.1016/j.neo.2022.01.001

Chen, Y., Xu, T., Xie, F., Wang, L., Liang, Z., Li, D., et al. (2021). Evaluating the biological functions of the prognostic genes identified by the Pathology Atlas in bladder cancer. *Oncol. Rep.* 45 (1), 191–201. doi:10.3892/or.2020.7853

Colwill, K., and Graslund, S.Renewable Protein Binder Working Group (2011). A roadmap to generate renewable protein binders to the human proteome. *Nat. Methods* 8 (7), 551–558. doi:10.1038/nmeth.1607

Edwards, N. J., Oberti, M., Thangudu, R. R., Cai, S., McGarvey, P. B., Jacob, S., et al. (2015). The CPTAC data portal: A resource for cancer proteomics research. *J. Proteome Res.* 14 (6), 2707–2713. doi:10.1021/pr501254j

Feng, A., He, L., Chen, T., and Xu, M. (2022). A novel cuproptosis-related lncRNA nomogram to improve the prognosis prediction of gastric cancer. *Front. Oncol.* 12, 957966. doi:10.3389/fonc.2022.957966

Gao, J., Aksoy, B. A., Dogrusoz, U., Dresdner, G., Gross, B., Sumer, S. O., et al. (2013). Integrative analysis of complex cancer genomics and clinical profiles using the cBioPortal. *Sci. Signal.* 6 (269), pl1. doi:10.1126/scisignal.2004088

Gupta, G., Cappellini, F., Farcal, L., Gornati, R., Bernardini, G., and Fadeel, B. (2022). Copper oxide nanoparticles trigger macrophage cell death with misfolding of Cu/Zn superoxide dismutase 1 (SOD1). *Part. Fibre Toxicol.* 19 (1), 33. doi:10.1186/s12989-022-00467-w

Habarou, F., Hamel, Y., Haack, T. B., Feichtinger, R. G., Lebigot, E., Marquardt, I., et al. (2017). Biallelic mutations in LIPT2 cause a mitochondrial lipoylation defect associated with severe neonatal encephalopathy. *Am. J. Hum. Genet.* 101 (2), 283–290. doi:10.1016/j.ajhg.2017.07.001

He, H., Zou, Z., Wang, B., Xu, G., Chen, C., Qin, X., et al. (2020). Copper oxide nanoparticles induce oxidative DNA damage and cell death via copper ion-mediated P38 MAPK activation in vascular endothelial cells. *Int. J. Nanomedicine* 15, 3291–3302. doi:10.2147/IJN.S241157

He, J., Ding, H., Li, H., Pan, Z., and Chen, Q. (2021). Intra-tumoral expression of SLC7A11 is associated with immune microenvironment, drug resistance, and prognosis in cancers: A pan-cancer analysis. *Front. Genet.* 12, 770857. doi:10.3389/fgene.2021.770857

Huang, X., Zhou, S., Toth, J., and Hajdu, A. (2022). Cuproptosis-related gene index: A predictor for pancreatic cancer prognosis, immunotherapy efficacy, and chemosensitivity. *Front. Immunol.* 13, 978865. doi:10.3389/fimmu.2022.978865

Jiang, Y., Huo, Z., Qi, X., Zuo, T., and Wu, Z. (2022). Copper-induced tumor cell death mechanisms and antitumor theragnostic applications of copper complexes. *Nanomedicine (Lond)* 17 (5), 303–324. doi:10.2217/nnm-2021-0374

Kahlson, M. A., and Dixon, S. J. (2022). Copper-induced cell death. *Science* 375 (6586), 1231–1232. doi:10.1126/science.abo3959

Kim, S. S., Sumner, W. A., Miyauchi, S., Cohen, E. E. W., Califano, J. A., and Sharabi, A. B. (2021). Role of B Cells in responses to checkpoint blockade immunotherapy and overall survival of cancer patients. *Clin. Cancer Res.* 27 (22), 6075–6082. doi:10.1158/1078-0432.CCR-21-0697

Lanczky, A., and Gyorffy, B. (2021). Web-based survival analysis tool tailored for medical research (KMplot): Development and implementation. *J. Med. Internet Res.* 23 (7), e27633. doi:10.2196/27633

Lei, L., Tan, L., and Sui, L. (2022). A novel cuproptosis-related gene signature for predicting prognosis in cervical cancer. *Front. Genet.* 13, 957744. doi:10.3389/fgene.2022.957744

Li, K., Tan, L., Li, Y., Lyu, Y., Zheng, X., Jiang, H., et al. (2022). Cuproptosis identifies respiratory subtype of renal cancer that confers favorable prognosis. *Apoptosis*. doi:10.1007/s10495-022-01769-2

Li, L., Yao, W., Yan, S., Dong, X., Lv, Z., Jing, Q., et al. (2021). Pan-cancer analysis of prognostic and immune infiltrates for CXCs. *Cancers (Basel)* 13 (16), 4153. doi:10.3390/cancers13164153

Li, T., Fu, J., Zeng, Z., Cohen, D., Li, J., Chen, Q., et al. (2020). TIMER2.0 for analysis of tumor-infiltrating immune cells. *Nucleic Acids Res.* 48 (W1), W509–W514. doi:10.1093/nar/gkaa407

Lv, H., Liu, X., Zeng, X., Liu, Y., Zhang, C., Zhang, Q., et al. (2022). Comprehensive analysis of cuproptosis-related genes in immune infiltration and prognosis in melanoma. *Front. Pharmacol.* 13, 930041. doi:10.3389/fphar.2022.930041

Mayr, J. A., Feichtinger, R. G., Tort, F., Ribes, A., and Sperl, W. (2014). Lipoic acid biosynthesis defects. *J. Inherit. Metab. Dis.* 37 (4), 553–563. doi:10.1007/s10545-014-9705-8

Ni, M., Solmonson, A., Pan, C., Yang, C., Li, D., Notzon, A., et al. (2019). Functional assessment of lipoyltransferase-1 deficiency in cells, mice, and humans. *Cell Rep.* 27 (5), 1376–1386. doi:10.1016/j.celrep.2019.04.005

Oughtred, R., Rust, J., Chang, C., Breitkreutz, B. J., Stark, C., Willems, A., et al. (2021). The BioGRID database: A comprehensive biomedical resource of curated protein, genetic, and chemical interactions. *Protein Sci.* 30 (1), 187–200. doi:10.1002/pro.3978

Ren, L., Yi, J., Yang, Y., Li, W., Zheng, X., Liu, J., et al. (2022). Systematic pan-cancer analysis identifies APOC1 as an immunological biomarker which regulates macrophage polarization and promotes tumor metastasis. *Pharmacol. Res.* 183, 106376. doi:10.1016/j.phrs.2022.106376

Shan, L., Lu, Y., Song, Y., Zhu, X., Xiang, C. C., Zuo, E. D., et al. (2022). Identification of nine m6a-related long noncoding RNAs as prognostic signatures associated with oxidative stress in oral cancer based on data from the cancer genome atlas. *Oxid. Med. Cell. Longev.* 2022, 9529814. doi:10.1155/2022/9529814

Shi, X., Zhang, J., Jiang, Y., Zhang, C., Luo, X., Wu, J., et al. (2021). Comprehensive analyses of the expression, genetic alteration, prognosis significance, and interaction networks of m(6)A regulators across human cancers. *Front. Genet.* 12, 771853. doi:10.3389/fgene.2021.771853

Shihab, I., Khalil, B. A., Elemam, N. M., Hachim, I. Y., Hachim, M. Y., Hamoudi, R. A., et al. (2020). Understanding the role of innate immune cells and identifying genes in breast cancer microenvironment. *Cancers (Basel)* 12 (8), E2226. doi:10.3390/cancers12082226

Smith, J., Sen, S., Weeks, R. J., Eccles, M. R., and Chatterjee, A. (2020). Promoter DNA hypermethylation and paradoxical gene activation. *Trends Cancer* 6 (5), 392–406. doi:10.1016/j.trecan.2020.02.007

Soreze, Y., Boutron, A., Habarou, F., Barnerias, C., Nonnenmacher, L., Delpech, H., et al. (2013). Mutations in human lipoyltransferase gene LIPT1 cause a Leigh disease with secondary deficiency for pyruvate and alpha-ketoglutarate dehydrogenase. *Orphanet J. Rare Dis.* 8, 192. doi:10.1186/1750-1172-8-192

Stenstrom, J., Hedenfalk, I., and Hagerling, C. (2021). Regulatory T lymphocyte infiltration in metastatic breast cancer-an independent prognostic factor that changes with tumor progression. *Breast Cancer Res.* 23 (1), 27. doi:10.1186/s13058-021-01403-0

Talty, R., and Olino, K. (2021). Metabolism of innate immune cells in cancer. *Cancers (Basel)* 13 (4), 904. doi:10.3390/cancers13040904

Tang, Z., Li, C., Kang, B., Gao, G., Li, C., and Zhang, Z. (2017). Gepia: A web server for cancer and normal gene expression profiling and interactive analyses. *Nucleic Acids Res.* 45 (W1), W98–W102. doi:10.1093/nar/gkx247

Tao, S., Ye, X., Pan, L., Fu, M., Huang, P., Peng, Z., et al. (2021). Construction and clinical translation of causal pan-cancer gene score across cancer types. *Front. Genet.* 12, 784775. doi:10.3389/fgene.2021.784775

Tort, F., Ferrer-Cortes, X., Thio, M., Navarro-Sastre, A., Matalonga, L., Quintana, E., et al. (2014). Mutations in the lipoyltransferase LIPT1 gene cause a fatal disease associated with a specific lipoylation defect of the 2-ketoacid dehydrogenase complexes. *Hum. Mol. Genet.* 23 (7), 1907–1915. doi:10.1093/hmg/ddt585

Tsvetkov, P., Coy, S., Petrova, B., Dreishpoon, M., Verma, A., Abdusamad, M., et al. (2022). Copper induces cell death by targeting lipoylated TCA cycle proteins. *Science* 375 (6586), 1254–1261. doi:10.1126/science.abf0529

Wang, Y., Zhang, Y., Wang, L., Zhang, N., Xu, W., Zhou, J., et al. (2022). Development and experimental verification of a prognosis model for cuproptosis-related subtypes in HCC. *Hepatol. Int.* doi:10.1007/s12072-022-10381-0

Yu, C. Y., and Mitrofanova, A. (2021). Mechanism-centric approaches for biomarker detection and precision therapeutics in cancer. *Front. Genet.* 12, 687813. doi:10.3389/fgene.2021.687813

Yuan, H., Yan, M., Zhang, G., Liu, W., Deng, C., Liao, G., et al. (2019). CancerSEA: A cancer single-cell state atlas. *Nucleic Acids Res.* 47 (D1), D900–D908. doi:10.1093/nar/gky939

frontiers | Frontiers in Genetics

TYPE Original Research
PUBLISHED 24 October 2022
DOI 10.3389/fgene.2022.998258

OPEN ACCESS

EDITED BY
Qian Wang,
Tai'an City Central Hospital, China

REVIEWED BY
Feng Jiang,
Fudan University, China
Shaonan Hu,
Southern Medical University, China
Xiangqiong Liu,
China Tibetology Research Center, China

*CORRESPONDENCE
Juanqing Yue,
lolayue@foxmail.com

†These authors have contributed equally to this work

SPECIALTY SECTION
This article was submitted to Cancer Genetics and Oncogenomics, a section of the journal Frontiers in Genetics

RECEIVED 19 July 2022
ACCEPTED 05 October 2022
PUBLISHED 24 October 2022

CITATION
Tao X, Huang R, Xu R, Zheng S and Yue J (2022), A novel m7G methylation–related signature associated with chromosome homeostasis in patients with lung adenocarcinoma.
Front. Genet. 13:998258.
doi: 10.3389/fgene.2022.998258

A novel m7G methylation–related signature associated with chromosome homeostasis in patients with lung adenocarcinoma

Xiaoying Tao[1†], Run Huang[2†], Rujun Xu[1], Shuang Zheng[1] and Juanqing Yue[1*]

[1]Department of Pathology, Affiliated Hangzhou First People's Hospital, Zhejiang University School of Medicine, Hangzhou, China, [2]Department of Infectious Diseases, Shanghai Jiao Tong University Affiliated Sixth People's Hospital, Shanghai, China

Lung adenocarcinoma (LUAD) is a malignant tumor of the respiratory system with poor prognosis. Recent studies have revealed that N7-methylguanosine (m7G) methylation is a widespread modification occurring in RNA. But the expression of m7G methylation–related genes in LUAD and their correlations with prognosis are still unclear. In this study, we found 12 m7G methylation–related regulators with differential expression between LUAD and normal lung tissues. According to differentially expressed genes (DEGs), all LUAD cases were separated into two subtypes. The prognostic value of each m7G methylation–related gene for survival was evaluated to construct a multigene signature using The Cancer Genome Atlas (TCGA) cohort. Finally, an m7G methylation–related prognostic signature based on three genes was built to classify LUAD patients into two risk groups. Patients in the high-risk group showed significantly reduced overall survival (OS) when compared with patients in the low-risk group ($p < 0.05$). The receiver operating characteristic (ROC) curve analysis confirmed the predictive capacity of the signature. The Gene Ontology (GO) functional annotation analysis disclosed that chromosome homeostasis plays an important role in this process. The gene set enrichment analysis (ssGSEA) implied that the immune status was decreased in the high-risk group. To sum up, m7G methylation–related genes play a vital role in tumor immunity and the related signature is a reliable predictor for LUAD prognosis.

KEYWORDS

lung adenocarcinoma, m7G methylation, gene signature, chromosome homeostasis, immune station

Introduction

Lung adenocarcinoma (LUAD) is the most common histological type of lung cancer. Despite advances in its pathogenesis and therapeutic approaches, it unfortunately remains one of the most aggressive and fatal tumors with an overall survival (OS) of less than 5 years (Denisenko et al., 2018). Therefore, it is important to understand the underlying molecular mechanisms and develop an accurate prognostic tool to improve the progression of LUAD.

To date, with a large number of RNA modifications, N7-methylguanosine (m7G) has been found to be the most common modification at the 5′ cap of mRNA and exert an important part in the multicellular processes and regulation of mRNA output, translation, transcriptional elongation, and splicing. METTL1/WDR4 has been identified as an m7G writer of mRNA. METTL1 acts as an m7G methyltransferase to install m7G modifications in target mRNAs, while WDR4 facilitates the binding of heterodimeric complexes to target mRNAs (Zhang et al., 2019a). Accumulating evidence point to the critical role of m7G in human disease development, especially cancer, and aberrant m7G levels are closely related to tumorigenesis and progression by regulating the expression of multiple oncogenes and tumor suppressor genes (Luo et al., 2022). Interestingly, various studies to date have shown that m7G modulators play different roles in different types of tumors. METTL1/WDR4 is the core regulator of m7G modification and exerts a powerful oncogenic role in acute myeloid leukemia (AML) (Orellana et al., 2021), bladder cancer (BC) (Ying et al., 2021), esophageal squamous cell carcinoma (ESCC) (Han et al., 2022), glioma (Li et al., 2021a), hepatocellular carcinoma (HCC) (Tian et al., 2019; Chen et al., 2021; Xia et al., 2021), head and neck squamous cell carcinoma (HNSCC) (Chen et al., 2022), etc., promoting the malignant phenotype and progression of tumors. However, a recent study investigated the functions of m7G regulators WBSCR22 and TRMT112 in pancreatic cancer (PC) and found that WBSCR22 was downregulated in PC samples when compared with adjacent normal pancreatic tissue and WBSCR22 cooperates with TRMT112 to exert a tumor suppressor effect in PC, associated with longer survival of patients (Khan et al., 2022).

Although evidence shows RNA modifications are critical to the development and progression of LUAD, few researchers have systematically explored the relationship between m7G methylation and LUAD. In this study, we systematically assessed the prognostic value of m7G regulatory genes for LUAD patients. The expression profiles and clinical information were obtained from the TCGA database. Additionally, online databases such as the R software package were used for bioinformatics analysis to study the characteristics of m7G regulatory factors. Besides, we assessed the association of the prognostic model based on m7G regulatory genes with survival outcomes, immune-related pathways, and immune cell infiltration. We found that m7G was involved in several aspects of LUAD, such as the formation of tumor microenvironment (TME). A better understanding of m7G modifications makes it possible to develop more effective personalized treatment strategies for LUAD.

Materials and methods

Data sets

In this study, we downloaded the RNA sequencing information and the corresponding clinical characteristics of LUAD patients from the TCGA database (https://portal.gdc.cancer.gov/), which included 535 tumors and 59 normal tissues (Cancer Genome Atlas Research Network and others, 2014; Campbell et al., 2016). The expression data sets could be normalized by fragment per kilobase million (FPKM) scores.

Identifying differentially expressed m7G methylation–related genes

We curated a total of 29 m7G methylation–related genes (Supplementary Table S1) by reviewing previous literature (Tomikawa, 2018; Rong et al., 2021; Wiener and Schwartz, 2021). These m7G methylation–related genes were studied using the Search Tool for the Retrieval of Interacting Genes (STRING). Using the "limma" R package, we identified differentially expressed m7G methylation–related genes among tumor and normal tissues with a false discovery rate (FDR) within 0.05 and $|\log FC| > 0.5$.

Development and validation of m7G methylation–related gene signature

The consensus cluster method was adopted to construct the consensus matrix according to the expression levels of the differentially expressed genes (DEGs). We evaluated clustering results with K values ranging from 2 to 9 in order to determine the optimal clustering results. A univariate Cox study of the OS was used to screen DEGs using prognostic values [adjusted p-value <0.05; p-values were adjusted using Benjamini and Hochberg (BH) correction]. Then, the DEGs with prognostic values were applied to construct a signature in prognostic prediction. By combining standard expressions of every gene and its relevant regression coefficients, the risk scores were calculated as follows:

$$\text{Risk Score} = \sum_{i=1}^{n} Coef\,i \times xi.$$

LUAD in TCGA could be regulated as two risk groups (high/low) based on the median value of the risk score. According to the gene expression in this signature, the principal component

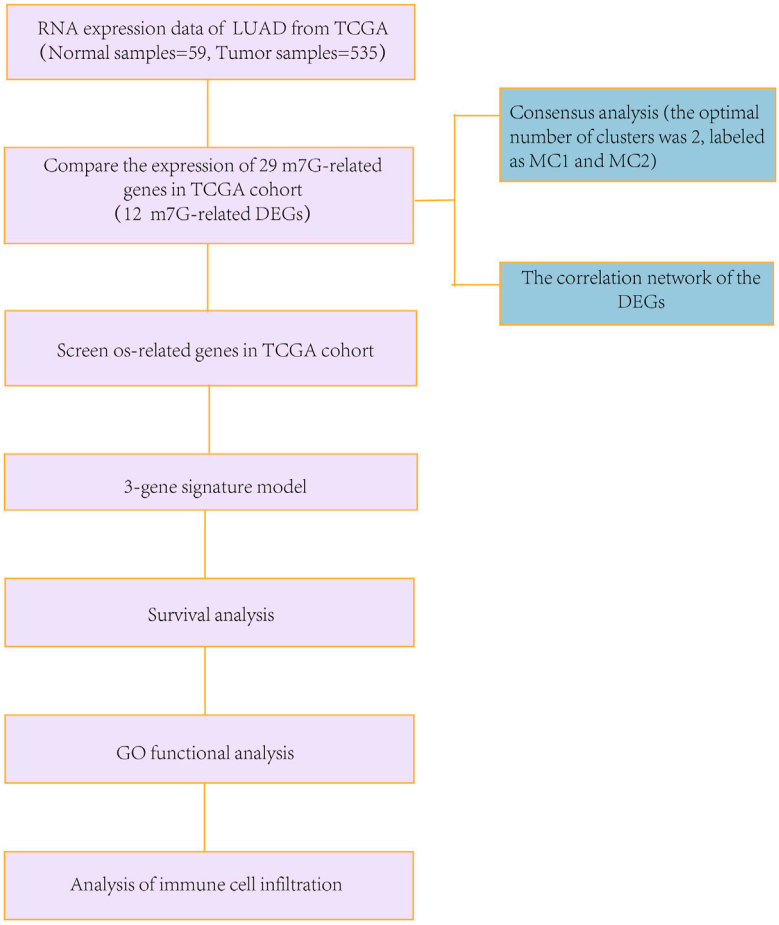

FIGURE 1
Detailed workflow of the flowchart for data analysis.

analysis (PCA) was conducted by means of the "prcomp" function of the R statistical package. The prognostic model of genes was assessed by the time-dependent receiver operating characteristic (ROC) profile analyses *via* the "survivalROC" R package. The nomogram was built by combining age, gender, risk scores, and pathology stages to forecast the living possibility of LUAD patients after 3 and 5 years. The Decision Curve Analysis (DCA) was carried out to evaluate the clinical implications of the prediction model.

Gene Ontology functional and immune analysis of differentially expressed genes among low- and high-risk groups

As aforementioned, LUAD patients were regulated as two risk groups based on the median value. The DEGs among the high-risk and low-risk groups could be determined with $|\log2FC| \geq 1$ and FDR <0.05. The GO annotation analysis of DEGs was achieved with an adjusted p-value < 0.05. Accumulating evidence have confirmed that tumor infiltrating immune cells were involved in cancer progression and correlated with the outcomes. Therefore, ssGSEA was used to estimate the permeation values for immunization-related cells and analyze the activity of immunization-related pathways. Supplementary Table S2 provides these annotated gene set files. Meanwhile, we conducted correlation analysis between immune cells and immune functions and between genes for signature construction and immune cells and immune function. Furthermore, we evaluated the infiltration level of immune cells between the high-risk and low-risk groups by using CIBERSORT, CIBERSORT-ABS, quanTIseq, MCP-counter, xCell, TIMER, and EPIC algorithms.

Statistical analysis

To compare the standards of gene expression among normal and LUAD tissues, a single-factor analysis of variance was used,

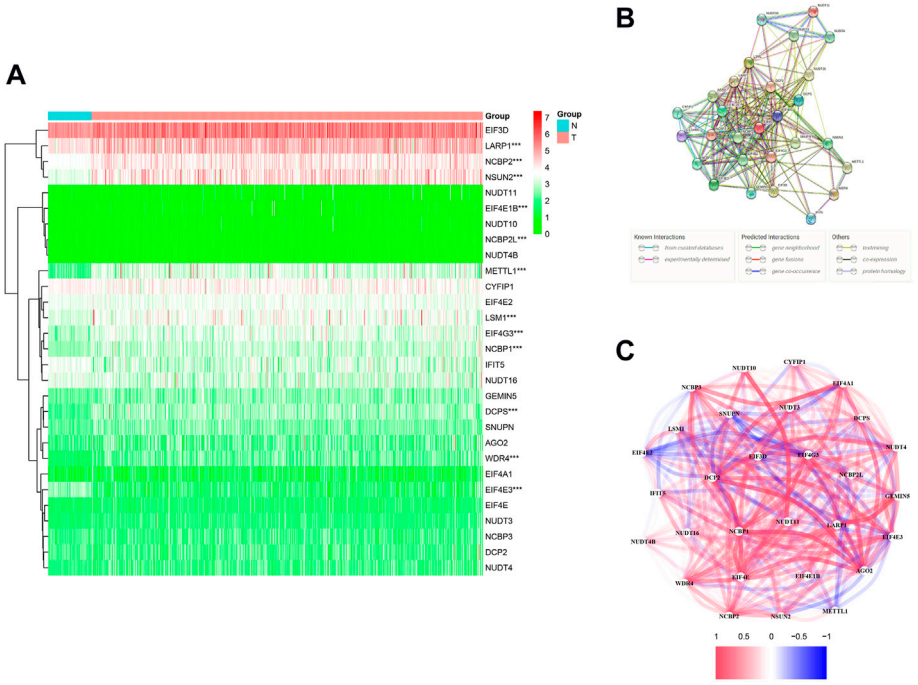

FIGURE 2
Expression and interaction of 29 m7G methylation–related genes. **(A)** Heatmap (green: low expression; red: high expression) of m7G methylation–related genes between normal (N, bright blue) and tumor (T, pink) tissue in the TCGA LUAD queue. **(B)** PPI network shows interactions of all m7G methylation–related genes. **(C)** Correlation network of all m7G methylation–related genes (red: positive relevance; blue: negative relevance. The shade of color reflects the strength of the correlation). *$p < 0.05$, **$p < 0.01$; * * *$p < 0.001$.

and the Pearson's Chi-square test was used to contrast the classified variances. Nomogram was constructed with the "RMS" R package. BH-adjusted Mann–Whitney tests were conducted to compare the ssGSEA scores between the high- and low-risk subgroups of immune cells or pathways. Kaplan–Meier analysis using log-rank tests were used to contrast the OS among different groups. Data analyses were carried out using the R software (v. 4.1.2). The flowchart is shown in Figure 1.

Results

m7G methylation–related differentially expressed genes in The Cancer Genome Atlas lung adenocarcinoma queue

We identified 12 m7G-related DEGs (FDR < 0.05) by comparing the expression levels of all m7G methylation–related genes in LUAD tissues (n = 535) with normal tissues (n = 59) in the TCGA database. The mRNA levels of all m7G methylation–related genes are presented as heatmaps (Figure 2A). The protein–protein interaction (PPI) network and gene correlation network showed the interaction relationships of all m7G methylation–related genes (Figures 2B,C).

Construction of three m7G methylation–related prognostic model in The Cancer Genome Atlas queue

We performed a consensus clustering analysis of all 535 LUAD from the TCGA cohort to investigate the relationship among expressions of 12 m7G methylation–related DEGs and the subtypes of LUAD. Adding the clustering variable (k) from 2 to 9, when k = 2, showed the highest intragroup relevance and the lowest intergroup relevance, hinting that the optimal number of clusters was two, defined as MC1 and MC2 (Figures 3A–C). The profile of the DEG expressions and clinical features such as age (≤60 or >60 years), the degree of cancer stage (stages 1–4), and living status (alive or dead) are shown in the heatmap (Figure 3D). The univariate Cox regression analysis identified three DEGs that were correlated with the OS, namely, LARP1, NCBP1, and WDR4 (Figure 4A). Therefore, these three DEGs were used to construct the risk model. Further multivariate Cox proportional hazards

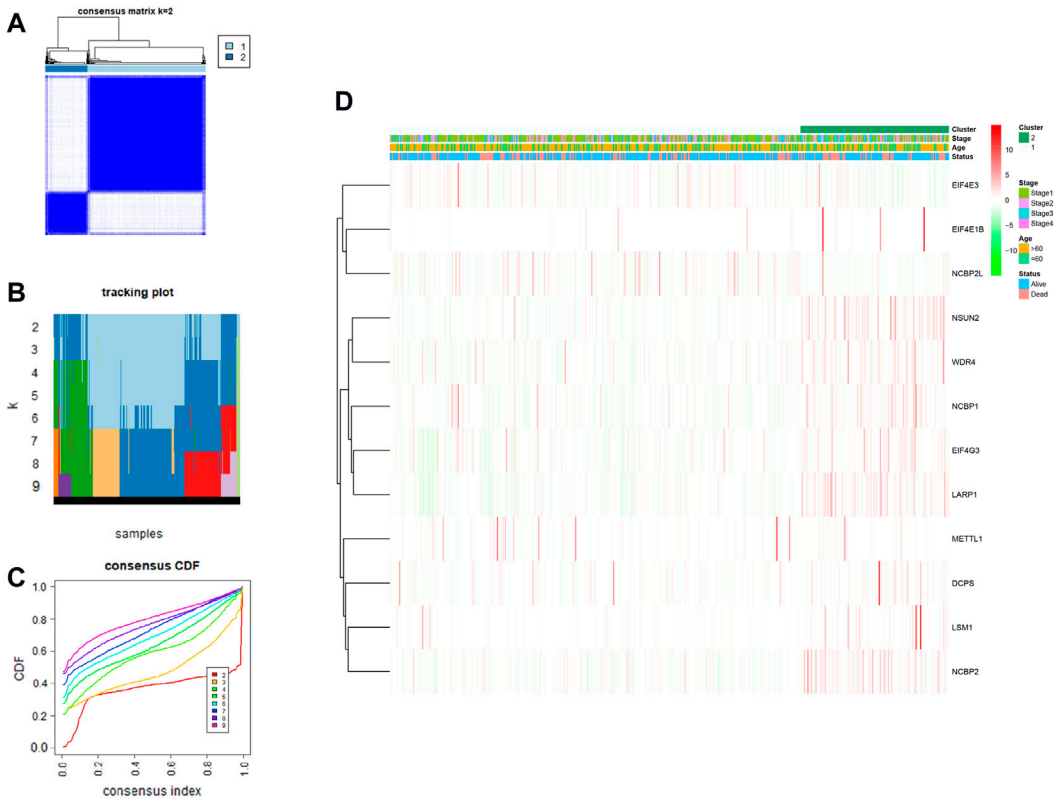

FIGURE 3
LUAD classification according to m7G methylated–associated DEGs. **(A–C)** Consensus clustering algorithm applied to cluster LUAD samples in the TCGA database. The best number of clusters was two, which are defined as MC1 and MC2, respectively. **(D)** Heatmap and clinicopathological characteristics of two clusters.

analysis suggested that all the three DEGs were related to increasing risk with HRs >1 (Supplementary Table S3). The formula used for risk value calculation is risk value = (0.0113 × LARP1 exp.) + (0.0255 × NCBP1 exp.) + (0.0817 × WDR4 exp.). The LUAD patients in the TCGA were separated into the high-risk group (n = 262) or low-risk group (n = 248) with a middle score (Figure 4B). The PCA showed that the different risk groups could be well divided into two clusters (Figure 4C), and patients in the high-risk group survived less and lived shorter than did those in the low-risk group. Consistently, the Kaplan–Meier profile indicated that the OS time difference between the low- and high-risk groups was statistically significant, and the high-risk group had worse OS than their low-risk counterparts (Figures 4D,E). Time-dependent ROC analysis was performed, and the area under the ROC curve (AUC) was 0.623, 0.639, and 0.607 for a 1-, 2-, and 3-year survival, respectively (Figure 4F). The clinicopathologic features, along with the associated risk groups, were mapped using a heatmap (Figure 4G). The nomogram was constructed for forecasting the 3- and 5-year living probability of LUAD patients (Figure 5A). The DCA for the 3- and 5-year prediction of m7G-related gene signature nomogram is illustrated in Figures 5B,C.

Functional analysis according to risk model

DEGs among low- and high-risk groups could be extracted by applying the "limma" R package with standards—FDR < 0.05 and | log2FC | ≥ 1. In total, there were 430 DEGs identified (the data are shown in Supplementary Table S4). The results of the GO analysis indicated that the DEGs were mainly enriched for chromosomal activity and homeostasis (Figure 6A). For exploring the relationships among the risk levels and the immune status in LUAD, the ssGSEA was used to compare the enrichment fractions of 16 kinds of immune cells and the activities of 13 kinds of immune-related pathways in the TCGA database. Interestingly, the low-risk subgroup had higher standards of aDCs, DCs, and iDCs, as did the mast cells. The HLA and type-2 IFN reaction pathway indicated higher activity in the low-risk group, while on the contrary, the MHC class-1 pathway showed

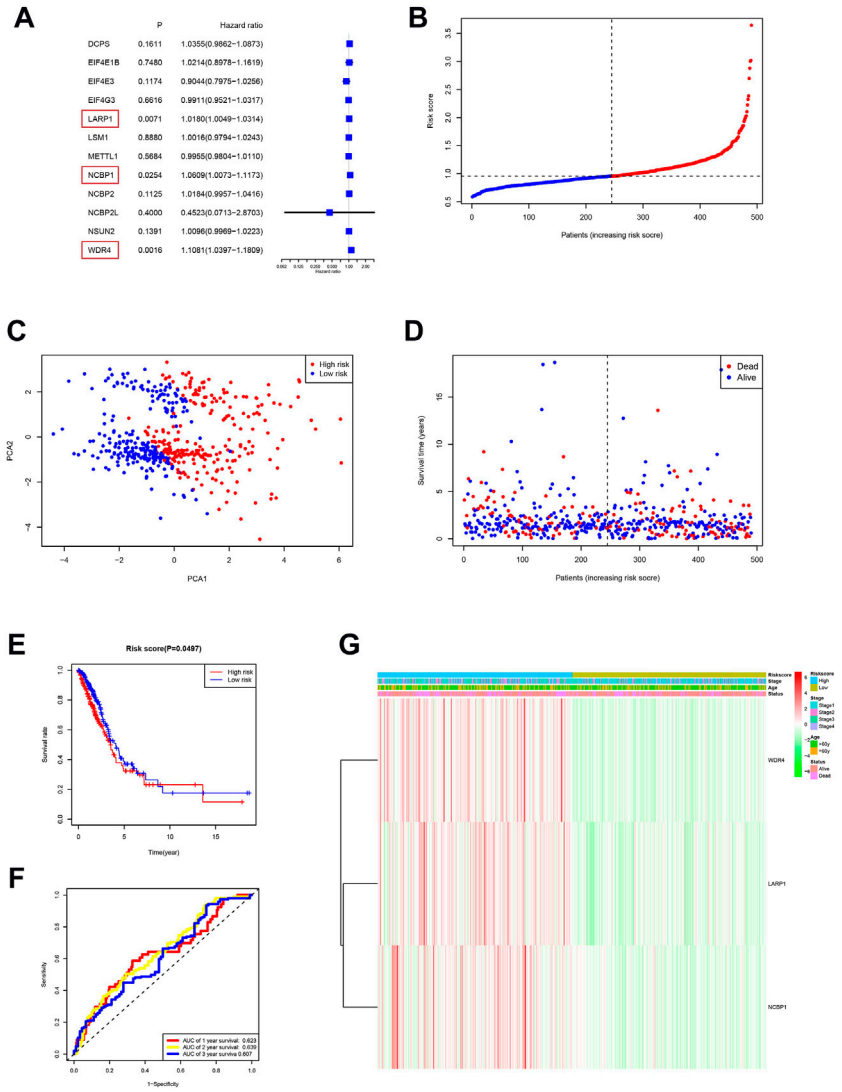

FIGURE 4
Risk signature establishment of the TCGA queue. **(A)** Single-variable Cox regression study of 12 m7G methylation–related DEGs and three genes with $p < 0.05$. **(B)** Patient distribution on the basis of risk score. **(C)** PCA diagram of LUADs on the basis of risk score. **(D)** Living situation of every patient (low-risk population: left dotted line; high-risk groups: right dotted line). **(E)** Kaplan–Meier survival analysis for patients with high- and low-risk groups. **(F)** ROC profile showing the forecasting power of risk scores. **(G)** The relationship among clinicopathological characteristics and risk groups is visualized with heatmaps (green: low expression; red: high expression).

higher activity in the high-risk group (Figures 6B,C). Tumor-infiltrating lymphocytes (TILs) and plasmacytoid dendritic cells (pDCs) had the highest correlation in the LUAD immune microenvironment with an R value of 0.86; the mast cells and Tfh were negatively correlated with an R value of −0.04 (Figure 6D). Immune checkpoints and T-cell coinhibition pathways showed the highest positive correlation with an R value of 0.9 (Figure 6E). *WDR4*, *LARP1*, and *NCBP1* were inversely correlated with most immune cells and immune functions (Figure 6F). The relationship between the signature and immune infiltration is displayed in the heatmap according to the analyses of TIMER, CIBERSORT, CIBERSORT-ABS, xCELL, quanTIseq, EPIC, and MCP-counter (Figure 7). The result of CIBERSORT indicated that the proportions of myeloid dendritic cells and active mast cells were higher in the low-risk group, whereas the proportion of neutrophils was higher in the high-risk group.

Discussion

As the most common histological subtype of lung cancer, LUAD results in a severe incidence rate and death rate (Bray

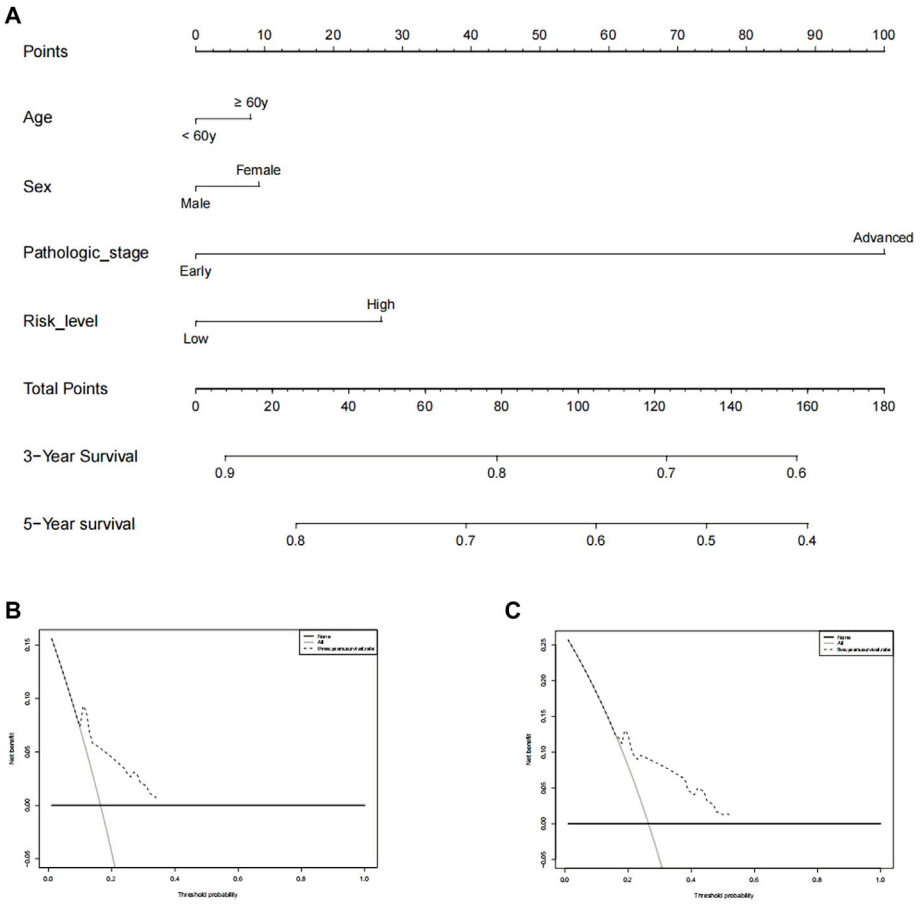

FIGURE 5
Prediction of 3- and 5-year survival probabilities for nomogram LUAD patients. **(A)** An upward line is drawn from these values to a "score" line based on age (≥60 or <60 years), sex, pathological stage (early stages include stages 1 and 2, advanced stages include stages 3 and 4), and risk levels. Points are calculated by drawing an upward vertical line on the "points" column. Adding these "points" gives the "total point" and a vertical line is drawn down from the "total point" line to count the 3-year and 5-year living probabilities. **(B,C)** Decision curve analysis of multi-Cox models for 3 and 5 years, respectively.

et al., 2018). In this study, we have shown the mRNA standards of 29 m7G methylation–related genes in LUAD tissues and found that 12 of them were differentially expressed when compared with normal tissues. In order to further evaluate the prognostic value of the m7G methylation–related regulators, we used Cox univariate analysis and finally constructed a three-gene risk signature.

m7G is a substantially positively charged modification on the 5′ cap of eukaryotic mRNA and also appears at defined internal locations of tRNA and rRNA (Malbec et al., 2019). In humans, m7G is catalyzed and set up *via* a complex composed of methyltransferase-like 1/WD repeat domain 4 (METTL1/WDR4) (Boulias and Greer, 2019). METTL1 serves as the m7G catalyzing enzyme but WDR4 acts as a stabilizer (Boulias and Greer, 2019; Zeng et al., 2021). Growing evidence indicates that a variety of disorders and tumors are associated with disturbances in RNA transcriptional modification and translational control (Bray et al., 2018; Obeng et al., 2019). It has been proposed that mutation in *WDR4* causes a unique microcephaly primitive dwarfism by impairing tRNA m7G46 methylation (Shaheen et al., 2015). Recently, increasing evidence have shown that *WDR4* plays a vital role in the occurrence and progression of tumors. An analysis of human pan-cancer based on TCGA, GTEx, and CCLE databases has revealed that except for the TCGA kidney chromophobe cohort, *WDR4* is continually upregulated in most cancer types. Besides, a higher expression level of *WDR4* is an adverse factor in many kinds of cancers, such as LUAD. More crucially, a link between *WDR4* and immune infiltration suggests *WDR4* as a target for immunotherapy in cancer (Zeng et al., 2021).

Accumulating evidence have verified that *WDR4* expression increased the m7G methylation level in tumors, promoting tumor cell proliferation and progression, such as in

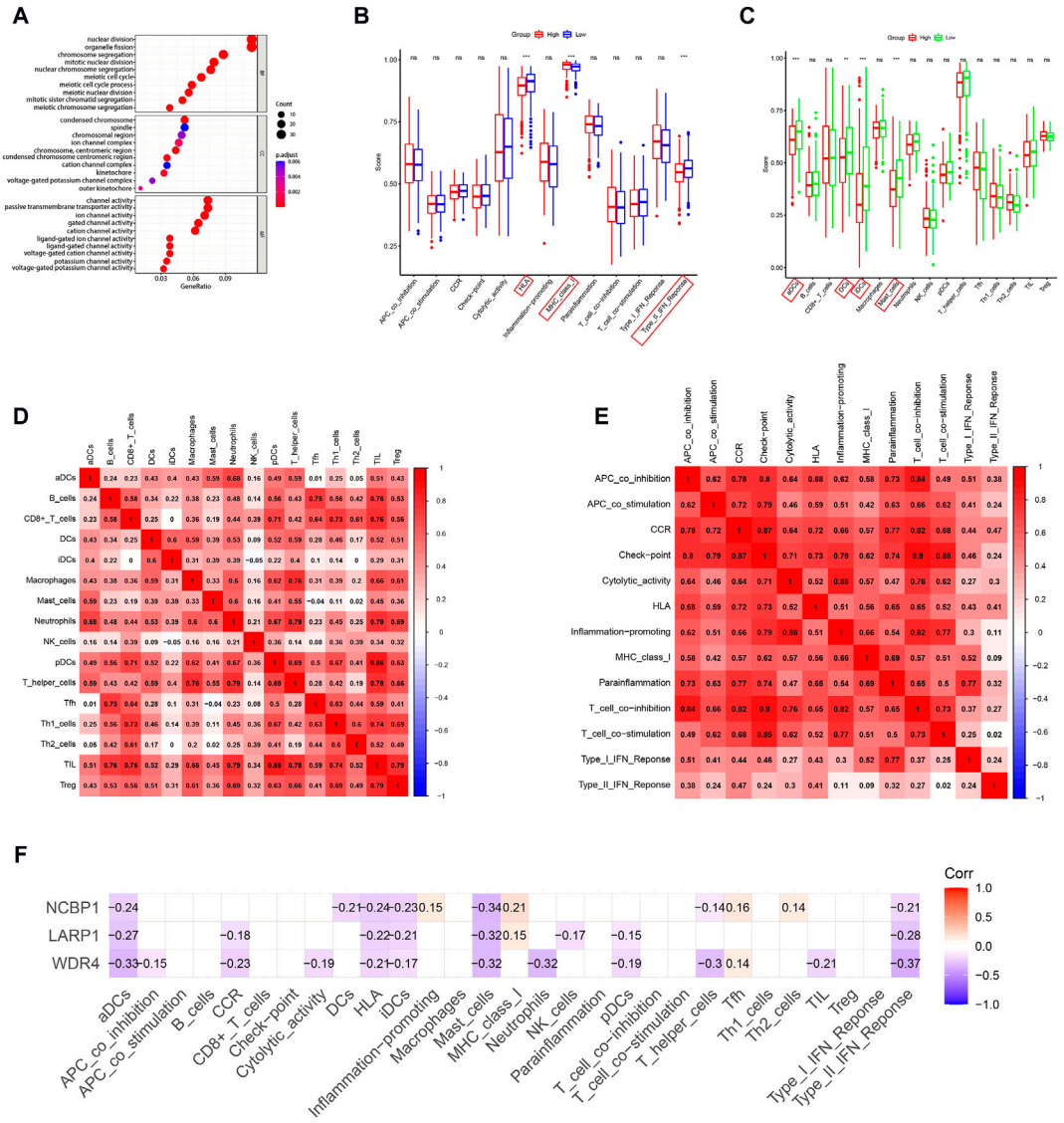

FIGURE 6
GO and immune analyses according to DEGs among two risk groups in the TCGA queue. **(A)** Bubble graph for GO functional annotation analysis (the smaller bubble means fewer genes are enriched, and the increasing depth of red means the differences are more obvious). **(B)** By contrast, enrichment fractions of 16 kinds of immune cells in the low- (bule box) and high-risk (red box) groups. **(C)** By contrast, enrichment values of 13 immune-related pathways among low-risk (green box) and high-risk (red box) groups. Correlations between **(D)** immune cells and **(E)** immune functions in LUAD patients. **(F)** Correlation analysis of *WDR4*, *LARP1*, and *NCBP1* with immune cells and immune function. *$p < 0.05$; **$p < 0.01$; ***$p < 0.001$.

hepatocellular carcinoma (HCC) (Xia et al., 2021) and neck squamous cell carcinoma (Chen et al., 2022). In addition, *WDR4* can enhance HCC metastasis and chemoresistance by epithelial–mesenchymal transition (EMT) (Xia et al., 2021). Importantly, a study by Ma et al. (2021) observed that in lung cancer samples of humans, *METTL1* and *WDR4* expression levels were significantly raised and negatively related to patient outcomes. Moreover, *METTL1* or *WDR4* depletion inhibited proliferation and invasion, as well as *in vivo* tumor growth of lung cancer cells. Their findings uncovered the oncogenic role of *METTL1/WDR4*-mediated m7G tRNA modification in lung cancer. The conclusions from these prior studies are consistent with the result that high expression levels of *WDR4* are connected with bad clinical outcomes of LUAD, such as in our study.

La-associated protein 1 (LARP1) is an m7G cap-binding protein, belonging to the LARP family and most widely studied RNA-binding protein (RBP) family (Cockman et al., 2020). We

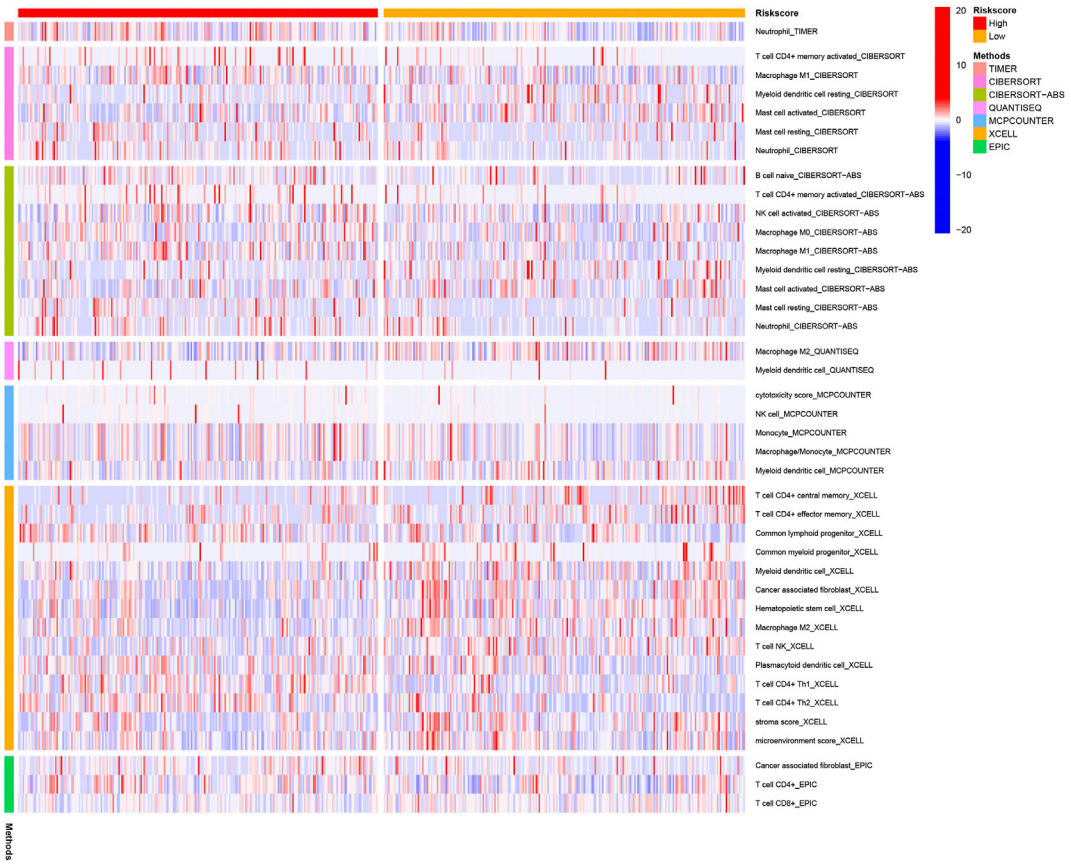

FIGURE 7
Immune cells' infiltration between high-risk and low-risk groups based on seven kinds of analyses.

found that LARP1 has a highly conserved DM15 region. Crystallographic studies have shown DM15 regionally binds 7-methylguanosine 5′-5′ triphosphate (m7Gppp) partial and terminal oligopyrimidine (TOP) mRNA-invariant first cytidine (Lahr et al., 2017). *LARP1* has attracted much attention in recent years due to its effect on the mTOR signaling cascade and TOP mRNA translation. These results suggest opportunities for further pharmacological development. However, the role of LARP1 in this process is controversial. Some scientists believe that LARP1 inhibits TOP translation, while others believe otherwise (Hong et al., 2017; Cassidy et al., 2019). Previous studies have found that LARP1 is overexpressed in most epithelial malignancies, and its expression level is correlated with clinical outcomes. The study by Xie et al. (2013)found that high levels of LARP1 protein in HCC tumor tissues were associated with decreased survival time and an increased risk of 5-year death, tumor size, and Child–Pugh score. These results are consistent with other malignant tumors, such as intrahepatic cholangiocarcinoma (Jiang et al., 2018), cervical cancer (Mura et al., 2015), and ovarian cancer (Hopkins et al., 2016). Importantly, there are some studies on LARP1 and LUAD. A study by Han et al. (2018) found that circ-BANP facilitates lung cancer cell living, proliferation, migration, and invasion by targeting miR-503/*LARP1*. Similarly, Xu et al. (2017) found that in contrast to normal control cells, non–small-cell lung cancer (NSCLC) cells had higher mRNA levels of LARP1. The knockout of LARP1 in NSCLC cells can inhibit cell proliferation, migration, invasion, and tumorigenesis. In further studies, LARP1 was found to be the target of miR-374A. Meanwhile, according to the study (Xu et al., 2017), the XIST/miR-374A/*LARP1* axis is associated with lung cancer. In keeping with previous findings, we found that in LUAD tissues, LARP1 was upregulated, and its high expression means unfavorable living outcomes, showing it has the function of a proto-oncogene. There is a consensus in these studies that LARP1 exerts a key part in LUAD progression and may be a valuable therapeutic strategy. However, whether/how LARP1 participates in LUAD promotion by m7G methylation has not been investigated before and is worthy of further exploration.

Nuclear cap-binding protein subunit 1 (NCBP1) is a kind of heterodimer of nuclear cap-binding proteins, which along with NCBP2 and NCBP3 constitute the nuclear cap-binding complex

(CBC), an important player in the RNA posttranscriptional regulation mechanism (Gebhardt et al., 2015; Dou et al., 2020). It was first discovered that CBC bound to the m7G 'cap structure' of the new transcription mRNA and controlled downstream RNA biological parent in HeLa cells (Izaurralde et al., 1994; Izaurralde et al., 1995). However, not much is considered as part of *NCBP1* in tumors. *NCBP1* silencing has been reported to suppress the growth of HeLa cells (Gebhardt et al., 2015). In a recent study, it was shown that downregulation of *NCBP1* reduced the proliferation and migration of LUAD cells, while overexpression of *NCBP1* did the opposite (Zhang et al., 2019b). This is consistent with our analysis, the expression of *NCBP1* is positively associated with patient risk, accompanying a poor prognosis. Mechanistically, they found cullin *4B* (*CUL4B*) could be a downstream target gene of *NCBP1* in NSCLC. Unfortunately, this study did not explore whether *NCBP1* affects LUAD cell proliferation through the mechanism of m7G methylation, which needs to be further verified (Zhang et al., 2019b). Our study may provide some insights for further research.

It is becoming increasingly apparent that the degree of malignancy of cancer is jointly determined by its intrinsic characteristics and the TME (Joyce and Fearon, 2015; Jiang et al., 2021; Jiang et al., 2022). TMEs, which include B lymphocytes, T lymphocytes, dendritic cells (DCs), natural killer (NK) cells, and macrophages, influence both the expression of tumor cells and clinical course of cancer (Binnewies et al., 2018; Li et al., 2021b). According to the DEGs among distinct risk groups, we conducted ssGSEA to compare the immunity of the two risk subgroups and unexpectedly discovered that the low-risk group in the TCGA queue had higher fractions of mast cells and DCs. Takahashi et al. (2016) illustrated the beneficial influence of the DC vaccine on the OS in 260 advanced NSCLC patients, suggesting a possible clinical benefit of DCs. However, few research studies have been concerned with the relationship between LUAD and DCs. In this study, we found that high infiltration of DCs was correlated to the low risk of LUAD, which indicates a good prognosis in lung cancer patients, suggesting a therapeutic advantage of activating DCs in the TME. Similarly, high mast cell infiltration has been reported as an indicator of good prognosis in NSCLC, independent of the tumor stage, which can be an explanation for mast cells having had high infiltration in low-risk groups of this study. In our study, we found that a high-risk level was associated with impaired antitumor immunity, containing type II interferon reaction, as well as HLA. In summary, based on this study and our analysis of immunity, we speculate that m7G methylation regulates the immune microenvironment of tumors and poor prognosis in high-risk patients may be related to the weakened antitumor immune ability.

There are few studies on methylation of m7G in tumors, especially on the mechanism of methylation in LUAD. Our research has shown three m7G methylation–related genes in LUAD and preliminarily assessed prognostic value of m7G methylation–related genes. Additionally, a conceptual framework for further investigation is also provided. However, due to the lack of data, we are still unable to clarify the role of these regulatory factors in the m7G methylation pathway in LUAD, and this issue needs further research.

Conclusion

In summary, this study demonstrates that m7G methylation–related genes are closely connected to LUAD. Moreover, it provides a novel three-gene signature (*WDR4*, *LARP1*, and *NCBP1*) for forecasting LUAD prognosis. M7G modification plays an important role in a variety of tumors, showing great potential in clinical diagnosis and treatment. Its role in chemotherapy resistance and TME remodeling suggests that targeting dysfunctional m7G sites through posttranscriptional editing is combined with chemotherapy or immunotherapy, which makes it possible to obtain better treatment results in the future. m7G modification is a research topic that is still in its preliminary stage, and the important role of m7G in tumor progression and its value in clinical pathology provide potential ideas for the clinical management and treatment of LUAD.

Data availability statement

The original contributions presented in the study are included in the article/Supplementary Material; further inquiries can be directed to the corresponding author.

Author contributions

XT and RH performed the research study, analyzed the data, and wrote the manuscript. RX and SZ downloaded the patient data. JY conceived and designed the study. All authors contributed to the article and approved the submitted version.

Funding

This study was supported by the Medical and Health Technology Project of Hangzhou (A20220598).

Acknowledgments

We want to thank and acknowledge patients and families affected by LUAD for their generous contributions to these studies. And we would like to acknowledge The Cancer Genome Atlas (TCGA) database for providing data.

Conflict of interest

The authors declare that the research was conducted in the absence of any commercial or financial relationships that could be construed as a potential conflict of interest.

Publisher's note

All claims expressed in this article are solely those of the authors and do not necessarily represent those of their affiliated organizations, or those of the publisher, editors, and reviewers. Any product that may be evaluated in this article, or claim that may be made by its manufacturer, is not guaranteed or endorsed by the publisher.

Supplementary material

The Supplementary Material for this article can be found online at: https://www.frontiersin.org/articles/10.3389/fgene.2022.998258/full#supplementary-material

References

Binnewies, M., Roberts, E. W., Kersten, K., Chan, V., Fearon, D. F., Merad, M., et al. (2018). Understanding the tumor immune microenvironment (TIME) for effective therapy. *Nat. Med.* 24 (5), 541–550. doi:10.1038/s41591-018-0014-x

Boulias, K., and Greer, E. L. (2019). Put the pedal to the METTL1: Adding internal m(7)G increases mRNA translation efficiency and augments miRNA processing. *Mol. Cell* 74 (6), 1105–1107. doi:10.1016/j.molcel.2019.06.004

Bray, F., Ferlay, J., Soerjomataram, I., Siegel, R. L., Torre, L. A., and Jemal, A. (2018). Global cancer statistics 2018: GLOBOCAN estimates of incidence and mortality worldwide for 36 cancers in 185 countries. *Ca. Cancer J. Clin.* 68 (6), 394–424. doi:10.3322/caac.21492

Campbell, J. D., Alexandrov, A., Kim, J., Wala, J., Berger, A. H., Pedamallu, C. S., et al. (2016). Distinct patterns of somatic genome alterations in lung adenocarcinomas and squamous cell carcinomas. *Nat. Genet.* 48 (6), 607–616. doi:10.1038/ng.3564

Cancer Genome Atlas Research Network and others (2014). Comprehensive molecular profiling of lung adenocarcinoma. *Nature* 511 (7511), 543–550. doi:10.1038/nature13385

Cassidy, K. C., Lahr, R. M., Kaminsky, J. C., Mack, S., Fonseca, B. D., Das, S. R., et al. (2019). Capturing the mechanism underlying TOP mRNA binding to LARP1. *Structure* 27 (12), 1771–1781. doi:10.1016/j.str.2019.10.006

Chen, Z., Zhu, W., Zhu, S., Sun, K., Liao, J., Liu, H., et al. (2021). METTL1 promotes hepatocarcinogenesis via m(7) G tRNA modification-dependent translation control. *Clin. Transl. Med.* 11 (12), e661. doi:10.1002/ctm2.661

Chen, J., Li, K., Wang, X., Ling, R., Cheng, M., et al. (2022). Aberrant translation regulated by METTL1/WDR4-mediated tRNA N7-methylguanosine modification drives head and neck squamous cell carcinoma progression. *Cancer Commun.* 42 (3), 223–244. doi:10.1002/cac2.12273

Cockman, E., Anderson, P., and Ivanov, P. (2020). TOP mRNPs: Molecular mechanisms and principles of regulation. *Biomolecules* 10 (7), E969. doi:10.3390/biom10070969

Denisenko, T. V., Budkevich, I. N., and Zhivotovsky, B. (2018). Cell death-based treatment of lung adenocarcinoma. *Cell Death Dis.* 9 (2), 117. doi:10.1038/s41419-017-0063-y

Dou, Y., Kalmykova, S., Pashkova, M., Oghbaie, M., Jiang, H., Molloy, K. R., et al. (2020). Affinity proteomic dissection of the human nuclear cap-binding complex interactome. *Nucleic Acids Res.* 48 (18), 10456–10469. doi:10.1093/nar/gkaa743

Gebhardt, A., Habjan, M., Benda, C., Meiler, A., Haas, D. A., Hein, M. Y., et al. (2015). mRNA export through an additional cap-binding complex consisting of NCBP1 and NCBP3. *Nat. Commun.* 6, 8192. doi:10.1038/ncomms9192

Han, H., Yang, C., Ma, J., Zhang, S., Zheng, S., Ling, R., et al. (2022). N(7)-methylguanosine tRNA modification promotes esophageal squamous cell carcinoma tumorigenesis via the RPTOR/ULK1/autophagy axis. *Nat. Commun.* 13 (1), 1478. doi:10.1038/s41467-022-29125-7

Han, J., Zhao, G., Ma, X., Dong, Q., Zhang, H., Wang, Y., et al. (2018). CircRNA circ-BANP-mediated miR-503/LARP1 signaling contributes to lung cancer progression. *Biochem. Biophys. Res. Commun.* 503 (4), 2429–2435. doi:10.1016/j.bbrc.2018.06.172

Hong, S., Freeberg, M A, Han, T, Kamath, A, Yao, Y, Fukuda, T, Suzuki, T, Kim, J K, et al. (2017). LARP1 functions as a molecular switch for mTORC1-mediated translation of an essential class of mRNA, *Elife*, 6,:e25237. doi:10.7554/eLife.25237

Hopkins, T. G., Mura, M., Al-Ashtal, H. A., Lahr, R. M., Abd-Latip, N., Sweeney, K., et al. (2016). The RNA-binding protein LARP1 is a post-transcriptional regulator of survival and tumorigenesis in ovarian cancer. *Nucleic Acids Res.* 44 (3), 1227–1246. doi:10.1093/nar/gkv1515

Izaurralde, E., Lewis, J., Gamberi, C., Jarmolowski, A., Mcguigan, C., and Mattaj, I. W. (1995). A cap-binding protein complex mediating U snRNA export. *Nature* 376 (6542), 709–712. doi:10.1038/376709a0

Izaurralde, E., Lewis, J., Mcguigan, C., JankowskaM, DarzynkiEwicz, E., and Mattaj, I. W. (1994). A nuclear cap binding protein complex involved in pre-mRNA splicing. *Cell* 78 (4), 657–668. doi:10.1016/0092-8674(94)90530-4

Jiang, F., Fang, D. B., Chen, Q., Zhu, L. X., and Yu, H. Z. (2018). Correlation of LARP1 and E-cadherin expression with prognosis of intrahepatic cholangiocarcinoma. *Int. J. Clin. Exp. Pathol.* 11 (7), 3559–3566.

Jiang, F., Hu, Y., Liu, X., Wang, M., and Wu, C. (2022). Methylation pattern mediated by m(6)A regulator and tumor microenvironment invasion in lung adenocarcinoma. *Oxid. Med. Cell. Longev.* 2022, 2930310. doi:10.1155/2022/2930310

Jiang, F., Miao, X. L., Zhang, X. T., Yan, F., Mao, Y., Wu, C. Y., et al. (2021). A hypoxia gene-based signature to predict the survival and affect the tumor immune microenvironment of osteosarcoma in children. *J. Immunol. Res.* 2021, 5523832. doi:10.1155/2021/5523832

Joyce, J. A., and Fearon, D. T. (2015). T cell exclusion, immune privilege, and the tumor microenvironment. *Science* 348 (6230), 74–80. doi:10.1126/science.aaa6204

Khan, A. A., Huang, H., Zhao, Y., Li, H., Pan, R., Wang, S., et al. (2022). WBSCR22 and TRMT112 synergistically suppress cell proliferation, invasion and tumorigenesis in pancreatic cancer via transcriptional regulation of ISG15. *Int. J. Oncol.* 60 (3), 24. doi:10.3892/ijo.2022.5314

Lahr, R. M., Fonseca, B. D., Ciotti, G. E., Al-Ashtal, H. A., Jia, J. J., Niklaus, M. R., et al. (2017). La-related protein 1 (LARP1) binds the mRNA cap, blocking eIF4F assembly on TOP mRNAs. *Elife* 6, e24146. doi:10.7554/eLife.24146

Li, L., Yang, Y., Wang, Z., Xu, C., and Huang, J. (2021). Prognostic role of METTL1 in glioma. *Cancer Cell Int.* 21 (1), 633. doi:10.1186/s12935-021-02346-4

Li, M. O., Wolf, N., Raulet, D. H., Akkari, L., Pittet, M. J., Rodriguez, P. C., et al. (2021). Innate immune cells in the tumor microenvironment. *Cancer Cell* 39 (6), 725–729. doi:10.1016/j.ccell.2021.05.016

Luo, Y., Yao, Y., Wu, P., Zi, X., and Sun, N. (2022). The potential role of N(7)-methylguanosine (m7G) in cancer. *J. Hematol. Oncol.* 15 (1), 63. doi:10.1186/s13045-022-01285-5

Ma, J., Han, H., Huang, Y., Yang, C., Zheng, S., Cai, T., et al. (2021). METTL1/WDR4-mediated m(7)G tRNA modifications and m(7)G codon usage promote mRNA translation and lung cancer progression. *Mol. Ther.* 29 (12), 3422–3435. doi:10.1016/j.ymthe.2021.08.005

Malbec, L., Zhang, T., Chen, Y. S., Zhang, Y., Sun, B. F., Shi, B. Y., et al. (2019). Dynamic methylome of internal mRNA N(7)-methylguanosine and its regulatory role in translation. *Cell Res.* 29 (11), 927–941. doi:10.1038/s41422-019-0230-z

Mura, M., Hopkins, T. G., Michael, T., Abd-LatipN, Weir, J., AboagyE, E., et al. (2015). LARP1 post-transcriptionally regulates mTOR and contributes to cancer progression. *Oncogene* 34 (39), 5025–5036. doi:10.1038/onc.2014.428

Obeng, E. A., Stewart, C., and Abdel-Wahab, O. (2019). Altered RNA processing in cancer pathogenesis and therapy. *Cancer Discov.* 9 (11), 1493–1510. doi:10.1158/2159-8290.CD-19-0399

Orellana, E. A., Liu, Q., Yankova, E., Pirouz, M., De Braekeleer, E., Zhang, W., et al. (2021). METTL1-mediated m(7)G modification of Arg-TCT tRNA drives oncogenic transformation. *Mol. Cell* 81 (16), 3323–3338.e14. doi:10.1016/j.molcel.2021.06.031

Rong, D., Sun, G., Wu, F., Cheng, Y., Sun, G., Jiang, W., et al. (2021). Epigenetics: Roles and therapeutic implications of non-coding RNA modifications in human cancers. *Mol. Ther. Nucleic Acids* 25, 67–82. doi:10.1016/j.omtn.2021.04.021

Shaheen, R., Abdel-Salam, G. M. H., Guy, M. P., Alomar, R., Abdel-Hamid, M. S., Afifi, H. H., et al. (2015). Mutation in WDR4 impairs tRNA m(7)G46 methylation and causes a distinct form of microcephalic primordial dwarfism. *Genome Biol.* 16, 210. doi:10.1186/s13059-015-0779-x

Takahashi, H., Shimodaira, S., Ogasawara, M., Ota, S., Kobayashi, M., Abe, H., et al. (2016). Lung adenocarcinoma may be a more susceptive subtype to a dendritic cell-based cancer vaccine than other subtypes of non-small cell lung cancers: A multicenter retrospective analysis. *Cancer Immunol. Immunother.* 65 (9), 1099–1111. doi:10.1007/s00262-016-1872-z

Tian, Q. H., Zhang, M. F., Zeng, J. S., Luo, R. G., Wen, Y., Chen, J., et al. (2019). METTL1 overexpression is correlated with poor prognosis and promotes hepatocellular carcinoma via PTEN. *J. Mol. Med.* 97 (11), 1535–1545. doi:10.1007/s00109-019-01830-9

Tomikawa, C. (2018). 7-Methylguanosine modifications in transfer RNA (tRNA). *Int. J. Mol. Sci.* 19 (12), E4080. doi:10.3390/ijms19124080

Wiener, D., and Schwartz, S. (2021). The epitranscriptome beyond m(6)A. *Nat. Rev. Genet.* 22 (2), 119–131. doi:10.1038/s41576-020-00295-8

Xia, P., Zhang, H., Xu, K., Jiang, X., Gao, M., Wang, G., et al. (2021). MYC-targeted WDR4 promotes proliferation, metastasis, and sorafenib resistance by inducing CCNB1 translation in hepatocellular carcinoma. *Cell Death Dis.* 12 (7), 691. doi:10.1038/s41419-021-03973-5

Xie, C., Huang, L., Xie, S., Xie, D., Zhang, G., Wang, P., et al. (2013). LARP1 predict the prognosis for early-stage and AFP-normal hepatocellular carcinoma. *J. Transl. Med.* 11, 272. doi:10.1186/1479-5876-11-272

Xu, Z., Xu, J., Lu, H., Lin, B., Cai, S., Guo, J., et al. (2017). LARP1 is regulated by the XIST/miR-374a axis and functions as an oncogene in non-small cell lung carcinoma. *Oncol. Rep.* 38 (6), 3659–3667. doi:10.3892/or.2017.6040

Ying, X., Liu, B., Yuan, Z., Huang, Y., Chen, C., Jiang, X., et al. (2021). METTL1-m(7) G-EGFR/EFEMP1 axis promotes the bladder cancer development. *Clin. Transl. Med.* 11 (12), e675. doi:10.1002/ctm2.675

Zeng, H., Xu, S., Xia, E., Hirachan, S., Bhandari, A., and Shen, Y. (2021). Aberrant expression of WDR4 affects the clinical significance of cancer immunity in pan-cancer. *Aging (Albany NY)* 13 (14), 18360–18375. doi:10.18632/aging.203284

Zhang, H., Wang, A., Tan, Y., Wang, S., Ma, Q., Chen, X., et al. (2019). NCBP1 promotes the development of lung adenocarcinoma through up-regulation of CUL4B. *J. Cell. Mol. Med.* 23 (10), 6965–6977. doi:10.1111/jcmm.14581

Zhang, L. S., Liu, C., Ma, H., Dai, Q., Sun, H. L., Luo, G., et al. (2019). Transcriptome-wide mapping of internal N(7)-methylguanosine methylome in mammalian mRNA. *Mol. Cell* 74 (6), 1304–1316. doi:10.1016/j.molcel.2019.03.036

frontiers | Frontiers in Genetics

TYPE Systematic Review
PUBLISHED 09 November 2022
DOI 10.3389/fgene.2022.1065320

OPEN ACCESS

EDITED BY
Simin Li,
Southern Medical University, China

REVIEWED BY
Chao Deng,
Wannan Medical College, China
Jin Liu,
Xian Jiaotong University, China

*CORRESPONDENCE
Bin Cheng,
chengbin@mail.sysu.edu.cn
Juan Wang,
wangj255@mail.sysu.edu.cn

SPECIALTY SECTION
This article was submitted to Cancer Genetics and Oncogenomics, a section of the journal Frontiers in Genetics

RECEIVED 09 October 2022
ACCEPTED 27 October 2022
PUBLISHED 09 November 2022

CITATION
Chen S, Hu Q, Tao X, Xia J, Wu T, Cheng B and Wang J (2022), Retinoids in cancer chemoprevention and therapy: Meta-analysis of randomized controlled trials.
Front. Genet. 13:1065320.
doi: 10.3389/fgene.2022.1065320

Retinoids in cancer chemoprevention and therapy: Meta-analysis of randomized controlled trials

Shuting Chen[1,2,3], Qinchao Hu[1,2,3], Xiaoan Tao[1,2,3], Juan Xia[1,2,3], Tong Wu[1,2,3], Bin Cheng[1,2,3]* and Juan Wang[1,2,3]*

[1]Hospital of Stomatology, Sun Yat-Sen University, Guangzhou, China, [2]Guangdong Provincial Key Laboratory of Stomatology, Guangzhou, China, [3]Guanghua School of Stomatology, Sun Yat-Sen University, Guangzhou, China

Retinoids, natural and synthetic derivatives of vitamin A, have many regulatory functions in human body, including regulating cellular proliferation, differentiation, apoptosis. Moreover, retinoids have been used successfully for the treatment of certain malignancies, especially acute promyelocytic leukemia (APL) in adults and neuroblastoma in children. However, retinoids have not yet been translated into effective systemic treatments for most solid cancers. Some recent studies have shown that retinoids promote tumorigenesis. Therefore, we performed this meta-analysis to systematically evaluate the efficacy of retinoids in the chemoprevention and treatment of cancers. We performed literature search of several electronic databases, including PubMed, Embase and Cochrane Library from 2000 January to 2021 November. Various outcomes were applied to investigate the potential of retinoids for prevention and treatment of cancers. The primary outcomes in this study were disease recurrence and clinical response. The secondary outcomes included overall survival (OS), cancer development, disease progression and event-free survival. We identified 39 randomized controlled trials with 15,627 patients in this study. Our results showed that lower recurrence rate and better clinical response were obtained in retinoids treated patients with cancer or premalignancy as compared with control. The differences were statistically significant (RR = 0.85, 95% CI = 0.74–0.96, p = 0.01; RR = 1.24, 95% CI = 1.03–1.49, p = 0.02, respectively). Retinoids treatment was not associated with improvement in overall survival, cancer development, disease progression or event-free survival. Subgroup analysis conducted based on cancer type showed that patients benefited from retinoids treatment in APL, renal cell carcinoma, hepatocellular carcinoma, lung cancer, Kaposi sarcoma, and complete hydatidiform mole. No significant therapeutic effect was noted in head and neck cancer, acute myeloid leukemia (AML), melanoma, breast cancer, bladder cancer, cervical intraepithelial neoplasia (CIN) or cervical carcinoma. Subgroup analysis based on tumor classification demonstrated that retinoids group obtained a lower recurrence rate and better clinical response than control group in solid cancers. In conclusion, clinical application of retinoids was associated with reduction in disease recurrence and improvement in clinical response, illustrating that retinoids play a key role in

cancer prevention and therapy. Further research is needed to broaden the utility of retinoids in other types of cancers.

Systematic Review Registration: PROSPERO, identifier CRD42022296706.

KEYWORDS

retinoids, vitamin A, cancer, treatment, prevention

Introduction

Retinoids are a family of signaling molecules in humans and they function *via* retinoic acid receptors (RARs) and retinoid X receptors (RXRs). Retinoids cannot be synthesized by mammals, they can only be metabolized and converted from vitamin A. Vitamin A can be absorbed from animal food sources and plants. In animal products, vitamin A exists in the form of retinyl palmitate initially, and then dietary retinyl palmitate is converted to retinol in the intestinal lumen (Harrison, 2005). Retinol ultimately metabolizes to retinoic acid and its derivatives, known as retinoids. Retinoids consist of the natural and synthetic analogues of vitamin A. There are many different types of retinoids, such as all trans retinoic acid (ATRA), 13-cis retinoic acid (13 cRA), etretinate, and fenretinide. They can be classified into three generations regarding the structures and properties. Now the fourth generation is under research with less toxicity and greater efficacy (Khalil et al., 2017).

Retinoids regulate a wide range of biological processes, including cell proliferation and differentiation, apoptosis, immune function, and embryonic development (Tang and Gudas, 2011). Retinoids play vital roles in regulating skin functions, including epidermal keratinization, differentiation and proliferation. Owing to these effects, they have been used to treat skin diseases such as acne vulgaris, psoriasis and photoaging, and show positive efficacy (Cosio et al., 2021).

The synthesis and metabolism of retinoids are aberrant in many human tumors, including oral cavity, skin, bladder, kidney and breast, suggesting that retinoids are closely related to the development and progression of cancer. Lecithin-retinol acyltransferase (LRAT) is an important enzyme of retinoid metabolism, and it increases retinol uptake. Abnormally low intracellular concentrations of retinoids and decreased LRAT expression have been confirmed in various types of cancers including oral cavity, bladder, skin, prostate and breast cancers (Tang and Gudas, 2011). Reduced protein levels of recombinant aldehyde dehydrogenase 1 family, member A2 (ALDH1A2), a key player in the retinoic acid (RA) pathway and retinoid metabolism, have been reported in human prostate and breast cancer. The upregulated expression of CYP26A1, an enzyme responsible for RA oxidation, has been proven to promote the progression of human primary breast cancer (Kim et al., 2005).

Previous studies have proven the potential antitumor effects of retinoids through inducing cell differentiation and inhibiting cell proliferation. Differentiation therapy with ATRA has shown great success in treating acute promyelocytic leukemia (APL) (Ni et al., 2019). Clinical trials using retinoids exerted beneficial therapeutic effects in solid tumors such as breast cancer, cervical cancer, renal cancer, head and neck cancer, basal cell skin cancer, and prostate cancer, but the therapy response to retinoids was often limited to a small part of treated patients (Tang and Gudas, 2011). However, a recent study has shown that retinoids promote tumorigenesis by suppressing the immune system (Devalaraja et al., 2020). Another study demonstrated that the treatment effects of retinoids were not predictable, due to their immune promoting or inhibiting actions, suggesting the complex roles of retinoids in innate and adaptive immunity (Larange and Cheroutre, 2016). The results of published studies are conflicting, and the potential effect of retinoids on prevention and therapy of cancer remains unclear. Thus, this updated meta-analysis will include more eligible RCTs, especially the new studies, to systematically evaluate the effect of retinoids in cancer prevention and therapy.

Materials and methods

Our meta-analysis was performed according to the PRISMA statement and Cochrane Collaboration Tool. The protocol of our research was registered at the PROSPERO (CRD42022296706).

Search strategy and selection criteria

We performed literature search of several electronic databases, including PubMed, Embase and Cochrane Library from 2000 January to 2021 November. We also searched ClinicalTrials.gov to further identify relevant registered randomized controlled trials (RCTs). Language and study region were not restricted in the search strategy. The search formula consists of three major parts: retinoids, cancer or premalignancy and RCT filter. Literature search was performed using following MeSH headings in the title or abstract: (retinoic OR retinoid* OR "retinoid derivative*") AND (neoplasm* OR cancer* OR carcino* OR tumo* OR premalignan* OR precancerous).

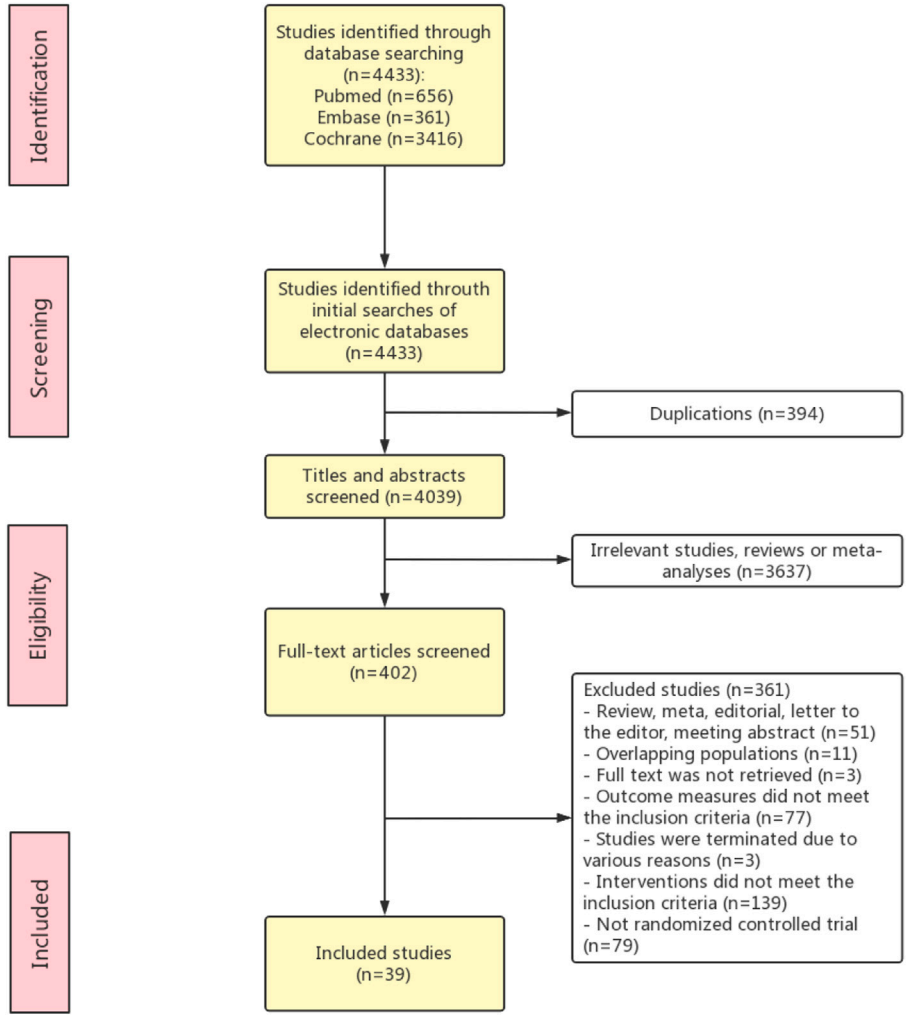

FIGURE 1
PRISMA flow diagram of study identification.

We included only these RCTs that reported extractable data on retinoids as treatment or prevention in patients with tumors or precancerous lesions, whereas review, meta-analysis, case report, editorials and conference papers were excluded. All these RCTs compared the efficacy of retinoids and no retinoids (defined as placebo or no treatment).

Data extraction and quality assessment

Two investigators (SC and QH) performed literature screening independently. Extracted data included author, year of publication, country, subject age, cancer type, intervention method, treatment duration, follow-up duration, sample size, sex ratio, and outcome. Any discrepancies and disagreements were resolved by discussion and consensus with the senior investigators (JW and BC). The methodological quality and internal validity of individual trials were independently assessed by two investigators using the Cochrane Collaboration's risk of bias tool. There were seven assessment components, each of which could be rated as high risk, low risk or unclear risk according to the criteria.

The primary outcomes in this study were disease recurrence and clinical response. Disease recurrence was defined as relapse of disease after treatment completion. Clinical response was assessed by clinicians in terms of relief or recovery of the disease, including complete resolution and partial resolution. The secondary outcomes were overall survival (OS), cancer development, disease progression and event-free survival. Overall survival was defined as the proportion of patients who were alive from randomization to the end of follow-up period. Cancer development referred to neoplasm events, which

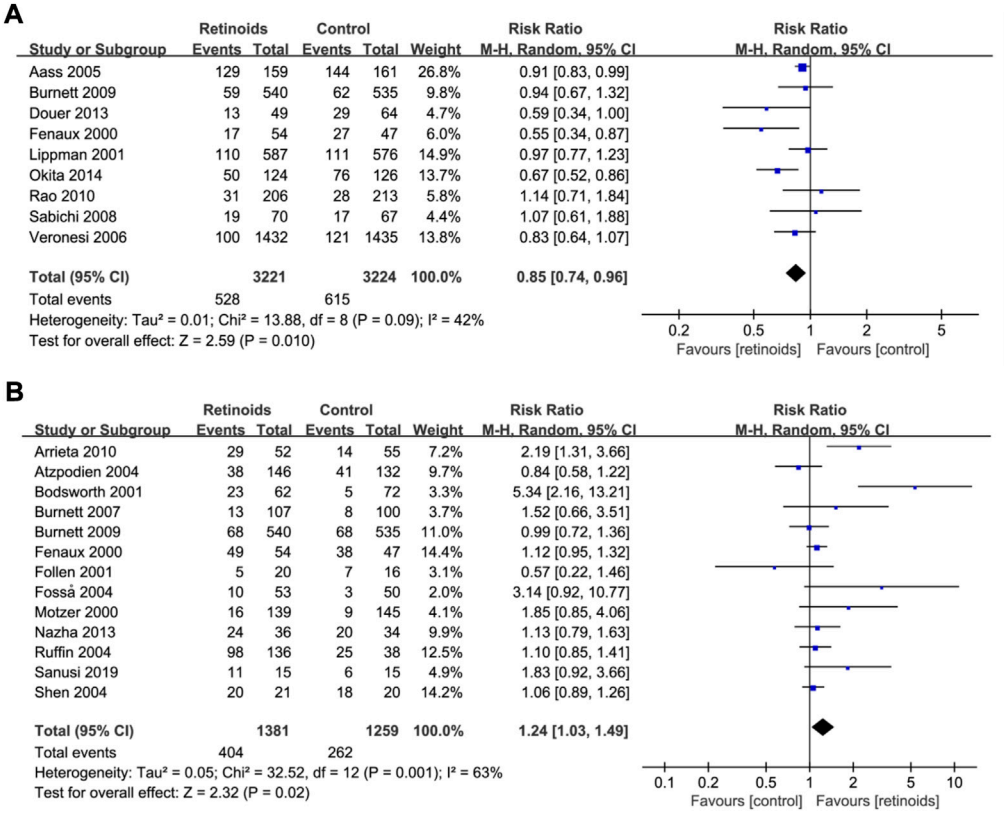

FIGURE 2
Forest plots showed the effects of retinoids application in cancers or precancerous lesions concerning primary outcomes. **(A)** disease recurrence, **(B)** clinical response. CI, confidence interval.

included new cancer development, second primary tumor (SPT) and malignant transformation. Disease progression refers to the progression and deterioration of the neoplasia confirmed by histologic examination. Event-free survival was characterized by the proportion of patients who are alive free of neoplasm events.

Statistical analysis

Review manager 5.4 and Stata 16.0 software were used to perform statistical analysis. We present the results using risk ratios (RR) with 95% confidence intervals (CI) to represent the estimated efficacy of the intervention. I^2 statistic was applied to evaluate the heterogeneity between studies. Heterogeneity was considered high if I^2 was greater than 50%. If heterogeneity was high, sensitivity analysis was performed by excluding studies one by one to find out the potential source of heterogeneity. L'Abbe plot was also used to detect the heterogeneity between studies. Random-effect model was applied to synthesize the data. Subgroup analysis was performed based on cancer type and tumor classification. Funnel plot asymmetry and Egger's test were used to detect potential publication bias. A two-tailed $p < 0.05$ was considered statistically significant.

Results

Studies characteristics

The literature searching and screening process is presented in Figure 1. Thirty-nine RCT studies with a total of 15,627 patients were included in this meta-analysis (Fenaux et al., 2000; Kohler et al., 2000; Motzer et al., 2000; van Zandwijk et al., 2000; Bodsworth et al., 2001; Follen et al., 2001; Lippman et al., 2001; Bernstein et al., 2002; George et al., 2002; Robinson et al., 2002; Atzpodien et al., 2004; Fosså et al., 2004; Ruffin et al., 2004; Shen et al., 2004; Toma et al., 2004; Aass et al., 2005; Chiesa et al., 2005; Perry et al., 2005; Richtig et al., 2005; Takai et al., 2005; Khuri et al., 2006; Scardina et al., 2006; Veronesi et al., 2006; Burnett et al., 2007; Sabichi et al., 2008; Decensi et al., 2009; Weinstock et al., 2009; Andrijono and Muhilal,

TABLE 1 Characteristics of included studies.

Author year	Country	Age	Cancer type	Intervention	Treatment duration	Follow-up duration	Sample size	Female,%	Outcome
Zandwijk 2000	Italy	Median age 61 years	Patient with head and neck cancer or lung cancer treated	Retinyl palmitate vs. no retinyl palmitate	2 years	49 months	1290/1283	13	OS, SPT
Khuri (2006)	United States	Mean ± SD 60.8 ± 10.9	Patients who had been treated for stage I or II HNSCC	Isotretinoin (30 mg/d) vs. placebo	3 years	4 years	590/600	21	OS, SPT
Perry (2005)	Australia	Unclear	Patients with their first head and neck squamous cell carcinoma treated	Isotretinoin (1.0 mg/kg/d) vs. isotretinoin (0.5 mg/kg/d) vs. placebo	3 years	Unclear	54/48/49	24	SPT
Bhatia (2017)	United States	Median age 60 years	Treated stage I/II SCC of the oral cavity, oropharynx, hypopharynx, larynx	13-Cis Retinoic Acid vs. placebo	2 years	5 years	91/85	22	OS, SPT
Lippman (2001)	United States	Mean ± SD 64.2 ± 8.8	Treated stage I non-small-cell lung cancer	Isotretinoin (30 mg/day) vs. placebo	3 years	3.5 years	589/577	43	OS, SPT, recurrence
Veronesi 1999/2006	Italy	Mean ± SD 51 ± 7.6/ 51 ± 7.8	Surgically removed stage I breast cancer or ductal carcinoma *in situ*	Fenretinide orally (200 mg/day) vs. no treatment	5 years	14.6 years	1432/1435	100	SPT, recurrence
Toma (2004)	Italy	Unclear	Squamous cell carcinoma of head and neck	Isotretinoin vs. control	unclear	39 months	126/126	Unclear	OS, disease progression
Sabichi (2008)	United States	Median age 70.9/64.0	Resected non-muscle-invasive bladder cancer	Fenretinide (200 mg/day orally) vs. placebo	12 months	15 months	70/67	0	Recurrence
Kohler (2000)	United Kingdom	Children	Advanced neuroblastoma after chemotherapy	13-Cis retinoic acid 0.75 mg/kg/ day vs. placebo	4 years	59 months	88/87	Unclear	EFS
Kadakia (2012)	United States	Mean ± SD 68.2 ± 9.48	Treated nonmelanoma skin cancers (NMSCs)	Acitretin 25 mg orally 5 days per week vs. placebo	2 years	Unclear	35/35	37	New NMSC development
Takai (2005)	Japan	Unclear	Treated Hepatocellular Carcinoma (HCC)	Acyclic Retinoid 600 mg/d vs. placebo	48 weeks	7 years	44/45	Unclear	OS, SPT
Weinstock (2012)	United States	Mean age 71 years	Patients with history of BCC or SCC of the skin	Topical 0.1% tretinoin cream vs. control	3 years	3.5 years	566/565	3	OS, cancer development
Douer (2013)	United States	Median age 36	Untreated acute promyelocytic leukemia (APL)	ATRA 45 mg/m^2/ d orally vs. observation	1 year	11.8 years	101/117	34	Relapse
George (2002)	Australia	Mean ± SD 56.7 ± 9.5 (Group1)/ 52.2 ± 10.2 (Group2)	Patients with history of non-melanoma skin cancers	Acitretin 25 mg orally, once daily vs. drug-free	2 years	Unclear	23/23	22	Cancer development
Dencensi (2009)	Italy	Mean ± SD 46.2 ± 5.2	Premenopausal Women at risk of breast cancer	fenretinide 200 mg/d vs. placebo	2 years	5.5 years	59/58	100	Breast cancer events
Shinagawa (2014)	Japan	Median age 48	Patients with newly diagnosed APL	ATRA or tamibarotene	2 years	1 year	135/134	47	Relapse, EFS
Okita 2014	Japan	Unclear	Treated hepatitis C-related hepatocellular carcinoma	peretinoin 600 mg/day, peretinoin 300 mg/day, or placebo	96 weeks	3 years	124/ 126/127	36	OS, EFS, recurrence

(Continued on following page)

TABLE 1 (*Continued*) Characteristics of included studies.

Author year	Country	Age	Cancer type	Intervention	Treatment duration	Follow-up duration	Sample size	Female,%	Outcome
Richtig (2005)	Austria	Mean ± SD 52.6 ± 13.8	Resected melanoma in stage IIA and IIB	IFN + isotretinoin vs. IFN + placebo	2 years	5 years	206/201	47	OS, disease progression
Rao (2011)	United States	Median age 72	Postmenopausal women with hormone receptor-positive breast cancer resected	Tamoxifen + fenretinide vs. tamoxifen + placebo	5 years	5 years	206/213	100	Recurrence, SPT
Aass (2005)	Norway	Median age 60	Progressive metastatic renal cell carcinoma treated	IFN-α-2a + 13-cRA vs. IFN-α-2a alone	13–15 weeks	3 months	159/161	31	Relapse, OS
Motzer (2000)	United States	Median age 60	Advanced renal cell carcinoma	13-cis-retinoic acid + IFN-α-2a vs. IFN-α-2a	60 months	Unclear	139/145	33	OS, CR
Atzpodien (2004)	Germany	Median age 59	Irresectable metastatic renal cell carcinoma	13 cRA + IFN-α-2a/IL-2/IV-FU vs. IFN-α-2a/IL-2/IV-FU	8 weeks	Unclear	146/132	25	OS, CR
Aviles (2015)	Mexico	Median age 63	Patients with refractory/relapsed, cutaneous T-cell lymphoma, with advanced stages	IFN + ATRA vs. IFN + MTX	6 months	12 months	176/201	32	OS
Bernstein (2002)	United States	Mean ± SD 37.5 ± 6.7/ 41.2 ± 6.7	Patients with AIDS-associated Kaposi sarcoma	ATRA once weekly vs. 3 times weekly	12 weeks	Unclear	30/46	3	CR
Bodsworth (2001)	Australia	Median age 38	Cutaneous AIDS-Related Kaposi Sarcoma	Alitretinoin gel 0.1% twice daily vs. vehicle gel	12 weeks	Unclear	62/72	0	CR
Sanusi (2019)	Indonesia	Mean ± SD 54.0 ± 9.2/ 47.7 ± 8.2	Locally advanced cervical carcinoma	NAC (cisplatin and paclitaxel) + vitamin A VS. NAC	64 weeks	Unclear	15/15	100	CR
Fosså (2004)	Norway	Median age 60	Progressive, metastatic renal cell carcinoma	IFN vs. IFN + 13-cis retinoic acid	3 months	1 year	53/50	43	CR
Arrieta (2010)	Mexico	Median age 59	Advanced non–small-cell lung cancer	Paclitaxel/ cisplatin (P/C) + ATRA vs. P/C + placebo	80–100 days	80–100 days	52/55	45	CR
Burnett 2009	United Kingdom	Median age 45	Acute Myeloid Leukemia	Treatment with ATRA or not	8 years	Unclear	540/535	49	OS, relapse, CR
Burnett (2007)	United Kingdom	Median age 65	Older patients Not Considered Fit for Intensive Treatment with acute myeloid leukemia	Cytarabine (Ara-C) or hydroxyurea with or without ATRA	3 years	Unclear	107/99	44	OS, CR
Nazha 2013	United States	Median age 66	Older patients with acute myeloid leukemia	Intensive chemotherapy with or without ATRA	Unclear	12.5 years	36/34	Unclear	CR
Fenaux (2000)	France	Unclear	Newly diagnosed APL	ATRA + chemotherapy vs. chemotherapy	Unclear	73 months	54/47	Unclear	Relapse, CR
Shen (2004)	China	Median age 32	Newly diagnosed APL	ATRA + As2O3 vs. As2O3	Unclear	18 months	21/20	49	CR

(Continued on following page)

TABLE 1 (*Continued*) Characteristics of included studies.

Author year	Country	Age	Cancer type	Intervention	Treatment duration	Follow-up duration	Sample size	Female,%	Outcome
Scardina (2006)	Italy	Unclear	Oral leukoplakia	Isotretinoin 0.18% vs. 0.05% (topical, twice a day)	3 months	10 years	20/20	Unclear	Malignant change
Chiesa (2005)	Italy	Median age 50	Oral leukoplakias	200 mg fenretinide daily vs. no intervention	1 year	5 years	84/86	29	Cancer development
Andrijono (2010)	Thailand	Median age 25	Complete hydatidiform mole	Vitamin A vs. placebo	Unclear	20 mon	32/35	100	Malignant disease
Robinson (2002)	United States	Unclear	HIV-positive women with low-grade squamous intraepithelial lesions of the cervix	Isotretinoin vs. observation	6 months	192 weeks	56/58	100	Disease progression
Ruffin (2004)	United States	Unclear	Women with biopsy-proven CIN II/III	ATRA (0.16%, 0.28%, 0.36%) vs. placebo	4 days	12 weeks	136/38	100	Regression rate
Follen (2001)	United States	Unclear	Biopsy-proven CIN-2/3 (High-Grade SIL)	4-HPR at 200 mg/day vs. placebo	6 months	12 months	20/16	100	CR, disease progression

OS, overall survival; SPT, second primary tumor; EFS, event-free survival; CR, clinical response; ATRA, all trans retinoic acid; IFN, interferon; 13-cRA, 13-cis retinoic acid; IL-2, interleukin-2; IV, intravenous; FU, fluorouracil; MTX, methotrexate; NAC, neoadjuvant chemotherapy; 4-HPR, N-(4-hydroxyphenyl) retinamide.

2010; Arrieta et al., 2010; Burnett et al., 2010; Lee et al., 2010; Rao et al., 2011; Kadakia et al., 2012; Weinstock et al., 2012; Douer et al., 2013; Nazha et al., 2013; Shinagawa et al., 2014; Aviles et al., 2015; Okita et al., 2015b; Bhatia et al., 2017; Sanusi, 2019). The characteristics of the included studies are shown in Table 1. The quality assessment of the included studies was shown in Supplementary Figure S1. Sixteen studies were conducted in North America, 14 studies were conducted in Europe, six studies were proceeded in Asia, and 3 studies were proceeded in Oceania. Among the 39 included studies, 14 studies described the overall survival, and others evaluated the cancer development (n = 14), clinical response (n = 13), disease recurrence (n = 9), disease progression (n = 4), and event-free survival (n = 3).

Primary outcomes

The association of retinoids and disease recurrence was supplied by nine studies (Fenaux et al., 2000; Lippman et al., 2001; Aass et al., 2005; Burnett et al., 2007; Sabichi et al., 2008; Rao et al., 2011; Douer et al., 2013; Okita et al., 2015a) with 6,445 patients. Data analysis revealed that retinoids usage was correlated with lower recurrence rate compared with control group (RR = 0.85, 95% CI = 0.74–0.96, p = 0.01) (Figure 2A). The heterogeneity was acceptable according to the statistic (I^2 = 42%) (Figure 2A).

Pooled data in 13 studies (Fenaux et al., 2000; Motzer et al., 2000; Bodsworth et al., 2001; Follen et al., 2001; Atzpodien et al., 2004; Fosså et al., 2004; Ruffin et al., 2004; Shen et al., 2004; Burnett et al., 2007; Arrieta et al., 2010; Burnett et al., 2010; Nazha et al., 2013; Sanusi, 2019) with 2,640 patients showed that retinoids group exhibited a better clinical response rate than control group (RR = 1.24, 95% CI = 1.03–1.49, p = 0.02) (Figure 2B). Heterogeneity among the above 13 studies was significant (I^2 = 63%) (Figure 2B).

Secondary outcomes

Fourteen studies (Motzer et al., 2000; van Zandwijk et al., 2000; Lippman et al., 2001; Atzpodien et al., 2004; Toma et al., 2004; Aass et al., 2005; Richtig et al., 2005; Takai et al., 2005; Khuri et al., 2006; Burnett et al., 2007; Weinstock et al., 2009; Burnett et al., 2010; Bhatia et al., 2017) with 9,521 patients reported the data of retinoids and overall survival. Synthesized data showed that there was no significant relation between retinoids usage and overall survival (RR = 0.98, 95% CI = 0.95–1.01, p = 0.23) (Figure 3A) without obvious heterogeneity (I^2 = 18%) (Figure 3A).

Fourteen studies (van Zandwijk et al., 2000; Lippman et al., 2001; George et al., 2002; Chiesa et al., 2005; Perry et al., 2005; Takai et al., 2005; Khuri et al., 2006; Veronesi et al., 2006; Decensi et al., 2009; Weinstock et al., 2009; Andrijono and Muhilal, 2010;

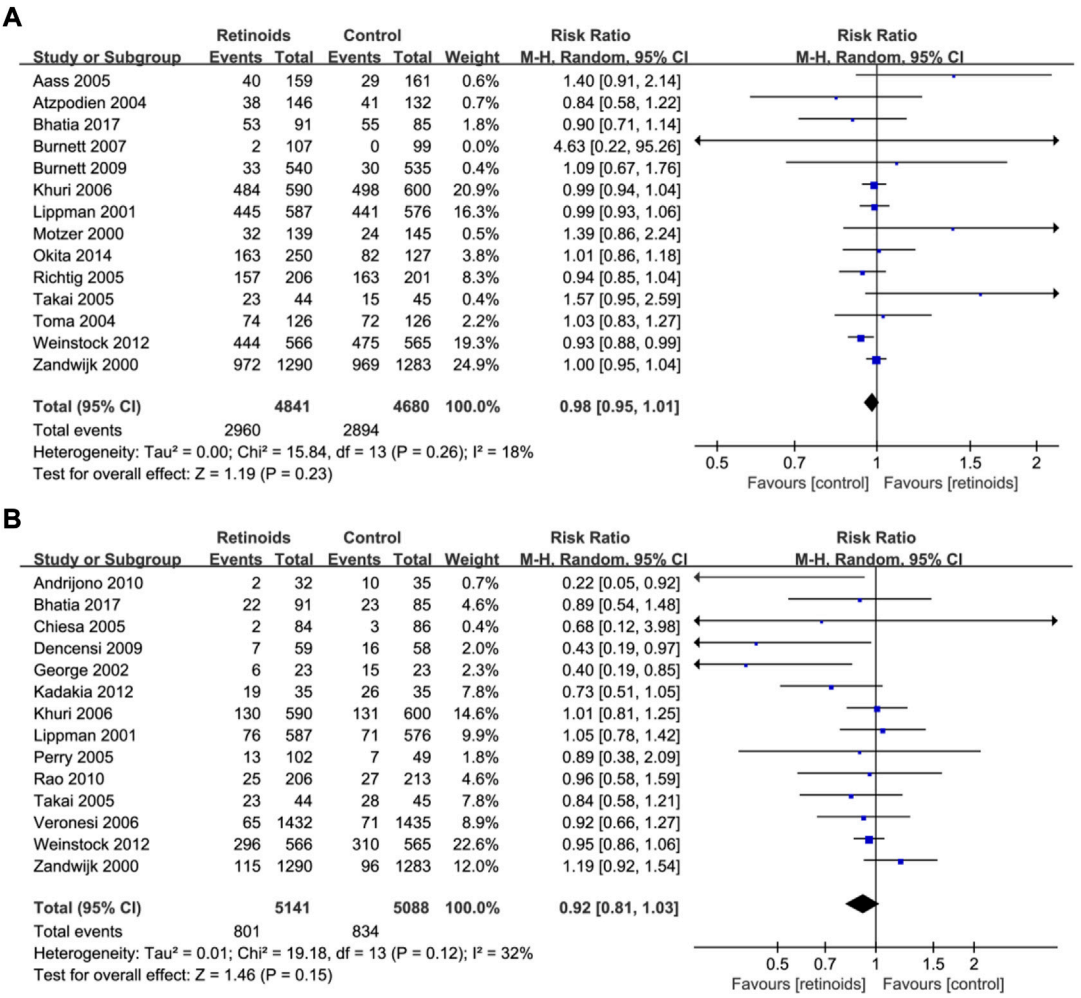

FIGURE 3
Forest plots showed the effects of retinoids application in cancers or precancerous lesions concerning secondary outcomes. **(A)** overall survival (OS), **(B)** cancer development. CI, confidence interval.

Rao et al., 2011; Kadakia et al., 2012; Bhatia et al., 2017) with 10,229 patients showed the relationship between retinoids and cancer development. Data analysis showed that there was no significant association between retinoids application and cancer development (RR = 0.92, 95% CI = 0.81–1.03, p = 0.15) (Figure 3B). Acceptable heterogeneity was presented (I^2 = 32%) (Figure 3B).

For the disease progression, four studies (Follen et al., 2001; Robinson et al., 2002; Toma et al., 2004; Richtig et al., 2005) with 798 patients reported that there was no significant relation between retinoids application and disease progression (RR = 1.17, 95% CI = 0.86–1.60, p = 0.32) (Supplementary Figure S2) without obvious heterogeneity (I^2 = 0%) (Supplementary Figure S2).

As for event-free survival, three studies (Kohler et al., 2000; Shinagawa et al., 2014; Okita et al., 2015b) with 556 patients evaluated the relationship between retinoids and event-free survival. No difference was observed statistically between retinoids group and control group based on the pooled data (RR = 0.94, 95% CI = 0.87–1.02, p = 0.13) (Supplementary Figure S3). No heterogeneity was found (I^2 = 0%) (Supplementary Figure S3).

Sensitivity analysis

Heterogeneity analysis as well as sensitivity analysis of our meta-analysis were conducted mainly based on overall survival as it has the maximum included studies. According to the statistics, heterogeneity was not significant (I^2 = 18%) (Figure 3A). Furthermore, L'Abbe plot also showed that there was no significant heterogeneity detected (Supplementary Figure S4). However, there is a considerable heterogeneity in the primary outcome clinical response (I^2 =

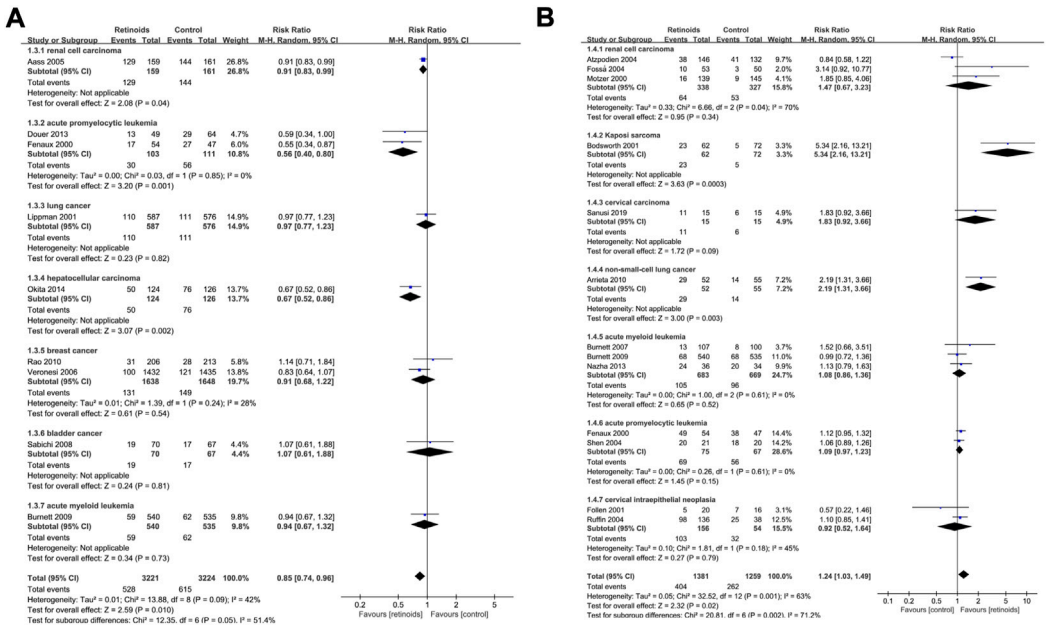

FIGURE 4
Subgroup analysis based on cancer type described the effects of retinoids application in cancers or precancerous lesions concerning primary outcomes. **(A)** disease recurrence, **(B)** clinical response. CI, confidence interval.

63%) (Figure 2B). Sensitivity analysis was performed by excluding studies one by one, and then we found that one RCT (Bodsworth et al., 2001) is the potential origin of heterogeneity. After removing it, the heterogeneity declined to 42%. Whether excluding this RCT or not, similar trends of retinoids treatment in clinical response were observed and it confirmed the robustness of our results (Supplementary Figure S5).

Subgroup analysis based on cancer type

Subgroup analysis based on cancer type of primary outcome disease recurrence showed that retinoids induced lower rate of recurrence in APL ($p = 0.001$), renal cell carcinoma ($p = 0.04$) and hepatocellular carcinoma ($p = 0.002$) (Figure 4A). On the contrary, no significant effect of retinoids was found in lung cancer ($p = 0.82$), breast cancer ($p = 0.54$), bladder cancer ($p = 0.81$) and AML ($p = 0.73$). As for primary outcome clinical response (Figure 4B), higher clinical response rate was detected in Kaposi sarcoma ($p = 0.0003$) and non-small-cell lung cancer ($p = 0.003$) owing to retinoids application. However, no difference was found between retinoids group and control group in renal cell carcinoma ($p = 0.34$), cervical carcinoma ($p = 0.09$), AML ($p = 0.52$), APL ($p = 0.15$), and cervical intraepithelial neoplasia ($p = 0.48$).

As for secondary outcome overall survival (Figure 5A), there was no significant association between retinoids usage and overall survival in head and neck cancer ($p = 0.66$), renal cell carcinoma ($p = 0.43$), AML ($p = 0.62$), lung cancer ($p = 0.76$), hepatocellular carcinoma ($p = 0.44$), and melanoma ($p = 0.23$). However, poorer overall survival was related to retinoids usage in keratinocyte carcinoma ($p = 0.02$). Pooled analysis on secondary outcome cancer development revealed that there was no difference between retinoids group and control group in head and neck cancer ($p = 0.53$), breast cancer ($p = 0.29$), non-melanoma skin cancer ($p = 0.14$), lung cancer ($p = 0.75$), and hepatocellular carcinoma ($p = 0.35$) (Figure 5B). Nevertheless, retinoids group showed a lower rate of cancer development in complete hydatidiform mole ($p = 0.04$).

Subgroup analysis based on tumor classification

The included cancers in this study can be divided into two general classifications: solid cancer and hematology malignancy. For primary outcome disease recurrence, subgroup analysis based on tumor classification demonstrated that retinoids group obtained a lower rate of recurrence than control group in solid cancers (RR = 0.88, 95% CI = 0.78–0.99, $p = 0.04$) (Table 2). The difference was statistically significant ($p = 0.04$). However, as for hematology malignancy, no significant difference was found between retinoids group and control group concerning disease recurrence (RR = 0.70, 95% CI =

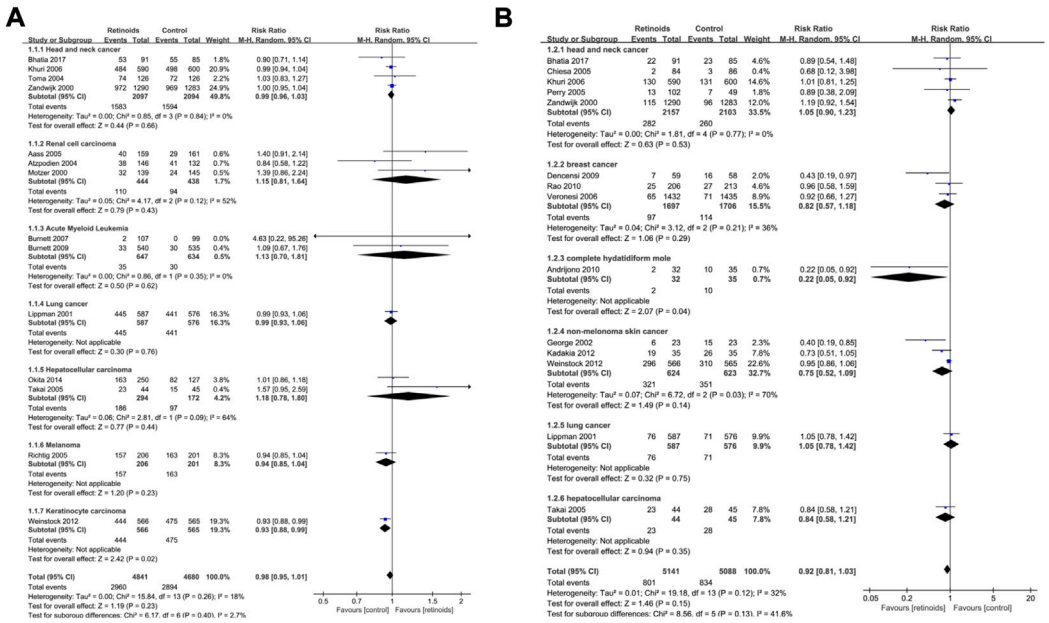

FIGURE 5
Subgroup analysis based on cancer type described the effects of retinoids application in cancers or precancerous lesions concerning secondary outcomes. **(A)** overall survival (OS), **(B)** cancer development. CI, confidence interval.

TABLE 2 Subgroup analysis of tumor classification.

Outcome	Subgroup	Study number	Sample size	RR (95%CI)	*p*-value	Heterogeneity	
						I^2 (%)	*p*-value
Disease recurrence	Overall	9	6445	0.85 (0.74–0.96)	0.01	42	0.09
	Tumor classification						
	Solid cancer	6	5156	0.88 (0.78–0.99)	0.04	31	0.2
	Hematology malignancy	3	1289	0.70 (0.48–1.02)	0.06	55	0.11
Clinical response	Overall	13	2640	1.24 (1.03–1.49)	0.02	63	0.001
	Tumor classification						
	Solid cancer	8	1146	1.56 (1.03–2.36)	0.04	75	0.0002
	Hematology malignancy	5	1494	1.09 (0.98–1.21)	0.11	0	0.87
Overall survival	Overall	14	9521	0.98 (0.95–1.01)	0.23	18	0.26
	Tumor classification						
	Solid cancer	12	9139	0.98 (0.95–1.02)	0.3	23	0.22
	Hematology malignancy	2	382	1.02 (0.42–2.47)	0.96	15	0.28

0.48–1.02, $p = 0.06$) (Table 2). Similar findings were also seen in primary outcome clinical response. Pooled data revealed that retinoids usage was correlated with a better clinical response rate in solid cancers (RR = 1.56, 95% CI = 1.03–2.36, $p = 0.04$) (Table 2) and exhibited statistically significant difference ($p = 0.04$). In hematology malignancy, there was no significant correlation between retinoids application and clinical response (RR = 1.09, 95% CI = 0.98–1.21, $p = 0.11$) (Table 2).

As for secondary outcome overall survival (OS), synthesized data showed that there was no difference statistically between retinoids group and control group in either solid cancers (RR = 0.98, 95% CI = 0.95–1.02, p = 0.30) (Table 2) or hematology malignancy (RR = 1.02, 95% CI = 0.42–2.47, p = 0.96) (Table 2).

Publication bias

We analyzed publication bias in studies regarding overall survival using funnel plot asymmetry. No obvious asymmetry was observed, indicating that there was no apparent publication bias, which was confirmed by Egger's test (p = 0.0784) (Supplementary Figure S6).

Discussion

Retinoids are a family of signaling molecules in human beings and they play vital roles in cell differentiation, proliferation, and apoptosis. The synthesis and metabolism of retinoids are impaired in various cancers (Tang and Gudas, 2011). It is critically necessary to clarify the correlation between retinoids and carcinogenesis risk. Many previous preclinical and clinical investigations revealed the great potential of retinoids in the chemoprevention and treatment of several types of cancers. However, a few recent studies have reported that retinoids promote tumorigenesis (Larange and Cheroutre, 2016; Devalaraja et al., 2020). Therefore, we performed this meta-analysis of RCTs to systematically evaluate the effects of retinoids on cancers. We investigated the association between disease recurrence, clinical response, overall survival, cancer development, disease progression, event-free survival, and retinoids application in patients with tumors or precancerous lesions. A more detailed subgroup analysis was also conducted based on cancer type. Our results showed that lower recurrence rate and better clinical response were obtained in retinoids group as compared with placebo group or no treatment group. However, retinoids application was not correlated with overall survival, cancer development, disease progression or event-free survival in patients with cancer or premalignancy.

According to our research, retinoids showed preventive and therapeutic effectiveness in certain cancers. Retinoids application lowered the rate of malignant transformation in patients with complete hydatidiform mole. Moreover, retinoids reduced tumor recurrence in renal cell carcinoma, APL and hepatocellular carcinoma. Better clinical response was obtained in Kaposi sarcoma and non-small-cell lung cancer in retinoids group. One previous study confirmed the benefit of retinoids in prolonging disease-free survival in patients with hepatocellular carcinoma (Chu et al., 2010). As for lung cancer, Yu et al. (2015) reported that dietary vitamin A intake could reduce the risk of lung cancer, however two other studies demonstrated the ineffectiveness of vitamin A in the treatment or prevention of lung cancer (Fritz et al., 2011; Cortés-Jofré et al., 2020). The studies mentioned above included cohort studies or case-control studies while our study was strictly restricted to RCTs. Thus, our meta-analysis could provide more reliable evidence to clarify the effectiveness of retinoids in cancer chemoprevention and therapy.

Subgroup analysis based on cancer type indicated that no significant difference was observed in any outcome between retinoids and control group in patients with head and neck cancer, AML, melanoma, breast cancer, bladder cancer, cervical intraepithelial neoplasia (CIN) or cervical carcinoma. Our study was consistent with the previous research reported by He et al. (2018), which showed that vitamin A derivatives intake had no effects on the survival of breast cancer patients. However, Fulan et al. (2011) claimed that both the total intake of retinol and vitamin A could reduce breast cancer risk. These contradictory studies suggested that retinol might have preventive effect rather than therapeutic effect on breast cancer. Similar contradictory findings were also seen in cervical diseases and bladder cancer. One study showed that retinoids had no effect in preventing the progression of CIN (Helm et al., 2013), while another study demonstrated that vitamin A intake was inversely associated with cervical cancer risk (Zhang et al., 2012). High vitamin A intake was also associated with low bladder cancer risk (Tang et al., 2014). As shown above, the antitumor efficacy of retinoids is limited to several types of cancers, which may be attributed to retinoid resistance. Patients treated with retinoids often exhibit or develop resistance to this therapy. The molecular mechanisms of this resistance remain incompletely understood and the following factors have been confirmed involved: increased expression of RA binding proteins, new mutations in retinoid receptors and the pharmacologic alteration in RA metabolism (Chlapek et al., 2018). Strategies to overcome retinoid resistance include combination therapy as well as the alternative use of non-classical retinoids. Combination of retinoids and interferon-α showed partial or complete response in lymphoid malignancy and preclinical studies indicated that non-classical retinoids can function as tumor suppressors in human cancers (Tang and Gudas, 2011). Well-designed comprehensive studies focused on combination retinoid therapy are recommended.

Subgroup analysis based on tumor classification revealed that retinoids group obtained a lower recurrence rate and better clinical response than control group in solid cancers. But in hematology malignancy, there was no significant difference between retinoids group and control group. We further analyze the possible causes. In our meta-analysis, the included hematology malignancies were consisted of APL and AML. Previous studies have shown that retinoids treatment acquires great success in APL but not in AML (Ni et al., 2019). These findings were also consistent with our subgroup analysis based on cancer type. Thus, the ineffectiveness of retinoids in hematology malignancy may be attributed to the synthesized analysis

integrating APL and AML. All in all, our work indicated the potential chemoprevention effect of retinoids for the treatment of solid cancers. Well-designed and large-scaled studies are warranted to confirm our findings.

It should be noted that one RCT included in this study showed that patients with keratinocyte carcinoma obtained a worse overall survival in tretinoin-treated group as compared with control group. However, further analysis by the investigator revealed that the increased mortality in tretinoin-treated group could hardly be attributed to retinoids application, owing to lack of additional supportive evidence and failing to specify the causes of deaths such as smoking status (Weinstock et al., 2009). A recent preclinical study also reported the tumorigenic role of retinoids in fibrosarcoma and melanoma *via* inhibiting immune system (Devalaraja et al., 2020). However, the finding of this study is still lack of support data from clinical research. More large-scale comprehensive RCTs are warranted to figure out whether retinoids have tumorigenic role.

The main limitation of our study may be heterogeneity in interventions and outcomes among studies, such as different categories of retinoids, drug dosage, application pattern, and frequency. The heterogeneity was not significant in any outcome except for clinical response. By excluding RCTs one by one, we found that one RCT study (Bodsworth et al., 2001) is the potential source of heterogeneity. This RCT demonstrated that the alitretinoin group showed a significant higher clinical response rate than control group, which made it distinct from other included studies. This remarkably high response rate of this RCT study may be the main cause of heterogeneity in clinical response. We searched more studies to clarify this problem and found that an approximate clinical response rate of alitretinoin was shown in a recent systematic review comprising three clinical trials and three case reports (Htet et al., 2022). Besides, alitretinoin is Food and Drug Administration-approved medication for Kaposi sarcoma. All these studies demonstrated that alitretinoin had a significant efficacy for the treatment of Kaposi sarcoma. Moreover, synthesized analysis showed that whether excluding or retaining the study (Bodsworth et al., 2001), the result of retinoids treatment in clinical response remained unchanged and this confirmed the robustness of our results.

Conclusion

Our meta-analysis of RCTs revealed the positive preventive and therapeutic effects of retinoids in several malignancies. Retinoids usage reduced disease recurrence and improved clinical response. Combination therapy containing retinoids may be promising cancer therapy in the future.

Data availability statement

The original contributions presented in the study are included in the article/Supplementary Material, further inquiries can be directed to the corresponding authors.

Author contributions

SC contributed to designing the study plan, data acquisition, analysis, and drafting the manuscript. QH, XT, JX, and TW contributed to data acquisition, analysis, and interpretation. BC and JW contributed to the project conception, writing manuscript, and supervision. All authors read and approved the final manuscript.

Funding

This work was supported by the National Natural Science Foundation of China (Grant No. 81800969), and the Major Research plan of Science and Technology Program of Guangzhou, China (Grant No. 202206080009).

Conflict of interest

The authors declare that the research was conducted in the absence of any commercial or financial relationships that could be construed as a potential conflict of interest.

Publisher's note

Supplementary material

The Supplementary Material for this article can be found online at: https://www.frontiersin.org/articles/10.3389/fgene.2022.1065320/full#supplementary-material

References

Aass, N., De Mulder, P. H., Mickisch, G. H., Mulders, P., van Oosterom, A. T., van Poppel, H., et al. (2005). Randomized phase II/III trial of interferon alfa-2a with and without 13-cis-retinoic acid in patients with progressive metastatic renal cell carcinoma: The European organisation for research and treatment of cancer genito-urinary tract cancer group (EORTC 30951). *J. Clin. Oncol.* 23 (18), 4172–4178. doi:10.1200/jco.2005.07.114

Andrijono, A., and Muhilal, M. (2010). Prevention of post-mole malignant trophoblastic disease with vitamin A. *Asian pac. J. Cancer Prev.* 11 (2), 567–570.

Arrieta, O., González-De la Rosa, C. H., Aréchaga-Ocampo, E., Villanueva-Rodríguez, G., Cerón-Lizárraga, T. L., Martínez-Barrera, L., et al. (2010). Randomized phase II trial of All-trans-retinoic acid with chemotherapy based on paclitaxel and cisplatin as first-line treatment in patients with advanced non-small-cell lung cancer. *J. Clin. Oncol.* 28 (21), 3463–3471. doi:10.1200/JCO.2009.26.6452

Atzpodien, J., Kirchner H Fau - Jonas, U., Jonas U Fau - Bergmann, L., BergmannFau - Schott, L. H., Schott H Fau - Heynemann, H., Heynemann H Fau - Fornara, P., et al. (2004). *Interleukin-2- and interferon alfa-2a-based immunochemotherapy in advanced renal cell carcinoma: A prospectively randomized trial of the German cooperative renal carcinoma chemoimmunotherapy group*. New York, NY: DGCIN. -183X (Print), 0732. doi:10.1200/JCO.2004.06.155

Aviles, A., Neri, N., Fernandez-Diez, J., Silva, L., and Nambo, M. J. (2015). Interferon and low doses of methotrexate versus interferon and retinoids in the treatment of refractory/relapsed cutaneous T-cell lymphoma. *Hematol. Amst. Neth.* 20 (9), 538–542. doi:10.1179/1607845415Y.0000000002

Bernstein, Z. P., Chanan-Khan, A., Miller, K. C., Northfelt, D. W., Lopez-Berestein, G., and Gill, P. S. (2002). A multicenter phase II study of the intravenous administration of liposomal tretinoin in patients with acquired immunodeficiency syndrome-associated Kaposi's sarcoma. *Cancer* 95 (12), 2555–2561. doi:10.1002/cncr.11009

Bhatia, A. K., Lee, J.-W., Pinto, H. A., Jacobs, C. D., Limburg, P. J., Rubin, P., et al. (2017). Double-Blind, randomized phase 3 trial of low-dose 13-cis retinoic acid in the prevention of second primaries in head and neck cancer: Long-term follow-up of a trial of the eastern cooperative oncology group-ACRIN cancer research group (C0590). *Cancer* 123 (23), 4653–4662. doi:10.1002/cncr.30920

Bodsworth, N. J., Bloch, M., Bower, M., Donnell, D., and Yocum, R. (2001). Phase III vehicle-controlled, multi-centered study of topical alitretinoin gel 0.1% in cutaneous AIDS-related Kaposi's sarcoma. *Am. J. Clin. Dermatol.* 2 (2), 77–87. doi:10.2165/00128071-200102020-00004

Burnett, A. K., Hills, R. K., Milligan, D. W., Goldstone, A. H., Prentice, A. G., McMullin, M. F., et al. (2010). Attempts to optimize induction and consolidation treatment in acute myeloid leukemia: Results of the MRC AML12 trial. *J. Clin. Oncol.* 28 (4), 586–595. doi:10.1200/JCO.2009.22.9088

Burnett, A. K., Milligan, D., Prentice, A. G., Goldstone, A. H., McMullin, M. F., Hills, R. K., et al. (2007). A comparison of low-dose cytarabine and hydroxyurea with or without all-trans retinoic acid for acute myeloid leukemia and high-risk myelodysplastic syndrome in patients not considered fit for intensive treatment. *Cancer* 109 (6), 1114–1124. doi:10.1002/cncr.22496

Chiesa, F., Tradati, N., Grigolato, R., Boracchi, P., Biganzoli, E., Crose, N., et al. (2005). Randomized trial of fenretinide (4-HPR) to prevent recurrences, new localizations and carcinomas in patients operated on for oral leukoplakia: Long-term results. *Int. J. Cancer* 115 (4), 625–629. doi:10.1002/ijc.20923

Chlapek, P., Slavikova, V., Mazanek, P., Sterba, J., and Veselska, R. (2018). Why differentiation therapy sometimes fails: Molecular mechanisms of resistance to retinoids. *Int. J. Mol. Sci.* 19 (1), E132. doi:10.3390/ijms19010132

Chu, K. J., Lai Ec Fau - Yao, X.-P., Yao Xp Fau - Zhang, H.-W., Zhang Hw Fau - Lau, W. Y., Lau Wy Fau - Fu, X.-H., Fu Xh Fau - Lu, C.-D., et al. (20100219). Vitamin analogues in chemoprevention of hepatocellular carcinoma after resection or ablation-a systematic review and meta-analysis–3108. *(Electronic)*.59.. doi:10.1016/S1015-9584(10)60021-8

Cortés-Jofré, M., Rueda, J. R., Asenjo-Lobos, C., Madrid, E., and Bonfill Cosp, X. (2020). Drugs for preventing lung cancer in healthy people, 1469–493X. *(Electronic)*.doi:10.1002/14651858.CD002141

Cosio, T. A.-O., Di Prete, M. A.-O., Gaziano, R. A.-O., Lanna, C., Orlandi, A. A.-O., Di Francesco, P., et al. (2021). *Trifarotene: A current review and perspectives in dermatology*, 2227–9059. LID -[doi] LID - 237(Print). doi:10.3390/biomedicines9030237

Decensi, A., Robertson C Fau - Guerrieri-Gonzaga, A., Guerrieri-Gonzaga A Fau - Serrano, D., Serrano D Fau - Cazzaniga, M., Cazzaniga M Fau - Mora, S., Mora S Fau - Gulisano, M., et al. (2009). Randomized double-blind 2 x 2 trial of low-dose tamoxifen and fenretinide for breast cancer prevention in high-risk premenopausal women, 1527–7755. *(Electronic)*.27. doi:10.1200/JCO.2008.19.3797

Devalaraja, S., To, T. K. J., Folkert, I. W., Natesan, R., Alam, M. Z., Li, M., et al. (2020). Tumor-derived retinoic acid regulates intratumoral monocyte differentiation to promote immune suppression. *Cell* 180 (6), 10981098–10981114. doi:10.1016/j.cell.2020.02.042

Douer, D., Zickl, L. N., Schiffer, C. A., Appelbaum, F. R., Feusner, J. H., Shepherd, L., et al. (2013). All-trans retinoic acid and late relapses in acute promyelocytic leukemia: Very long-term follow-up of the North American intergroup study I0129. *Leuk. Res.* 37 (7), 795–801. doi:10.1016/j.leukres.2013.03.001

Fenaux, P., Chevret, S., Guerci, A., Fegueux, N., Dombret, H., Thomas, X., et al. (2000). Long-term follow-up confirms the benefit of all-trans retinoic acid in acute promyelocytic leukemia. European APL group. *Leukemia* 14 (8), 1371–1377. doi:10.1038/sj.leu.2401859

Follen, M., Atkinson, E. N., Schottenfeld, D., Malpica, A., West, L., Lippman, S., et al. (2001). A randomized clinical trial of 4-hydroxyphenylretinamide for high-grade squamous intraepithelial lesions of the cervix. *Clin. Cancer Res.* 7 (11), 3356–3365.

Fosså, S. D., Mickisch, G. H., De Mulder, P. H., Horenblas, S., van Oosterom, A. T., van Poppel, H., et al. (2004). Interferon-alpha-2a with or without 13-cis retinoic acid in patients with progressive, measurable metastatic renal cell carcinoma. *Cancer* 101 (3), 533–540. doi:10.1002/cncr.20307

Fritz, H., Kennedy D Fau - Fergusson, D., Fergusson D Fau - Fernandes, R., Fernandes R Fau - Doucette, S., Doucette S Fau - Cooley, K., CooleyFau - Seely, K. A., et al. (2011). Vitamin A and retinoid derivatives for lung cancer: A systematic review and meta analysis, 1932–6203. *(Electronic)*.6, doi:10.1371/journal.pone.0021107

Fulan, H., Changxing J Fau - Baina, W. Y., Baina Wy Fau - Wencui, Z., WencuiFau - Chunqing, Z. L., ChunqingFau - Fan, L. W., Fan W Fau - Dandan, L., et al. (2011).Retinol, vitamins A, C, and E and breast cancer risk: A meta-analysis and meta-regression, 1573–7225. *(Electronic)*. doi:10.1007/s10552-011-9811-y

George, R., Weightman, W., Russ, G. R., Bannister, K. M., and Mathew, T. H. (2002). Acitretin for chemoprevention of non-melanoma skin cancers in renal transplant recipients. *Australas. J. Dermatol.* 43 (4), 269–273. doi:10.1046/j.1440-0960.2002.00613.x

Harrison, E. H. (2005). *Mechanisms of digestion and absorption of dietary vitamin A*, 0199–9885. (Print). doi:10.1146/annurev.nutr.25.050304.092614

He, J., Gu, Y., and Zhang, S. (20181938). Vitamin A and breast cancer survival: A systematic review and meta-analysis–0666. *(Electronic)*.7. doi:10.1016/j.clbc.2018.07.025

Helm, C. W., Lorenz Dj Fau - Meyer, N. J., Meyer Nj Fau - Rising, W. W. R., Rising Ww Fau - Wulff, J. L., and Wulff, J. L. (2013). Retinoids for preventing the progression of cervical intra-epithelial neoplasia, 1469–493X. *(Electronic)*.10.doi:10.1002/14651858.CD003296.pub3

Htet, K. Z., Waul, M. A., and Leslie, K. S. (2022). Topical treatments for Kaposi sarcoma: A systematic review. *Skin. Health Dis.* 2 (2), e107. doi:10.1002/ski2.107

Kadakia, K. C., Barton, D. L., Loprinzi, C. L., Sloan, J. A., Otley, C. C., Diekmann, B. B., et al. (2012). Randomized controlled trial of acitretin versus placebo in patients at high-risk for basal cell or squamous cell carcinoma of the skin (North Central Cancer Treatment Group Study 969251). *Cancer* 118 (8), 2128–2137. doi:10.1002/cncr.26374

Khalil, S., Bardawil, T., Stephan, C., Darwiche, N., Abbas, O., Kibbi, A. G., et al. (2017). Retinoids: A journey from the molecular structures and mechanisms of action to clinical uses in dermatology and adverse effects, 1471–1753. *(Electronic)*.28. doi:10.1080/09546634.2017.1309349

Khuri, F. R., Lee, J. J., Lippman, S. M., Kim, E. S., Cooper, J. S., Benner, S. E., et al. (2006). Randomized phase III trial of low-dose isotretinoin for prevention of second primary tumors in stage I and II head and neck cancer patients. *J. Natl. Cancer Inst.* 98 (7), 441–450. doi:10.1093/jnci/djj091

Kim, H., Lapointe J Fau - Kaygusuz, G., Kaygusuz G Fau - Ong, D. E., Ong De Fau - Li, C., Li C Fau - van de Rijn, M., van de Rijn M Fau - Brooks, J. D., et al. (2005). The retinoic acid synthesis gene ALDH1a2 is a candidate tumor suppressor in prostate cancer, 0008–5472. *(Print)*.65. doi:10.1158/0008-5472.CAN-04-4562

Kohler, J. A., Imeson, J., Ellershaw, C., and Lie, S. O. (2000). A randomized trial of 13-Cis retinoic acid in children with advanced neuroblastoma after high-dose therapy. *Br. J. Cancer* 83 (9), 1124–1127. doi:10.1054/bjoc.2000.1425

Larange, A., and Cheroutre, H. (2016). Retinoic acid and retinoic acid receptors as pleiotropic modulators of the immune system, 1545–3278. *(Electronic)*.36. doi:10.1146/annurev-immunol-041015-055427

Lee, J. J., Feng, L., Reshef, D. S., Sabichi, A. L., Williams, B., Rinsurongkawong, W., et al. (2010). Mortality in the randomized, controlled lung intergroup trial of isotretinoin. *Cancer Prev. Res.* 3 (6), 738–744. doi:10.1158/1940-6207.Capr-09-0124

Lippman, S. M., Lee, J. J., Karp, D. D., Vokes, E. E., Benner, S. E., Goodman, G. E., et al. (2001). Randomized phase III intergroup trial of isotretinoin to prevent second primary tumors in stage I non-small-cell lung cancer. *J. Natl. Cancer Inst.* 93 (8), 605–618. doi:10.1093/jnci/93.8.605

Motzer, R. J., Murphy, B. A., Bacik, J., Schwartz, L. H., Nanus, D. M., Mariani, T., et al. (2000). Phase III trial of interferon alfa-2a with or without 13-cis-retinoic acid for patients with advanced renal cell carcinoma. *J. Clin. Oncol.* 18 (16), 2972–2980. doi:10.1200/JCO.2000.18.16.2972

Nazha, A., Bueso-Ramos, C., Estey, E., Faderl, S., O'Brien, S., Fernandez, M. H., et al. (2013). The addition of all-trans retinoic acid to chemotherapy may not improve the outcome of patient with NPM1 mutated acute myeloid leukemia. *Front. Oncol.* 3, 218. doi:10.3389/fonc.2013.00218

Ni, X., Hu, G., and Cai, X. (2019). The success and the challenge of all-trans retinoic acid in the treatment of cancer, 1549–7852. *(Electronic)*.59. doi:10.1080/10408398.2018.1509201

Okita, K., Izumi, N., Ikeda, K., Osaki, Y., Numata, K., Ikeda, M., et al. (2015b). Survey of survival among patients with hepatitis C virus-related hepatocellular carcinoma treated with peretinoin, an acyclic retinoid, after the completion of a randomized, placebo-controlled trial. *J. Gastroenterol.* 50 (6), 667–674. doi:10.1007/s00535-014-0996-1

Okita, K., IzumiFau - Matsui, N. O., O Fau - Tanaka, MatsuiK., TanakaFau - Kaneko, K. S., Kaneko S Fau - Moriwaki, H., H Fau - Ikeda, MoriwakiK., et al. (2015a).Peretinoin after curative therapy of hepatitis C-related hepatocellular carcinoma: A randomized double-blind placebo-controlled study, 1435–5922. *(Electronic)*.50. doi:10.1007/s00535-014-0956-9

Perry, C. F., Stevens, M., Rabie, I., Yarker, M. E., Cochrane, J., Perry, E., et al. (2005). Chemoprevention of head and neck cancer with retinoids: A negative result. *Arch. Otolaryngol. Head. Neck Surg.* 131 (3), 198–203. doi:10.1001/archotol.131.3.198

Rao, R. D., Cobleigh, M. A., Gray, R., Graham Ii, M. L., Norton, L., Martino, S., et al. (2011). Phase III double-blind, placebo-controlled, prospective randomized trial of adjuvant tamoxifen vs. tamoxifen and fenretinide in postmenopausal women with positive receptors (EB193): An intergroup trial coordinated by the Eastern Cooperative Oncology Group. *Med. Oncol.* 28 (1), S39–S47. doi:10.1007/s12032-010-9682-1

Richtig, E., Soyer, H. P., Posch, M., Mossbacher, U., Bauer, P., Teban, L., et al. (2005). Prospective, randomized, multicenter, double-blind placebo-controlled trial comparing adjuvant interferon alfa and isotretinoin with interferon alfa alone in stage IIA and IIB melanoma: European cooperative adjuvant melanoma treatment study group. *J. Clin. Oncol.* 23 (34), 8655–8663. doi:10.1200/JCO.2004.00.8128

Robinson, W. R., Andersen, J., Darragh, T. M., Kendall, M. A., Clark, R., and Maiman, M. (2002). Isotretinoin for low-grade cervical dysplasia in human immunodeficiency virus-infected women. *Obstet. Gynecol.* 99 (5 1), 777–784. doi:10.1016/s0029-7844(02)01949-x

Ruffin, M. T., Bailey, J. M., Normolle, D. P., Michael, C. W., Bieniasz, M. E., Kmak, D. C., et al. (2004). Low-dose topical delivery of all-trans retinoic acid for cervical intraepithelial neoplasia II and III. *Cancer Epidemiol. Biomarkers Prev.* 13 (12), 2148–2152. doi:10.1158/1055-9965.2148.13.12

Sabichi, A. L., Lerner, S. P., Atkinson, E. N., Grossman, H. B., Caraway, N. P., Dinney, C. P., et al. (2008). Phase III prevention trial of fenretinide in patients with resected non-muscle-invasive bladder cancer. *Clin. Cancer Res.* 14 (1), 224–229. doi:10.1158/1078-0432.CCR-07-0733

Sanusi, R. S. (2019). Outcome of combined neoadjuvant chemotherapy and vitamin A in advanced cervical carcinoma: A randomized double-blind clinical trial. *Asian pac. J. Cancer Prev.* 20 (7), 2213–2218. doi:10.31557/apjcp.2019.20.7.2213

Scardina, G. A., Carini, F., Maresi, E., Valenza, V., and Messina, P. (2006). Evaluation of the clinical and histological effectiveness of isotretinoin in the therapy of oral leukoplakia: Ten years of experience: Is management still up to date and effective? *Methods Find. Exp. Clin. Pharmacol.* 28 (2), 115–119. doi:10.1358/mf.2006.28.2.977843

Shen, Z. X., Shi, Z. Z., Fang, J., Gu, B. W., Li, J. M., Zhu, Y. M., et al. (2004). All-trans retinoic acid/As2O3 combination yields a high quality remission and survival in newly diagnosed acute promyelocytic leukemia. *Proc. Natl. Acad. Sci. U. S. A.* 101 (15), 5328–5335. doi:10.1073/pnas.0400053101

Shinagawa, K., Yanada, M., Sakura, T., Ueda, Y., Sawa, M., Miyatake, J., et al. (2014). Tamibarotene as maintenance therapy for acute promyelocytic leukemia: Results from a randomized controlled trial. *J. Clin. Oncol.* 32 (33), 3729–3735. doi:10.1200/JCO.2013.53.3570

Takai, K., Okuno, M., Yasuda, I., Matsushima-Nishiwaki, R., Uematsu, T., Tsurumi, H., et al. (2005). Prevention of second primary tumors by an acyclic retinoid in patients with hepatocellular carcinoma: Updated analysis of the long-term follow-up data. *Intervirology* 48 (1), 39–45. doi:10.1159/000082093

Tang, J. E., Wang, R. J., ZhongFau - Yu, H. B., YuFau - Chen, B. Y., and Chen, Y. (2014). Vitamin A and risk of bladder cancer: A meta-analysis of epidemiological studies, 1477–7819. *(Electronic)*. doi:10.1186/1477-7819-12-130

Tang, X. H., and Gudas, L. J. (2011). Retinoids, retinoic acid receptors, and cancer. *Annu. Rev. Pathol.* 6, 345–364. doi:10.1146/annurev-pathol-011110-130303

Toma, S., Bonelli, L., Sartoris, A., Mira, E., Antonelli, A., Beatrice, F., et al. (2004). 13-cis retinoic acid in head and neck cancer chemoprevention: Results of a randomized trial from the Italian head and neck chemoprevention study group. *Oncol. Rep.* 11 (6), 1297–1305. doi:10.3892/or.11.6.1297

van Zandwijk, N., Dalesio, O., Pastorino, U., de Vries, N., and van Tinteren, H. (2000). EUROSCAN, a randomized trial of vitamin A and N-acetylcysteine in patients with head and neck cancer or lung cancer. For the European organization for research and treatment of cancer head and neck and lung cancer cooperative groups. *J. Natl. Cancer Inst.* 92 (12), 977–986. doi:10.1093/jnci/92.12.977

Veronesi, U., Mariani, L., Decensi, A., Formelli, F., Camerini, T., Miceli, R., et al. (2006). Fifteen-year results of a randomized phase III trial of fenretinide to prevent second breast cancer. *Ann. Oncol.* 17 (7), 1065–1071. doi:10.1093/annonc/mdl047

Weinstock, M. A., Bingham, S. F., Digiovanna, J. J., Rizzo, A. E., Marcolivio, K., Hall, R., et al. (2012). Tretinoin and the prevention of keratinocyte carcinoma (basal and squamous cell carcinoma of the skin): A veterans affairs randomized chemoprevention trial. *J. Investig. Dermatol.* 132 (6), 1583–1590. doi:10.1038/jid.2011.483

Weinstock, M. A., Bingham, S. F., Lew, R. A., Hall, R., Eilers, D., Kirsner, R., et al. (2009). Topical tretinoin therapy and all-cause mortality. *Arch. Dermatol.* 145 (1), 18–24. doi:10.1001/archdermatol.2008.542

Yu, N., Su, X., Wang, Z., Dai, B., and Kang, J. (20152072).Association of dietary vitamin A and β-carotene intake with the risk of lung cancer: A meta-analysis of 19 publications–6643. *(Electronic)*.7. doi:10.3390/nu7115463

Zhang, X., DaiFau - Zhang, B. B., ZhangFau - Wang, B. Z., and Wang, Z. (2012). Vitamin A and risk of cervical cancer: A meta-analysis, 1095–6859. *Electronic*.124, 2. doi:10.1016/j.ygyno.2011.10.012

frontiers | Frontiers in Genetics

TYPE Original Research
PUBLISHED 16 November 2022
DOI 10.3389/fgene.2022.997739

OPEN ACCESS

EDITED BY
Simin Li,
Southern Medical University, China

REVIEWED BY
Yupei Deng,
China Tibetology Research Center, China
Zhixiang Yu,
Fourth Military Medical University, China

*CORRESPONDENCE
Dongfang Wu,
wudf@yucebio.com
Yu Peng,
pengyu20220718@163.com

†These authors have contributed equally to this work

SPECIALTY SECTION
This article was submitted to Cancer Genetics and Oncogenomics, a section of the journal Frontiers in Genetics

RECEIVED 19 July 2022
ACCEPTED 17 October 2022
PUBLISHED 16 November 2022

CITATION
Liang H, Zhao Y, Liu K, Xiao Y, Chen K, Li D, Zhong S, Zhao Z, Wu D and Peng Y (2022), The mechanism of lncRNAs in the crosstalk between epithelial-mesenchymal transition and tumor microenvironment for early colon adenocarcinoma based on molecular subtyping.
Front. Genet. 13:997739.
doi: 10.3389/fgene.2022.997739

The mechanism of lncRNAs in the crosstalk between epithelial-mesenchymal transition and tumor microenvironment for early colon adenocarcinoma based on molecular subtyping

Hanlin Liang[1†], Yi Zhao[2†], Kai Liu[3†], Yajie Xiao[4†], Kexu Chen[1], Delan Li[1], Shupeng Zhong[1], Zhikun Zhao[4], Dongfang Wu[4*] and Yu Peng[5*]

[1]Chemotherapy Department, Zhongshan City People's Hospital, Zhongshan, China, [2]GI Medicine, The Third Hospital Affiliated to Naval Medical University, Shanghai, China, [3]Department of Colorectal Oncology, National Clinical Research Center for Cancer, Key Laboratory of Cancer Prevention and Therapy of Tianjin, Tianjin's Clinical Research Center for Cancer, Tianjin Medical University Cancer Institute and Hospital, Tianjin, China, [4]Department of Medicine, YuceBio Technology Co., Ltd., Shenzhen, China, [5]Oncology Department, Jiangmen Central Hospital, Jiangmen, China

A large number of colon adenocarcinoma (COAD) patients are already advanced when diagnosed. In this study, we aimed to further understand the mechanism of tumor development in early COAD by focusing on epithelial-mesenchymal transition (EMT) and long non-coding RNAs (lncRNAs). Expression profiles of early COAD patients were obtained from public databases. EMT-related lncRNAs were used as a basis for constructing molecular subtypes through unsupervised consensus clustering. Genomic features, pathways and tumor microenvironment (TME) were compared between two subtypes. LncATLAS database was applied to analyze the relation between lncRNAs and transcription factors (TFs). First order partial correlation analysis was conducted to identify key EMT-related lncRNAs.C1 and C2 subtypes with distinct prognosis were constructed. Oncogenic pathways such as EMT, KRAS signaling, JAK-STAT signaling, and TGF-β signaling were significantly enriched in C2 subtype. Higher immune infiltration and expression of immune checkpoints were also observed in C2 subtype, suggesting the key EMT-related lncRNAs may play a critical role in the modulation of TME. In addition, JAK-STAT signaling pathway was obviously enriched in upregulated TFs in C2 subtype, which indicated a link between key lncRNAs and JAK-STAT signaling that may regulate TME. The study further expanded the research on the role of EMT-related lncRNAs in the early COAD. The six identified EMT-related lncRNAs could serve as biomarkers for early screening COAD.

KEYWORDS

colon adenocarcinoma, epithelial-mesenchymal transition, long non-coding RNAs, tumor microenvironment, transcription factors, biomarkers, bioinformatics analysis

Introduction

According to the global cancer statistics, colon adenocarcinoma (COAD) is the sixth most diagnosed cancer with 1,148,515 new cases in 2020, contributing 6.0% of all new diagnosed cancer cases (Sung et al., 2021). Simultaneously, the death cases contribute 5.8% (576,858) of all deaths by cancer, which is the fifth leading cause of cancer death in 2020. Although the 5-year overall survival (OS) is upon 75% of American Joint Committee on Cancer (AJCC) stage I and II, a dramatically decreased survival of distant metastasis is shown with only less than 20% of AJCC stage IV (Ulanja et al., 2019). Prognostic difference is shown between right-sided and left-sided colon cancer, and left-sided colon cancer has a lower death risk than right-sided colon cancer (Petrelli et al., 2017), which may result from their genetic and immunological differences (Lee et al., 2015). Screening techniques for colon cancer include invasive and non-invasive tests. Colonoscopic tests are recommended for high-risk individuals and non-colonoscopic tests are recommended in average-risk individuals according to European Society for Medical Oncology (EMSO) clinical practice guidelines (Argilés et al., 2020). However, they are not sensitive in the diagnosis of early colon cancer. Actually, a number of patients are already advanced when diagnosed as COAD. Therefore, early screening of COAD is of great value for improving prognosis and releasing cancer burden worldwide.

To reach accurate screening, comprehensive understanding of COAD tumorigenesis and development is a basis for identifying effective biomarkers for COAD screening. Of the hallmarks of cancers, epithelial-mesenchymal transition (EMT) is one of the most important features contributing for metastasis (Dongre and Weinberg, 2019). Tumor microenvironment (TME), another important component in cancer tissue, has been demonstrated to have a strong correlation with EMT through the linkages of proinflammatory factors such as TGF-β, TNF-α, and IL-6 (Jung et al., 2015). Among these interactions, long non-coding RNAs (lncRNAs) are considered as critical regulators for modulating TME and managing EMT (Sun et al., 2018; O'Brien et al., 2020). Oncogenic pathways involving in EMT such as WNT signaling, JAK-STAT3 signaling (Xue et al., 2018), mTOR signaling and MAPK/ERK signaling have been illustrated to be regulated by various lncRNAs (O'Brien et al., 2020). In colon cancer, lncRNA-HOTAIR associated with EMT was identified as a predictor of metastasis and prognosis (Wu et al., 2014).

As lncRNAs are of potential to serve as biomarkers for COAD prognosis, we consider that lncRNAs involving in EMT process may also be effective predictors for COAD. Therefore, in this study, we tried to construct a novel molecular subtyping system based on EMT-related lncRNAs. Compared to pathological subtyping or clinical features, molecular subtyping is more accurate for classifying cancer patients into different classes with different prognosis. By exploring the mechanisms of EMT-related lncRNAs in tumorigenesis in COAD, we further identified six key EMT-related lncRNAs that could serve as biomarkers for early screening COAD.

Materials and methods

Sample collection

COAD samples were obtained from public databases through Sangerbox platform (Shen et al., 2022). RNA-seq data with clinical information was downloaded from The Cancer Genome Atlas (TCGA) database. GSE17538 with gene expression profiles was downloaded from Gene Expression Omnibus (GEO) database. In TCGA-COAD and GSE17538 cohorts, only samples of stage I and II were retained, and samples without survival information were removed. The clinical information of COAD samples was shown in Table 1.

TABLE 1 The clinical information of COAD samples.

Clinical features	TCGA-COAD	GSE17538
OS		
0 (alive)	199	80
1 (dead)	26	20
T Stage		
T1	8	
T2	61	
T3	145	
T4	10	
TX	1	
N Stage		
N0	225	
M Stage		
M0	204	
MX	21	
Stage		
I	70	28
II	155	72
Gender		
Female	99	47
Male	126	53
Age		
<=70	117	53
>70	108	47

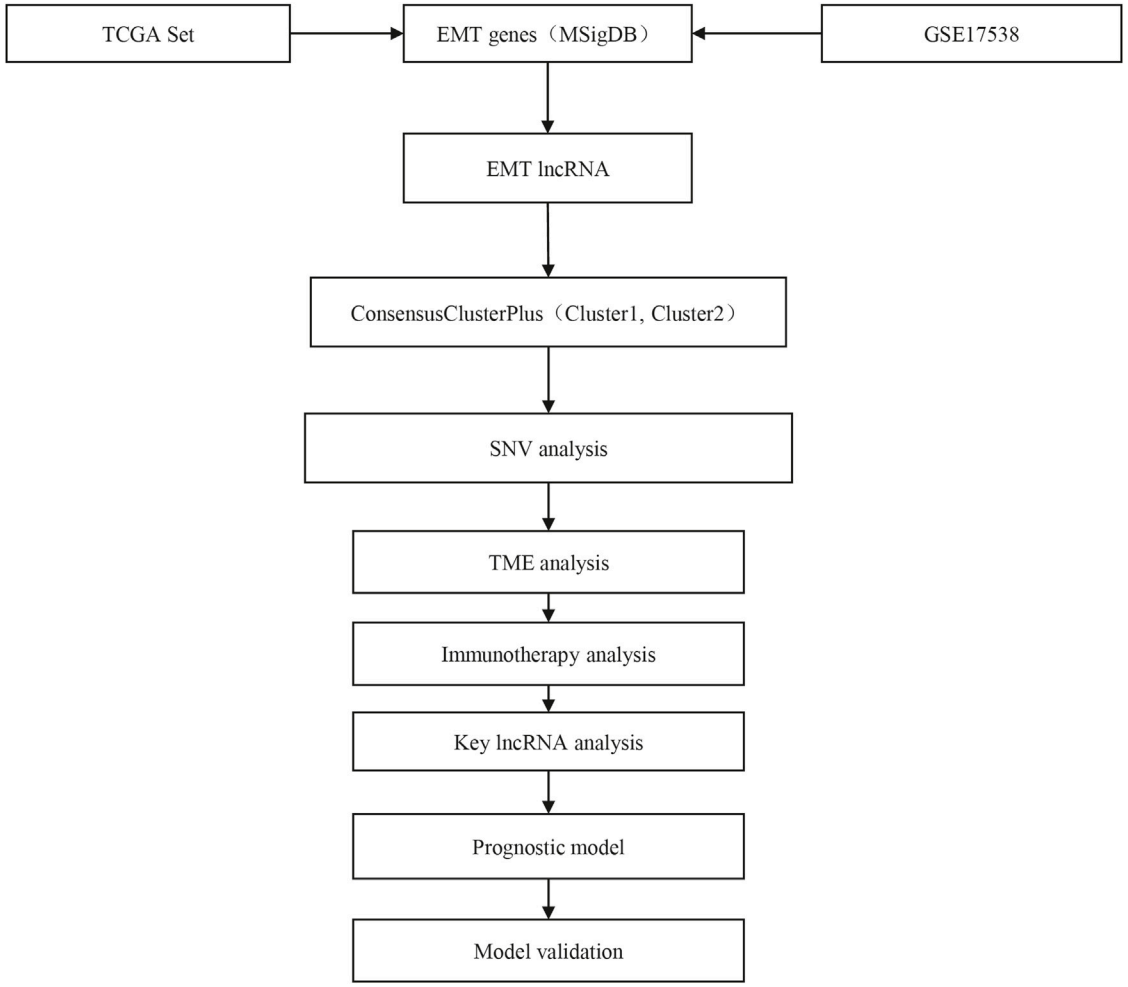

FIGURE 1
The work flow of this study.

Identification of epithelial-mesenchymal transition-related lncRNAs

EMT-related genes in hallmark EMT pathway were obtained from Molecular Signatures Database (MSigDB, v7.4, https://www.gsea-msigdb.org/gsea/msigdb/) (Liberzon et al., 2015). LncRNAs and mRNAs in TCGA-COAD and GSE17538 cohorts were annotated by gene transfer format (GTF, v32) file which was downloaded from GENCODE (https://www.gencodegenes.org/).

EMT score of each sample was calculated by single sample gene set enrichment analysis (ssGSEA) in GSVA R package (Hänzelmann et al., 2013). Then Pearson correlation analysis was employed to calculate correlation coefficients between EMT score and expression of lncRNAs. EMT-related lncRNAs were determined by the conditions of |coefficient| > 0.25 and $p < 0.05$.

Identification of molecular subtypes based on epithelial-mesenchymal transition-related lncRNAs

Screened EMT-related lncRNAs that were overlapped in TCGA-COAD and GSE17538 cohorts were used as a basis to construct molecular subtypes. Unsupervised consensus clustering in ConsensusClusterPlus R package was implemented to construct consensus matrix (Wilkerson and Hayes, 2010). KM algorithm and Euclidean distance were used to conduct 500 bootstraps with each bootstrap containing 80% samples. Cluster number k from 2 to 10 was included to screen the optimal cluster according to consensus matrix and cumulative distribution function (CDF).

Gene set enrichment analysis

GSEA is a powerful analytical method for interpreting biological processes based on gene expression profiles (Subramanian et al., 2005), which was applied to assess hallmark pathways for two subtypes. Hallmark pathways with a series of gene sets were obtained from MSigDB (Liberzon et al., 2015). The proportion of 28 immune cells was estimated by GSEA based on gene signatures of different cell types (Şenbabaoğlu et al., 2016). Estimation of STromal and Immune cells in MAlignant Tumours using Expression data (ESTIMATE) (Yoshihara et al., 2013), also based on GSEA was used to calculate stromal score and immune score of two subtypes. ClusterProfiler R package was used to annotate Kyoto Encyclopedia of Genes and Genomes (KEGG) pathways on TFs and EMT-related lncRNAs (Yu et al., 2012).

Localization of lncRNAs and calculation of transcription factor activity

Relative concentration index (RCI) based on LncATLAS database was introduced to measure the localization of lncRNAs (Mas-Ponte et al., 2017). RCI >0 indicates lncRNAs localizing in the cytoplasm and RCI <0 indicates the nuclear. The TF activity was assessed according to the algorithm from Garcia-Alonso et al. Garcia-Alonso et al. (2018). Pearson correlation analysis was conducted to analyze the association between EMT-related lncRNAs and TFs.

Identification of key epithelial-mesenchymal transition-related lncRNAs

First order partial correlation analysis was used to evaluate the linkage among EMT-related lncRNAs, EMT score and EMT-related genes (Reverter and Chan, 2008). The association between two variables were largely decreased when eliminating the effect of another variable, and the variable was considered as key EMT-related lncRNA strongly associated with EMT score and EMT-related genes.

The identified key EMT-related lncRNAs were used to construct a prognostic model for predicting OS. Univariate Cox regression analysis was conducted on these lncRNAs and coefficients were generated for building the model, defining as: risk score =Σ (beta i × exp i). Beta represents coefficients and exp represents the expression of lncRNAs.

Statistical analysis

Statistical analysis was performed in R (4.1.1) software. Parameters of R packages and software were default if no

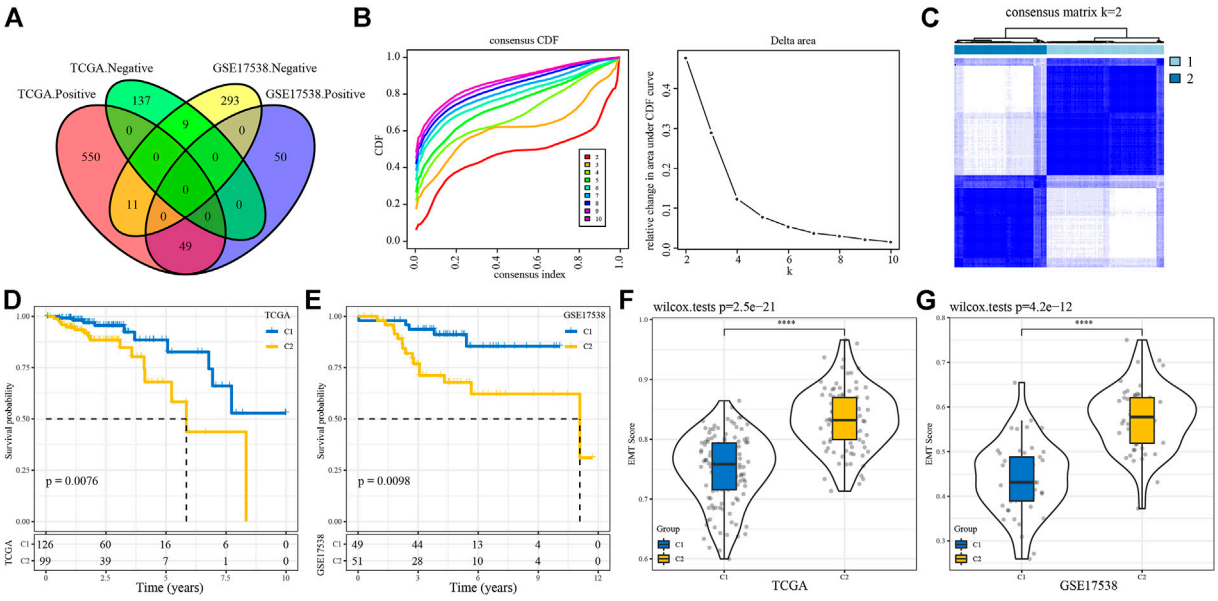

FIGURE 2
Construction of molecular subtypes based on EMT-related lncRNAs **(A)** Venn plot of lncRNAs positively or negatively correlated with EMT activity. **(B)** CDF curves of different cluster numbers (k) from 2 to 10 **(C)** Consensus matrix when cluster number k = 2. **(D–E)** Kaplan-Meier survival curves of C1 and C2 subtypes in TCGA-COAD **(D)** and GSE17538 **(E)** cohorts. Log-rank test was conducted. **(F–G)** Differential EMT score of C1 and C2 subtypes in two cohorts. Wilcoxon test was conducted. ****$p < 0.0001$.

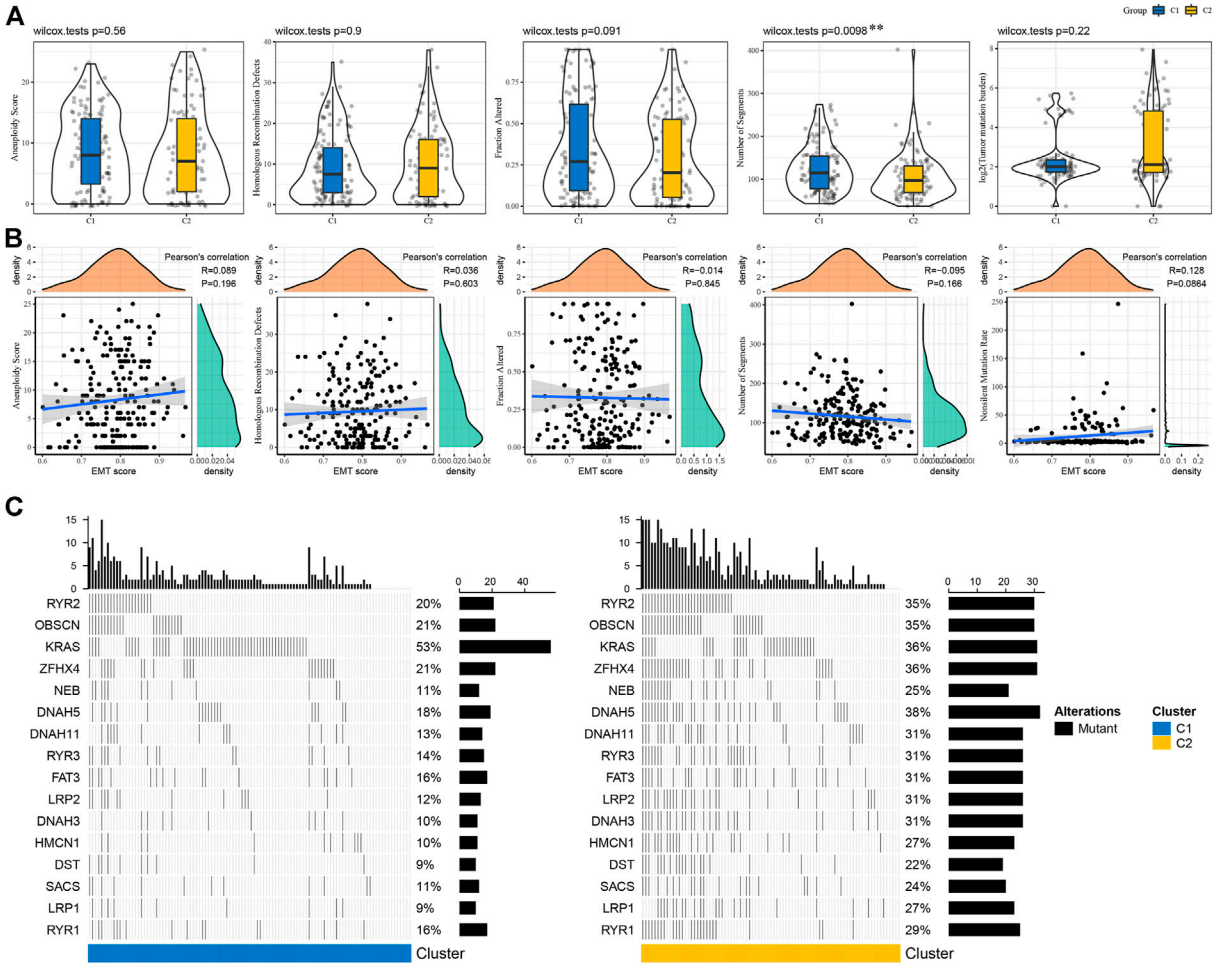

FIGURE 3
Mutation patterns of C1 and C2 subtypes **(A)** Genomic features of two subtypes including aneuploidy, homologous recombination defects, fraction altered, number of segments and tumor mutation burden. Wilcoxon test was performed. **(B)** Pearson correlation analysis between genomic features and EMT score. **(C)** The top 20 significantly mutated genes in C1 and C2 subtypes. Fisher exact test was conducted. $^{**}p < 0.01$.

introduce. Statistical methods were indicated in the corresponding figure legends. $p < 0.05$ was considered as significant. ns, no sifnificance. $^{*}p < 0.05$, $^{**}p < 0.01$, $^{***}p < 0.001$, $^{****}p < 0.0001$.

Results

Constructing two molecular subtypes based on epithelial-mesenchymal transition-related lncRNAs

The work flow of this study was shown in Figure 1. To identify EMT-related lncRNAs, Pearson correlation analysis was conducted between EMT activity and lncRNA expression. A total of 756 and 412 EMT-related lncRNAs were identified in TCGA-COAD and GSE17538 cohorts respectively (Figure 2A). Then the intersected part of 58 EMT-related lncRNAs were used as a basis for unsupervised consensus clustering. The optimal cluster number (k) was determined according to CDF curve and consensus matrix (Figures 2B,C). When k = 2, samples were obviously divided into two groups. Kaplan-Meier survival analysis of two groups showed a significance of OS in both two cohorts ($p = 0.0076$ and $p = 0.0098$ in TCGA-COAD and GSE17538 respectively, Figures 2D,E). Finally, COAD samples were classified into two molecular subtypes (C1 and C2), with C1 subtype had a superior OS than C2 subtype. EMT activity shown as EMT score also varied largely between two subtypes. Not surprisingly, C2 subtype exhibited a significantly higher EMT score than C1 subtype, indicating that EMT pathway was more activated in C2 subtype ($p < 0.0001$, Figures 2F,G).

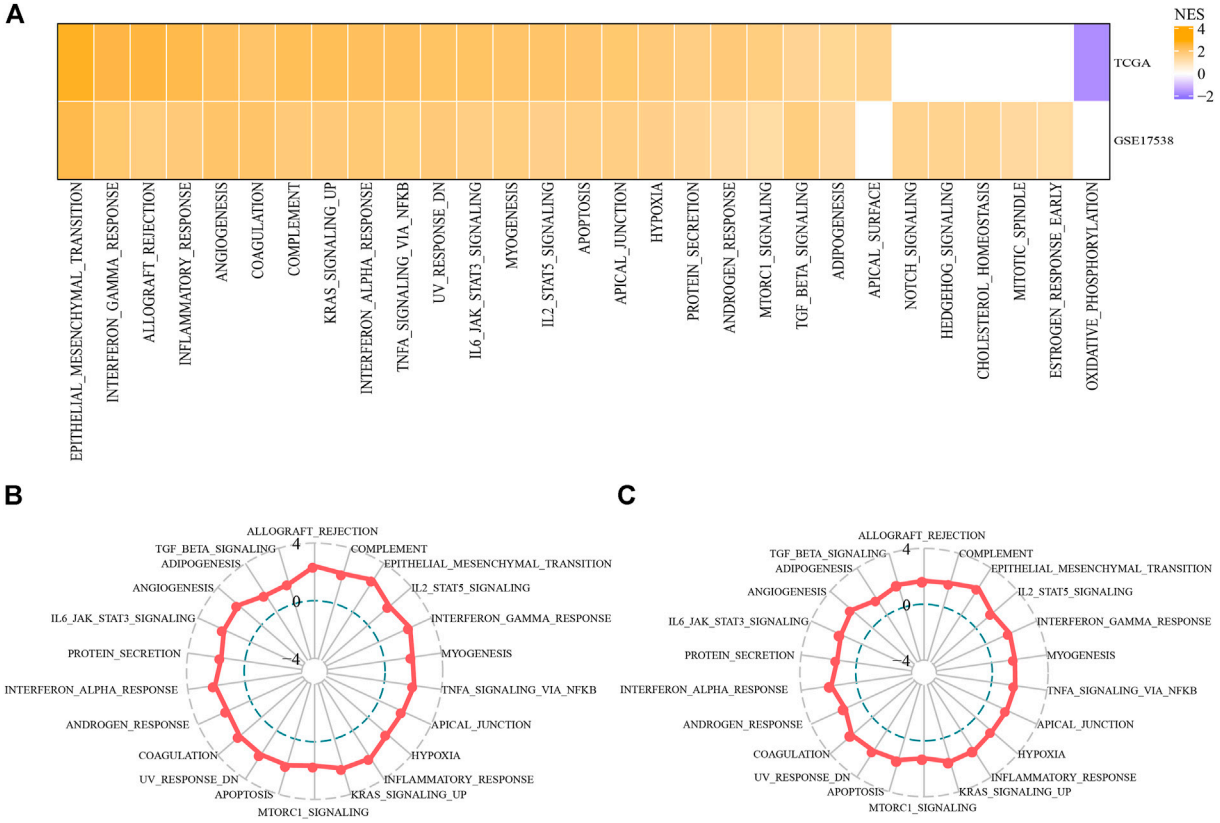

FIGURE 4
Differentially enriched pathways between C1 and C2 subtypes **(A)** Activated hallmark pathways by comparing C2 with C1 based on normalized enrichment score (NES). Orange indicates upregulated pathways in C2 and purple indicates the reverse **(B–C)** Rader plots of activated pathways of C2 subtype in TCGA-COAD **(B)** and GSE17538 **(C)** cohorts. NES was indicated as −4, 0 and 4 from inside to outside. Hallmark pathways were shown around rader plots.

In addition, the result also demonstrated that these 58 EMT-related lncRNAs may play a key role in regulating EMT activity.

Characterizing gene mutations of two molecular subtypes

We compared the genomic features between C1 and C2 subtypes in TCGA-COAD cohort on five aspects including aneuploidy, fraction altered, tumor mutation burden, homologous recombination defects and number of segments. We observed that only a significant difference was shown in number of segments between two subtypes (Figure 3A). No obvious correlation was manifested between genomic features and EMT score (Figure 3B). Gene mutation analysis revealed that samples in C2 subtype had a higher mutated proportion than C1 subtype, except for *KRAS* mutations contributing for 53% samples in C1 subtype (Figure 3C).

Oncogenic pathways were more enriched in C2 subtype

Next we tried to know if there was a difference of activated pathways between two subtypes. Hallmark pathways from MSigDB were included for GSEA and significantly enriched pathways were outpuuted with false discovery rate (FDR) < 0.05. By comparing C2 subtype with C1 subtype, we observed that C2 subtype had 23 activated and 11 suppressed pathways in TCGA-COAD cohort, and 27 activated and 9 suppressed pathways in GSE17538 cohort. Of these activated pathways, we found that oncogenic pathways and immune-related pathways were greatly enriched, such as EMT, angiogenesis, KRAS signaling, hypoxia, interferon response, TNF-α signaling, IL6-JAK-STAT3 signaling, IL2-STAT5 signaling, and TGF-β signaling pathways (Figure 4A). Overall, C2 subtype had significantly higher normalized enrichment scores (NES) of these pathways than C1 in both two cohorts (Figures 4B,C), suggesting that EMT-related lncRNAs may be extensively involved in the regulation of these pathways especially EMT.

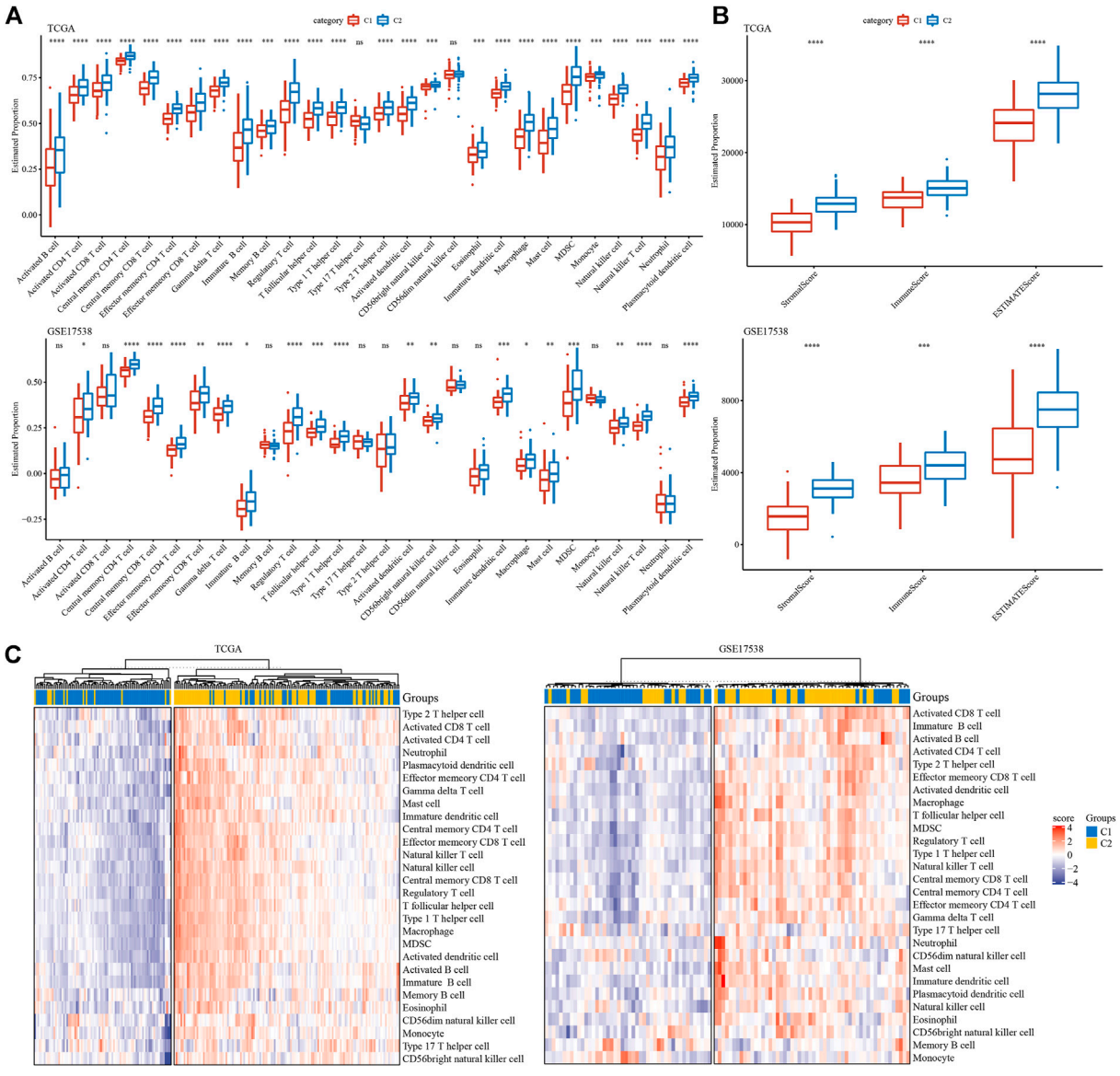

FIGURE 5
Tumor microenvironment of C1 and C2 subtypes **(A)** Estimated proportion of 28 immune cells in TCGA-COAD and GSE17538 cohorts. **(B)** Stromal score and immune score in TCGA-COAD and GSE17538 cohorts calculated by ESTIMATE. **(C)** Unsupervised consensus clustering based on gene signatures of immune cells in two cohorts. Red and purple indicates relatively high and low enrichment. Student *t* test was conducted between two groups. ns, no significance. *$p < 0.05$, **$p < 0.01$, ***$p < 0.001$, ****$p < 0.0001$.

C2 subtype had higher infiltration of immune cells

To evaluate the tumor microenvironment of C1 and C2 subtypes, we assessed the estimated proportions of a series immune cells based on gene signatures from Şenbabaoğlu et al. Şenbabaoğlu et al. (2016). To our surprise, C2 subtype had extremely higher proportions of most immune cells in both two cohorts (Figure 5A). Specifically, activated CD4 T cells, activated CD8 T cells, regulatory T cells, dendritic cells, macrophages, myeloid-derived suppressor cells (MDSCs) and natural killer cells were all more enriched in C2 subtype. ESTIMATE evaluation also supported the result that C2 subtype had higher stromal score and immune score than C1 subtype in both two cohorts ($p < 0.001$, Figure 5B). Furthermore, unsupervised consensus clustering based on these immune cells clearly divided samples into two groups of high and low immune infiltration (Figure 5C). Obviously, samples in high immune infiltration group largely belonged to C2 subtype.

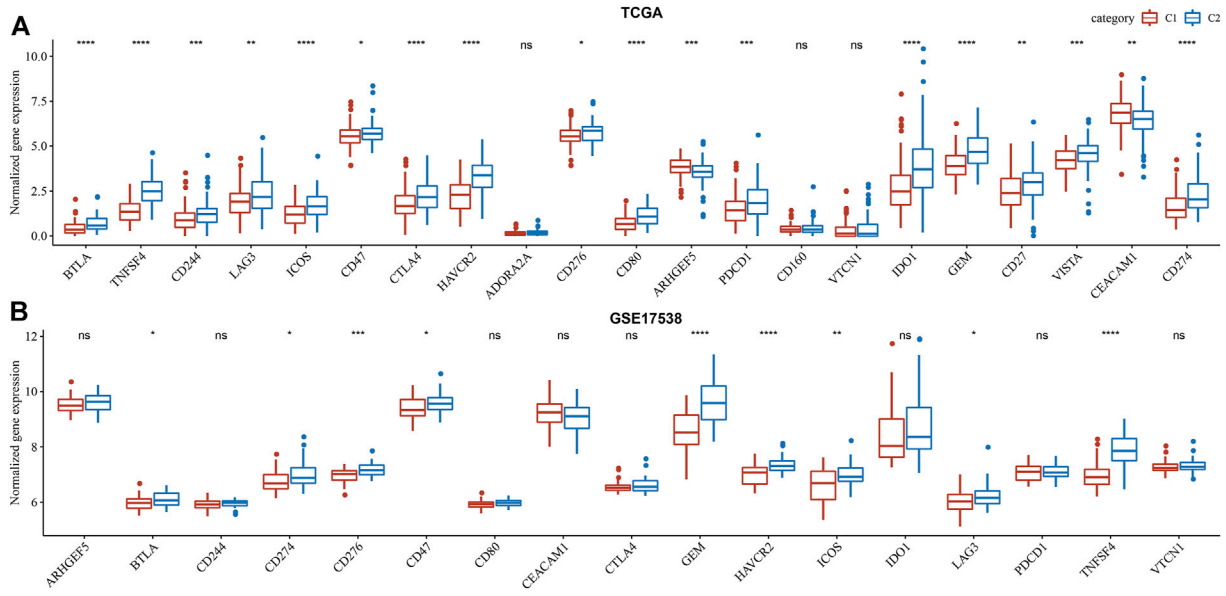

FIGURE 6
Comparison of immune checkpoint expression between two subtypes in TCGA-COAD **(A)** and GSE17538 **(B)** cohorts. Student *t* test was conducted. ns, no significance. *$p < 0.05$, **$p < 0.01$, ***$p < 0.001$, ****$p < 0.0001$.

These results implicated a close link between EMT-related lncRNAs and TME modulation.

Commonly, high immune infiltration of cytotoxic immune cells has favorable prognosis. However, immunosuppressive immune cells such as regulatory T cells and MDSCs were simultaneously increased in C2 subtype. In addition, we analyzed the expression of immune checkpoints obtained from HisgAtlas database (Liu et al., 2017). Higher expression of many important immune checkpoints was observed in C2 subtype, such as LAG3, ICOS, CTLA4, CD276, PDCD1, IDO1 and CD274 (Figure 6).

The crosstalk between epithelial-mesenchymal transition-related lncRNAs and transcription factors

Given that we have illustrated distinct molecular features of different subtypes, we implicated that EMT-related lncRNAs were greatly involved in modulating oncogenic pathways or the expression of immune-related genes. Actually, close associations (both negative and positive) were observed between EMT-related lncRNAs and protein-coding genes (PCGs) (Figure 7A). It is known that the function of lncRNAs is highly associated with their subcellular locations. Therefore, to evaluate the possible mechanism of the regulation, we assessed the locations of these 58 identified EMT-related lncRNAs. We found over a half of lncRNAs localized in the nuclear with 61.59% and 63.30% in TCGA-COAD and GSE17538 cohorts respectively (Figure 7B). As most of EMT-related lncRNAs localized in the nuclear, we supposed that they possibly regulated gene expression by interacting with TFs. We then analyzed the TF activity and screened differentially expressed TFs between two subtypes (131 TFs in TCGA-COAD and 106 TFs in GSE17538). Correlation analysis between 58 EMT-related lncRNAs and dysregulated TFs discovered a group of important TFs and lncRNAs that may closely interact with each other. The top 10 identified TFs in two cohorts were listed (Figure 7C), and 19 EMT-related lncRNAs were screened to have a close relation to differentially expressed TFs (Figure 7D). By comparing C2 with C1 subtype, we found that a majority of TFs were upregulated in C2 with 7 same TFs upregulated in both two cohorts (Figure 7E). Functional analysis on the genes targeting by these 7 upregulated TFs showed that tumor-related pathways of Jak-STAT signaling and transcriptional misregulation in cancer were significantly enriched (Figures 7F,G). The above results indicated that the 19 identified EMT-related lncRNAs may regulate oncogenic pathways through interacting with the 7 upregulated TFs.

Six epithelial-mesenchymal transition-related lncRNAs were identified to serve as prognostic biomarkers

In the previous section, we identified 19 EMT-related lncRNAs with a relation to TFs. To understand which

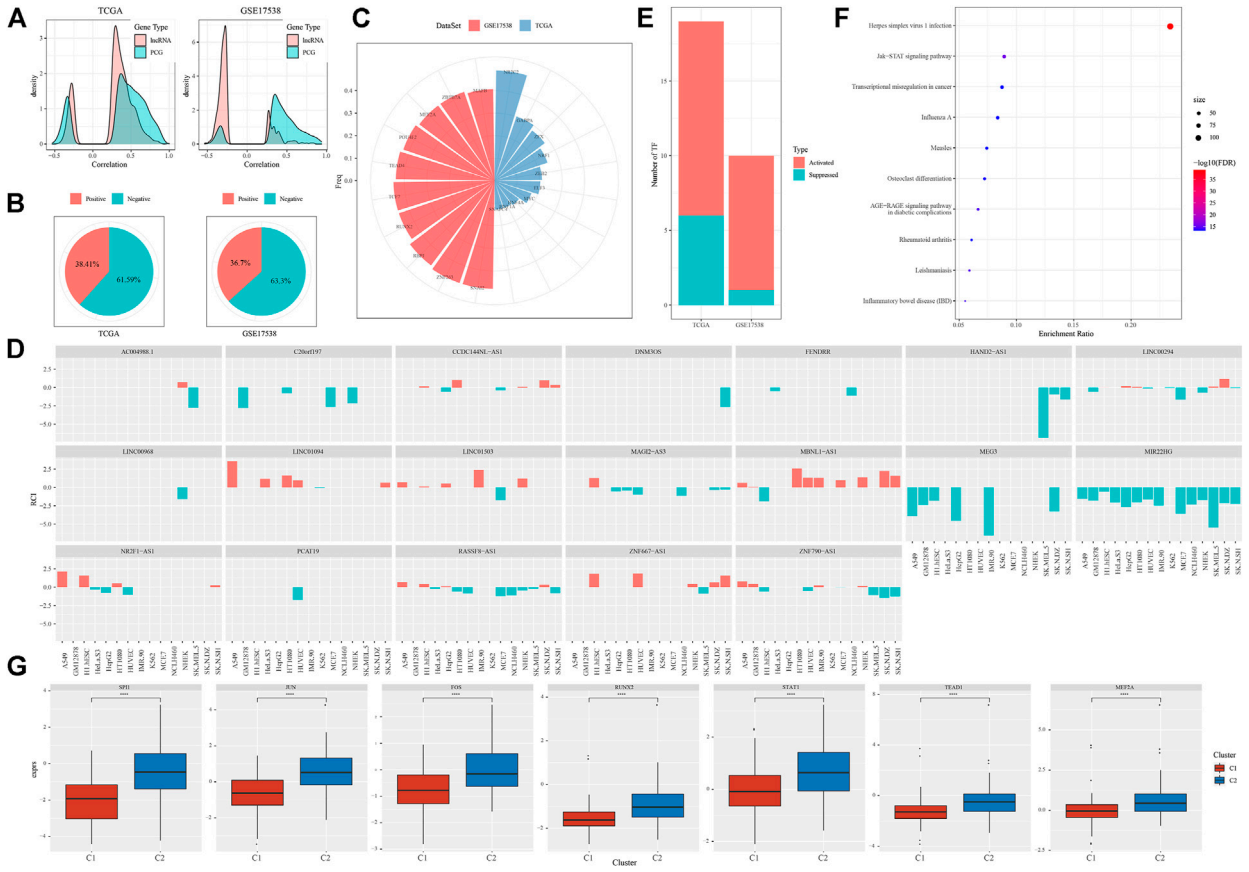

FIGURE 7
The relation between EMT-related lncRNAs and TFs **(A)** Pearson correlation analysis between EMT-related lncRNAs and PCGs in two cohorts. **(B)** Proportion of nuclear (negative) and cytoplasmic (positive) lncRNAs in two cohorts **(C)** The top 10 differentially expressed TFs associated with EMT-related lncRNAs of two cohorts. **(D)** 19 of 58 identified EMT-related lncRNA with close relations to differentially expressed TFs **(E)** Activated and suppressed TFs by comparing C2 with C1. **(F)** GSEA of genes targeted by 7 upregulated TFs. Size indicates gene counts. **(G)** Comparison of expression of 7 upregulated TFs between C1 and C2 subtypes in TCGA-COAD cohort. Student *t* test was conducted. ****$p < 0.0001$.

lncRNAs among them acted a key role between EMT-related genes and EMT activity, we applied first order partial correlation analysis on them. When eliminating some of lncRNAs, the correlation between EMT activity and EMT-related genes greatly decreased. As a result, six EMT-related lncRNAs were identified, including ZNF667-AS1, CCDC144NL-AS1, MAGI2-AS3, HAND2-AS1, LINC01094 and PCAT19 (Figure 8A). Not surprisingly, GSEA on EMT-related genes associated with these 6 lncRNAs dug out that tumor- and immune-related pathways including proteoglycans in cancer, leukocyte transendothelial migration and focal adhesion were significantly enriched (Figure 8B). Finally, based on the expression of the 6 lncRNAs, we constructed a prognostic model. Samples in two cohorts could be both clearly stratified into high-risk and low-risk groups ($p = 0.0058$ and $p = 0.00052$ in TCGA-COAD and GSE17538 respectively, Figures 8C,D), implicating robust performance of the prognostic model.

Discussion

A number of studies have found the regulatory role of lncRNAs in EMT and thus promotes tumor development and metastasis. Usually, the function of lncRNAs can be divided into two classifications, EMT promoters or suppressors (Cheng et al., 2019). However, some of lncRNAs are controversial that they act different roles varied by cancer types, indicating the complication of tumor development. To further understand the role of lncRNAs in EMT in colon cancer with early stages (I and II), we identified 58 lncRNAs that were possibly involved in EMT process, and constructed two molecular subtypes based on these EMT-related lncRNAs.

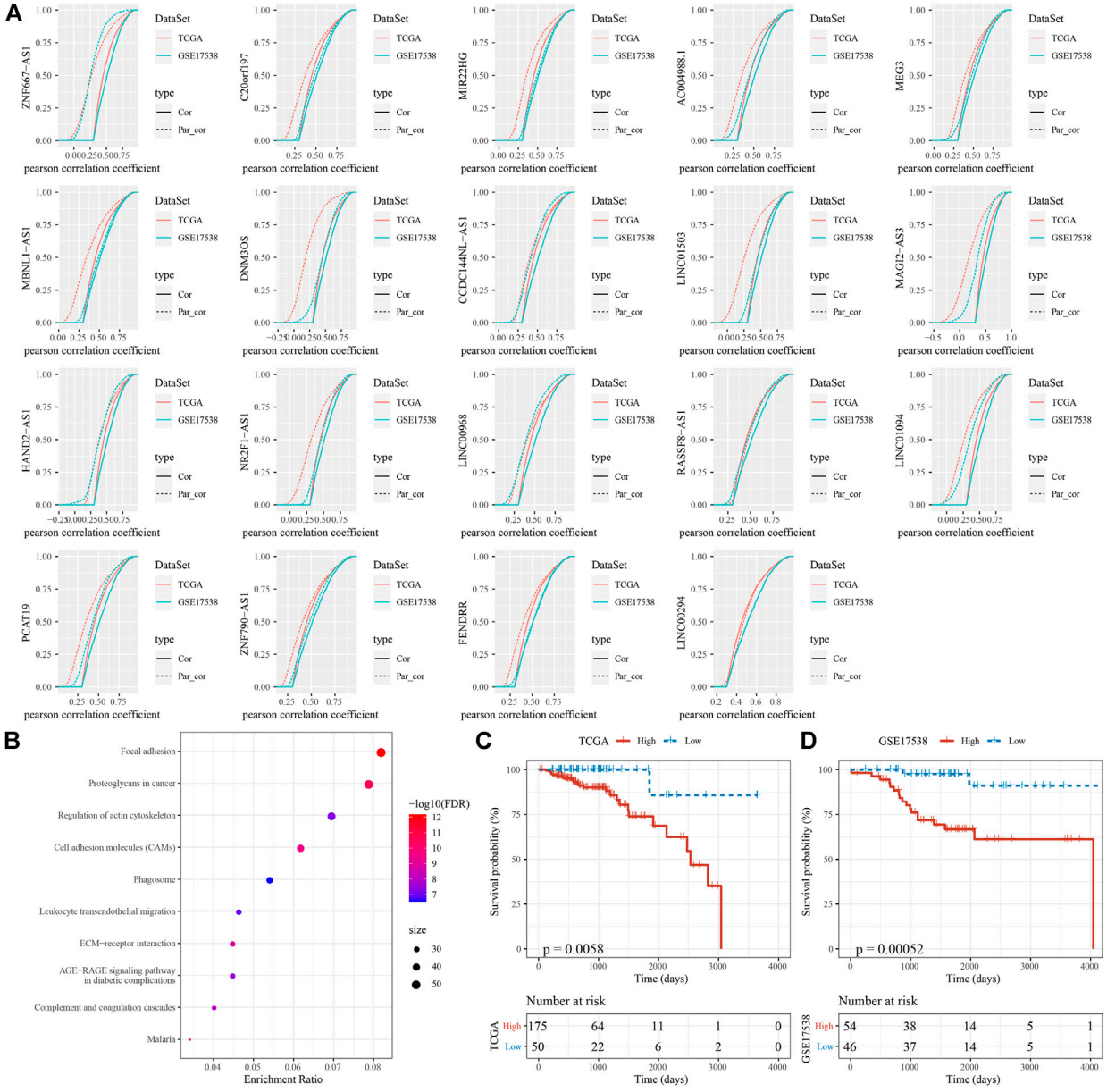

FIGURE 8
Identification of key EMT-related lncRNAs **(A)** First order partial correlation analysis on the 19 identified EMT-related lncRNAs with EMT score and EMT-related genes. Four CDF curves were presented. Solid and dashed lines represents CDF of correlation coefficients between EMT score and EMT-related genes, without and with adjustment respectively. Kolmogorov-Smirnov test was performed between solid and dashed lines. Vertical axis indicates cumulative probabilities. **(B)** GSEA on EMT-related genes associated with the 6 EMT-related lncRNAs. **(C–D)** Kaplan-Meier survival analysis of high-risk and low-risk groups stratified by the 6-gene prognostic model in two cohorts. Log-rank test was conducted.

In the comparison between two subtypes, it was reasonable that C1 subtype had more favorable OS, with lower EMT activity than C2. However, two subtypes displayed no obvious difference on genomic features. Notably, pathways activated in cancer development were observed to be more enriched in C2 subtype, indicating higher invasive activity of tumor cells leading to migration in C2 subtype. There was no doubt in the results that EMT pathway was the most enriched in C2 subtype compared with other enriched tumor-related pathways such as angiogenesis, hypoxia, TNF-α signaling and TGF-β signaling. These pathways were all reported to be associated with EMT process under the regulation of lncRNAs or miRNAs.

Vascular endothelial growth factor (VEGF) contributing for angiogenesis is demonstrated to be linked with Twist2 expression and the reduction of E-cadherin levels (Rojas-Puentes et al., 2016). It has been reported that VEGF upregulation in solid tumors with hypoxia can stimulate the transformation of endothelial cells to mesenchymal cells (Holderfield and Hughes, 2008). Multiple studies on different cancer types demonstrated that VEGF administration induced the detection of EMT markers (Yang et al., 2006; Gonzalez-Moreno et al., 2010; Desai et al., 2013). Hypoxia is a critical hallmark of solid tumors, and are illustrated to induce EMT through hypoxia-inducible factor-1α (HIF-1α) activating SNAI1 (Zhang et al., 2013; Tam et al., 2020). Notably, HIF-1α is a mediator of E-cadherin expression, a major epithelial tumor suppressor, whose reduction can promote angiogenesis (Evans et al., 2007). Links among hypoxia, HIF-1α, E-cadherin, angiogenesis and EMT are shown to promote tumor invasion.

Techasen et alhave demonstrated that tumor necrosis factor-α (TNF-α), an inflammatory cytokine largely secreted from tumor stromal cells, stimulates EMT activation and significantly upregulated Snail expression in cholangiocarcinoma tissues (Techasen et al., 2012). Another critical cytokine tumor growth factor-β (TGF-β) expressing by tumor-infiltrating immune cells also serves as an inducer of EMT through forming EMT-permissive microenvironment, which creates a linkage between EMT and TME (Fuxe and Karlsson, 2012). Moreover, we found that JAK-STAT signaling controlling immune response was highly enriched in C2 subtype. JAK-STAT signaling mediates immune cells in response to cytokines and growth factors, which is involved in metastasis and EMT (Jin, 2020). Xue et alhave revealed that lncRNA-AB073614 promotes EMT through JAK-STAT3 signaling pathway in colorectal cancer cells (Xue et al., 2018). These associations support the reliability of EMT-related lncRNAs for classifying COAD patients into two subtypes where EMT-related pathways were highly enriched in C2 subtype.

Besides enriched pathways, two subtypes also showed distinct TME with high immune infiltration in C2 subtype. A series of cytokines, chemokines and immune checkpoints secreted by tumor cells and tumor-infiltrated immune cells contribute EMT-permissive TME (Jung et al., 2015). Although C2 subtype was highly infiltrated with higher proportion of cytotoxic immune cells, immunosuppressive cells such as macrophages, regulatory T cells, and MDSCs were also highly enriched. In addition, higher expression of immune checkpoints was shown in C2, further supporting the close relation between TME and EMT. In lung adenocarcinoma, Lou et alfound that multiple immune checkpoints associating with increased regulatory T cells including PD-L1, PD-1, TIM-3, B7-H3, BTLA and CTLA-4 displayed EMT phenotype (Lou et al., 2016). Similarly, C2 subtype with high EMT activity also shown increased expression of BTLA, CD274 (PD-L1) and CTLA-4, suggesting that these immune checkpoints may be involved in EMT process.

To understand the possible mechanism of EMT-related lncRNAs regulating EMT-related genes, we investigated the relation between lncRNAs and TFs. We discovered that 7 TFs were significantly upregulated in C2 subtype, and JAK-STAT signaling pathway was found to be enriched in these TFs, which was consistent with the previous findings. Among the 19 identified lncRNAs correlated with TF expression, MEG3 and MIR22HG were massively expressed in the nuclear. MEG3, considering as an oncogenic lncRNA (Al-Rugeebah et al., 2019), is indicated to affect EMT in various cancer types such as breast cancer (Zhang et al., 2017), ovarian cancer (Wang et al., 2019), lung cancer (Terashima et al., 2017) and gastric cancer (Xu et al., 2018). However, it has not been reported in colon cancer, which may serve as a novel direction for further characterizing the mechanism of EMT. MIR22HG is demonstrated as a tumor suppressor through TGF-β/SMAD signaling in colorectal cancer, whose depletion can promote EMT process and tumor metastasis (Xu et al., 2020). We speculated that these 19 lncRNAs are highly involved in regulating EMT through interacting with TFs or other regulators.

Furthermore, to identify key EMT-related lncRNAs, we used first-order partial correlation analysis and dug out six key lncRNAs including ZNF667-AS1, CCDC144NL-AS1, MAGI2-AS3, HAND2-AS1, LINC01094, and PCAT19. These six lncRNAs were all reported to be involved in cancer progression. ZNF667-AS1 was reported to be involved in cancer progression and migration in laryngeal squamous cell carcinoma and cervical cancer (Li et al., 2019; Meng et al., 2019). CCDC144NL-AS1 was identified as a prognostic biomarker in non-small cell lung cancer and it could also promote hepatocellular carcinoma development (Zhang et al., 2021a; Zhang et al., 2021b). MAGI2-AS3 and HAND2-AS1 were dysregulated in many cancer types and were suggested as potential biomarkers for cancer prognosis (Gu et al., 2021; Kai-Xin et al., 2021). LINC01094 could promote the progression of ovarian cancer (Chen et al., 2021), breast cancer (Wu et al., 2021), pancreatic cancer (Luo et al., 2021), and other cancers. PCAT19 could activate cell-cycle genes thereby promoting cancer cell growth and cancer metastasis in pancreatic cancer (Hua et al., 2018).

In conclusion, this study proposed two novel molecular subtypes based on EMT-related lncRNAs. The distinct features of enriched pathways and TME between two subtypes supported that EMT-related lncRNAs played important roles in EMT process through regulating TFs involved in JAK-STAT signaling. Moreover, we identified six key EMT-related lncRNAs associated overall survival and the six lncRNAs could serve as a prognostic signature for COAD patients. As the study focused on COAD samples with stage I and II, we expanded the fundamental research on the early stages of COAD and the six lncRNAs may

serve as biomarkers for early diagnose of COAD. However, the limitation was that only pure bioinformatics analysis was applied in the present study. In addition, we did not distinguish left-sided and right-sided colon cancer, which may lower the accuracy of our results. In the future work, the role and prognostic value of six key EMT-related lncRNAs needed to be further explored and validated in more clinical patients.

Data availability statement

The datasets presented in this study can be found in online repositories. The names of the repository/repositories and accession number(s) can be found in the article/ Supplementary Material.

Author contributions

All authors contributed to the study conception and design. Material preparation, data collection and analysis were performed by KL, KC, DL, SZ, and ZZ. The first draft of the manuscript was written by HL, YZ, and YX, DW and YP revised the manuscript. All authors read and approved the final manuscript.

Conflict of interest

Authors YX, ZZ, and DW were employed by the company YuceBio Technology Co., Ltd.

The remaining authors declare that the research was conducted in the absence of any commercial or financial relationships that could be construed as a potential conflict of interest.

Publisher's note

All claims expressed in this article are solely those of the authors and do not necessarily represent those of their affiliated organizations, or those of the publisher, the editors and the reviewers. Any product that may be evaluated in this article, or claim that may be made by its manufacturer, is not guaranteed or endorsed by the publisher.

Supplementary material

The Supplementary Material for this article can be found online at: https://www.frontiersin.org/articles/10.3389/fgene.2022.997739/full#supplementary-material

References

Al-Rugeebah, A., Alanazi, M., and Parine, N. R. (2019). MEG3: An oncogenic long non-coding RNA in different cancers. *Pathol. Oncol. Res.* 25, 859–874. doi:10.1007/s12253-019-00614-3

ArgiléS, G., Tabernero, J., Labianca, R., Hochhauser, D., Salazar, R., Iveson, T., et al. (2020). Localised colon cancer: ESMO clinical practice guidelines for diagnosis, treatment and follow-up. *Ann. Oncol.* 31, 1291–1305. doi:10.1016/j.annonc.2020.06.022

Chen, H., Liu, Y., Liu, P., Dai, Q., and Wang, P. (2021). LINC01094 promotes the invasion of ovarian cancer cells and regulates the Wnt/β-catenin signaling pathway by targeting miR-532-3p. *Exp. Ther. Med.* 22, 1228. doi:10.3892/etm.2021.10662

Cheng, J. T., Wang, L., Wang, H., Tang, F. R., Cai, W. Q., Sethi, G., et al. (2019). Insights into biological role of LncRNAs in epithelial-mesenchymal transition, *Cells*, 8. E1178. doi:10.3390/cells8101178

Desai, S., Laskar, S., and Pandey, B. N. (2013). Autocrine IL-8 and VEGF mediate epithelial-mesenchymal transition and invasiveness via p38/JNK-ATF-2 signalling in A549 lung cancer cells. *Cell. Signal.* 25, 1780–1791. doi:10.1016/j.cellsig.2013.05.025

Dongre, A., and Weinberg, R. A. (2019). New insights into the mechanisms of epithelial-mesenchymal transition and implications for cancer. *Nat. Rev. Mol. Cell Biol.* 20, 69–84. doi:10.1038/s41580-018-0080-4

Evans, A. J., Russell, R. C., Roche, O., Burry, T. N., Fish, J. E., Chow, V. W., et al. (2007). VHL promotes E2 box-dependent E-cadherin transcription by HIF-mediated regulation of SIP1 and snail. *Mol. Cell. Biol.* 27, 157–169. doi:10.1128/MCB.00892-06

Fuxe, J., and Karlsson, M. C. (2012). TGF-β-induced epithelial-mesenchymal transition: A link between cancer and inflammation. *Semin. Cancer Biol.* 22, 455–461. doi:10.1016/j.semcancer.2012.05.004

Garcia-Alonso, L., Iorio, F., Matchan, A., Fonseca, N., Jaaks, P., Peat, G., et al. (2018). Transcription factor Activities enhance markers of drug sensitivity in cancer. *Cancer Res.* 78, 769–780. doi:10.1158/0008-5472.CAN-17-1679

Gonzalez-Moreno, O., Lecanda, J., Green, J. E., Segura, V., Catena, R., Serrano, D., et al. (2010). VEGF elicits epithelial-mesenchymal transition (EMT) in prostate intraepithelial neoplasia (PIN)-like cells via an autocrine loop. *Exp. Cell Res.* 316, 554–567. doi:10.1016/j.yexcr.2009.11.020

Gu, X., Zheng, Q., Chu, Q., and Zhu, H. (2021). HAND2-AS1: A functional cancer-related long non-coding rna. *Biomed. Pharmacother.* 137, 111317. doi:10.1016/j.biopha.2021.111317

HäNZELMANN, S., Castelo, R., and Guinney, J. (2013). Gsva: Gene set variation analysis for microarray and RNA-seq data. *BMC Bioinforma.* 14, 7. doi:10.1186/1471-2105-14-7

Holderfield, M. T., and Hughes, C. C. (2008). Crosstalk between vascular endothelial growth factor, notch, and transforming growth factor-beta in vascular morphogenesis. *Circ. Res.* 102, 637–652. doi:10.1161/CIRCRESAHA.107.167171

Hua, J. T., Ahmed, M., Guo, H., Zhang, Y., Chen, S., Soares, F., et al. (2018). Risk SNP-mediated promoter-enhancer switching drives prostate cancer through lncRNA PCAT19. *Cell* 174, 564–575. doi:10.1016/j.cell.2018.06.014

Jin, W. (2020). Role of JAK/STAT3 signaling in the regulation of metastasis, the transition of cancer stem cells, and chemoresistance of cancer by epithelial-mesenchymal transition. *Cells* 9, E217. doi:10.3390/cells9010217

Jung, H. Y., Fattet, L., and Yang, J. (2015). Molecular pathways: Linking tumor microenvironment to epithelial-mesenchymal transition in metastasis. *Clin. Cancer Res.* 21, 962–968. doi:10.1158/1078-0432.CCR-13-3173

Kai-Xin, L., Cheng, C., Rui, L., Zheng-Wei, S., Wen-Wen, T., and Peng, X. (2021). Roles of lncRNA MAGI2-AS3 in human cancers. *Biomed. Pharmacother.* 141, 111812. doi:10.1016/j.biopha.2021.111812

Lee, G. H., Malietzis, G., Askari, A., Bernardo, D., Al-Hassi, H. O., and Clark, S. K. (2015). Is right-sided colon cancer different to left-sided colorectal cancer? - a systematic review. *Eur. J. Surg. Oncol.* 41, 300–308. doi:10.1016/j.ejso.2014.11.001

Li, Y. J., Yang, Z., Wang, Y. Y., and Wang, Y. (2019). Long noncoding RNA ZNF667-AS1 reduces tumor invasion and metastasis in cervical cancer by counteracting microRNA-93-3p-dependent PEG3 downregulation. *Mol. Oncol.* 13, 2375–2392. doi:10.1002/1878-0261.12565

Liberzon, A., Birger, C., ThorvaldsdóTTIR, H., Ghandi, M., Mesirov, J. P., and Tamayo, P. (2015). The Molecular Signatures Database (MSigDB) hallmark gene set collection. *Cell Syst.* 1, 417–425. doi:10.1016/j.cels.2015.12.004

Liu, Y., He, M., Wang, D., Diao, L., Liu, J., Tang, L., et al. (2017). HisgAtlas 1.0: A human immunosuppression gene database. *Database.* 2017, bax094. doi:10.1093/database/bax094

Lou, Y., Diao, L., Cuentas, E. R., Denning, W. L., Chen, L., Fan, Y. H., et al. (2016). Epithelial-mesenchymal transition is associated with a distinct tumor microenvironment including elevation of inflammatory signals and multiple immune checkpoints in lung adenocarcinoma. *Clin. Cancer Res.* 22, 3630–3642. doi:10.1158/1078-0432.CCR-15-1434

Luo, C., Lin, K., Hu, C., Zhu, X., Zhu, J., and Zhu, Z. (2021). LINC01094 promotes pancreatic cancer progression by sponging miR-577 to regulate LIN28B expression and the PI3K/AKT pathway. *Mol. Ther. Nucleic Acids* 26, 523–535. doi:10.1016/j.omtn.2021.08.024

Mas-Ponte, D., Carlevaro-Fita, J., Palumbo, E., Hermoso Pulido, T., Guigo, R., and Johnson, R. (2017). LncATLAS database for subcellular localization of long noncoding RNAs. *Rna* 23, 1080–1087. doi:10.1261/rna.060814.117

Meng, W., Cui, W., Zhao, L., Chi, W., Cao, H., and Wang, B. (2019). Aberrant methylation and downregulation of ZNF667-AS1 and ZNF667 promote the malignant progression of laryngeal squamous cell carcinoma. *J. Biomed. Sci.* 26, 13. doi:10.1186/s12929-019-0506-0

O'Brien, S. J., Bishop, C., Hallion, J., Fiechter, C., Scheurlen, K., Paas, M., et al. (2020). Long non-coding RNA (lncRNA) and epithelial-mesenchymal transition (EMT) in colorectal cancer: A systematic review. *Cancer Biol. Ther.* 21, 769–781. doi:10.1080/15384047.2020.1794239

Petrelli, F., Tomasello, G., Borgonovo, K., Ghidini, M., Turati, L., Dallera, P., et al. (2017). Prognostic survival associated with left-sided vs right-sided colon cancer: A systematic review and meta-analysis. *JAMA Oncol.* 3, 211–219. doi:10.1001/jamaoncol.2016.4227

Reverter, A., and Chan, E. K. (2008). Combining partial correlation and an information theory approach to the reversed engineering of gene co-expression networks. *Bioinformatics* 24, 2491–2497. doi:10.1093/bioinformatics/btn482

Rojas-Puentes, L., Cardona, A. F., Carranza, H., Vargas, C., Jaramillo, L. F., Zea, D., et al. (2016). Epithelial-mesenchymal transition, proliferation, and angiogenesis in locally advanced cervical cancer treated with chemoradiotherapy. *Cancer Med.* 5, 1989–1999. doi:10.1002/cam4.751

Şenbabaoğlu, Y., Gejman, R. S., Winer, A. G., Liu, M., Van Allen, E. M., De Velasco, G., et al. (2016). Erratum to: Tumor immune microenvironment characterization in clear cell renal cell carcinoma identifies prognostic and immunotherapeutically relevant messenger RNA signatures. *Genome Biol.* 17, 46. doi:10.1186/s13059-017-1180-8

Shen, W., Song, Z., Xiao, Z., Huang, M., Shen, D., Gao, P., et al. (2022). Sangerbox: A comprehensive, interaction-friendly clinical bioinformatics analysis platform. *iMeta* 3, e36. doi:10.1002/imt2.36

Subramanian, A., Tamayo, P., Mootha, V. K., Mukherjee, S., Ebert, B. L., Gillette, M. A., et al. (2005). Gene set enrichment analysis: A knowledge-based approach for interpreting genome-wide expression profiles. *Proc. Natl. Acad. Sci. U. S. A.* 102, 15545–15550. doi:10.1073/pnas.0506580102

Sun, Z., Yang, S., Zhou, Q., Wang, G., Song, J., Li, Z., et al. (2018). Emerging role of exosome-derived long non-coding RNAs in tumor microenvironment. *Mol. Cancer* 17, 82. doi:10.1186/s12943-018-0831-z

Sung, H., Ferlay, J., Siegel, R. L., Laversanne, M., Soerjomataram, I., Jemal, A., et al. (2021). Global cancer statistics 2020: GLOBOCAN estimates of incidence and mortality worldwide for 36 cancers in 185 countries. *Ca. Cancer J. Clin.* 71, 209–249. doi:10.3322/caac.21660

Tam, S. Y., Wu, V. W. C., and Law, H. K. W. (2020). Hypoxia-induced epithelial-mesenchymal transition in cancers: HIF-1α and beyond. *Front. Oncol.* 10, 486. doi:10.3389/fonc.2020.00486

Techasen, A., Namwat, N., Loilome, W., Bungkanjana, P., Khuntikeo, N., Puapairoj, A., et al. (2012). Tumor necrosis factor-α (TNF-α) stimulates the epithelial-mesenchymal transition regulator Snail in cholangiocarcinoma. *Med. Oncol.* 29, 3083–3091. doi:10.1007/s12032-012-0305-x

Terashima, M., Tange, S., Ishimura, A., and Suzuki, T. (2017). MEG3 long noncoding RNA contributes to the epigenetic regulation of epithelial-mesenchymal transition in lung cancer cell lines. *J. Biol. Chem.* 292, 82–99. doi:10.1074/jbc.M116.750950

Ulanja, M. B., Rishi, M., Beutler, B. D., Sharma, M., Patterson, D. R., Gullapalli, N., et al. (2019). Colon cancer sidedness, presentation, and survival at different stages. *J. Oncol.* 2019, 4315032. doi:10.1155/2019/4315032

Wang, L., Yu, M., and Zhao, S. (2019). lncRNA MEG3 modified epithelial-mesenchymal transition of ovarian cancer cells by sponging miR-219a-5p and regulating EGFR. *J. Cell. Biochem.* 120, 17709–17722. doi:10.1002/jcb.29037

Wilkerson, M. D., and Hayes, D. N. (2010). ConsensusClusterPlus: A class discovery tool with confidence assessments and item tracking. *Bioinformatics* 26, 1572–1573. doi:10.1093/bioinformatics/btq170

Wu, Z. H., Wang, X. L., Tang, H. M., Jiang, T., Chen, J., Lu, S., et al. (2014). Long non-coding RNA HOTAIR is a powerful predictor of metastasis and poor prognosis and is associated with epithelial-mesenchymal transition in colon cancer. *Oncol. Rep.* 32, 395–402. doi:10.3892/or.2014.3186

Wu, X., Kong, C., and Wu, Y. (2021). Long intergenic non-protein coding RNA 1094 (LINC01094) promotes the progression of breast cancer (BC) by regulating the microRNA-340-5p (miR-340-5p)/E2F transcription factor 3 (E2F3) axis. *Bioengineered* 12, 9046–9057. doi:10.1080/21655979.2021.1993715

Xu, G., Meng, L., Yuan, D., Li, K., Zhang, Y., Dang, C., et al. (2018). MEG3/miR-21 axis affects cell mobility by suppressing epithelial-mesenchymal transition in gastric cancer. *Oncol. Rep.* 40, 39–48. doi:10.3892/or.2018.6424

Xu, J., Shao, T., Song, M., Xie, Y., Zhou, J., Yin, J., et al. (2020). MIR22HG acts as a tumor suppressor via TGFβ/SMAD signaling and facilitates immunotherapy in colorectal cancer. *Mol. Cancer* 19, 51. doi:10.1186/s12943-020-01174-w

Xue, J., Liao, L., Yin, F., Kuang, H., Zhou, X., and Wang, Y. (2018). LncRNA AB073614 induces epithelial- mesenchymal transition of colorectal cancer cells via regulating the JAK/STAT3 pathway. *Cancer Biomark.* 21, 849–858. doi:10.3233/CBM-170780

Yang, A. D., Camp, E. R., Fan, F., Shen, L., Gray, M. J., Liu, W., et al. (2006). Vascular endothelial growth factor receptor-1 activation mediates epithelial to mesenchymal transition in human pancreatic carcinoma cells. *Cancer Res.* 66, 46–51. doi:10.1158/0008-5472.CAN-05-3086

Yoshihara, K., Shahmoradgoli, M., MartíNEZ, E., Vegesna, R., Kim, H., Torres-Garcia, W., et al. (2013). Inferring tumour purity and stromal and immune cell admixture from expression data. *Nat. Commun.* 4, 2612. doi:10.1038/ncomms3612

Yu, G., Wang, L. G., Han, Y., and He, Q. Y. (2012). clusterProfiler: an R package for comparing biological themes among gene clusters. *Omics* 16, 284–287. doi:10.1089/omi.2011.0118

Zhang, L., Huang, G., Li, X., Zhang, Y., Jiang, Y., Shen, J., et al. (2013). Hypoxia induces epithelial-mesenchymal transition via activation of SNAI1 by hypoxia-inducible factor -1α in hepatocellular carcinoma. *BMC Cancer* 13, 108. doi:10.1186/1471-2407-13-108

Zhang, W., Shi, S., Jiang, J., Li, X., Lu, H., and Ren, F. (2017). LncRNA MEG3 inhibits cell epithelial-mesenchymal transition by sponging miR-421 targeting E-cadherin in breast cancer. *Biomed. Pharmacother.* 91, 312–319. doi:10.1016/j.biopha.2017.04.085

Zhang, L., Chi, B., Chai, J., Qin, L., Zhang, G., Hua, P., et al. (2021a). LncRNA ccdc144nl-AS1 serves as a prognosis biomarker for non-small cell lung cancer and promotes cellular function by targeting miR-490-3p. *Mol. Biotechnol.* 63, 933–940. doi:10.1007/s12033-021-00351-6

Zhang, Y., Zhang, H., and Wu, S. (2021b). LncRNA-CCDC144NL-AS1 promotes the development of hepatocellular carcinoma by inducing WDR5 expression via sponging miR-940. *J. Hepatocell. Carcinoma* 8, 333–348. doi:10.2147/JHC.S306484

frontiers | Frontiers in Genetics

TYPE Systematic Review
PUBLISHED 28 November 2022
DOI 10.3389/fgene.2022.1069780

OPEN ACCESS

EDITED BY
Simin Li,
Southern Medical University, China

REVIEWED BY
Zhinuan Hong,
Fujian Medical University Union Hospital, China
Ju Wang,
Sapienza University of Rome, Italy

*CORRESPONDENCE
Kunyang Li,
15567592115@163.com
Zhifeng Yu,
YUzf1986@tjutcm.edu.cn

SPECIALTY SECTION
This article was submitted to Cancer Genetics and Oncogenomics, a section of the journal Frontiers in Genetics

RECEIVED 14 October 2022
ACCEPTED 10 November 2022
PUBLISHED 28 November 2022

CITATION
Feng N, Wang S, Liu C, Xu Z, Song Z, Li K and Yu Z (2022), A network meta-analysis to evaluate the efficacy of traditional Chinese medicine on intestinal flora in patients with gastrointestinal cancer.
Front. Genet. 13:1069780.
doi: 10.3389/fgene.2022.1069780

A network meta-analysis to evaluate the efficacy of traditional Chinese medicine on intestinal flora in patients with gastrointestinal cancer

Niran Feng[1], Shurui Wang[1], Chengjiang Liu[2], Zixin Xu[3], Zhijie Song[1], Kunyang Li[4]* and Zhifeng Yu[4]*

[1]Graduate College, Tianjin University of Traditional Chinese Medicine, Tianjin, China, [2]Department of Gastroenterology, Anhui Medical University, Hefei, China, [3]Graduate College, Shaanxi University of Traditional Chinese Medicine, Xi'an, China, [4]Department of Chinese Medicine, School of Chinese Medicine Engineering, Tianjin University of Traditional Chinese Medicine, Tianjin, China

Background and Purpose: Traditional Chinese medicine (TCM) can regulate intestinal flora so as to affect the occurrence, progression, and prognosis of gastrointestinal cancer. According to clinical studies, TCM oral administration, TCM external treatment, and TCM injections, can adjust intestinal flora disorders in patients with gastrointestinal cancer. This network meta-analysis aims to evaluate the effect of three treatments on the intestinal flora in gastrointestinal cancer patients.

Methods: This meta-analysis was registered in PROSPERO (CRD42022332553). Six electronic databases, namely CNKI, Wanfang, CSTJ, PubMed, Cochrane Library, and EMBASE, were searched from their inception to 1 April 2022. We identified randomized controlled trials (RCT) used to compare the efficacy of three TCM treatment methods—oral administration, external therapy and injections—on the intestinal flora in gastrointestinal cancer patients. The main outcome indicators were *Bifidobacteria*, *Lactobacilli*, *Escherichia coli*, and *Enterococci*. Stata (15.1) and the Cochrane risk of bias assessment tool were employed.

Results: We identified 20 eligible RCTs with a total of 1,774 patients. According to network meta-analysis results, TCM injection plus common treatment (CT) or oral administration of TCM plus CT was superior to CT alone for supporting *Bifidobacterium*. In supporting *Lactobacillus*, TCM injection plus CT demonstrated more obvious effect relative to oral administration of TCM plus CT; TCM injection plus CT was more effective than CT only; and oral administration of TCM plus CT was superior to CT only.The inhibitory effect of TCM injection plus CT on *Escherichia coli* was better compared with CT only. In terms of inhibiting *Enterococci,* oral administration of TCM plus CT was superior to CT only.The difference in efficacy among the above treatments was statistically significant. In the SUCRA probability ranking, TCM injection plus CT had the best ranking curve among the three treatments and was the most effective in supporting *Bifidobacteria* (Sucra = 90.08%), *Lactobacilli* (Sucra =

96.4%), and regulating *Escherichia coli* (Sucra = 86.1%) and *Enterococci* (Sucra = 87.1%).

Conclusion: TCM injections plus CT is the most effective therapy in balancing the intestinal flora of gastrointestinal cancer patients. However, the current results deserve further validation through high-quality research.

Systematic Review Registration: http://www.prisma-statement.org/, identifier 10.1136/bmj.n71.

KEYWORDS

gastrointestinal cancers, intestinal flora, systematic review, treatment, traditional Chinese medicine (TCM)

1 Introduction

Gastrointestinal (GI) cancers, including gastric cancer, colon cancer, and colorectal cancer (Soleimanpour et al., 2020), are among the most common cancers (Wang et al., 2020a), accounting for approximately 26% of total cancer incidence and about 36.4% of cancer-related deaths (Arnold et al., 2020). Recently, the incidence and mortality of GI cancers have been increasing (Bray et al., 2018), so exploring the protective factors and risk factors for the occurrence and development of GI cancers will be conducive to effectively preventing and treating these cancers. Clinically, GI cancers are usually treated by radiotherapy, chemotherapy, surgery, drugs, and immunotherapy, while TCM, generally considered as an adjuvant therapy combined with radiotherapy and chemotherapy, plays an effective anti-tumor role by inducing tumor cell apoptosis and inhibiting tumor angiogenesis (Wang S. et al., 2021). At the same time, it decreases the gastrointestinal reactions caused by radiotherapy and chemotherapy (Zhang et al., 2021). However, with the in-depth study of the relationship between TCM and intestinal flora and gastrointestinal cancers, we found that TCM can adjust intestinal flora, promote beneficial bacteria to produce more Short-chain fatty acids (SCFAs) (Martin-Gallausiaux et al., 2021), mainly including acetate (C2), propionate (C3) and butyrate (C4), and improve the microenvironment of the gastrointestinal tumors, thereby having a certain beneficial impact on the occurrence, development, and prognosis of GI cancers (Sivan et al., 2015). In addition, intestinal flora also has a therapeutic effect on radiation enteritis caused by radiotherapy (Jian et al., 2021). Therefore, we believe that TCM can treat patients with gastrointestinal cancers by regulating intestinal flora in multiple ways.

Human intestinal microbes constitute a complex ecosystem, with around 800 species and more than 7,000 bacterial strains (Ley et al., 2006). In the intestine, symbiotic microorganisms are dynamic, which can maintain intestinal stability and inhibit pathogen colonization. When the balance is broken, the intestinal mucosal barrier and immune function will be undermined, leading to additional pathogenic factors, which are risk factors for colorectal cancer as well (Si et al., 2021).Clinical studies have found significant changes in the structure and characteristics of the intestinal flora in gastrointestinal cancer patients (Ferreira et al., 2018). Additionally, intestinal flora affects the absorption of anticancer drugs and correlates with the prognosis of these patients (Wertman et al., 2021). The pathological mechanisms by which intestinal flora affects colorectal cancer are currently thought to be achieved through multiple pathways, such as the induction of inflammation and immunity (Meng et al., 2018). Notably, intestinal pathogenic bacteria can drive tumorigenesis by shaping the tumor microenvironment or forming biofilms, such as *Bacteroides*, *Escherichia coli*, and *Clostridium difficile*, which can secrete a variety of virulence factors that damage intestinal epithelial cells and trigger chronic inflammatory responses, and develop into colorectal cancers (Hayase and Jenq, 2021). Meanwhile, some intestinal probiotics can directly produce tumor suppressive substances or enhance related antigens to achieve anti-tumor effects (Song et al., 2021). The ferritin produced by *Lactobacillus* casei ATCC334, for instance, can act as a tumor suppressor through the JNK signaling pathway (Konishi et al., 2016). Therefore, we consider how to balance the environment of intestinal microbiota deserves further exploration.

Among many pathogenic bacteria, *Escherichia coli* and *Enterococcus*, belonging to neutral bacteria, are not pathogenic when their population is within a certain range, however, an excessive number of these bacteria may produce *Enterotoxin* that are highly pathogenic (Wassenaar, 2018; Alhinai et al., 2019). *Bifidobacteria* and *Lactic acid bacteria*, as probiotics, produce a large amount of SCFAs, which are beneficial to intestinal health (Zaharuddin et al., 2019). Because of their large number, more in-depth basic research, and easy clinical detection, when intestinal pathology changes, the flora changes significantly, so they are commonly used as clinical indicators for evaluation of intestinal flora (Kuugbee et al., 2016).

In fact, the TCM adjuvant therapy for cancer has achieved a remarkable clinical efficacy (Wang S. et al., 2020c). Nowadays, the main TCM therapies commonly used in the clinics are oral therapy, external therapy and injection therapy (Huang et al., 2018). The classification is based on different routes of

administration. Oral treatments of TCM are absorbed through the gastrointestinal tract, external treatments of TCM are absorbed through the skin and mucosa by physical therapy or enema, and TCM injections are the components directly enter the bloodstream. To the best of our knowledge, most of the previous studies have focused more on TCM oral administration, and less on external treatments and TCM injections. It has been shown that TCM can inhibit the development of cancer by regulating intestinal microbes (Chen et al., 2021). XiaoYao decoction (a medicinal diet with Ginseng, Atractylodes and Fushen as the main ingredients), for instance, can increase the abundance of *Bacteroides, Lactobacillus*, and *Proteobacteria*, and reduce the abundance of *Desulfovibrio* and *Rickerella* (Zhang Z. et al., 2020).

Given that the evidence in the current literature not able to determine which one is the most effective Therefore, we tried to select the best treatment by counting and analyzing the changes of 4 indicators in intestinal flora after the application of three TCM treatments in the previous literature. To date, no meta-analysis has been conducted to compare the effects of CT in combination with each of these three TCM methods on intestinal flora in gastrointestinal cancer patients. We present the paper on the basis of the checklist of the extended PRISMA for network meta-analysis.

2 Materials and methods

This meta-analysis was registered in PROSPERO (CRD42022332553).

2.1 Search strategies

We searched three English databases (PubMed, Cochrane Library and Embase) and three Chinese electronic databases (CNKI, Wanfang and Chinese Science and Technology Journal Database). The search period started from the establishment of the database until 1 April 2022.

Our search strategy contains comprehensive terms in the English database as follows: (Medical, Chinese traditional or Chinese medicine) and (gastric or colorectal or colorectal or gastrointestinal tumors) or (intestinal flora or gut microbes or *Bifidobacterium* or *Lactobacillus* or *Escherichia* coli or *Enterococcus*). A comprehensive search with subject terms, joint keywords and free words was conducted according to different databases to ensure the systematization and integrity of the search.

2.2 Inclusion standards

(1) The symptoms and clinical indicators of patients were in accordance with the newly compiled guideline *The Diagnostic Criteria of Gastrointestinal Tumors.*
(2) Randomized controlled trial.
(3) The control group was treated with CT, and the treatment group with one of three TCM intervention methods, namely CT + Oral administration of TCM, CT + external therapy of TCM (e.g., enema of TCM, acupoint catgut embedding, cutaneous scraping therapy, acupuncture, and moxibustion), and CT + TCM injection.
(4) The observation indicators are the numbers of *Bifidobacterium*, *Lactobacillus*, *Escherichia coli* and *Enterococcus.* At least one result was available in the literature.
(5) The intestinal microbiota numbers in fecal samples of patients can only be analyzed by 16SrDNA sequencing.

2.3 Exclusion standards

(1) Literature review, animal experiment, experience summary and other types of literature are excluded.
(2) Patients with non-simple gastrointestinal cancer.
(3) The treatment group did not meet the requirements of combined TCM and common treatment or did not use one of the 3 treatment methods of TCM, or the control group was treated with TCM.
(4) Articles with multiple publications and those with full text unavailable or with incomplete data were excluded.
(5) None of the four selected indicators of intestinal flora (*Bifidobacteria*, *Lactobacilli*, *Escherichia coli*, and *Enterococci*) was found in the outcome indicators of RCT.

2.4 Types of outcome measures

The outcome indicators of this study were determined based on the frequency of outcome indicators in the articles involved and the 2020 AGA clinical practice guidelines. The main outcome indicators are as follows: 1) *Bifidobacteria* and *Lactobacilli* (increased number) and 2) *Escherichia coli* and *Enterococci* (decreased number).

2.5 Literature screening and data extraction

According to the search strategy, relevant literature was found in the database and the bibliography was exported. Duplicate literature was excluded using Endnotex9 software.The literature that met the inclusion criteria were downloaded for comparison, and the full text was ultimately read for exclusion.

Two reviewers (Niran Feng and Kunyang Li) independently searched the database and the selected articles. If there was any disagreement between them, a third party (Shurui Wang) would

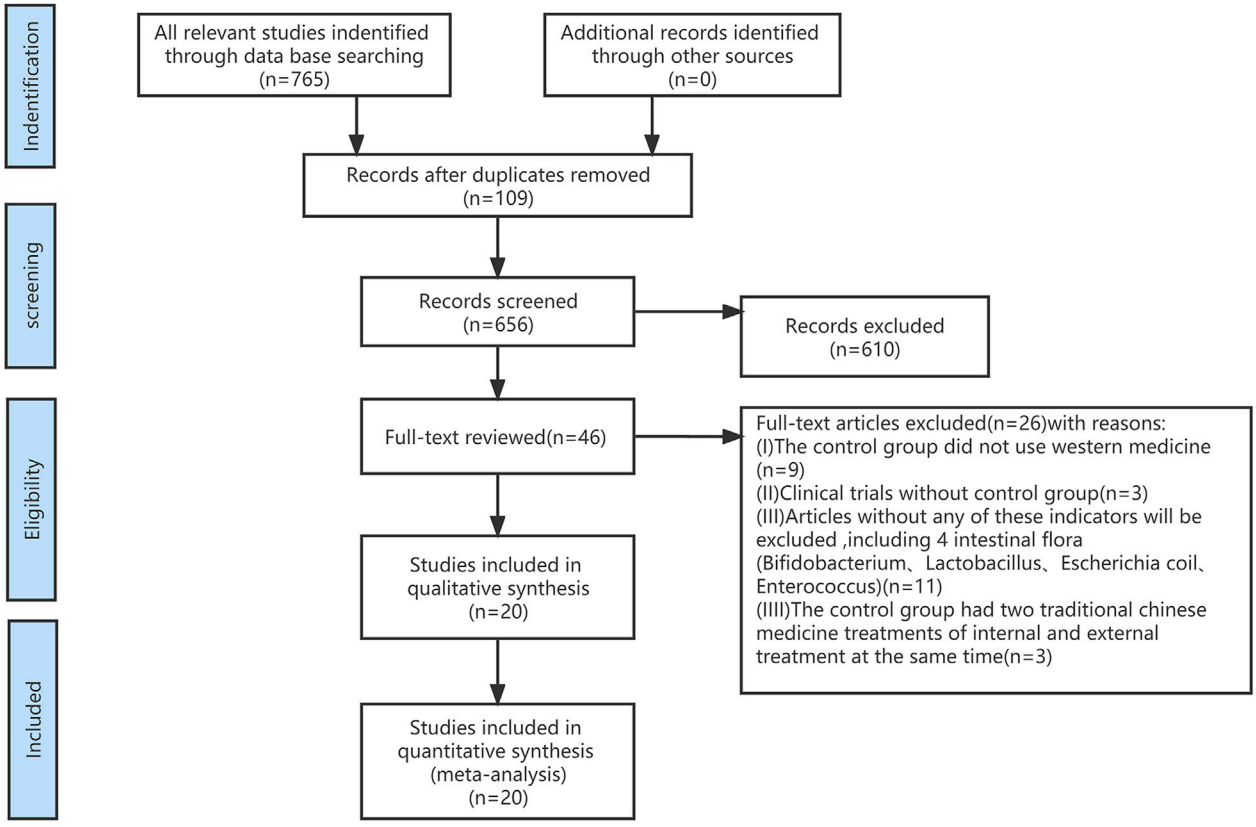

FIGURE 1
The process of literature filtering.

participate in the discussion and propose a solution to resolve their differences. Furthermore, the references in the selected studies were examined to incorporate literature missing from the main studies.

Data extraction criteria included: first author, publication year, country, title, number of cases, treatment duration, intervention measures in both the experimental group and the control group, and treatment results.

2.6 Quality assessment

Two researchers (Niran Feng and Zixin Xu) independently assessed the literature according to the inclusion and exclusion criteria. A third party participated in the discussion and decided whether there was any objection. We used the Revman software 5.2 and the "bias risk assessment" tool recommended by the Cochrane manual as the evaluation index for the quality assessment for all included studies. We evaluated the content of the literature with high risk, low risk, and unknown risk. In the case of incomplete data during the evaluation process, we obtained data by contacting the authors.

2.7 Statistical investigation

Considering the data of the four intestinal microbiota as continuous variables, the weighted mean difference (WMD) and 95% CI were used as effect size indicators for continuous variables. The difference was considered statistically significant, when the confidence interval (CI) was set to 95% and 0 was excluded. The data extracted from the article were ranked for efficacy and ranked cumulative probabilities using stata15.0 (Stata Corporation, College Station, TX, United States). Heterogeneity was assessed using funnel plots, where I^2 values greater than 50% represented considerable statistical heterogeneity. In addition, data processing, network link graph, forest graph and surface under the curve ranking (Sucra) were completed sequentially.

3 Results

3.1 Literature search of the included studies

First, we screened out 765 articles and eliminated 109 duplicates according to the search criteria. Next, after

TABLE 1 Characteristics of the 20 trials included in the network meta-analysis.

Study	Patients		Interventions		Duration (days)	Outcomes							
	IG	CG	IG	CG		Bifidobacterim IG/CG		*Lactobacillus* IG/CG		*Escherichia coli* IG/CG		*Enterococcus* IG/CG	
Sun et al. (2021) China	40	40	BZYQ + CT	CT	90	7.15 ± 0.63	8.77 ± 0.24	7.01 ± 0.45	8.55 ± 0.71	10.76 ± 0.89	9.04 ± 0.63	–	–
Li et al. (2020) China	56	56	SLBZ + CT	CT	84	9.04 ± 0.68	7.10 ± 0.89	9.65 ± 0.64	7.50 ± 0.65	7.56 ± 0.34	9.05 ± 0.41	8.50 ± 0.43	9.93 ± 0.89
Hu and Hao, (2021) China	39	39	DGBX + CT	CT	12	8.5 ± 1.12	7.94 ± 1.05	7.57 ± 1.26	7.00 ± 1.22	8.75 ± 1.35	9.45 ± 1.54	9.03 ± 1.25	9.74 ± 1.34
Yang et al. (2018) China	42	42	Enema therapy with TCM (EHT)+CT	CT	7	8.46 ± 0.71	7.61 ± 0.73	8.25 ± 0.63	7.14 ± 0.55	9.05 ± 0.82	9.73 ± 0.75	7.89 ± 0.67	7.42 ± 0.65
Wang et al. (2020a) China	43	43	Acupoint catgut embedding + CT	CT	21	8.23 ± 0.26	7.38 ± 1.85	8.08 ± 1.96	7.02 ± 1.84	9.04 ± 2.58	10.53 ± 2.96	7.89 ± 1.81	7.14 ± 1.67
Han et al. (2017) China	75	75	GGQLT + CT	CT	84	7.21 ± 0.33	6.56 ± 0.38	6.31 ± 0.22	5.81 ± 0.26	8.25 ± 0.56	9.1 ± 0.47	9.26 ± 0.25	10.21 ± 0.35
He et al. (2021) China	43	43	cutaneous scraping therapy + Moxibustion therapy + CT	CT	21	8.94 ± 0.56	7.91 ± 0.64	8.97 ± 0.46	7.76 ± 0.62	6.23 ± 1.56	8.14 ± 1.32	4.26 ± 0.54	5.93 ± 0.74
Miao et al. (2019) China	30	30	JS + CT	CT	112	9.12 ± 1.11	8.04 ± 0.91	8.29 ± 0.94	7.26 ± 0.76	8.82 ± 0.97	9.39 ± 1.21	8.44 ± 0.91	7.56 ± 0.81
Song et al. (2021) China	75	75	JPJD + CT	CT	21	5.02 ± 1.31	7.62 ± 1.34	5.18 ± 0.13	6.57 ± 0.11	9.58 ± 0.16	8.26 ± 0.17	–	–
Chen et al. (2021) China	28	28	JPJD + CT	CT	56	8.18 ± 1.35	6.54 ± 0.51	7.89 ± 1.41	6.22 ± 0.68	6.21 ± 0.92	8.32 ± 1.41	4.71 ± 0.97	5.95 ± 0.84
Wang J. et al. (2021) China	33	36	JPJD + CT	CT	90	8.30 ± 1.13	7.78 ± 0.97	7.99 ± 0.81	7.60 ± 0.75	6.31 ± 0.97	7.35 ± 0.95	4.81 ± 0.95	5.33 ± 0.97
Hai et al. (2010) China	30	30	JPSS + CT	CT	28	6.86 ± 0.32	5.86 ± 0.32	8.12 ± 0.39	7.33 ± 0.23	7.65 ± 0.18	7.80 ± 0.19	–	–
Zhang F. et al. (2020) China	30	30	SJZ + CT	CT	10	8.12 ± 0.31	5.83 ± 0.36	8.62 ± 0.36	6.94 ± 0.21	7.01 ± 0.15	6.92 ± 0.21	5.94 ± 0.3	5.84 ± 0.25
Wu et al. (2021) China	44	43	SJZ + CT	CT	8	7.59 ± 2.68	5.14 ± 1.48	6.64 ± 2.27	5.38 ± 1.77	6.85 ± 1.66	7.51 ± 2.1	6.30 ± 1.28	7.51 ± 2.1
Lin et al. (2020) China	109	109	Enema therapy with TCM (XZHJ)+CT	CT	7days	8.89 ± 0.74	7.64 ± 0.76	8.28 ± 0.66	7.17 ± 0.58	9.08 ± 0.85	9.76 ± 0.78	7.92 ± 0.7	7.45 ± 0.68
Liu et al. (2021) China	39	39	YQJP + CT	CT	21days	9.96 ± 1.78	8.31 ± 1.12	9.78 ± 1.42	8.32 ± 1.14	4.32 ± 0.56	6.25 ± 0.78	3.21 ± 0.41	4.96 ± 0.65
Gao et al. (2020) China	40	40	CJZQKA + CT	CT	21	7.42 ± 1.28	6.23 ± 1.16	5.27 ± 0.64	4.35 ± 0.67	7.23 ± 1.14	5.07 ± 0.76	6.03 ± 0.72	4.83 ± 0.56
Li (2013) China	30	30	AD injection + CT	CT	-	8.48 ± 0.21	4.84 ± 0.24	7.82 ± 0.34	3.87 ± 0.36	3.05 ± 0.24	5.28 ± 0.29	2.86 ± 0.42	5.98 ± 0.25
Yanjie et al. (2008) China	30	30	AD injection + CT	CT	10	6.73 ± 0.12	6.00 ± 0.36	8.46 ± 0.32	7.49 ± 0.18	7.76 ± 0.21	7.78 ± 0.25	9.07 ± 0.2	8.96 ± 0.22
Minghong (2014) China	30	30	AD injection + CT	CT	10	8.48 ± 0.21	6.94 ± 0.24	7.82 ± 0.34	5.84 ± 0.31	3.15 ± 0.24	5.28 ± 0.29	3.16 ± 0.42	3.25 ± 0.25

Abbreviations: CT, common treatment (radiotherapy-chemotherapy-surgery). Traditional chinese medicine of oral administration: BCYQ, Bu-Zhong-Yi-Qi Decoction; SLBZ, Shen-ling-bai-zhu Decoction; DGBX, Dang-Gui-Bu-Xue Decoction; GGQL, Ge-Gen-Qin-Lian Decoction; JS, Ji-Shen Decoction; PJD, Jian-Pi-Jie-Du Decoction; JPSS, Jian-Pi-Shen-Shi Decoction; SJZ, Si-Jun-Zi Decoction; YQJP, Yi-Qi-Jian-Pi Decoction; CJZQKA, Chong-Jian-Zhong-Qi-Kang-Ai Decoction. External therapy of TCM: EH, Ehuang-Decoction of enema; XZHJ, Xiao-Zheng-Hua-Ji Decoction of enema.

10.3389/fgene.2022.1069780

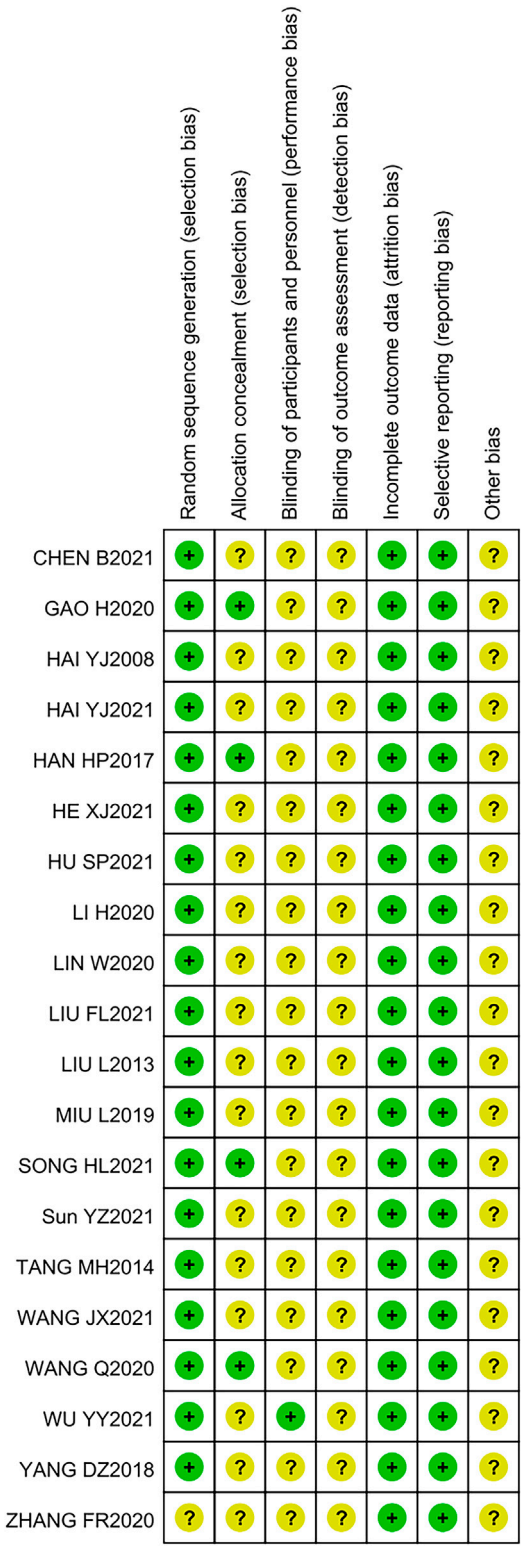

FIGURE 2
Quality assessment of inclusive literature.

reading the titles and abstracts, another 610 references were excluded. Finally, the remaining 46 articles were read and 20 eligible RCTs were included (Figure 1). The 20 RCTs comprised a total of 1,774 patients, including 888 in the treatment group and 886 in the control group. All included studies were conducted in China, with a sample size range of 30–109 entries. The duration of medication varied from 7 days to 3 months. 20 studies were RCTs, and 2 studies had no Enterococci-related data.

3.2 Characteristics of included literature

A total of 20 studies (Yanjie et al., 2008; Hai et al., 2010; Li et al., 2013; Minghong, 2014; Han et al., 2017; Yang et al., 2018; Miao et al., 2019; Wang et al., 2020b; Chen et al., 2020; Gao et al., 2020; Li et al., 2020; Lin et al., 2020; Zhang F. et al., 2020; He et al., 2021; Hu and Hao, 2021; Liu et al., 2021; Song, 2021; Sun et al., 2021; Wang S. et al., 2021; Wu et al., 2021) were included, and 14 RCT experiments of oral medicine use 10 TCM prescriptions: Buzhong yiqi Decoction (BZYQ), Shenling bai zhu Decoction (SLBZ), Danggui buxue Decoction (DGBX), Gegen qinlian Decoction (GGQL), Jishen Decoction (JS), Jianpi jiedu Decoction (JPJD), Jianpi shenshi Decoction (JPSS), Sijunzi Decoction (SJZ), Yiqi jianpi Decoction (YQJP), and Chongjian zhongqi kangai Decoction (CJZQKA). Three RCT experiments used external treatment methods, including Ehuang Decoction (EH) of enema, Xiaozheng Huaji Decoction (XZHJ) of enema, acupoint catgut embedding, skin scraping therapy and ginger separated moxibustion. Three RCT experiments involved TCM injection: Aidi injection. The treatment duration ranged from 7 to 90 days. Table 1 gives the basic information about the involved literature.

3.3 Risk of basis

The results of the quality assessment are presented in Figure 2, which shows that the risks of a large proportion of the studies were unclear and low. However, the overall quality of the 20 RCTs was acceptable.

3.4 Outcome indicators

3.4.1 Data analysis

The network diagram includes 20 RCTs. The line between two points indicates the evidence for direct comparison between the two methods. There is no closed loop between interventions; that is, there is no direct comparison between interventions (Figure 3). Among the four bacteria, the three types of TCM

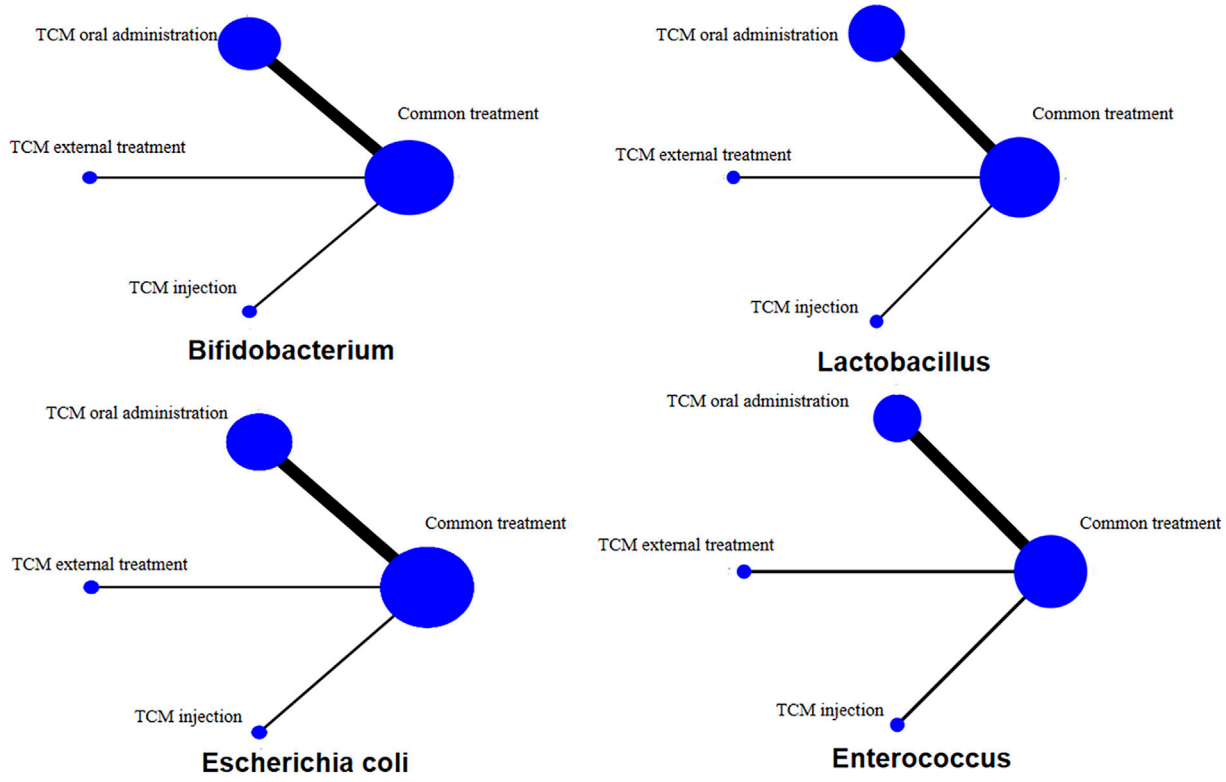

FIGURE 3
Network diagram.

treatment measures (oral administration, external treatment and injection) plus CT are directly compared with CT only, and the thickness of the line indicates the number of RCTs. This shows that the number of treatment methods using oral Chinese medicine is the largest, followed by external treatment and injection. All pairwise comparisons between interventions were from indirect comparisons. Therefore, statistical analysis can be performed directly under the consistency model.

3.4.2 Publication bias

Publication bias was assessed by the comparative-adjusted funnel method. Comparative correction charts were prepared for the included studies to evaluate the small sample effects. As shown in Figure 4, the RCTs with *Lactobacillus* and *Bifidobacterium* as outcome indicators in this study are roughly symmetrically distributed on both sides of the midline, indicating that the possibility of a small sample effect is low, and RCTs with *Escherichia coli* and *Enterococcus* as outcome indicators are not symmetrically distributed on both sides of the midline, indicating that the possibility of a small sample effect is high.

3.4.3 Network meta-analysis

In the comparison of pairwise methods, a total of 6 groups are meaningful (Table 2). In the *bifidobacteria* group, there were 2 pairs of comparison with statistically significant differences. CT only was compared with TCM injection in combination with CT, which the MD is 1.97 [MD = 1.97, 95% CI (0.48, 3.46)]. CT only was compared with oral administration of TCM in combination with CT, which MD is 0.83 [MD = 0.83, 95% CI (0.13,1.53)]. In *Lactobacillus*, 3 pairs of comparison showed statistically significant differences. TCM injection plus CT was compared with oral administration of TCM plus CT, which the MD is 1.55 [MD = 1.55 95% CI (0.20, 2.89)]. TCM injection combined with CT only was compared with CT, which the MD is 2.3 [MD = 2.30, 95% CI (1.08, 3.51)]. Oral administration of TCM combined with CT was compared with CT, which the MD is 0.75 [MD = 0.75, 95% CI (0.18, 1.32)]. In *Escherichia coli*, there is a statistically significant difference in one pair of comparison, the curative effect of TCM injection combined with CT was compared with CT only, which the MD is -1.46 [MD = -1.46, 95% CI (- 2.88, - 0.03)]. Among enterococci, one pair of comparison indicated a statistically significant difference. Oral administration combined with CT of TCM Compare with

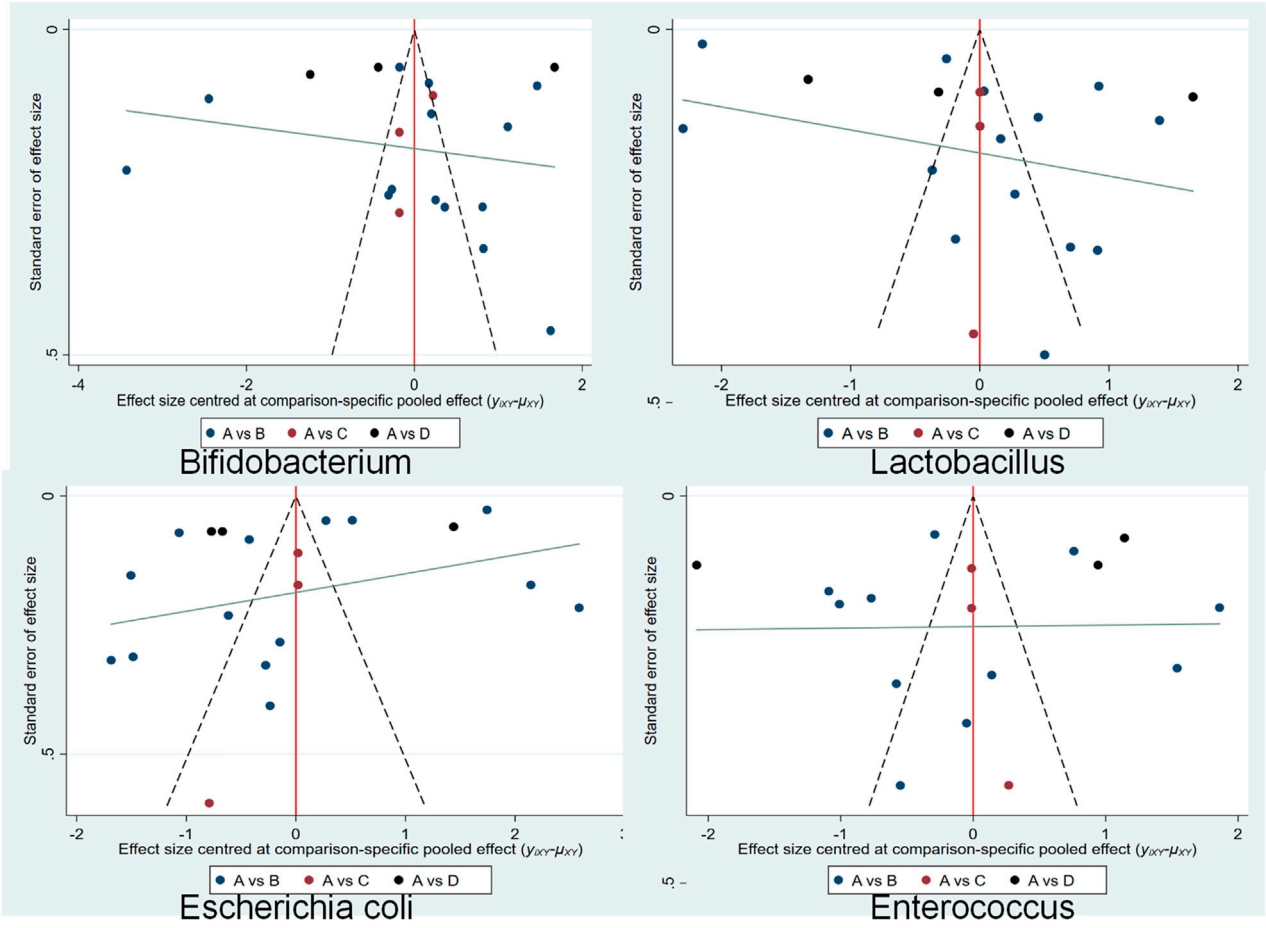

FIGURE 4
Funnel chart for comparison and correction of bifidobacteria, *Lactobacillus*, *Escherichia coli* and *Enterococcus*. **(A)** conventional treatment, **(B)** conventional treatment + TCM oral administration, **(C)** conventional treatment + TCM external treatment, **(D)** conventional treatment + TCM injection.

Common treatment, which the MD is -0.66 [MD = -0.66, 95% CI (- 1.31, - 0.01)].

3.4.4 SUCRA probability ranking

The cumulative ranking of the four methods is shown in Figure 5. High SUCRA values are correlated with good efficacy of this treatment for this type of gut microbiota. According to Sucra values, the total ranking of the four methods (A, Common Treatment; B, Common treatment plus TCM oral prescription; C, Common treatment plusTCM external treatment; D, Common treatment + TCM injection treatment) in supporting *bifidobacteria* was: D (Sucra = 90.08) > C (Sucra = 55.9) > B (Sucra = 49.7) > A (Sucra = 3.6); in supporting *Lactobacillus*, the total ranking of four methods was: D (Sucra = 96.4) > C (Sucra = 58.4) > B (Sucra = 43.7) > A (Sucra = 1.5); for *Escherichia coli*, the total ranking was: D (Sucra = 86.1) > C (Sucra = 63.2) > B (Sucra = 42.4) >A (Sucra = 8.3); and in inhibiting *Enterococcus*, the total ranking was: D (Sucra = 87.1) > B (Sucra = 74.3) > A (Sucra = 29.6) > C (Sucra = 8.9); To sum up, CT plus TCM injection can increase the probiotics (bifidobacteria and lactic acid bacteria) and reduce the pathogens (*Escherichia coli* and *Enterococcus*) in the intestinal tract of patients with gastric cancer. Thus, it is the best choice.

3.4.5 Comparative effect of colorectal cancer and gastric cancer

To make the results more stable and credible, we performed a meta-analysis supplementing the intestinal flora of colorectal and gastric cancers (Table 3). The random-effects model shows that TCM injection plus CT (WMD = 1.97, 95% CI (0.273, 3.667), $p < 0.05$] or TCM external treatment plus CT (WMD = 1.046, 95% CI (0.843,1.249), $p < 0.05$] is compared with CT, the amount of *Bifidobacteria* and *Lactobacillus* in feces of colorectal cancer patients are higher than those of the control group. For

TABLE 2 Network meta-analysis matrix of results Comparison of treatments: Mean difference (95% confidence intervals).

Bifidobacterium			
TCM injection treatment + CT			
0.98 (−1.13, 3.10)	TCM external treatment + CT		
1.14 (−0.51, 2.79)	0.16 (−1.50, 1.82)	TCM oral prescription + CT	
1.97 (0.48, 3.46)	0.99 (−0.52, 2.49)	0.83 (0.13, 1.53)	Common treatment
Lactobacillus			
TCM injection treatment + CT			
1.20 (−0.53, 2.94)	TCM external treatment + CT		
1.55 (0.20, 2.89)	0.34 (−1.03, 1.71)	TCM oral prescription + CT	
2.30 (1.08, 3.51)	1.09 (−0.15, 2.34)	0.75 (0.18, 1.32)	Common treatment
Escherichia coli			
TCM injection treatment + CT			
−0.54 (−2.59, 1.51)	TCM external treatment + CT		
−1.03 (−2.61, 0.54)	-0.49 (−2.11, 1.13)	TCM oral prescription + CT	
−1.46 (−2.88, −0.03)	-0.92 (−2.39, 0.56)	−0.43 (−1.09,0.24)	Common treatment
Enterococcus			
TCM injection treatment + CT			
−1.59 (−3.35, 0.17)	TCM external treatment + CT		
−0.37 (−1.76, 1.02)	1.22 (−0.20, 2.63)	TCM oral prescription + CT	
−1.03 (−2.26, 0.20)	0.56 (−0.70, 1.81)	0.66 (−1.31, −0.01)	Common treatment

Abbreviations: TCM, traditional chinese medicine; CT, common treatment.

Escherichia coli, the amount of *Escherichia coli* in colorectal cancer patients treated with external treatment plus CT (WMD = -1.070, 95% CI (- 1.579, - 0.561), $p < 0.05$] is lower than that in the control group. As compared to CT only, colorectal cancer patients treated with TCM external therapy plus CT (WMD = 0.627,95% CI (0.35,0.904), $p < 0.05$] have significant differences in *Enterococcus* in the treatment group. Conclusion: compared with CT only, the combination of TCM injection or external treatment with CT is more effective for supporting the number of *Bifidobacterium* and *Lactobacillus* in colorectal cancer. Similarly, as compared to CT, the effect of external treatment of TCM combined with CT is better for inhibiting the number of *Enterococcus* and *Escherichia coli* in intestinal cancer.

4 Discussion

A total of 20 RCTs with 1774 patients was included in this paper. Through the comparison of SUCRA results, Aidi injection is the most effective in increasing the number of *Bifidobacteria* and *Lactobacillus*, and in inhibiting the number of *Escherichia coli* and *Enterococcus*. In the pairwise comparison of three TCM treatments, injection of TCM plus CT or oral Chinese medicine plus CT are effective for *Bifidobacteria* and *Lactobacillus*. For *Escherichia coli*, TCM injection plus CT takes effect. For *Enterococcus*, TCM oral treatment plus CT is practical.

There are three treatments of TCM, including internal treatment (oral absorption), external treatment (physical therapy or skin mucosal absorption), and injection (direct blood injection). Internal treatment mainly uses oral Chinese medicine decoction, the preparation of which is to soak the traditional Chinese medicine in boiling water or hot water to produce an aqueous extract containing a mixture of chemical components (Zhou et al., 2016; Deng et al., 2019). Specifically, after oral administration of TCM into the colon, intestinal microbiota converts carbohydrates, proteins, lipids and small non-nutritive compounds from TCM into chemical metabolites that may have beneficial or adverse effects on human health (Wang et al., 2013). For example, the continuous digestion of polysaccharides and carbohydrates (PS) produces many short-chain oligosaccharides, which can promote the growth of probiotics such as *Bifidobacteria* and *Bacteroides*. Shorter PSs are digested to form monosaccharides, which can be continuously catabolized to form short-chain fatty acids (SCFA) (e.g., formate, acetate, propionate, butyrate), lactic

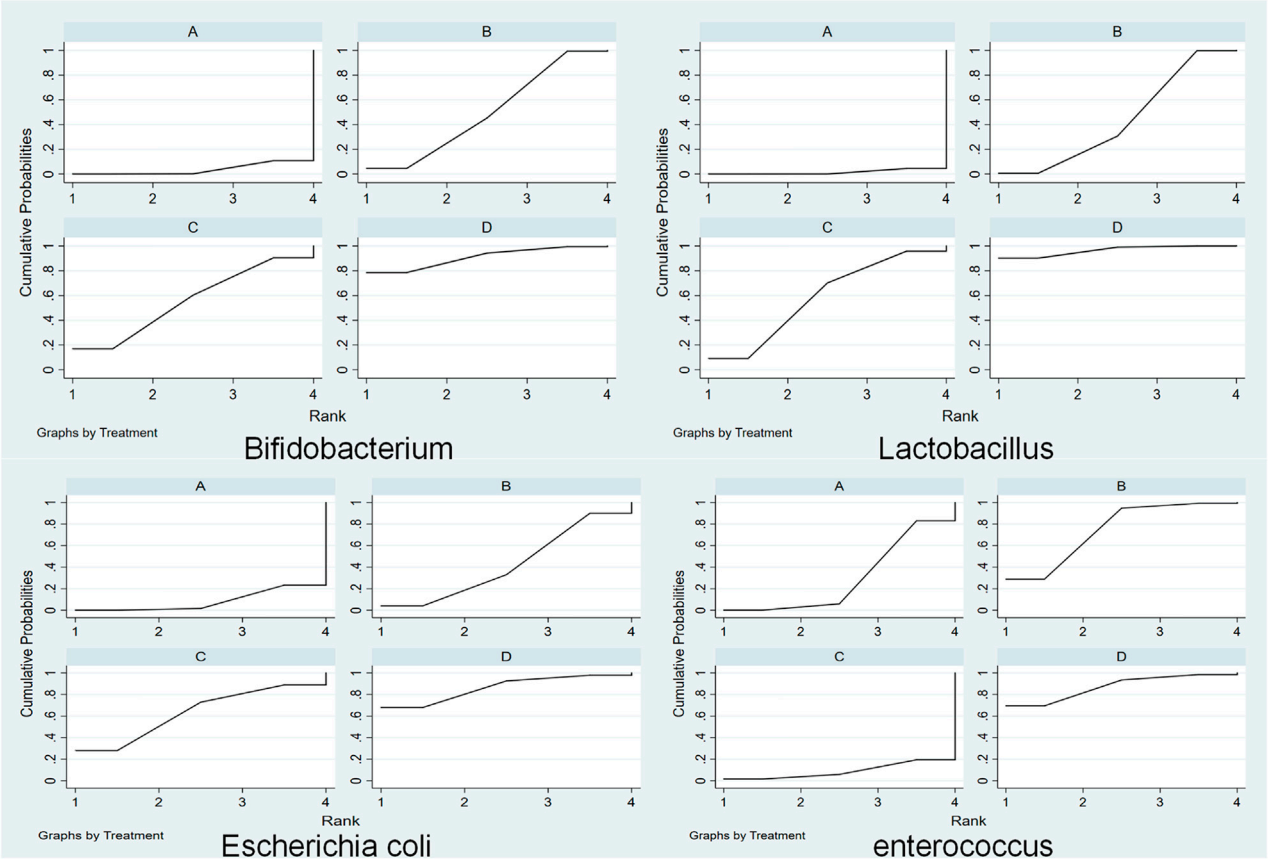

FIGURE 5
Cumulative probability of total effective rate (Abbreviations: **(A)** traditional therapy; **(B)** traditional therapy + traditional Chinese medicine (TCM) oral prescription; **(C)** common treatment + TCM external treatment; **(D)** common treatment + TCM injection treatment).

acid, hydrogen, carbon dioxide and other metabolites. Valproic acid, a kind of SCFAs, has antitumor activity, and its main mechanism is to inhibit histone deacetylase (Gurvich et al., 2004). These metabolites may directly affect the host intestinal environment and improve the microenvironment of gastrointestinal cancer (Vernocchi et al., 2016; Feng et al., 2019).

Aidi injection is mainly composed of ginseng, *Astragalus* membranaceus, canthatis, and acanthopanax senticosus. The active components are ginsenoside, astragalus polysaccharide, astragalus saponin, cantharidin and Acanthopanax Senticosus Polysaccharide (Quirke et al., 2007). *Astragalus* polysaccharides can increase the number of *lactic acid bacteria* and *Bifidobacteria*, thereby reducing pro-inflammatory factors, such as interleukin-6 and tumor necrosis factor-α. Therefore, as an inflammatory response inhibitor, it can also reduce the inflammatory response by reducing *Salmonella typhi* in the intestine (Tang et al., 2021). Ginsenoside-rb3 and ginsenoside Rd can promote the growth of beneficial bacteria, such as *Bifidobacterium*, *Lactobacillus*, *Acidophilus* and *Anisoid*, and can also reduce a number of cancer-related pathogens and *Helicobacter pylori spp* to prevent the development of colorectal cancer (CRC) (Huang et al., 2017). There are few studies on other drugs. We attribute the better effect of Aidi injection to its high bioavailability compared with the other two methods. When it comes to the cold and hot nature of the drug, all four drugs in the prescription are warm products. Therefore, it can be inferred that Aidi injection is hot and may be more suitable for the body of cancer patients undergoing radiotherapy and chemotherapy. External treatments include enema, acupoint embedding, skin scratching and ginger moxibustion. These methods are rarely studied in the field of intestinal flora research.

Many studies have shown that there is a causal relationship between changes in the intestinal flora and colorectal cancer. Patients with colorectal cancer have poor nutritional status and low systemic and partial resistance, which inhibit the growth of intestinal dominant bacteria, such as *Lactobacillus* and *Bifidobacterium*, resulting in the imbalance of the intestinal microenvironment. Meanwhile, intestinal flora imbalance will decrease the immune function of the body, and the decline of immune function will aggravate the flora imbalance, thus

TABLE 3 Comparative Effect of Colorectal Cancer and Gastric Cancer in the meta-analysis.

Outcome	Disease	Treatment	WMD	[95% Conf.	interval]	p
Bifidobacterium	Colorectal cancer	TCM oral treatment + CT vs. CT	0.648	−0.114	1.409	0.096
Bifidobacterium	Colorectal cancer	TCM injection + CT vs. CT	1.970	0.273	3.667	0.023
Bifidobacterium	Colorectal cancer	TCM external treatment + CT vs. CT	1.046	0.843	1.249	0
Bifidobacterium	Gastric cancer	TCM oral treatment + CT vs. CT	0.975	−1.269	3.218	0.394
Lactobacillus	Gastric cancer	TCM oral treatment + CT vs. CT	0.650	−0.384	1.683	0.218
Lactobacillus	Colorectal cancerr	TCM injection + CT vs. CT	2.299	0.605	3.994	0.008
Lactobacillus	Colorectal cancer	TCM external treatment + CT vs. CT	1.135	1.017	1.252	0
Lactobacillus	Colorectal cancer	TCM oral treatment + CT vs. CT	0.691	−1.174	2.557	0.468
Escherichia coli	Colorectal cancer	TCM oral treatment + CT vs. CT	−0.475	−1.182	0.232	0.188
Escherichia coli	Colorectal cancer	TCM injection + con CT CT	−1.460	−2.934	−0.015	0.052
Escherichia coli	Colorectal cancer	TCM external treatment + CT vs. CT	−1.070	−1.579	−0.561	0
Escherichia coli	Gastric cancer	TCM oral treatment + CT vs. CT	0.436	−1.734	2.606	0.694
Enterococcus	Colorectal cancer	TCM oral treatment + CT vs. CT	−0.402	−1.005	0.201	0.191
Enterococcus	Gastric cancer	TCM oral treatment + CT vs. CT	−0.471	−2.440	1.499	0.693
Enterococcus	Colorectal cancer	TCM external treatment + CT vs. CT	0.627	0.350	0.904	0
Enterococcus	Gastric cancer	TCM injection + CT vs. CT	−1.033	−2.969	0.903	0.296

Abbreviations: CT, common treatment; adiotherapy-chemotherapy-surgery. TCMoraltreatment; BZYQ, Bu-Zhong-Yi-QiDecoction; SLBZ, Shen-ling-bai-zhu Decoction; DGBX, Dang-Gui-Bu-Xue Decoction; GGQL, Ge-gen-Qin-lian Decoction; JS, Ji-Shen Decoction; JPJD, Jian-Pi-Jie-Du Decoction; JPSS, Jian-Pi-Shen-Shi Decoction; SJZ, Si-Jun-Zi Decoction; YQJP, Yi-Qi-Jian-Pi Decoction; CJZQKA, Chong-Jian-Zhong-Qi-Kan-Ai Decoction. TCM, injection, Eddie injection; TCM, external treatment; EH, Ehuang Decoction of enema; XZHJ, Xiaozheng Huaji Decoction of enema acupoint catgut embedding, cutaneous scraping therapy and ginger separated moxibustion.

forming a vicious circle. In addition, chemotherapy drugs further reduce the immunity of patients and interfere with the proportion of normal intestinal flora. Moreover, the more obvious the imbalance is before chemotherapy, the more serious the imbalance is after chemotherapy. Therefore, the anti-cancer research of intestinal flora is of great significance. *Lactic acid bacteria* and *Bifidobacterium* strains induce dendritic cell (DC) to mature (Hickey et al., 2021) and produce IFN- γ (IFN- γ), enhancing the cytolytic potential of NK cells (Zhou et al., 2019). Probiotics induce apoptosis by inhibiting the expression of COX-2, NF KB, and MAPK, suppressing the inactivation of inflammatory bodies, and activating Caspase-3 (Iyer et al., 2008). It also induces cell death through autophagy (Engevik et al., 2019). *Bifidobacterium* can increase anti-PD-L1 and inhibit tumor volume by inducing anti-inflammatory activity of macrophages and dendritic cells (Xu et al., 2020). Probiotics such as *Lactobacillus* and *Bifidobacterium* inhibit the growth of colorectal cancer by suppressing inflammation and angiogenesis, and enhance the intestinal barrier function by secreting short-chain fatty acids (SCFAs) (Koh et al., 2016). *Escherichia coli* is more prevalent in colorectal cancer tissues (Buc et al., 2013). *Enterococcus faecalis* produces enterotoxins (e.g., tartary buckwheat glucoside) and reactive oxygen species, which can lead to DNA oxidative damage and intestinal epithelial cell inflammation (Baldassarri et al., 2005). *Enterococcus faecalis* is responsible for producing reactive oxygen species and superoxide anions, resulting in DNA damage and genomic instability in colorectal cancer (Geravand et al., 2019). Fecal *Escherichia coli* induces mucosal macrophages to produce DNA damage inducers (Goodwin et al., 2011), such as 4-hydroxy-2-nonyl, through COX-2 (Yang et al., 2013).

We did a general meta-analysis, separating the patients with gastric cancer and colorectal cancer, to compare the differences between CT only and the three methods combined with CT. For colorectal cancer patients, in *Bifidobacteria* and *Lactobacillus*, external treatment plus CT or injection of TCM plus CT, are more effective than CT. For *Escherichia coli*, the TCM external treatment plus CT and the TCM injection plus CT are more effective than CT only. For *Enterococci*, We prefer TCM injection plus CT because it exhibits better effect than CT only.

5 Limitations

The following limitations should be considered in this study. The methodological quality of the effect of TCM on intestinal flora of gastrointestinal cancers is subject to some risk deviation, such as insufficient sample size and short duration. In addition, gastrointestinal cancers are subdivided into gastric and colorectal cancers. Because the number of articles is too small to perform a heterogeneity testing, we did a general meta-analysis to assist the results. TCM is divided into three categories. The external treatment includes enema, the effect of which overlaps with that of oral TCM. However, considering its direct effect on

intestinal flora and its short duration, it is placed in the external treatment.

6 Conclusion

In this study, *Bifidobacteria* and *Lactobacilli*, *Escherichia coli* and *Enterococci* were used as the main therapeutic indicators for comprehensive evaluation. Overall, TCM injection may be the best treatment, followed by TCM external treatment. TCM plays a certain role in the intestinal flora of patients with gastrointestinal cancers through multi-targeted comprehensive intervention. Clinically, it can be used in combination with other therapies depending on the actual situation of patients, and is suitable for the whole treatment process for gastrointestinal cancer patients.

Data availability statement

The original contributions presented in the study are included in the article/supplementary material, further inquiries can be directed to the corresponding authors.

Author contributions

All authors contributed to the study conception and design. NF and SW: Conceptualization, Methodology, Software, Writing—Original draft, Data curation, Visualization were performed; CL, ZX, and ZS: Methodology, Software, Writing—Original draft were performed; KL and ZY: Concetualization, Supervision, Project administration, Funding acquisition were performed. All authors read and approved the final manuscript.

Funding

This overview was funded by the Special Support Plan for National 12th Five Year Plan Project (No. 2012BAI25B05).

Acknowledgments

Thanks to the authors of the included studies to provide primary data.

Conflict of interest

The authors declare that the research was conducted in the absence of any commercial or financial relationships that could be construed as a potential conflict of interest.

Publisher's note

References

Alhinai, E. A., Walton, G. E., and Commane, D. M. (2019). The role of the gut microbiota in colorectal cancer causation. *Int. J. Mol. Sci.* 20 (21), E5295. doi:10.3390/ijms20215295

Arnold, M., Abnet, C. C., Neale, R. E., Vignat, J., Giovannucci, E. L., McGlynn, K. A., et al. (2020). Global burden of 5 major types of gastrointestinal cancer. *Gastroenterology* 159 (1), 335–349.e315. doi:10.1053/j.gastro.2020.02.068

Baldassarri, L., Bertuccini, L., Creti, R., Filippini, P., Ammendolia, M. G., Koch, S., et al. (2005). Glycosaminoglycans mediate invasion and survival of *Enterococcus faecalis* into macrophages. *J. Infect. Dis.* 191 (8), 1253–1262. doi:10.1086/428778

Bray, F., Ferlay, J., Soerjomataram, I., Siegel, R. L., Torre, L. A., and Jemal, A. (2018). Global cancer statistics 2018: GLOBOCAN estimates of incidence and mortality worldwide for 36 cancers in 185 countries. *Ca. Cancer J. Clin.* 68 (6), 394–424. doi:10.3322/caac.21492

Buc, E., Dubois, D., Sauvanet, P., Raisch, J., Delmas, J., Darfeuille-Michaud, A., et al. (2013). High prevalence of mucosa-associated *E. coli* producing cyclomodulin and genotoxin in colon cancer. *PLoS One* 8 (2), e56964. doi:10.1371/journal.pone.0056964

Chen, B., Liang, F., Yuan, X., Wan, G., Yu, H., and Xie, M. (2020). Effects of modified Jianpi Jiedu formula on intestinal flora and immune function in advanced colorectal cancer chemotherapy with spleen Qi deficiency syndrome. *J. traditional Chin. Med.* 61 (05), 423–427. doi:10.13288/j.11-2166/r.2020.05.013

Chen, Y. Z., Yuan, M. Y., Chen, Y. L., Zhang, X., Xu, X. T., Liu, S. L., et al. (2021). The gut microbiota and traditional Chinese medicine: A new clinical frontier on cancer. *Curr. Drug Targets* 22 (11), 1222–1231. doi:10.2174/1389450122666210412141304

Deng, Z., Jing, W. G., Wang, S. H., Jiao, M. J., Zhang, Q., Zhou, H. Y., et al. (2019). Discussion and research progress in standard decoction of medicinal slices. *Zhongguo Zhong Yao Za Zhi* 44 (2), 242–248. doi:10.19540/j.cnki.cjcmm.20181108.005

Engevik, M. A., Luk, B., Chang-Graham, A. L., Hall, A., Herrmann, B., Ruan, W., et al. (2019). Bifidobacterium dentium fortifies the intestinal mucus layer via autophagy and calcium signaling pathways. *mBio* 10 (3), e01087-19. doi:10.1128/mBio.01087-19

Feng, W., Ao, H., Peng, C., and Yan, D. (2019). Gut microbiota, a new frontier to understand traditional Chinese medicines. *Pharmacol. Res.* 142, 176–191. doi:10.1016/j.phrs.2019.02.024

Ferreira, R. M., Pereira-Marques, J., Pinto-Ribeiro, I., Costa, J. L., Carneiro, F., Machado, J. C., et al. (2018). Gastric microbial community profiling reveals a dysbiotic cancer-associated microbiota. *Gut* 67 (2), 226–236. doi:10.1136/gutjnl-2017-314205

Gao, H., Yin, D., Xin, X., and Zhou, L. (2020). Adverse reactions of postoperative chemotherapy of chongjian zhongqi kang'ai decoction I in the treatment of gastric cancer. *ACTA Chin. Med.* 35 (03), 637–641. doi:10.16368/j.issn.1674-8999.2020.03.144

Geravand, M., Fallah, P., Yaghoobi, M. H., Soleimanifar, F., Farid, M., Zinatizadeh, N., et al. (2019). Investigation of enterococcus faecalis population

in patients with polyp and colorectal cancer in comparison of healthy individuals. *Arq. Gastroenterol.* 56 (2), 141–145. doi:10.1590/s0004-2803.201900000-28

Goodwin, A. C., Destefano Shields, C. E., Wu, S., Huso, D. L., Wu, X., Murray-Stewart, T. R., et al. (2011). Polyamine catabolism contributes to enterotoxigenic Bacteroides fragilis-induced colon tumorigenesis. *Proc. Natl. Acad. Sci. U. S. A.* 108 (37), 15354–15359. doi:10.1073/pnas.1010203108

Gurvich, N., Tsygankova, O. M., Meinkoth, J. L., and Klein, P. S. (2004). Histone deacetylase is a target of valproic acid-mediated cellular differentiation. *Cancer Res.* 64 (3), 1079–1086. doi:10.1158/0008-5472.can-03-0799

Hai, Y., Lu, L., and Ding, Y. (2010). Study on Intestinal flora of Jianpishenshi decoction in patients advanced colorectal cancer. *Chin. Pharm.* 13 (11), 1545–1547. doi:10.3969/j.issn.1005-376X.2008.04.029

Han, H., Zhang, L., Dong, J., Yingchun, L., and Fang, W. (2017). Effect of compound glutamin entersoluble capsule combined with Gegen Qinlian Decoction on prevention and treatment of advanced colorectal cancer with FOLFIRI chemotherapy related diarrhea and its influence on intestinal permeability and immune cytokine. *Mod. J. Integr. Traditional Chin. West. Med.* 26 (33), 3667–3670+3739.

Hayase, E., and Jenq, R. R. (2021). Role of the intestinal microbiome and microbial-derived metabolites in immune checkpoint blockade immunotherapy of cancer. *Genome Med.* 13 (1), 107. doi:10.1186/s13073-021-00923-w

He, X., Qin, M., Tang, X., Jie, C., and Lin, Y. (2021). Clinical study on scraping therapy combined with ginger-separated moxibustion for improve immune function after chemotherapy of colorectal cancer. *J. Sichuan Traditional Chin. Med.* 39 (12), 217–220.

Hickey, A., Stamou, P., Udayan, S., Ramón-Vázquez, A., Esteban-Torres, M., Bottacini, F., et al. (2021). Bifidobacterium breve exopolysaccharide blocks dendritic cell maturation and activation of CD4(+) T cells. *Front. Microbiol.* 12, 653587. doi:10.3389/fmicb.2021.653587

Hu, S., and Hao, Y. (2021). Effect of Danggui buxue decoction on intestinal flora and immune function of perioperative patients with colorectal cancer. *Guangming J. Chin. Med.* 36 (14), 2362–2364.

Huang, G., Khan, I., Li, X., Chen, L., Leong, W., Ho, L. T., et al. (2017). Ginsenosides Rb3 and Rd reduce polyps formation while reinstate the dysbiotic gut microbiota and the intestinal microenvironment in Apc(Min/+) mice. *Sci. Rep.* 7 (1), 12552. doi:10.1038/s41598-017-12644-5

Huang, Y., Zhang, L., and Tang, E. (2018). Reflections on classification of TCM treatment methods. *J. Nanjing Univ. traditional Chin. Med.* 34 (05), 436–439+479. doi:10.14148/j.issn.1672-0482.2018.0436

Iyer, C., Kosters, A., Sethi, G., Kunnumakkara, A. B., Aggarwal, B. B., and Versalovic, J. (2008). Probiotic Lactobacillus reuteri promotes TNF-induced apoptosis in human myeloid leukemia-derived cells by modulation of NF-kappaB and MAPK signalling. *Cell. Microbiol.* 10 (7), 1442–1452. doi:10.1111/j.1462-5822.2008.01137.x

Jian, Y., Zhang, D., Liu, M., Wang, Y., and Xu, Z. X. (2021). The impact of gut microbiota on radiation-induced enteritis. *Front. Cell. Infect. Microbiol.* 11, 586392. doi:10.3389/fcimb.2021.586392

Koh, A., De Vadder, F., Kovatcheva-Datchary, P., and Bäckhed, F. (2016). From dietary fiber to host physiology: Short-chain fatty acids as key bacterial metabolites. *Cell* 165 (6), 1332–1345. doi:10.1016/j.cell.2016.05.041

Konishi, H., Fujiya, M., Tanaka, H., Ueno, N., Moriichi, K., Sasajima, J., et al. (2016). Probiotic-derived ferrichrome inhibits colon cancer progression via JNK-mediated apoptosis. *Nat. Commun.* 7, 12365. doi:10.1038/ncomms12365

Kuugbee, E. D., Shang, X., Gamallat, Y., Bamba, D., Awadasseid, A., Suliman, M. A., et al. (2016). Structural change in microbiota by a probiotic cocktail enhances the gut barrier and reduces cancer via TLR2 signaling in a rat model of colon cancer. *Dig. Dis. Sci.* 61 (10), 2908–2920. doi:10.1007/s10620-016-4238-7

Ley, R. E., Peterson, D. A., and Gordon, J. I. (2006). Ecological and evolutionary forces shaping microbial diversity in the human intestine. *Cell* 124 (4), 837–848. doi:10.1016/j.cell.2006.02.017

Li, L. (2013). Aidi's effect on intestinal flora after radiotherapy for colorectal cancer. *Henan Tradit. Chin. Med.* 33, 126.

Li, H., Li, G., Han, B., Lei, L., and Li, L. (2020). Regulation of shenling baizhu powder on intestinal microflora, intestinal barrier and immune function in gastric cancer patients with chemotherapy after operation. *Anti-tumor Pharm.* 10 (04), 477–482.

Li, L., Hu, J., Huang, H., and He, Y. (2013). Effect of Jinlong capsule on proliferation and apoptosis of human pancreatic cancer cells BxPC-3. *J. Traditional Chin. Med.* 33 (0), 205–210. doi:10.1016/s0254-6272(13)60126-0

Lin, W., Qiu, Z., Chen, J., Li, Z., and Zhao, T. (2020). Effect of Xiaozheng Huaji recipe enema combined with Bifidobacterium on intestinal microecology and mucosal immune function in patients with colorectal cancer after surgery. *Oncol. Progress.* 18 (11), 1163–1166.

Liu, F., Ma, L., Song, R., and Yan, H. (2021). Effect of Yiqi Jianpi Decoction on immune function of patients with spleen deficiency syndrome after colorectal cancer operation flora, and intestinal flora. *J. Sichuan Traditional Chin. Med.* 39 (11), 102–105.

Martin-Gallausiaux, C., Marinelli, L., Blottière, H. M., Larraufie, P., and Lapaque, N. (2021). Scfa: Mechanisms and functional importance in the gut. *Proc. Nutr. Soc.* 80 (1), 37–49. doi:10.1017/s0029665120006916

Meng, C., Bai, C., Brown, T. D., Hood, L. E., and Tian, Q. (2018). Human gut microbiota and gastrointestinal cancer. *Genomics Proteomics Bioinforma.* 16 (1), 33–49. doi:10.1016/j.gpb.2017.06.002

Miao, X., Tao, Y., Gu, X., and Shen, S. (2019). Jisheng decoction combined with postoperative adjuvant chemotherapy in treating patients undergoing chemotherapy post II period colorectal cancer operation and its effect on intestinal flora. *Chin. J. Surg. Oncol.* 11 (05), 346–349.

Minghong, T. (2014). The effect of Aidi injection on intestinal flora of patients with colorectal cancer after radiotherapy. *J. Clin. Med. Pract.* 18 (0), 107–108.

Quirke, P., Williams, G. T., Ectors, N., Ensari, A., Piard, F., and Nagtegaal, I. (2007). The future of the TNM staging system in colorectal cancer: Time for a debate? *Lancet. Oncol.* 8 (7), 651–657. doi:10.1016/s1470-2045(07)70205-x

Si, H., Yang, Q., Hu, H., Ding, C., Wang, H., and Lin, X. (2021). Colorectal cancer occurrence and treatment based on changes in intestinal flora. *Semin. Cancer Biol.* 70, 3–10. doi:10.1016/j.semcancer.2020.05.004

Sivan, A., Corrales, L., Hubert, N., Williams, J. B., Aquino-Michaels, K., Earley, Z. M., et al. (2015). Commensal Bifidobacterium promotes antitumor immunity and facilitates anti-PD-L1 efficacy. *Science* 350 (6264), 1084–1089. doi:10.1126/science.aac4255

Soleimanpour, S., Hasanian, S. M., Avan, A., Yaghoubi, A., and Khazaei, M. (2020). Bacteriotherapy in gastrointestinal cancer. *Life Sci.* 254, 117754. doi:10.1016/j.lfs.2020.117754

Song, H. (2021). Effects of Jianpi Jiedu decoction on clinical symptoms, intestinal flora and T lymphocyte sub- sets in patients with colorectal cancer. *Med. J. Liaoning* 35 (06), 44–47.

Song, P., Wang, Q. B., Liang, B., and Jiang, S. J. (2021). Advances in research on the relationship between the gut microbiome and cancer. *Eur. Rev. Med. Pharmacol. Sci.* 25 (16), 5104–5112. doi:10.26355/eurrev_202108_26521

Sun, Y., Li, B., and Chen, L. (2021). Efficacy ang safety of modified Buzhong yiqi decoction on patients with spleen and stomach qi deficiency syndrome after grastric cancer chemotherapy. *World J. Integr. Traditional West. Med.* 16 (12), 2308–2313+2319. doi:10.13935/j.cnki.sjzx.211230

Tang, S., Liu, W., Zhao, Q., Li, K., Zhu, J., Yao, W., et al. (2021). Combination of polysaccharides from Astragalus membranaceus and Codonopsis pilosula ameliorated mice colitis and underlying mechanisms. *J. Ethnopharmacol.* 264, 113280. doi:10.1016/j.jep.2020.113280

Vernocchi, P., Del Chierico, F., and Putignani, L. (2016). Gut microbiota profiling: Metabolomics based approach to unravel compounds affecting human health. *Front. Microbiol.* 7, 1144. doi:10.3389/fmicb.2016.01144

Wang, J., Cao, L., Han, J., and Shen, Q. (2021). Clinical efficacy of Jianpi Jiedu formula combined with FOLFOX4 regimen in patients with colorectal cancer undergoing chemotherapy. *Chin. Tradit. Pat. Med.* 43 (11), 3258–3261.

Wang, Q., Geng, W., Guo, H., Wang, Z., Xu, K., Chen, C., et al. (2020a). Emerging role of RNA methyltransferase METTL3 in gastrointestinal cancer. *J. Hematol. Oncol.* 13 (1), 57. doi:10.1186/s13045-020-00895-1

Wang, Q., Kuang, H., Su, Y., Sun, Y., Feng, J., Guo, R., et al. (2013). Naturally derived anti-inflammatory compounds from Chinese medicinal plants. *J. Ethnopharmacol.* 146 (1), 9–39. doi:10.1016/j.jep.2012.12.013

Wang, Q., Luo, M., Li, W., Jiwen, Z., and Weizhong, S. (2020b). Effect of Ehuang Decoction Retention enema combined with acupoint catgut embedding at Zusanli on postoperative short-term rehabilitation and quality of life in patients with colorectal cancer. *Chin. J. Clin. Oncol. Rehabilitation* 27 (01), 48–51. doi:10.13455/j.cnki.cjcor.2020.01.14

Wang, S., Fu, J. L., Hao, H. F., Jiao, Y. N., Li, P. P., and Han, S. Y. (2021). Metabolic reprogramming by traditional Chinese medicine and its role in effective cancer therapy. *Pharmacol. Res.* 170, 105728. doi:10.1016/j.phrs.2021.105728

Wang, S., Long, S., Deng, Z., and Wu, W. (2020c). Positive role of Chinese herbal medicine in cancer immune regulation. *Am. J. Chin. Med.* 48 (7), 1577–1592. doi:10.1142/s0192415x20500780

Wassenaar, T. M. (2018). *E. coli* and colorectal cancer: A complex relationship that deserves a critical mindset. *Crit. Rev. Microbiol.* 44 (5), 619–632. doi:10.1080/1040841x.2018.1481013

Wertman, J. N., Dunn, K. A., and Kulkarni, K. (2021). The impact of the host intestinal microbiome on carcinogenesis and the response to chemotherapy. *Future Oncol.* 17 (32), 4371–4387. doi:10.2217/fon-2021-0087

Wu, Y., Yang, J., and Zhou, W. (2021). Clinical study on Sijunzi decoction combined enteral nutrition in the treatment of gastric cancer with spleen deficiency syndrome. *World Chin. Med.* 16 (07), 1104–1108.

Xu, D., Zou, W., Luo, Y., Gao, X., Jiang, B., Wang, Y., et al. (2020). Feasibility between bifidobacteria targeting and changes in the acoustic environment of tumor tissue for synergistic HIFU. *Sci. Rep.* 10 (1), 7772. doi:10.1038/s41598-020-64661-6

Yang, D., Junming, H., Yong, J., Fu, T., Ming, D., Yuanwei, L., et al. (2018). Effect of ehuang decoction retention enema on intestinal flora and intestinal mucosal permeability after colorectal cancer surgery. *Guid. J. Traditional Chin. Med.* 24 (10), 46–49. doi:10.13862/j.cnki.cn43-1446/r.2018.10.012

Yang, Y., Wang, X., Huycke, T., Moore, D. R., Lightfoot, S. A., and Huycke, M. M. (2013). Colon macrophages polarized by commensal bacteria cause colitis and cancer through the bystander effect. *Transl. Oncol.* 6 (5), 596–606. doi:10.1593/tlo.13412

Yanjie, H., Baoling, J., and Lin, L. (2008). Study on intestinal flora and immune function of Aidi injection combined with chemotherapy in colorectal cancer patients. *Chin. J. Microecology* 20 (4), 400–401.

Zaharuddin, L., Mokhtar, N. M., Muhammad Nawawi, K. N., and Raja Ali, R. A. (2019). A randomized double-blind placebo-controlled trial of probiotics in post-surgical colorectal cancer. *BMC Gastroenterol.* 19 (1), 131. doi:10.1186/s12876-019-1047-4

Zhang, F., Xie, A., Zhang, J., Cai, X., Chen, J., and Li, W. (2020). Clinical study on the influence of Sijunzi decoction on gut microbiota and immune function of postoperative patients with colorectal cancer chemotherapy. *J. Shantou Univ. Med. Coll.* 33 (04), 206–208. doi:10.13401/j.cnki.jsumc.2020.04.004

Zhang, X., Qiu, H., Li, C., Cai, P., and Qi, F. (2021). The positive role of traditional Chinese medicine as an adjunctive therapy for cancer. *Biosci. Trends* 15 (5), 283–298. doi:10.5582/bst.2021.01318

Zhang, Z., Shao, S., Zhang, Y., Jia, R., Hu, X., Liu, H., et al. (2020). Xiaoyaosan slows cancer progression and ameliorates gut dysbiosis in mice with chronic restraint stress and colorectal cancer xenografts. *Biomed. Pharmacother.* 132, 110916. doi:10.1016/j.biopha.2020.110916

Zhou, S. S., Xu, J., Zhu, H., Wu, J., Xu, J. D., Yan, R., et al. (2016). Gut microbiota-involved mechanisms in enhancing systemic exposure of ginsenosides by coexisting polysaccharides in ginseng decoction. *Sci. Rep.* 6, 22474. doi:10.1038/srep22474

Zhou, X., Li, W., Wang, S., Zhang, P., Wang, Q., Xiao, J., et al. (2019). YAP aggravates inflammatory bowel disease by regulating M1/M2 macrophage polarization and gut microbial homeostasis. *Cell Rep.* 27 (4), 1176–1189.e1175. doi:10.1016/j.celrep.2019.03.028

frontiers | Frontiers in Genetics

TYPE Review
PUBLISHED 04 January 2023
DOI 10.3389/fgene.2022.1077419

OPEN ACCESS

EDITED BY
Simin Li,
Southern Medical University, China

REVIEWED BY
Tiankui Qiao,
Lung Cancer Research Foundation, United States
Xiaoli Lou,
Shanghai Jiao Tong University, China
Anna Maria Corsale,
University of Palermo, Italy
Xiaofei Liu,
Affiliated Hospital of Shandong University of Traditional Chinese Medicine, China
Jianwei Dou,
Xi'an Jiaotong University, China

*CORRESPONDENCE
Keqiang Wang,
wkqsd@163.com

SPECIALTY SECTION
This article was submitted to Cancer Genetics and Oncogenomics, a section of the journal Frontiers in Genetics

RECEIVED 23 October 2022
ACCEPTED 13 December 2022
PUBLISHED 04 January 2023

CITATION
Zhu R, Yan Q, Wang Y and Wang K (2023), Biological characteristics of γδT cells and application in tumor immunotherapy.
Front. Genet. 13:1077419.
doi: 10.3389/fgene.2022.1077419

Biological characteristics of γδT cells and application in tumor immunotherapy

Renhong Zhu[1,2], Qian Yan[3], Yashu Wang[4] and Keqiang Wang[1]*

[1]Department of Laboratory Medicine, Second Affiliated Hospital of Shandong First Medical University, Tai'an, China, [2]Department of Laboratory Medicine, Tai'an Tumor Prevention and Treatment Hospital, Tai'an, China, [3]Department of Laboratory Medicine, Second Hospital of Traditional Chinese Medicine, Tai'an, China, [4]Department of Laboratory Medicine, The Affiliated Tai'an City Central Hospital of Qingdao University, Tai'an, China

Human γδT cells are a special immune cell type which exist in small quantities in the body, do not require processing and presentation for antigen recognition, and have non-major histocompatibility complex (MHC)-restricted immune response. They play an important role in the body's anti-tumor, anti-infection, immune regulation, immune surveillance and maintenance of immune tolerance. This article reviews the generation and development of human γδT cells, genetic characteristics, classification, recognition and role of antigens, and research progress in tumor immunotherapy.

KEYWORDS

γδT cells, tumor, immunotherapy, progress, biological

1 Introduction

T cells are classified into αβT cells and γδT cells according to the differences in the types of their cell receptors (T cell receptor, TCR). γδT cells are considered to be special immune cells between acquired immunity and natural immunity due to their distribution characteristics in the body and the non-MHC restricted characteristics of immune response. They both play a unique role in innate immunity and in acquired immunity. The role of the response is gradually revealed. Numerous studies have shown that γδT cells play an important role in the body's anti-infection, anti-tumor, immune surveillance and regulation (Wang K. Q et al., 2017; Wang et al., 2018; Wang Y. R et al., 2019; Wang Y. S et al., 2019; Zhao et al., 2021a; Zhao et al., 2021b). This article reviews the generation and development of human γδT cells, genetic characteristics, classification, recognition and role of antigens, and research progress in tumor immunotherapy.

2 Biological characteristics of γδT cells

2.1 The production and development of γδT cells

Human γδT cells occur in the thymus medulla of normal fetuses at 7–8 weeks, and their development process are similar to that of αβT cells. Before gaining autoimmune

tolerance, they not only need to undergo functional TCR expression, but also need to undergo negative selection. The point is that some γδT cells have not undergone double positive selection, so that γδT cells have non-limiting MHC when recognizing antigens. Studies have found that the formation of various functions of γδT cells begins in the thymus and matures in the peripheral blood. In the thymus, thymic precursor cells differentiate into γδTCR + thymocytes under the control of the TCR signal pathway. After leaving the thymus, they enter the peripheral blood circulation and become γδT cells in the peripheral blood circulation. So far, the immune function of various γδT cell subtypes has been basically perfected. Subsequently, these cells can differentiate into a single oligoclonal cell subtype under the induction of TCR ligand-related molecules, and further develop under the action of various hormones released by the thymus, and finally have the function of mature immune cells (Cook et al., 2008; Narayan et al., 2012; Shekhar et al., 2012).

2.2 The genetic characteristics of γδT cells

The TCRγδ gene contains four groups of genes V (variable region), D (diversity region), J (joining region) and C (constant region). The *γ* chain gene consists of 10 V gene segments, 2 D gene segments, Two J gene segments are composed of C, while the delta chain gene is composed of only 7 V gene segments, 2 J gene segments and C. The combination of these gene segments and the diversity of junction regions make TCRγδ have the potential for diversity. However, because γδT cell subsets often only use a specific combination of VγVδ and J region sequences, the TCRγδ structure lacks diversity (Chen et al., 2012). The gene recombination and matching of γδT cells are highly coordinated. Vγ9 and Cγ1 are linked and almost all combine with Vδ2 to form TCR dimers. Studies have confirmed that the Vγ9Vδ2 subtype in adult peripheral blood accounts for more than 90% of the total number of γδT cells (Yang et al., 2011). Therefore, the γδT gene lacks diversity with limited gene rearrangement, MHC non-restrictive reaction with antigen (Davey et al., 2018), and similar functions to cells related to natural immunity, so it was initially considered to be an important part of the body's innate immunity.

2.3 Recognition and effect of γδT cells on antigen

γδT cells are not only an important cell group involved in innate immune response, but also a key component of non-specific immune response. The recognition of γδT cells to antigens is not restricted by MHC and can directly recognize antigens. Not only can they recognize complete polypeptides, they can respond to certain MHC-like molecules, and they also show special affinity for heat shock proteins. The recognition of γδT cells to antigens shows certain tissue specificity: γδT cells from the same tissue express the same TCR to recognize antigens of the same nature, while γδT cells from different tissues can express different TCRs to recognize antigens of different properties (Khatri et al., 2010). The antigens recognized by γδT cells currently found mainly include MHC and MHC-like molecules, heat shock proteins (HSP), DNA mismatch repair related proteins (MSH2), phosphorylated antigens, and those presented by CD1a, CD1c, and CD1d in the CD1 family Lipid antigens and so on (Sebestyen et al., 2020). These antigens bind to T cell receptors or NK cell receptors on the surface of γδT cells to cause the activation of γδT. Natural killer receptors (NKR) and Toll-like receptors (TLR) can provide costimulatory signals to participate in the activation process. Parts of the mechanisms of the activation of Vγ9Vδ2+ T cells by phosphoantigens are mediated through the B7 immunoglobulin family-like butyrophilin 2A1 (BTN2A1) and BTN3A1 complexes. Following phosphoantigen binding to the intracellular B30.2 domains of BTN3A1 in tumor cells, BTN3A1 undergoes a conformational change (Sandstrom et al., 2014; Gu et al., 2017) and promotes the interaction between BTN2A1 and BTN3A1 intracellular domains (Rigau et al., 2020). Subsequently, the germline-encoded regions of the TCR Vγ9 chain directly bind to BTN2A1 on tumor cells (Rigau et al., 2020), then leads to Vγ9Vδ2+ T Cell activation. Activated γδT cells exhibit a variety of biological and immunological functions: 1) Non-specific immune response: Without the presentation of APC, it can be activated directly through TCR to recognize multiple antigen components, participate in non-specific immune response and play an important role. 2) Secretion of a variety of cytokines: by secreting cytokines such as TNF-α, IFN-γ, IL-4, IL-10, etc., it can not only directly inhibit tumor growth, but also promote the maturation of dendritic cells and enhance natural killer cell-mediated cytotoxicity (Maniar et al., 2010; McCarthy et al., 2013). 3) Promote target cell apoptosis: destroy the cell structure of target cells by secreting perforin and granzyme B; exert antibody-dependent cell-mediated cytotoxicity through certain membrane surface receptors such as FcγR; through Fas/FasL Pathways, expression-related apoptosis-inducing ligand CD95 ligand and TNF-related apoptosis-inducing ligand (TRAIL), etc. cause programmed apoptosis of target cells (Pennington et al., 2005; Poonia and Pauza, 2012). 4) Antigen presentation: partially activated γδT cells are specialized antigen presenting cells, and their surface highly expresses chemokine receptors CCR7, MHC-II molecules, CD80 and CD86, etc., and processes the antigens and cross-presents them to αβT cells thus stimulate a specific immune response (Brandes et al., 2009; Wu et al., 2009). 5) Immune surveillance and immunomodulation: Activated γδ T cells exert immune surveillance through the high expression of CCR7 and CD161 on their surface (Chodaczek et al., 2012); through the production of IL-10, transforming growth factor-β

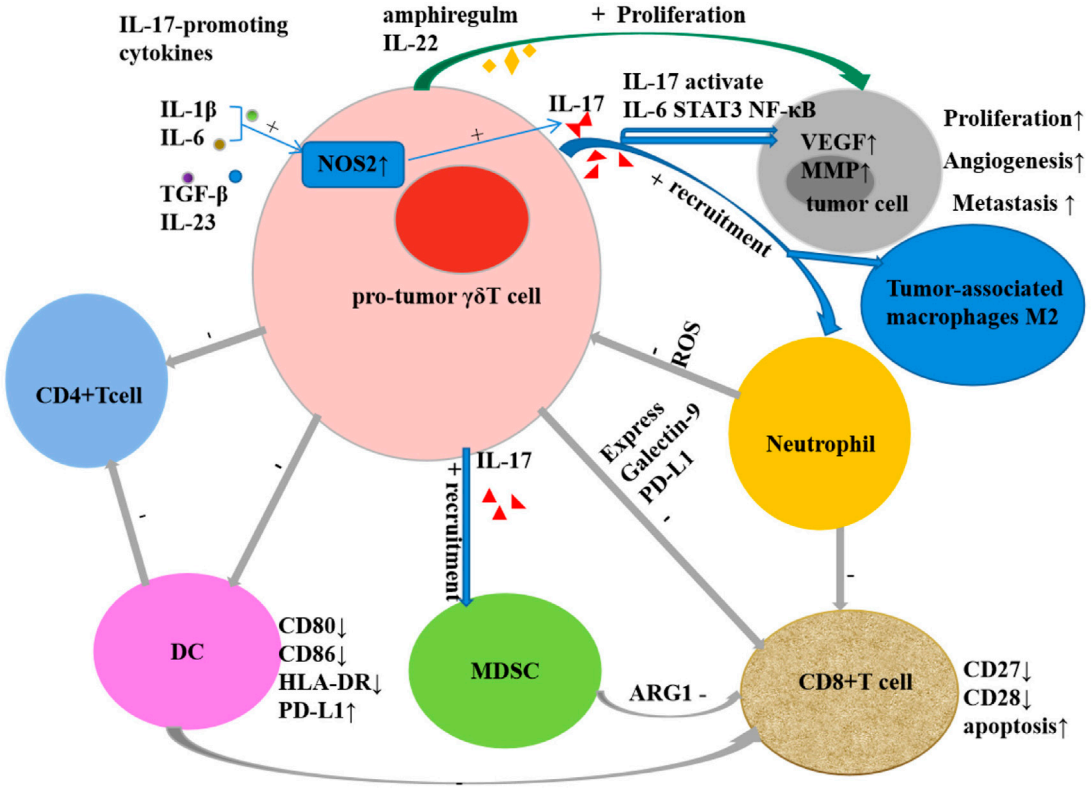

FIGURE 1
The tumor-promoting effect of γδT cells.

(TGF-β) and other cells factors play an immunomodulatory role (Kühl et al., 2009). 6) Tumor-promoting effect (Figure 1): The tumor-promoting effect of γδT cells is mainly related to the production of IL-17. It not only induces tumor angiogenesis, stimulates tumor cell proliferation, and promotes tumor cell metastasis (Welte and Zhang, 2015; Qian et al., 2017), but also mobilizes pro-inflammatory neutrophils or immunosuppressive myeloid cells. Myeloid-derived suppressor cells inhibit the activation of CD8+T cells through high expression of ARG1 (Romano et al., 2018; Sacchi et al., 2018), and reactive oxygen species (ROS) produced by neutrophils have a certain inhibitory effect on IL-17-producing γδT cells (Wakita et al., 2010; Benevides et al., 2015; Coffelt et al., 2015). Other tumor-promoting effects of γδT cells include inhibiting the maturation of DCs, the senescent DCs can further suppress CD4+T cells and CD8+T cells (Peng et al., 2007; Ye et al., 2013a; Ye et al., 2013b), inhibiting T cell responses by secreting galectin and expressing programmed cell death protein ligand 1 (PDL1); and inducing tumor cell proliferation by expressing IL-22 and biregulin (Daley et al., 2016; Khosravi et al., 2018; Chen et al., 2019; Silva-Santos et al., 2019; Zhang et al., 2020). 7) Anti-tumor effect (Figure 2): Direct anti-tumor effect: activated γδT cells can secrete perforin, granzyme B and IFN-γ or express CD95 ligand (CD95L) and TRAIL to directly kill tumor cells (Gao et al., 2003); Indirect anti-tumor effect: Activated γδT cells induce DC maturation and infiltration by the secretion of TNF-α and IFN-γ (Conti et al., 2005; Münz et al., 2005; Nussbaumer et al., 2011); induce robust NK cell-mediated anti-tumor cytotoxicity through CD137 engagement (Maniar et al., 2010); efficiently processed and displayed antigens and provided co-stimulatory signals sufficient for strong induction of naïve αβT cell proliferation and differentiation (Brandes et al., 2005; Khan et al., 2014; Mao et al., 2014); γδT cells can target tumor associated macrophages and MDSCs to improve their anti-tumor ability. The enhanced killing capacity was correlated with the increased CD25 expression and IFN-γ secretion of γδT cells (Li et al., 2022).

3 γδT cells and tumors

3.1 Digestive system

1) Gastric cancer: Compared with normal gastric mucosa, the γδT cells in gastric cancer tissue are mainly Vδ1+T cells. The frequency of Vδ1γδT cells in gastric cancer tissue is reduced,

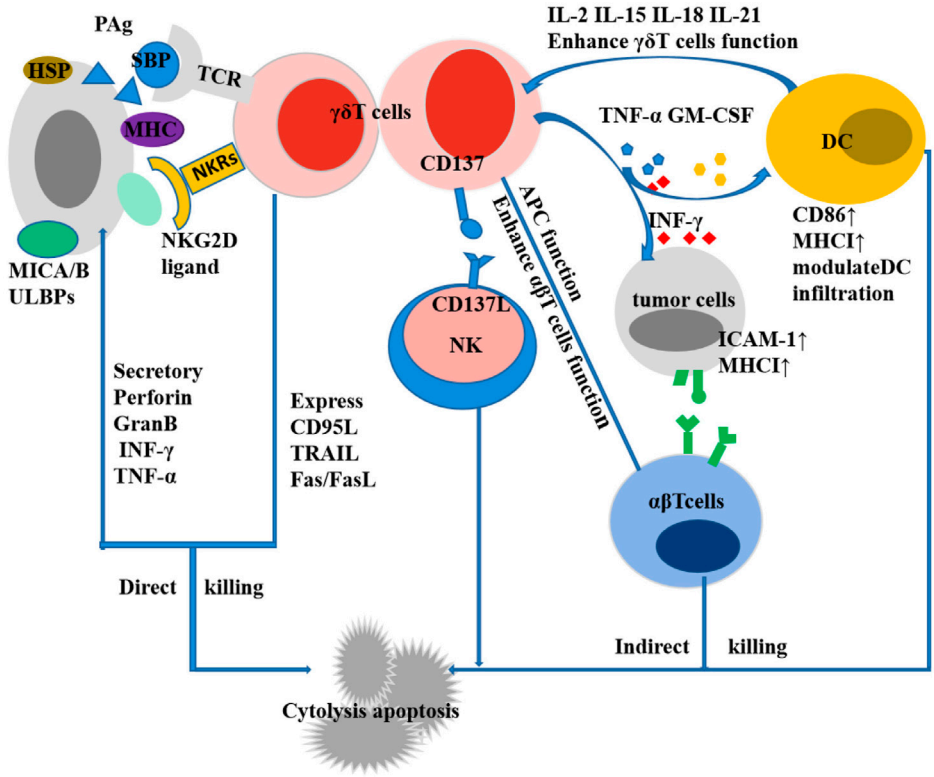

FIGURE 2
Anti-tumor effect of γδT cells.

the function is impaired, the secretion of IFN-γ and the expression of NKG2D are reduced. Reduced NKG2D expression may be one of the mechanisms of impaired function. The γδT cells infiltrated in gastric cancer tissue are also related to the prognosis of patients and can be used as an independent factor to judge the prognosis of patients (Kuroda et al., 2012; Wang. J et al., 2017; Chen et al., 2017). *In vitro*, γδT cells induced by pyrophosphate combined with IL-2 exhibited killing activity against gastric cancer cell line SGC-7901. The cytotoxicity of the cell line SGC-7901 was enhanced (Wu et al., 2016). Peripheral-derived γδT cells activated by gastric tumors can not only effectively kill tumor cells, but also induce the activation and proliferation of $CD4^+$ and CD8+αβT cells through the antigen-presenting cell properties of Vγ9Vδ2 T cells, and enhance the cytotoxic function of CD8+αβT cells (Mao et al., 2014). *In vivo*, γδT cells also showed a certain anti-tumor effect, Wada et al. (Wada et al., 2014) used Vδ2+γδT cells induced and cultured *in vitro* to immunotherapy patients with advanced gastric cancer with malignant ascites. After treatment, the number of tumor cells in the patients' ascites was significantly reduced and the ascites of some patients were controlled. Postoperative recurrence of gastric cancer is still a common problem, and cellular immunotherapy combined with chemotherapy seems to benefit patients after gastric cancer surgery. Oxaliplatin, a platinum drug for the treatment of gastric cancer, can upregulate the expression of NKG2D in tumor cells, thereby enhancing the sensitivity of tumor cells to kill mediated by γδT cells, NK cells, or cytokine-induced killer (CIK) cells (Gasser et al., 2005). When γδT cells, NK cells, and CIK cells combined with chemotherapy (5-FU and platinum) were used as adjuvant therapy after gastric cancer surgery, the adjuvant therapy showed good resistance compared with chemotherapy alone. Receptivity and safety can improve the quality of life of patients, significantly reduce the risk of recurrence and metastasis of stage II/III gastric cancer, and significantly improve the clinical prognosis of patients with stage II/III gastric cancer (Cui et al., 2015; Wang. Y et al., 2017).

2) Hepatocellular carcinoma: γδT cells can effectively kill a variety of liver cancer cell lines *in vitro* (Bouet-Toussaint et al., 2008; Hoh et al., 2013; Honda et al., 2015), and the presence of low concentrations of zoledronate can enhance the sensitivity of HCC cells to Vγ9Vδ2 T cell-mediated killing (Sugai et al., 2016). However, liver cancer infiltrating γδT cells

have defects in killing function and secretion of IFN-γ. This defect is caused by the following factors such as the damage of "T cell receptor pathway", "natural killer cell pathway" and "primary immunodeficiency pathway". It may be caused by a large number of infiltrating Treg cells in liver cancer tissues. Treg cells directly inhibit the effector function of γδT cells through cytokines TGFβ and IL-10 (Yi et al., 2013). Studies have found that allogeneic Vδ2 + γδT cells can complement the loss of anti-tumor function of liver cancer-infiltrating γδT cells (He et al., 2022). HCC tissue-resident γδT cells exhibit the characteristics of tissue-resident memory T cells and can effectively target ZOL-sensitized HCC tumor cells (Zakeri et al., 2022). Higher frequency of intratumoral γδT cells in HCC is associated with improved survival in HCC patients (Zakeri et al., 2022), The presence of γδT cells in adjacent tissues is related to the recurrence rate of hepatocellular carcinoma patients after surgery. The ratio of peritumoral hepatic stellate cells (HSCs) to γδT cells affects the invasiveness and recurrence of hepatocellular carcinoma, and the levels of IFN-γ, IL-17 and TNF-α secreted by γδT cells increased after cultured in HSC-containing medium, and greatly reduced the proliferation and invasiveness of liver cancer cells (Cai et al., 2014; Zhou et al., 2019). Increasing the number and function of γδT cells may become a new way to treat hepatocellular carcinoma.

3) Colorectal cancer: The study of Wu et al. (Wu et al., 2014a) proved that Vδ1 T cells induced and cultured *in vitro* by PHA combined with IL-7 showed a significant inhibitory effect on NOD/SCID mouse transplanted tumors established with the human colon cancer cell line HT29. Vγ9Vδ2T cells isolated from ascites have a killing effect on most colon cancer cell lines. This effect is related to the accumulation of IPP in tumor cells and the expression of ICAM-1, but there is no effect on normal colon cells (Corvaisier et al., 2005). Most colorectal cancer tissues express chemokines CCR5 and CXCR3 ligands, and CCR5 and CXCR3 receptors are expressed on the surface of γδT cells. The combination of the two promotes the migration of γδT cells to the tumor tissue and migrates to the γδT cells around the tumor tissue. The binding of NKG2D receptor to MICA/B and ICAM-1 on the surface of colon cancer cells is activated. The activated γδT cells release perforin and granzyme B to secrete cytokines IFN-γ, TNF-α, as well as TRAIL, Fas/FasL and many other ways to exert an effect on colon cancer cells (Todaro et al., 2009; Wu et al., 2014a). However, B7-H3+γδT cells and γδT17 are present in colon cancer that play the opposite role. The proportion of γδT cells expressing the immunomodulatory protein B7-H3 (CD276) in the peripheral blood and tumor tissues of colon cancer patients was significantly increased, and B7-H3 inhibited T-bet (a transcription factor of the T-box gene family) in Vδ2 T cells by inhibiting to inhibit the expression of IFN-γ and Vδ2 T cytotoxicity by downregulating the expression of perforin/granzyme B (Lu et al., 2020). Tumor-infiltrating γδT17 cells are the main IL-17-producing cells in human colorectal cancer, and activated γδT17 cells promote the proliferation of PMN-MDSCs by secreting cytokines such as IL-17, IL-8, TNF-α and GM-CSF, and maintain its immunosuppressive activity, promoting tumor progression (Wu et al., 2014b). The study of γδT cells with different functions provides more possible potential immunotherapies for colon cancer.

4) Pancreatic cancer: Oberg et al. (Oberg et al., 2014) used pancreatic cancer cell lines PancTu-I and SCID-Beige mice to establish a nude mouse tumor model, and used γδT cells, IL-2 and [(Her2)2xVγ9] to treat the above-mentioned tumor-bearing mice. This study found that the tumors in all mice were inhibited, and the significantly inhibited, moderately inhibited, and slightly inhibited patients accounted for 2/5, 1/5, and 2/5, respectively. However, the γδT cells infiltrated in pancreatic ductal adenocarcinoma (PDA) have a promoting effect on the occurrence and development of tumors. The cells are widely distributed in the interstitium of PDA, accounting for about 75% of infiltrating T cells, and the effective memory γδT cells are the main ones. These cells highly express IL-10, IL-17, FoxP3, PDL1 and galectin 9 (Gal-9). The interaction of these factors can cause adaptive immune suppression, thereby promoting the occurrence and development of PDA (Daley et al., 2016).

5) Esophageal cancer: The killing effect of γδT cells on esophageal tumor cells is mainly related to the expression of HSP on the surface of tumor cells. There may be γδT cell subsets expressing two phenotypes (Vγ9/Vδ2, Vγ9/Vδ1) in the peripheral blood of patients with esophageal cancer. These γδT cells recognize the HSP-60 and HSP-70 that expressed on the surface of tumor cells, shows cytotoxicity against autologous and allogeneic esophageal cancer cells (Thomas et al., 2000). In two phase 1 clinical trials of adoptive cellular immunotherapy using autologous γδT cells for recurrent or metastatic esophageal cancer (r/mEC), γδT cells with or without chemotherapy (docetaxel, cisplatin, and 5-fluorouracil) (DCF) in combination with chemotherapy) are safe and feasible, and γδT cells combined with chemotherapy can benefit patient survival (Sato et al., 2021).

3.2 Reproductive system

1) Ovarian cancer: A number of studies have shown that, γδT cells have a killing effect on ovarian cancer cells. *In vitro*, polyclonal γδT cells proliferated and activated by γ-irradiated k562-derived artificial antigen-presenting cells (aAPCs) showed a wide range of anti-tumor activities, and had certain anti-tumor activity against various ovarian cancer cell lines, such as CAOV3, EFO21, UPN251, IGROV1, and OC314. There are obvious inhibitory effects on the

transplanted tumor of NSG mice established with ovarian cancer cells CAOV3-effLuc-mKate, and significantly reducing the tumor burden in mice (Deniger et al., 2014). *In vitro*, Free or liposomal aminobisphosphonic acid salts such as zoledronic acid (ZA) and alendronic acid (AA) can enhance the killing effect of γδT cells on ovarian cancer cell lines SKOV-3 and IGROV1, and patient-derived γδT cells can also kill autologous cells after activation ovarian cancer cells. Intraperitoneal administration of low doses of AA or liposomal AA (L-AA) with γδT cells resulted in modest tumor regression in many SKOV-3-luc xenograft mice, and higher doses of AA or L-AA Intravenous administration with γδT cells resulted in marked and sustained tumor regression in SKOV-3-luc xenograft mice and prolonged survival of the mice. Activation of γδT cells by L-AA was also demonstrated in mice with a more aggressive IGROV-1-luc tumor model. The low maximum tolerated dose of liposomal ZA in SCID mice limits its application *in vivo* (Parente-Pereira et al., 2014). Foord et al. found that ascites-derived γδT cells had higher killing ability than CD8 + T cells in killing mature ovarian cancer cell line OVCAR-3, produced a higher proportion of IFN-γ, and derived from long-term survivors. γδT cells showed higher killing capacity than deceased patients (Foord et al., 2021). Another study found (Lai et al., 2012) that γδT cells also had an inhibitory effect on cells expressing stem cell markers in ovarian cancer. Researchers co-cultured γδT cells with microspheres with stem cell characteristics induced under certain conditions and found that the microspheres proliferation rate and the expression of stem cell-related genes were significantly reduced, the sensitivity to paclitaxel and cisplatin was increased, and the expression of antigens HLA-DR, B7-1, and B7-2 were significantly increased. It can be seen that γδT cells have a clear inhibitory effect on putative cancer stem cells.

2) Cervical cancer: One of the main risk factors for cervical cancer is the persistent infection of high-risk HPV. HPV-positive cervical cancer cells have low expression of MHC class I antigens, which limits the tumor recognition and anti-tumor effects of conventional T cells. The non-MHC restricted properties of γδT cells may play an important role in the immunotherapy of cervical cancer. In the research on cervical cancer, it was found that both bisphosphonate chemotherapeutics and galectin-1 (Gal-1) monoclonal antibody can enhance the anti-tumor effect of γδT cells. The immunosuppressive factor Gal-1 has been widely concerned. There is an inhibitory effect on the activity of γδT cells. When Gal-1 monoclonal antibody and γδT cells are used in combination with SiHa and HeLa cells *in vitro*, the killing activity of γδT cells is enhanced. Bisphosphonate chemotherapeutics such as pamidronate can increase the sensitivity of various cervical cancer cell lines such as HeLa, SiHa and CaSki to Vγ9Vδ2T cells, and enhance the antitumor activity of γδT cells. The enhancing effect of Gal-1 monoclonal antibody and bisphosphonate chemotherapeutics on the anti-tumor activity of γδT cells has been confirmed in mouse tumor-bearing experiments (Li et al., 2010; Lertworapreecha et al., 2013). However, it is worth noting that there are γδT17 cells in HPV-related cervical squamous cell carcinoma, which play a role in promoting the occurrence and development of tumors (Van Hede et al., 2017).
3) Prostate cancer: The use of syngeneic γδT cells for adoptive immunotherapy in a mouse prostate cancer model inhibited the growth of cancer cells (Liu et al., 2008). Zol combined with IL-2 *in vivo* expansion γδT cell therapy has a certain effect on hormone refractory prostate cancer. The effect is related to the maintenance or increase of the number of γδT cells during the treatment period. Moreover the increased γδT cells were mainly CD45RA-CD27-effect memory type and CD45RA+CD27-terminally differentiated type with direct effector functions and cytotoxic effects (Dieli et al., 2007). The inhibitory effect of γδT cells on prostate cancer has been confirmed in mice and clinical trials. However, the inhibitory effect of γδT cells on prostate cancer is different among different prostate cancer cell lines. DU145 is sensitive to the cytotoxicity of γδT cells, while PC-3 is characterized by its low activity of the melanic acid pathway and low IPP content in the body without sensitive (Arkko et al., 2015). Therefore, when using bisphosphonates to activate γδT for tumor immunotherapy, the type of tumor cells is an important consideration.

3.3 Urinary system

The research on the effect of γδT cells on urinary system tumors is mainly in kidney cancer. Peripheral blood γδT cells of patients with metastatic renal cell carcinoma (MRCC) can selectively act on kidney cancer cells after being activated by nitrogen-containing bisphosphonate and IL-2, but there are no effect on normal kidney cells. The above-mentioned selectivity may be related to the high expression of MICA/B and ULBP in renal cancer cells. γδT cells combine with MICA/B and ULBP through the NKG2D receptor to provide costimulatory signals to enhance the lysis of tumor cells by TCR signals (Viey et al., 2005). Zoledronate combined with IL-15 to induce γδT cells from healthy volunteer PBMCs effectively inhibited the growth of tumors in mice bearing renal cell carcinoma patient-derived xenografts and prolonged the survival time of tumor-bearing mice (Zhang et al., 2021).

The inhibitory effect of γδT cells on renal cell carcinoma has also been studied in a small clinical scale. Kobayashi et al. (Kobayashi et al., 2007) used γδT cells to treat patients with advanced renal cancer after radical nephrectomy. Among the 7 patients, 3 patients had prolonged tumor doubling time and

increased the number of γδT cells in peripheral blood. The study also found that the proportion of γδT cells in the peripheral blood of patients was related to the rate of tumor metastasis and the occurrence of tumor-related deaths in patients, which is one of the important factors to improve the prognosis of renal cancer patients. Bennouna et al. (Bennouna et al., 2008) used γδT cells combined with IL-2 to immunotherapy in 10 patients with metastatic renal cell carcinoma. 6 patients were in stable condition and the tumor progression time was prolonged. The immunotherapy of γδT cells may be the gospel for patients with advanced renal cancer.

3.4 Respiratory system

1) Nasopharyngeal carcinoma: Zheng B et al. (Zheng et al., 2001a) experimentally confirmed that γδT cells obtained by selective expansion of healthy human peripheral blood mononuclear cells *in vitro* had a certain cytotoxic effect on nasopharyngeal carcinoma cell lines CNE2 and 915, and this effect was related to the number of CD56-γδ T cells. Zheng BJ et al. (Zheng et al., 2001b) found that the use of nasopharyngeal carcinoma cell line CNE2 to establish a nude mouse tumor model, 5 days after CNE2 cell inoculation, tumors were seen subcutaneously in nude mice, and nude mice that were not treated with γδT cells had progressive tumors growth, the average lifespan of mice was 35 ± 3.4 days; CNE2 cells were inoculated with γδT cell treatment on the 10th day, and only a single dose of γδT cell treatment was given to the group. The tumor resumed growth 1 week later, and the average lifespan of mice was 61 ± 15.7 days; Once every other week, the group who was given γδT cell treatment twice resulted in delayed tumor recovery and growth, and the average life span of mice was prolonged by 74 ± 12.9 days. The results of immunohistochemistry showed that the tumor specimens on the second day of γδT cell treatment showed γδT cell accumulation and local necrosis, while on the sixth day, the infiltrating cells in the tumor tissue disappeared and the tumor cell mitosis increased. The above studies suggest that γδT cells exert a certain inhibitory effect on nasopharyngeal carcinoma cell lines both *in vivo* and *in vitro*.
2) Lung cancer: The inhibitory effect of γδT cells on lung cancer has been confirmed *in vitro*, mice and lung cancer patients. *In vitro* studies have shown (Xie et al., 2018) that the expanded γδT cells have a certain killing effect on the lung squamous cell line SK-MES-1 and the lung adenocarcinoma cell line A549; the use of *in vitro* expanded γδT cells on the human lung cancer cell A549, the mice were subjected to immunotherapy and found that the tumor growth rate slowed down, and the tested mice had no acute adverse reactions; Nakajima et al. (Nakajima et al., 2010) used γδT cells to perform adoptive immunotherapy on 10 patients with advanced lung cancer, and 3 patients were in stable condition. The inhibitory effect of γδT cells on lung cancer was related to the expression of HSP72 on the surface of lung cancer cells to varying degrees, a platelet-like receptor with a relative molecular mass of 67000 and a high affinity, and human MutS homologous protein 2 (hMSH2) molecules. After the T cell receptor TCRγδ or the natural killer receptor NKG2D is recognized, γδT cells are activated, and the levels of the activated γδT cells expressing CD69 and CD107a are significantly increased, and the secretion of IFN-γ and TNF-α increases, thereby killing and eliminating target cells (Ferrarini et al., 1996; Wei et al., 2018). The effects of γδT cells on lung cancer cells have been studied in depth, and how to better apply them in clinical practice needs to be further studied.
3) Breast cancer: The most effective treatment for breast cancer is surgery. Chemotherapy and immunotherapy are indispensable consolidation treatments after surgery. Studies have found that γδT cells have different inhibitory effects on different breast cancer cell lines. They have obvious inhibitory effects on breast cancer cell lines SkBr7, MCF7 and MDA-MB-231, while their inhibitory effects on BrCa-MZ01 are not obvious. The existence of this phenomenon may be related to the expression level of MICA/B and ICAM1 on the surface of breast cancer cells. γδT cells can up-regulate the expression of MICA/B and ICAM1 on the surface of the sensitive strain SkBr7. These molecules bind to the NKG2D receptor on the surface of γδT cells to trigger changes in intracellular signal molecules, protein kinases AKT, ERK and other signal molecules related to cell proliferation. The phosphorylation level of signal transduction and activator of transcription 3 (STAT3) decreased, and the expression level of pro-apoptotic molecules such as PARP and Caspase3 increased. Therefore, the recognition and binding of NKG2D receptors of γδT cells with MICA molecules expressed by tumor cells may be a necessary condition for their anti-tumor effects. The immunotherapy of NOD/SCID mouse xenograft model established by the sensitive strain SkBr7 and the resistant strain BrCa-MZ01 using γδT cells showed that γδT cells had a significant inhibitory effect on the tumor formation of the sensitive strain SkBr7, which was manifested by accelerated tumor cell apoptosis. Angiogenesis was inhibited, and tumor burden decreased. The non-sensitive cells did not appear to be suppressed. The appearance of these phenomena was not only related to the above analysis factors, but also related to the secretion of chemokines, tumor macrophage infiltration, etc. They act together on the tumor microenvironment, enhance the immune surveillance of tumors, inhibit tumor cell proliferation and induce them apoptosis (Aggarwal et al., 2013). In addition, activated γδT cells secreted IFN-γ, stimulated cancer stem cells (CSCs) to up-regulate the expression of MHC class I molecules and ICAM-1, and

enhanced the killing effect of CD8+T cells, both of which synergistically targeted breast cancer stem-like cells (Chen et al., 2017). The study of these mechanisms provides a theoretical basis for the clinical application of γδT cells. Meraviglia et al. (Meraviglia et al., 2010) used zoledronic acid combined with IL-2 *in vivo* proliferation and activation of γδT cells for immunotherapy of 10 patients with advanced breast cancer, and found that the progression of the patient's condition was related to the number of peripheral Vγ9Vδ2 T cells, and the condition was partially relieved or stable. The number of Vγ9Vδ2 T cells in the peripheral blood of 3 patients was maintained at a high level and the level of CA153 decreased. The number of Vγ9Vδ2 T cells in the peripheral blood of the 7 patients whose condition deteriorated could not be maintained continuously. Another study found that γδT cells could enhance the efficacy of trastuzumab in patients with HER-2 positive breast cancer, and the tumor volume of patients was significantly reduced (Capietto et al., 2011). Rukangyin and its disassembled prescriptions can inhibit the proliferation of triple-negative breast MDA-MB-231 cells and induce their apoptosis (Li et al., 2020). After Rukangyin activates γδT, it improves the killing rate of breast cancer MDA-MB-231 cells (Li et al., 2020; Chen et al., 2021). It can be seen that immunotherapy based on γδT cells may become a new method for breast cancer treatment.

3.5 Nervous system

The research on the effect of γδT cells on nervous system tumors is more common in neuroblastoma (neurobiastoma, NB). Many studies have confirmed (Schilbach et al., 2000; Chargui et al., 2010) that γδT cells proliferated and activated *in vitro* are highly cytotoxic to human neuroblastoma cells. They can effectively kill a variety of NB cell lines. γδT cells mainly recognize the target of NB cell line through their TCRγδ, and NKG2D has a weak role in NB cell lysis. This may be related to the lack of MICA on NB cells. These studies show the feasibility of using γδT cells to treat patients with neuroblastoma. Pressey et al. (Pressey et al., 2016) used phosphoantigen combined with IL-2 to perform immunotherapy on patients with refractory neuroblastoma and found that the therapy was well tolerated. The number of γδT cells in the patient increased significantly, and the patient had experienced remission. No toxic side effects of the therapy were found.

3.6 Blood system

γδT cells not only show inhibitory effects on solid tumors, but also have clear killing activity on hematological tumors. γδT cells are effective against many types of acute leukemia cell lines such as Jurkat cell line, THP-1 cell line, HL-60 cell line, chronic myeloid leukemia K562 cell line, multiple myeloma RPMI-8226 cell line and histiocytic lymphoma U-937 cell line, and it has strong killing effect on Jurkat cell line and U-937 cell line (Xiao et al., 2017). D'Asaro et al. (D'Asaro et al., 2010) confirmed that Vγ9Vδ2 T cells could recognize, phagocytose and effectively kill imatinib-sensitive CML cell line K562S and imatinib-resistant CML cell line K562R after pretreatment with zoledronate, KCL22R and LAMA84R, and prolong the survival of Nod/SCID mice bearing the CML cell line MM-1. Almeida et al. (Almeida et al., 2016) found that DOT cells had high cytotoxicity to CLL cell line MEC-1, autologous and allogeneic CLL cells, and had a significant inhibitory effect on NSG mouse xenografts established by MEC-1 cell line. DOT cells selectively target transformed B lymphocytes through their specific TCR mechanism and NKR mechanism, but there was no effect on normal B lymphocytes. DOT cells also showed a certain inhibitory effect on various AML cell lines such as THP-1, HEL, AML-193, MV4-11, HL-60, U-937, OCI-AML3, Kasumi-1 and KG-1, did not respond to normal leukocytes including $CD33^{+}$ or CD123+ myeloid cells. Adoptive cell therapy with DOT cells reduces AML burden in blood and target organs in various human AML xenograft models and significantly prolongs host survival without significant toxic effects. DOT cells can also target chemoresistance AML cells. These provide a theoretical basis for the application of DOT cells in the treatment of CLL and AML (Lorenzo et al., 2019). γδT cells can directly kill leukemia cells through perforin/granzyme-dependent cytolysis, and they can also act on hematological tumors by secreting cytokines IFN-γ and TNF-α (Gertner-Dardenne et al., 2012; Xiao et al., 2017). Tokuyama et al. (Tokuyama et al., 2008) found that the killing effect of γδT cells on lymphoma was related to the expression level of CD16 molecules on the cell surface. Trastuzumab and tuximab can enhance the killing activity of γδT cells against lymphoma. Wilhelm et al. (Wilhelm et al., 2003) used pamidronate (PAM) combined with IL-2 proliferation and activation of γδT cells in patients with immunotherapy of 19 patients with refractory non-Hodgkin's lymphoma and multiple myeloma, and found that PAM combined with low. The dose of IL-2 can specifically induce the proliferation of γδT cells, so that the patient's condition was stable or partially relieved without obvious adverse reactions. These studies have laid the foundation for the clinical application of γδT cells for immunotherapy of hematological tumors.

3.7 Other

Jiang Hui et al. (Jiang et al., 2010) found that γδT cells had a strong killing effect on the osteosarcoma cell line HOS, whether

TABLE 1 Preclinical trials based on γδT-cells.

Year	Author	Effector cells	Tumor type	Outcome
2016	Almeida Almeida et al., 2016	DOT (Vδ1T)	CLL-MEC-1 NSG mice, various human AML xenograft models	prolongs host survival without significant toxic effects
2022	Sánchez Martínez Sánchez Martínez et al., 2022	CD123 CAR-DOT (Vδ1T)	AML-PDX^{Luc} NSG mice	complete control of leukemia in mice
2004	Rischer Rischer et al., 2004	CD19 CAR-γδT (Vγ9Vδ2T) G_{D2} CAR-γδT (Vγ9Vδ2T)	Raji Reh LAN-1 JF	Efficiently and specifically lyse antigen-expressing tumour cells
2017	Harrer Harrer et al., 2017	gp100/HLA-A2 TCR-γδT MCSP CAR-γδT (Vγ9Vδ2T)	Mel 526 A375M	specifically lyse melanoma cells
2020	Ang Ang et al., 2020	$NKG2D_Z$ CAR-γδT (Vγ9Vδ2T)	HCT116-Luc NSG mice SKOV3-Luc NSG mice	1/5 tumor growth inhibition,4/5 tumor growth slowing down; median survival extend significantly
2020	Rozenbaum Rozenbaum et al., 2020	CD19 CAR-γδT (Vγ9Vδ2T)	$CD19^{+/-}$tumor cells B- ALL-Nalm6 NSG mice	highly reactive against good anti-leukemic activity but limited persistence of γδ CAR-T cells
2021	Makkouk Makkouk et al., 2021	GPC-3 CAR/SIL-15 Vδ1T	HCC-HepG2-NSG mice	controlled tumor growth
2021	Wallet Wallet et al., 2021	γδ CAR-iT	B-ALL-Nalm6 NSG mice	potent tumor growth inhibition

CAR, chimeric antigen receptor; $G_{D2,}$ ganglioside antigen; LAN-1 JF, neuroblastoma cell lines; Raji, Burkitt's lymphoma cell lines; Reh acute lymphocytic leukaemia cell lines; Mel526 A375M, melanoma cell lines; gp100, glycoprotein 100; MCSP, melanoma associated chondroitin sulfate proteoglycan; HCT116, Colorectal cancer cell lines; SKOV3, ovarian cancer cell lines; +, Positive; -, negtive; GPC-3, Glypican-3; HCC, hepatocellular carcinoma; γδ CAR-iT, Pluripotent stem cell-derived γδ CAR-T-cells.

in vitro or in tumor-bearing mice. Studies by Lozupone et al. (Lozupone et al., 2004) confirmed that both *in vivo* activation and adoptive infusion of γδT cells could inhibit the growth of tumors in melanoma-bearing mice and prolong the survival time of tumor-bearing mice. Malignant melanoma cell lines express NKG2D ligand and low expression of MHC-I related antigen A. These molecules bind to the NKG2D receptor of γδT cells to activate the body's anti-tumor immunity. Compared with healthy people, the peripheral blood γδT cells of melanoma patients increased significantly, and the increased γδT cells were mainly CD3 + CD28-γδT cells, which exerted anti-tumor effects through the expression of a large amount of perforin (Campillo et al., 2007). In B16 melanoma, IFN-γ produced by γδT cells serves as an early and important source of IFN-γ in tumor immune surveillance, plays a critical role in protecting immune responses against tumor development, and modulates tumor antigen-triggered $CD4^+$ and $CD8^+$ T cells response, thereby enhancing the recognition and potency of cytotoxic T cells against cancer cells (Khan et al., 2014).

4 γδT-cell-based cellular strategies

Evaluation of adoptive transfer and *in vivo* amplification of Vδ2+T cell efficacy Phase II trials showed that although Vδ2 + T Cells continue to activate and proliferate, but the clinical response of solid tumors is limited (Dieli et al., 2007; Bennouna et al., 2008; Kobayashi et al., 2011; Lang et al., 2011; Noguchi et al., 2011; Sakamoto et al., 2011; Scheper et al., 2014; Lo Presti et al., 2017; Zou et al., 2017; Hoeres et al., 2018). The mechanisms of preventing activation of Vδ2 + T cells inducing long-term anti-tumor immunity in cancer (Hayday and Tigelaar, 2003; Pennington et al., 2006; Kabelitz et al., 2013; Wesch et al., 2014; Peters et al., 2018) include the immunosuppressive function of γδT cells (Wu et al., 2014b; Daley et al., 2016), especially after TCR stimulation in different environments (Casetti et al., 2009; Traxlmayr et al., 2010; Peters et al., 2014), a study showed that TCR stimulation alone led to immunosuppressive behavior, and the degree of immunosuppression was related to the intensity of TCR signal (Schilbach et al., 2020). Even a single TCR crosslinking will produce inhibition behavior (Schilbach et al., 2020). However, several new immunotherapy strategies based on γδT cells have emerged. The application of γδT cells in tumor immunotherapy brings new hope. Almeida et al. (Almeida et al., 2016) used a 3-week culture program to obtain DOT cell products that showed inhibitory effects on a variety of CLL and AML cell lines; Chimeric antigen receptor (CAR) γδT cells can improve the efficacy of CAR-T cells and reduce their side effects (Rischer et al., 2004; Harrer et al., 2017; Ang et al., 2020; Rozenbaum et al., 2020; Makkouk et al., 2021; Sánchez Martínez et al., 2022); Wallet et al. described the generation of induced pluripotent stem cell-derived γδ CAR-T-cells (γδCAR-iT). They demonstrated a single dose of γδ CAR-T-cells resulted in potent tumor growth inhibition in a xenograft mouse model (Wallet et al., 2021);

TABLE 2 Ongoing clinical trials based on γδT-cells.

Title	Cellular strategies	Intervention	Malignancy	Phase	Organization	Start date	Recruitment status	Study identifier
A Safety and Efficacy Study of ADI-001, an Anti-CD20 Allogeneic Gamma Delta CAR-T, in Subjects With B cell Malignancies (GLEAN-1)	γδ CAR-T Cells	ADI-001. Anti-CD20 CAR-T + Lymphodeple-tion	B-NHL	I	Adicet Bio, Inc	4 March2021	Recruiting	NCT 04735471
Study of GDX012 in Patients With MRD Positive AML	Allogeneic γδT-cell transfer	GDX012. Allogeneic cell therapy enriched for Vd1+	AML	I	Gamma Delta Therapeutics Limited	13 August 2021	Teminated	NCT 05001451
Safety and Efficacy of *Ex-vivo* Expanded Allogeneic γδ T-lymphocytes (OmnImmune®) in Patients With Acute Myeloid Leukaemia (AML)	Allogeneic γδT-cell transfer	OmnImmune®	AML	I	TC Biopharm	Novem-ber 27, 2018	Completed	NCT 03790072
Trial of LAVA-051 in Patients With Relapsed/ Refractory CLL, MM, AML	Antibody-based strategies	LAVA-051. Bispecifific γδT-cell engager	CLL, AML, MM	I/II	Lava Therapeutics	12 July 2021	Recruiting	NCT 04887259
Trial of LAVA-1207 in Patients With Therapy Refractory Metastatic Castration Resistant Prostate Cancer	Antibody-based strategies	LAVA-1207. Bispecifific γδT-cell engager	mCRPC	I/IIa	Lava Therapeutics	27 June 2022	Recruiting	NCT 05369000
Phase 1/2a Study of ICT01 Plus Low Dose SC IL-2 in Patients With Advanced Solid Tumors (EVICTION-2)	Antibody-based strategies	ICT01.anti-BTN3A mAb + IL-2	Solid Tumor, Adult	I/IIa	ImCheck Therapeutics	19 April 2022	Recruiting	NCT 05307874
A Study to Investigate the Safety and Effificacy of TEG002 in Relapsed/ Refractory Multiple Myeloma Patients	Alternative γδT-cell-related strategies	TEG002	RR MM	I	Gadeta B.V.	13 May 2021	Active, not Recruiting	NCT 04688853

B-NHL, B cell Non-Hodgkin lymphoma; AML, acute myeloid leukemia; CLL, chronic lymphocytic leukemia; MM, multiple myeloma; mCRPC, metastatic castration resistant prostate cancer.

Bispecific γδT lymphocyte conjugator (bsTCE) optimizes Vγ9Vδ2 Tumor targeted activation of T cells not only preserves the ability of immune cells to recognize and kill tumors, but also promotes the immune response against tumors (Labrijn et al., 2019); Humanized anti BTN3A (also called CD277) monoclonal antibody can selectively activate Vγ9Vδ2 T cells, and further stimulate the immune system to kill tumor cells (Harly et al., 2012). These therapeutic strategies show promising anti-tumor activity *in vitro* and *in vivo* (Table 1). These therapeutic strategies will be evaluated in Phase I/Phase II clinical trials (Table 2), and the results of these trials will determine whether the potential of γδT cells can be translated into clinical benefits.

5 Conclusion

The role of γδT cells in tumor immunotherapy has gradually been recognized, but due to the lack of continuous and effective amplification methods, the complexity of γδT cell secretion factors, the various inhibitory factors existing in tumors, and the complexity of tumor microenvironment, etc. Existence limits the anti-tumor effect of γδT cells. How to establish and optimize a continuous and effective amplification method and further clarifying its mechanism of action is the direction of the researchers' unremitting efforts. The synergistic anti-tumor effect between chemotherapeutic drugs and γδT cells provides new ideas for the application of γδT cells. In clinical applications, whether γδT cell immunotherapy, radiotherapy, surgery and other combined treatments are synergistic and whether they can improve the prognosis of patients is also one of the future research directions.

Author contributions

RZ, QY, and YW drafted the manuscript. KW revised the manuscript.

Funding

This research was supported by the National Natural Science Foundation of China (grant number 82274538 and 81473687), the Natural Science Foundation of Shandong Province (grant numbers ZR2020MH312 and ZR2020MH357), and the Tai'an Science and Technology Plan (grant number 2020NS129).

Conflict of interest

The authors declare that the research was conducted in the absence of any commercial or financial relationships that could be construed as a potential conflict of interest.

Publisher's note

All claims expressed in this article are solely those of the authors and do not necessarily represent those of their affiliated organizations, or those of the publisher, the editors and the reviewers. Any product that may be evaluated in this article, or claim that may be made by its manufacturer, is not guaranteed or endorsed by the publisher.

References

Aggarwal, R., Lu, J., Kanji, S., Das, M., Joseph, M., Lustberg, M. B., et al. (2013). Human Vγ2Vδ2 T cells limit breast cancer growth by modulating cell survival-apoptosis-related molecules and microenvironment in tumors. *Int. J. Cancer* 133 (9), 2133–2144. doi:10.1002/ijc.28217

Almeida, A. R., Correia, D. V., Fernandes-Platzgummer, A., da Sliva, C. L., da Sliva, M. G., Anjos, D. R., et al. (2016). Delta one T cells for immunotherapy of chronic lymphocytic leukemia: Clinical-grade expansion/differentiation and preclinical proof of concept. *Clin. Cancer Res.* 22 (23), 5795–5804. doi:10.1158/1078-0432.CCR-16-0597

Ang, W. X., Ng, Y. Y., Xiao, L., Chen, C., Li, Z., Chi, Z., et al. (2020). Electroporation of Nkg2d rna car improves Vγ9vδ2 T cell responses against human solid tumor xenografts. *Mol. Ther. Oncolytics* 17, 421–430. doi:10.1016/j.omto.2020.04.013

Arkko, S., Zlatev, H. P., Mönkkönen, H., Räikkönen, J., Benzaïd, I., Clézardin, P., et al. (2015). Upregulation of the mevalonate pathway by cholesterol depletion abolishes tolerance to N-bisphosphonate induced Vγ9Vδ2 T cell cytotoxicity in PC-3 prostate cancer cells. *Cancer Lett.* 357 (1), 279–285. doi:10.1016/j.canlet.2014.11.030

Benevides, L., da Fonseca, D. M., Donate, P. B., Tiezzi, D. G., De Carvalho, D. D., de Andrade, J. M., et al. (2015). IL17 promotes mammary tumor progression by changing the behavior of tumor cells and eliciting tumorigenic neutrophils recruitment. *Cancer Res.* 75 (18), 3788–3799. doi:10.1158/0008-5472.CAN-15-0054

Bennouna, J., Bompas, E., Neidhardt, E. M., Rolland, F., Philip, I., Galéa, C., et al. (2008). Phase-I study of Innacell gammadelta, an autologous cell-therapy product highly enriched in gamma9delta2 T lymphocytes, in combination with IL-2, in patients with metastatic renal cell carcinoma. *Cancer Immunol. Immunother.* 57 (11), 1599–1609. doi:10.1007/s00262-008-0491-8

Bouet-Toussaint, F., Cabillic, F., Toutirais, O., LeGallo, M., Thomasde la Pintière, C., Daniel, P., et al. (2008). Vgamma9Vdelta2 T cell-mediated recognition of human solid tumors. Potential for immunotherapy of hepatocellular and colorectal carcinomas. *Cancer Immunol. Immunother.* 57 (4), 531–539. doi:10.1007/s00262-007-0391-3

Brandes, M., Willimann, K., Bioley, G., Lévy, N., Eberl, M., Luo, M., et al. (2009). Cross-presenting human gammadelta T cells induce robust CD8+ alphabeta T cell responses. *Pro Natl. Acad. Sci. U. S. A.* 106 (7), 2307–2312. doi:10.1073/pnas.0810059106

Brandes, M., Willimann, K., and Moser, B. (2005). Professional antigen-presentation function by human gammadelta T Cells. *Science* 309 (5732), 264–268. doi:10.1126/science.1110267

Cai, X., Wang, J., Yi, Y., He, H. W., Ni, X. C., Zhou, J., et al. (2014). Low counts of γδ T cells in peritumoral liver tissue are related to more frequent recurrence in patients with hepatocellular carcinoma after curative resection. *Asian Pac J. Cancer Prev.* 15 (2), 775–780. doi:10.7314/apjcp.2014.15.2.775

Campillo, J. A., Martínez-Escribano, J. A., Minguela, A., López-Alvarez, R., Marín, L. A., García-Alonso, A. M., et al. (2007). Increased number of cytotoxic CD3+ CD28- gammadelta T cells in peripheral blood of patients with cutaneous malignant melanoma. *Dermatology* 214 (4), 283–288. doi:10.1159/000100878

Capietto, A. H., Martinet, L., and Fournié, J. J. (2011). Stimulated gammadelta T cells increase the *in vivo* efficacy of trastuzumab in HER-2$^+$ breast cancer[J]. *J. Immunol.* 187 (2), 1031–1038. doi:10.4049/jimmunol.1100681

Casetti, R., Agrati, C., Wallace, M., Sacchi, A., Martini, F., Martino, A., et al. (2009). Cutting edge: TGF-beta1 and IL-15 induce FOXP3+ gammadelta regulatory T cells in the presence of antigen stimulation. *J. Immunol.* 183 (6), 3574–3577. doi:10.4049/jimmunol.0901334

Chargui, J., Combaret, V., Scaglione, V., Iacono, I., Péri, V., Valteau-Couanet, D., et al. (2010). Bromohydrin pyrophosphate-stimulated Vgamma9delta2 T cells expanded *ex vivo* from patients with poor-prognosis neuroblastoma lyse autologous primary tumor cells. *J. Immunother.* 33 (6), 591–598. doi:10.1097/CJI.0b013e3181dda207

Chen, H., Bernstein, H., Ranganathan, P., and Schluter, S. F. (2012). Somatic hypermutation of TCR γ V genes in the sandbar shark. *Dev. Comp. Immunol.* 37 (1), 176–183. doi:10.1016/j.dci.2011.08.018

Chen, H. C., Joalland, N., Bridgeman, J. S., Alchami, F. S., Jarry, U., Khan, M. W. A., et al. (2017). Synergistic targeting of breast cancer stem-like cells by human γδ T cells and CD8+ T cells. *Immunol. Cell Biol.* 95 (7), 620–629. doi:10.1038/icb.2017.21

Chen, X., Shang, W., Xu, R., Wu, M., Zhang, X., Huang, P., et al. (2019). Distribution and functions of γδ T cells infiltrated in the ovarian cancer microenvironment. *J. Transl. Med.* 17 (1), 144. doi:10.1186/s12967-019-1897-0

Chen, Z. W., Zhao, Y. J., Li, X. Q., and Wang, K. Q. (2021). Study on the killing effect of *γδ*T cells activated by rukangyin on breast cancer MDA-MB-231 cells. *Dis. Markers* 2021, e5838582. doi:10.1155/2021/5838582

Chodaczek, G., Papanna, V., Zal, M. A., and Zal, T. (2012). Body-barrier surveillance by epidermal γδ TCRs. *Nat. Immunol.* 13 (3), 272–282. doi:10.1038/ni.2240

Coffelt, S. B., Kersten, K., Doornebal, C. W., Weiden, J., Vrijland, K., Hau, C. S., et al. (2015). IL-17-producing γδ T cells and neutrophils conspire to promote breast cancer metastasis. *Nature* 522 (7556), 345–348. doi:10.1038/nature14282

Conti, L., Casetti, R., Cardone, M., Varano, B., Martino, A., Belardelli, F., et al. (2005). Reciprocal activating interaction between dendritic cells and pamidronate-stimulated gammadelta T cells: Role of CD86 and inflammatory cytokines. *J. Immunol.* 174 (1), 252–260. doi:10.4049/jimmunol.174.1.252

Cook, L., Miyahara, N., Jin, N., Wands, J. M., Taube, C., Roark, C. L., et al. (2008). Evidence that CD8+ dendritic cells enable the development of gammadelta T cells that modulate airway hyperresponsiveness. *J. Immunol.* 181 (1), 309–319. doi:10.4049/jimmunol.181.1.309

Corvaisier, M., Moreau-Aubry, A., Diez, E., Bennouna, J., Mosnier, J. F., Scotet, E., et al. (2005). V gamma 9V delta 2 T cell response to colon carcinoma cells. *J. Immunol.* 175 (8), 5481–5488. doi:10.4049/jimmunol.175.8.5481

Cui, J., Li, L., Wang, C., Jin, H., Yao, C., Wang, Y., et al. (2015). Combined cellular immunotherapy and chemotherapy improves clinical outcome in patients with gastric carcinoma. *Cytotherapy* 17 (7), 979–988. doi:10.1016/j.jcyt.2015.03.605

Daley, D., Zambirinis, C. P., Seifert, L., Akkad, N., Mohan, N., Werba, G., et al. (2016). Γδ T cells support pancreatic oncogenesis by restraining αβ T cell activation. *Cell* 166 (6), 1485–1499. doi:10.1016/j.cell.2016.07.046

D'Asaro, M., Mendola, C. L., Liberto, D. D., Orlando, V., Todaro, M., Spina, M., et al. (2010). V gamma 9V delta 2 T lymphocytes efficiently recognize and kill zoledronate-sensitized, imatinib-sensitive, and imatinib-resistant chronic myelogenous leukemia cells. *J. Immunol.* 184, 3260–3268. doi:10.4049/jimmunol.0903454

Davey, M. S., Willcox, C. R., Hunter, S., Kasatskaya, S. A., Remmerswaal, E. B. M., Salim, M., et al. (2018). The human Vδ2+ T-cell compartment comprises distinct innate-like Vγ9+ and adaptive Vγ9- subsets. *Nat. Commun.* 9 (1), 1760. doi:10.1038/s41467-018-04076-0

Deniger, D. C., Maiti, S. N., Mi, T., Switzer, K. C., Ramachandran, V., Hurton, L. V., et al. (2014). Activating and propagating polyclonal gamma delta T cells with broad specificity for malignancies. *Clin. Cancer Res.* 20 (22), 5708–5719. doi:10.1158/1078-0432.CCR-13-3451

Dieli, F., Vermijlen, D., Fulfaro, F., Caccamo, N., Meraviglia, S., Cicero, G., et al. (2007). Targeting human {gamma}delta} T cells with zoledronate and interleukin-2 for immunotherapy of hormone-refractory prostate cancer. *Cancer Res.* 67 (15), 7450–7457. doi:10.1158/0008-5472.CAN-07-0199

Ferrarini, M., Heltai, S., Pupa, S. M., Mernard, S., and Zocchi, R. (1996). Killing of lamininreceptor-positive human lung cancers by tumor infiltrating lymphocytes bearing γδ⁺T-cell receptors[J]. *J. Natl. Cancer Inst.* 88 (7), 436–441. doi:10.1093/jnci/88.7.436

Foord, E., Arruda, L. C. M., Gaballa, A., Klynning, C., and Uhlin, M. (2021). Characterization of ascites- and tumor-infiltrating γδ T cells reveals distinct repertoires and a beneficial role in ovarian cancer. *Sci. Transl. Med.* 13 (577), eabb0192. doi:10.1126/scitranslmed.abb0192

Gao, Y. F., Yang, W. C., Pan, M., Scully, E., Girardi, M., Augenlicht, L. H., et al. (2003). Gamma delta T cells provide an early source of interferon gamma in tumor immunity. *J. Exp. Med.* 198 (3), 433–442. doi:10.1084/jem.20030584

Gasser, S., Orsulic, S., Brown, E. J., and Raulet, D. H. (2005). The DNA damage pathway regulates innate immune system ligands of the NKG2D receptor. *Nature* 436, 1186–1190. doi:10.1038/nature03884

Gertner-Dardenne, J., Castellano, R., Mamessier, E., Garbit, S., Kochbati, E., Etienne, A., et al. (2012). Human Vγ9Vδ2 T cells specifically recognize and kill acute myeloid leukemic blasts. *J. Immunol.* 188 (9), 4701–4708. doi:10.4049/jimmunol.1103710

Gu, S., Sachleben, J. R., Boughter, C. T., Nawrocka, W. I., Borowska, M. T., Tarrasch, J. T., et al. (2017). Phosphoantigen-induced conformational change of butyrophilin 3A1 (BTN3A1) and its implication on Vγ9Vδ2 T cell activation. *Proc. Natl. Acad. Sci.* 114 (35), E7311–E7320. doi:10.1073/pnas.1707547114

Harly, C., Guillaume, Y., Nedellec, S., Peigne, C. M., Mönkkönen, H., Mönkkönen, J., et al. (2012). Key implication of CD277/butyrophilin-3 (BTN3A) in cellular stress sensing by a major human γδ T-cell subset. *Blood* 120 (11), 2269–2279. doi:10.1182/blood-2012-05-430470

Harrer, D. C., Simon, B., Fujii, S-I., Shimizu, K., Uslu, U., Schuler, G., et al. (2017). RNA-Transfection of γ/δ T cells with a chimeric antigen receptor or an α/β T-cell receptor: A safer alternative to genetically engineered α/β T cells for the immunotherapy of melanoma. *BMC Cancer* 17 (1), 551. doi:10.1186/s12885-017-3539-3

Hayday, A., and Tigelaar, R. (2003). Immunoregulation in the tissues by gammadelta T cells. *Nat. Rev. Immunol.* 3 (3), 233–242. doi:10.1038/nri1030

He, W. J., Hu, Y., Chen, D., Li, Y., Ye, D., Zhao, Q., et al. (2022). Hepatocellular carcinoma-infiltrating γδ T cells are functionally defected and allogenic Vδ2 $^{+}$ γδ T cell can be a promising complement. *Clin. Transl. Med.* 12 (4), e800. doi:10.1002/ctm2.800

Hoeres, T., Smetak, M., Pretscher, D., and Wilhelm, M. (2018). Improving the efficiency of Vγ9Vδ2 T-cell immunotherapy in cancer. *Front. Immunol.* 9, 800. doi:10.3389/fimmu.2018.00800

Hoh, A., Dewerth, A., Vogt, F., Wenz, J., Baeuerle, P. A., Warmann, S. W., et al. (2013). The activity of γδ T cells against paediatric liver tumour cells and spheroids in cell culture. *Liver Int.* 33 (1), 127–136. doi:10.1111/liv.12011

Honda, Y., Takahashi, S., Zhang, Y., Ono, A., Murakami, E., Shi, N., et al. (2015). Effects of bisphosphonate zoledronic acid in hepatocellular carcinoma, depending on mevalonate pathway. *J. Gastroenterol. Hepatol.* 30, 619–627. doi:10.1111/jgh.12715

Jiang, H., Xu, Q., Yang, C., Cao, Z. G., Li, C. X., and Ye, Z. M. (2010). Gammadelta T cells stimulated by zoledronate kill osteosarcoma cells. *Chin. J. Cell Mol. Immunol.* 26 (12), 1195–1197. doi:10.13423/j.cnki.cjcmi.005670

Kabelitz, D., Peters, C., Wesch, D., and Oberg, H. H. (2013). Regulatory functions of γδ T cells. *Int. Immunopharmacol.* 16 (3), 382–387. doi:10.1016/j.intimp.2013.01.022

Khan, M. W., Curbishley, S. M., Chen, H. C., Thomas, A. D., Pircher, H., Mavilio, D., et al. (2014). Expanded human blood-derived γδT cells display potent antigen-presentation functions. *Front. Immunol.* 5, 344. doi:10.3389/fimmu.2014.00344

Khatri, M., Dwivedi, V., Krakowka, S., Manickam, C., Ali, A., Wang, L., et al. (2010). Swine influenza H1N1 virus induces acute inflammatory immune responses in pig lungs: A potential animal model for human H1N1 influenza virus. *J. Virol.* 84 (21), 11210–11218. doi:10.1128/JVI.01211-10

Khosravi, N., Caetano, M. S., Cumpian, A. M., Unver, N., Dela GarzaRamos, C., Noble, O., et al. (2018). IL22 promotes kras-mutant lung cancer by induction of a protumor immune response and protection of stemness properties. *Cancer Immunol. Res.* 6 (7), 788–797. doi:10.1158/2326-6066.CIR-17-0655

Kobayashi, H., Tanaka, Y., Yagi, J., Minato, N., and Tanabe, K. (2011). Phase I/II study of adoptive transfer of γδ T cells in combination with zoledronic acid and IL-2 to patients with advanced renal cell carcinoma. *Cancer Immunol. Immunother.* 60 (8), 1075–1084. doi:10.1007/s00262-011-1021-7

Kobayashi, H., Tanaka, Y., Yagi, J., Osaka, Y., Nakazawa, H., Uchiyama, T., et al. (2007). Safety profile and anti-tumor effects of adoptive immunotherapy using gamma-delta T cells against advanced renal cell carcinoma: A pilot study. *Cancer Immunol. Immunother.* 56 (4), 469–476. doi:10.1007/s00262-006-0199-6

Kühl, A. A., Pawlowski, N. N., Grollich, K., Blessenohl, M., Westermann, J., Zeitz, M., et al. (2009). Human peripheral gammadelta T cells possess regulatory potential. *Immunology* 128 (4), 580–588. doi:10.1111/j.1365-2567.2009.03162.x

Kuroda, H., Saito, H., and Ikeguchi, M. (2012). Decreased number and reduced NKG2D expression of Vδ1 γδ T cells are involved in the impaired function of Vδ1 γδ T cells in the tissue of gastric cancer. *Gastric Cancer* 15, 433–439. doi:10.1007/s10120-011-0138-x

Labrijn, A. F., Janmaat, M. L., Reichert, J. M., and Parren, P. (2019). Bispecific antibodies: A mechanistic review of the pipeline. *Nat. Rev. Drug Discov.* 18 (8), 585–608. doi:10.1038/s41573-019-0028-1

Lai, D., Wang, F., Chen, Y., Wang, C., Liu, S., Lu, B., et al. (2012). Human ovarian cancer stem-like cells can be efficiently killed by γδ T lymphocytes. *Cancer Immunol. Immunother.* 61 (7), 979–989. doi:10.1007/s00262-011-1166-4

Lang, J. M., Kaikobad, M. R., Wallace, M., Staab, M. J., Horvath, D. L., Wilding, G., et al. (2011). Pilot trial of interleukin-2 and zoledronic acid to augment γδ T cells as treatment for patients with refractory renal cell carcinoma. *Cancer Immunol. Immunother.* 60 (10), 1447–1460. doi:10.1007/s00262-011-1049-8

Lertworapreecha, M., Patumraj, S., Niruthisard, S., Hansasuta, P., and Bhattarakosol, P. (2013). Cytotoxic function of gamma delta (gamma/delta) T cells against pamidronate-treated cervical cancer cells. *Indian J. Exp. Biol.* 51 (8), 597–605.

Li, H., Wang, Y. B., and Zhou, F. X. (2010). Effect of *ex vivo*-expanded γδ-T cells combined with galectin-1 antibody on the growth of human cervical cancer xenografts in SCID mice. *Clin. Invest. Med.* 33 (5), E280–E289. doi:10.25011/cim.v33i5.14353

Li, X. Q., Wei, C. R., Zhang, M., Wang, Y., and Guo, G. L. (2020). Role of serum containing rukangyin on invasion of breast cancer MDA-MB-231 cells[J]. *J. Med. Res.* 49 (2), 59–63. doi:10.11969/j.issn.1673-548X.2020.02.014

Li, Y. R., Brown, J., Yu, Y., Lee, D., Zhou, K., Dunn, Z. S., et al. (2022). Targeting immunosuppressive tumor-associated macrophages using innate T cells for enhanced antitumor reactivity. *Cancers* 14 (11), 2749. doi:10.3390/cancers14112749

Liu, Z., Eltoum, I. E., Guo, B., Beck, B. H., Cloud, G. A., and Lopez, R. D. (2008). Protective immunosurveillance and therapeutic antitumor activity of gammadelta

T cells demonstrated in a mouse model of prostate cancer. *J. Immunol.* 180 (9), 6044–6053. doi:10.4049/jimmunol.180.9.6044

Lo Presti, E., Pizzolato, G., Gulotta, E., Cocorullo, G., Gulotta, G., Dieli, F., et al. (2017). Current advances in γδ T cell-based tumor immunotherapy. *Front. Immunol.* 8, 1401. doi:10.3389/fimmu.2017.01401

Lorenzo, B. D., Simoes, A. E., Caiado, F., Tieppo, P., Correia, D. V., Carvalho, T., et al. (2019). Broad cytotoxic targeting of acute myeloid leukemia by polyclonal delta one T cells. *Cancer Immunol. Res.* 7 (4), 552–558. doi:10.1158/2326-6066.CIR-18-0647

Lozupone, F., Pende, D., Burgio, V. L., Castelli, C., Spada, M., Venditti, M., et al. (2004). Effect of human natural killer and gammadelta T cells on the growth of human autologous melanoma xenografts in SCID mice. *Cancer Res.* 64 (1), 378–385. doi:10.1158/0008-5472.can-03-1501

Lu, H. M., Shi, T. G., Wang, M. Y., Li, X., Gu, Y., Zhang, X., et al. (2020). B7-H3 inhibits the IFN-γ-dependent cytotoxicity of Vγ9Vδ2 T cells against colon cancer cells. *OncoImmunology* 9 (1), 1748991. doi:10.1080/2162402X.2020.1748991

Makkouk, A., Yang, X. C., Barca, T., Lucas, A., Turkoz, M., Wong, J. T. S., et al. (2021). Off-the-shelf Vδ1 gamma delta T cells engineered with glypican-3 (GPC-3)-specific chimeric antigen receptor (CAR) and soluble IL-15 display robust antitumor efficacy against hepatocellular carcinoma. *J. Immunother. Cancer* 9 (12), e003441. doi:10.1136/jitc-2021-003441

Maniar, A., Zhang, X., Lin, W., Gastman, B. R., Pauza, C. D., Strome, S. E., et al. (2010). Human gammadelta T lymphocytes induce robust NK cell-mediated antitumor cytotoxicity through CD137 engagement. *Blood* 116 (10), 1726–1733. doi:10.1182/blood-2009-07-234211

Mao, C. M., Mou, X., Zhou, Y. P., Yuan, G., Xu, C., Liu, H., et al. (2014). Tumor-activated TCRγδ$^+$ T cells from gastric cancer patients induce the antitumor immune response of TCRαβ$^+$ T cells via their antigen-presenting cell-like effects. *J. Immunol. Res.* 2014, 593562. doi:10.1155/2014/593562

McCarthy, N. E., Bashir, Z., Vossenkämper, A., Hedin, C. R., Giles, E. M., Bhattacharjee, S., et al. (2013). Proinflammatory Vδ2$^+$T cells populate the human intestinal mucosa and enhance IFN-γ production by colonic αβT cells[J]. *J. Immunol.* 191 (5), 2752–2763. doi:10.4049/jimmunol.1202959

Meraviglia, S., Eberl, M., Vermijlen, D., Todaro, M., Buccheri, S., Cicero, G., et al. (2010). *In vivo* manipulation of Vgamma9Vdelta2 T cells with zoledronate and low-dose interleukin-2 for immunotherapy of advanced breast cancer patients. *Clin. Exp. Immunol.* 161 (2), 290–297. doi:10.1111/j.1365-2249.2010.04167.x

Münz, C., Steinman, R. M., and Fujii, S. (2005). Dendritic cell maturation by innate lymphocytes: Coordinated stimulation of innate and adaptive immunity. *J. Exp. Med.* 202 (2), 203–207. doi:10.1084/jem.20050810

Nakajima, J., Murakawa, T., Fukami, T., Goto, S., Kaneko, T., Yoshida, Y., et al. (2010). A phase I study of adoptive immunotherapy for recurrent non-small-cell lung cancer patients with autologous gammadelta T cells. *Eur. J. Cardiothorac. Surg.* 37 (5), 1191–1197. doi:10.1016/j.ejcts.2009.11.051

Narayan, K., Sylvia, K. E., Malhotra, N., Yin, C. C., Martens, G., Vallerskog, T., et al. (2012). Intrathymic programming of effector fates in three molecularly distinct γδ T cell subtypes. *Nat. Immunol.* 13 (5), 511–518. doi:10.1038/ni.2247

Noguchi, A., Kaneko, T., Kamigaki, T., Fujimoto, K., Ozawa, M., Saito, M., et al. (2011). Zoledronate-activated Vγ9γδ T cell-based immunotherapy is feasible and restores the impairment of γδ T cells in patients with solid tumors. *Cytotherapy* 13 (1), 92–97. doi:10.3109/14653249.2010.515581

Nussbaumer, O., Gruenbacher, G., Gander, H., and Thurnher, M. (2011). DC-like cell-dependent activation of human natural killer cells by the bisphosphonate zoledronic acid is regulated by γδ T lymphocytes. *Blood* 118 (10), 2743–2751. doi:10.1182/blood-2011-01-328526

Oberg, H. H., Peipp, M., Kellner, C., Sebens, S., Krause, S., Petrick, D., et al. (2014). Novel bispecific antibodies increase γδ T-cell cytotoxicity against pancreatic cancer cells. *Cancer Res.* 74 (5), 1349–1360. doi:10.1158/0008-5472.CAN-13-0675

Parente-Pereira, A. C., Shmeeda, H., Whilding, L. M., Zambirinis, C. P., Foster, J., van der Stegen, S. J., et al. (2014). Adoptive immunotherapy of epithelial ovarian cancer with Vγ9Vδ2 T cells, potentiated by liposomal alendronic acid. *J. Immunol.* 193 (11), 5557–5566. doi:10.4049/jimmunol.1402200

Peng, G., Wang, H. Y., Peng, W., Kiniwa, Y., Seo, K. H., and Wang, R. F. (2007). Tumor-infiltrating gammadelta T cells suppress T and dendritic cell function via mechanisms controlled by a unique toll-like receptor signaling pathway. *Immunity* 27 (2), 334–348. doi:10.1016/j.immuni.2007.05.020

Pennington, D. J., Silva-Santos, B., Silberzahn, T., Escórcio-Correia, M., Woodward, M. J., Roberts, S. J., et al. (2006). Early events in the thymus affect the balance of effector and regulatory T cells. *Nature* 444 (7122), 1073–1077. doi:10.1038/nature06051

Pennington, D. J., Vermijlen, D., Wise, E. L., Clarke, S. L., Tigelaar, R. E., and Hayday, A. C. (2005). The integration of conventional and unconventional T cells that characterizes cell-mediated responses. *Adv. Immunol.* 87, 27–59. doi:10.1016/S0065-2776(05)87002-6

Peters, C., Kabelitz, D., and Wesch, D. (2018). Regulatory functions of γδ T cells. *Cell Mol. Life Sci.* 75 (12), 2125–2135. doi:10.1007/s00018-018-2788-x

Peters, C., Oberg, H. H., Kabelitz, D., and Wesch, D. (2014). Phenotype and regulation of immunosuppressive Vδ2-expressing γδ T cells. *Cell Mol. Life Sci.* 71 (10), 1943–1960. doi:10.1007/s00018-013-1467-1

Poonia, B., and Pauza, C. D. (2012). Gamma delta T cells from HIV+ donors can be expanded *in vitro* by zoledronate/interleukin-2 to become cytotoxic effectors for antibody-dependent cellular cytotoxicity. *Cytotherapy* 14 (2), 173–181. doi:10.3109/14653249.2011.623693

Pressey, J. G., Adams, J., Harkins, L., Kelly, D., You, Z., and Lamb, L. S. (2016). *In vivo* expansion and activation of γδ T cells as immunotherapy for refractory neuroblastoma: A phase 1 study. *Medicine* 95 (39), e4909. doi:10.1097/MD.0000000000004909

Qian, X., Chen, H., Wu, X., Hu, L., Huang, Q., and Jin, Y. (2017). Interleukin-17 acts as double-edged sword in anti-tumor immunity and tumorigenesis. *Cytokine* 89, 34–44. doi:10.1016/j.cyto.2015.09.011

Rigau, M., Ostrouska, S., Fulford, T. S., Johnson, D. N., Woods, K., Ruan, Z., et al. (2020). Butyrophilin 2A1 is essential for phosphoantigen reactivity by γδ T cells. *Science* 367 (6478), eaay5516. doi:10.1126/science.aay5516

Rischer, M., Pscherer, S., Duwe, S., Vormoor, J., Jurgens, H., and Rossig, C. (2004). Human gammadelta T cells as mediators of chimaeric-receptor redirected anti-tumour immunity. *Br. J. Haematol.* 126 (4), 583–592. doi:10.1111/j.1365-2141.2004.05077.x

Romano, A., Parrinello, N. L., La Cava, P., Tibullo, D., Giallongo, C., Camiolo, G., et al. (2018). PMN-MDSC and arginase are increased in myeloma and may contribute to resistance to therapy. *Expert Rev. Mol. Diagn* 18 (7), 675–683. doi:10.1080/14737159.2018.1470929

Rozenbaum, M., Meir, A., Aharony, Y., Itzhaki, O., Schachter, J., Bank, I., et al. (2020). Gamma-delta CAR-T cells show CAR-directed and independent activity against leukemia. *Front. Immunol.* 11, 1347. doi:10.3389/fimmu.2020.01347

Sacchi, A., Tumino, N., Sabatini, A., Cimini, E., Casetti, R., Bordoni, V., et al. (2018). Myeloid-derived suppressor cells specifically suppress IFN-γ production and antitumor cytotoxic activity of vδ2 T cells. *Front. Immunol.* 9, 1271. doi:10.3389/fimmu.2018.01271

Sakamoto, M., Nakajima, J., Murakawa, T., Fukami, T., Yoshida, Y., Murayama, T., et al. (2011). Adoptive immunotherapy for advanced non-small cell lung cancer using zoledronate-expanded γδTcells: a phase I clinical study. *J. Immunother.* 34 (2), 202–211. doi:10.1097/cji.0b013e318207ecfb

Sánchez Martínez, D., Tirado, N., Mensurado, S., Martínez-Moreno, A., Romecín, P., Gutiérrez Agüera, F., et al. (2022). Generation and proof-of-concept for allogeneic CD123 CAR-Delta One T (DOT) cells in acute myeloid leukemia. *J. Immunother. Cancer* 10 (9), e005400. doi:10.1136/jitc-2022-005400

Sandstrom, A., Peigné, C-M., Léger, A., Crooks, J. E., Konczak, F., Gesnel, M-C., et al. (2014). The intracellular B30.2 domain of butyrophilin 3A1 binds phosphoantigens to mediate activation of human Vγ9Vδ2 T cells. *Immunity* 40 (4), 490–500. doi:10.1016/j.immuni.2014.03.003

Sato, Y., Mori, K., Hirano, K., Yagi, K., Kobayashi, Y., Nagaoka, K., et al. (2021). Adoptive γδT-cell transfer alone or combined with chemotherapy for the treatment of advanced esophageal cancer. *Cytotherapy* 23 (5), 423–432. doi:10.1016/j.jcyt.2021.02.002

Scheper, W., Sebestyen, Z., and Kuball, J. (2014). Cancer immunotherapy using γδT cells: Dealing with diversity. *Front. Immunol.* 5, 601. doi:10.3389/fimmu.2014.00601

Schilbach, K., Krickeberg, N., Kaißer, C., Mingram, S., Kind, J., Siegers, G. M., et al. (2020). Suppressive activity of Vδ2+ γδ T cells on αβ T cells is licensed by TCR signaling and correlates with signal strength. *Cancer Immunol. Immunother.* 69 (4), 593–610. doi:10.1007/s00262-019-02469-8

Schilbach, K. E., Geiselhart, A., Wessels, J. T., Niethammer, D., and Handgretinger, R. (2000). Human gammadelta T lymphocytes exert natural and IL-2-induced cytotoxicity to neuroblastoma cells. *J. Immunother.* 23 (5), 536–548. doi:10.1097/00002371-200009000-00004

Sebestyen, Z., Prinz, I., Déchanet-Merville, J., Silva-Santos, B., and Kuball, J. (2020). Translating gammadelta (γδ) T cells and their receptors into cancer cell therapies. *Nat. Rev. Drug Discov.* 19 (3), 169–184. doi:10.1038/s41573-019-0038-z

Shekhar, S., Milling, S., and Yang, X. (2012). Migration of γδ T cells in steady-state conditions. *Vet. Immunol. Immunopathol.* 147 (1-2), 1–5. doi:10.1016/j.vetimm.2012.03.016

Silva-Santos, B., Mensurado, S., and Coffelt, S. B. (2019). Γδ T cells: Pleiotropic immune effectors with therapeutic potential in cancer. *Nat. Rev. Cancer* 19, 392–404. doi:10.1038/s41568-019-0153-5

Sugai, S., Yoshikawa, T., Iwama, T., Tsuchiya, N., Ueda, N., Fujinami, N., et al. (2016). Hepatocellular carcinoma cell sensitivity to Vγ9Vδ2 T lymphocyte-mediated killing is increased by zoledronate. *Int. J. Oncol.* 48 (5), 1794–1804. doi:10.3892/ijo.2016.3403

Thomas, M. L., Samant, U. C., Deshpande, R. K., and Chiplunkar, S. V. (2000). Gammadelta T cells lyse autologous and allogenic oesophageal tumours: involvement of heat-shock proteins in the tumour cell lysis. *Cancer Immunol. Immunother.* 48, 653–659. doi:10.1007/s002620050014

Todaro, M., D'Asaro, M., Caccamo, N., Lovino, F., Francipane, M. G., Meraviglia, S., et al. (2009). Efficient killing of human colon cancer stem cells by gammadelta T lymphocytes. *J. Immunol.* 182 (11), 7287–7296. doi:10.4049/jimmunol.0804288

Tokuyama, H., Hagi, T., Mattarollo, S. R., Morley, J., Wang, Q., So, H. F., et al. (2008). V gamma 9 V delta 2 T cell cytotoxicity against tumor cells is enhanced by monoclonal antibody drugs-rituximab and trastuzumab. *Int. J. Cancer* 122 (11), 2526–2534. doi:10.1002/ijc.23365

Traxlmayr, M. W., Wesch, D., Dohnal, A. M., Funovics, P., Fischer, M. B., Kabelitz, D., et al. (2010). Immune suppression by gammadelta T-cells as a potential regulatory mechanism after cancer vaccination with IL-12 secreting dendritic cells. *J. Immunother.* 33 (1), 40–52. doi:10.1097/CJI.0b013e3181b51447

Van Hede, D., Polese, B., Humblet, C., Wilharm, A., Renoux, V., Dortu, E., et al. (2017). Human papillomavirus oncoproteins induce a reorganization of epithelial-associated γδ T cells promoting tumor formation. *Proc. Natl. Acad. Sci. U. S. A.* 114 (43), E9056–E9065. doi:10.1073/pnas.1712883114

Viey, E., Fromont, G., Escudier, B., Morel, Y., DaRocha, S., Chouaib, S., et al. (2005). Phosphostim-activated gamma delta T cells kill autologous metastatic renal cell carcinoma. *J. Immunol.* 174 (3), 1338–1347. doi:10.4049/jimmunol.174.3.1338

Wada, I., Matsushita, H., Noji, S., Mori, K., Yamashita, H., Nomura, S., et al. (2014). Intraperitoneal injection of *in vitro* expanded Vγ9Vδ2 T cells together with zoledronate for the treatment of malignant ascites due to gastric cancer. *Cancer Med.* 3 (2), 362–375. doi:10.1002/cam4.196

Wakita, D., Sumida, K., Iwakura, Y., Nishikawa, H., Ohkuri, T., Chamoto, K., et al. (2010). Tumor-infiltrating IL-17-producing gammadelta T cells support the progression of tumor by promoting angiogenesis. *Eur. J. Immunol.* 40 (7), 1927–1937. doi:10.1002/eji.200940157

Wallet, M., Nishimura, T., Del Casale, C., Lebid, A., Salantes, B., Santostefano, K., et al. (2021). Induced pluripotent stem cell-derived gamma delta CAR-T cells for cancer immunotherapy. *Blood* 138, 2771. doi:10.1182/blood-2021-149095

Wang, J., Lin, C., Li, H., Li, R., Wu, Y., Liu, H., et al. (2017). Tumor-infiltrating γδT cells predict prognosis and adjuvant chemotherapeutic benefit in patients with gastric cancer. *OncoImmunology* 6 (11), e1353858. doi:10.1080/2162402X.2017.1353858

Wang, K. Q., Hou, Y. Q., Duan, Y. C., Wang, Y. R., and Li, X. Q. (2018). A method for detecting intracellular IL-2 in γδT cells. *Biomed. Res.* 29 (15), 3144–3148. doi:10.4066/biomedicalresearch.29-18-921

Wang, K. Q., Hou, Y. Q., Gu, C. X., Zhao, D. P., Duan, Y. C., Ran, Z. S., et al. (2017). Inhibitory effect of the mitogen activated protein kinase specific inhibitor PD98059 on Mtb-Ag-activated γδT cells. *Int. J. Clin. Exp. Pathol.* 10 (9), 9644–9648.

Wang, Y., Wang, C., Xiao, H., Niu, C., Wu, H., Jin, H., et al. (2017). Adjuvant treatment combining cellular immunotherapy with chemotherapy improves the clinical outcome of patients with stage II/III gastric cancer. *Cancer Med.* 6 (1), 45–53. doi:10.1002/cam4.942

Wang, Y. R., Wang, Y. S., and Wang, K. Q. (2019). Research progress on the mechanism of γδT cells inpathogenic microbial infection[J]. *Int. J. Clin. Exp. Med.* 12 (8), 9597–9606.

Wang, Y. S., Bu, W. J., Wang, Y. R., Hu, J. G., and Wang, K. Q. (2019). Increased values of peripheral blood γδT cells, Th17 cells, IL-17, ALT, AST, TB, and DB are closely related to the severity of chronic Hepatitis B[J]. *Int. J. Clin. Exp. Med.* 12 (6), 7374–7382.

Wei, L., Wang, K. Q., Ran, Z. S., Liu, Q. H., Chen, Y. Y., Ji, B., et al. (2018). Auxiliary diagnostic value of γδT cell, IL-17, and IFN-γ levels in peripheral blood and bronchoalveolar lavage fluid for lung cancer complicated with chronic obstructive pulmonary disease[J]. *Int. J. Clin. Exp. Med.* 11 (7), 7183–7191.

Welte, T., and Zhang, X. H. (2015). Interleukin-17 could promote breast cancer progression at several stages of the disease. *Mediat. Inflamm.* 2015, 804347. doi:10.1155/2015/804347

Wesch, D., Peters, C., and Siegers, G. M. (2014). Human gamma delta T regulatory cells in cancer: Fact or fiction[J]? *Front. Immunol.* 5, 598. doi:10.3389/fimmu.2014.00598

Wilhelm, M., Kunzmann, V., Eckstein, S., Reimer, P., Weissinger, F., Ruediger, T., et al. (2003). Gammadelta T cells for immune therapy of patients with lymphoid malignancies. *Blood* 102 (1), 200–206. doi:10.1182/blood-2002-12-3665

Wu, D., Wu, P., Wu, X. G., Ye, J., Wang, Z., Zhao, S., et al. (2014). *Ex vivo* expanded human circulating Vδ1 γδT cells exhibit favorable therapeutic potential for colon cancer. *OncoImmunology* 4 (3), e992749. doi:10.4161/2162402X.2014.992749

Wu, P., Wu, D., Ni, C., Ye, J., Chen, W., Hu, G., et al. (2014). γδT17 cells promote the accumulation and expansion of myeloid-derived suppressor cells in human colorectal cancer. *Immunity* 40 (5), 785–800. doi:10.1016/j.immuni.2014.03.013

Wu, X., Sun, H., Zhang, B., Jia, F. Y., and Wu, P. (2016). The effect of activated Mϕ1 on γδT cell-mediated killing of gastric cancer cells *in vitro*. *Oncol. Lett.* 12, 3368–3372. doi:10.3892/ol.2016.5066

Wu, Y., Wu, W., Wong, W. M., Ward, E., Thrasher, A. J., Goldblatt, D., et al. (2009). Human gamma delta T cells: A lymphoid lineage cell capable of professional phagocytosis. *J. Immunol.* 183, 5622–5629. doi:10.4049/jimmunol.0901772

Xiao, L., Zhang, B., and Chen, H. (2017). Killing activity *in vitro* of γδ T cells against human hematologic neoplasms cells[J]. *Chin. J. Cancer Biother* 24 (3), 230–236. doi:10.3872/j.issn.1007-385X.2017.03.003

Xie, L., Chen, W., Wang, L., Cheng, M., Hu, S. L., and Shen, G. (2018). Establishment of the culture system of γδ T cells *in vitro* and the anti-tumor effect. *Chin. J. Oncol.* 40 (4), 247–251. doi:10.3760/cma.j.issn.0253-3766.2018.04.002

Yang, Q. T., Huang, X. K., Li, P., Chen, Y. L., and Zhang, G. H. (2011). Distribution and clonality of T cell receptor Vγ and Vδ subfamily in peripheral blood of patients with allergic rhinitis before and after immunotherapy. *Chin J Otolaryngology Head Neck Surg.* 46 (12), 992–997.

Ye, J., Ma, C., Hsueh, E. C., Eickhoff, C. S., Zhang, Y., Varvares, M. A., et al. (2013). Tumor-derived γδ regulatory T cells suppress innate and adaptive immunity through the induction of immunosenescence. *J. Immunol.* 190 (5), 2403–2414. doi:10.4049/jimmunol.1202369

Ye, J., Ma, C., Wang, F., Hsueh, E. C., Toth, K., Huang, Y., et al. (2013). Specific recruitment of γδ regulatory T cells in human breast cancer. *Cancer Res.* 73 (20), 6137–6148. doi:10.1158/0008-5472.CAN-13-0348

Yi, Y., He, H. W., Wang, J. X., Cai, X. Y., Li, Y. W., Zhou, J., et al. (2013). The functional impairment of HCC-infiltrating γδ T cells, partially mediated by regulatory T cells in a TGFβ- and IL-10-dependent manner. *J. Hepatol.* 58, 977–983. doi:10.1016/j.jhep.2012.12.015

Zakeri, N., Hall, A., Swadling, L., Pallett, L. J., Schmidt, N. M., Diniz, M. O., et al. (2022). Characterisation and induction of tissue-resident gamma delta T-cells to target hepatocellular carcinoma. *Nat. Commun.* 13 (1), 1372. doi:10.1038/s41467-022-29012-1

Zhang, B. F., Li, H. Z., Liu, W. B., Tian, H., Li, L., Gao, C., et al. (2021). Adoptive cell therapy of patient-derived renal cell carcinoma xenograft model with IL-15-induced γδT cells. *Med. Oncol.* 38, 30. doi:10.1007/s12032-021-01474-1

Zhang, M., Lu, X. L., Wei, C. R., and Li, X. Q. (2020). Association between αβ and γδ T-cell subsets and clinicopathological characteristics in patients with breast cancer. *Oncol. Lett.* 20 (6), 325–3258. doi:10.3892/ol.2020.12188

Zhao, N. G., Zhang, J. P., Zhang, T. T., Yin, Y., and Wang, K. Q. (2021). Expression of γδT and CD4+ CD25+ T cells in peripheral blood of HIV-infected patients/AIDS patients and their correlation[J]. *Chin. J. Microbiol. Immunol.* 41 (7), 524–530. doi:10.3760/cma.j.cn112309-20200618-00322

Zhao, N. G., Zhang, T. T., Zhao, Y. J., Zhang, J. P., and Wang, K. Q. (2021). $CD3^+T$, $CD4^+T$, $CD8^+T$, and $CD4^+T/CD8^+T$ ratio and quantity of *γδ*T cells in peripheral blood of HIV-infected/AIDS patients and its clinical significance. *Comput. Math. Methods Med.* 2021, 8746264. doi:10.1155/2021/8746264

Zheng, B., Lam, C., Im, S., Huang, J., Luk, W., Lau, S. Y., et al. (2001). Distinct tumour specificity and IL-7 requirements of CD56(-)and CD56(+) subsets of human gamma delta T cells. *Scand. J. Immunol.* 53 (1), 40–48. doi:10.1046/j.1365-3083.2001.00827.x

Zheng, B. J., Chan, K. W., Im, S., Chua, D., Sham, J. S., Tin, P. C., et al. (2001). Anti-tumor effects of human peripheral gammadelta T cells in a mouse tumor model. *Int. J. Cancer* 92 (3), 421–425. doi:10.1002/ijc.1198

Zhou, B. Y., Gong, J. H., Cai, X. Y., Wang, J. X., Luo, F., Jiang, N., et al. (2019). An imbalance between stellate cells and γδT cells contributes to hepatocellular carcinoma aggressiveness and recurrence. *Hepatol. Int.* 13 (5), 631–640. doi:10.1007/s12072-019-09969-w

Zou, C., Zhao, P., Xiao, Z., Han, X., Fu, F., and Fu, L. (2017). γδ T cells in cancer immunotherapy. *Oncotarget* 8 (5), 8900–8909. doi:10.18632/oncotarget.13051

frontiers | Frontiers in Genetics

TYPE Original Research
PUBLISHED 09 January 2023
DOI 10.3389/fgene.2022.1036408

OPEN ACCESS

EDITED BY
Qian Wang,
Tai'an City Central Hospital, China

REVIEWED BY
Shilin Xu,
Xichang People's Hospital·Liangshan High-tech Tumor Hospital, China
Peng-fei Liu,
First Affiliated Hospital of Harbin Medical University, China

*CORRESPONDENCE
Yujie Li,
libeng8465@163.com

SPECIALTY SECTION
This article was submitted to Cancer Genetics and Oncogenomics, a section of the journal Frontiers in Genetics

RECEIVED 04 September 2022
ACCEPTED 12 December 2022
PUBLISHED 09 January 2023

CITATION
Fan K, Dong Y, Li T and Li Y (2023), Cuproptosis-associated CDKN2A is targeted by plicamycin to regulate the microenvironment in patients with head and neck squamous cell carcinoma. *Front. Genet.* 13:1036408. doi: 10.3389/fgene.2022.1036408

Cuproptosis-associated CDKN2A is targeted by plicamycin to regulate the microenvironment in patients with head and neck squamous cell carcinoma

Kaihui Fan, Yuke Dong, Tao Li and Yujie Li*

Department of Otorhinolaryngology, Head and Neck Surgery, Zhengzhou Central Hospital affiliated with Zhengzhou University, Zhengzhou, Henan, China

Head and neck squamous cell carcinoma (HNSCC), the most common malignancy of the head and neck, has an overall 5-year survival rate of <50%. Genes associated with cuproptosis, a newly identified copper-dependent form of cell death, are aberrantly expressed in various tumours. However, their role in HNSCC remains unknown. In this study, bioinformatic analysis revealed that the cuproptosis-related gene CDKN2A was correlated with the malignant behaviour of HNSCC. Kaplan-Meier (KM) curves showed that patients with high CDKN2A expression had a better prognosis. Multiomic analysis revealed that CDKN2A may be associated with cell cycle and immune cell infiltration in the tumour microenvironment and is important for maintaining systemic homeostasis in the body. Furthermore, molecular docking and molecular dynamics simulations suggested strong binding between plicamycin and CDKN2A. And plicamycin inhibits the progression of HNSCC in cellular assays. In conclusion, this study elucidated a potential mechanism of action of the cuproptosis-associated gene CDKN2A in HNSCC and revealed that plicamycin targets CDKN2A to improve the prognosis of patients.

KEYWORDS

CDKN2A, head and neck squamous cell carcinoma (HNSCC), Cuproptosis, systemic homeostasis, multiomics

Background

Head and neck squamous cell carcinoma (HNSCC) is the most common malignant tumour of the head and neck that develops in the mucosal epithelium of the mouth, pharynx, larynx, nasal cavity, and sinus cavities (Taberna et al., 2017). It is the sixth most common malignancy worldwide, with approximately 890,000 new cases and 450,000 deaths owing to HNSCC reported worldwide in 2018 (Bray et al., 2018; Ferlay et al., 2019). Although significant progress has been made in the combined use of surgery, radiotherapy, chemotherapy and targeted therapy for the treatment of HNSCC, 40%–50% of patients have post-treatment relapse, and the overall 5-year

survival rate is <50% (Canning et al., 2019). Therefore, biomarkers that can improve HNSCC prognosis need to be identified.

Tsvetkov et al., (2022) recently described a new copper-dependent type of cell death, cuproptosis, closely related to mitochondrial respiration. Copper binds to fatty acylated proteins in the tricarboxylic acid cycle during mitochondrial respiration, resulting in the aggregation of fatty acylated proteins and low expression of iron–sulfur cluster proteins, thereby inducing proteotoxic stress and eventually leading to cell death (Tsvetkov et al., 2022). There have been four genes identified for cuproptosis that are positively regulated (*FDX1*, *LIAS*, *LIPT1*, *DLD*, *DLAT*, *PDHA1*, *PDHB* and *ATP7B*) and eight genes that are negatively regulated (*MTF1*, *GLS*, cyclin-dependent kinase inhibitor 2A [*CDKN2A*] and *SLC31A1*) (Tsvetkov et al., 2022). Biological processes such as tumour cell proliferation, vascular growth, and metastasis have been shown to be significantly affected by copper, an essential element for mitochondrial respiration and iron uptake (Ruiz et al., 2021; Oliveri, 2022). There are a number of factors that regulate and maintain the body's intake, excretion, and metabolism of copper. Copper-induced cell death or abnormal copper metabolism can occur when copper homeostasis is disrupted in the body. Previous research reported that the cuproptosis-related gene *LIPT1* is significantly correlated with prognosis and immune infiltration in melanoma (Lv et al., 2022). Similar findings have been reported by Yun Y et al. indicating that SLC31A1, DX1 and TP7B0 are associated with lung cancer (Yun et al., 2022). Several studies have shown that cuproptosis-related genes are associated with poor prognosis, reduced drug sensitivity, and tumor microenvironment in renal clear cell carcinoma (Ji et al., 2022). However, further studies are needed to determine the effects of cuproptosis on HSNCC.

Bioinformatic tools have become increasingly popular with the rapid development of high-throughput technology for assessing prognostic markers and studying mechanisms (Wei et al., 2019; Shi et al., 2021; Luo et al., 2022a; Luo et al., 2022b; Chen et al., 2022; Lin et al., 2022; Mei et al., 2022; Xuan et al., 2022; Zhao and Jiang, 2022). In melanoma, lung cancer, and renal clear cell carcinoma, cuproptosis-related genes have been studied. In recent studies, researchers examined ten cuproptosis-related lncRNAs associated with immune function and prognosis in HNSCC (Li et al., 2022). However, the functions and mechanisms of action of cuproptosis-related genes in HNSCC warrant further investigation. Molecular dynamics simulation serves as one of the important tools for assessing the stability of drug-targeting ligands for the development of oncological therapeutics (Chikan and Vipperla, 2015; Thai et al., 2015). The aim of this study was to identify cuproptosis-related genes associated with poor prognosis of HNSCC and screen for potential candidate drugs for its treatment using molecular docking and molecular dynamics simulations.

Materials and methods

Gene identification and data acquisition

TCGA-HNSCC data were analyzed to identify differentially expressed genes (DEGs) between tumours and healthy tissues as previous researches (Tomczak et al., 2015; Kang et al., 2021). Based on the intersection of tumour-associated DEGs and cuproptosis-associated genes, *CDKN2A* was identified as a key gene. We investigated the correlation between *CDKN2A* expression and clinical staging of HNSCC. *CDKN2A* prognostic significance was evaluated using KM curves. In order to investigate the performance of CDKN2A for predicting 1, 3 and 5 year overall survival (OS), ROC curves were plotted using the time ROC package. Furthermore, ROC curves were used to assess the relationship between *CDKN2A* and HNSCC clinical characteristics.

CDKN2A function assessment

For further analysis, RNA-seq data were extracted from TCGA, and log2-transformed gene expression data were obtained (Tomczak et al., 2015). Based on the median CDKN2A expression, tumour samples were divided into high and low-expression groups for survival analysis. In the high and low CNKN2A expression groups, DEGs were screened using the limma R package. Adjusted p-values of <.05 and |logFC| values of >1 were used as the screening criteria for significant DEGs (Ritchie et al., 2015). The ggplot2 package was used to plot volcano and heat maps to visualise the expression of 17 significant DEGs. Data on CDKN2A mutations was downloaded from TCGAbiolinks and visualized using track Viewer (Colaprico et al., 2016; Ou and Zhu, 2019).

Gene set variation analysis (GSVA)

The "GSVA" package was used to analyze all CDKN2A-associated DEGs, followed by the "limma" package to identify high and low CDKN2A expression levels (Hänzelmann et al., 2013; Lin et al., 2021).

GSEA and KEGG enrichment analysis

GSEA was performed on DEGs associated with *CDKN2A*, KEGG enrichment analysis was performed with gseKEGG, and pathways of interest were visualized using ggplot2 (Subramanian et al., 2005; Ito and Murphy, 2013).

Immuno-infiltration analysis

In order to calculate 28 immune cells, ssGSEA was used on gene expression profile data (Barbie et al., 2009). Based on *CDKN2A* expression levels, 28 immune cells were compared between groups with high and low expression levels of the protein. The Pearson correlation coefficient was used to examine the correlation between CDKN2A and immune cell infiltration further. Pearson correlation coefficient was used to analyze the correlation between each type of immune cell.

Acquisition and optimization of FDA structures

Food and Drug Administration (FDA) approved 2,568 small molecules (as of 2022-01-04). We downloaded the small molecule structures from Drug Bank (http://www.drugbank.com/) in SDF format (Luo et al., 2022b). In RDKit, the Experimental-Torsion Basic Knowledge Distance Geometry (ETKDG) algorithm was used to generate 3D conformations based on the modified distance geometry algorithm, while the MMFF94 stand was used to optimize small molecule structure and energy using the MMFFOptimize Molecule module (Li et al., 2022).

The structures of the proteins were obtained from the Uniport website (https://www.uniprot.org/). PDB structure 1A5E obtained under CDKN2A entry (P42771) using gene name query. Docking was carried out using Smina Chikan and Vipperla, (2015). Protein-Ligand Interaction Profiler (Plip, https://plip-tool.biotec.tu-dresden.de/plip-web/plip) was used to analyze docking results.

Analysis of PPI networks and gene networks

By using the STRING website and cytoscape software, we explored CDKN2A's protein-protein interaction network (Shannon et al., 2003; Szklarczyk et al., 2021). Genemania was used to analyze the *CDKN2A* network (Warde-Farley et al., 2010).

Construction of ceRNA network

Firstly, the multiMiR package was used to find miRNAs related to *CDKN2A* (Huang et al., 2019a). The LncRNADisease database was then used to identify HNSCC-related LncRNAs, and the miRTarBase database was used to identify shared miRNAs with HNSCC-related LncRNAs (Bao et al., 2019; Huang et al., 2019b). Cytoscape is used for the final visualization (Shannon et al., 2003).

Drug analysis

To identify drugs that may act on DEGs (99 highly expressed genes and 56 lowly expressed genes) between high and low expression groups of CDKN2A, the cmap website was accessed (http://clue.io/).

Molecular dynamics simulation (MDS)

The lowest energy conformation was selected as the kinetic initial conformation. The quantitative software Orca was used to perform quantum chemical optimization for small molecules under B3LYP/6-31G* basis set conditions, involving corrections for bond lengths, bond angles, dihedral angles, and calculations of RESP2 at 0 fixed charges. Gromacs 2019.6 was chosen as the kinetic simulation software, amber14sb was chosen as the protein force field, and Gaff2 force field was chosen for small molecules, and the TIP3P water model was used to add TIP3P water model to the complex system to build a water box and add sodium ions to equilibrate the system. Under elastic simulation by Verlet and cg algorithms, Particle-mesh Ewald (PME) deals with electrostatic interactions using the steepest descent method for energy minimization for the maximum number of steps (50,000 steps). The Coulomb force cutoff distance and van der Waals radius cutoff distance were both 1.4 nm. Finally the system was equilibrated with the regular system (NVT) and isothermal isobaric system (NPT), and the MD simulations were performed at room temperature and pressure for 100 ns. During the MD simulation, the hydrogen bonds involved were constrained using the LINCS algorithm with an integration step of 2 fs. The PME method was calculated with a cutoff value set to 1.2 nm and a non-bond interaction cutoff value set to 10 Å. The V-rescale temperature coupling method was used to control the simulation temperature at 300 K and the Berendsen method to control the pressure at 1 bar. Additionally, 30 ps of NVT and NPT equilibrium simulations were performed at 300 K. Finally, 50 ns of finished MD simulations were performed for the protein–ligand complex system. Root mean square fluctuations (RMSF) were used to observe the local loci variation structure of the system during the simulation (the fluctuation cutoff was set to 0.2). The radius of gyration (Rg) was used to evaluate the tightness of the system structure. The RMSF can observe the local loci variation of the system during the simulation.

Calculation of free energy of binding of proteins and small molecules

The MD trajectory operation is calculated by the following equation:

$$\Delta G_{bind} = \Delta G_{complex} - \left(\Delta G_{receptor} + \Delta G_{ligand}\right) = \Delta E_{internal} + \Delta E_{VDW} + \Delta E_{elec} + \Delta G_{GB} + \Delta G_{SA}$$

In the above equation, $\Delta E_{internal}$ represents internal energy, ΔE_{VDW} represents van der Waals interaction, and ΔE_{elec} represents electrostatic interaction. Internal energy includes bond energy (Ebond), angular energy (Eangle), and torsion energy (Etorsion). ΔG_{GB} and ΔG_{SA} are collectively referred to as the solvation free energy. G_{GB} is the polar solvation free energy and G_{SA} is the non-polar solvation free energy. We used the GB model for calculating ΔG_{GB} (Weiser et al., 1999). The ΔG_{SA} was calculated based on the product of surface tension (γ) and solvent accessible surface area (SA): $\Delta G_{SA} = 0.0072 \times \Delta SA$. The entropy variation was neglected in this study due to the high consumption of computational resources with low accuracy.

Cell culture and wound-healing assay

Human laryngeal cancer cell lines (TU212) were obtained from the Cell Bank of the Chinese Academy of Sciences. For cell culture, Dulbecco's modified Eagle's medium (DMEM) containing 10% fetal bovine serum (FBS) was used. In an incubator with 5% CO2 and 37°C, 10%FBS and 1% penicillin all cell lines were cultured. In TU212 cells, plicamycin was applied for 14 days at 10 nmol/L. Incubation at 37°C was carried out for both treated and untreated cells plated on 10-cm culture dishes. With a plastic pipette tip, a lane was scratched through the confluent monolayers, followed by addition of DMEM, 1% FBS, and 10 nmol/L plicamycin. Several wounded areas were observed and then photographed through a microscope 24 h after the scratch.

Statistical analysis

Standard error of the mean is indicated by bars on figures, and was calculated using Microsoft Office Excel 2016. All experiments were performed with at a minimum of triplicate samples, and all *p*-values were calculated with two-tailed t-tests.

Results

Data acquisition and screening of DEGs

After intersecting tumour-associated DEGs with cuproptosis-related genes, CDKN2A was identified as a key gene (Figure 1A), which may play a critical role in tumour development through cuproptosis. CDKN2A expression was significantly higher among patients with T2-stage HNSCC than among patients with T3-and T4-stage HNSCC (Figure 1B), indicating that CDKN2A expression is high in early malignant tumours and low in advanced malignant tumours. KM curves demonstrated that high CDKN2A expression was associated with a better clinical prognosis (Figure 1C). The area under the ROC curves indicated a more significant protective effect of CDKN2A on 1-, 3- and 5-year OS (Figure 1D). In addition, age; sex; T, N, and M stages and CDKN2A were found to have predictive significance for the prognosis of HNSCC (Figure 1E).

Characterisation of CDKN2A expression and enrichment analysis

HNSCC samples in TCGA cohort were divided into the high- and low-CDKN2A-expression groups based on the median CDKN2A expression. The scatter plot demonstrated differences in the survival status of patients between the two groups (Figures 2A, B). A total of 155 DEGs were identified in the two groups; of which, 99 were upregulated and 56 were downregulated (Figure2D). The top 17 genes with the most significant differences in expression were visualised on a heat map (Figure 2C). GSEA suggested that these genes were significantly enriched in pathways associated with cell cycle and DNA replication in the high-CDKN2A-expression group (Figure 2E). In addition, GSVA suggested that the genes were enriched in pathways associated with DNA repair, E2F targets and the G2M checkpoint in the high-CDKN2A-expression group and pathways associated with coagulation, apical junction and inflammatory response in the low-CDKN2A-expression group (Figure 2F). These results suggest that high CDKN2A expression is associated with activation of the cell cycle in HNSCC.

Immune infiltration analysis

ssGSEA revealed that the infiltration of memory B cell was higher in the low-CDKN2A-expression group; however, no significant difference was observed in the infiltration of other immune cells between the two groups (Figure 3A and Supplementary Figure S1A). Correlation analysis revealed a co-expression relationship among 28 immune cell types (Supplementary Figure S1B), and the correlation between CDKN2A and immune cells indicated that CDKN2A promoted immune cell infiltration (Figure 3B). CDKN2A was significantly positively correlated with activated B-cell (cor = 0.182, $p < 0.001$) and activated CD4 T-cell (cor = 0.160, $p < 0.001$) (Figures 3C, D) and significantly negatively correlated with

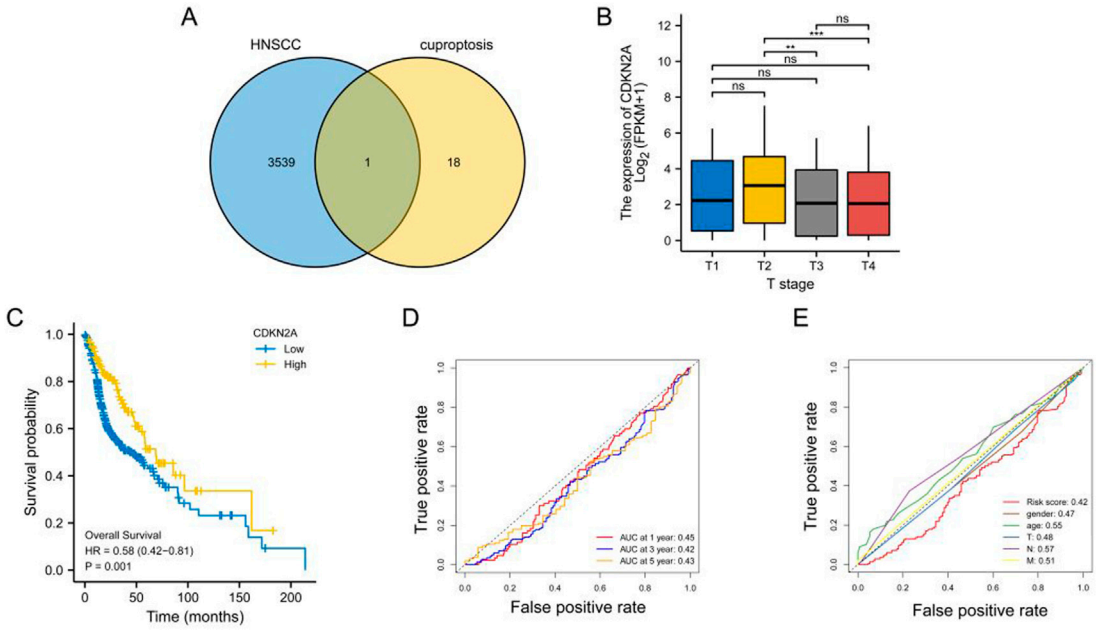

FIGURE 1
Identification of key genes. **(A)** Venn diagram demonstrating the results of intersection analysis of differentially expressed genes and cuproptosis-related genes; **(B)** Bar graph demonstrating the difference in CDKN2A expression among patients with different T stages; **(C)** KM curve demonstrating a better prognosis for patients with head and neck squamous cell carcinoma with high CDKN2A expression; **(D)** ROC curve demonstrating the predictive performance of CDKN2A for 1-, 3- and 5-year OS; **(E)** ROC curves demonstrating the relationship between clinical characteristics and the predictive performance of CDKN2A for clinical prognosis.

neutrophils (cor = −0.262, $p < 0.001$) and gamma-delta T-cell (cor = −0.166, $p < 0.001$) (Figures 3E, F). This suggests that CDKN2A is involved in tumor immune microenvironment homeostasis.

Gene network and mutation analysis of CDKN2A

A protein–protein interaction (PPI) network is shown in Figure 4A. The gene interaction network of CDKN2A was visualised using geneMANIA (Figure 4B). In the ceRNA network of CDKN2A, HOTAIR was found to be closely associated with has-miR-34a and has-miR-125a (Figures 4C, D). HOTAIR may regulate has-miR-34a and has-miR-125a in HNSCC, thus exerting a regulatory effect on CDKN2A expression (Figure 4D). In addition, CDKN2A had a higher mutation rate at the *p*. R80 locus than at the *p*. R58 and *p*. W110 loci (Supplementary Figure S2).

Molecular docking results

The distribution of docking fractions for virtual screening is shown in Figure 5. The binding affinity of proteins and small molecules can be obtained after molecular docking. The docking fraction for each ordinal number corresponds to −5.42 kcal/mol, with a mean value of −5.42 kcal/mol. Based on a potential screening threshold of −7 kcal/mol, the screening rate is 12.13% (308/2,539), i.e., 12.13% of small molecules have the potential for precursor optimization as Potential dead drug set (PLDS). The mid-docking effects of PLDS were examined to avoid analytical bias caused by transient false-positive docking results. There were 104 residue sites contacted (Supplementary Figure S3). A cut-off of 20 was selected to exclude transient positive contacts. The results are shown in Figure 6. The orange colour represents hydrogen bonds; the number share is the main interaction force [47.41% (1427/3010)] and the amino acid residue contact sites include 46-ARG, 47-ARG, 54-MET, 84-ASP, 87-ARG, 88-GLU, 105-ASP, 111-GLY, 116-ASP, 131-ARG, 138-ARG, 139-GLY, 142-HIS, 144-ARG and 147-ALA. The blue colour represents hydrophobic interactions, which are the main interaction forces [38.27% (1152/3010)], and the amino acid residue contact sites include 21-ALA, 44-TYR, 51-VAL, 77-THR, 79-THR, 107-ARG, 110-TRP, 112-ARG, 113-LEU, 117-LEU, 121-LEU, 137-THR, 148-ALA, 149-GLU, 151-PRO and 154-ILE. Molecular docking analysis suggests that plicamycin binds CDKN2A most strongly.

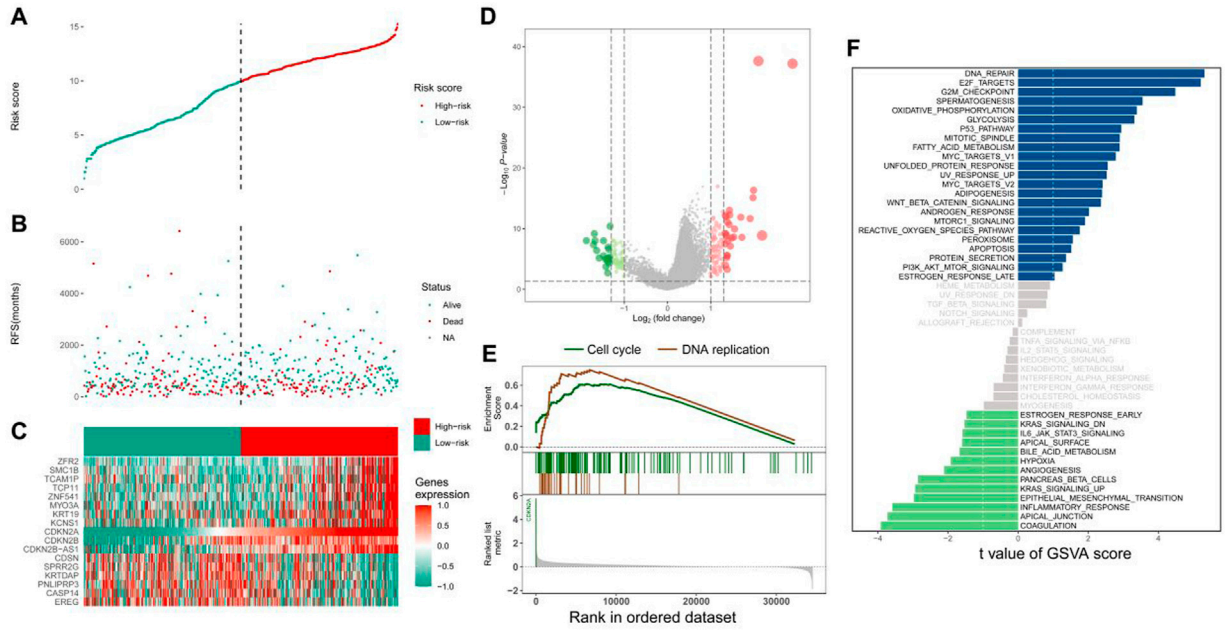

FIGURE 2
Relevant functions of CDKN2A. **(A)** Tumour samples in TCGA database were divided into the high- and low-expression groups according to median CDKN2A expression; **(B)** Scatter plot demonstrating the difference in survival status between the two groups; **(C)** Top 17 differentially expressed genes; **(D)** Volcano plot demonstrating the distribution of differentially expressed genes; **(E)** GSEA; **(F)** Bar graph demonstrating the differentially enriched pathways between the two groups.

Molecular dynamics and cellular effects of plicamycin

Molecular dynamics simulation (MDS) is an important method for assessing the stability of complexes in an aqueous solution (Hollingsworth and Dror, 2018; Hildebrand et al., 2019; Huang et al., 2022; Kang et al., 2022; Zhang et al., 2022). Stability of a system can be measured by the atomic root-mean-square deviation (RMSD). In Figure 7A, RMSD values fluctuated between 20 and 30 ns due to transient instability and then remained stable at 30–50 ns. Root-mean-square fluctuations (RMSF) reflect changes in the local sites of the system during MDS. According to Figure 7B, amino acids at positions 1–15, 33–44, 58, 90, 107, and 124–156 fluctuated more than other amino acids. Figure 7C shows that the radius of rotation (Rg) is an important measure of architecture tightness. In Figure 7D, the solvent-accessible surface area (SASA) of the protein decreases steadily over 0–100 ns, indicating favourable binding and progressive protein tightening. Figure 7E shows the potential-energy curve of hydrogen bonded complexes in their steady state. Figures 8A, B show the binding site, docking pose, and overall protein structure.

We compared the binding free energies of the two solvated molecules in their bound and free states, as well as the binding free energies of various solvated conformations of plicamycin (Figure 9A). Analysis of the variation of the binding free energy with MDS revealed that the total free energy (G_{total}) was <0, indicating a likely interaction between the CDKN2A protein and plicamycin. The binding energy of both van der Waals and electrostatic interactions was <0, indicating that hydrophobic interactions and electrostatic energy contribute to the binding between CDKN2A and plicamycin. Non-polar interactions favored binding, whereas polar solvation didn't. Positive values of polar solvation energy (EGB) indicate that non-polar interactions favored binding. MET-52, MET-53, MET-54, and ASP-84 contact residues of the complex have free energies of zero, indicating they are the major binding sites for CDKN2A and plicamycin (Figure 9B). There was a positive free energy difference between ARG-46 and ARG-87, indicating that plicamycin binds poorly to CDKN2A at these sites. In the stable complex, the contact residue MET-52 contributes to the major binding force (Figure 9B). Furthermore, we found that plicamycin treatment reduced the mobility of TU212 cells in scratch experiments (Figure 10A, B). Accordingly, plicamycin inhibited HNSCC progression in cellular assays. Based on molecular dynamics simulations, this study shows that plicamycin targets CDKN2A to improve patient outcomes.

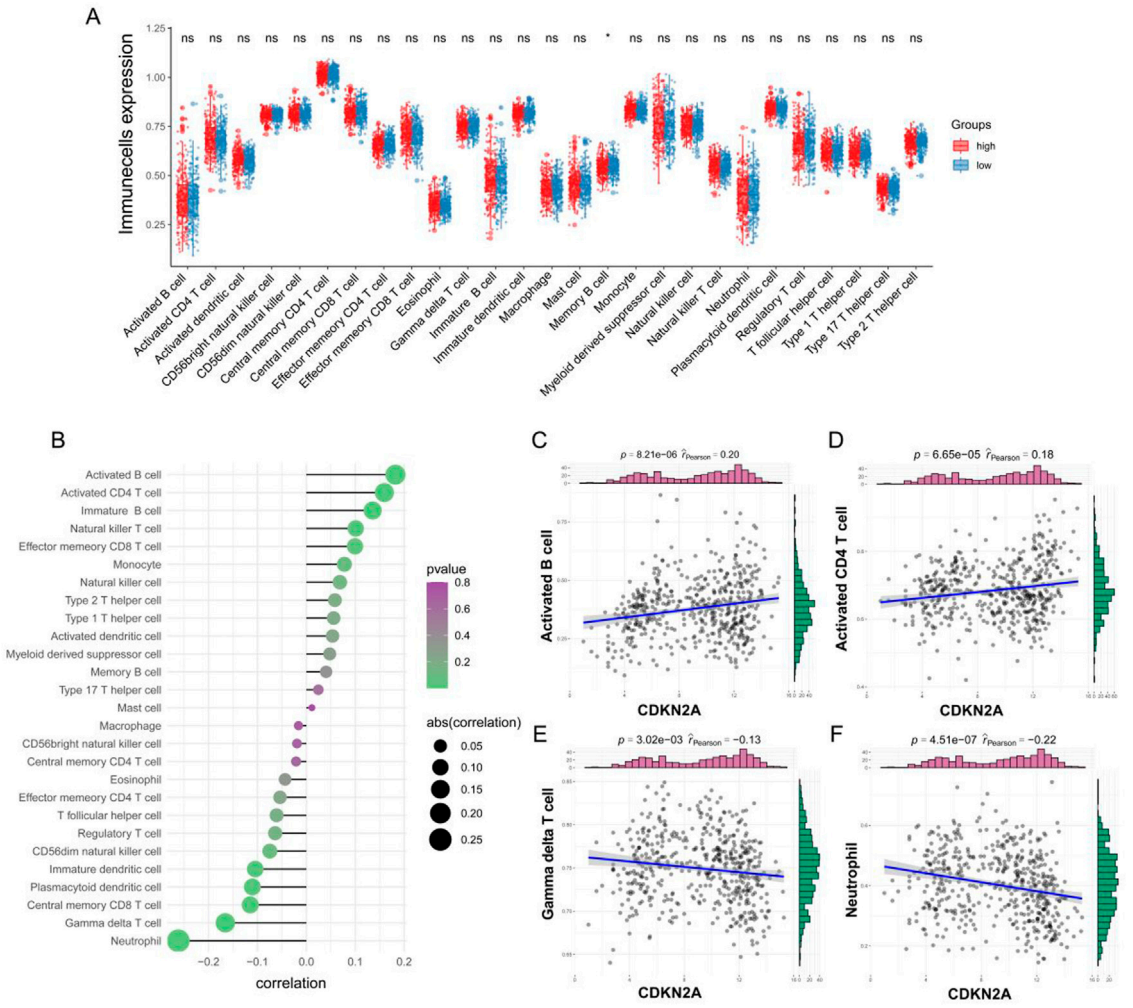

FIGURE 3
Correlation between CDKN2A and immune cells. **(A)** Differences in immune cell infiltration between the high- and low-CDKN2A-expression groups were examined *via* ssGSEA; **(B)** Correlation between CDKN2A and the infiltration of immune cells; **(C–F)** Correlation plots demonstrating the relationship between the top four immune cell types and CDKN2A.

Discussion

Cuproptosis, a newly discovered form of cell death, is involved in the accumulation of intracellular copper and possesses the common features of multiple regulated cell death (RCD) mechanisms. Genes associated with cuproptosis play an important role in the prognosis of various tumours such as melanoma and lung cancer. (Shanbhag et al., 2021; Yun et al., 2022). In this study, CDKN2A, a cuproptosis-associated gene, was identified as a novel biological marker for predicting the prognosis of patients with T2-stage HNSCC compared with T3- and T4-stage HNSCC. GSEA and GSVA revealed that CDK2NA overexpression was associated with the cell cycle. Positive correlations were found between CDKN2A expression and activated B and CD4 T cells, but negative correlations were found between CDKN2A expression and neutrophils and gamma-delta T cells. Molecular docking and MDS analysis revealed that plicamycin inhibits HNSCC progression by acting on CDKN2A.

CDKN2A contributes to cell proliferation and angiogenesis by being a member of the INK4 family of tumour suppressor genes (Zhang et al., 2016; Zhao et al., 2016). CDKN2A contains four exons, namely, exons 1α, 1β, 2 and 3. It possesses independent promoters for their respective proteins: exons 1, 2 and 3 encode P16INK4a and exons 1, 2 and 3 encode P14ARF, thus they are both independent proteins (Li et al., 2011). The cyclin-dependent kinase (CDK) inhibitor p16INK4a inhibits the phosphorylation of retinoblastoma protein (pRb) by binding to CDK4 and CDK6. Hypophosphorylated pRb inhibits the transcription factor family E2F, impairing cell cycle

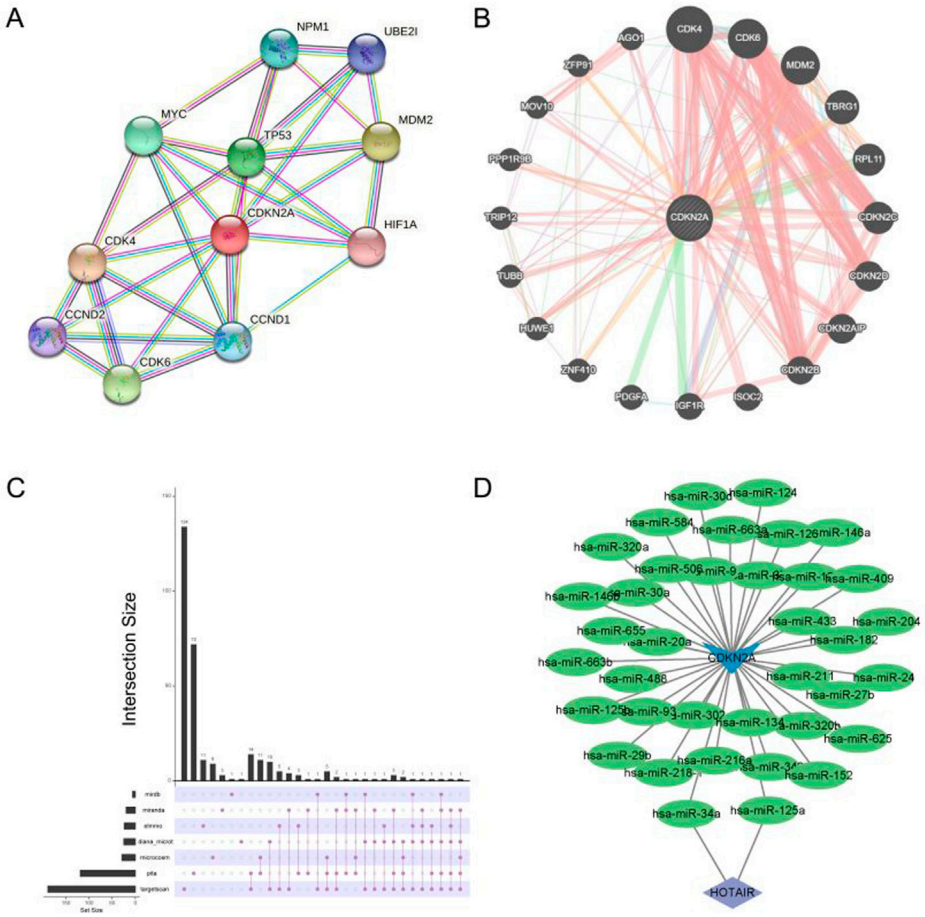

FIGURE 4
Single gene network diagram. **(A)** PPI network analysis of CDKN2A; **(B)** Gene interaction analysis of CDKN2A using geneMANIA; **(C)** miRNAs targeted by CDKN2A were predicted based on data extracted from seven databases; **(D)** Visualization of the ceRNA network maps using Cytoscape.

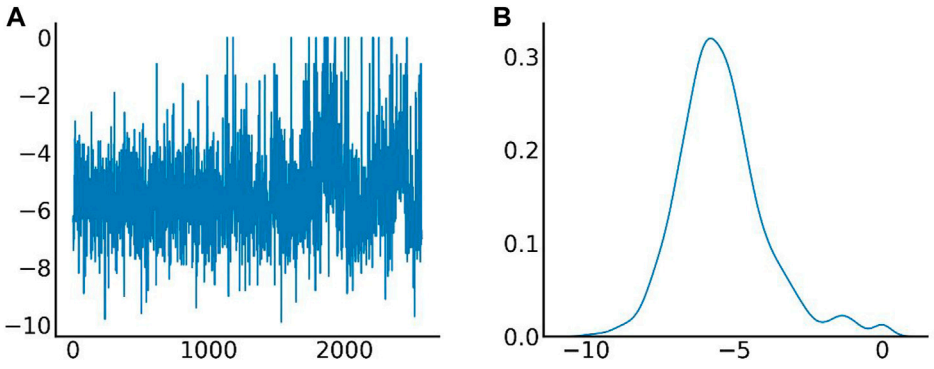

FIGURE 5
Different amino acid binding modes. **(A)** The X-axis represents the serial number of FDA-approved drugs, and the *Y*-axis represents the docking fraction (unit: kcal/mol); **(B)** Distribution of docking fractions. The horizontal coordinate represents the docking fraction (unit: kcal/mol), and the vertical coordinate represents the distribution probability.

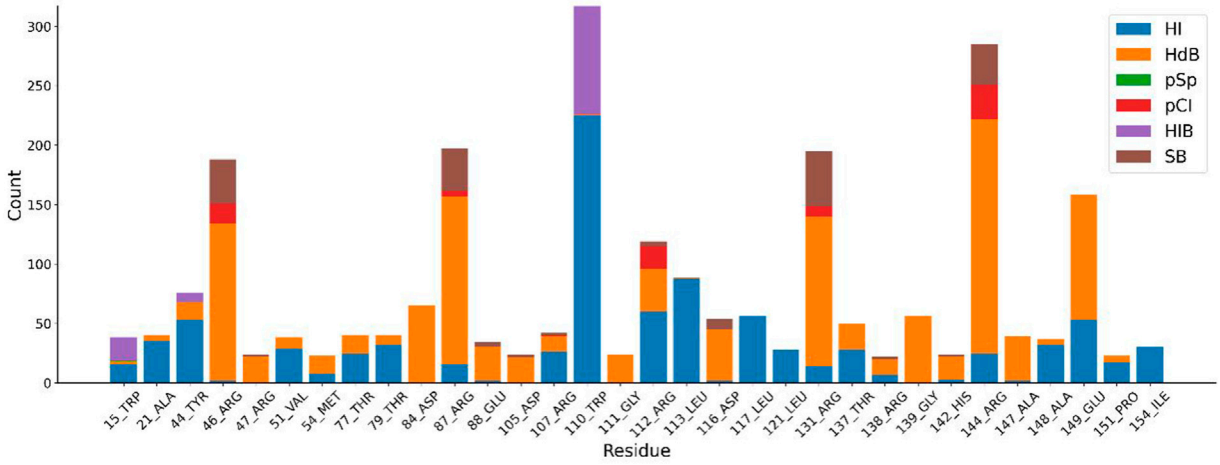

FIGURE 6
Different amino acid binding modes. Blue represents hydrophobic interactions (HI), orange represents hydrogen bonds (HdB), green represents π-π stacking (pSp), red represents π-cation interactions (pCI), purple represents halogen bonds (HIB) and brown represents salt bridge (SB).

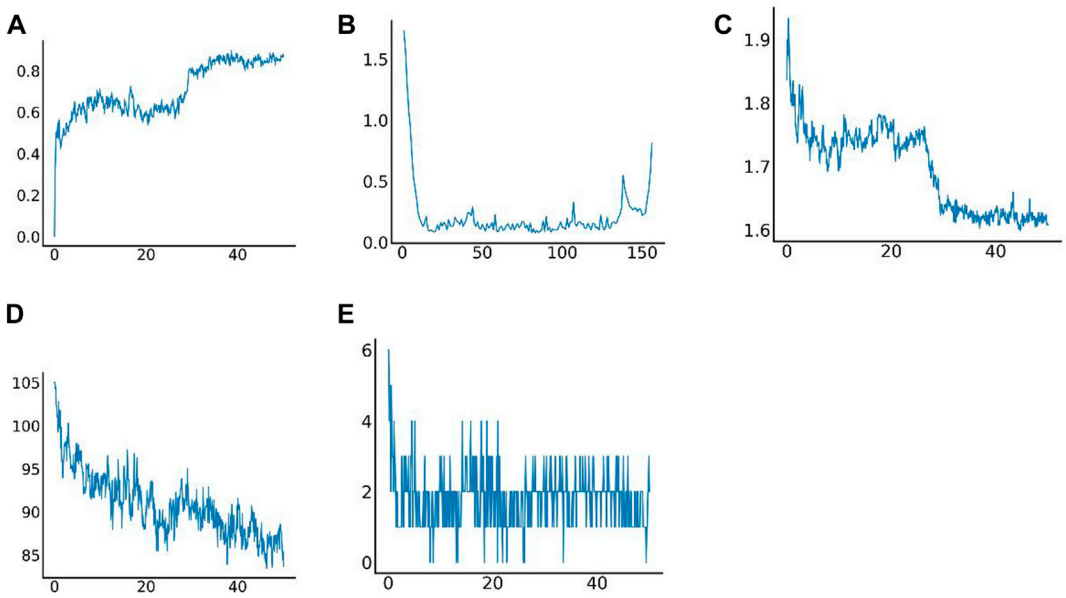

FIGURE 7
Results of molecular dynamics simulation. **(A)** Root-mean-square deviation (RMSD) of complex MDS; **(B)** Root-mean-square fluctuation (RMSF) of complex MDS; **(C)** Variations in the radius of gyration (Rg) of complex MDS; **(D)** Variations in SASA of the protein in 0–100 ns of complex MDS; **(E)** Variations in hydrogen bonding in the stable complex.

progression from G1 to S phase (Rubin, 2013; van den Heuvel and Dyson, 2008). By forming a trimeric complex with MDM2 and p53, P14ARF inhibits the degradation of P53 by MDM2, resulting in G1 and G2 arrest (Pollice et al., 2008). CDKN2A expression is correlated with the development and prognosis of various tumours, including hepatocellular carcinoma, pancreatic cancer and melanoma (Zeng et al., 2018; Kimura et al., 2021; Luo et al., 2021). Copy number deletion in CDKN2A and low expression of p16INK4a indicate a poor prognosis and can be used as independent

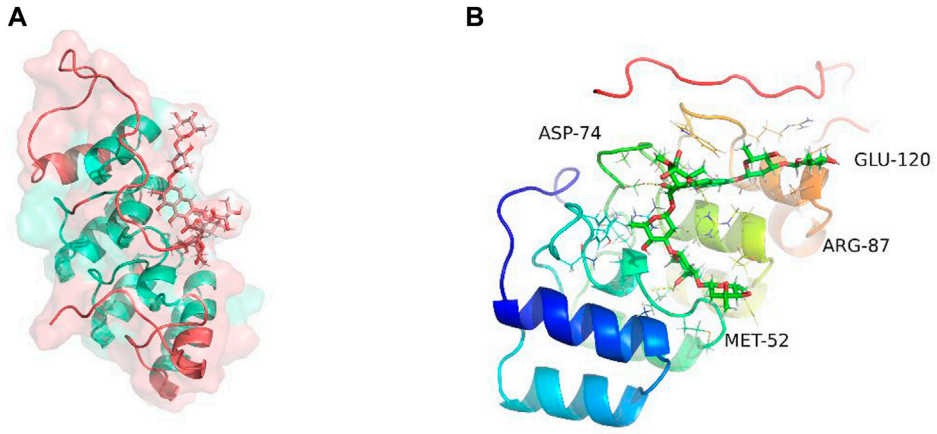

FIGURE 8
Binding site of plicamycin on the CDKN2A protein. **(A)** Docking pose; **(B)** Amino acids and docking sites.

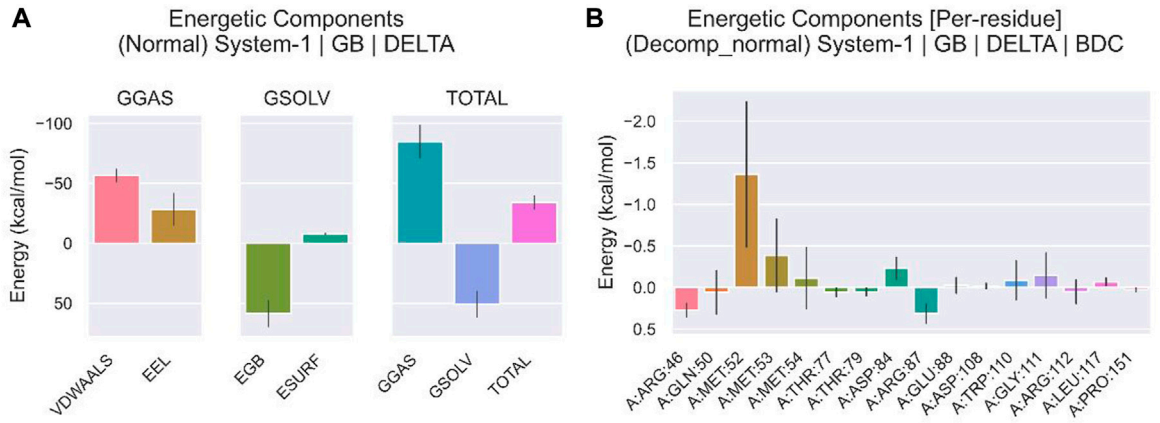

FIGURE 9
Energy analysis of molecular dynamics simulations. **(A)** Binding free energy of protein–ligand complexes. VDWAALS, van der Waals energy; EEL, electrostatic energy; EGB, polar solvation energy; ESURF, non-polar solvation energy; GGAS, total gas phase free energy; GSOLV, total solvation free energy; G_{total} free energy = GSOLV + GGAS. **(B)** The relationship between each contact residue and the binding energy.

prognostic predictors in HNSCC (Chen et al., 2018; Cury et al., 2021). A meta-analysis on HNSCC reported that methylation of CDKN2A is significantly correlated with tumorigenesis, progression and metastasis and can be used as a potential diagnostic marker (Zhou et al., 2018). Similar results were obtained in this study, indicating that CDKN2A plays an important role in regulating the tumour cell cycle and may serve as a prognostic marker in HNSCC.

Tumor-infiltrating immune cells are critical components of the tumour microenvironment and are highly predictive of prognosis and treatment outcomes (Nguyen et al., 2016; Guo et al., 2020). In this study, CDKN2A was positively correlated with the infiltration of activated B and CD4 T cells in the tumour microenvironment, leading to a better prognosis of HNSCC. The IGJ gene encodes CD19 and the J-chain gene, typical markers of B cells. In HNSCC, CD19 and J-chain expression were studied, and B cell infiltration in the tumor microenvironment indicated a better prognosis (Kim et al., 2020). Moreover, anti-blockade of PD-1/PD-L1 immune checkpoints in an AT-84-E7 murine model of HNSCC led to tumor enlargement by depleting B cells in the tumor microenvironment by regulating B cell activation and germinal center formation (Kim et al., 2020). This suggests that B cell infiltration and activity play an important role in the treatment of tumors. Hladíková et al., (2019) observed a high abundance of tumor-infiltrating B cells (TIL-Bs) in the HNSCC tumor microenvironment, which may

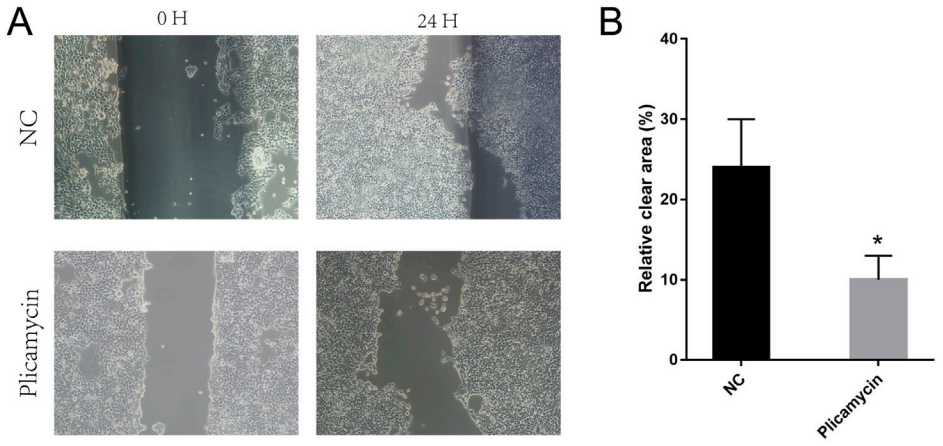

FIGURE 10
Pplicamycin treatment reduced the mobility of TU212 cells. **(A)** Wound-healing assay for migration activity of untreated (upper panel) and treated (lower panel) TU212 cells. After 24 h, we captured representative images of the migrating cells. **(B)** Quantitative analysis of untreated TU212 invasion effects compared to treated TU212 invasion effects. Invasive cells were counted on average.

interact with $CD8^+$ T cells to promote tumor growth (). They produce tumour-associated antibodies and cytokines, which exert cytotoxic effects on tumours, as well as presenting tumour-associated antigens (TAA) (Candolfi et al., 2011; Mahmoud et al., 2012; Shi et al., 2013; Germain et al., 2014). Infection with the human papillomavirus (HPV) is causing an increase in HNSCC. HNSCC with HPV-positive microenvironment contain more $CD4^+$ T cells, which result in a better prognosis and response to radiotherapy than those with HPV-negative microenvironment. However, whether this better prognostic performance is related to $CD4^+$ T cell infiltration remains unclear (van Kempen et al., 2016). Multiple studies have shown that neutrophils can promote tumour development and angiogenesis through the secretion of cytokines such as vascular endothelial growth factor, hepatocyte growth factor, IL-6 and IL-8 (McCourt et al., 1999; McCourt et al., 2001; Schaider et al., 2003). Low CDKN2A expression was associated with neutrophil infiltration and poorer prognosis in the present study. Yang et al. reported in a previous study that high neutrophil infiltration can result in the generation of reactive oxygen species, arginase and nitric oxide, causing lymphocytes to be suppressed, T cells to be activated, and, ultimately, tumour growth (Gooden et al., 2011; Yang et al., 2019). Watermann et al., (2021) also found a link between neutrophil infiltration and tumour malignancy in the microenvironment of recurrent HNSCC.

There is a positive correlation between CDKN2A expression and activation of B cells and $CD4^+$ T cells. There is evidence that $CD8^+$ and $CD4^+$ T cells infiltrate the microenvironment to ensure the beneficial effects of gamma-delta T cells on prognosis (Nielsen et al., 2017; Lu et al., 2020). Gamma-delta T cells are important immune cells in the mucosal region responsible for removing pathogens and maintaining the integrity of the epithelium. Lu et al. found a high abundance of gamma-delta T cells infiltration in the tumour microenvironment of patients with HNSCC with a better prognosis. However, Bas et al. examined gamma-delta T cell in the peripheral blood of patients with HNSCC and found that their high abundance was associated with the recurrence of HNSCC (Bas et al., 2006). Therefore, CDKN2A, an immune cell related gene, can aid in improving the prognosis and microenvironment of tumors by inhibiting immune cells that activate B and CD4 T cell, neutrophils and gamma-delta T cells.

Plicamycin, also known as mithramycin A, is a natural polycyclic aromatic polyketide compound that inhibits SP1 transcription factor binding to DNA, which interferes with biological processes like tumour cell proliferation, apoptosis, angiogenesis, invasion, and metastasis (Beishline and Azizkhan-Clifford, 2015; Schweer et al., 2021). Plicamycin is a natural polycyclic aromatic polyketide that inhibits SP1 transcription factor binding to DNA, impeding apoptosis, angiogenesis, invasion, and metastatic processes in cancer cells (Saha et al., 2015). In mouse models of lung cancer, low SP1 expression can effectively inhibit tumour growth and nicotine-induced lung cancer cell growth (Brown et al., 2013). The histone methyltransferase gene SETDB1 is an important gene in the development and metastasis of melanoma *in vivo*. Several studies have shown that plicamycin can effectively target the activity of SP-1 protein on the SETDB1 promoter to inhibit SETDB1 expression, thus offering a beneficial therapeutic strategy for melanoma (Federico et al., 2020). Plicamycin, an inhibitor of SP1, can inhibit tumour progression in several cancer types and has been used for the treatment of lung, breast and gastrointestinal tract cancers in phase II clinical trials, with good efficacy. However, the role and mechanisms of action of

plicamycin in HNSCC remain to be elucidated. In this study, strong binding was observed between plicamycin and CDKN2A through molecular docking and MDS, suggesting that plicamycin improves the prognosis of HNSCC by targeting CDKN2A at the molecular level. However, the relationship between CDKN2A and SP1 warrants further investigation. The results of this study are mainly based on bioinformatics analysis and MDS, and they aren't validated *in vivo* or *in vitro*. Additionally, plicamycin's effects on HNSCC should be studied in large clinical trials.

Conclusion

CDKN2A, which is closely related to the maintenance of copper metabolic homeostasis in the body, is a biomarker of HNSCC and may improve its prognosis by regulating the cell cycle and immune cell infiltration. Further, plicamycin targets and binds CDKN2A, offering a novel strategy for the treatment of HNSCC in the future.

Data availability statement

Publicly available datasets were analyzed in this study. This data can be found here: Head and neck squamous cell carcinoma data were obtained from TCGA database (https://portal.gdc.cancer.gov).

Author contributions

KF and YL conceived and designed the analysis; KF, TL, and YL collected the data; TL, YL, and YD contributed data or analysis tools; KF, TL, YL, and YD performed the analysis; KF, TL, YL, and YD wrote the paper.

Conflict of interest

The authors declare that the research was conducted in the absence of any commercial or financial relationships that could be construed as a potential conflict of interest.

Publisher's note

All claims expressed in this article are solely those of the authors and do not necessarily represent those of their affiliated organizations, or those of the publisher, the editors and the reviewers. Any product that may be evaluated in this article, or claim that may be made by its manufacturer, is not guaranteed or endorsed by the publisher.

Supplementary material

The Supplementary Material for this article can be found online at: https://www.frontiersin.org/articles/10.3389/fgene.2022.1036408/full#supplementary-material

SUPPLEMENTARY FIGURE S1
Correlation among immune cell types. **(A)** Heat map demonstrating immune cell infiltration in the high- and low-CDKN2A-expression groups; **(B)** Correlation among different immune cell types.

SUPPLEMENTARY FIGURE S2
CDKN2A mutation sites.

SUPPLEMENTARY FIGURE S3
PLDS shows a medium docking effect with a total of 104 residue sites.

References

Bao, Z., Yang, Z., Huang, Z., Zhou, Y., Cui, Q., and Dong, D. (2019). LncRNADisease 2.0: An updated database of long non-coding RNA-associated diseases. *Nucleic Acids Res.* 47, D1034–D1037. doi:10.1093/nar/gky905

Barbie, D. A., Tamayo, P., Boehm, J. S., Kim, S. Y., Moody, S. E., Dunn, I. F., et al. (2009). Systematic RNA interference reveals that oncogenic KRAS-driven cancers require TBK1. *Nature* 462, 108–112. doi:10.1038/nature08460

Bas, M., Bier, H., Schirlau, K., Friebe-Hoffmann, U., Scheckenbach, K., Balz, V., et al. (2006). Gamma–delta T-cells in patients with squamous cell carcinoma of the head and neck. *Oral Oncol.* 42, 691–697. doi:10.1016/j.oraloncology.2005.11.008

Beishline, K., and Azizkhan-Clifford, J. (2015). Sp1 and the 'hallmarks of cancer. *FEBS J.* 282, 224–258. doi:10.1111/febs.13148

Bray, F., Ferlay, J., Soerjomataram, I., Siegel, R. L., Torre, L. A., and Jemal, A. (2018). Global cancer statistics 2018: GLOBOCAN estimates of incidence and mortality worldwide for 36 cancers in 185 countries. *CA A Cancer J. Clin.* 68, 394–424. doi:10.3322/caac.21492

Brown, K. C., Perry, H. E., Lau, J. K., Jones, D. V., Pulliam, J. F., Thornhill, B. A., et al. (2013). Nicotine induces the up-regulation of the α7-nicotinic receptor (α7-nAChR) in human squamous cell lung cancer cells via the Sp1/GATA protein pathway. *J. Biol. Chem.* 288, 33049–33059. doi:10.1074/jbc.M113.501601

Candolfi, M., Curtin, J. F., Yagiz, K., Assi, H., Wibowo, M. K., Alzadeh, G. E., et al. (2011). B cells are critical to T-cell—mediated antitumor immunity induced by a combined immune-stimulatory/conditionally cytotoxic therapy for glioblastoma. *Neoplasia* 13, 947–960. doi:10.1593/neo.11024

Canning, M., Guo, G., Yu, M., Myint, C., Groves, M. W., Byrd, J. K., et al. (2019). Heterogeneity of the head and neck squamous cell carcinoma immune landscape and its impact on immunotherapy. *Front. Cell Dev. Biol.* 7, 52. doi:10.3389/fcell.2019.00052

Chen, W. S., Bindra, R. S., Hayman, T., Husain, Z., Contessa, J. N., Mo, A., et al. (2018). CDKN2A copy number loss is an independent prognostic factor in HPV-negative head and neck squamous cell carcinoma. *Front. Oncol.* 8, 95. doi:10.3389/fonc.2018.00095

Chen, Y., Sun, Y., Luo, Z., Lin, J., Qi, B., Kang, X., et al. (2022). Potential mechanism underlying exercise upregulated circulating blood exosome miR-215-5p to prevent necroptosis of neuronal cells and a model for early diagnosis of alzheimer's disease. *Front. Aging Neurosci.* 14, 860364. doi:10.3389/fnagi.2022.860364

Chikan, N. A., and Vipperla, B. (2015). KAISO inhibition: An atomic insight. *J. Biomol. Struct. Dyn.* 33, 1794–1804. doi:10.1080/07391102.2014.974072

Colaprico, A., Silva, T. C., Olsen, C., Garofano, L., Cava, C., Garolini, D., et al. (2016). TCGAbiolinks: An R/bioconductor package for integrative analysis of TCGA data. *Nucleic Acids Res.* 44, e71. doi:10.1093/nar/gkv1507

Cury, S. S., Miranda, P. M. d., Marchi, F. A., Canto, L. M. d., Chulam, T. C., Petersen, A. H., et al. (2021). Germline variants in DNA repair genes are associated with young-onset head and neck cancer. *Oral Oncol.* 122, 105545. doi:10.1016/j.oraloncology.2021.105545

Federico, A., Steinfass, T., Larribere, L., Novak, D., Moris, F., Nunez, L. E., et al. (2020). Mithramycin A and mithralog EC-8042 inhibit SETDB1 expression and its oncogenic activity in malignant melanoma. *Mol. Ther. - Oncolytics* 18, 83–99. doi:10.1016/j.omto.2020.06.001

Ferlay, J., ColoMbetM., Soerjomataram, I., Mathers, C., Parkin, D. M., PinerosM., et al. (2019). Estimating the global cancer incidence and mortality in 2018: GLOBOCAN sources and methods. *Int. J. Cancer* 144, 1941–1953. doi:10.1002/ijc.31937

Germain, C., Gnjatic, S., Tamzalit, F., Knockaert, S., Remark, R., Goc, J., et al. (2014). Presence of B Cells in tertiary lymphoid structures is associated with a protective immunity in patients with lung cancer. *Am. J. Respir. Crit. Care Med.* 189, 832–844. doi:10.1164/rccm.201309-1611OC

Gooden, M. J. M., de Bock, G. H., Leffers, N., Daemen, T., and Nijman, H. W. (2011). The prognostic influence of tumour-infiltrating lymphocytes in cancer: A systematic review with meta-analysis. *Br. J. Cancer* 105, 93–103. doi:10.1038/bjc.2011.189

Guo, L., Li, X., Liu, R., Chen, Y., Ren, C., and Du, S. (2020). TOX correlates with prognosis, immune infiltration, and T cells exhaustion in lung adenocarcinoma. *Cancer Med.* 9, 6694–6709. doi:10.1002/cam4.3324

Hänzelmann, S., Castelo, R., and Guinney, J. (2013). Gsva: Gene set variation analysis for microarray and RNA-seq data. *BMC Bioinforma.* 14, 7. doi:10.1186/1471-2105-14-7

Hildebrand, P. W., Rose, A. S., and Tiemann, J. K. S. (2019). Bringing molecular dynamics simulation data into view. *Trends Biochem. Sci.* 44, 902–913. doi:10.1016/j.tibs.2019.06.004

Hladíková, K., Koucky, V., Boucek, J., Laco, J., Grega, M., Hodek, M., et al. (2019). Tumor-infiltrating B cells affect the progression of oropharyngeal squamous cell carcinoma via cell-to-cell interactions with CD8+ T cells. *J. Immunother. cancer* 7, 261. doi:10.1186/s40425-019-0726-6

Hollingsworth, S. A., and Dror, R. O. (2018). Molecular dynamics simulation for all. *Neuron* 99, 1129–1143. doi:10.1016/j.neuron.2018.08.011

Huang, H.-Y., Lin, Y. C. D., Li, J., Huang, K. Y., Shrestha, S., Hong, H. C., et al. (2019). miRTarBase 2020: updates to the experimentally validated microRNA-target interaction database. *Nucleic Acids Res.* 48, D148. doi:10.1093/nar/gkz896

Huang, J., Lin, W., Sun, Y., Wang, Q., He, S., Han, Z., et al. (2022). Quercetin targets VCAM1 to prevent diabetic cerebrovascular endothelial cell injury. *Front. Aging Neurosci.* 14, 944195. doi:10.3389/fnagi.2022.944195

Huang, Z., Shi, J., Gao, Y., Cui, C., Zhang, S., Li, J., et al. (2019). HMDD v3.0: A database for experimentally supported human microRNA–disease associations. *Nucleic Acids Res.* 47, D1013–D1017. doi:10.1093/nar/gky1010

Ito, K., and Murphy, D. (2013). Application of *ggplot2* to pharmacometric graphics. *CPT Pharmacometrics Syst. Pharmacol.* 2, 79. doi:10.1038/psp.2013.56

Ji, Z.-H., Ren, W.-Z., Wang, H.-Q., Gao, W., and Yuan, B. (2022). Molecular subtyping based on cuproptosis-related genes and characterization of tumor microenvironment infiltration in kidney renal clear cell carcinoma. *Front. Oncol.* 12, 919083. doi:10.3389/fonc.2022.919083

Kang, X., Chen, Y., Yi, B., Yan, X., Jiang, C., Chen, B., et al. (2021). An integrative microenvironment approach for laryngeal carcinoma: The role of immune/methylation/autophagy signatures on disease clinical prognosis and single-cell genotypes. *J. Cancer* 12, 4148–4171. doi:10.7150/jca.58076

Kang, X., Sun, Y., Yi, B., Jiang, C., Yan, X., Chen, B., et al. (2022). Based on network pharmacology and molecular dynamics simulations, baicalein, an active ingredient of yiqi qingre ziyin method, potentially protects patients with atrophic rhinitis from cognitive impairment. *Front. Aging Neurosci.* 14, 880794. doi:10.3389/fnagi.2022.880794

Kim, S. S., Shen, S., Miyauchi, S., Sanders, P. D., Franiak-Pietryga, I., Mell, L., et al. (2020). B cells improve overall survival in HPV-associated squamous cell carcinomas and are activated by radiation and PD-1 blockade. *Clin. Cancer Res.* 26, 3345–3359. doi:10.1158/1078-0432.CCR-19-3211

Kimura, H., Klein, A. P., Hruban, R. H., and Roberts, N. J. (2021). The role of inherited pathogenic CDKN2A variants in susceptibility to pancreatic cancer. *Pancreas* 50, 1123–1130. doi:10.1097/MPA.0000000000001888

Li, J., Poi, M. J., and Tsai, M.-D. (2011). Regulatory mechanisms of tumor suppressor P16 ^{INK4A} and their relevance to cancer. *Biochemistry* 50, 5566–5582. doi:10.1021/bi200642e

Li, Y., Jun, L., Yan, H., Zhang, Q., and Wei, S. L. (2022). The prognostic value and immune landscape of a cuproptosis-related lncRNA signature in head and neck squamous cell carcinoma. *Front. Genet.* 13, 942785. doi:10.3389/fgene.2022.942785

Lin, W., Liu, J., Oualha, N., and Balesdent, M. (2021). Study on the effect of composite nanoparticles on corneal epithelial cell immune mechanism based on dectin-1 signaling pathway. *Oxid. Med. Cell Longev.* 2021, 1148–1153. doi:10.1166/jnn.2021.18703

Lin, W., Wang, Q., Chen, Y., Wang, N., Ni, Q., Qi, C., et al. (2022). Identification of a 6-RBP gene signature for a comprehensive analysis of glioma and ischemic stroke: Cognitive impairment and aging-related hypoxic stress. *Front. Aging Neurosci.* 14, 951197. doi:10.3389/fnagi.2022.951197

Lu, H., Dai, W., Guo, J., Wang, D., Wen, S., Yang, L., et al. (2020). High abundance of intratumoral γδ T cells favors a better prognosis in head and neck squamous cell carcinoma: A bioinformatic analysis. *Front. Immunol.* 11, 573920. doi:10.3389/fimmu.2020.573920

Luo, J., Wang, J., and Huang, J. (2021). CDKN2A is a prognostic biomarker and correlated with immune infiltrates in hepatocellular carcinoma. *Biosci. Rep.* 41, BSR20211103. doi:10.1042/BSR20211103

Luo, Q., Ma, H., Guo, E., Yu, L., Jia, L., Zhang, B., et al. (2022). MicroRNAs promote the progression of sepsis-induced cardiomyopathy and neurovascular dysfunction through upregulation of NF-kappaB signaling pathway-associated HDAC7/ACTN4. *Front. Neurol.* 13, 909828. doi:10.3389/fneur.2022.909828

Luo, Z., He, Z., Qin, H., Chen, Y., Qi, B., Lin, J., et al. (2022). Exercise-induced IL-15 acted as a positive prognostic implication and tumor-suppressed role in pan-cancer. *Front. Pharmacol.* 13, 1053137. doi:10.3389/fphar.2022.1053137

Lv, H., Liu, X., Zeng, X., Liu, Y., Zhang, C., Zhang, Q., et al. (2022). Comprehensive analysis of cuproptosis-related genes in immune infiltration and prognosis in melanoma. *Front. Pharmacol.* 13, 930041. doi:10.3389/fphar.2022.930041

Mahmoud, S. M. A., Lee, A. H. S., Paish, E. C., Macmillan, R. D., Ellis, I. O., and Green, A. R. (2012). The prognostic significance of B lymphocytes in invasive carcinoma of the breast. *Breast Cancer Res. Treat.* 132, 545–553. doi:10.1007/s10549-011-1620-1

McCourt, M., Wang, J. H., Sookhai, S., and Redmond, H. P. (2001). Activated human neutrophils release hepatocyte growth factor/scatter factor. *Eur. J. Surg. Oncol. (EJSO)* 27, 396–403. doi:10.1053/ejso.2001.1133

McCourt, M., Wang, J. H., Sookhai, S., and Redmond, H. P. (1999). Proinflammatory mediators stimulate neutrophil-directed angiogenesis. *Arch. Surg.* 134, 1325–1331. doi:10.1001/archsurg.134.12.1325

Mei, S., Li, Y., and Kang, X. (2022). Prognostic and functional analysis of NPY6R in uveal melanoma using bioinformatics. *Dis. Markers* 2022, 4143447–4143514. doi:10.1155/2022/4143447

Nguyen, N., Bellile, E., Thomas, D., McHugh, J., Rozek, L., Virani, S., et al. (2016). Tumor infiltrating lymphocytes and survival in patients with head and neck squamous cell carcinoma: Tumor infiltrating lymphocytes. *Head. Neck* 38, 1074–1084. doi:10.1002/hed.24406

Nielsen, M. M., Witherden, D. A., and Havran, W. L. (2017). γδ T cells in homeostasis and host defence of epithelial barrier tissues. *Nat. Rev. Immunol.* 17, 733–745. doi:10.1038/nri.2017.101

Oliveri, V. (2022). Selective targeting of cancer cells by copper ionophores: overview. *Front. Mol. Biosci.* 9, 841814. doi:10.3389/fmolb.2022.841814

Ou, J., and Zhu, L. J. (2019). trackViewer: a Bioconductor package for interactive and integrative visualization of multi-omics data. *Nat. Methods* 16, 453–454. doi:10.1038/s41592-019-0430-y

Pollice, A., Vivo, M., and Mantia, G. L. (2008). The promiscuity of ARF interactions with the proteasome. *FEBS Lett.* 582, 3257–3262. doi:10.1016/j.febslet.2008.09.026

Ritchie, M. E., Phipson, B., Wu, D., Hu, Y., Law, C. W., Shi, W., et al. (2015). Limma powers differential expression analyses for RNA-sequencing and microarray studies. *Nucleic Acids Res.* 43, e47. doi:10.1093/nar/gkv007

Rubin, S. M. (2013). Deciphering the retinoblastoma protein phosphorylation code. *Trends Biochem. Sci.* 38, 12–19. doi:10.1016/j.tibs.2012.10.007

Ruiz, L. M., Libedinsky, A., and Elorza, A. A. (2021). Role of copper on mitochondrial function and metabolism. *Front. Mol. Biosci.* 8, 711227. doi:10.3389/fmolb.2021.711227

Saha, S., Mukherjee, S., Mazumdar, M., Manna, A., Khan, P., Adhikary, A., et al. (2015). Mithramycin A sensitizes therapy-resistant breast cancer stem cells toward genotoxic drug doxorubicin. *Transl. Res.* 165, 558–577. doi:10.1016/j.trsl.2014.10.011

Schaider, H., Oka, M., Bogenrieder, T., Nesbit, M., Satyamoorthy, K., Berking, C., et al. (2003). Differential response of primary and metastatic melanomas to neutrophils attracted by IL-8. *Int. J. Cancer* 103, 335–343. doi:10.1002/ijc.10775

Schweer, D., McCorkle, J. R., Rohr, J., Tsodikov, O. V., Ueland, F., and Kolesar, J. (2021). Mithramycin and analogs for overcoming cisplatin resistance in ovarian cancer. *Biomedicines* 9, 70. doi:10.3390/biomedicines9010070

Shanbhag, V. C., Gudekar, N., Jasmer, K., Papageorgiou, C., Singh, K., and Petris, M. J. (2021). Copper metabolism as a unique vulnerability in cancer. *Biochimica Biophysica Acta (BBA) - Mol. Cell Res.* 1868, 118893. doi:10.1016/j.bbamcr.2020.118893

Shannon, P., Markiel, A., Ozier, O., Baliga, N. S., Wang, J. T., Ramage, D., et al. (2003). Cytoscape: A software environment for integrated models of biomolecular interaction networks. *Genome Res.* 13, 2498–2504. doi:10.1101/gr.1239303

Shi, J.-Y., Gao, Q., Wang, Z. C., Zhou, J., Wang, X. Y., Min, Z. H., et al. (2013). Margin-infiltrating CD20+ B cells display an atypical memory phenotype and correlate with favorable prognosis in hepatocellular carcinoma. *Clin. Cancer Res.* 19, 5994–6005. doi:10.1158/1078-0432.CCR-12-3497

Shi, Q., Yan, X., Wang, J., and Zhang, X. (2021). Collagen family genes associated with risk of recurrence after radiation therapy for vestibular schwannoma and pan-cancer analysis. *Dis. Markers* 2021, 7897994–7898015. doi:10.1155/2021/7897994

Subramanian, A., Tamayo, P., Mootha, V. K., Mukherjee, S., Ebert, B. L., Gillette, M. A., et al. (2005). Gene set enrichment analysis: A knowledge-based approach for interpreting genome-wide expression profiles. *Proc. Natl. Acad. Sci. U.S.A.* 102, 15545–15550. doi:10.1073/pnas.0506580102

Szklarczyk, D., Gable, A. L., Nastou, K. C., Lyon, D., Kirsch, R., Pyysalo, S., et al. (2021). The STRING database in 2021: Customizable protein–protein networks, and functional characterization of user-uploaded gene/measurement sets. *Nucleic Acids Res.* 49, D605–D612. doi:10.1093/nar/gkaa1074

Taberna, M., MenaM.Pavon, M. A., Alemany, L., Gillison, M. L., and Mesia, R. (2017). Human papillomavirus-related oropharyngeal cancer. *Ann. Oncol.* 28, 2386–2398. doi:10.1093/annonc/mdx304

Thai, K.-M., Le, D. P., Tran, N. V. K., Nguyen, T. T. H., and Tran, T. D. (2015). Computational assay of Zanamivir binding affinity with original and mutant influenza neuraminidase 9 using molecular docking. *J. Theor. Biol.* 385, 31–39. doi:10.1016/j.jtbi.2015.08.019

Tomczak, K., Czerwińska, P., and Wiznerowicz, M. (2015). Review the cancer genome atlas (TCGA): An immeasurable source of knowledge. *Contemp. Oncol. Pozn.* 19, 68–77. doi:10.5114/wo.2014.47136

Tsvetkov, P., Coy, S., Petrova, B., Dreishpoon, M., Verma, A., Abdusamad, M., et al. (2022). Copper induces cell death by targeting lipoylated TCA cycle proteins. *Science* 375, 1254–1261. doi:10.1126/science.abf0529

van den Heuvel, S., and Dyson, N. J. (2008). Conserved functions of the pRB and E2F families. *Nat. Rev. Mol. Cell Biol.* 9, 713–724. doi:10.1038/nrm2469

van Kempen, P. M. W., Noorlag, R., Swartz, J. E., Bovenschen, N., Braunius, W. W., Vermeulen, J. F., et al. (2016). Oropharyngeal squamous cell carcinomas differentially express granzyme inhibitors. *Cancer Immunol. Immunother.* 65, 575–585. doi:10.1007/s00262-016-1819-4

Warde-Farley, D., Donaldson, S. L., Comes, O., Zuberi, K., Badrawi, R., Chao, P., et al. (2010). The GeneMANIA prediction server: Biological network integration for gene prioritization and predicting gene function. *Nucleic Acids Res.* 38, W214–W220. doi:10.1093/nar/gkq537

Watermann, C., Pasternack, H., Idel, C., Ribbat-Idel, J., Bragelmann, J., Kuppler, P., et al. (2021). Recurrent HNSCC harbor an immunosuppressive tumor immune microenvironment suggesting successful tumor immune evasion. *Clin. Cancer Res.* 27, 632–644. doi:10.1158/1078-0432.CCR-20-0197

Wei, C.-Y., Zhu, M. X., Lu, N. H., Peng, R., Yang, X., Zhang, P. F., et al. (2019). Bioinformatics-based analysis reveals elevated MFSD12 as a key promoter of cell proliferation and a potential therapeutic target in melanoma. *Oncogene* 38, 1876–1891. doi:10.1038/s41388-018-0531-6

Weiser, J., Shenkin, P. S., and Still, W. C. (1999). Approximate atomic surfaces from linear combinations of pairwise overlaps (LCPO). *J. Comput. Chem.* 20, 217–230. doi:10.1002/(sici)1096-987x(19990130)20:2<217::aid-jcc4>3.0.co;2-a

Xuan, Z., Ma, T., Qin, Y., and Guo, Y. (2022). Role of ultrasound imaging in the prediction of TRIM67 in brain metastases from breast cancer. *Front. Neurol.* 13, 889106. doi:10.3389/fneur.2022.889106

Yang, L., Huang, Y., Zhou, L., Dai, Y., and Hu, G. (2019). High pretreatment neutrophil-to-lymphocyte ratio as a predictor of poor survival prognosis in head and neck squamous cell carcinoma: Systematic review and meta-analysis. *Head Neck* 41, 1525–1535. doi:10.1002/hed.25583

Yun, Y., Wang, Y., Yang, E., and Jing, X. (2022). Cuproptosis-related gene – SLC31A1, FDX1 and ATP7B – polymorphisms are associated with risk of lung cancer. *PGPM* 15, 733–742. doi:10.2147/PGPM.S372824

Zeng, H., Jorapur, A., Shain, A. H., Lang, U. E., Torres, R., Zhang, Y., et al. (2018). Bi-Allelic loss of CDKN2A initiates melanoma invasion via BRN2 activation. *Cancer Cell* 34, 56e9–68. doi:10.1016/j.ccell.2018.05.014

Zhang, L., Zeng, M., and Fu, B. M. (2016). Inhibition of endothelial nitric oxide synthase decreases breast cancer cell MDA-MB-231 adhesion to intact microvessels under physiological flows. *Am. J. Physiology-Heart Circulatory Physiology* 310, H1735–H1747. doi:10.1152/ajpheart.00109.2016

Zhang, Y., Zhang, J., Sun, C., and Wu, F. (2022). Identification of the occurrence and potential mechanisms of heterotopic ossification associated with 17-beta-estradiol targeting MKX by bioinformatics analysis and cellular experiments. *PeerJ* 9, e12696. doi:10.7717/peerj.12696

Zhao, B., and Jiang, X. (2022). hsa-miR-518-5p/hsa-miR-3135b regulates the REL/SOD2 pathway in ischemic cerebral infarction. *Front. Neurol.* 13, 852013. doi:10.3389/fneur.2022.852013

Zhao, R., Choi, B. Y., Lee, M.-H., Bode, A. M., and Dong, Z. (2016). Implications of genetic and epigenetic alterations of CDKN2A (p16 INK4a) in cancer. *EBioMedicine* 8, 30–39. doi:10.1016/j.ebiom.2016.04.017

Zhou, C., Shen, Z., Ye, D., Li, Q., Deng, H., Liu, H., et al. (2018). The association and clinical significance of CDKN2A promoter methylation in head and neck squamous cell carcinoma: A meta-analysis. *Cell Physiol. Biochem.* 50, 868–882. doi:10.1159/000494473

frontiers | Frontiers in Genetics

TYPE Original Research
PUBLISHED 20 January 2023
DOI 10.3389/fgene.2023.1107294

OPEN ACCESS

EDITED BY
Aneesha Acharya,
Dr D. Y. Patil Dental College & Hospital, India

REVIEWED BY
Hanluo Li,
Hubei University of Technology, China
Yifan Zhao,
Guangzhou Regenerative Medicine and Health Guangdong Laboratory, China

*CORRESPONDENCE
Tao Wang,
smu02204633@i.smu.edu.cn
Qing Li,
liq73@163.com

SPECIALTY SECTION
This article was submitted to Cancer Genetics and Oncogenomics, a section of the journal Frontiers in Genetics

RECEIVED 24 November 2022
ACCEPTED 11 January 2023
PUBLISHED 20 January 2023

CITATION
Liu Y, Wu D, Chen H, Yan L, Xiang Q, Li Q and Wang T (2023), Construction and verification of a novel prognostic risk model for kidney renal clear cell carcinoma based on immunity-related genes.
Front. Genet. 14:1107294.
doi: 10.3389/fgene.2023.1107294

Construction and verification of a novel prognostic risk model for kidney renal clear cell carcinoma based on immunity-related genes

Yufeng Liu, Dali Wu, Haiping Chen, Lingfei Yan, Qi Xiang, Qing Li* and Tao Wang*

Department of Urology, The Fifth Affiliated Hospital, Southern Medical University, Guangzhou, China

Background: Currently, there are no useful biomarkers or prognostic risk markers for the diagnosis of kidney renal clear cell carcinoma (KIRC), although recent research has shown that both, the onset and progression of KIRC, are substantially influenced by immune-associated genes (IAGs).

Objective: This work aims to create and verify the prognostic value of an immune risk score signature (IRSS) based on IAGs for KIRC using bioinformatics and public databases.

Methods: Differentially expressed genes (DEGs) related to the immune systems (IAGs) in KIRC tissues were identified from The Cancer Genome Atlas (TCGA) databases. The DEGs between the tumor and normal tissues were identified using gene ontology (GO) and Kyoto Encyclopaedia of Genes and Genomes (KEGG) enrichment analyses. Furthermore, a prognostic IRSS model was constructed and its prognostic and predictive performance was analyzed using survival analyses and nomograms. Kidney renal papillary cell carcinoma (KIRP) sets were utilized to further validate this model.

Results: Six independent immunity-related genes (PAEP, PI3, SAA2, SAA1, IL20RB, and IFI30) correlated with prognosis were identified and used to construct an IRSS model. According to the Kaplan-Meier curve, patients in the high-risk group had significantly poorer prognoses than those of patients in the low-risk group in both, the verification set (p <0.049; HR = 1.84; 95% CI = 1.02–3.32) and the training set (p < 0.001; HR = 3.12, 95% CI = 2.23–4.37). The numbers of regulatory T cells (Tregs) were significantly positively correlated with the six immunity-related genes identified, with correlation coefficients were 0.385, 0.415, 0.399, 0.451, 0.485, and 0.333, respectively (p <0.001).

Conclusion: This work investigated the association between immune infiltration, immunity-related gene expression, and severity of KIRC to construct and verify a prognostic risk model for KIRC and KIRP.

KEYWORDS

kidney renal clear cell carcinoma, risk model, prognostic biomarker, immune infiltration, KIRC

Introduction

Renal cell carcinomas (RCCs) are malignancies in the kidneys; globally, the incidence of RCC has been steadily rising over the last few decades. The most common types of RCCs are kidney renal clear cell carcinomas (KIRCs) and kidney renal papillary cell carcinomas (KIRPs). Although in the early stages of both diseases, patients often display no clinical symptoms, the prognosis for those with KIRP is better than for those with KIRC. It is also unclear if KIRC and KIRP have similar pathogenesis pathways.

KIRC represents about 80% of all RCC cases in adults, whereas KIRP about 10%–15% (Ricketts et al., 2018). For most cases of localized KIRC, the primary treatment consists of surgical removal of the tumor; for advanced and metastatic cases, however, chemotherapy, targeted medication, and immunotherapy are usually used (Chen et al., 2019). When diagnosed at an advanced stage, RCC is a fatal illness with a dismal 5-year survival rate of 11.7% (Siegel et al., 2017). Currently, combinations of anti-VEGF (Vascular Endothelial Growth Factor, VEGF) and immune checkpoint inhibitor treatments are under investigation, which if successful, will significantly alter the therapeutic landscape for RCC treatment (Motzer et al., 2015).

Since immune-associated genes (IAGs) are known to significantly influence the onset and progression of KIRC, (Ghatalia et al., 2019; Xu et al., 2019), several types of immunotherapies, including the use of programmed death-1 (PD-1) inhibitors, cytotoxic T-lymphocyte associated protein 4 (CTLA-4) inhibitors, or programmed death-ligand 1 (PD-L1) inhibitors, are proving to be effective treatment options (Atkins and Tannir, 2018). Recently, a multicentre, randomized, double-blind, placebo-controlled, phase 3 trial has shown that Pembrolizumab is an effective immunotherapeutic agent for KIRC (Powles et al., 2022). However, poor long-term response rates and the absence of efficient prognostic predictors have restricted the use of such first-generation immunotherapies. Therefore, there is an urgent need for identifying new biomarkers, especially immune-related ones, to track disease development, prognosis, and therapy response in KIRC patients.

In recent years, many studies have reported on how prognostic models can be valuable clinical tools in the treatment of various conditions (Huang et al., 2019; Shen et al., 2019; Xu et al., 2020a; Liu et al., 2020; Qu et al., 2020; Wang et al., 2020; Jia et al., 2022; Zhang et al., 2022). However, there have been few investigations on establishing prognostic models for KIRC, especially those related to the immune system. To investigate the relationships between the immune system and the progression of KIRC, we used data from The Cancer Genome Atlas (TCGA) database to construct a risk score model relying on immunity-related genes. Collectively, our results demonstrate the functional significance of immunity-related signatures as prognostic biomarkers for KIRC and kidney renal papillary cell carcinoma (KIRP).

Materials and methods

Data compilation and handling

We retrieved data on gene expression, clinicopathology, and survival of patients with KIRC and KIRP from The Cancer Genome Atlas (TGCA) database and the University of California Santa Cruz (UCSC)database. The KIRC samples with prognostic data, comprising 172 normal samples and 539 tumor samples, were integrated to form a training set. A verification set containing prognostic data on 256 KIRP patients was also established.

In total, the expression profiles of 2,483 immunity-related genes were retrieved, with the complete gene names obtained from the Immunology Database and Analysis Portal (ImmPort) database's Gene List module (Supplementary Table S1).

The human protein atlas (HPA) databases

The HPA contains extensive data on the transcriptome and proteome of various human specimens, including tissue, cell, and pathology atlases. Moreover, the database also provides data on protein immunohistochemistry in tumors and normal human tissue samples.

Differential gene expression analysis

Differential gene expression analysis was used to identify the differentially expressed genes (DEGs) between the tumor and normal groups. We used the 'limma' software package in R (v. 3.6.3), With a false discovery rate (FDR) < 0.25 and Log2| Fold Change | > 2. The DEGs were visualized through volcano plots using the "ggplot2," "Cairo," and "ggrepel" packages in R (v. 3.6.3).

Gene ontology (GO) and kyoto encyclopedia of genes and genomes (KEGG) analysis

We used the 'clusterProfiler' package (v. 3.14.3) to perform GO and KEGG analyses to discover the prospective biological functions and enrichment pathways of the identified DEGs. The KEGG database incorporates information on chemical, genomic, and systematic functional data. The molecular functions, biological processes, and cell composition are gene features that are primarily described by the GO analysis. An adjusted p-value of <0.05 indicated significance. We used the "ggplot2" package (version 3.3.3) for visualization.

Establishment of immune risk score signature (IRSS) for prognosis

To identify the differentially expressed immunity-related genes (DEIGs), a total of 1734 genes associated with immunity were identified in KIRC tissues and compared with the DEGs obtained in the previous analysis. Univariate Cox regression analysis was then used to identify immunity-related genes that had significant relationships with prognosis. Following this, we used LASSO (least absolute shrinkage and selection operator) regression analysis to identify a subset of genes that could be used as independent prognostic indicators. The LASSO regression allowed us to improve our model's accuracy and interpretability, while also addressing the issue of collinearity among the independent variables (Alhamzawi and Ali, 2018). Independent prognostic factor-related regression coefficients were then obtained from multivariate Cox regression

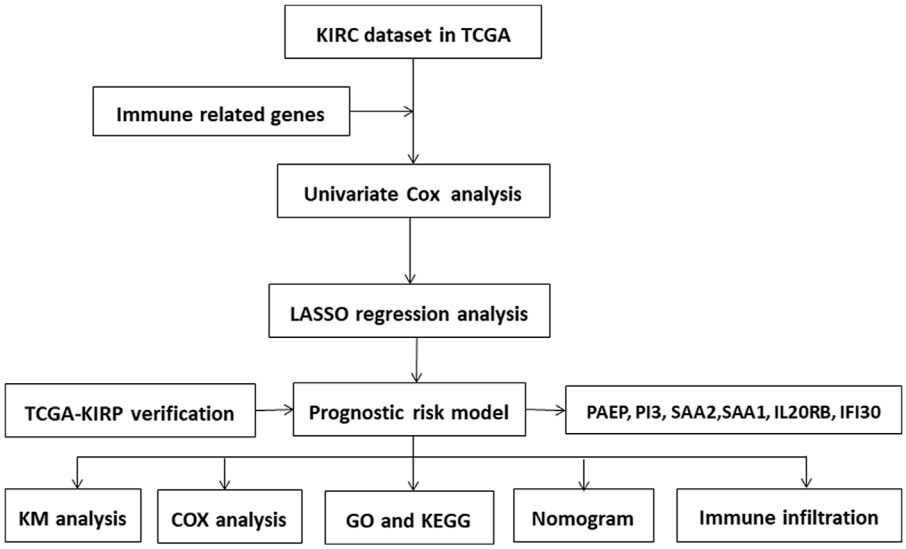

FIGURE 1
Flow chart of steps followed for data collection and analysis in this study.

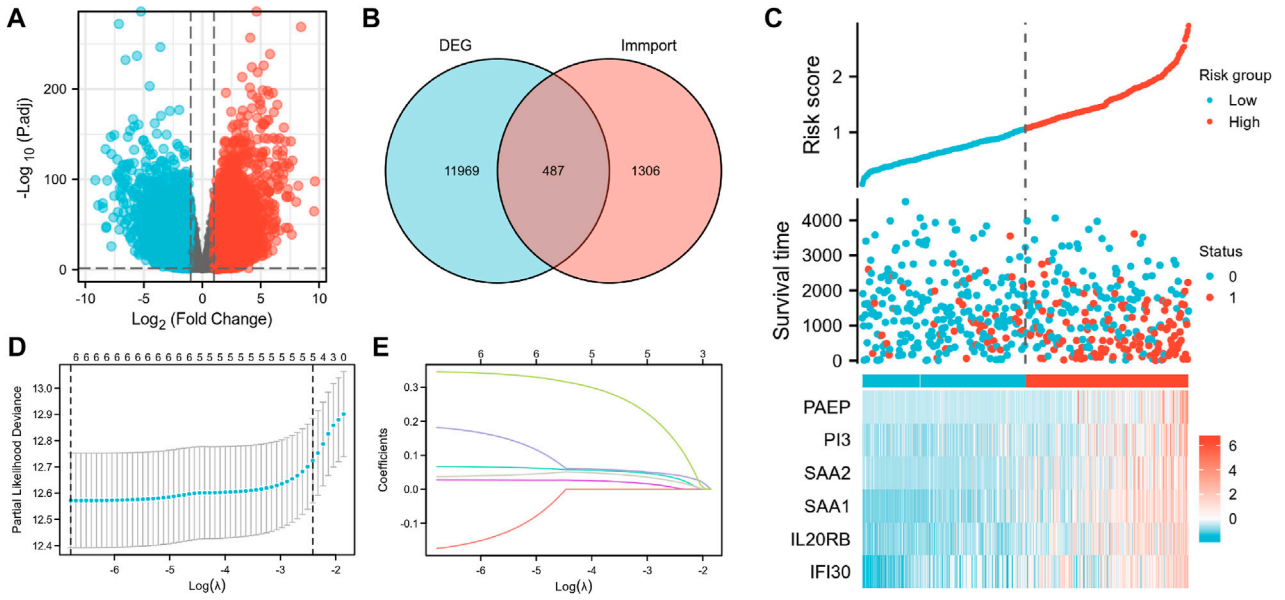

FIGURE 2
Construction of the IRSS. **(A)** Volcano plot of differentially expressed genes. **(B)** Intersection Venn diagram of DEGs and immunity-related genes. **(C)** Risk scores, survival status, and heat maps of six immunity-related genes in KIRC patients. **(D)** Ten-fold cross-validation of the LASSO model-related optimized parameter selection. **(E)** LASSO coefficient profiles. 0 represents survival status "alive," one represents survival status "dead".

analysis. Lastly, the formula for an IRSS, which was established using the multivariate Cox regression coefficient beta value as:

$$\text{IRSS} = \text{EXPgene1}^{*}\beta 1 + \text{EXPgene2}^{*}\beta 2 + \text{EXPgene3}^{*}\beta 3 + \cdots + \text{EXPgenen}^{*}\beta \text{n}$$

wherein this formula, EXP denotes the expression level of the gene and β signifies the regression coefficient from the multivariate Cox regression analysis (Zeng et al., 2017).

Groups with high-IRSS and low-IRSS were established where the risk score for each TCGA-KIRC sample was computed using the above formula; the median risk score was used as the cut-off value for the establishment of these groups. Additionally, the log-rank test was used for comparing overall survival (OS) rates between the two groups, which was visualized using Kaplan-Meier (KM) curves. The AUC (area under the curve) for the receiver operating characteristic (ROC) was used to analyze the prognostic value of the six immunity-related genes identified in this study and the IRSS

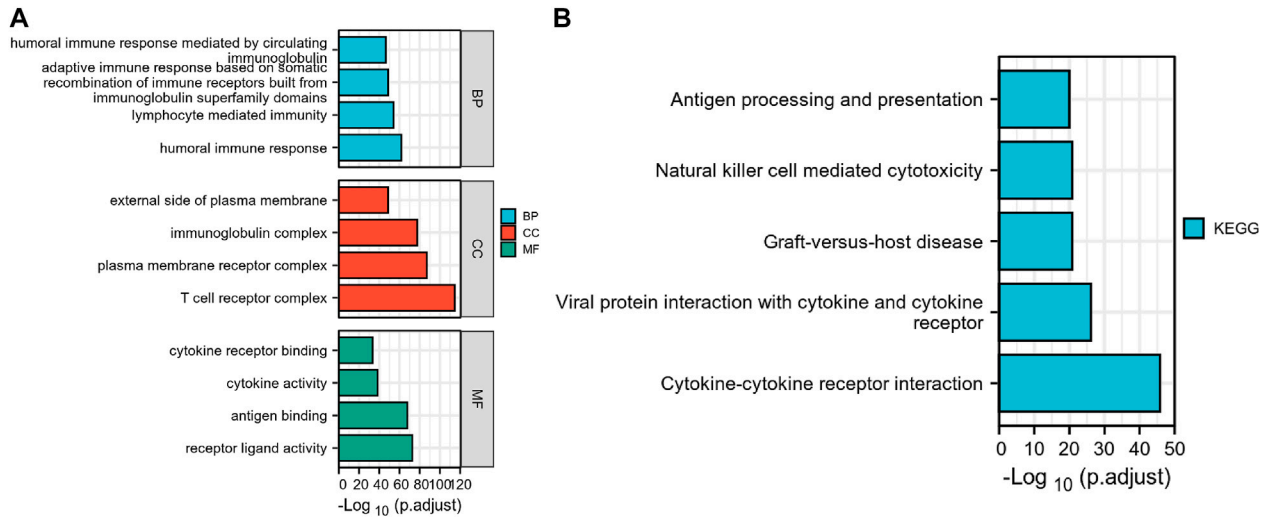

FIGURE 3
Differential genes expressed in normal and KIRC tissues are involved in immune-related pathways. **(A)** GO, Gene Ontology; **(B)** KEGG, Kyoto Encyclopedia of Genes and Genomes.

in KIRC patients. The horizontal and vertical axes of the ROC curve denote specificity and sensitivity, respectively (DeLong et al., 1988). The AUC provides a probability value that can be used to assess the model's predictive accuracy and varies in value from 0.5 to 1, where the larger the value, the better the model's accuracy. In our study, larger AUC values denote higher levels of agreement between the actual OS and the predicted OS. For these analyses, we used the "glmnet" package (version 4.1-2) and the 'survival' package (version 3.2-10).

Immune cell infiltration analysis

Marker genes for each of the 24 types of immune cells were obtained from a research report by Bindea et al. (2013). We used the single sample Gene Set Enrichment Analysis (ssGSEA) method to identify the different immune cells that infiltrated KIRC tumors. We used Wilcoxon's signed-rank sum test and Spearman's correlation to analyze the associations between the gene expression profiles of the six DIEGs and immune infiltration patterns. The analysis was performed using the "Xiantao tool" module (https://www.xiantao.love/products) and the 'GSVA' package (version 1.34.0).

Analyzing the relationships between clinicopathological data and the IRSS

We screened for KIRC-related prognostic predictors, specifically clinical characteristics, and examined their association with the IRSS that we have developed. We paid special attention to the relationship between the OS and the IRSS, which was examined with the univariate Cox proportional risk model. Multivariate Cox regression analysis was used to establish the potential of the IRSS as an independent prognostic predictor. A nomogram was constructed by incorporating clinicopathological data from KIRC patients, including age, gender, histologic grade of the tumor, pathologic stage of the tumor, and IRSS; this was used to comprehensively evaluate patients' survival data. We used the "rms" package [version 6.2-0] and the 'survival' package [version 3.2-10] for these analyses.

In addition, decision curve analysis (DCA) were also generated across 1, 3, and 5 years to assess the suitability of nomograms for clinical use. The threshold probability percentage and net income are displayed in a graph (Figure 8) on the *x* and *y*-axes, respectively.

Verification of the IRSS

The TCGA-KIRP dataset (n = 256) was chosen to verify our IRSS model and assess the generalization of the signature since KIRC and KIRP tumors are anatomically and histologically quite similar. Every patient's risk score in the KIRP cohort was computed and ranked using the IRSS formula that we developed using the TCGA-KIRC dataset. The TCGA-KIRP cohort's cutoff values were used to classify the KIRP samples into groups with high- and low-risk as per the scores. The KM curve was used to compare survival across the two groups. The ROC curve was used to evaluate the precision of the signature prediction. In addition, the nomogram was used to evaluate the survival probabilities of the KIRP patients using clinicopathological data, including age, gender, histologic grade of the tumor, pathologic stage of the tumor, and the IRSS.

Results

Differential gene expression analysis

We first created a flow chart (Figure 1) to illustrate the steps followed in this study. The training set had samples from 539 KIRC patients along with 172 normal samples with data on gene expression, prognosis, and survival. A risk score model was

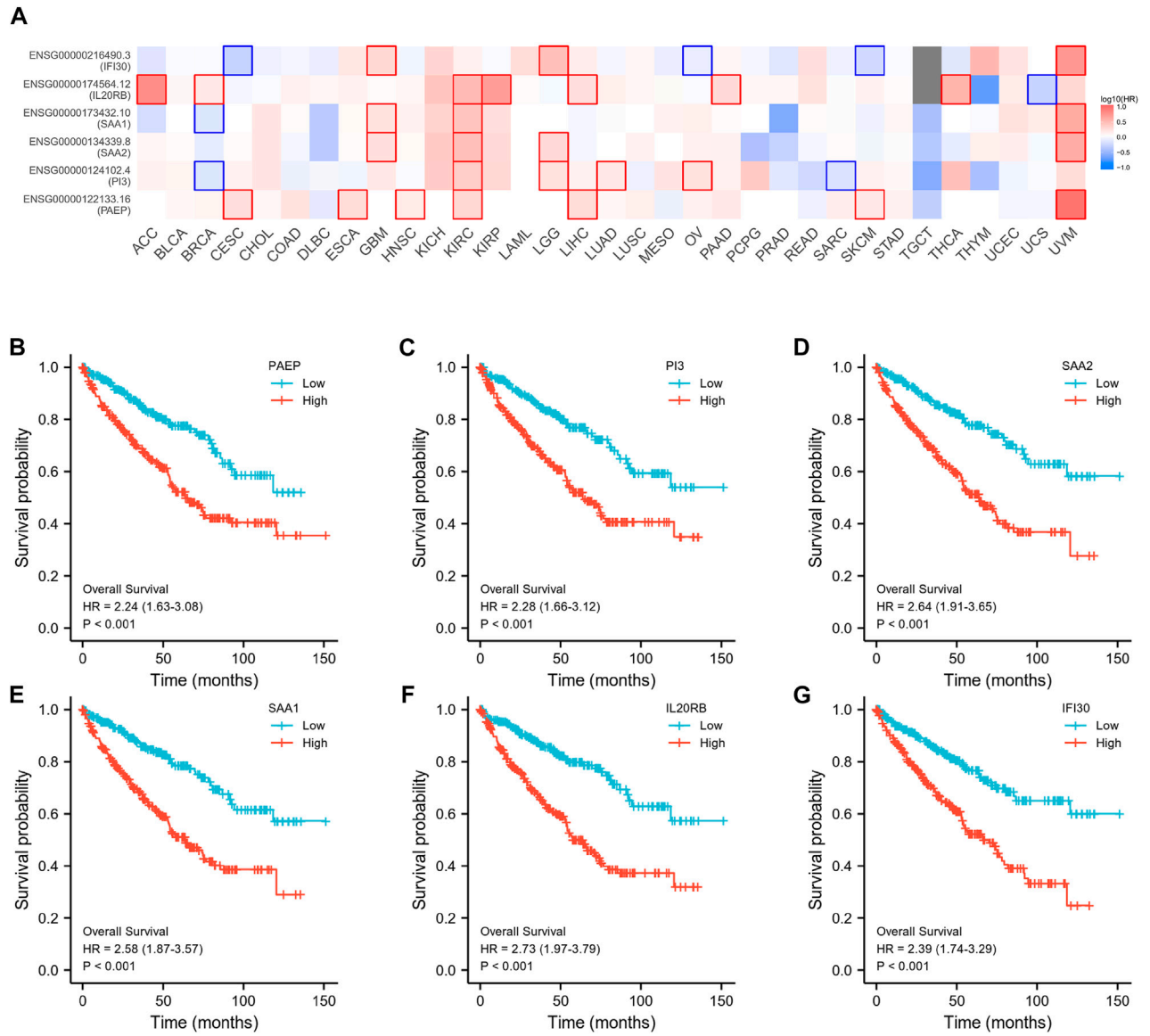

FIGURE 4
Prognostic analysis of six immunity-related genes in KIRC. **(A)** Establishment of an OS heatmap of these genes. **(B–G)** Survival analysis to investigate the association between the expression levels of PAEP, PI3, SAA2, SAA1, IL20RB, IFI30, and overall survival of KIRC.

developed based on the expression patterns of the immunity-related genes to predict the prognoses of the KIRC patients to examine if these genes can be used as biomarkers. The differential gene expression analysis identified 6,533 DEGs (|log2(FC)|>2 and p <0.05) as depicted in the volcano plot (Figure 2A) Supplementary Table S2. Of these, 5,055 were upregulated (logFC positive) and 1,478 were downregulated (logFC negative).

GO and KEGG analysis

GO and KEGG enrichment analyses were conducted to investigate the prospective relationship between immune activity and gene expression in the tumor and normal tissues in the TCGA-KIRC cohort. The DEGs were enriched in a range of processes in both tissue types, with immune-related pathways making up the majority of these processes. As per the KEGG enrichment analysis (Figure 3), natural killer cell-mediated cytotoxicity, cytokine-cytokine receptor interaction, BP modules implicated in receptor-ligand activity, cytokine receptor binding, and cytokine activity, in GO enrichment analysis. Collectively, these results demonstrate that certain immune genes are differentially expressed in KIRC tumors. Supplementary Table S3, S4 provide more details on the enrichment analysis results.

Construction and prognostic value of IRSS

According to the Venn diagram showing the overlay of the immunity-related genes and DEGs (Figure 2B); 487 DEIGs were

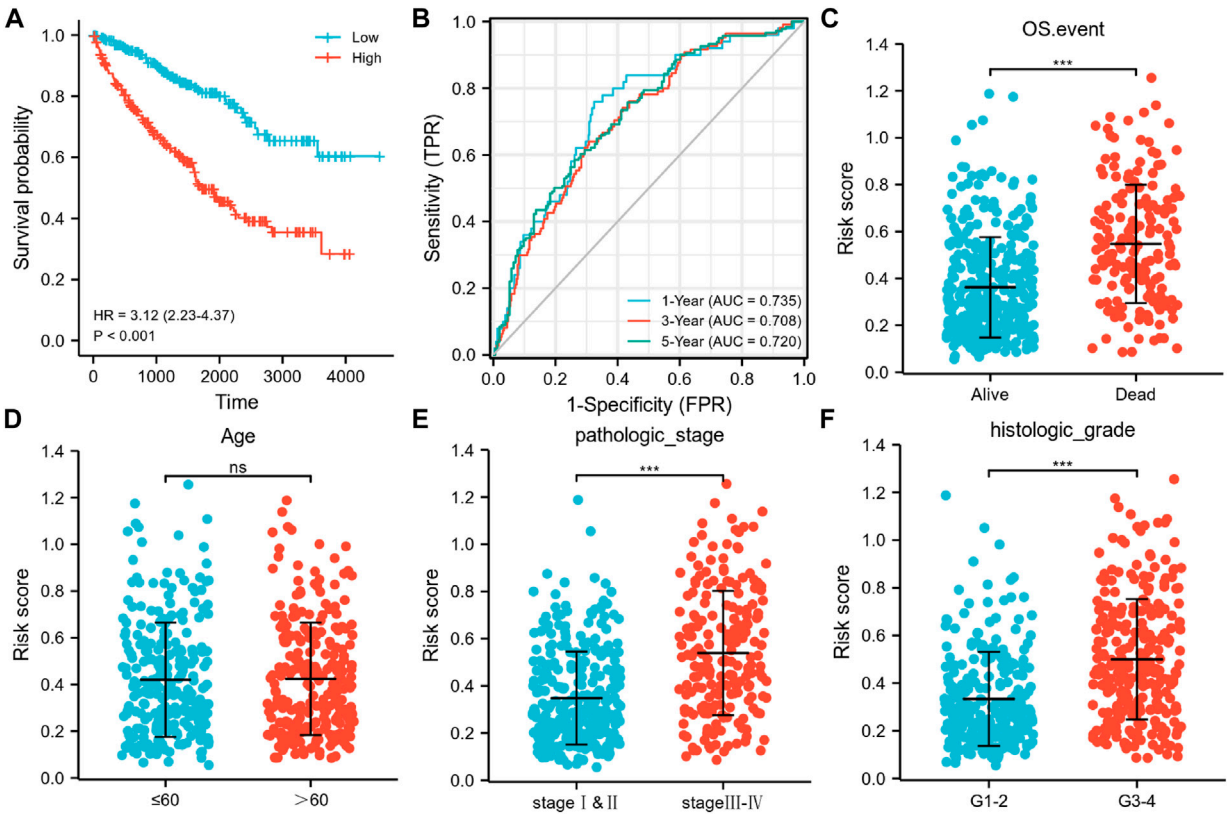

FIGURE 5
Associations of the six immunity-related genes signatures with OS, AUC curves, and clinicopathological features in KIRC. **(A)** Kaplan-Meier curve exhibited substantial variation in OS across the high- and low-risk groups in the TCGA-KIRC cohort. **(B)** Time-dependent ROC curves for predicting 1-, 3-, and 5-year survival rates. Relationship between signature risk scores and clinicopathological features in **(C)** OS events (Alive vs. Dead; unpaired Student's t-test, p <0.001), **(D)** age (>60 vs. ≤60; unpaired Student's t-test, p >0.05), **(E)** Pathological stage of tumor (stage I–II vs stage III–IV; unpaired Student's t-test, p <0.001), **(F)** Histological grade of tumor (G1–2 vs G3–4; unpaired Student's t-test, p <0.001).

identified (Supplementary Table S5; Figure 2B). Of these, six genes that had a strong link to prognosis were found during the LASSO regression analysis. Merging the results depicted in Figures 2D, E, the six immunity-related genes that were selected and included in the model were PAEP, PI3, SAA2, SAA1, IL20RB, and IFI30 (Figure 2C; Supplementary Table S6). The associated regression coefficients for these genes (β1–β6) were 0.067, 0.027, −0.174, 0.182, 0.038, and 0.346, respectively (Supplementary Table S7). The IRSS was developed using the following formula:

$$\begin{aligned}\text{IRSS} = {} & \text{EXP PAEP}*0.067 + \text{EXP PI3}*0.027 + \text{EXP SAA2} * -0.174 \\ & + \text{EXP SAA1}*0.182 + \text{EXP IL20RB} * 0.038 \\ & + \text{EXP IFI30}*0.346\end{aligned}$$

Subsequently, an OS heatmap of the six immune-related genes was generated (Figure 4A) and the relationship between the IRSS and prognosis in KIRC patients was examined using the Kaplan-Meier (K-M) plotter. As shown in Figures 4B–G, high expression levels of PAEP, PI3, SAA2, SAA1, IL20RB, and IFI30 is correlated with poor prognosis in patients with KIRC. We also analyzed the relationships between the expression levels of the six immunity-related genes and overall survival outcomes in KIRP. The results showed that high expression levels of SAA2, SAA1, and IL20RB are linked to poor prognosis (Supplementary Figure S1). Additionally, when the KIRC samples were split into low- and high-risk groups based on the IRSS, we found that patients in the high-risk group had poorer prognoses than those in the low-risk group (Figure 5A, log-rank p < 0.001; HR = 3.12, 95% CI = 2.23–4.37). Subsequently, the single-indicator ROC curve analysis indicated that AUC (Area under curve) values were 0.764, 0.521, 0.474, 0.568, 0.957, and 0.891, respectively. (Figure 6). Following this, the effectiveness of our model in predicting OS for KIRC patients was evaluated using the ROC curves. As shown in Figure 5B, the 1-, 3-, and 5-year AUC values were 0.735, 0.708, and 0.720, respectively, which demonstrates the model's reliability and accuracy in predicting patient prognosis.

Associations between the IRSS and the clinicopathological characteristics of KIRC

An investigation of the relationships between the clinicopathological characteristics and the IRSS revealed that the progression of KIRC was closely associated with the six immunity-related genes identified in this study. Patients with pathological stage III–IV and histologic grade G three to four tumors, and those

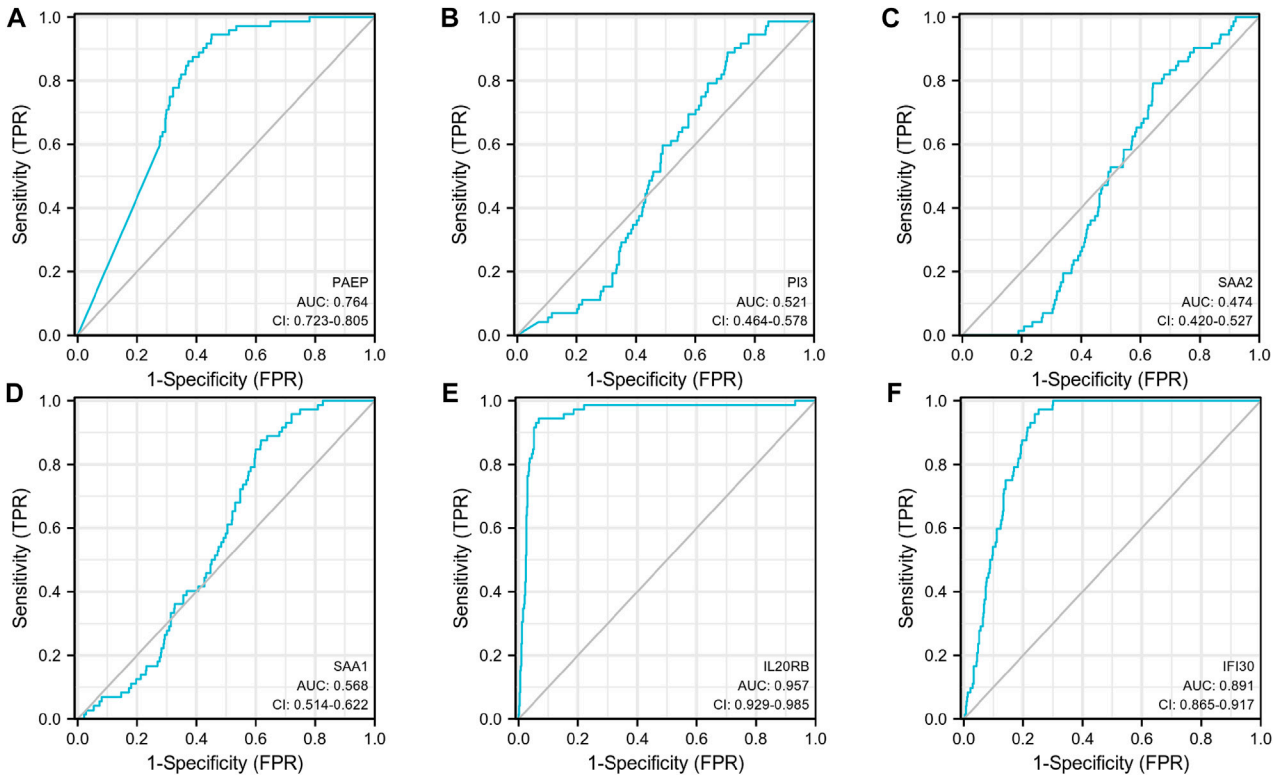

FIGURE 6
Single-indicator ROC curves for PAEP, PI3, SAA2, SAA1, IL20RB, and IFI30 for diagnosis of KIRC. **(A)** PAEP, **(B)** PI3, **(C)** SAA2, **(D)** SAA1, **(E)** IL20RB, **(F)** IFI30.

who died because of KIRC were found to have greater risk scores as compared to those with pathological stage I–II (p <0.001) and histologic grade G 1–2 (p <0.001) tumors and patients who survived (p <0.001; Figures 5C, E, F). No significant association between age and the IRSS were observed (p >0.05; Figure 5D). Overall, our findings demonstrated that the six immunity-related genes identified in this study are strongly linked to KIRC progression.

Correlations between immune infiltration and expression levels of PAEP, PI3, SAA2, SAA1, IL20RB, and IFI30

As shown in Figure 7, PAEP expression was significantly positively correlated with infiltration by regulatory T cells (Tregs), Th2 cells, and Th1 cells (p <0.001); PI3 expression was significantly positively correlated with infiltration by Tregs, macrophages, and Th2 cells (p <0.001); SAA2 expression was significantly positively correlated with infiltration by macrophages, Tregs, and B cells (p <0.001); SAA1 expression was significantly positively correlated with infiltration by Tregs, macrophages, and B cells (p <0.001); IL20RB expression was significantly positively correlated with infiltration of Tregs, Th1 cells, and macrophages (p <0.001); IFI30 expression was significantly positively correlated with infiltration by Tregs, NK CD56 bright cells, and T helper cells (p <0.001). Interestingly, we found that Tregs were positively associated with all the six genes identified in this study, with correlation coefficients of 0.385, 0.415, 0.399, 0.451, 0.485, and 0.333, respectively. We also analyzed the relationships between the six immunity-related genes identified here and 24 tumor-infiltrating immune cells in KIRP tissues. The results showed that the six immunity-related genes were also associated with multiple immune cell infiltration in KIRP (Supplementary Figure S2).

Prognostic significance of IRSS

We used univariate and multivariate Cox regression analyses to evaluate the prognostic significance of the IRSS that we have developed. According to univariate Cox regression analysis, in the TGGA-KIRC dataset, age, histologic grade, pathologic stage, and risk score, were all prognostic predictors, although gender was not (Figure 8A). According to the multivariate Cox regression analysis (Figure 8B, log-rank p < 0.001; HR = 3.334, 95% CI = 1.785–6.229; Table 1), the risk score was an independent prognostic predictor. According to the DCA (Figure 8C), the IRSS in combination with various clinicopathological characteristics has greater clinical applicability. According to the aforementioned findings, our IRSS can be employed as a robust and innovative prognostic biomarker for KIRC.

Nomograms are useful because they simplify statistical prediction models to single numerical estimates of event possibilities suited to specific patient characteristics (Iasonos et al., 2008). Since numerous clinical characteristics have prognostic significance in clinical practice, we constructed a

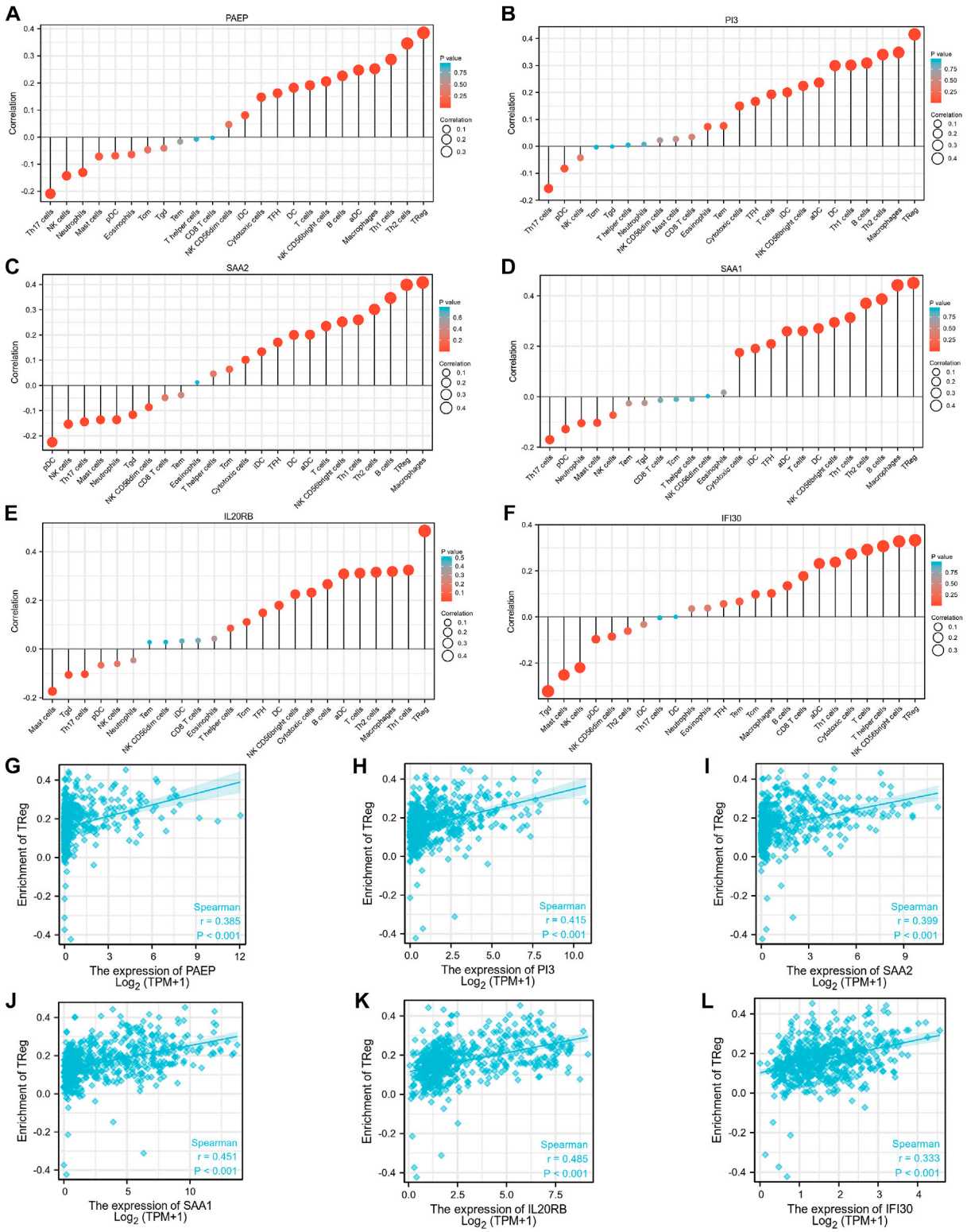

FIGURE 7
Associations between expression levels of the six immunity-related genes and infiltrating immune cells in patients with KIRC. **(A–F)** The associations between the expression levels of PAEP, PI3, SAA2, SAA1, IL20RB, and IFI30 and infiltration by immune cells. **(G–L)** The associations between expression levels of PAEP, PI3, SAA2, SAA1, IL20RB, IFI30 and infiltration by regulatory T cells in KIRC tissues.

nomogram using numerous clinicopathological characteristics and the IRSS to predict patient prognosis in KIRC. As depicted in Figure 8D, it is possible to compute and combine the scores of each variable to generate a prognosis. According to the DCA (Figure 8E), the nomogram's clinical application value is also higher when in combination with a variety of clinical variables.

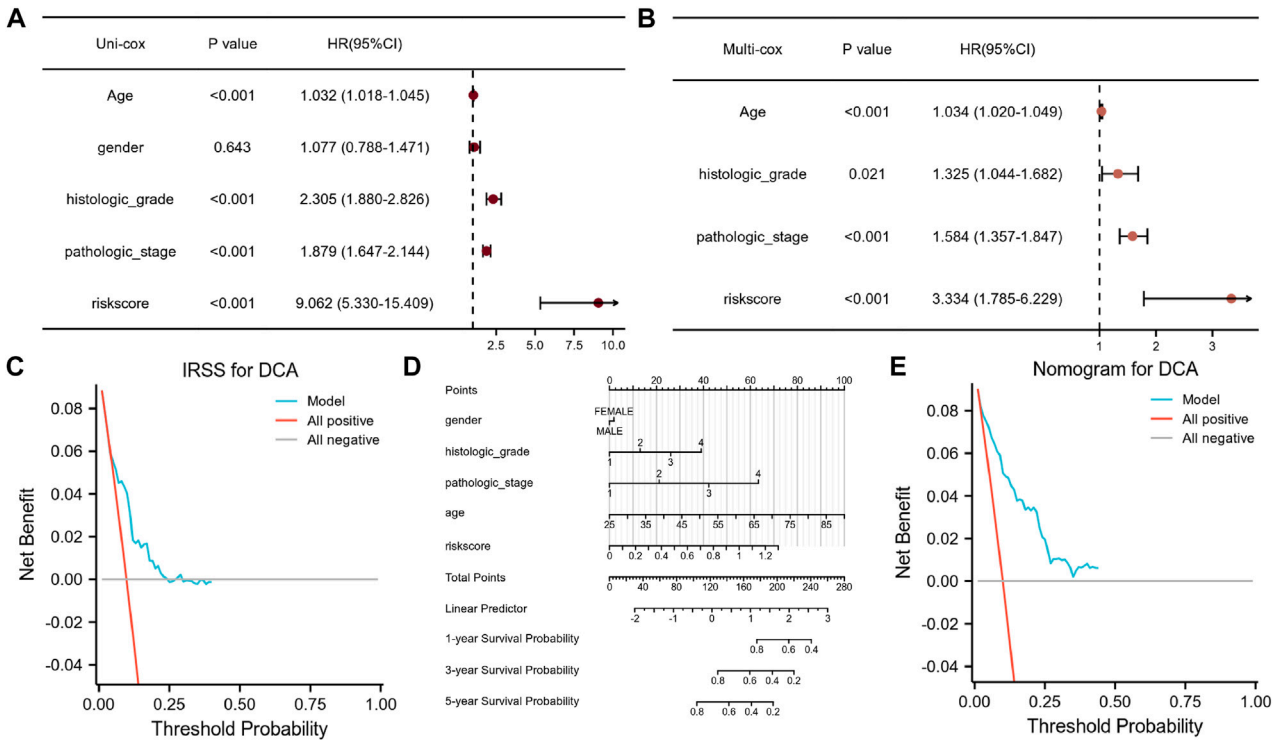

FIGURE 8
Assessment of the IRSS along with establishment and assessment of nomograms. **(A)** Univariate Cox regression analysis indicated that age, gender, histological grade of the tumor, pathological stage of the tumor, and risk score were correlated with OS in KIRC patients. **(B)** Multivariate Cox regression analysis indicated that the risk score was correlated with the OS in KIRC patients. **(C)** Decision curve analysis (DCA) for assessing the performance of the IRSS in prognostic prediction. **(D)** 1-, 3-, and 5-year nomograms for predicting OS in patients with KIRC. This nomogram incorporates the following five variables: Age, gender, histological grade of the tumor, pathological stage of the tumor, and IRSS. **(E)** Decision curve analysis (DCA) for the assessing the performance of the nomogram.

TABLE 1 Univariate and multivariate Cox regression analysis.

Characteristics	Total(N)	Univariate analysis		Multivariate analysis	
		Hazard ratio (95% CI)	*p*-value	Hazard ratio (95% CI)	*p*-value
gender	526				
MALE	346	Reference			
FEMALE	180	1.077 (0.788–1.471)	0.643		
histologic_grade	526	2.305 (1.880–2.826)	**<0.001**	1.325 (1.044–1.682)	**0.021**
pathologic_stage	526	1.879 (1.647–2.144)	**<0.001**	1.584 (1.357–1.847)	**<0.001**
age	526	1.032 (1.018–1.045)	**<0.001**	1.034 (1.020–1.049)	**<0.001**
riskscore	526	9.062 (5.330–15.409)	**<0.001**	3.334 (1.785–6.229)	**<0.001**

Bolded font means statistically significant.

Verification of IRSS using the TCGA-KIRP cohort

Data from the TCGA-KIRP cohort were used as a verification dataset to validate the usability of the IRSS that we have developed for RCCs. After the individual patients' risk scores were computed as per the IRSS equation mentioned before (Supplementary Table S8), the KIRP samples were classified into low- and high-risk groups using the median IRSS value. We found that the risk score was negatively correlated with the OS rates (Figure 9A). In addition, the KM analysis (Figure 9B) indicated that the patients in the low-risk group had significantly better prognoses than those in the high-risk group (log-rank $p = 0.049$; HR = 1.84, 95% CI = 1.02–3.32. The model performed well in predicting OS as demonstrated by the AUCs of the survival ROC curves which were 0.601, 0.571, and 0.518 over 1, 3, and 5 years, respectively (Figure 9C). Several clinical features including

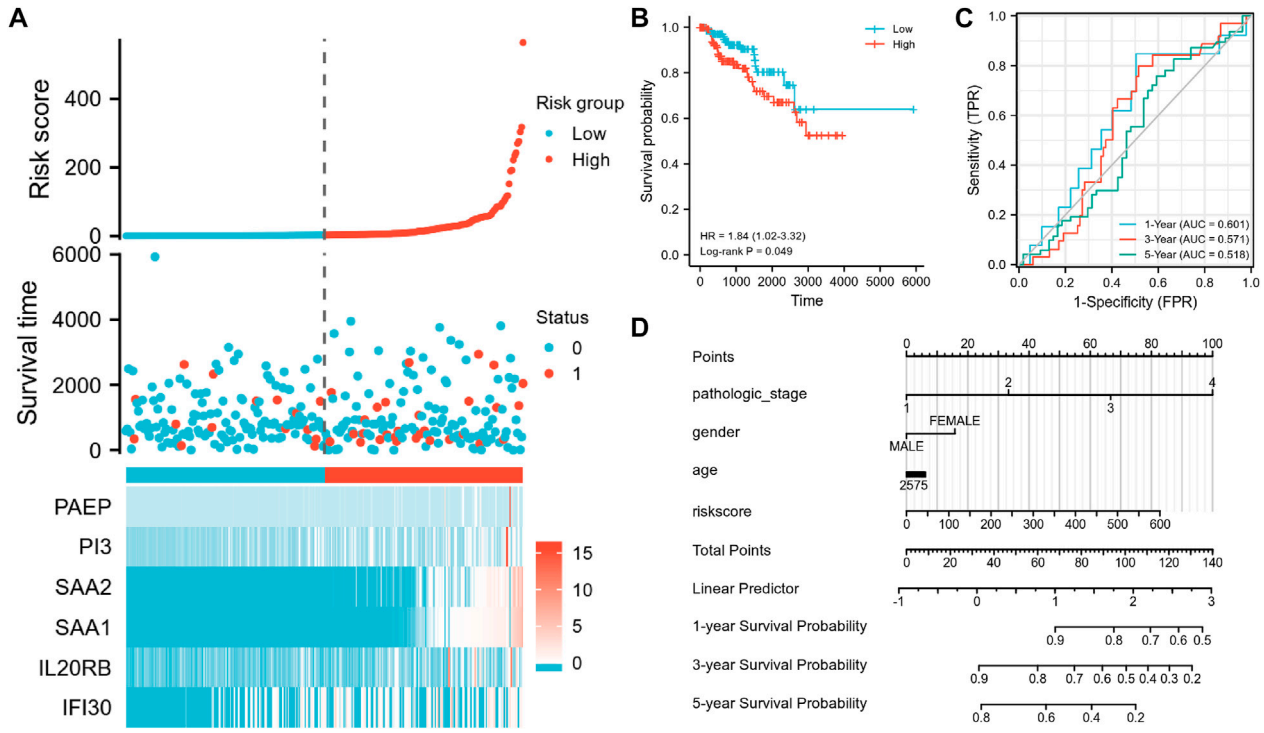

FIGURE 9
Validation of the IRSS signature with the TCGA-KIRP dataset. **(A)** Risk scores, survival status, and heat maps of the six immunity-related genes in KIRP patients. **(B)** Kaplan-Meier curve exhibited significant differences in OS between the high- and low-risk groups in TCGA-KIRP. **(C)** Time-dependent ROC curves for predicting 1-, 3- and 5-year survival rates. **(D)** 1-,3-, and 5-year nomograms for predicting OS in patients with KIRP. This nomogram incorporates the following four variables: Age, gender, pathology stage, and IRSS. 0 represents the survival status "alive" and one represents the survival status "dead."

age, gender, and pathologic stage of the tumor together with IRSS were utilized to construct a nomogram for predicting prognostic survival over 1, 3, and 5 years (Figure 9D).

Collectively, the IRSS that we have developed has potential as a prognostic predictive biomarker for both KIRC and KIRP and may be useful in other RCCs also.

Discussion

In this study, we investigated the possibility of using immunity-related genes in developing a prognostic biomarker for RCCs. To do this, we used the TCGA-KIRC database as a training set. The differential gene analysis was performed to identify DEGs between the tumor and normal tissues in KIRC patients. Following this, GO and KEGG enrichment analyses were conducted on the DEGs to identify immune and tumor-related genes which were upregulated. Our results support earlier reports that IAGs are vital to the onset and advancement of KIRC (Shen et al., 2020).

Subsequently, we used the Cox proportional hazard model and LASSO regression analysis to select immunity-related genes from the DEGs identified through the previous analyses. We identified six independent immunity-related genes associated with KIRC prognosis. Data on these genes were integrated to create an IRRS model to predict patient prognosis for KIRC.

The progestagen-associated endometrial protein (PAEP), which is a member of the lipocalin family of glycoproteins, is one of the six genes identified in this study and functions as a negative controller of T cell receptor-mediated activation. In melanomas, tumor cells secrete PAEP which can inhibit the activation, proliferation, and cytotoxicity of T lymphocytes (Ren et al., 2015). The PI3-kinase/Akt signaling pathway is active in most RCCs. A recent study showed that dual inhibition of PI3K/mTOR by NVP-BEZ235 triggered growth arrest in RCC cell lines both *in vivo* and *in vitro* (Cho et al., 2010). SAA2 expression was positively linked to the disease stage of non-small cell lung cancer (Zhang et al., 2021). Another study has shown that SAA1 may be used as a biomarker for diagnosis and prognosis in advanced KIRC cases (Li et al., 2021). Many human malignancies exhibit dysregulated IL20RB expression, which is remarkably high in KIRC. Previous work has shown that IL20RB can be used as a prognostic biomarker for tracking KIRC treatment (Guo et al., 2022). Abnormal expression of IFI30 has also been found in many human tumors. For example, IFI30 overexpression is linked to the occurrence of high-grade tumors, immune infiltration, and worse OS in glioma (Jiang et al., 2021).

The KM analysis indicates that the IRSS model that we have developed is a robust biomarker for predicting patient prognosis in KIRC. The differences in OS between the high- and low-risk groups were statistically significant. Additionally, the survival ROC data showed that our model's ability to predict prognosis was in line with real-world outcomes. Furthermore, survival analysis with clinicopathological data (such as age, histologic grade of tumor, pathologic stage of tumor, and gender) as covariates, showed that our IRSS model was still a reliable and independent prognostic predictor. We also developed a nomogram to predict patient survival using the IRSS and clinicopathologic data. The DCA results demonstrated that the IRSS that we have developed had

greater accuracy in predicting patient prognosis than the conventional prediction using (tumor node metastasis, TNM) stage. Furthermore, we also found that the nomogram using clinical data along with the IRSS could make better predictions of patient prognosis for KIRC.

We have also investigated the relationships between the expression levels of six IAGs in KIRC and tumor infiltration by 24 different types of immune cells. Our results show that the expression levels of these six IAGvary substantially in the different infiltrating immune cells and that these expression levels were significantly and positively correlated with immune infiltration by Tregs. Immune homeostasis is influenced by Treg cells, which have high expression levels of the forkhead box P3 transcription factor (FOXP3) (Kasagi et al., 2014; Li et al., 2015; Ni et al., 2018). In the supplementary material, we also provide the results of an analysis that looks at the relationship between FOXP3 expression and the expression levels of the six IAGs in KIRC tissues. The results show a significantly positive association between these variables (Supplementary Figure S3). Similar results were found in KIRP tissues also (Supplementary Figure S4). Previous research has demonstrated that there are various mechanisms by which Treg cells can control the growth of tumors, including affecting the expression of immune checkpoint molecules (CTLA-4, ICOS, LAG-3) and secreting immunosuppressive cytokines (IL-10 and TGF-β) (Gu et al., 2022). Therefore, targeting these six IAGs may become an alternative strategy for tumor immunotherapy in treating KIRC.

The highly complex processes of tumor development and progression in RCCs are regulated by several genes. Currently, there are numerous relevant prognostic models for patients with KIRC as a result of an increase in interest in this area of research (Xu et al., 2020b; Wu et al., 2021). We used the LASSO regression analysis to establish a risk model linked to immunity-related genes for patients with KIRC. LASSO regression is a compressed estimation technique. By creating a penalty mechanism, constricting a few coefficients, and zeroing out some coefficients, it can produce a more refined model than univariate and multifactorial regression. It can also perform variable selection simultaneously with parameter estimation and is thus better at addressing the multicollinearity problems in regression analysis than univariate and multifactorial regression. The drawbacks, however, of this model are that it is difficult to calibrate when some coefficients are compressed, which results in underfitting of the data.

Our work has used the expression profiles of PAEP, PI3, SAA2, SAA1, IL20RB, and IFI30 to develop an IRSS model to predict the prognoses of patients with KIRC. In addition, we also generated 1-, 3- and 5-year ROC curves for patients with KIRC on the basis of the risk model; we find that our prognostic model is likely to offer a more thorough and individualized scheme of treatment. The IRSS that we have developed can not only predict clinical prognosis but can also reflect the immune status of patients with KIRC. However, the interaction among these six genes and their potential role in predicting prognosis, especially response to immunotherapy for KIRC, still needs to be investigated.

We also analyzed the mRNA expression levels of the six immunity-related genes identified in this study in KIRC and KIRP tissues. We find that the expression levels of all six immunity-related genes expression were higher in KIRP tumor tissues than in normal tissues (Supplementary Figure S5). However, only PAEP, SAA1, and IL20RB were overexpressed in KIRC tissues as compared to normal tissues (Supplementary Figure S6). These differences in expression need to be further verified. In addition, we investigated the protein levels of these six immunity-related genes in tumor tissues (KIRC/KIRP) and normal tissues using data from the human protein atlas (HPA) database (Supplementary Figure S7). We find that the protein levels and mRNA levels are not always consistent; this needs to be further investigated through immunohistochemistry studies.

Conclusion

In summary, we have developed a new and reliable biomarker for predicting the prognosis of patients with KIRC using six immunity-related genes. The IRSS model developed was found to be quite robust and may be useful for clinical application. Our observations need to be verified with further research and additional experimental investigation.

Data availability statement

The datasets presented in this study can be found in online repositories. The names of the repository/repositories and accession number(s) can be found in the article/Supplementary Material.

Author contributions

TW and YL wrote the main manuscript text and DW prepared Figures 1–3, HP C prepared Figures 4–6, LY prepared Figures 7–9, QX prepared Supplementary tables and figures. QL supervised this work. All authors have read and approved the manuscript.

Funding

This study was supported by the President Foundation of The Fifth Affiliated Hospital, Southern Medical University (YZ2022ZX09).

Conflict of interest

The authors declare that the research was conducted in the absence of any commercial or financial relationships that could be construed as a potential conflict of interest.

Publisher's note

Supplementary material

The Supplementary Material for this article can be found online at: https://www.frontiersin.org/articles/10.3389/fgene.2023.1107294/full#supplementary-material

References

Alhamzawi, R., and Ali, H. T. M. (2018). The Bayesian adaptive lasso regression. *Math. Biosci.* 303, 75–82. doi:10.1016/j.mbs.2018.06.004

Atkins, M. B., and Tannir, N. M. (2018). Current and emerging therapies for first-line treatment of metastatic clear cell renal cell carcinoma. *Cancer Treat. Rev.* 70, 127–137. doi:10.1016/j.ctrv.2018.07.009

Bindea, G., Mlecnik, B., Tosolini, M., Kirilovsky, A., Waldner, M., Obenauf, A. C., et al. (2013). Spatiotemporal dynamics of intratumoral immune cells reveal the immune landscape in human cancer. *Immunity* 39, 782–795. doi:10.1016/j.immuni.2013.10.003

Chen, V. J., Hernandez-Meza, G., Agrawal, P., Zhang, C. A., Xie, L., Gong, C. L., et al. (2019). Time on therapy for at least three months correlates with overall survival in metastatic renal cell carcinoma. *Cancers (Basel)* 11 (7), 1000. doi:10.3390/cancers11071000

Cho, D. C., Cohen, M. B., Panka, D. J., Collins, M., Ghebremichael, M., Atkins, M. B., et al. (2010). The efficacy of the novel dual PI3-kinase/mTOR inhibitor NVP-BEZ235 compared with rapamycin in renal cell carcinoma. *Clin. Cancer Res.* 16 (14), 3628–3638. doi:10.1158/1078-0432.CCR-09-3022

DeLong, E. R., DeLong, D. M., and Clarke-Pearson, D. L. (1988). Comparing the areas under two or more correlated receiver operating characteristic curves: A nonparametric approach. *Biometrics* 44, 837–845.

Ghatalia, P., Gordetsky, J., Kuo, F., Dulaimi, E., Cai, K. Q., Devarajan, K., et al. (2019). Prognostic impact of immune gene expression signature and tumor infiltrating immune cells in localized clear cell renal cell carcinoma. *J. Immunother. Cancer* 7 (1), 139. doi:10.1186/s40425-019-0621-1

Gu, J., Zhou, J., Chen, Q., Xu, X., Gao, J., Li, X., et al. (2022). Tumor metabolite lactate promotes tumorigenesis by modulating MOESIN lactylation and enhancing TGF-β signaling in regulatory T cells. *Cell Rep.* 39 (12), 110986. doi:10.1016/j.celrep.2022.110986

Guo, H., Jiang, S., Sun, H., Shi, B., Li, Y., Zhou, N., et al. (2022). Identification of IL20RB as a novel prognostic and therapeutic biomarker in clear cell renal cell carcinoma. *Dis. Markers* 2022, 9443407. doi:10.1155/2022/9443407

Huang, H., Liu, Q., Zhu, L., Zhang, Y., Lu, X., Wu, Y., et al. (2019). Prognostic value of preoperative systemic immune-inflammation index in patients with cervical Cancer. *Sci. Rep.* 9, 3284. doi:10.1038/s41598-019-39150-0

Iasonos, A., Schrag, D., Raj, G. V., and Panageas, K. S. (2008). How to build and interpret a nomogram for cancer prognosis. *J. Clin. Oncol.* 26, 1364–1370. doi:10.1200/JCO.2007.12.9791

Jia, E., Ren, N., Guo, B., Cui, Z., Zhang, B., and Xue, J. (2022). Construction and validation of a novel prognostic model for lung squamous cell cancer based on N6-methyladenosine-related genes. *World J. Surg. Oncol.* 20 (1), 59. doi:10.1186/s12957-022-02509-1

Jiang, W., Zheng, F., Yao, T., Gong, F., Zheng, W., and Yao, N. (2021). IFI30 as a prognostic biomarker and correlation with immune infiltrates in glioma. *Ann. Transl. Med.* 9 (22), 1686. doi:10.21037/atm-21-5569

Kasagi, S., Zhang, P., Che, L., Abbatiello, B., Maruyama, T., Nakatsukasa, H., et al. (2014). *In vivo*-generated antigen-specific regulatory T cells treat autoimmunity without compromising antibacterial immune response. *Sci. Transl. Med.* 6, 241ra78. doi:10.1126/scitranslmed.3008895

Li, S., Cheng, Y., Cheng, G., Xu, T., Ye, Y., Miu, Q., et al. (2021). High SAA1 expression predicts advanced tumors in renal cancer. *Front. Oncol.* 11, 649761. doi:10.3389/fonc.2021.649761

Li, Z., Li, D., Tsun, A., and Li, B. (2015). FOXP3+ regulatory T cells and their functional regulation. *Cell. Mol. Immunol.* 12, 558–565. doi:10.1038/cmi.2015.10

Liu, J., Nie, S., Wu, Z., Jiang, Y., Wan, Y., Li, S., et al. (2020). Exploration of a novel prognostic risk signatures and immune checkpoint molecules in endometrial carcinoma microenvironment. *Genomics* 112 (5), 3117–3134. doi:10.1016/j.ygeno.2020.05.022

Motzer, R. J., Escudier, B., McDermott, D. F., George, S., Hammers, H. J., Srinivas, S., et al. (2015). Nivolumab versus everolimus in advanced RenalCell carcinoma. *N. Engl. J. Med.* 373, 1803–1813. doi:10.1056/NEJMoa1510665

Ni, X., Tao, J., Barbi, J., Chen, Q., Park, B. V., Li, Z., et al. (2018). YAP is essential for Treg-mediated suppression of antitumor immunity. *Cancer Discov.* 8, 1026–1043. doi:10.1158/2159-8290.cd-17-1124

Powles, T., Tomczak, P., Park, S. H., Venugopal, B., Ferguson, T., Symeonides, S. N., et al. (2022). Pembrolizumab versus placebo as post-nephrectomy adjuvant therapy for clear cell renal cell carcinoma (KEYNOTE-564): 30-month follow-up analysis of a multicentre, randomised, double-blind, placebo-controlled, phase 3 trial. *Lancet Oncol.* 23 (9), 1133–1144. doi:10.1016/S1470-2045(22)00487-9

Qu, Y., Zhang, S., Zhang, Y., Feng, X., and Wang, F. (2020). Identification of immune-related genes with prognostic significance in the microenvironment of cutaneous melanoma. *Virchows Arch.* 478, 943–959. doi:10.1007/s00428-020-02948-2949

Ren, S., Chai, L., Wang, C., Li, C., Ren, Q., Yang, L., et al. (2015). Human malignant melanoma-derived progestagen-associated endometrial protein immunosuppresses T lymphocytes *in vitro*. *PLoS One* 10 (3), e0119038. doi:10.1371/journal.pone.0119038

Ricketts, C. J., De Cubas, A. A., Fan, H., Smith, C. C., Lang, M., Reznik, E., et al. (2018). The cancer Genome atlas comprehensive molecular characterization of renal cell carcinoma. *Cell Rep.* 23, 313–326.e5. e5. doi:10.1016/j.celrep.2018.03.075

Shen, C., Liu, J., Wang, J., Zhong, X., Dong, D., Yang, X., et al. (2020). Development and validation of a prognostic immune-associated gene signature in clear cell renal cell carcinoma. *Int. Immunopharmacol.* 81, 106274. doi:10.1016/j.intimp.2020.106274

Shen, S., Wang, G., Zhang, R., Zhao, Y., Yu, H., Wei, Y., et al. (2019). Identification of immune-related genes with prognostic significance in the microenvironment of cutaneous melanoma. *EBioMedicine* 40, 318–326. doi:10.1007/s00428-020-02948-9

Siegel, R. L., Miller, K. D., and Jemal, A. (2017). Cancer statistics. *CA Cancer J. Clin.* 67, 7–30. doi:10.3322/caac.21387

Wang, J., Yu, S., Chen, G., Kang, M., Jin, X., Huang, Y., et al. (2020). A novel prognostic signature of immune-related genes for patients with colorectal cancer. *J. Cell Mol. Med.* 24 (15), 8491–8504. doi:10.1111/jcmm.15443

Wu, G., Xu, Y., Zhang, H., Ruan, Z., Zhang, P., Wang, Z., et al. (2021). A new prognostic risk model based on autophagy-related genes in kidney renal clear cell carcinoma. *Bioengineered* 12 (1), 7805–7819. doi:10.1080/21655979.2021.1976050

Xu, K., He, J., Zhang, J., Liu, T., Yang, F., and Ren, T. (2020). A novel prognostic risk score model based on immune-related genes in patients with stage IV colorectal cancer. *Biosci. Rep.* 40 (10), BSR20201725. doi:10.1042/BSR20201725

Xu, W. H., Xu, Y., Wang, J., Wan, F. N., Wang, H. K., Cao, D. L., et al. (2019). Prognostic value and immune infiltration of novel signatures in clear cell renal cell carcinoma microenvironment. *Aging (Albany NY)* 11 (17), 6999–7020. doi:10.18632/aging.102233

Xu, Y., Li, X., Han, Y., Wang, Z., Han, C., Ruan, N., et al. (2020). A new prognostic risk model based on PPAR pathway-related genes in kidney renal clear cell carcinoma. *PPAR Res.* 2020, 6937475. doi:10.1155/2020/6937475

Zeng, J. H., Liang, L., He, R. Q., Tang, R. X., Cai, X. Y., Chen, J. Q., et al. (2017). Comprehensive investigation of a novel differentially expressed lncRNA expression profile signature to assess the survival of patients with colorectal adenocarcinoma. *Oncotarget* 8, 16811–16828. doi:10.18632/oncotarget.15161

Zhang, F. F., Han, B., Xu, R. H., Zhu, Q. Q., Wu, Q. Q., Wei, H. M., et al. (2021). Identification of plasma SAA2 as a candidate biomarker for the detection and surveillance of non-small cell lung cancer. *Neoplasma* 68 (6), 1301–1309. doi:10.4149/neo_2021_210228N263

Zhang, J., Huang, C., Yang, R., Wang, X., Fang, B., Mi, J., et al. (2022). Identification of immune-related subtypes and construction of a novel prognostic model for bladder urothelial cancer. *Biomolecules* 12 (11), 1670. doi:10.3390/biom12111670

frontiers | Frontiers in Genetics

TYPE Systematic Review
PUBLISHED 20 January 2023
DOI 10.3389/fgene.2022.1072229

OPEN ACCESS

EDITED BY
Simin Li,
Southern Medical University, China

REVIEWED BY
Maher Hendi,
Sir Run Run Shaw Hospital, China
Mingqiang Kang,
Fujian Medical University Union Hospital, China
Xiaopei Liu,
Shaanxi University of Chinese Medicine, China

*CORRESPONDENCE
Yu Zhang,
yuzhang0106@163.com

SPECIALTY SECTION
This article was submitted to Cancer Genetics and Oncogenomics, a section of the journal Frontiers in Genetics

RECEIVED 17 October 2022
ACCEPTED 07 December 2022
PUBLISHED 20 January 2023

CITATION
Qiu H, Zhang L, Wang D, Miao H and Zhang Y (2023), Comparisons of short-term and long-term results between laparoscopic between open pancreaticoduodenectomy for pancreatic tumors: A systematic review and meta-analysis.
Front. Genet. 13:1072229.
doi: 10.3389/fgene.2022.1072229

Comparisons of short-term and long-term results between laparoscopic between open pancreaticoduodenectomy for pancreatic tumors: A systematic review and meta-analysis

Hongquan Qiu[1], Liang Zhang[2], Dongzhi Wang[3], Haiyan Miao[4] and Yu Zhang[5]*

[1]Department of Surgery, Liuqiao Central Hospital, Nantong, China, [2]Department of General Surgery, Tengzhou Central People's Hospital, Tengzhou, China, [3]Department of Hepatobiliary and Pancreatic Surgery, Affiliated Hospital of Nantong University, Nantong, China, [4]Department of General Surgery, The Sixth People's Hospital of Nantong, Nantong, China, [5]Department of Laboratory Medicine, Haimen Hospital Affiliated to Xinglin College of Nantong University, Nantong, China

Objective: The efficacy of pancreaticoduodenectomy and open pancreaticoduodenectomy for pancreatic tumors is controversial. The study aims to compare the efficacy of laparoscopic pancreaticoduodenectomy (LPD) and open pancreaticoduodenectomy (OPD) in the treatment of pancreatic tumors through systematic evaluation and meta-analysis.

Methods: PubMed, Embase, Cochrane Library and Web of science databases were searched for clinical studies on the treatment of pancreatic tumors with LPD and OPD. The end time for the searches was 20 July 2022. Rigorous inclusion and exclusion criteria were used to screen the articles, the Cochrane manual was used to evaluate the quality of the included articles, and the stata15.0 software was used for statistical analysis of the indicators.

Results: In total, 16 articles were included, including two randomized controlled trials and 14 retrospective studies. Involving a total of 4416 patients, 1275 patients were included in the LPD group and 3141 patients in the OPD group. The results of the meta-analysis showed that: the operation time of LPD was longer than that of OPD [WMD = 56.14,95% CI (38.39,73.89), $p = 0.001$]; the amount of intraoperative blood loss of LPD was less than that of OPD [WMD = −120.82,95% CI (−169.33, −72.30), $p = 0.001$]. No significant difference was observed between LPD and OPD regarding hospitalization time [WMD = −0.5,95% CI (−1.35, 0.35), $p = 0.250$]. No significant difference was observed regarding postoperative complications [RR = 0.96,95% CI (0.86,1.07, $p = 0.463$]. And there was no significant difference regarding 1-year OS and 3-year OS: 1-year OS [RR = 1.02,95% CI (0.97,1.08), $p = 0.417$], 3-year OS [RR = 1.10 95% CI (0.75, 1.62), $p = 0.614$%].

Conclusion: In comparison with OPD, LPD leads to less blood loss but longer operation time, therefore the bleeding rate per unit time of LPD is less than that

of OPD. LPD has obvious advantages. With the increase of clinical application of LPD, the usage of LPD in patients with pancreatic cancer has very good prospect. Due to the limitations of this paper, in future studies, more attention should be paid to high-quality, multi-center, randomized controlled studies.

KEYWORDS

laparoscopic, pancreaticoduodenectomy, pancreatic tumors, meta-analysis, surgery

1 Introduction

Pancreatic cancer is the 12th most common malignant tumor in the world, and the seventh leading cause of death from cancer, with a 5-year survival rate of only 10% (Chang et al., 2022). In the past 25 years, the global burden of pancreatic cancer has doubled, and it is now ranking among the top 10 cancer deaths in more than 130 countries (Klein, 2021). According to the latest data of the American *Cancer* Association, there were about 60,430 new patients with pancreatic cancer in 2021, of which 48,220 died. It is expected that it will become the second leading cause of death from cancer in the United States within the next 20–30 years (Siegel et al., 2021). Among the European Union, pancreatic cancer is expected to surpass breast cancer and become the third leading cause of death related to cancer (Carioli et al., 2021). In China, the 5-year survival rate of pancreatic cancer has not been significantly ameliorated in the past 10 years, with a number of only 9.9%. With population growth, the growth of the aging propulation and the influence of Western lifestyles, the incidence rate of pancreatic cancer is expected to continue to rise in the next few years (Sun et al., 2020). As a digestive tract tumor with extremely poor prognosis, the main treatment for pancreatic cancer is still a multidisciplinary approach based on traditional open surgery (Neoptolemos et al., 2018; Chang et al., 2022). Pancreatoduodenectomy is the conventional surgical treatment for periampullary malignant tumors (Kawai and Yamaue, 2011). However, due to the limitations of OPD, such as the strong trauma that it causes, slow postoperative recovery, and long hospitalization time, as well as the continuously rising expectations for diagnosis and treatment methods from the patients, surgeons are constantly pursuing to make surgeries as minimally invasive as possible (Scialpi et al., 2016; Iovanna and Dusetti, 2017; Miller et al., 2020).

In recent years, surgical treatment for pancreatic cancer has gradually developed towards minimally invasive (Heestand et al., 2015). Minimally invasive surgery does not involve digestive tract anastomosis and reconstruction, with little technical difficulty and small incisions. The visual field can be magnified by 5–10 times under laparoscopy, which can enter into narrow spaces to obtain a field of vision unmatched by open surgery. The operative field is clearer, and the surgeries are more refined. Combined with advanced medical devices such as endoscopic cutter-staplers, ultrasonic knives, energy platforms, etc., it can very well achieve the dissection, dissociation, resection and anastomosis of some particular places, reduce the pain at the site of incision after surgery, contribute to the aesthetic appearance of the incision, and reduce trauma to the patients' minds (Harrison et al., 2022). In addition, the magnified vision of laparoscopy provides more detailed anatomical opportunities for operators, and improves the safety of the surgery and the thoroughness of clearing (Pisters et al., 2001; Zhang et al., 2011; Cesaretti et al., 2017). However, the high recurrence rate after minimally invasive surgery, the high incidence of severe pancreatic fistula and the long operation time are still unsolved problems (Sciuto et al., 2014; Kuesters et al., 2018). Although the operation time of open surgery is short, the amount of blood loss during operation is large. Therefore, whether to choose open surgery or minimally invasive surgery for the treatment of pancreatic cancer is still a subject of great controversy (Zhang et al., 2011; Zhou et al., 2019). It is hoped that through this study, we can solve this controversy and provide a foundation for the selection of intervention (surgery) for the treatment of pancreatic cancer in clinic.

2 Methods

The study was registered with PROSPERO and followed PRISMA-P (the preferred reporting project for system review and meta-analysis scheme) guidelines.

2.1 Literature search

We searched the following English databases: PubMed, EMBASE, Cochrane Library and Web of science, with keywords such as laparoscopy, pancreatoduodenectomy, pancreatic cancer, etc. The search period was set from the foundation of the database to 20 July 2022. We searched the databases for clinical studies about LPD and OPD as treatment methods for pancreatic cancer. See Supplementary Table S1 for PubMed retrieval strategy.

2.2 Inclusion and exclusion criteria

Inclusion criteria: for those who met the diagnostic criteria for pancreatic cancer (Okusaka et al., 2020) and were older than

18 years old, LPD and OPD were used as intervention. The primary outcome indicators were: operation time, amount of intraoperative blood loss, hospitalization time, overall survival rate (OS). The secondary outcome indicators were: postoperative complications. Randomized controlled trials and retrospective studies were included in this study. Systematic reviews, repeatedly published articles, case reports, protocols, animal experiments, conference summaries, full texts unable to be obtained, articles without usable data; articles meeting the above criteria were excluded.

2.3 Literature and data extraction

Two researchers (HQQ and LZ) independently screened the studies to extract data. Preliminary screening was conducted by reading the titles and abstracts of the different literature, and for the ones that were easy to judge, literature screening was directly conducted; for literature that raised objections about whether they could be included, relevant teachers were consulted, and they were screened by directly downloading and reading the full texts. During the screening process, all the inclusion and exclusion criteria were strictly followed. Two researchers independently extracted the outcome indicators' data from the studies, and the extracted information were cross checked in order to ensure the consistency of the extracted data. The extracted data included: first author, year of publication, experimental design, country, sample size, age, follow-up and outcome indicators.

2.4 Quality evaluation of the included literature

The quality evaluation of the included studies was independently completed by two researchers. For randomized controlled trials, the bias analysis evaluation tool provided by Cochrane Handbook for Systematic Reviews of Interventions 5.1.0 was used, in an effort to evaluate the quality of the included studies. The evaluation included seven aspects: generation of random sequence (selection bias), allocation concealment (selection bias), blinding of the implementers and participants (implementation bias), blinding of outcome evaluators (observation bias), integrity of data results (follow-up bias), selective reporting of research results (reporting bias), and other sources of bias. For retrospective studies, the Newcastle Ottawa Scale (NOS) was utilized to evaluate the quality of the cohort studies or case-control studies. The NOS scale includes two forms: one for cohort studies and one for case-control studies. The cohort study form includes eight items within three domains: study population selection, comparability between groups and result measurement. The case-control study form also includes eight items within three domains: study population selection, comparability between groups, and measurement of exposure factors. If the requirements are met, one point is scored, with a full score of nine points, and ≥five points is considered as high-quality literature.

2.5 Statistical analysis

Meta-analysis of data was carried out by using the Stata15.0 software. Continuous variables were expressed by weighted mean difference (WMD) and 95% confidence interval (CI), and binary variables were represented by relative risk (RR) and 95% confidence interval (CI). The heterogeneity of each study was tested. When $p \geq 0.1$ and I2<50%, the heterogeneity was regarded as low, and the fixed effects model was used. When $p < 0.1$ and I2>50%, heterogeneity was considered to be present, therefore sensitivity analysis was used to investigate the source of heterogeneity. If the source of heterogeneity could not be determined, a random effects model was used to conduct meta-analysis for the literature. By observing whether the two sides of the funnel chart were symmetrical, it was judged whether or not the meta-analysis' results contained publication bias. A value of $p < 0.05$ was considered as significant difference.

3 Results

3.1 Literature screening results

A total of 1809 articles were obtained through preliminary retrieval from the databases, 592 remained after removing duplicate articles, then 36 were obtained through preliminary screening by reading the titles and abstracts of the studies, and 16 (20–35) articles were finally included after reading the full texts. See Figure 1 for the flow diagram of literature screening.

3.2 Basic characteristics and quality evaluation of the included literature

Among the 16 included controlled studies about LPD and OPD for the treatment of pancreatic cancer, two were randomized controlled experiments (Palanivelu et al., 2017; Wang et al., 2021), and 14 were retrospective studies (Cho et al., 2009; Bao et al., 2014; Croome et al., 2014; Mendoza et al., 2015; Stauffer et al., 2017; Chapman et al., 2018; Kim et al., 2019; Tan et al., 2019; Choi et al., 2020; El Nakeeb et al., 2020; Han et al., 2020; Kwon et al., 2020; Weng et al., 2021; Zhang et al., 2022), involving a total of 4416 patients, including 1275 in the LPD group and 3141 in the OPD group. See Table 1 for literature characteristics, see Supplementary Table S2 and Supplementary Figures S1, S2 for the quality evaluation of the included studies.

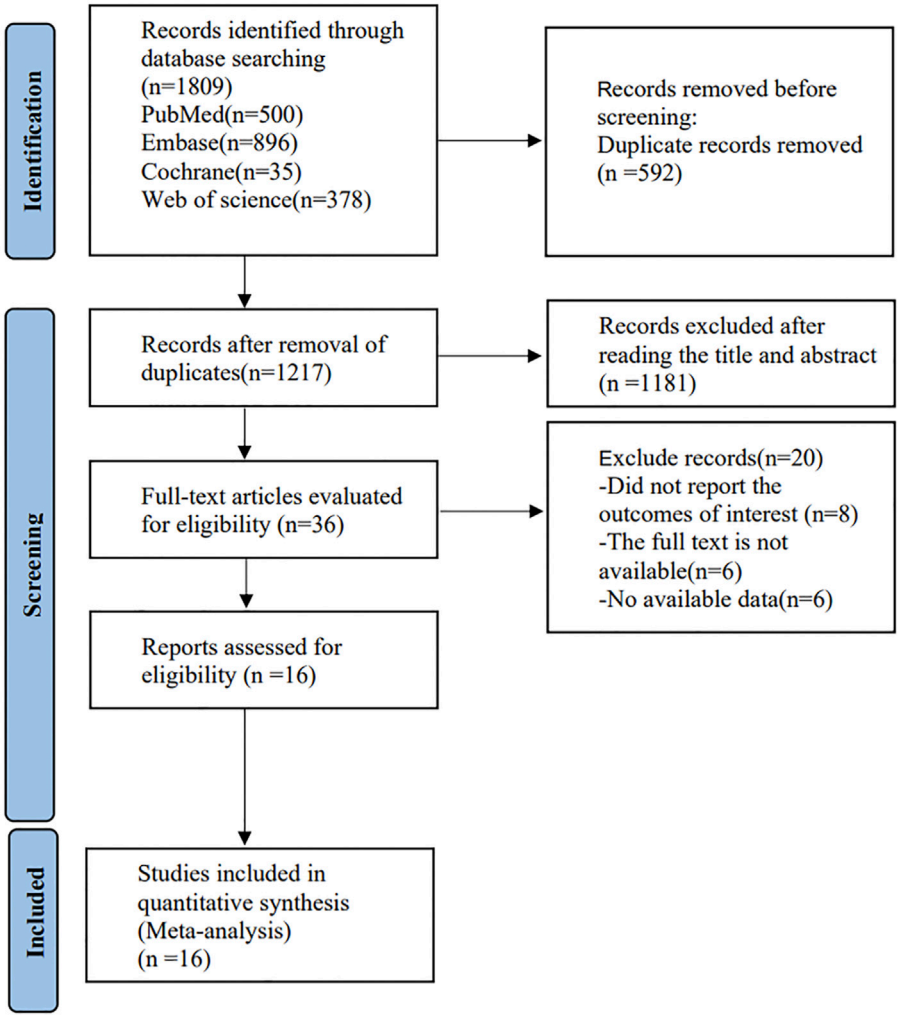

FIGURE 1
Flow chart of literature retrieval.

3.3 Meta-analysis

3.3.1 Operation time

Among the included studies, a total of 13 articles (Cho et al., 2009; Bao et al., 2014; Croome et al., 2014; Mendoza et al., 2015; Palanivelu et al., 2017; Stauffer et al., 2017; Kim et al., 2019; Tan et al., 2019; Choi et al., 2020; El Nakeeb et al., 2020; Han et al., 2020; Wang et al., 2021; Weng et al., 2021) mentioned the index of operation time. Among them, 907 cases were part of the LPD group and 1355 cases were in the OPD group. Therefore, the random effects model was used for meta-analysis. According to the heterogeneity test (I2 = 97.1%, $p = 0.0001$), the analysis results showed that the difference between the two groups was statistically significant [WMD = 56.14,95% CI (38.39,73.89), $p = 0.001$], indicating that the operation time of LPD was longer than that of OPD. As shown in Figure 2, subgroup analysis was then conducted according to literature type. The randomized controlled trial subgroup [WMD = 32.01,95% CI (18.99,45.02), $p = 0.001$], and the retrospective study subgroup [WMD = 62.45,95% CI (18.21106.70), $p = 0.006$]; the results showing that the operation time of LPD was longer than that of OPD in both randomized controlled studies and retrospective studies. The sensitivity analysis of this indicator was carried out after removing literature one by one, as shown in Figure 3.

3.3.2 Intraoperative blood loss

14 (20, 22–28, 30, 31, 36) articles mentioned intraoperative blood loss as an indicator, including 954 cases in the LPD group and 1402 cases in the OPD group. The random effect model was used for meta-analysis. According to the heterogeneity test (I2 = 96.2%, $p = 0.0001$), the analysis results showed that the difference between the two groups was statistically significant [WMD = −120.82, 95% CI

TABLE 1 Characteristics of studies included.

Study	Study design	Country	Sample size (male)		Mean age (year)		Follow-up(M)	Outcome
			LPD	OPD	LPD	OPD		
Palanivelu et al (2017)	RCT	India	32 (18)	32 (22)	57.8	58.6	3	F1; F2; F3; F4; F5; F6; F7
Wang et al (2021)	RCT	China	297 (171)	297 (193)	61	60	3	F1; F2; F4; F5; F6; F8
Bao et al (2014)	Retrospective study	United States	28 (13)	28 (13)	68	67.7	3	F1; F2; F4; F5; F7; F8
Chapman et al (2018)	Retrospective study	United States	248 (132)	1520 (721)	79.6	79.5	60	F5; F7; F8; F9
Cho et al (2009)	Retrospective study	Japan	15 (6)	15 (7)	64	68	NA	F1; F2; F4; F5; F6
Choi et al (2020)	Retrospective study	Korea	27 (12)	34 (18)	63.35	63.35	60	F1; F2; F4; F5; F9; F10
Croome et al. (2014)	Retrospective study	United States	108 (51)	214 (131)	66.6	65.4	60	F1; F2; F4; F5; F9; F10
El Nakeeb et al. (2020)	Retrospective study	Egypt	37 (22)	74 (40)	NA	NA	NA	F1; F2; F4; F5; F6; F7
Han et al. (2020)	Retrospective study	Korea	104 (53)	113 (70)	61.5	64.5	3	F1; F2; F5; F6; F7; F8
Kim et al. (2019)	Retrospective study	Korea	58 (18)	91 (42)	49.5	56	60	F1; F2; F5; F6; F7; F9; F10
Kwon et al (2020)	Retrospective study	Korea	73 (41)	219 (114)	62.4	63.3	60	F6; F9; F10
Mendoza et al (2015)	Retrospective study	Korea	18 (10)	34 (21)	63.7	68.4	NA′	F1; F2; F4; F5; F8
Stauffer et al. (2017)	Retrospective study	United States	58 (32)	193 (96)	69.9	68.9	60	F1; F2; F5; F6; F9
Tan et al. (2019)	Retrospective study	Singapore	20 (11)	20 (11)	65	64	NA	F1; F2; F4; F5
Weng et al. (2021)	Retrospective study	China	105 (66)	210 (135)	64	62	60	F1; F2; F8; F9; F10
Zhang et al. (2022)	Retrospective study	China	47 (31)	47 (30)	57.64	57.57	50	F2; F4; F7; F9

F1: duration of operation; F2: blood loss; F3: Duration of ICU, stay; F4: blood transfusion; F5: duration of hospital stay; F6: postoperative complications; F7: readmission; F8: 90-Mortality; F9: overall survival; F10: disease-free survival.

(−169.33, −72.30), p = 0.001], indicating that the amount of intraoperative blood loss in LPD was less than OPD. As shown in Figure 4, subgroup analysis was then conducted according to literature type. The randomized controlled trial subgroup [WMD = −116.25,95% CI (−183.38, −49.13), p = 0.013], and the retrospective study subgroup [WMD = −1114.45,95% CI (−204.55, −24.35), p = 0.006]; the results showing that the blood loss during LPD operation was less than that of OPD, in both randomized controlled studies and retrospective studies. Sensitivity analysis was conducted for this indicator by removing literature one by one, as shown in Figure 5.

3.3.3 Hospitalization time

12 (20–23, 26, 27, 29, 30, 32–35) articles mentioned hospitalization time (length of stay in hospital), including 1030 cases from the LPD group and 2045 cases in the OPD group. The random effects model was used for meta-analysis. According to the heterogeneity test (I2 = 90.1%, p = 0.0001), the analysis results showed that the difference between the two groups was not statistically significant [WMD = −0.5,95% CI (−1.35,0.35), p = 0.250], indicating that there was no significant difference regarding the length of hospitalization between LPD and OPD. Subgroup analysis was then conducted according to literature type, as shown in Figure 6. The randomized controlled trial subgroup [WMD = −2.96,95% CI (−7.74,1.83), p = 0.226], and the retrospective study subgroup [WMD = 0.21,95% CI (−1.42,1.84), p = 0.801]; the results showing that, whether in randomized controlled trials or retrospective studies, there was no difference in hospilization time between LPD and OPD. Sensitivity analysis of this indicator was carried out by removing literature one by one, as shown in Figure 7.

3.3.4 Postoperative complications

A total of 8 (23–28, 32, 35) studies mentioned postoperative complications, including 674 cases in the LPD group and 1034 cases in the OPD group. Therefore, meta-analysis was carried out on the fixed effects model. According to the heterogeneity test (I2 = 0%, p = 0.480), the analysis results showed that the difference between the two groups was not statistically significant [RR = 0.96,95% CI (0.86,1.07), p = 0.463], indicating that there no significant difference was observed between LPD and OPD regarding postoperative complications. As shown in Figure 8, subgroup analysis was carried out according to literature type. The randomized controlled trial subgroup [RR = 1.06,95% CI (0.90,1.24), p = 0.483], and the retrospective study subgroup [RR = 0.88,95% CI (0.76,1.03), p =

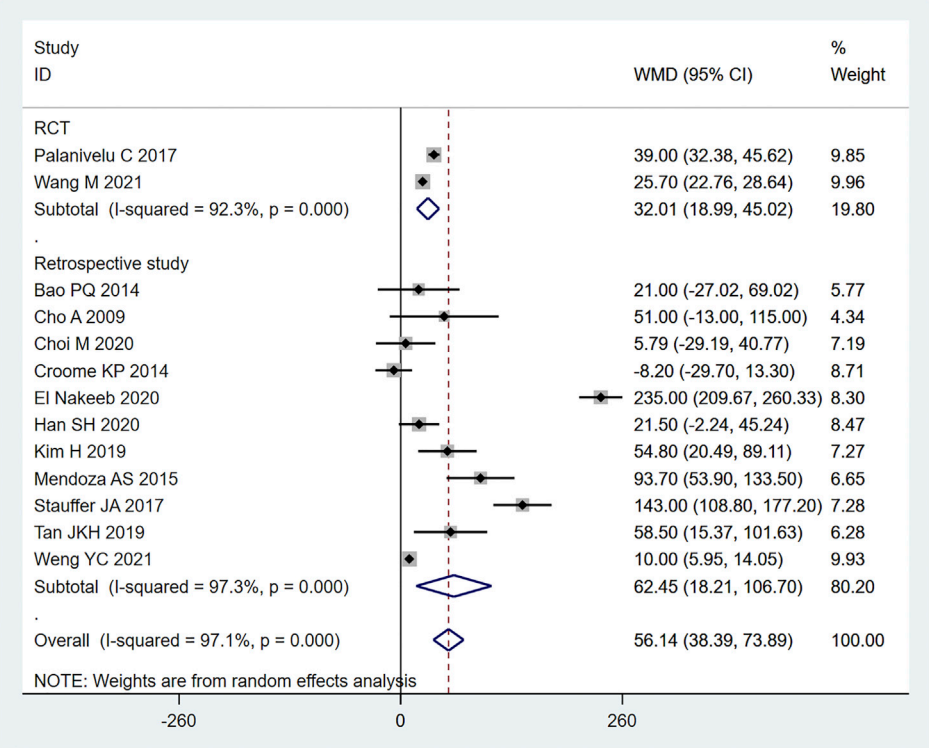

FIGURE 2
Forest plot of Meta-analysis of operation time.

0.108]; the results showing that there was no difference regarding postoperative complications between LPD and OPD, whether in randomized controlled studies or retrospective studies.

3.3.5 OS (overall survival)

A total of 8 (20–22, 24, 26, 27, 30, 34) retrospective studies mentioned OS, respectively recording their 1-year OS and 3-year OS. Therefore, the random effects model was used for meta-analysis. According to the heterogeneity test (I2 = 55.4%, p = 0.005), the analysis results showed that the difference between the two groups was not statistically significant [RR = 1.96,95% CI (0.96,1.17), p = 0.216]. In the 1-year OS subgroup [RR = 1.02,95% CI (0.97,1.08), p = 0.417], and in the 3-year OS subgroup [RR = 1.10,95% CI (0.75, 1.62), p = 0.614]; whether in the 1-year OS or 3-year OS, no significant difference was observed between LPD and OPD, as shown in Figure 9. Sensitivity analysis was conducted for this indicator by removing the literature one by one, as shown in Figure 10.

3.4 Publication bias

The egger test was used to evaluate the publication deviation of the operative time and intraoperative blood loss in the article, and it was found that the operative blood loss p = 0.475 and the operative time egger test p = 0.147, which suggested that there was no publication bias in these two indexes. See Supplementary Figures S3, S4.

4 Discussion

Surgery is gradually heading towards a minimally invasive era, and the advantages of laparoscopic surgery are becoming increasingly prominent (Sammut et al., 2017). Before that, LPD has already been widely used to treat benign and low-grade malignant tumors located at the body and tail of the pancreas. Croome et al. (Croome et al., 2014) retrospectively analyzed clinical data of pancreatic cancer patients who underwent laparoscopic duodenectomy and open resection at Mayo Clinic from January 2008 to July 2013. They found that patients who underwent minimally invasive surgery recovered quickly after surgery, could receive adjuvant treatment sooner, and had their disease-free survival time after surgery extended.

Pancreatoduodenectomy involves many vessels and organs, with complex spatial structure. Laparoscopic technic can enlarge the visual field during operation, only causes little trauma, and results in fast postoperative recovery (Jiang et al., 2019). In this

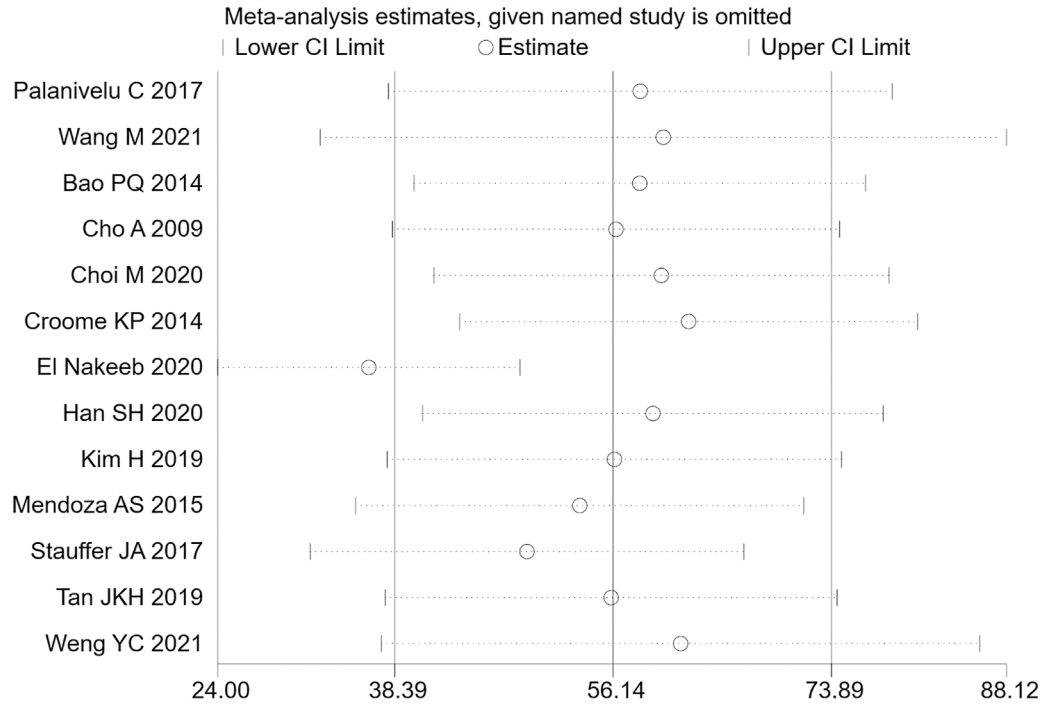

FIGURE 3
Sensitivity analysis of operation time.

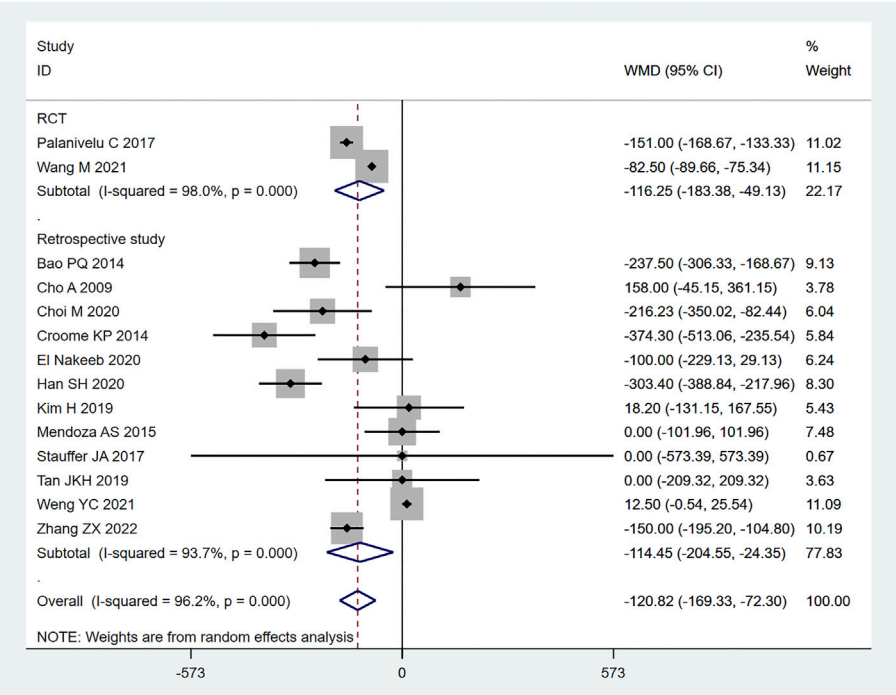

FIGURE 4
Forest plot of Meta-analysis of intraoperative blood loss.

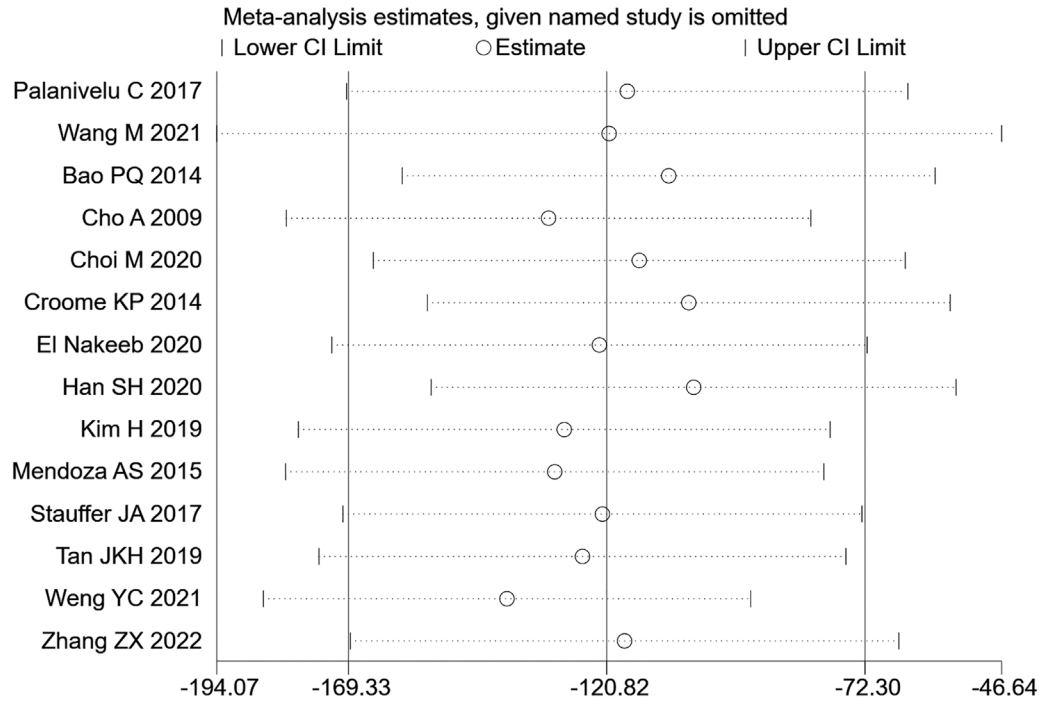

FIGURE 5
Sensitivity analysis of intraoperative blood loss.

study, the amount of blood loss of pancreatic cancer patients during LPD was remarkably less than that of OPD [WMD = −120.82,95% CI (−169.33, −72.30), p = 0.001], but the operation time of LPD was longer than that of OPD [WMD = 56.14,95% CI (38.39,73.89), p = 0.001]. We believe that with an accumulation of operation volume, after passing through the learning curve of the challenge period of the third stage, the operation time of LPD can be significantly shortened, and will get closer to, or even less than that of OPD. Moreover, the bleeding volume of LPD is far less than that of OPD, so the bleeding rate of LPD per unit time should be lower than that of OPD. Therefore, it can be considered that LPD has obvious advantages over OPD. Nagakawa et al. (Nagakawa et al., 2021) conducted a cohort study on 42 patients (21 patients in the left superior mesenteric artery group and 21 patients in the right superior mesenteric artery group), and pointed out that jejunal vein and lower pancreaticoduodenal artery hemorrhage often occurred on the left side of the mesenteric artery. Nussbaum D et al. (Nussbaum et al., 2014) pointed out that a lesser amount of blood loss is related to lower complication rate; reducing pancreaticoduodenal bleeding during operation can reduce the incidence of serious postoperative complications. During LPD, it is easier to find important tissues such as blood vessels and nerves, due to a clearer fenestration and higher fineness, thus reducing the quantity of intraoperative blood loss. In addition, the amount of intraoperative blood loss is related to the surgical proficiency of the operator. Some studies have pointed out that the amount of intraoperative blood loss can be decreased with the increase of learning time. Overly long operation time, an increase of blood loss during operation, and occurrence of postoperative complications will all prolong the patient's hospitalization time (Yeo et al., 1993). Therefore, the requirements for doctors' surgical skills are also very high. The amount of time it takes to operate is closely related to the learning curve. Some scholars have divided the learning curve of LPD into three periods: 1–11 cases is considered as the initial learning period, 12–38 cases the period of technical competency, and 39–57 cases the challenge period (Godhi et al., 2017). At the initial stage, the operation time of LPD can be long. First, because the degree of freedom and agility that endoscopic surgery allows is not as good as that of laparotomy, and second, because of the complexity and difficulty of LPD itself. For LPD beginners, when dealing with the operation difficulties, such as separation and resection of the pancreatic uncinate process, clearing of deep abdominal lymph nodes, reconstruction of digestive tract (especially pancreaticoduodenal anastomosis), it will inevitably consume a lot of the surgeon's time (Gerstenhaber et al., 2013; Meng et al., 2022), which further explains the results we obtained this time. For long-term outcomes, our study obtained: 1-year OS [RR = 1.02, 95% CI (0.97, 1.08), p = 0.417] and 3-year OS [RR = 1.10,95% CI (0.75, 1.62), p = 0.614], for which no significant difference was observed. It may be that the number of included

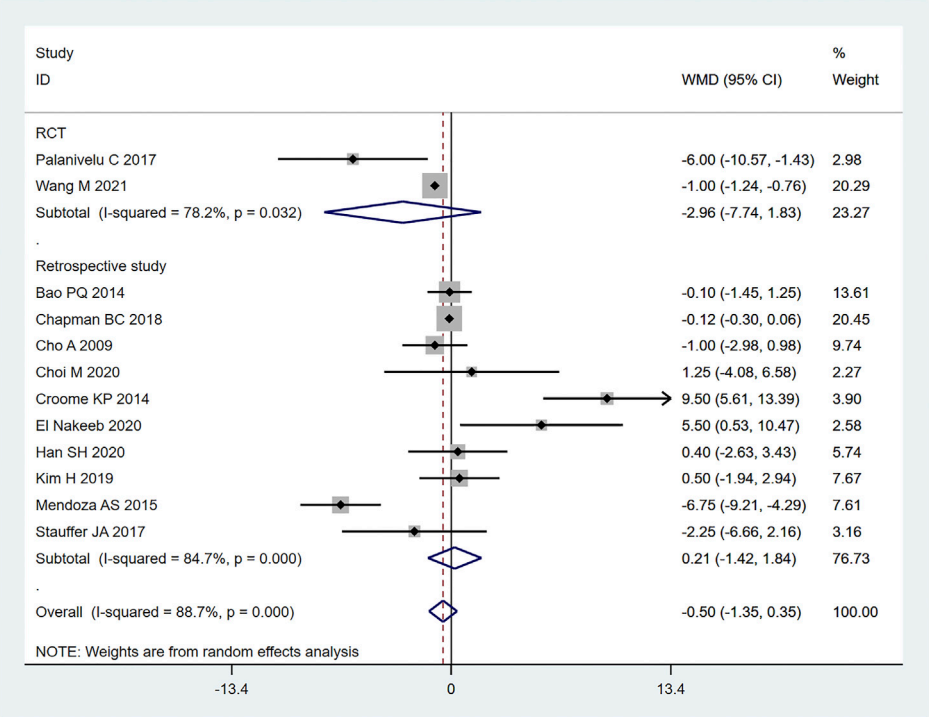

FIGURE 6
Forest plot of Meta-analysis of hospitalization time.

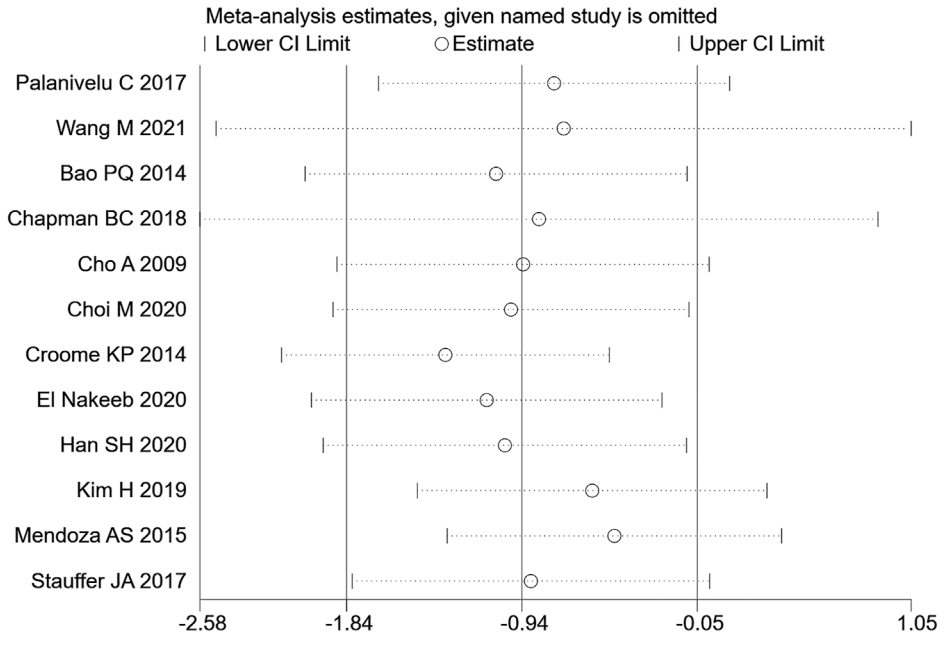

FIGURE 7
Sensitivity analysis of hospitalization time.

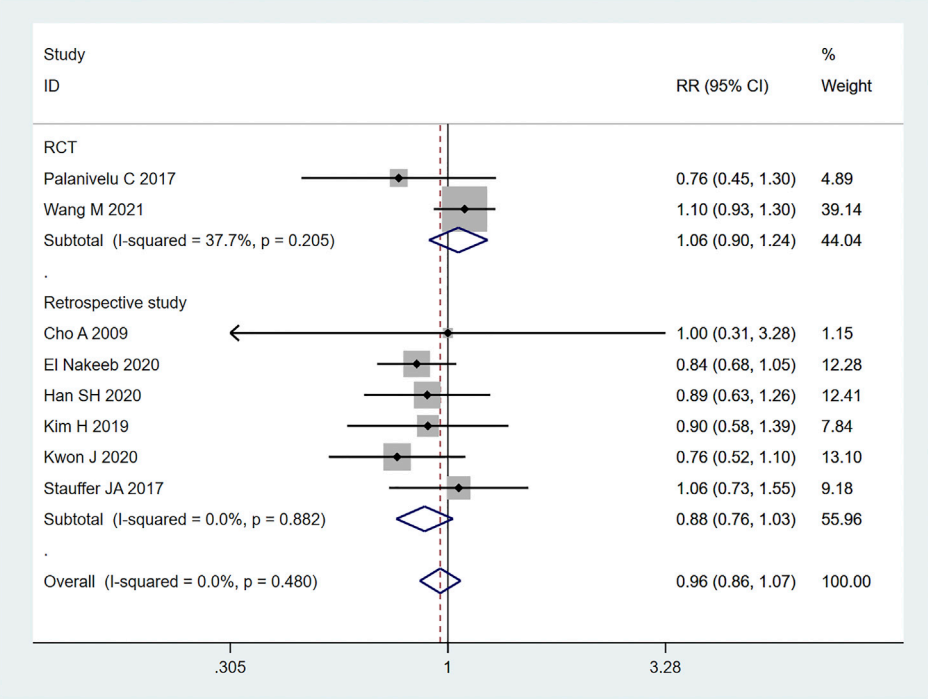

FIGURE 8
Forest plot of Meta-analysis of postoperative complications.

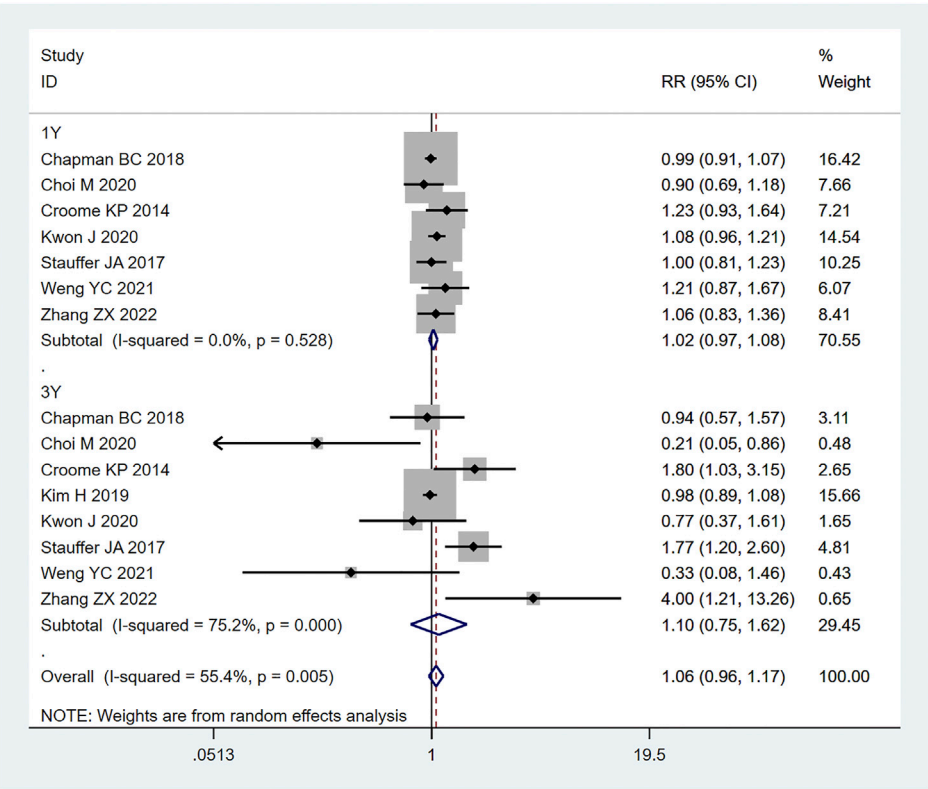

FIGURE 9
Forest plot of Meta-analysis of OS.

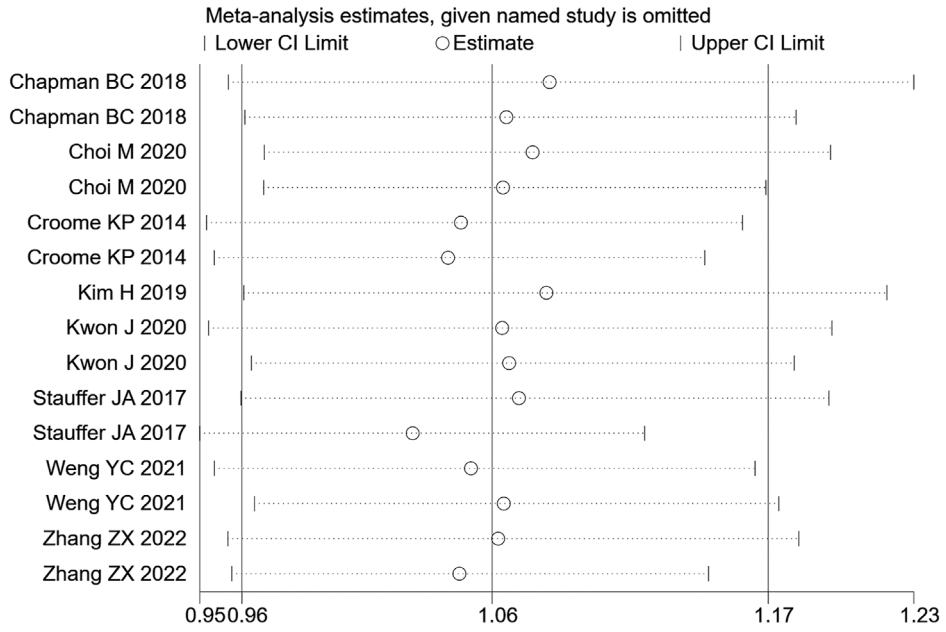

FIGURE 10
Sensitivity analysis of OS.

studies was small, and the included articles did not fully and clearly record the factors that may affect the prognosis of patients, such as the learning curve of the surgeon, the degree of tumor differentiation after surgery, the tumor stage, or the integrity of clinical data (such as whether or not the patient received adjuvant therapy). In short, even if it is impossible to assume that patients of the LDP group had a longer survival time, the current studies show that LDP has no weaker oncological outcome than ODP regarding the treatment of pancreatic cancer.

This study still contains some limitations. First of all, the included articles did not include retrospective studies, and the sample size of some studies was small, with inevitable presence of selection bias, which lead to the lower evidence quality of this research. Second, most studies were single center studies, leading to high heterogeneity between studies. The number of cases included in most studies was small, therefore it was impossible to analyze the incidence of various types of postoperative complications in detail. Third, the follow-up time after surgery was inconsistent, which may be the source of potential heterogeneity of the study.

5 Conclusion

In summary, LPD involves less blood loss and longer operation time when compared with OPD, therefore the bleeding rate per unit time of LPD is less than that of OPD. LPD has obvious advantages. With the increase of clinical application of LPD, the usage of LPD in patients with pancreatic cancer has a good prospect. Due to the limitations of this paper, in future studies, more attention should be paid to high-quality, multi-center, randomized controlled studies.

Data availability statement

The original contributions presented in the study are included in the article/Supplementary Material, further inquiries can be directed to the corresponding author.

Author contributions

HQ conceptualized and designed the study, designed the data collection instruments, collected the data, summarized the data, drafted the initial manuscript, reviewed, and revised the manuscript. DW, LZ and HM screened the manuscripts, reviewed, and revised the manuscript. YZ provided methodological support including overseeing the search strategy, reviewed, and revised the manuscript. HQ conceptualized the study, reviewed, and revised the manuscript. HQ and YZ oversaw the project, conceptualized and designed the study, screened the manuscripts, reviewed, and revised the manuscript. All authors approved the final

manuscript as submitted and agree to be accountable for all aspects of the work.

Funding

This work is supported by Nantong Municipal Commission of Health and Family Planning (QA2020040).

Conflict of interest

The authors declare that the research was conducted in the absence of any commercial or financial relationships that could be construed as a potential conflict of interest.

Publisher's note

Supplementary material

The Supplementary Material for this article can be found online at: https://www.frontiersin.org/articles/10.3389/fgene.2022.1072229/full#supplementary-material

References

Bao, P. Q., Mazirka, P. O., and Watkins, K. T. (2014). Retrospective comparison of robot-assisted minimally invasive versus open pancreaticoduodenectomy for periampullary neoplasms. *J. Gastrointest. Surg.* 18 (4), 682–689. doi:10.1007/s11605-013-2410-3

Carioli, G., Malvezzi, M., Bertuccio, P., Boffetta, P., Levi, F., La Vecchia, C., et al. (2021). European cancer mortality predictions for the year 2021 with focus on pancreatic and female lung cancer. *Ann. Oncol.* 32 (4), 478–487. doi:10.1016/j.annonc.2021.01.006

Cesaretti, M., Bifulco, L., Costi, R., and Zarzavadjian Le Bian, A. (2017). Pancreatic resection in the era of laparoscopy: State of Art. A systematic review. *Int. J. Surg.* 44, 309–316. doi:10.1016/j.ijsu.2017.07.028

Chang, A., Sherman, S. K., Howe, J. R., and Sahai, V. (2022). Progress in the management of pancreatic neuroendocrine tumors. *Annu. Rev. Med.* 73, 213–229. doi:10.1146/annurev-med-042320-011248

Chapman, B. C., Gajdos, C., Hosokawa, P., Henderson, W., Paniccia, A., Overbey, D. M., et al. (2018). Comparison of laparoscopic to open pancreaticoduodenectomy in elderly patients with pancreatic adenocarcinoma. *Surg. Endosc.* 32 (5), 2239–2248. doi:10.1007/s00464-017-5915-0

Cho, A., Yamamoto, H., Nagata, M., Takiguchi, N., Shimada, H., Kainuma, O., et al. (2009). Comparison of laparoscopy-assisted and open pylorus-preserving pancreaticoduodenectomy for periampullary disease. *Am. J. Surg.* 198 (3), 445–449. doi:10.1016/j.amjsurg.2008.12.025

Choi, M., Hwang, H. K., Rho, S. Y., Lee, W. J., and Kang, C. M. (2020). Comparing laparoscopic and open pancreaticoduodenectomy in patients with pancreatic head cancer: Oncologic outcomes and inflammatory scores. *J. Hepatobiliary. Pancreat. Sci.* 27 (3), 124–131. doi:10.1002/jhbp.697

Croome, K. P., Farnell, M. B., Que, F. G., Reid-Lombardo, K. M., Truty, M. J., Nagorney, D. M., et al. (2014). Total laparoscopic pancreaticoduodenectomy for pancreatic ductal adenocarcinoma: Oncologic advantages over open approaches? *Ann. Surg.* 260 (4), 633–638. doi:10.1097/SLA.0000000000000937

El Nakeeb, A., Attia, M., El Sorogy, M., Ezzat, H., Shehta, A., Salem, A., et al. (2020). Laparoscopic pancreaticodudenectomy for periampullary tumor: Should it be a routine? A propensity score-matched study. *Surg. Laparosc. Endosc. Percutan. Tech.* 30 (1), 7–13. doi:10.1097/SLE.0000000000000715

Gerstenhaber, F., Grossman, J., Lubezky, N., Itzkowitz, E., Nachmany, I., Sever, R., et al. (2013). Pancreaticoduodenectomy in elderly adults: Is it justified in terms of mortality, long-term morbidity, and quality of life? *J. Am. Geriatr. Soc.* 61 (8), 1351–1357. doi:10.1111/jgs.12360

Godhi, S. A., Nadi, P. R., Saluja, S., and Mishra, P. (2017). Minimally invasive versus open pancreaticoduodenectomy for cancer. Practice patterns and short-term outcomes among 7061 patients. *Ann. Surg.* 266 (2), e26. doi:10.1097/SLA.0000000000001315

Han, S. H., Kang, C. M., Hwang, H. K., Yoon, D. S., and Lee, W. J. (2020). The yonsei experience of 104 laparoscopic pancreaticoduodenectomies: A propensity score-matched analysis with open pancreaticoduodenectomy. *Surg. Endosc.* 34 (4), 1658–1664. doi:10.1007/s00464-019-06942-4

Harrison, J. M., Harris, C., and Castillo, C. F. (2022). A pancreatic tail mass in a young male. *Gastroenterology* 162 (1), e1–e3. doi:10.1053/j.gastro.2021.04.073

Heestand, G. M., Murphy, J. D., and Lowy, A. M. (2015). Approach to patients with pancreatic cancer without detectable metastases. *J. Clin. Oncol.* 33 (16), 1770–1778. doi:10.1200/JCO.2014.59.7930

Iovanna, J., and Dusetti, N. (2017). Speeding towards individualized treatment for pancreatic cancer by taking an alternative road. *Cancer Lett.* 410, 63–67. doi:10.1016/j.canlet.2017.09.016

Jiang, J., Upfill-Brown, A., Dann, A. M., Kim, S. S., Girgis, M. D., King, J. C., et al. (2019). Association of hospital length of stay and complications with readmission after open pancreaticoduodenectomy. *JAMA Surg.* 154 (1), 88–90. doi:10.1001/jamasurg.2018.3213

Kawai, M., and Yamaue, H. (2011). Pancreaticoduodenectomy versus pylorus-preserving pancreaticoduodenectomy: The clinical impact of a new surgical procedure; pylorus-resecting pancreaticoduodenectomy. *J. Hepatobiliary. Pancreat. Sci.* 18 (6), 755–761. doi:10.1007/s00534-011-0427-0

Kim, H., Song, K. B., Hwang, D. W., Lee, J. H., Alshammary, S., and Kim, S. C. (2019). Laparoscopic versus open pancreaticoduodenectomy for pancreatic neuroendocrine tumors: A single-center experience. *Surg. Endosc.* 33 (12), 4177–4185. doi:10.1007/s00464-019-06969-7

Klein, A. P. (2021). Pancreatic cancer epidemiology: Understanding the role of lifestyle and inherited risk factors. *Nat. Rev. Gastroenterol. Hepatol.* 18 (7), 493–502. doi:10.1038/s41575-021-00457-x

Kuesters, S., Chikhladze, S., Makowiec, F., Sick, O., Fichtner-Feigl, S., Hopt, U. T., et al. (2018). Oncological outcome of laparoscopically assisted pancreatoduodenectomy for ductal adenocarcinoma in a retrospective cohort study. *Int. J. Surg.* 55, 162–166. doi:10.1016/j.ijsu.2018.05.026

Kwon, J., Song, K. B., Park, S. Y., Shin, D., Hong, S., Park, Y., et al. (2020). Comparison of minimally invasive versus open pancreatoduodenectomy for pancreatic ductal adenocarcinoma: A propensity score matching analysis. *Cancers* 12 (4), 982. doi:10.3390/cancers12040982

Mendoza, A. S., 3rd, Han, H. S., Yoon, Y. S., Cho, J. Y., and Choi, Y. (2015). Laparoscopy-assisted pancreaticoduodenectomy as minimally invasive surgery for periampullary tumors: A comparison of short-term clinical outcomes of laparoscopy-assisted pancreaticoduodenectomy and open pancreaticoduodenectomy. *J. Hepatobiliary. Pancreat. Sci.* 22 (12), 819–824. doi:10.1002/jhbp.289

Meng, H., Wang, S., Liu, J., Zhao, X., Rong, Z., Xu, Y., et al. (2022). Laparoscopic pancreaticoduodenectomy with transanal specimen extraction for periampullary tumors. *Ann. Surg.* 275 (3), e596–e598. doi:10.1097/SLA.0000000000004886

Miller, A. L., Garcia, P. L., and Yoon, K. J. (2020). Developing effective combination therapy for pancreatic cancer: An overview. *Pharmacol. Res.* 155, 104740. doi:10.1016/j.phrs.2020.104740

Nagakawa, Y., Jang, J. Y., Kawai, M., Kim, S. C., Inoue, Y., Yabushita, Y., et al. (2021). Surgical outcomes of pancreatectomy with resection of the portal vein and/or superior mesenteric vein and jejunal vein for pancreatic head cancer: A multicenter study. *Ann. Surg.* doi:10.1097/SLA.0000000000005330

Neoptolemos, J. P., Kleeff, J., Michl, P., Costello, E., Greenhalf, W., and Palmer, D. H. (2018). Therapeutic developments in pancreatic cancer: Current and future

perspectives. *Nat. Rev. Gastroenterol. Hepatol.* 15 (6), 333–348. doi:10.1038/s41575-018-0005-x

Nussbaum, D. P., Penne, K., Speicher, P. J., Stinnett, S. S., Perez, A., White, R. R., et al. (2014). The role of clinical care pathways: An experience with distal pancreatectomy. *J. Surg. Res.* 190 (1), 64–71. doi:10.1016/j.jss.2014.02.026

Okusaka, T., Nakamura, M., Yoshida, M., Kitano, M., Uesaka, K., Ito, Y., et al. (2020). Clinical practice guidelines for pancreatic cancer 2019 from the Japan pancreas society: A synopsis. *Pancreas* 49 (3), 326–335. doi:10.1097/MPA.0000000000001513

Palanivelu, C., Senthilnathan, P., Sabnis, S. C., Babu, N. S., Srivatsan Gurumurthy, S., Anand Vijai, N., et al. (2017). Randomized clinical trial of laparoscopic versus open pancreatoduodenectomy for periampullary tumours. *Br. J. Surg.* 104 (11), 1443–1450. doi:10.1002/bjs.10662

Pisters, P. W., Lee, J. E., Vauthey, J. N., Charnsangavej, C., and Evans, D. B. (2001). Laparoscopy in the staging of pancreatic cancer. *Br. J. Surg.* 88 (3), 325–337. doi:10.1046/j.1365-2168.2001.01695.x

Sammut, M., Sammut, M., and Andrejevic, P. (2017). The benefits of being a video gamer in laparoscopic surgery. *Int. J. Surg.* 45, 42–46. doi:10.1016/j.ijsu.2017.07.072

Scialpi, M., Reginelli, A., D'Andrea, A., Gravante, S., Falcone, G., Baccari, P., et al. (2016). Pancreatic tumors imaging: An update. *Int. J. Surg.* 28 (1), S142–S155. doi:10.1016/j.ijsu.2015.12.053

Sciuto, A., Abete, R., Reggio, S., Pirozzi, F., Settembre, A., and Corcione, F. (2014). Laparoscopic spleen-preserving distal pancreatectomy for insulinoma: Experience of a single center. *Int. J. Surg.* 12, S152–S155. doi:10.1016/j.ijsu.2014.05.023

Siegel, R. L., Miller, K. D., Fuchs, H. E., and Jemal, A. (2021). Cancer statistics, 2017. *Ca. Cancer J. Clin.* 71 (1), 7–30. doi:10.3322/caac.21387

Stauffer, J. A., Coppola, A., Villacreses, D., Mody, K., Johnson, E., Li, Z., et al. (2017). Laparoscopic versus open pancreaticoduodenectomy for pancreatic adenocarcinoma: Long-term results at a single institution. *Surg. Endosc.* 31 (5), 2233–2241. doi:10.1007/s00464-016-5222-1

Sun, D., Cao, M., Li, H., He, S., and Chen, W. (2020). Cancer burden and trends in China: A review and comparison with Japan and South Korea. *Chin. J. cancer Res. = Chung-kuo yen cheng yen chiu* 32 (2), 129–139. doi:10.21147/j.issn.1000-9604.2020.02.01

Tan, J. K. H., Ng, J. J., Yeo, M., Koh, F. H. X., Bonney, G. K., Ganpathi, I. S., et al. (2019). Propensity score-matched analysis of early outcomes after laparoscopic-assisted versus open pancreaticoduodenectomy. *ANZ J. Surg.* 89 (5), E190–E194. doi:10.1111/ans.15124

Wang, M., Li, D., Chen, R., Huang, X., Li, J., Liu, Y., et al. (2021). Laparoscopic versus open pancreatoduodenectomy for pancreatic or periampullary tumours: A multicentre, open-label, randomised controlled trial. *Lancet. Gastroenterol. Hepatol.* 6 (6), 438–447. doi:10.1016/S2468-1253(21)00054-6

Weng, Y., Jiang, Y., Fu, N., Jin, J., Shi, Y., Huo, Z., et al. (2021). Oncological outcomes of robotic-assisted versus open pancreatoduodenectomy for pancreatic ductal adenocarcinoma: A propensity score-matched analysis. *Surg. Endosc.* 35 (7), 3437–3448. doi:10.1007/s00464-020-07791-2

Yeo, C. J., Barry, M. K., Sauter, P. K., Sostre, S., Lillemoe, K. D., Pitt, H. A., et al. (1993). Erythromycin accelerates gastric emptying after pancreaticoduodenectomy. A prospective, randomized, placebo-controlled trial. *Ann. Surg.* 218 (3), 229–237. doi:10.1097/00000658-199309000-00002

Zhang, T., Du, X., and Zhao, Y. (2011). Laparoscopic surgery for pancreatic lesions: Current status and future. *Front. Med.* 5 (3), 277–282. doi:10.1007/s11684-011-0147-5

Zhang, Z., Yin, T., Qin, T., Pan, S., Wang, M., Zhang, H., et al. (2022). Comparison of laparoscopic versus open pancreaticoduodenectomy in patients with resectable pancreatic ductal adenocarcinoma: A propensity score-matching analysis of long-term survival. *Pancreatology* 22 (2), 317–324. doi:10.1016/j.pan.2021.12.005

Zhou, W., Jin, W., Wang, D., Lu, C., Xu, X., Zhang, R., et al. (2019). Laparoscopic versus open pancreaticoduodenectomy for pancreatic ductal adenocarcinoma: A propensity score matching analysis. *Cancer Commun.* 39 (1), 66. doi:10.1186/s40880-019-0410-8

frontiers | Frontiers in Genetics

TYPE Original Research
PUBLISHED 19 April 2023
DOI 10.3389/fgene.2023.1122758

OPEN ACCESS

EDITED BY
Qian Wang,
Tai'an City Central Hospital, China

REVIEWED BY
Ihtisham Bukhari,
Fifth Affiliated Hospital of Zhengzhou University, China
Farhan Ullah Khan,
University of Sherbrooke, Canada

*CORRESPONDENCE
Xinrui Zhang,
zxr9047@163.com
Andreas Melzer,
andreas.melzer@medizin.uni-leipzig.de

†These authors have contributed equally to this work

‡These authors share senior authorship

SPECIALTY SECTION
This article was submitted to Cancer Genetics and Oncogenomics, a section of the journal Frontiers in Genetics

RECEIVED 13 December 2022
ACCEPTED 21 March 2023
PUBLISHED 19 April 2023

CITATION
Hu S, Zhang X, Melzer A and Landgraf L (2023), Ultrasound-induced cavitation renders prostate cancer cells susceptible to hyperthermia: Analysis of potential cellular and molecular mechanisms. *Front. Genet.* 14:1122758. doi: 10.3389/fgene.2023.1122758

Ultrasound-induced cavitation renders prostate cancer cells susceptible to hyperthermia: Analysis of potential cellular and molecular mechanisms

Shaonan Hu[1†], Xinrui Zhang[1*†], Andreas Melzer[1,2*‡] and Lisa Landgraf[1‡]

[1]Innovation Center Computer Assisted Surgery (ICCAS), University of Leipzig, Leipzig, Germany, [2]Institute for Medical Science and Technology (IMSaT), University of Dundee, Dundee, United Kingdom

Background: Focused ultrasound (FUS) has become an important non-invasive therapy for prostate tumor ablation *via* thermal effects in the clinic. The cavitation effect induced by FUS is applied for histotripsy, support drug delivery, and the induction of blood vessel destruction for cancer therapy. Numerous studies report that cavitation-induced sonoporation could provoke multiple anti-proliferative effects on cancer cells. Therefore, cavitation alone or in combination with thermal treatment is of great interest but research in this field is inadequate.

Methods: Human prostate cancer cells (LNCap and PC-3) were exposed to 40 s cavitation using a FUS system, followed by water bath hyperthermia (HT). The clonogenic assay, WST-1 assay, and Transwell® invasion assay, respectively, were used to assess cancer cell clonogenic survival, metabolic activity, and invasion potential. Fluorescence microscopy using propidium iodide (PI) as a probe of cell membrane integrity was used to identify sonoporation. The H2A.X assay and Nicoletti test were conducted in the mechanism investigation to detect DNA double-strand breaks (DSBs) and cell cycle arrest. Immunofluorescence microscopy and flow cytometry were performed to determine the distribution and expression of 5α-reductase (SRD5A).

Results: Short FUS shots with cavitation **(**FUS-Cav) in combination with HT resulted in, respectively, a 2.2, 2.3, and 2.8-fold decrease (LNCap) and a 2.0, 1.5, and 1.6-fold decrease (PC-3) in the clonogenic survival, cell invasiveness and metabolic activity of prostate cancer cells when compared to HT alone. FUS-Cav immediately induced sonoporation in 61.7% of LNCap cells, and the combination treatment led to a 1.4 (LNCap) and 1.6-fold (PC-3) increase in the number of DSBs compared to HT alone. Meanwhile, the combination therapy resulted in 26.68% of LNCap and 31.70% of PC-3 with cell cycle arrest in the Sub-G1 phase and 35.37%

Abbreviations: AR, androgen receptor; Cdk, cyclin-dependent kinases; cyto-c, cytochrome c; DAPI, 4, 6-diamidino-2-phenylindole; DHT, dihydrotestosterone; DSBs, DNA double-strand breaks; FBS, fetal bovine serum; FDA, food and drug administration; FOH, fiber-optic hydrophone; FUS, focused ultrasound; FUS-Cav, short FUS shots with cavitation; HIFU, high-intensity focused ultrasound; HT, hyperthermia; MMP, matrix metalloproteinase; MR, magnetic resonance; MRI, magnetic resonance imaging; PARP, polyadenosine diphosphate ribose polymerase; PBS, phosphate-buffered saline; SEM, standard error of the mean; SF, clonogenic survival fraction; SRD5A, 5α-reductase; SRD5A1, type I 5α-reductase; SRD5A2, type II 5α-reductase; SRD5A3, type III 5α-reductase; T, testosterone; US, ultrasound.

of PC-3 with cell cycle arrest in the G2/M phase. Additionally, the treatment of FUS-Cav combined with HT block the androgen receptor (AR) signal pathway by reducing the relative Type I 5α-reductase (SRD5A1) level to 38.28 ± 3.76% in LNCap cells, and decreasing the relative Type III 5α-reductase 3 (SRD5A3) level to 22.87 ± 4.88% in PC-3 cells, in contrast, the relative SRD5A level in untreated groups was set to 100%.

Conclusion: FUS-induced cavitation increases the effects of HT by interrupting cancer cell membranes, inducing the DSBs and cell cycle arrest, and blocking the AR signal pathway of the prostate cancer cells, with the potential to be a promising adjuvant therapy in prostate cancer treatment.

KEYWORDS

focused ultrasound, cavitation, hyperthermia, combination, mechanisms, prostate cancer

Introduction

The mechanism of focused ultrasound or high-intensity focused ultrasound (FUS/HIFU) for medical applications is based on thermal and mechanical effects (Gourevich et al., 2013). In current clinical practice, HIFU-induced thermal ablation (at a temperature above 55°C) of the targeted tissue has been approved for the clinical treatment of uterine myomas, prostate diseases, bone metastasis-related pain, essential tremor, and Parkinson's disease, and the techniques of magnetic resonance (MR) or ultrasound (US) imaging are used to anatomical guide the FUS waves to the target and simultaneously enable therapy control (Siedek et al., 2019). Currently, further applications of FUS e.g., blood-brain barrier opening, immune stimulation, and neuromodulation are in the preclinical and clinical research phases. More biological and physical understanding is required for the investigation of FUS application in cancer therapy.

As one of the most crucial mechanical effects caused by FUS/HIFU, cavitation is described as the linear or non-linear oscillation of small vapor-filled cavities in the effects of expansion and compression cycles traveling through a medium in an acoustic field (Izadifar et al., 2019). Stable oscillations of small vapor-filled cavities at low acoustic pressures induce micro-streaming around cavitation nuclei and increase mass transmission through micromixing and convection (Wiggins and Ottino, 2004). This effect is named stable cavitation, which is applied for the induction of cell sonoporation and to support drug delivery. At high acoustic pressures, the small-sized vapor-filled cavities will expand rapidly over a few acoustic cycles and collapse violently. The phenomenon is termed inertial cavitation (Wiggins and Ottino, 2004), during which the generation of shock waves and liquid microjets are applied for histotripsy (Schade et al., 2012) and induction of anti-vascular (Daecher et al., 2017) effects. Hydrophones (Lai et al., 2006; Morris et al., 2009; Bull et al., 2011; Maxwell et al., 2013; Lo et al., 2014) were utilized to investigate cavitation dose quantification previously. Lo et al. (2014) a needle hydrophone to measure and control the cavitation events that occurred in a 24-well plate. The results showed that accurate, stable, and repeatable cavitation levels could be obtained using the hydrophone method. In contrast to the needle hydrophone, the fiber-optic hydrophone (FOH) with a thin optic fiber sensor was able to be located inside the 96-well plate, allowing low interference to the acoustic field and more accurate determination of cavitation dose for the limited space (Bull et al., 2011). A lot of prior research manifested that the hydrophone technique could also be utilized to determine the cavitation activity within *ex vivo* tissues or tissue-mimicking phantom, and the FOH sensor showed an advantage of the ease of positioning within the tissues or phantom and higher spatial sensitivity to cavitation occurring within samples (Lai et al., 2006; Morris et al., 2009; Bull et al., 2011; Maxwell et al., 2013). The technique of passive cavitation detection was also reported to determine the cavitation activity precisely *in vivo*.

Thermal ablation is currently the most commercially available FUS application in the clinic, with several devices approved by the FDA for clinical use and a total of 374,812 patients treated with HIFU thermal ablation by 2020 [FUS foundation]. In the clinical context of HIFU treatment, cavitation is so far a problem and is avoided during clinical thermal ablation with existing HIFU systems since it can interfere with magnetic resonance imaging (MRI) thermometry and is difficult to forecast and manage throughout the treatment process (Izadifar et al., 2019). However, this does not imply that cavitation is an undesirable event for the treatment of tumors; in fact, histotripsy—the non-invasive mechanical destruction of diseased tissue using the cavitation effect has been clinically accomplished (Schuster et al., 2018). The non-thermal characteristics of cavitation overcome all the drawbacks of thermal effects, including the heat sink effect, lack of predictability of margins, and thermal spread, etc. (Xu et al., 2021). In addition to histotripsy, cavitation is also used in drug delivery, blood–brain barrier opening, lithotripsy, and the induction of blood vessel destruction during cancer treatment. Thermal and cavitation effects are frequently concomitant during FUS therapy, where the cavitation effect is also one of the mechanisms for thermal effect generation (Farny et al., 2009; Izadifar et al., 2019). With the development of clinical cavitation detection techniques such as passive cavitation detection, active cavitation detection, and MRI techniques, precise detection and control of cavitation events for their clinical use is becoming possible. It is feasible that cavitation will no longer be considered a "useless and to be avoided" form in future HIFU therapeutic applications, but rather could synergistically work in combination with thermal effects in therapies. Because numerous studies reported anti-proliferative effects on cancer cells (e.g., cell apoptosis, cell-cycle arrest, and clonogenicity suppression) caused by cavitation-induced sonoporation (Miller and Dou, 2009; Karshafian et al., 2010;

Zhong et al., 2011; Chen et al., 2013), making it a potential adjuvant therapy to sensitize cancer cells in combination treatment regimes.

Hyperthermia (HT) refers to the generation of moderate heat in a range of 40°C–47°C where treatment time varies between a few minutes to 1 h (Hurwitz and Stauffer, 2014). HT technology can be classified into whole-body HT, localized HT, and regional HT, which are regularly employed to treat solid tumors in deep tissue with an external heat source to kill cancer cells or suppress their proliferation (Hegyi et al., 2013; Peeken et al., 2017). State-of-the-art of HT techniques includes electromagnetic equipment such as radiofrequency and microwave, ultrasound-induced HT, and novel magnetic nanoparticle heating (Peeken et al., 2017). Compared to other techniques, FUS-induced HT shows the benefit of non-invasive tissue penetration, and allowance of beamforming as well as shaping for both superficial and deep HT treatment. The HT caused by FUS has also been reported to induce cancer cell apoptosis by triggering intracellular oxidative stress (Hildebrandt et al., 2002; Saliev et al., 2013). HT inhibited the repair of DNA damage induced by radiotherapy and enhanced tissue oxygenation by improving blood flow, thus boosting the radiotherapy's cytotoxic effect (Song et al., 1997; Kampinga and Dikomey, 2001). HT was also reported to render cancer cells susceptible to chemotherapeutic drugs, accelerating tumor cell death. Thus, HT is generally used as adjuvant therapy to improve radiation or chemotherapy (Peeken et al., 2017). Additionally, HT induces changes in the tumor microenvironment and stimulation of immune response (Peeken et al., 2017). Due to the good linearity and temperature dependence, proton resonance frequency (PRF) shift MR thermometry is widely used in MRI-guided HIFU for non-invasive temperature monitoring inside the body by measuring the phase change resulting from temperature-induced PRF shift (Rieke and thermometry., 2011).

The AR signaling pathway plays a unique role in the development, functionality, and homeostasis of the prostate (Lonergan and Tindall, 2011). The conventional functions of the AR signaling pathway include modulation of lipid and protein biosynthesis and coordination of cell division, differentiation, proliferation, and apoptosis (Meehan and Sadar, 2003). Both testosterone (T) and dihydrotestosterone (DHT) can bind to the AR to activate the AR signaling pathway. The dissociation rate of the AR-DHT complex is much lower than the AR-T complex. Therefore, DHT is regarded as the primary ligand for binding with the AR due to the more stable AR-DHT complex (Wu et al., 2013). The binding of DHT to the AR promotes the dissociation of heat-shock proteins, and thereafter the AR-DHT complex is transferred into the cell nucleus to bind with androgen response elements and other complex response elements. By this time, the AR is trans-activated by the co-activators located on the DNA to modulate the transcription and expression of corresponding genes. Using various techniques, 146 to 517 genes and 44 proteins regulated by the AR signaling pathway have been detected in human prostate cancer cells (Meehan and Sadar, 2003). The AR signaling pathway is crucial to the initiation and development of prostate cancer. Maintaining of AR protein and activation of the AR signaling pathway are in every stage of prostate cancer, even after androgen deprivation therapy (Wu et al., 2013). The AR signaling pathway is indispensable for normal prostate development and function but also crucial for the initiation and progression of prostate cancer. DHT is responsible for activating the AR and is generated from testosterone (T) by the enzyme 5α-reductase (SRD5A), playing a vital role in the AR signaling pathway (Li et al., 2011). Three isozymes of 5α-reductase have been identified inside the human body till now. Type I and type III 5α-reductase (SRD5A1 and SRD5A3) were discovered to be correlated with DHT generation and AR activation in malignant prostate tumors (Uemura et al., 2008; Godoy et al., 2011), while type II (SRD5A2) is primarily expressed in normal prostate tissues (Thigpen et al., 1993; Chen et al., 1998). Immunofluorescence is a widely used technique to visualize the distribution of SRD5A in the cytoplasm and quantify the SRD5A level *via* flow cytometry.

In contrast, the effect of cavitation in combination with the thermal effect has not been sufficiently investigated till now. Our previous study (Hu et al., 2020) indicated that FUS-induced cavitation can improve the treatment outcome of HT (Hyperthermia, 45°C for 30 min) on prostate cancer cell PC-3, it is still necessary to explore the mechanism of the synergistic effects of the combination treatment of FUS-induced cavitation and HT. Therefore, in this study, we investigated the therapeutic effect of combination treatment on prostate cancer cell line LNCap and PC-3, as well as the mechanisms of enhanced efficacy by combination treatment.

Materials and methods

Prostate cancer cell lines and cell culture

The human prostate cancer cell lines PC-3 and LNCap were purchased from the European Collection of Authenticated Cell Cultures (ECACC, Salisbury, United Kingdom). PC-3 is a cell line established from bone metastasis of grade IV prostatic adenocarcinoma from a 62-year-old male Caucasian and cells were cultured in Ham's F-12 K (Kaighn's) medium (Gibco, Thermo Fisher Scientific, Germany). LNCap is a cell line isolated from metastasis at the left supraclavicular lymph node of a 50-year-old patient with a confirmed diagnosis of metastatic prostate carcinoma and cells were cultured in RPMI 1640 medium (Gibco, Thermo Fisher Scientific, Germany). All cell culture media were supplemented with 10% (v/v) fetal bovine serum (FBS, Gibco, Thermo Fisher Scientific, Dreieich, Germany), 100 U/mL penicillin, and 100 mg/mL streptomycin (Biochrom GmbH, Berlin, Germany) and all cultures were maintained at 37°C with 5% (v/v) CO_2 in humidified air. Cell culture mediums were changed every 2–3 days. For sub-cultivation and experiments, cells were routinely washed with phosphate-buffered saline (PBS) without Ca^+, Mg^+, and phenol red (Biozym Scientific GmbH, Germany) and detached using trypsin/EDTA (Biozym Scientific GmbH, Germany). Cells were routinely tested for *mycoplasma*.

FUS *in vitro* system

The *in vitro* FUS apparatus includes a Perspex® water bath compartment, where the ultrasound source (transducer) and a

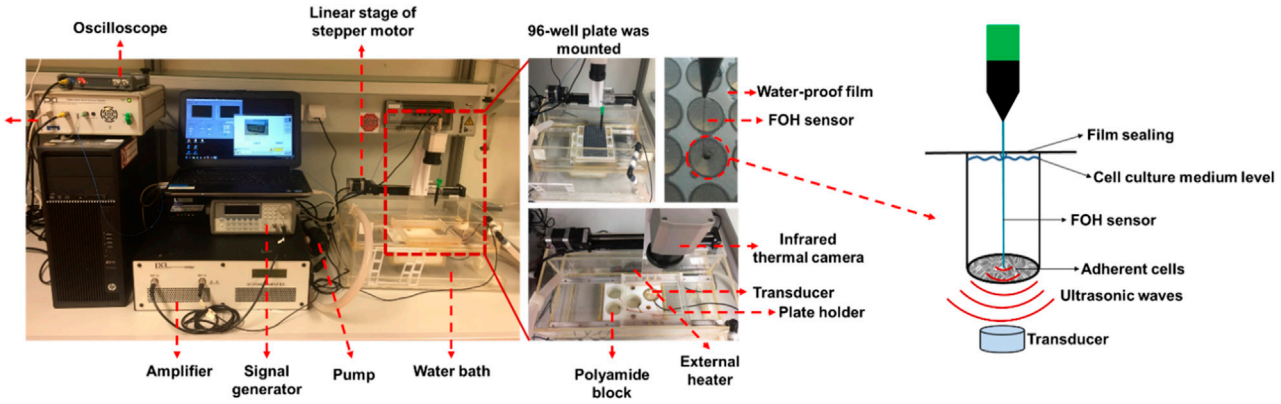

FIGURE 1
In vitro focused ultrasound (FUS) apparatus displaying experimental configuration for cavitation detection and FUS treatment. The FUS system is composed of a Perspex® water bath compartment with pump and adjustable heater, a customized single-element FUS transducer at 1.467 MHz, a small polyamide block worked to detachably accommodate the transducer, a 3D-printed plate holder, and a stepper motor to move the 96-well plate. The continuous ultrasound waves were emitted from the transducer using the FUS signal generator and a radiofrequency power amplifier. A 96-well μclear plate was used for the FUS treatment of cells. To retain the cells in a sterile environment, the plate was protected with a water-proof film. A fiber-optic hydrophone system connected to an oscilloscope was utilized to calibrate the transducer and measure the dose of cavitation that occurs on the adherent cells. The right diagram shows the measurement position of the FOH sensor and the focused ultrasonic action site. A thermal camera was mounted to measure the temperature in real time. The LabView application was utilized to control the FUS treatment using a feedback loop to the thermal camera.

96-well cell culture plate located in a 3D-printed plate holder were placed. Degassed water was used as the transport medium that transferred ultrasonic waves to the cells, and also contributed to the creation of an environment with stable temperature during the treatment. A self-priming water pump (Lei Te Co., Ltd., Guangdong, China) was employed for the circulation of degassed water to prevent bubble formation beneath the plate from interfering with the FUS wave propagation. The circulating water passed through an external heater (Hydor, Salisbury, United Kingdom) to hold the water temperature at 34°C. A small polyamide block inside the water bath was used to detachably accommodate the customized single FUS transducer. The FUS transducer was made from Perspex® tubes with geometrically-focused piezoceramic bowls positioned at the top of each tube with a frequency of 1.467 MHz. Adapted lengths of transducers were designed to precisely position the focus spot at the bottom of the 96-well plate. Various waveforms could be generated by a FUS signal generator (33120A, Agilent Technologies, Edinburgh, United Kingdom) and amplified by an A075 RF power amplifier (A075, Electronics and Innovation, Rochester, NY, United States). An X-slide linear stage connected to a programmable VXM motor controller and a NEMA 17 stepper motor (all VELMEX Inc., Bloomfield, NY, United States) were the main components of the motion system, which was used to move the 96-well plate for precise positioning of the focal regions at wells in different lines. Four starting positions of transducers on the polyamide block were alternated to sonicate selected wells in different columns of a 96-well plate. An infrared thermal camera (Optris PI450, Optris GmbH, Berlin, Germany) was mounted above the 96-well plates to monitor the real-time temperature in the wells during FUS treatments (Figure 1).

FUS-Cav treatment of prostate cancer cells

Ultrasound penetrable 96-well plates (Greiner Bio-One, Frickenhausen, Germany) with μ-clear bottom were used for the FUS treatment of prostate cancer cells. Cancer cells were seeded at a concentration of 6,000–10,000 cells/well in 100 μL corresponding cell culture medium to reach 80%–100% of cell confluency at the desired time point post-treatment. The seeding was performed 24–48 h before treatment. The 96-well plates for culturing of LNCap cells were coated with 40 μL/cm^2 poly-L-lysine solutions for 30 min at 37°C and washed twice with distilled water (Song and Khera, 2014) to improve the adherence of LNCap cells. Before sonication, up to 420 μL/well of cell culture medium was added in the wells and the 96-well plate was sealed with Titer Top® film (Sigma-Aldrich, Munich, Germany). To separate the FUS-induced thermal and mechanical effects, an infrared thermal camera was mounted above the 96-well plate to monitor the real-time temperature in the wells during FUS treatments. When the temperature in the wells reached 39°C, the sonication stopped until the temperature decreased to the baseline of 34°C. In prior work (Hu et al., 2020), the FOH system was used to determine the cavitation dose at various focused acoustic intensities of 129, 344, 539, 1,136, and 1704 W/cm^2. While accounting for the consistency and stability of the cavitation events at the focused acoustic field, a FUS treatment protocol (Hu et al., 2020) was designed to induce the cavitation on the adherent cancer cells: a segmental FUS treatment (FUS-Cav) at the acoustic intensity of 1136 W/cm^2 and an active sonication duration of 40 s. The cavitation dose of FUS-Cav was 62.6 mV*s (stable cavitation dose: 16.33 ± 4.29 mV*s; inertial cavitation dose: 46.27 ± 17.17 mV*s). The active sonication duration of each segment was 0.86 s and the treatment duration was 126.7 s with a temperature of 36.50°C ± 1.53°C.

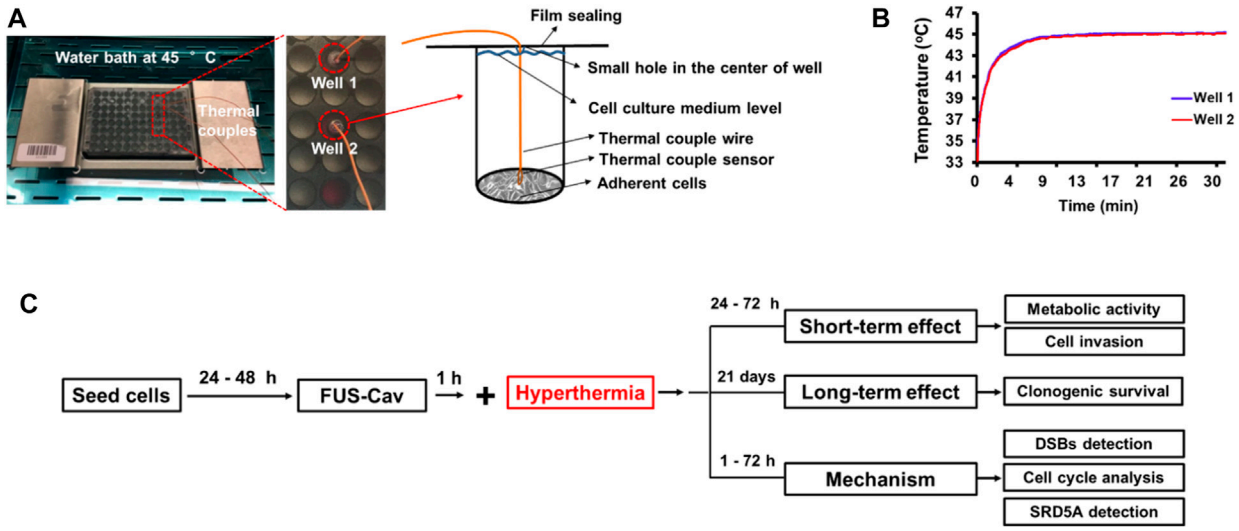

FIGURE 2
Experimental setup of water bath hyperthermia with 96-well plate at 45°C. **(A)** The real-time temperatures in two reference wells were measured with inserted thermal couples close to monolayer cells. **(B)** Temperature curves in two reference wells. **(C)** The timeline of the combined treatment and biological experimentation is depicted in the flow chart for the experimental plan.

HT treatment with water bath and protocol of combination treatment for prostate cancer cells

In order to investigate whether cavitation treatment could benefit from HT, cancer cells were treated with conventional HT in a water bath (Perspex International, Lancashire, United Kingdom). Cells were seeded at a density of 6,000–10,000 cells/well in a 96-well plate to reach 80%–100% of cell confluency at the desired time point post-treatment. To maintain the sterile environment and prevent evaporation of the cell culture medium, 96-well plates were sealed with Titer Top® films before water bath HT treatment and then carefully placed in a pre-warmed water bath. Type T PTFE-insulated Copper-Constantan precision fine wire thermocouples (diameter 0.07 mm, Pico Technology, St Neots, United Kingdom) were used to measure the temperature inside two reference wells (Figure 2A), and a Pico data logger was used to record real-time temperature and collect data (Figure 2B). Based on the literature (Cihoric et al., 2015) and preliminary experiments (Hu et al., 2020), water bath HT treatment was performed at the temperature of 45°C for 30 min. In order to examine the additive effects of FUS-Cav to HT, water bath HT treatment was performed 60 min after FUS-Cav. Measurements of metabolic activity and cell invasion were utilized to assess the short-term effect 24–48 h after treatment, and a clonogenic assay was used to evaluate the long-term effect 21 days after treatment. DSBs detection, cell cycle analysis, and measurement of SRD5A expression were conducted to investigate the underlying mechanism of FUS-Cav induced additive effect to HT treatment (Figure 2C).

Evaluation of cell ability to reproduce with clonogenic assay

To examine the reproductive ability of a single cell in the long-term after different treatment regimes, clonogenic assay was performed according to the procedure reported by Franken et al. (Franken et al., 2006). Cell suspensions were harvested from 96-well plates with 100 µL trypsin/EDTA (×1) per well immediately after treatment and were seeded with a density of 500–1,000 cells/well into 6-well plates in triplicates. The 6-well plates were incubated for 21 days to allow colony formation, while the cell culture medium was changed twice per week. Colonies were gently rinsed with PBS twice before fixation with ice-cold methanol/acetone (1:1, V/V) for 5 min, afterward stained with 0.5% crystal violet solution in water for 30 min at room temperature and washed with deionized water to remove the unbound stain. Colonies in dried plates were scored if they exceeded a threshold number of 50 cells.

Cell invasion assay

The potential of prostate cancer LNCap and PC-3 cells to migrate was evaluated by the *in vitro* Transwell® invasion assay (Yu et al., 2013). The Transwell® chamber system (Corning, New York, United States) consists of a Transwell® insert mounted on the 24-well plate. The upper and lower chambers are divided by a polycarbonate porous membrane pre-coated with 100 µg/cm^2 matrigel (Corning, New York, United States) at 37°C for 4 h. Cells were harvested from 96-well plates immediately post-treatment (FUS-Cav, HT, FUS-Cav + HT). Approximately 1 ×

10^5 cells were resuspended in 100 µL serum-free cell culture medium and seeded in the upper Transwell® chamber. 600 µL medium was supplemented with 10% FBS as a chemo-attractant source in the lower chamber. After the incubation at 37°C for 48 h for the Transwell® chamber system, a sterile cotton swab was used to remove the non-invaded cells on the upper surface of the polycarbonate porous membrane. The invaded cells on the lower surface of the membrane were fixed with 600 µL of methanol (Carl Roth, Karlsruhe, Germany) and stained with 0.1% crystal violet (Sigma-Aldrich, Munich, Germany) for 15 min at room temperature. The invaded cells were visualized with a microscope (Zeiss, Axioobserver), and five bright light images of random fields of view were taken at 200-fold magnification in each Transwell® insert. The stained invaded cells were counted in ImageJ. All data were normalized to untreated control, which was set to 100%.

Determination of impact on cell metabolic activity

To evaluate the short-term effects of the various treatments on the cellular metabolic activity of the human prostate cancer cell line LNCap and PC-3, the WST-1 assay was conducted 24, 48, and 72 h post-treatment. The cellular enzyme of mitochondrial dehydrogenases cleaved WST-1 reagent (tetrazolium salt) to formazan dye in the sample, quantification of formazan dye was directly correlated to the number of metabolically active cells in the culture medium. Based on the manufacturers' instructions, the cell culture medium was discarded and cells were incubated with 100 µL fresh culture medium containing 10% WST-1 reagent (Carl Roth, Karlsruhe, Germany) in the 96-well plates at 37°C for 30 min. The absorbance of the formazan product was measured at 435 nm with a reference wavelength of 680 nm using a microplate reader (BioTek Instruments, Inc., Bad). All data were normalized to untreated control which was set as 100%.

Detection of DSBs

To investigate the DSBs induced by FUS, HT or the combination treatment, γH2A.X assay was conducted 1 and 24 h after each treatment. Cell culture medium in 96-well plate was aspirated and discarded from each well, and cells were fixed with 4% formaldehyde for 10 min at 37°C. The cells were chilled on ice for 1 min, the fixative was discarded and cells were washed 3 times with ×1 PBS. The 90% methanol was added to each well to permeabilize cells on ice for 30 min, and cells were washed 3 times with ×1 phosphate-buffered saline (PBS) again. Non-specific bindings of antibodies were blocked with blocking buffer (0.5% bovine serum albumin solution (BSA, Cell Signalling Technology, Danvers, MA, United States, 100 µL/well) in PBS) at room temperature for 10 min. Following removing the blocking buffer, cells were incubated with 50 µL/well phospho-histone H2A.X (Ser139) rabbit primary monoclonal antibody (#9718, Cell Signalling Technology, Danvers, MA, United States) at the concentration of 1:400 diluted with blocking buffer at room temperature for 1 h. Cells were washed 3 times with anti-body free blocking buffer, and incubated with 50 µL/well of fluorescently conjugated secondary antibodies (Anti-Rabbit IgG (H + L), F (ab')2 Fragment (Alexa Fluor® 594 Conjugate); #8889, Cell Signalling Technology, Danvers, MA, United States) at the concentration of 1:1,000 diluted with blocking buffer for 30 min at room temperature in the dark. After the incubation, the secondary antibody solutions were discarded and cells were washed 3 times with blocking buffer. Cell nuclei were stained with the nuclear stain 4, 6-diamidino-2-phenylindole (Fluoromount-G™ including DAPI, Thermo Fisher Scientific, Darmstadt, Germany) for 5 min. The foci representing DSBs were visualized at ex 561/em 594 nm and cell nuclei were stained by DAPI at ex 358/em 461 nm using a fluorescence microscope with 400-fold magnification. Semi-quantitative analysis was performed to calculate the mean numbers of stained foci per cell nucleus by the ImageJ software. All nuclei were counted in each image (80–120 nuclei).

Cell cycle analysis detection

Nicoletti assay was performed 72 h after each treatment to explore the impact of FUS, HT or the combination treatment on cell cycle phase distribution and apoptosis-induced DNA fragmentation. After the trypsinization with 100 µL trypsin/EDTA per well, cell suspensions were harvested to the 1.5 mL microtube from a 96-well plate, cells were washed twice with PBS and fixed using 70% ethanol overnight at –20°C. Afterward, cells were washed twice with PBS again and incubated at 37°C for 20 min, with 60 µL RNaseA solution (Sigma-Aldrich GmbH, Munich, Germany) at a concentration of 0.1 mg/mL diluted with PBS. Next, the propidium iodide solution (PI, Sigma-Aldrich GmbH, Munich, Germany) at a concentration of 50 µg/mL in PBS was used to stain the DNA content of cells at 4°C for 5 min and cells were analyzed by flow cytometry (AttuneNxT, Thermo Fisher Scientific, Darmstadt, Germany).

Visualization of SRD5A distribution

The impact of FUS-induced cavitation and HT on the SRD5A enzyme in prostate cancer cell lines was investigated using immunofluorescence microscopy. Cells in the 96-well plate were incubated at 37°C for 24 h after treatments. Cells in a 96-well plate were fixed on ice with 100 µL/well of 4% formaldehyde (Carl Roth, Karlsruhe, Germany) in PBS for 15 min, and the cells were permeabilized with 0.1% Triton® X-100 (Carl Roth, Karlsruhe, Germany) in PBS for 10 min. Non-specific bindings of the antibodies were blocked by the blocking buffer (4% FBS in PBS) for 1 h at room temperature. Cells were incubated overnight with blocking buffer containing 2 µg/mL 5α-reductase-1 primary antibody (Anti-SRD5A1 antibody produced in rabbit; Sigma-Aldrich, Munich, Germany) or 5-reductase-3 primary antibody (Anti-SRD5A3 antibody produced in rabbit; Sigma-Aldrich, Munich, Germany) at 4°C. After washing four times with PBS, cells were incubated with 2 µg/mL secondary antibodies (Anti-Rabbit IgG (H + L), F (ab')2 Fragment (Alexa Fluor® 594 Conjugate); #8889, Cell Signalling Technology, Danvers, MA, United States) in blocking buffer for 3 h at room temperature in the dark. The secondary antibody was removed, and the cell nuclei were

stained with the nuclear stain 4, 6-diamidino-2-phenylindole (DAPI) for 5 min. Immunofluorescence in the absence of primary antibodies was used as the negative control. The expressions of SRD5A1 and SRD5A3 proteins labeled by Alexa Fluor® 594 were visualized at ex 561/em 594 nm and cell nuclei were stained by DAPI at ex 358/em 461 nm using a fluorescence microscope with 400-fold magnification.

Quantification for the reduction of SRD5A proteins with flow cytometry

Flow cytometry was performed to quantify the SRD5A positive cells. Cell suspensions were harvested in a 1.5 mL microtube from a 96-well plate 24 h incubation after treatments. Cell supernatants were discarded after centrifuging at 2000 rpm, for 5 min. The cells were fixed on ice with 4% formaldehyde solution in PBS for 15 min and permeabilized with 0.1% Triton® X-100 in PBS for 10 min. The non-specific binding of antibodies was blocked with a blocking buffer at room temperature for 1 h. The cells were incubated with 2 μg/mL 5α-reductase-1 primary antibody (Anti-SRD5A1 antibody produced in rabbit) or 5α-reductase-3 primary antibody (Anti-SRD5A3 antibody produced in rabbit) dissolved in blocking buffer overnight at 4°C. Next, cells were washed four times with PBS and incubated with 2 μg/mL secondary antibodies (Anti-Rabbit IgG (H + L), F (ab')2 Fragment (Alexa Fluor® 594 Conjugate)) in a blocking buffer for 3 h at room temperature in the dark. Samples without incubation of primary antibody were used as the background control, and cells with higher fluorescence intensity than the background group were the fluorescent dye positive cells, the percentage of which indicated the overall SRD5A level 24 h after all treatments. Cell doublets and debris were excluded from the analysis of forward-scattered light (FSC) versus side-scattered light (SSC) using flow cytometry (AttuneNxT, Thermo Fisher Scientific, Darmstadt, Germany). Analysis of the percent dye positive cells was performed on at least 20,000 single cells. All data were normalized to untreated control which was set to 100%.

Cell sonoporation investigation

Sonoporation is defined as the recoverable perforation of the cell membrane created by FUS-induced stable cavitation. In order to investigate this phenomenon on cell membranes post-FUS exposure, PI was employed as a probe of cell membrane integrity in this study. PI cannot penetrate the intact cell membranes of living cells (Van Wamel et al., 2006) but is permeant to the sonoprated cells due to the perforation of the cell membranes. After the cell membrane is restored from sonoporation, PI remains inside the cells and stains the cell nucleus. CellMask™ Green Plasma Membrane Stain (Thermo Fisher Scientific, Darmstadt, Germany) was used to visualize cell membranes in this experiment. Cancer cells were seeded at a density of 5,000 cells/well in an ultrasound-permeable 96-well plate with a μ-clear bottom 24 h before sonication. Cells were treated with the FUS-Cav protocol as described above for 40 s in the cell culture medium, and the cells were gently washed with 100 μL of PBS. PI (Cayman Chemical, Ann Arbor, Michigan, United States) at a final concentration of 1 μg/mL and CellMask™ at a final concentration of 5 μg/mL were added to the cell culture medium before or 30 min after FUS-Cav treatment. PI-stained cell nuclei were visualized immediately at the excitation/emission at 535/617 nm, and cell plasma membranes were stained with CellMask™ at ex 522/em 535 nm using a fluorescence microscope and ZEN2.3 software. Since the focused spot of FUS exactly covers one well bottom of the 96-well plate, five random-field fluorescence images were taken at 200-fold magnification. Cells stained with PI and CellMask™ (approximately 150 cells in each field) were calculated to quantify the percentage of PI-positive cells.

Statistical analysis

The results of all measurements, including the survival fraction (clonogenic assay), cell invasion (transwell assay), metabolic activity (WST-1 assay), DNA double-strand breaks (H2A.X assay), cell cycle (Nicoletti assay), SRD5A visualization and quantification (immunofluorescence assay with microscopy and flow cytometry), and sonoporation efficiency (PI uptake assay), were expressed as mean ± SEM (Standard Error of the mean) of three independent experiments in two replicates. One-way ANOVA and the Tukey test for *post hoc* analysis were used to evaluate the significant differences between the mean values in any two groups. The non-parametric Mann-Whitney test was used in the statistical analysis of the clonogenic survival data in SPSS statistical software version 24. Statistical significance was defined as a p-value ≤ 0.05.

Results

FUS-Cav increases the effects of HT by reducing the clonogenic survival of prostate cancer cells

To investigate whether the treatment of short FUS-induced cavitation owns the long-term additional benefits to HT, the clonogenic survival fraction (SF) of cancer cells was assessed based on the number of cell colonies (Figure 3Aa) post-treatment. Although FUS-Cav alone only showed a limited impact on the clonogenic survival of LNCap cells, a significant decrease in SF was observed after the combination of FUS-Cav and HT in comparison to all single treatment groups. The effect on clonogenic survival following HT (SF: 0.40 ± 0.030) was enhanced by combining FUS-Cav (FUS-Cav + HT) revealing a 2.2-fold reduction of SF to 0.18 ± 0.028 (Figure 3Ab). For another prostate cancer cell line PC-3, the long-term increasing effects of FUS-Cav to HT were reported in our previous research (Hu et al., 2020): the combination of FUS-Cav and HT results in a 2-fold (SF: 0.37 ± 0.080) decrease of clonogenic survival compared to HT alone (0.74 ± 0.042) (Figure 3Ab).

FUS-Cav supports HT to diminish cell potential to invade and metabolic activity of prostate cancer cells

The short-term additive effects induced by FUS-Cv to HT were investigated *via* the evaluation of LNCap and PC-3 cell invasion (Figure 3Ba) 48 h post-treatment. Similar to the results of long-term

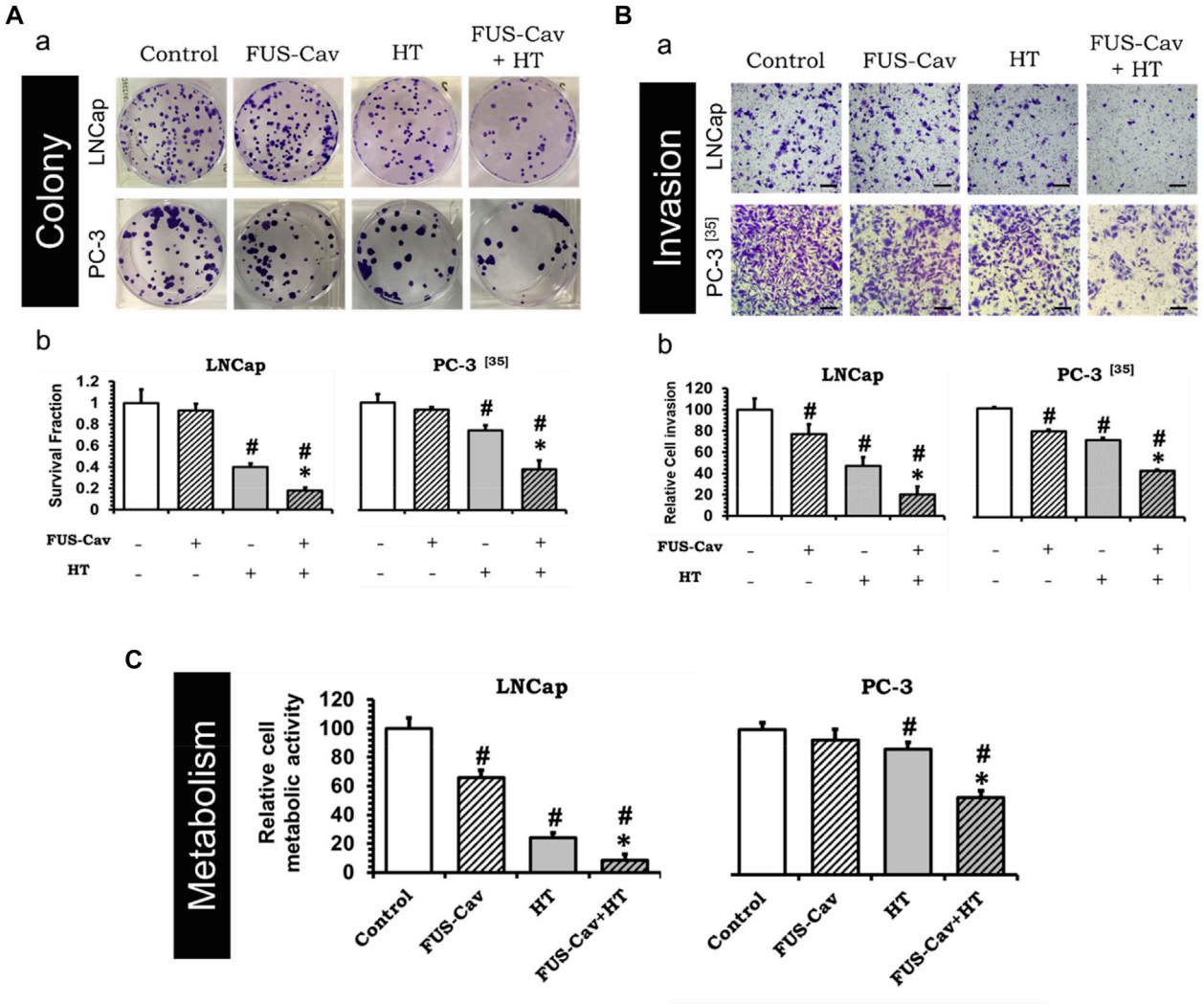

FIGURE 3
FUS-Cav (1136 W/cm^2, 40 s) demonstrated additive effect to HT (45°C, 30 min). **(A)** a: Representative images of colony formation in LNCap and PC-3 cells 21 days post-treatment. Cell survival fraction was calculated as the counted colonies divided by the product of the seeding number and the plating efficiency. b: Cell survival fraction diagrams of LNCap and PC-3 (Hu et al., 2020) cells, suggesting the ability of a single cell to grow into a colony after various treatments. **(B)** a: Representative microscopy images of Transwell® assay in LNCap and PC-3 (Hu et al., 2020) cells 48 h post-treatment. Scale bar = 100 μm. b: Relative cell invasion of LNCap and PC-3 (Hu et al., 2020) cells derived from semi-quantitative analysis of the Transwell® assay revealing cell invasive potential 48 h post-treatment. **(C)** Relative cellular metabolic activity was detected by WST-1 assay 72 h (for LNCap) or 48 h (for PC-3) post-treatment. Data were normalized to untreated control, which was set to 100%, and relative values are presented as mean ± SEM, n = 6, *significantly different from HT ($p \leq 0.05$), #significantly different from control ($p \leq 0.05$).

effects evaluation, FUS-Cav treatment also showed a significant additive effect on HT in the short term. The FUS-Cav alone leads to a significant loss of cell potential to invade (relative cell invasion of FUS-Cav: 77.19 ± 9.25%) compared to control, and the cavitation also enhanced the effects of HT, reducing the relative cell invasion from 46.87 ± 8.42% (HT) to 20.30 ± 7.16% (FUS-Cav + HT) (Figure 3Bb). Comparable effects were observed in the PC-3 cell line as described in detail previously (Hu et al., 2020): the combination treatment of FUS-Cav and HT leads to a significant decline of cell relative invasion (46.67 ± 1.17%) in comparison to single HT (70.73 ± 2.14%) (Figure 3Bb).

Another approach to evaluate the short-term additive effects induced by FUS-Cv to HT was WST-1 assay, which was performed 24, 48, and 72 h after each treatment. For both prostate cancer cell lines, the relative cell metabolic activities in the combination groups (FUS-Cav + HT) were significantly decreased at each incubation time point compared to the single treatment groups. Nevertheless, the magnitude of the decline varies depending on the incubation time. For LNCap cells, the relative cell metabolic activities were reduced from 97.62 ± 16.54% (24 h), 28.17 ± 4.38% (48 h), and 24.00 ± 3.60% (72 h) in the single treatments (HT alone) to 52.60 ± 13.43% (24 h), 19.08 ± 10.57% (48 h), and 8.54 ± 4.34% (72 h) in the combination groups (FUS- Cav + HT), respectively (Figure 3C). And for PC-3 cells (Hu et al., 2020), the relative cell metabolic activities declined from 81.60 ± 7.92% (24 h), 86.26 ± 4.84% (48 h), and 78.38 ± 10.56% (72 h) in the single HT treatments to 64.09 ±

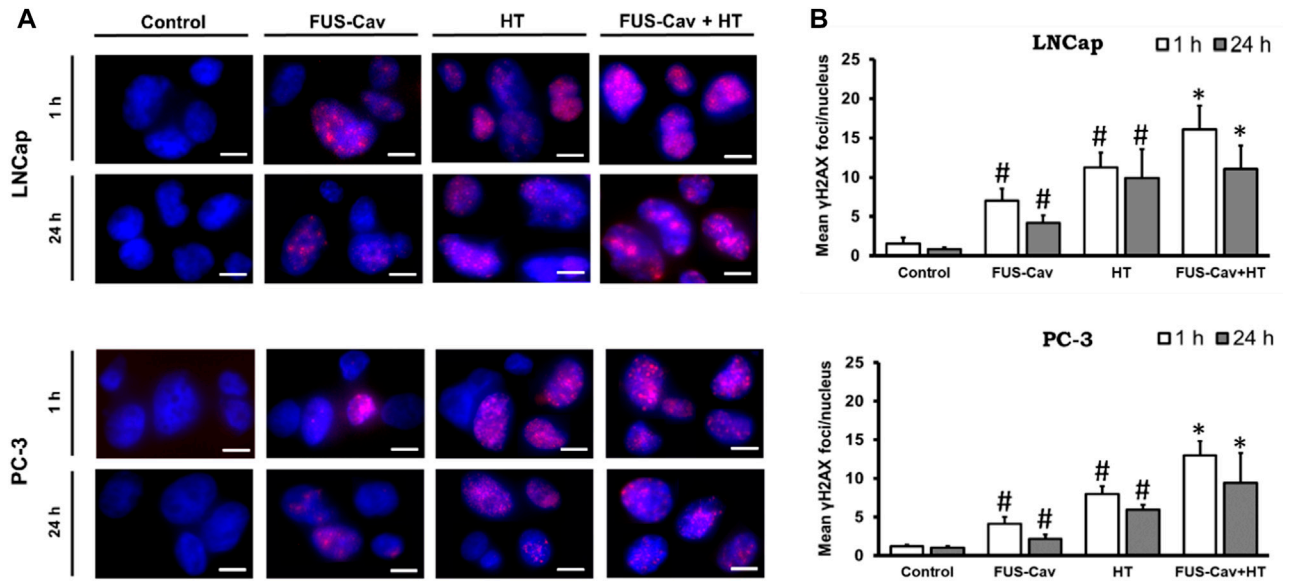

FIGURE 4
DSBs increased when FUS and HT were combined as opposed to when they were administered separately. **(A)** H2A.X foci (Alexaflour568 red) in the cell nucleus (blue) after single FUS or single HT is shown in representative microscopic fluorescence images, with the combined treatment (FUS + HT) displaying a greater amount of H2A.X foci than every single treatment. Scale bar = 10 μm. **(B)** Semi-quantitative analysis of H2A.X foci at 1- and 24- hours post-treatment. Data were presented as mean ± SEM, $n = 6$, *significantly different from HT ($p \leq 0.05$), #significantly different from control ($p \leq 0.05$).

1.84% (24 h), 53.20 ± 21.49% (48 h), and 66.76 ± 11.28% (72 h) in the combination treatment of FUS-Cav and HT (Figure 3C).

Boost of DSBs by the combination treatment of FUS-Cav and HT

The formation of γH2A.X represented an early cellular response event against DSB and was used as a biomarker to monitor DNA damage and repair. The effects of FUS-induced cavitation and its combined therapy with HT on the mechanism of sensing and repairing DNA damage were evaluated by counting the number of γH2A.X foci at 1 and 24 h after treatment in this study. Representative fluorescent microscopy images of stained γH2A.X foci (Figure 4A) display low levels of stained initial (1 h) and residual (24 h) foci in both cell lines in the untreated groups, with foci numbers ranging only from 0.85 to 1.53 foci/nuclei. Higher numbers of initial and residual γH2A.X foci were observed in the LNCap cell nucleus (initial foci number: 7.03 foci/nuclei; residual foci number: 4.19 foci/nuclei) than PC-3 cell (initial foci number: 4.15 foci/nuclei; residual foci number: 2.18 foci/nuclei) after a single FUS-Cav treatment (Figure 4B). The number of initial foci detected in LNCap (1.4-fold) and PC-3 (1.6-fold) cells was significantly enhanced after combining FUS and HT (LNCap: 16.07 foci/nuclei; PC-3: 12.97 foci/nuclei) compared to HT alone (LNCap: 11.22 foci/nuclei; PC-3: 8.00 foci/nuclei) (Figure 4A). Residual lesions, defined as foci scoring 24 h after treatment, revealed a similar trend to the result of initial lesions, with a slight decline in the number of foci compared to initial lesions (Figure 4A). Hence the highest numbers of stained initial and residual foci in both cell lines were observed in the combined group (FUS-Cav + HT).

Sub-G1 apoptosis and G2/M phase arrest induced by the combination treatment of FUS-Cav and HT

Flow cytometry was performed to analyze the regulation of cell cycle distribution and sub-G1 fraction representing apoptotic cells 24 h after the combination treatment of FUS-Cav and HT (Figure 5A). For LNCap cells, single HT treatment showed a significant accumulation of cells in the G2/M phase compared to the untreated control but no change in the Sub-G1 phase. Interestingly, single FUS-Cav (10.22 ± 1.60) led to a significantly increased percentage of cells in the Sub-G1 phase compared to untreated cells (6.28 ± 1.94) (Figure 5B). And the combination treatment of FUS-Cav and HT exhibited a dramatic accumulation of cells in Sub-G1, the percentage of cells arrested in the Sub-G1 phase increased from 6.28 ± 1.94% in untreated cells and 6.13 ± 1.93% in the HT group to 26.68 ± 4.38%. This was accompanied by a concomitant decline in the percentage of cells in the G0/G1 phase (Figure 5B). For PC-3 cells, a significant enhancement of the percentage of cells in the Sub-G1 phase was observed in the treatment of HT combined with FUS-Cav (FUS-Cav + HT: 31.7 ± 6.40%) compared to single treatment and untreated control (FUS-Cav: 13.35 ± 2.75%; HT: 20.88 ± 7.31%; Untreated control: 4.89 ± 2.00%). Notice that there was a significant increase in the percentage of cells at the G2/M phase from 26.02 ± 6.47% in HT alone to 35.37 ± 9.30% in

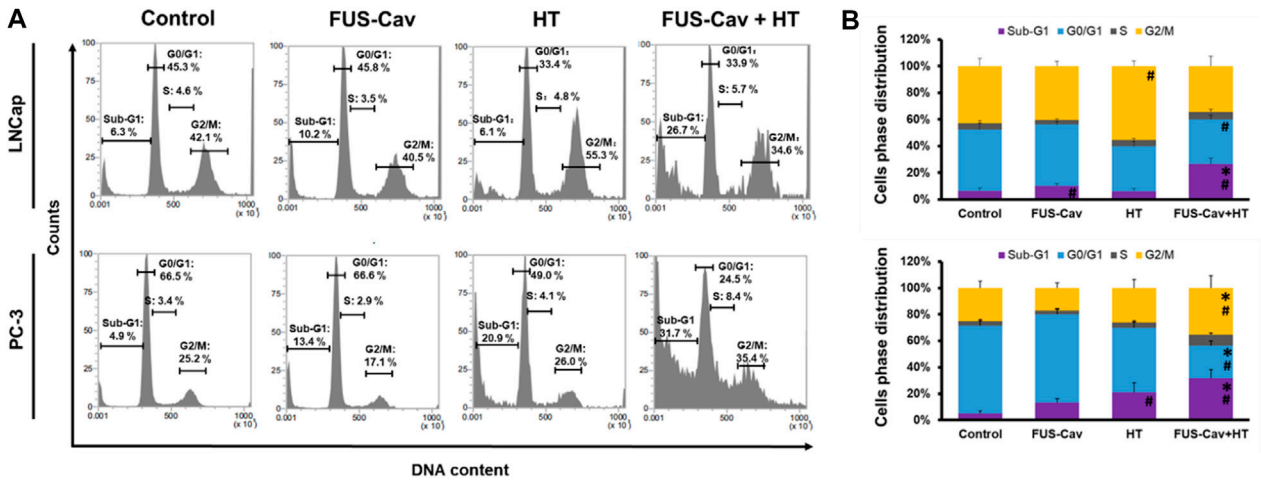

FIGURE 5
The combination of FUS-Cav and HT impacts the cell cycle phase in apoptotic sub-G1 and G2/M. **(A)** Representative flow cytometry results exhibit the percentage of cells in various cell cycles following each treatment. **(B)** Graphical columns show the cell cycle distribution of LNCap and PC-3 cells 48 h post-treatment. The count of cells in each cell cycle was presented as a percentage of the total cell amount. Data were presented as mean ± SEM, $n = 6$, *significantly different from HT ($p \leq 0.05$), #significantly different from control ($p \leq 0.05$).

HT combined with FUS-Cav, accompanied by a decrease in the percentage of cells in the G0/G1 phase (Figure 5B).

FUS-Cav enhances the effects of HT by inhibiting the SRD5A protein level in prostate cancer cell lines

After various treatment regimes, fluorescent microscopy was performed to visualize the subcellular localization of immunofluorescence-tagged SRD5A1 and SRD5A3 in the prostate cancer PC-3 and LNCap cell lines. Figure 6A shows the Alexa Fluor® 594-tagged SRD5A1 and SRD5A3 protein, and the fluorescence is distributed diffusely throughout the cytoplasm. In the fluorescent microscopy images for both PC-3 and LNCap cell lines, the distribution of SRD5A1 and SRD5A3 proteins were downregulated 24 h post single treatment of water bath HT. The effects of water bath HT treatment on reducing the SRD5A level were seemingly enlarged by adding short FUS-Cav treatment in terms of the visualization of SRD5A protein distributions (Figure 6A). In order to quantify the percentage of dye-positive cells in the total number of cells collected for analysis, flow cytometry was performed for the fluorescence-activated cell sorting after each treatment. Figure 6B shows the percentage of cells with immunofluorescence-tagged SRD5A1 or SRD5A3 protein for PC-3 and LNCap cell lines 24 h post-treatment. Figure 6C demonstrates the relative level of these two isozymes to untreated control in both cell lines after various treatments.

For the LNCap cell line, the relative SRD5A1 level was slightly decreased to 91.19 ± 2.98% by single treatment of FUS-Cav compared to untreated control (100 ± 5.39%). Nevertheless, FUS-Cav strengthened the impacts of combination treatment of FUS-Cav + HT, significantly reducing the relative SRD5A1 level from 51.21 ± 6.47% (HT) to 38.28 ± 3.76% (FUS-Cav + HT). FUS-Cav treatment alone significantly reduced the SRD5A3 level to 87.93 ± 4.58% compared to the untreated control. However, the combination treatment of FUS-Cav and water bath HT resulted in a decrease in SRD5A3 level from 26.78 5.03% (HT) to 23.32 1.76% (FUS-Cav + HT), indicating that FUS-Cav had no significant additive effects on water bath HT (Figure 6C).

For the PC-3 cell line, the relative SRD5A1 level was significantly diminished to 52.94 ± 2.84% by the single treatment of water bath HT compared to the untreated sample (100 ± 2.22%). Single FUS-Cav did not show significant suppressive effects on the expression of SRD5A1 compared to untreated control, and the combinatory treatment of FUS-Cav and water bath HT was not able to significantly reduce the SRD5A1 level compared to single treatment of water bath HT as well, indicating FUS-Cav had no additive effects to water bath HT suppressing the SRD5A1 expression. Single treatment of FUS-Cav induced a slight decline in SRD5A3 expression. The relative SRD5A3 level was significantly decreased by the combinatory treatments to 22.87 ± 4.88% (FUS-Cav + HT) compared to single water bath HT (55.70 ± 4.70%), denoting a significant additive effect of FUS-Cav to water bath HT in reducing the SRD5A3 expression (Figure 6C).

FUS-Cav induces sonoporation in prostate cancer cells

The sonoporation phenomenon induced by FUS-Cav was investigated exemplarily in prostate cancer cells. PI, which initially cannot penetrate the intact cell membrane, can pass through the pores created temporarily in the cell membrane by sonoporation and stain the cell nucleus. Therefore, PI staining was employed as an indicator to explore the phenomenon of sonoporation, and CellMask™ staining was used to visualize cell

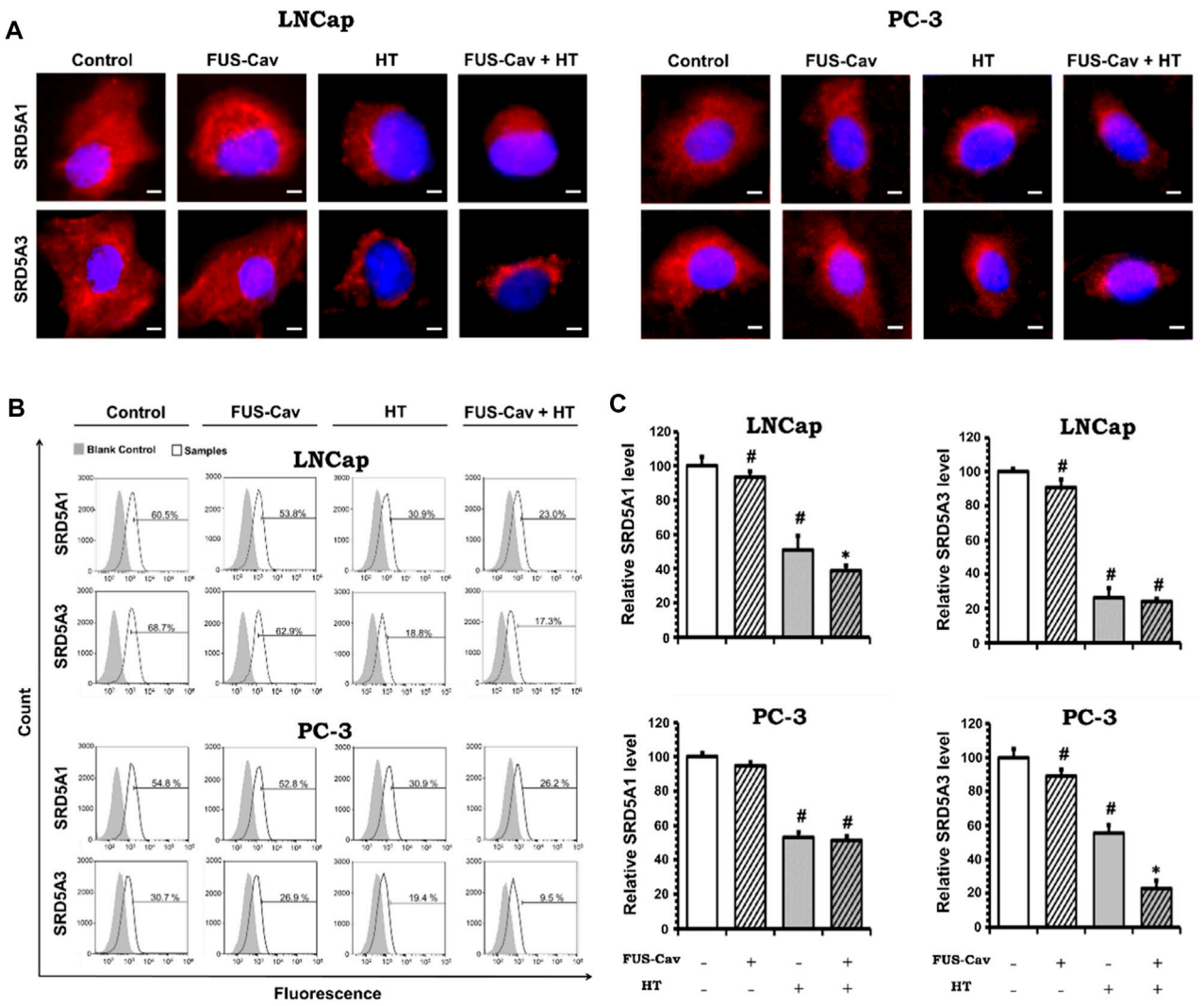

FIGURE 6
Effects of FUS-Cav to water bath HT decreasing the SRD5A distribution and expression were associated with cancer cell type. **(A)** Representative fluorescence microscopy images for LNCap and PC-3 cells showing the distribution of SRD5A1 and SRD5A3 proteins in the cytoplasm 24 h post-treatment. Scale bar = 5 μm. **(B)** Flow cytometry results exhibit the percentage of immunofluorescence-positive cells in all collected LNCap and PC-3 cells for analysis: histograms of immunofluorescence-positive cells showing the SRD5A level (percentage of fluorescence-positive cells indicated in each plot) after each treatment. The fluorescence-negative cells immune-stained in the absence of a primary antibody were set as the background control. **(C)** Statistical results of quantitative analysis with flow cytometry indicate SRD5A1 and SRD5A3 levels in LNCap and PC-3 cells 24 h post-treatment. Data were normalized to untreated control, which was set to 100%, and relative values are presented as mean ± SEM, $n = 6$, *significantly different from HT ($p \leq 0.05$), #significantly different from control ($p \leq 0.05$).

membranes (Figure 7A). Since the area of one well of the 96-well plate was exactly covered by the dimension of the focal field, the fluorescent images were taken randomly in the visualized view of the wells. Compared to untreated control, FUS-Cav treatment immediately led to an enhanced percentage of LNCap cells with a PI stained nucleus (Figure 7A) suggesting the occurrence of sonoporation. In the semi-quantitative results (Figure 7B), the percentage of PI-positive cells was significantly enhanced to 61.7% in LNCap cells immediately after exposure to FUS-Cav, and only 3.7% PI-positive cells were observed 30 min post-treatment suggesting the recovery of sonoporation in LNCap cells. The sonoporation effects induced by FUS-Cav in PC-3 cell line were reported in previous research (Hu et al., 2020): FUS-Cav treatment induced sonoporation effects (PI-positive) were observed in 49.9% of PC-3 cells, and the percentage of PI-positive cells is only 4% left 30 min after FUS-Cav indicating the resealing of cell membranes in PC-3 cells.

Discussion

The mechanisms of FUS/HIFU in medical sectors are mostly separated into i) thermal and ii) mechanical effects., with the cavitation effects being the emphasis of research and application in mechanical effects. Clinically, the intense heat generated by HIFU is utilized non-invasively and accurately to ablate prostate tumors

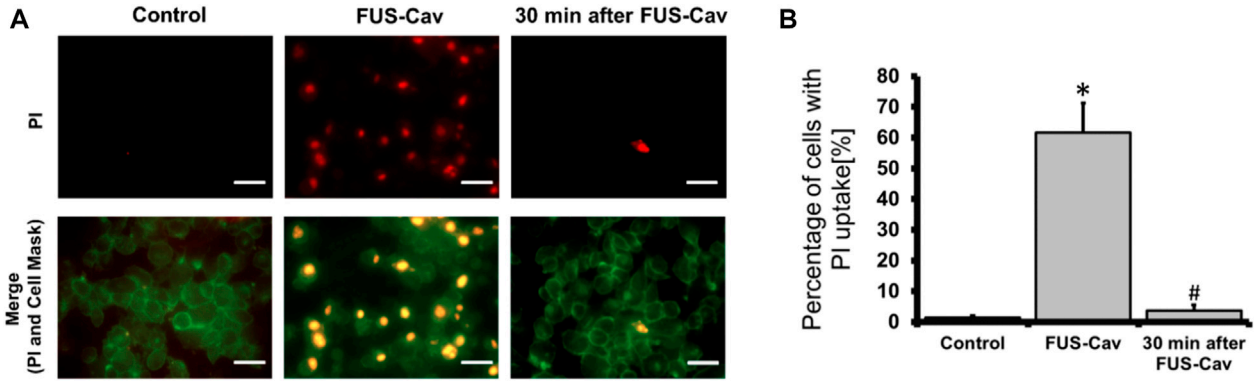

FIGURE 7
FUS-Cav induced sonoporation in LNCap cells. **(A)** Representative fluorescence microscopy images for LNCap cells showing an increase in red PI fluorescence during FUS-Cav; red: PI-stained cell nucleus; green: CellMask™ stained cell membranes, scale bar = 30 μm. **(B)** Semi-quantitative analysis of PI-positive percentage representing the quantity of sonoporated LNCap cells. Data were normalized to total cell number as 100% and relative values presented as mean ± SEM, n = 6, *significantly different from control ($p \leq 0.05$), #significantly different from FUS-Cav ($p \leq 0.05$).

under the guidance of MRI (Zhang et al., 2021). FUS allows for targeted treatment, causing thermal tissue coagulation, necrosis, and heat shock by raising the temperature by 55°C–80°C (Bakavicius et al., 2022). The majority of preclinical applications of cavitation effects have been focused on drug delivery (Xia et al., 2021; Wang et al., 2022), histotripsy (Xu et al., 2021), lithotripsy and application of anti-vascular effects (Tung et al., 2011; Kwok et al., 2013; Daecher et al., 2017). Cavitation is not regarded as having a favorable impact in the clinical application of HIFU thermal ablation of prostate cancers due to the lack of relevant studies demonstrating the synergistic effect between the two concomitant FUS-induced mechanisms i.e., cavitation and thermal effects. A PCI (passive cavitation imaging) system is utilized to monitor the broadband emissions to avoid cavitation-induced inadvertent tissue injury (Izadifar et al., 2019). *In vitro*, a short FUS shot (with cavitation) can support standard hyperthermia (HT) to reduce cell clonogenicity, metabolic activity, and cell potential to invade in human prostate cancer (PC-3), glioblastoma (T98G), and head and neck cancer (FaDu) cells, according to our previous study (Hu et al., 2020). The mechanisms of treatment could be linked to cavitation-induced sonoporation, which has been shown to induce several anti-proliferative effects on cancer cells but no more molecular mechanisms have been identified (Feril and Kondo, 2004; Miller and Dou, 2009; Karshafian et al., 2010; Zhong et al., 2011; Chen et al., 2013; Saliev et al., 2013). In this study, the effect of FUS-induced cavitation in combination with HT in the treatment of prostate cancer was further investigated using another prostate cancer cell line LNCap, and the therapeutic mechanism was evaluated from the perspectives of cell membrane disruption, DSBs, cell cycle arrest, and inhibiting the AR signal pathway of prostate cancer cells.

Currently, a lot of research about cavitation mainly focuses on its effects on cell membranes. Cavitation was reported to induce the deformation, damage, or sonoporation on the membrane of cancer cells and was usually used to deliver therapeutic agents (e.g., drugs or gene fragments) to targeted cells (Zolochevska et al., 2011; Wang et al., 2013; Yu et al., 2016). Sonoporation is a unique effect induced by FUS on cells: when the cavitation occurs near cell membranes, the extraction and contraction of the gas-filled cavities create the pores on the cell membrane temporarily (Tu and Yu, 2022). PI, a fluorescent dye with a molecular diameter of 0.8 nm, was used to investigate the sonoporation effect *in vitro* (Van Wamel et al., 2006). Pores created by sonoporation were reported to be 110 ± 40 nm in size, allowing PI molecules to pass through the cell membrane (Zhou et al., 2009). Sonoporated cells reseal the cell membrane within minutes after being exposed to ultrasound. However, the self-repairing of the cell membrane does not signify that sonoporation has no impact on cell survival. Papers are reporting the anti-proliferative effects of sonoporation or cavitation on cancer cells (Miller and Dou, 2009; Karshafian et al., 2010; Zhong et al., 2011; Chen et al., 2013). Sonoporation-induced apoptosis of human leukemia cells was associated with the decreased expression of polyadenosine diphosphate ribose polymerase (PARP) protein, which is a pro-apoptotic marker correlated to the impairment of DNA repair functionality (Figure 8). Sonoporation was also found to suppress the expression of a variety of checkpoint proteins such as cyclin and Cdk (cyclin dependent kinase) which play a vital role in cell cycle progression and prolong the DNA synthesis, thereby inducing cell cycle arrest in leukemia cells (Figure 8) (Zhong et al., 2011; Chen et al., 2013). Similarly, the percentages of sub-G1 phase in both sonoporated prostate cancer cell lines (apoptotic cells) (Plesca et al., 2008) increased significantly after treatment with FUS-induced cavitation compared to untreated groups, according to our findings. Sonoporation triggered cell cycle arrest on prostate cancer cells predominantly in the sub-G1 phase of apoptotic cells, whereas leukemia cells mostly in the G2/M and G1/S phases, implying that the cavitation-induced sonoporation effect on the cancer cell cycle arrest is cell type-dependent. Furthermore, when FUS-generated cavitation is combined with thermal effects (45°C for 30 min) that belongs to another mechanism of FUS, a substantial accumulation of cells in the Sub-G1 phase was observed in prostate cancer cells compared to a single treatment of HT or FUS-Cav. This is believed to be one of the potential mechanisms underlying the combined effects of HT treatment and FUS-induced cavitation on the inhibition of cell metabolic activity and clonogenic survival in prostate cancer cells *in vitro*.

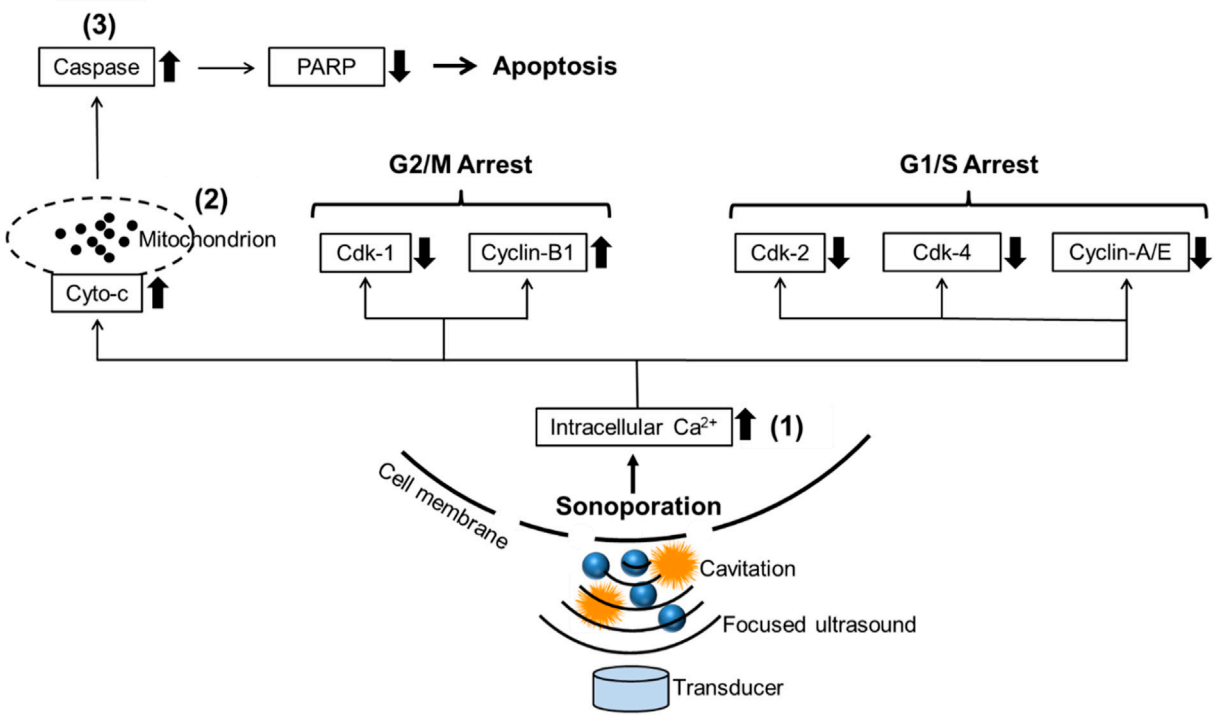

FIGURE 8
Schematic diagram reveals the potential mechanism of sonoporation-induced cell apoptosis and cell-cycle arrest. The transduction of intracellular signaling molecules involves 1) intracellular Ca^{2+} signaling system, 2) mitochondrion biology, and 3) apoptosis signaling pathway. Cyto-c: cytochrome c, PARP: polyadenosine diphosphate ribose polymerase, Cdk: Cyclin-dependent kinases. Adapted from (Zhong et al., 2011).

DSBs are randomly repaired in the absence of an intact template copy, wherefore they are considered one of the most dangerous forms of DNA damage. Incorrect gene repair can result in genomic rearrangements (deletions, translocations, fusions of DNA, etc.), leading to cell death potentially (Furusawa et al., 2014). Previous research on the mechanical effects of ultrasound on cells focused mainly on the impairment of cell membrane permeability and the consequent triggering of several biochemical responses, such as cell cycle arrest caused by sonoporation as mentioned above, as well as apoptosis (Zhong et al., 2011; Chen et al., 2013). However, it has been demonstrated that ultrasonic can penetrate the nuclear territory deeply, leading to alterations in genes and protein expression while also enhancing macromolecular localization. Previously, it was shown that DSBs occurred in pure DNA solution irradiated by ultrasound (Kondo et al., 1985). A neutral comet test was recently employed by Yukihiro Furusawa et al. to confirm the occurrence of DSBs in various leukemia cell lines exposed to ultrasonic irradiation *in vitro*. DNA damage was not highly associated with apoptosis and was primarily induced by the cavitation effect rendered by ultrasound waves penetrating deep into the nuclear territory (Furusawa et al., 2014). The occurrence of DSBs after the FUS-Cav treatment on prostate cancer cell lines (PC-3 and LNCap) was confirmed by the detection of DSBs events using γH2A.X as a biomarker, and the occurrence of DSBs in the nuclei of both prostate cancer cell lines was significantly increased when FUS-Cav was combined with thermal therapy compared to any single treatment in our study. This is in line with the findings of Yukihiro Furusawa, who suggested that cavitation may be a worrying sign as it shakes the safety of ultrasound in diagnostic applications, but maximized DNA damage induced by FUS-induced thermal effect combined with cavitation may eventually lead to cell death, which is beneficial for cancer eradication potentially. And unquestionably advantageous for the use of therapeutic ultrasound (i.e., HIFU) to treat tumors.

Zhou et al. (2012), reported that approximately half of the sonoporated KHT C (mouse fibrosarcoma) cells could not maintain long-term cell survival after the ultrasound-mediated MBs. The potential impacts of ultrasound mechanical effects also include changes in cell ultrastructure, division ability, chromosomal and cytogenetic effects, and functions (Izadifar et al., 2017). In our previous research (Hu et al., 2020), sonoporation occurred in more PC-3 cells (49.9%) than FaDu cells (23.3%) immediately after short FUS shots with cavitation (FUS-Cav) revealing that PC-3 cells are more susceptible to cavitation, which might be the biophysical mechanism at the cellular level here leading to lower survival of PC-3 compared to FaDu cells in the combination treatments. The extents and types of anti-proliferative effects induced by sonoporation vary depending on cancer cell types (Miller and Dou, 2009; Karshafian et al., 2010; Zhong et al., 2011; Chen et al., 2013). In the current investigation, FUS-Cav was able to induce sonoporation in 61.7% of LNCap cells, and more than 49.9% of PC-3 cells. Our findings suggest that LNCap is more susceptible to cavitation than PC-3, and when cavitation is combined with thermal effects on LNCap, it inhibits cell metabolic activity, clonogenic

survival, and invasion potential to a greater extent than PC-3. Although FUS-induced cavitation was proved to induce sonoporation in prostate cancer cell lines and head and neck cancer cell lines in our studies, the subsequent anti-proliferative effects (e.g., cancer cell apoptosis, cell-cycle arrest or prolong of DNA-synthesis) are still required to be clarified in future research and validated in animal models.

In our experiment, the treatment of water bath HT at 45°C for 30 min led to a significant reduction of cell invasion of prostate cancer cells LNCap and PC-3 compared to untreated control. Short FUS shots with cavitation (FUS-Cav) also demonstrated a significant suppressive effect on the invasion of prostate cancer cells, the pre-treatment to LNCap and PC-3 cells with FUS-Cav significantly expanded the impact of the subsequent HT treatment to inhibit cell invasion, exhibiting the additive effects of FUS-Cav to HT on the suppression of prostate cancer cell potential to invade in our study. In some other research, the activation of the phosphatidylinositol-3-kinase/AKT (PI3K/AKT) signaling pathway was discovered to be responsible for the migration and invasion of prostate cancer cells (Zhou et al., 2017). Ogata et al. (2005); Ogata et al. (2011) described that the inhibition of invasiveness of small cell lung cancer cell line A594 was induced by the downregulation of the matrix metalloproteinase (MMP)-2, which was attributed to the inactivation of the PI3K/AKT signaling pathway. HT was previously shown to inhibit cancer cell invasion *via* the downregulation of metastatic-related proteins, MMP-2 and MMP-9 (Xie et al., 2011). In numerous studies, the expression of MMP-2/9 has usually associated with the PI3K/AKT signaling pathway (Ogata et al., 2005; Adya et al., 2008; Chen et al., 2009; Zhu et al., 2019), the suppression of the PI3K/AKT signaling pathway in prostate cancer cells could result in the downregulation of MMP-2/9 (Chien et al., 2010). It has been previously reported that the cavitation effects were able to hinder the invasion and migration of PC-3 cells *via* downregulation of the MMP-2/9 (Wei et al., 2014). Based on the literature reports, HT as well as cavitation could inhibit the invasion of cancer cells in varying degrees by hindering cancer metastatic-related proteins MMPs. We assume that the combination of cavitation with HT carries the potential to reduce the expression of MMPs compared to single treatments, which is supposed to be the underlying mechanism of cavitation-induced additive effects to HT on the inhibition of the prostate cancer cell potential to invade. The inhibition of MMPs might be associated with the inactivation of the PI3K/AKT signaling pathway.

5α-reductase (SRD5A) proteins were discovered to be associated with dihydrotestosterone generation and activation of the AR signaling pathway in the prostate. SRD5A2 was the predominant form of 5α-reductase in healthy prostate tissue and benign prostatic diseases. SRD5A1 and SRD5A3 were the primary isozymes in the prostate cancer cells, and suppression of SRD5A1 and SRD5A3 protein levels was reported to be a promising alternative therapy to block the AR signaling pathway and inhibit the growth of malignant prostate tumors (Uemura et al., 2008; Godoy et al., 2011). In our experiment, a single FUS-Cav treatment demonstrated a minor inhibitory effect on the expression of SRD5A1 and SRD5A3 in prostate cancer cells, and the combination treatment of FUS-Cav and water bath HT led to a significant reduction of SRD5A protein compared to single HT, but the suppressive effects of combination treatment for an isoform of SRD5A are cell-type dependent. FUS with cavitation supported HT to reduce SRD5A1 level but had no impact on SRD5A3 in the LNCap cell line. In contrast, FUS-Cav combined with HT resulted in the decrease of SRD5A3 level compared to single HT, but no additive effect to HT treatment in inhibiting SRD5A1. Type I and III of SRD5A coexist in prostate cancer cells to boost the AR pathway and support prostate cancer initiation and progression, thus downregulating either SRD5A1 or SRD5A3 may restrict the AR pathway and further inhibit the growth of prostate cancer cells (Uemura et al., 2008; Godoy et al., 2011). SRD5A protein was significantly decreased by FUS-Cav + HT treatment in prostate cancer cells, which might result in the inactivation of the AR signaling pathway and a reduction in cell survival.

In clinical practice, the leading cause of prostate cancer-related death is cancer metastasis (Li et al., 2014). Patients with metastatic prostate cancer have a poor quality of life and usually suffer from urinary retention and bone pain (Kiljunen et al., 2015). Cancer cell migration is the crucial step for cancer progression to a metastatic state (Dirat et al., 2015). It is necessary to find an approach to reduce the potential of cancer cells to invade for slowing the progression of prostate cancer. From our studies, short FUS shots with cavitation sensitize prostate cancer LNCap and PC-3 cells to HT, inhibiting not only the short- and long-term survival as mentioned above but also the cell potential to invade. It provides a novel strategy combining the use of HIFU-induced cavitation and thermal effects to reduce the potential to spread the prostate cancer cells through the body leading to cancer metastasis. The potential of FUS-induced cavitation as an HT therapy sensitizer was demonstrated by using an *in vitro* cell culture model in our prior study (Hu et al., 2020). Biological analyses at the cellular and molecular levels (e.g., apoptosis, DNA damage, cell cycle, and AR pathway) were performed in the current study to uncover the underlying mechanisms of cavitation-induced additive effect on HT. It is also worthwhile to mention the limitation of the current study. The current findings obtained by *in vitro* experiments warrant being validated by *in vivo* experiments, where the ultrasound parameters should be optimized in accordance with the tissues' properties for ultrasound propagation. Microbubble administration should be taken into consideration to generate constrained cavitation effects in animals or humans with reduced acoustic intensities. However, it should be noted that our *in vitro* study provided the first evidence that FUS-Cav sensitizes cancer cells to HT and revealed its underlying mechanisms, thereby offering a solid foundation for future *in vivo* and clinical studies.

Conclusion

Our findings demonstrated the additive effect of FUS-induced cavitation when it was applied together with moderate heating, which was displayed in a reduction of the metabolic activity, invasiveness, and clonogenic survival of LNCap cells (a cell line with lymph node metastasis from prostate cancer). Compared with PC-3 cells (a cell line with bone metastases from prostate cancer) investigated in our previous study, FUS-Cav showed a stronger additive effect on HT treatment for the LNCap cell line in this study. Our findings further imply that the cavitation-induced sonoporation may be connected to the additive effects of FUS on HT, with potential mechanisms including

the induction of DSBs, cell cycle arrest, and blocking of the AR signaling pathway in prostate cancer cells.

Data availability statement

The raw data supporting the conclusion of this article will be made available by the authors, without undue reservation.

Author contributions

Conceptualization, XZ and LL; Methodology, SH; Formal analysis, SH; Investigation, SH; Data curation, SH; Writing—original draft preparation, SH; Writing—review and editing, LL, XZ, and AM; Visualization, XZ; Supervision, XZ and AM; Funding acquisition, AM. All authors have read and agreed to the published version of the manuscript.

Funding

We appreciate the funding by the German Federal Ministry of Education and Research (BMBF) under the grant No. 03Z1L511 (SONO-RAY project). This article was supported by the Publication Fund of the University of Leipzig and the Deutsche Forschungsgemeinschaft (DFG, German Research Foundation)-funded.

Conflict of interest

The authors declare that the research was conducted in the absence of any commercial or financial relationships that could be construed as a potential conflict of interest.

Publisher's note

All claims expressed in this article are solely those of the authors and do not necessarily represent those of their affiliated organizations, or those of the publisher, the editors and the reviewers. Any product that may be evaluated in this article, or claim that may be made by its manufacturer, is not guaranteed or endorsed by the publisher.

Supplementary material

The Supplementary Material for this article can be found online at: https://www.frontiersin.org/articles/10.3389/fgene.2023.1122758/full#supplementary-material

References

Adya, R., Tan, B. K., Punn, A., Chen, J., and Randeva, H. S. (2008). Visfatin induces human endothelial VEGF and MMP-2/9 production via MAPK and PI3K/akt signalling pathways: Novel insights into visfatin-induced angiogenesis. *Cardiovasc. Res.* 78 (2), 356–365. doi:10.1093/cvr/cvm111

Bakavicius, A., Marra, G., Macek, P., Robertson, C., Abreu, A. L., George, A. K., et al. (2022). Available evidence on HIFU for focal treatment of prostate cancer: A systematic review. *Int. braz J. Urol.* 48, 263–274. doi:10.1590/S1677-5538.IBJU.2021.0091

Bull, V., Civale, J., Rivens, I., and ter Haar, G. R. (2011). "Cavitation detection using a fibre-optic hydrophone: A pilot study," in AIP Conference Proceedings., Tokyo, 9–12 June 2011.

Chen, J. s., Wang, Q., Fu, X. H., Huang, X. H., Chen, X. L., Cao, L. Q., et al. (2009). Involvement of PI3K/PTEN/AKT/mTOR pathway in invasion and metastasis in hepatocellular carcinoma: Association with MMP-9. *Hepatology Res.* 39 (2), 177–186. doi:10.1111/j.1872-034X.2008.00449.x

Chen, W., Zouboulis, C. C., Fritsch, M., Blume-Peytavi, U., Kodelja, V., Goerdt, S., et al. (1998). Evidence of heterogeneity and quantitative differences of the type 1 5alpha-reductase expression in cultured human skin cells-evidence of its presence in melanocytes. *J. investigative dermatology* 110 (1), 84–89. doi:10.1046/j.1523-1747.1998.00080.x

Chen, X., Wan, J. M., and Alfred, C. (2013). Sonoporation as a cellular stress: Induction of morphological repression and developmental delays. *Ultrasound Med. Biol.* 39 (6), 1075–1086. doi:10.1016/j.ultrasmedbio.2013.01.008

Chien, C.-S., Shen, K. H., Huang, J. S., Ko, S. C., and Shih, Y. W. (2010). Antimetastatic potential of fisetin involves inactivation of the PI3K/Akt and JNK signaling pathways with downregulation of MMP-2/9 expressions in prostate cancer PC-3 cells. *Mol. Cell. Biochem.* 333 (1), 169–180. doi:10.1007/s11010-009-0217-z

Cihoric, N., Tsikkinis, A., van Rhoon, G., Crezee, H., Aebersold, D. M., Bodis, S., et al. (2015). Hyperthermia-related clinical trials on cancer treatment within the ClinicalTrials. gov registry. *Int. J. Hyperth.* 31 (6), 609–614. doi:10.3109/02656736.2015.1040471

Daecher, A., Stanczak, M., Liu, J. B., Zhang, J., Du, S., Forsberg, F., et al. (2017). Localized microbubble cavitation-based antivascular therapy for improving HCC treatment response to radiotherapy. *Cancer Lett.* 411, 100–105. doi:10.1016/j.canlet.2017.09.037

Dirat, B., Ader, I., Golzio, M., Massa, F., Mettouchi, A., Cormont, M., et al. (2015). Inhibition of the GTPase Rac1 mediates the anti-migratory effects of metformin in prostate cancer cells. *Mol. Cancer Ther.* 14, 586–596. doi:10.1158/1535-7163.MCT-14-0102

Farny, C. H., Holt, R. G., and Roy, R. A. (2009). The correlation between bubble-enhanced HIFU heating and cavitation power. *IEEE Trans. Biomed. Eng.* 57 (1), 175–184. doi:10.1109/TBME.2009.2028133

Feril, L. B., and Kondo, T. (2004). Biological effects of low intensity ultrasound: The mechanism involved, and its implications on therapy and on biosafety of ultrasound. *J. Radiat. Res.* 45 (4), 479–489. doi:10.1269/jrr.45.479

Franken, N. A., Rodermond, H. M., Stap, J., Haveman, J., and van Bree, C. (2006). Clonogenic assay of cells *in vitro*. *Nat. Protoc.* 1 (5), 2315–2319. doi:10.1038/nprot.2006.339

Furusawa, Y., Hassan, M. A., Zhao, Q. L., Ogawa, R., Tabuchi, Y., and Kondo, T. (2014). Effects of therapeutic ultrasound on the nucleus and genomic DNA. *Ultrason. sonochemistry* 21 (6), 2061–2068. doi:10.1016/j.ultsonch.2014.02.028

Godoy, A., Kawinski, E., Li, Y., Oka, D., Alexiev, B., Azzouni, F., et al. (2011). 5α-reductase type 3 expression in human benign and malignant tissues: A comparative analysis during prostate cancer progression. *Prostate* 71 (10), 1033–1046. doi:10.1002/pros.21318

Gourevich, D., Dogadkin, O., Volovick, A., Wang, L., Gnaim, J., Cochran, S., et al. (2013). Ultrasound-mediated targeted drug delivery with a novel cyclodextrin-based drug carrier by mechanical and thermal mechanisms. *J. Control. release* 170 (3), 316–324. doi:10.1016/j.jconrel.2013.05.038

Hegyi, G., Szigeti, G. P., and Szász, A. (2013). Hyperthermia versus oncothermia: Cellular effects in complementary cancer therapy. *Evidence-Based Complementary Altern. Med.* 2013, 1–12. doi:10.1155/2013/672873

Hildebrandt, B., Wust, P., Ahlers, O., Dieing, A., Sreenivasa, G., Kerner, T., et al. (2002). The cellular and molecular basis of hyperthermia. *Crit. Rev. oncology/hematology* 43 (1), 33–56. doi:10.1016/s1040-8428(01)00179-2

Hu, S., Zhang, X., Unger, M., Patties, I., Melzer, A., and Landgraf, L. (2020). Focused ultrasound-induced cavitation sensitizes cancer cells to radiation therapy and hyperthermia. *Cells* 9 (12), 2595. doi:10.3390/cells9122595

Hurwitz, M., and Stauffer, P. (2014). "Hyperthermia, radiation and chemotherapy: The role of heat in multidisciplinary cancer care," in *Seminars in oncology* (Netherlands: Elsevier).

Izadifar, Z., Babyn, P., and Chapman, D. (2017). Mechanical and biological effects of ultrasound: A review of present knowledge. *Ultrasound Med. Biol.* 43 (6), 1085–1104. doi:10.1016/j.ultrasmedbio.2017.01.023

Izadifar, Z., Babyn, P., and Chapman, D. (2019). Ultrasound cavitation/microbubble detection and medical applications. *J. Med. Biol. Eng.* 39 (3), 259–276. doi:10.1007/s40846-018-0391-0

Kampinga, H., and Dikomey, E. (2001). Hyperthermic radiosensitization: Mode of action and clinical relevance. *Int. J. Radiat. Biol.* 77 (4), 399–408. doi:10.1080/09553000010024687

Karshafian, R., Samac, S., Bevan, P. D., and Burns, P. N. (2010). Microbubble mediated sonoporation of cells in suspension: Clonogenic viability and influence of molecular size on uptake. *Ultrasonics* 50 (7), 691–697. doi:10.1016/j.ultras.2010.01.009

Kiljunen, T., Kangasmaki, A., Aaltonen, A., Kairemo, K., Partanen, K., Joensuu, G., et al. (2015). VMAT technique enables concomitant radiotherapy of prostate cancer and pelvic bone metastases. *Acta Oncol.* 54 (6), 847–853. doi:10.3109/0284186X.2014.962665

Kondo, T., Arai, S., Kuwabara, M., Yoshii, G., and Kano, E. (1985). Damage in DNA irradiated with 1.2 MHz ultrasound and its effect on template activity of DNA for RNA synthesis. *Radiat. Res.* 104 (3), 284–292. doi:10.2307/3576590

Kwok, S. J., El Kaffas, A., Lai, P., Al Mahrouki, A., Lee, J., Iradji, S., et al. (2013). Ultrasound-mediated microbubble enhancement of radiation therapy studied using three-dimensional high-frequency power Doppler ultrasound. *Ultrasound Med. Biol.* 39 (11), 1983–1990. doi:10.1016/j.ultrasmedbio.2013.03.025

Lai, C.-Y., Wu, C. H., Chen, C. C., and Li, P. C. (2006). Quantitative relations of acoustic inertial cavitation with sonoporation and cell viability. *Ultrasound Med. Biol.* 32 (12), 1931–1941. doi:10.1016/j.ultrasmedbio.2006.06.020

Li, D., Zhao, L. N., Zheng, X. L., Lin, P., Lin, F., Li, Y., et al. (2014). Sox2 is involved in paclitaxel resistance of the prostate cancer cell line PC-3 via the PI3K/Akt pathway. *Mol. Med. Rep.* 10 (6), 3169–3176. doi:10.3892/mmr.2014.2630

Li, J., Ding, Z., Wang, Z., Lu, J. F., Maity, S. N., Navone, N. M., et al. (2011). Androgen regulation of 5α-reductase isoenzymes in prostate cancer: Implications for prostate cancer prevention. *PloS one* 6 (12), e28840. doi:10.1371/journal.pone.0028840

Lo, C.-W., Desjouy, C., Chen, S. R., Lee, J. L., Inserra, C., Bera, J. C., et al. (2014). Stabilizing *in vitro* ultrasound-mediated gene transfection by regulating cavitation. *Ultrason. sonochemistry* 21 (2), 833–839. doi:10.1016/j.ultsonch.2013.10.017

Lonergan, P. E., and Tindall, D. J. (2011). Androgen receptor signaling in prostate cancer development and progression. *J. Carcinog.* 10 (1), 20. doi:10.4103/1477-3163.83937

Maxwell, A. D., Cain, C. A., Hall, T. L., Fowlkes, J. B., and Xu, Z. (2013). Probability of cavitation for single ultrasound pulses applied to tissues and tissue-mimicking materials. *Ultrasound Med. Biol.* 39 (3), 449–465. doi:10.1016/j.ultrasmedbio.2012.09.004

Meehan, K. L., and Sadar, M. D. (2003). Androgens and androgen receptor in prostate and ovarian malignancies. *Front. Bioscience-Landmark* 8 (4), 780–800. doi:10.2741/1063

Miller, D. L., and Dou, C. (2009). Induction of apoptosis in sonoporation and ultrasonic gene transfer. *Ultrasound Med. Biol.* 35 (1), 144–154. doi:10.1016/j.ultrasmedbio.2008.06.007

Morris, P., Hurrell, A., Shaw, A., Zhang, E., and Beard, P. (2009). A Fabry–Pérot fiber-optic ultrasonic hydrophone for the simultaneous measurement of temperature and acoustic pressure. *J. Acoust. Soc. Am.* 125 (6), 3611–3622. doi:10.1121/1.3117437

Ogata, T., Teshima, T., Inaoka, M., Minami, K., Tsuchiya, T., Isono, M., et al. (2011). Carbon ion irradiation suppresses metastatic potential of human non-small cell lung cancer A549 cells through the phosphatidylinositol-3-kinase/Akt signaling pathway. *J. Radiat. Res.* 52 (3), 374–379. doi:10.1269/jrr.10102

Ogata, T., Teshima, T., Kagawa, K., Hishikawa, Y., Takahashi, Y., Kawaguchi, A., et al. (2005). Particle irradiation suppresses metastatic potential of cancer cells. *Cancer Res.* 65 (1), 113–120. doi:10.1158/0008-5472.113.65.1

Peeken, J. C., Vaupel, P., and Combs, S. E. (2017). Integrating hyperthermia into modern radiation oncology: What evidence is necessary? *Front. Oncol.* 7, 132. doi:10.3389/fonc.2017.00132

Plesca, D., Mazumder, S., and Almasan, A. (2008). DNA damage response and apoptosis. *Methods Enzym.* 446, 107–122. doi:10.1016/S0076-6879(08)01606-6

Rieke, V., and thermometry., M. R. (2011). *Interventional magnetic resonance imaging*.

Saliev, T., Feril, L. B., Jr, Nabi, G., and Melzer, A. (2013). Targeted manipulation of apoptotic pathways by using High Intensity Focused Ultrasound in cancer treatment. *Cancer Lett.* 338 (2), 204–208. doi:10.1016/j.canlet.2013.04.016

Schade, G. R., Keller, J., Ives, K., Cheng, X., Rosol, T. J., Keller, E., et al. (2012). Histotripsy focal ablation of implanted prostate tumor in an ACE-1 canine cancer model. *J. urology* 188 (5), 1957–1964. doi:10.1016/j.juro.2012.07.006

Schuster, T. G., Wei, J. T., Hendlin, K., Jahnke, R., and Roberts, W. W. (2018). Histotripsy treatment of benign prostatic enlargement using the vortx rx system: Initial human safety and efficacy outcomes. *Urology* 114, 184–187. doi:10.1016/j.urology.2017.12.033

Siedek, F., Heijman, E., Grinstein, O., Bratke, G., Heneweer, C., Puesken, M., et al. (2019). "Magnetic resonance-guided high-intensity focused ultrasound (MR-HIFU): Technical background and overview of current clinical applications (part 1)," in *RöFo-Fortschritte auf dem Gebiet der Röntgenstrahlen und der bildgebenden Verfahren* (New York: © Georg Thieme Verlag KG).

Song, C. W., Shakil, A., Griffin, R. J., and Okajima, K. (1997). Improvement of tumor oxygenation status by mild temperature hyperthermia alone or in combination with carbogen. *Seminars Oncol.* 24, 626–632.

Song, W., and Khera, M. (2014). Physiological normal levels of androgen inhibit proliferation of prostate cancer cells *in vitro*. *Asian J. Androl.* 16 (6), 864–868. doi:10.4103/1008-682X.129132

Thigpen, A. E., Silver, R. I., Guileyardo, J. M., Casey, M. L., McConnell, J. D., and Russell, D. W. (1993). Tissue distribution and ontogeny of steroid 5 alpha-reductase isozyme expression. *J. Clin. investigation* 92 (2), 903–910. doi:10.1172/JCI116665

Tu, J., and Yu, A. C. (2022). Ultrasound-mediated drug delivery: Sonoporation mechanisms, biophysics, and critical factors. *BME Front.* 2022, 2022. doi:10.34133/2022/9807347

Tung, Y.-S., Vlachos, F., Feshitan, J. A., Borden, M. A., and Konofagou, E. E. (2011). The mechanism of interaction between focused ultrasound and microbubbles in blood-brain barrier opening in mice. *J. Acoust. Soc. Am.* 130 (5), 3059–3067. doi:10.1121/1.3646905

Uemura, M., Tamura, K., Chung, S., Honma, S., Okuyama, A., Nakamura, Y., et al. (2008). Novel 5α-steroid reductase (SRD5A3, type-3) is overexpressed in hormone-refractory prostate cancer. *Cancer Sci.* 99 (1), 81–86. doi:10.1111/j.1349-7006.2007.00656.x

Van Wamel, A., Kooiman, K., Harteveld, M., Emmer, M., ten Cate, F. J., Versluis, M., et al. (2006). Vibrating microbubbles poking individual cells: Drug transfer into cells via sonoporation. *J. Control. release* 112 (2), 149–155. doi:10.1016/j.jconrel.2006.02.007

Wang, Y., Bai, W. K., Shen, E., and Hu, B. (2013). Sonoporation by low-frequency and low-power ultrasound enhances chemotherapeutic efficacy in prostate cancer cells *in vitro*. *Oncol. Lett.* 6 (2), 495–498. doi:10.3892/ol.2013.1389

Wang, Z., Chen, C., Zou, P., Tao, Y., Gao, F., Jia, C., et al. (2022). Ultrasound-induced microbubble cavitation combined with paclitaxel-loaded nanoparticles for the elimination of PC-3 cells *in vitro*. *Nano LIFE* 12 (01), 2150006. doi:10.1142/s1793984421500069

Wei, C., Bai, W. K., Wang, Y., and Hu, B. (2014). Combined treatment of PC-3 cells with ultrasound and microbubbles suppresses invasion and migration. *Oncol. Lett.* 8 (3), 1372–1376. doi:10.3892/ol.2014.2310

Wiggins, S., and Ottino, J. M. (2004). Foundations of chaotic mixing. *Philosophical Trans. R. Soc. Lond. Ser. A Math. Phys. Eng. Sci.* 362 (1818), 937–970. doi:10.1098/rsta.2003.1356

Wu, Y., Godoy, A., Azzouni, F., Wilton, J. H., Ip, C., and Mohler, J. L. (2013). Prostate cancer cells differ in testosterone accumulation, dihydrotestosterone conversion, and androgen receptor signaling response to steroid 5α-reductase inhibitors. *Prostate* 73 (13), 1470–1482. doi:10.1002/pros.22694

Xia, H., Yang, D., He, W., Zhu, X., Yan, Y., Liu, Z., et al. (2021). Ultrasound-mediated microbubbles cavitation enhanced chemotherapy of advanced prostate cancer by increasing the permeability of blood-prostate barrier. *Transl. Oncol.* 14 (10), 101177. doi:10.1016/j.tranon.2021.101177

Xie, X., Shao, X., Gao, F., Jin, H., Zhou, J., Du, L., et al. (2011). Effect of hyperthermia on invasion ability and TGF-β1 expression of breast carcinoma MCF-7 cells. *Oncol. Rep.* 25 (6), 1573–1579. doi:10.3892/or.2011.1240

Xu, Z., Hall, T. L., Vlaisavljevich, E., and Lee, F. T., Jr (2021). Histotripsy: The first noninvasive, non-ionizing, non-thermal ablation technique based on ultrasound. *Int. J. Hyperth.* 38 (1), 561–575. doi:10.1080/02656736.2021.1905189

Yu, F. T., Chen, X., Wang, J., Qin, B., and Villanueva, F. S. (2016). Low intensity ultrasound mediated liposomal doxorubicin delivery using polymer microbubbles. *Mol. Pharm.* 13 (1), 55–64. doi:10.1021/acs.molpharmaceut.5b00421

Yu, S., Xia, S., Yang, D., Wang, K., Yeh, S., Gao, Z., et al. (2013). Androgen receptor in human prostate cancer-associated fibroblasts promotes prostate cancer epithelial cell growth and invasion. *Med. Oncol.* 30 (3), 674–677. doi:10.1007/s12032-013-0674-9

Zhang, X., Landgraf, L., Bailis, N., Unger, M., Jochimsen, T. H., and Melzer, A. (2021). Image-guided high-intensity focused ultrasound, A novel application for interventional nuclear medicine? *J. Nucl. Med.* 62 (9), 1181–1188. doi:10.2967/jnumed.120.256230

Zhong, W., Sit, W. H., Wan, J. M. F., and Yu, A. C. H. (2011). Sonoporation induces apoptosis and cell cycle arrest in human promyelocytic leukemia cells. *Ultrasound Med. Biol.* 37 (12), 2149–2159. doi:10.1016/j.ultrasmedbio.2011.09.012

Zhou, Y., Gu, P., Li, J., Li, F., Zhu, J., Gao, P., et al. (2017). Suppression of STIM1 inhibits the migration and invasion of human prostate cancer cells and is associated with PI3K/Akt signaling inactivation. *Oncol. Rep.* 38 (5), 2629–2636. doi:10.3892/or.2017.5961

Zhou, Y., Kumon, R. E., Cui, J., and Deng, C. X. (2009). The size of sonoporation pores on the cell membrane. *Ultrasound Med. Biol.* 35 (10), 1756–1760. doi:10.1016/j.ultrasmedbio.2009.05.012

Zhou, Y., Yang, K., Cui, J., Ye, J. Y., and Deng, C. X. (2012). Controlled permeation of cell membrane by single bubble acoustic cavitation. *J. Control. release* 157 (1), 103–111. doi:10.1016/j.jconrel.2011.09.068

Zhu, W., Wu, X., Yang, B., Yao, X., Cui, X., Xu, P., et al. (2019). miR-188-5p regulates proliferation and invasion via PI3K/Akt/MMP-2/9 signaling in keloids. *Acta Biochimica Biophysica Sinica* 51 (2), 185–196. doi:10.1093/abbs/gmy165

Zolochevska, O., Xia, X., Williams, B. J., Ramsay, A., Li, S., and Figueiredo, M. L. (2011). Sonoporation delivery of interleukin-27 gene therapy efficiently reduces prostate tumor cell growth *in vivo*. *Hum. gene Ther.* 22 (12), 1537–1550. doi:10.1089/hum.2011.076

Frontiers in Genetics

Highlights genetic and genomic inquiry relating to all domains of life

The most cited genetics and heredity journal, which advances our understanding of genes from humans to plants and other model organisms. It highlights developments in the function and variability of the genome, and the use of genomic tools.

Discover the latest Research Topics

See more →

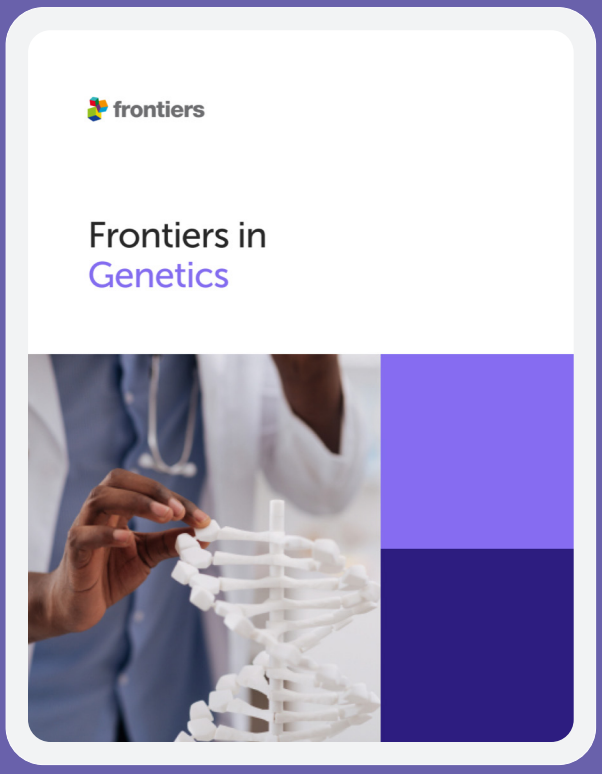

Frontiers

Avenue du Tribunal-Fédéral 34
1005 Lausanne, Switzerland
frontiersin.org

Contact us

+41 (0)21 510 17 00
frontiersin.org/about/contact